A novel role for the Parkinson disease-linked and neuromelanin-associated parkin protein as a cysteine-dependent redox-state regulator

Jacqueline M. Tokarew, M.Sc., M.D.

This thesis is being submitted to the Faculty of Medicine Graduate and Postdoctoral Studies in partial fulfillment of the requirements for the Doctorate in Philosophy degree in Cellular and Molecular Medicine

Department of Cellular and Molecular Medicine

Faculty of Medicine

University of Ottawa

Abstract

Parkinson disease (PD) is an incurable disease, second only to Alzheimer's disease as the most common neurodegenerative disease in adults. Unfortunately, the course of disease is significantly longer for individuals diagnosed at an early age (20-40 years of age). Although early-onset, recessively inherited cases represent a small subset of individuals with PD (~5-10%), their clinical presentation is unique, with symptoms being almost exclusively motor-related. The expressivity of early-onset PD is partially explained by post-mortem neuropathological findings, which demonstrate a specific loss of dopamine synthesizing cells in brainstem nuclei that also produce neuromelanin (i.e. *Substantia nigra* and *Locus coeruleus*). With the majority of early-onset PD cases being caused by homozygous and biallelic heterozygous mutations in the *PRKN* gene, its gene product, parkin, has been extensively studied. It is generally accepted that loss of its E3 ligase function leads to neurodegeneration by either one of the following two mechanisms: i) toxic substrate accumulation from the loss of target protein ubiquitination (and related degradation), or ii) accumulation of dysfunctional mitochondria due to impaired mitophagy initiation. However, whether these mechanisms lead to selective neuronal loss within the human brain remains unknown. This thesis represents a body of work that supports a novel role for parkin as a thiol-based anti-oxidant and redox homeostasis regulator, which helps explain the cell-specificity observed in recessive, *PRKN*-linked PD. These findings include: i) evidence that human brain parkin uniquely and natively undergoes age-associated aggregation beginning at 40 years of age (Chapter 2); ii) identification of multiple, reversible and irreversible oxidative modifications of parkin cysteines, both in cells and tissues, including dopamine-adduct conjugation on primate sequence-specific cysteine 95 (Chapter 2); iii) the demonstration that irreversible oxidation of parkin cysteines causes aggregate formation

in cells and mice exposed to exogenous and/or endogenous sources of oxidative and dopamine stress (Chapter 2 and 3); iv) evidence that parkin functions as a thiol-dependent anti-oxidant similar to glutathione (Chapter 2), which lowers oxidation state in cells and tissues under native and stress conditions (Chapter 2 and 3); v) the demonstration that parkin cysteines, notably C95, directly bind glutathione and regulate glutathione redox homeostasis in cells and tissues in a dynamic fashion (Chapter 3); and vi) the development of novel, human-specific, anti-parkin monoclonal antibodies that preferentially detect oxidized and aggregated forms of parkin found associated with neuromelanin and lysosomal storage vesicles within neurons of human *Substantia nigra* (Chapter 2 and 4). Future studies focusing on further validation of *in situ* oxidative modifications of parkin cysteines and their effect on protein structure, notably the poorly studied linker region that contains C95, will provide insight into how these oxidative modifications affect the function of parkin *in vivo*, including in adult human brain. Also, identifying the *bona fide* intracellular redox partners of parkin will be crucial to understanding how this protein regulates cellular redox state. Of clinical importance, the findings presented here indicate a potential, human-specific link between parkin and neuromelanin formation, which deserves to be further explored, such as with parkin mouse models engineered to produce neuromelanin. Finally, designing clinical trials using anti-oxidants specifically in individuals affected by *PRKN*-associated PD represents a logical, translational treatment approach to explore.

Table of Contents

Acknowledgements

Like many big projects, successful completion of this thesis was helped by the support of others. I would like to extend a heartfelt thank you to the following individuals:

First and foremost, I would like to dedicate this thesis to my family and close friends (son Theodore Tam, husband Roger Tam, parents Anne and Michael Tokarew, brother Daniel Tokarew and family, my kickboxing sister Zhaoyi , Taline, and my tight-knit gals Liliane, Annie, Taz and Elyse), who have supported me with their unconditional love, presence and encouragement. Without this, very little would have been accomplished professionally and personally.

Secondly, I want to thank my supervisor Dr. Michael Schlossmacher for welcoming me into his research group and providing me with many collaborative opportunities and the freedom to peer into many different rabbit-holes in pursuit of answers. I will never forget your dedication to finding a cure for your patients and hope to emulate this in my future career as clinician-scientist.

To all Schlossmacher lab members with whom I have worked with, I extend a big thank you! Dr. Julianna Tomlinson, Dr. Qiubo Jiang, Dr. Bojan Shutinoski and Dr. Andy Ng, thank you for technical support, scientific discussions and help with manuscript editing. A special thanks to Dr. Daniel El-Kodsi “my partner in parkin crime”, for being a friend, with whom I would spend many hours with running and discussing experiments. Thank you to Nathalie Lengacher, Angela Nguyen, Travis Fehr, Juan Li and undergraduate students Jasmine, Kelsey, Saba and Hoda for your technical support.

Thank you to my thesis advisory committee members, Dr. Steffany Bennett, Dr. Diane Lagace and Dr. Derek Pratt for your advice and guidance throughout my PhD journey. Additionally, I would like to acknowledge the funding received through the Canadian Institutes of Health Research, the Queen Elizabeth II Graduate Scholarship Fund, the Parkinson Research Consortium and the Michael J. Fox Foundation for Parkinson's Research, along with the many collaborators without whom the completion of this thesis would not have been possible.

Finally, a sincere thank you to all Parkinson disease patients and their families. Your testimonies, your time, your money and your brain donations are all enormously generous gifts and I hope that in-return my work will, in some small way, bring you closer to a cure.

Lists of Manuscripts

Lists of Figures

Lists of Tables

List of Abbreviations

$^{\bullet}OH$	hydroxyl radical
$^{\bullet}O_2^-$	superoxide
6-OHDA	6-hydroxydopamine
aa	amino acid
Aco2	aconitase-2
ACT	activating element
AD	Alzheimer's Disease
ADPD	autosomal dominant Parkinson Disease
AM	aminochrome
amu	atomic mass units
ARIH1	ariadne-1 homolog 1
ARPD	autosomal recessive Parkinson Disease
AT	amino-triazole
ATP	adenosine triphosphate
BSA	bovine serum albumin
BSO	buthionine sulfoximine
CCCP	carbonyl cyanide m-chlorophenyl hydrazine
CHO	Chinese hamster ovary cell line
CHOmP or CHO-parkin	CHO stably expressing myc parkin
CNS	central nervous system
COMT	catecholamine-*O*-methyltransferase
DA	dopamine
DAB	3'-Diaminobenzidine
DAM	dopamine-associated melanin
DAT	dopamine transporter
DCFH-DA	dichlorofluorescin diacetate
DJ-1	deglycase-1
DLB	Dementia with Lewy Body
DNTB	5,5'-dithio-bis-[2-nitrobenzoic acid]
DRD	dopa-responsive dystonia
DRT	dopamine replacement therapy
DTT	dithiothreitol
E1	ubiquitin-activating enzyme
E2	ubiquitin-conjugating enzyme
E3	ubiquitin ligase enzyme
EDTA	ethylenediaminetetraacetic acid
EOPD	early-onset Parkinson Disease

GCLC	glutamate cysteine ligase catalytic
GCLM	glutamate cysteine ligase modifier
GR	glutathione reductase
Grx	glutaredoxin
GSH	glutathione (reduced form)
GSH + GSSG	total glutathione
GSH-Px or GPx	glutathione peroxidase
GSSG	glutathione disulfide
H_2O_2	hydrogen peroxide
HECT	homologous to E6AP C-terminus
HEK-293	human embryonic kidney cell line 293
HMW	high molecular weight
HOIP	heme-oxidized IRP2 ubiquitin ligase 1-interacting protein
HRP	horseradish peroxidase
IAA	iodoacetamide
IBR	in-between RING
IHC	immunohistochemistry
IIF	indirect immunofluorescence
IMM	inner mitochondrial membrane
IP	immunoprecipitation
LAMP	Lysosomal-associated membrane protein
LB	Lewy Body
LC	*locus coeruleus*
LC3	microtubule-associated protein 1A/1B-light chain 3
LC-MS/MS	liquid chromatography with tandem mass spectrometry
L-dopa	L-3,4-dihydroxyphenylalanine
LN	Lewy Neurite
LRRK2	leucine-rich repeat kinase 2
M17	subcloned human neuroblastoma cell line
MAO	monoamine oxidase
MCB	monochlorobimane
MnSOD	manganese superoxide dismutase
MPP^+	1-methyl-4-phenylpyridinium
MPTP	N-methyl-4-phenyl-1,2,3,6-tetrahydropyridine
MS	mass spectrometry
NA	noradrenaline
NADPH	nicotinamide adenine dinucleotide phosphate
NEM	N-ethyl maleimide
NEMO	nuclear factor-κB (NF-κB) essential molecule
NF-kB	nuclear factor kappa B

NM	neuromelanin
NO	nitric oxide
OMM	outer mitochondrial membrane
$ONOO^-$	peroxynitrite
OS	oxidative stress
OXPHOS	oxidative phosphorylation
PACRG	parkin coregulated gene
PD	Parkinson Disease
PDD	Parkinson Disease with dementia
PINK1	PTEN-induced kinase-1
PMI	post-mortem interval
Prk8	monoclonal antibody clone 8
PRKN	parkin gene human homolog
prkn	parkin gene murine, rat and drosophila homolog
prkn -/-	*prkn* knockout mice
PTEN	phosphate and tensin homolog
PTM	post-translational modification
pUb	phosphorylated Ub
pUbl	phosphorylated ubiquitin-like domain
RBR	RING-between-RING
Rcat	required for catalysis
REP	repressor element of parkin
RES	reactive electrophilic species
RING	really interesting new gene
RNF43	ring finger protein 43
RNS	reactive nitrogen species
ROS	reactive oxygen species
r-parkin	recombinant parkin
RSH	thiol residue
S. nigra	*Substantia nigra*
SAG	sensitive to apoptosis gene
SDS	sodium dodecyl sulfate
SH-SY5Y	human neuroblastoma cell line
SNCA	a-synuclein gene name
SOD	superoxide dismutase
sod2 +/-	manganese superoxide dismutase haploinsufficiency
STN	subthalamic nucleus
SUMO	small ubiquitin-modifier
syn	α-synuclein protein
TCEP	tris(2-carboxyethyl)phosphine

TH	tyrosine hydroxylase
TNB	5-thio-2-nitrobenzoic-acid
TOMM	translocase of outer mitochondrial membrane
Tris	2-Amino-2-(hydroxymethyl)-1,3-propanediol
TS	Tris saline
TX	Triton X
Ub	ubiquitin
Ubl	ubiquitin-like
UIM	Ub-interacting motif
UPD	unique parkin domain
UPR	unfolded protein response
UPS	ubiquitin proteasome system
VDAC	voltage-dependent anion-selective channel
VMAT	vesicular monoamine transporter
VTA	ventral tegmental area

Chapter 1: General Introduction

1.1 Parkinson disease (PD)

Parkinson disease (PD) is a heterogeneous disease that affects >110,000 Canadians annually, representing 1-2 % of the population over the age of 65. It is one of the most prevalent, degenerative central nervous system (CNS) disorders in humans, second only to Alzheimer's disease (AD),[1] and affects men twice as much as women. Its annual incidence increases with the population age, from 0.1 to 2.9% of individuals between the 7th and 9th decades of life.[2] It is predicted that PD will affect nearly 9 million people globally in 2030.[3] Although this disease does not typically lower life expectancy, PD-associated symptoms can increase the risk of death caused by aspiration pneumonia, other forms of infections (e.g., urosepsis), malignancies (e.g., melanoma), or mechanical falls.[4-7]. The frequent association of advanced PD with dementia represents the number one cause for loss of independent living.

1.1.1 Clinical manifestations, diagnosis and pathophysiology of PD

This neurodegenerative disease was first described as the "Shaking Palsy" in 1817 by James Parkinson in An Essay on the Shaking Palsy[8] and later named PD by the French neurologist, Dr. Jean-Martin Charcot.[9] Historically, individuals were clinically diagnosed based on the presence of four key motor symptoms, now defined as the classic symptoms of PD: tremor, rigidity, bradykinesia (slow movement), and followed later by postural instability.[8] Currently, clinical diagnosis is confirmed based on the Movement Disorder Society-PD criteria, which includes the presence of bradykinesia, in combination with either resting tremor, rigidity, or both, as well as, the presence of other supportive criteria (e.g. responsive dopamine replacement therapy, DRT), absence of symptoms suggesting a non-PD etiology (e.g. respiratory dysfunction, dysphagia, dystonia or bilateral motor symptoms), and progression.[4,10]

Unfortunately, motor symptoms of 'typical' PD can be difficult to distinguish from other neurodegenerative motor-type diseases, termed parkinsonisms,[11] like progressive supranuclear palsy (PSP, caused by neuronal loss due to tauopathy in the basal ganglia, brainstem and cortex)[12] and multiple system atrophy (MSA, caused by neuronal and glial cell loss in the nigrostriatal tract, cerebellum and spinal cord).[13] In fact, roughly 10-20% of clinical diagnoses of PD are re-classified upon autopsy.[14,15] Areas of research involved in the development of novel diagnostic tools include neuroimaging (e.g. magnetic resonance imaging, radionuclide positron emission tomography, single photon emission computed tomography), [16-18] and cerebral spinal fluid (CSF) analyses[19] (e.g. α-synuclein,[20-24] C-reactive protein[25,26] and neurofilament light chain,[27,28]).

Definitive post-mortem diagnosis of PD is made based on histopathological findings within the brain, including: i) the selective loss of the dark brown pigmented neurons in the *Substantia nigra* (*S. nigra*, **Fig. 1.1a-d**), ii) the presence of protein-rich aggregates (*aka* inclusions) accumulated within neuronal cell bodies (Lewy Body, or LB, **Fig. 1.1e**) and neuronal projections (Lewy Neurites, or LN)[29,30], iii) loss of synapses in the neostriatum; and iv) gliosis. Lewy inclusions are composed predominantly of the presynaptic protein called α-synuclein[31] and ubiquitin, and are a common feature found in other neurodegenerative diseases as well (e.g. AD, MSA, and Dementia with Lewy Bodies or DLB); grouped together, these diseases are commonly referred to as synucleinopathies[32]. LB and LN are, however, not specific as they can also be found incidentally in age-matched neurological controls, albeit at a lesser rate and without neuronal loss in the latter.[33-35]

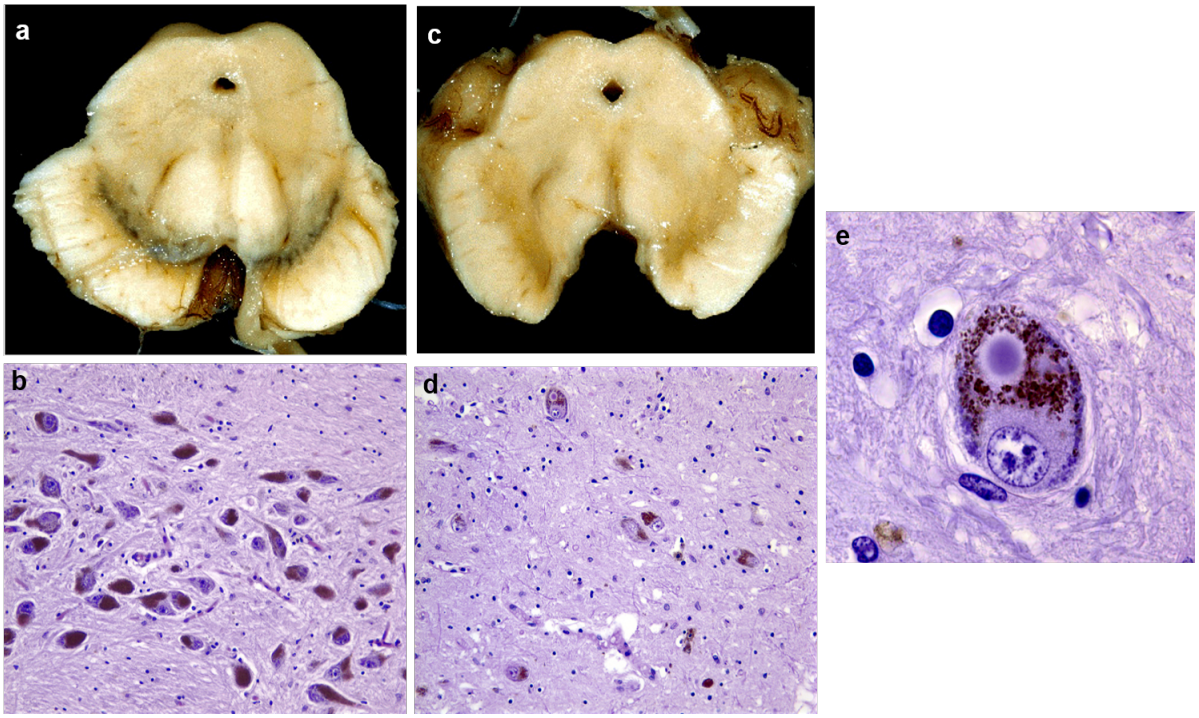

Figure 1.1. Neuropathological findings in Parkinson disease.
Gross anatomical appearance of a transverse section of a control (**a**) or Parkinson disease (c) human midbrain specimen. Immunohistological staining of the substantia nigra of control (**b**) and Parkinson disease (**d**) specimens, corresponding to (**a**) and (**c**), respectively. Immunohistological staining demonstrating the typical appearance of a Lewy Body, (**e**). Images obtained with permission from Agamanolis 2020.[30]

The late Dr. Hornykiewicz's hypothesis that loss of DA production caused PD led to the initial success of DRT trials and the later discovery that dopamine (DA) auto-oxidation is involved in the production of the dark pigment deposits (called neuromelanin, NM) found within the *S. nigra* neurons.[36-41] In mammalian CNS, DA is predominantly produced in neurons found within the *S. nigra* and the ventral tegmental area (VTA) DA pathways (**Fig. 1.2**),[42,43] which are both located in the mid-brain. Key structural characteristics of DA neurons help facilitate continual production and delivery of DA to multiple areas within the brain that rely on this neurotransmitter for regulating movement and behaviour.[44-46]

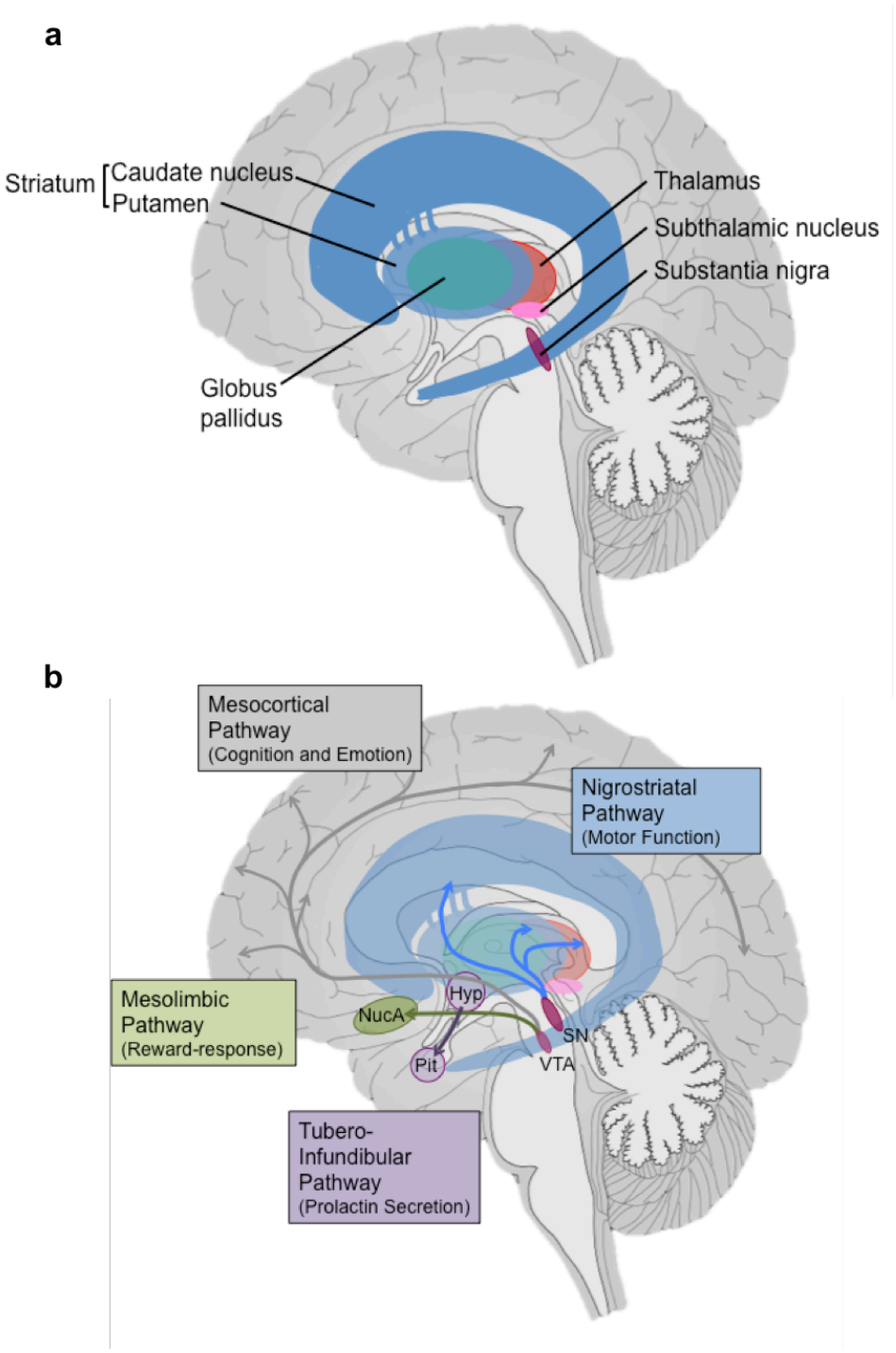

Figure 1.2. Basal ganglia structures and dopamine signaling pathways
(**a**) Structures of the basal ganglia shown in a sagittal plane of the brain. (**b**) The four major dopamine-dependent signaling pathways within the central nervous system. Nigrostriatal pathway connects the substantia nigra (SN) to the basal ganglia. The ventral tegmental area (VTA) projects to the cortex in the mesocortical pathway, or to the nucleus accumbens (NucA) in the mesolimbic pathway. The tubero-infundibular pathway links the hypothalamus (Hyp) to the pituitary gland (Pit) to regulate prolactin secretion.

Whereas the *S. nigra* DA neurons project onto the surrounding basal ganglia structures (**Fig. 1.2b**), known as the nigrostriatal pathway, to predominantly govern motor function, DA neurons within the VTA project to brain areas responsible for non-motor functions such as cognition, emotion (mesocortial pathway), and reward-response (mesolimbic pathway).[42,47] Not surprisingly, progressive *S. nigra* cell loss leads to worsening motor symptoms, such as tremor, bradykinesia and changes in muscle tone.[47,48] VTA DA neuron loss, on the other hand, is linked to the development of non-motor symptoms, such as impaired cognition, emotional dysregulation, and auditory and visual hallucinations.[49] The progressive development of cognitive symptoms following motor symptoms leads to a diagnosis of PD with dementia (or PDD). Progression to PDD is quite common, and patients with PD are at a six-time elevated risk of developing dementia compared to the general population.[50] In contrast, if cognitive impairment proceeds motor symptoms, a diagnosis of DLB is typically given, as long as, other core clinical features and biomarkers, which suggest a DA dysregulation etiology, are also present (e.g. fluctuating cognitive function, recurrent visual hallucinations and reduced dopamine transporter (DAT) uptake in the midbrain).[51] Given the close relationship between PDD and DLB clinical phenotypes, they are considered to share a common underlying pathophysiology and part of an α-synuclein-associated disease spectrum (synucleinopathies), which ranges from the least severe being incidental LB disease and non-demented Parkinson diseases to PDD, DLB, and finally, mixed dementia (with features of AD) as the most severe form.[52,53]

It is now well established that PD-specific motor symptoms usually develop when >70%, of *S. nigra* DA neurons (specifically within the *pars compacta*) are lost and caused by reduced motor activation within the basal ganglia.[54-57] The basal ganglia are a collection of distinct regions located centrally within the brain that share a collective purpose of regulating voluntary and involuntary motor signals arising from the cortex (see **Fig. 1.3a**).[58-60]

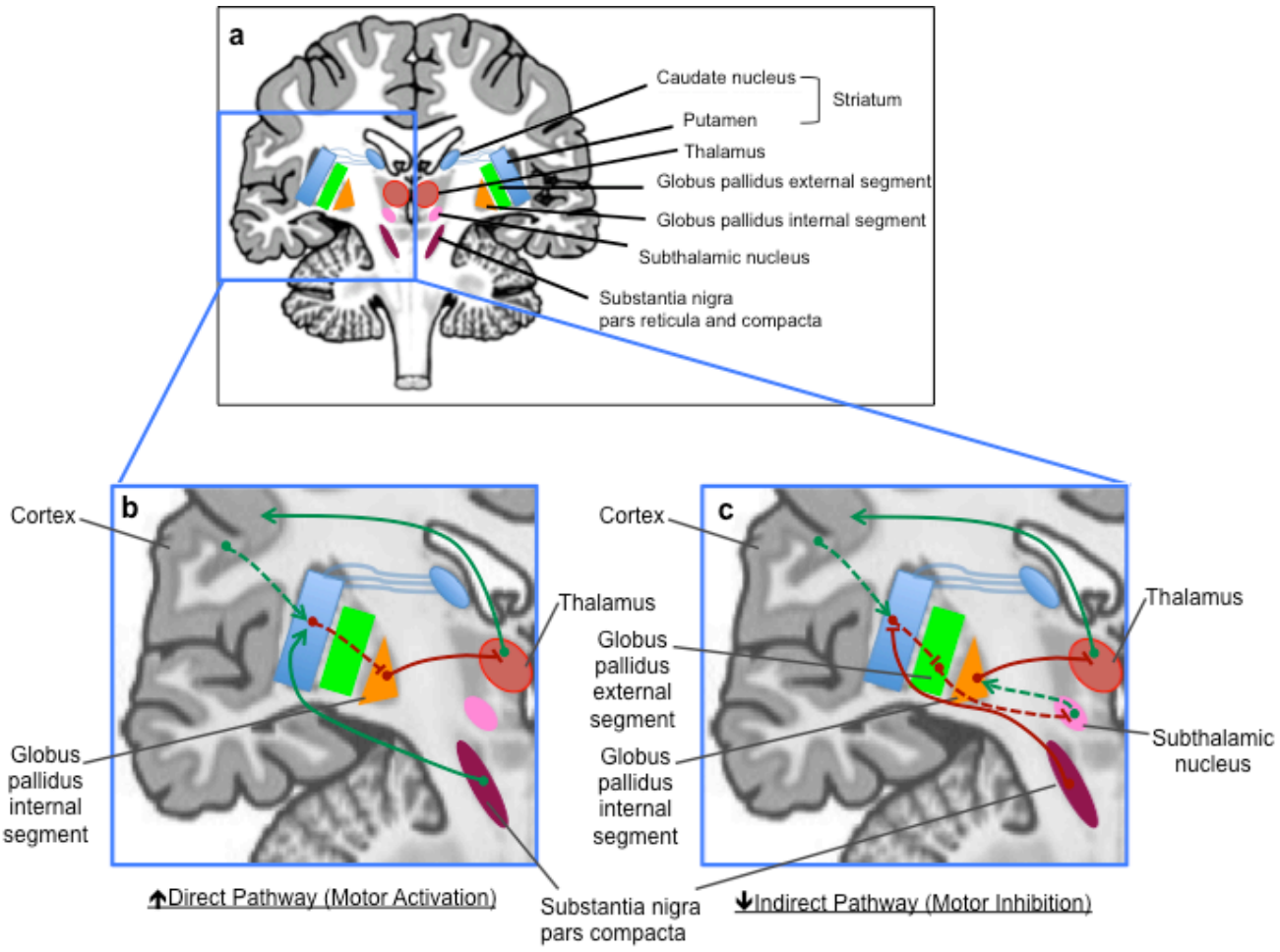

Figure 1.3. Direct and indirect pathways within the nigrostriatum
(**a**) Structures of the basal ganglia shown in a frontal section of the brain. Connections between substantia nigra pars compacta and other basal ganglial structures is shown for the direct pathway (**b**) and the indirect pathway (**c**). Activating connections are shown in green and inhibiting connections in red. D1 activating receptors within the striatum leads to increased activation of the direct pathway by substantia nigra pars compacta dopamine release, while D2 inhibiting receptors in the striatum of the indirect pathway results in inhibition. The resulting effect of substantia nigra signaling is overall motor activation. Modified from Knierim 1997.[60]

Signals sent from cortical neurons will synapse onto either the caudate nucleus or the putamen (known collectively as the striatum) and initiate one of two pathways, direct or indirect, causing activation or inhibition of movement respectively. As shown in **Fig. 1.3b and c**, the *S. nigra* has the ability to alter the activity of both the direct and indirect pathways via DA signaling due to the presence of different DA receptors within each pathway.[60,61] Whereas neurons involved in the direct pathway contain activating D1 DA receptors, neurons involved in the indirect pathway contain inhibiting D2 DA receptors. The resulting effect of *S. nigra* DA signaling, therefore, is the enhancement of motor activation by activating the direct pathway and inhibiting the indirect pathway. Loss of *S. nigra* signaling thus results in a net decrease in motor activation.[58,62]

Despite the clear pathophysiological link between dopaminergic nigrostriatal pathway dysregulation and PD, patients also present non-motor symptoms.[63,64] Intriguingly, many of these symptoms appear prior to classic motor symptoms presentation and are often considered prodromal in nature. These symptoms include: psychiatric manifestations (e.g. depression),[65] impairments of gastrointestinal (GI) motility (e.g. constipation), autonomic dysregulation,[66] sleep dysregulation (e.g. rapid-eye-movement, REM, behaviour disorder)[67,68] and hyposmia. REM behaviour disorder, which is characterized as the loss of motor inhibition during REM sleep phase leading to individuals unconsciously acting out their dreams, is considered a highly predictive risk factor for developing a neurodegenerative synucleinopathy such as PD (66% risk at 7.5 years from diagnosis of REM sleep disorder).[69] Interestingly, the most salient, pre-clinical, neurological sign of PD (90% prevalence in PD) is hyposmia, or loss of smell.[70] Although some non-motor symptoms are considered sensitive predictive risk factors for developing PD, they are not specific and are therefore unreliable for predicting early-stage PD.[63,69,70]

While some of these non-motor symptoms, such as emotional and cognitive dysfunction, can be partially explained by the loss of DA neurons in the VTA[42,47], the majority of these symptoms are not caused by CNS DA dysregulation.[71] There is strong evidence linking the loss of noradrenergic neurons in the *Locus coeruleus* (*L. coeruleus*),[53] and to a lesser extent the loss of serotonergic neurons in the *Raphe nuclei* (RN), to the development of non-motor PD symptoms.[72,73] As shown in **Fig. 1.4**, the noradrenergic signaling from the *L. coeruleus* is linked to a large number of other brain regions involved in regulating wakefulness, sleep, as well as, physiological and emotional responses to stress and pain.[74,75] The RN, on the other hand, form connections to the cerebral cortex and *L. coeruleus* to promote sleep and pain regulation.[74,75]

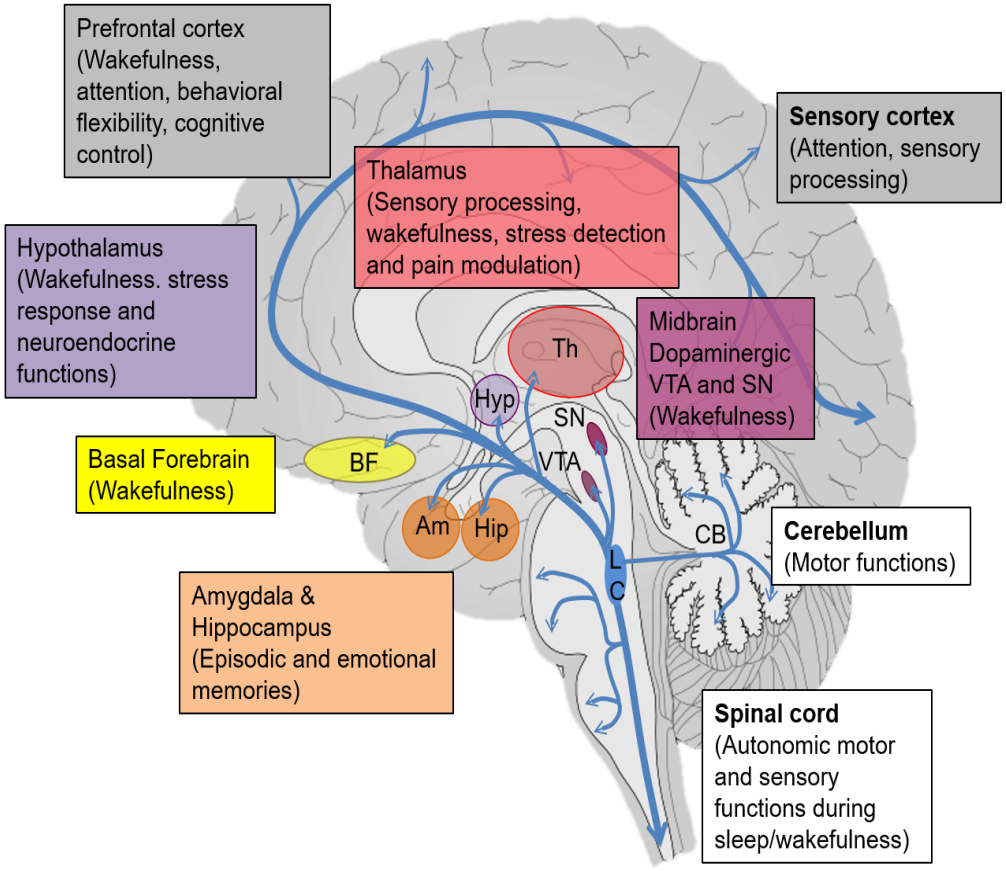

Figure 1.4. Locus coeruleus signaling pathways within the central nervous system
Locus coeruleus (LC) projects to three main pathways: 1) The ascending pathway, projecting to the ventral tegmental area (VTA) and substantia nigra (SN), amygdala (Am), hippocampus (Hip), hypothalamus (Hyp), thalamus (Th), basal forebrain (BF), prefrontal cortex and sensory cortices. 2) The cerebellar pathway, projecting to the cerebellum, and 3) the descending pathway, projecting to the spinal cord. Modified from Bari 2020.[75]

Interestingly, both *S. nigra* and *L. coeruleus* are the main sources of DA and noradrenaline (NA), respectively, within the CNS, and share a common synthesis pathway as shown in **Fig. 1.5**.[76] The presence of vesicular monoamine transporter (VMAT) protein facilitates the vesicular transport and release of these neurotransmitters into the synapse.[77] If DA or NA is prematurely released into the cytosol it can undergo: i) vesicular re-uptake, ii) partial degradation by catecholamine-*O*-methyltransferase (COMT) and monoamine oxidase (MAO) to homovanilic acid and vanillylmandelic acid, respectively, or iii) formation of NM (**Fig. 1.5**).[78] Most importantly, the *S. nigra* and *L. coeruleus* are the only primate brain regions to contain NM in macroscopically visible clusters.[79]

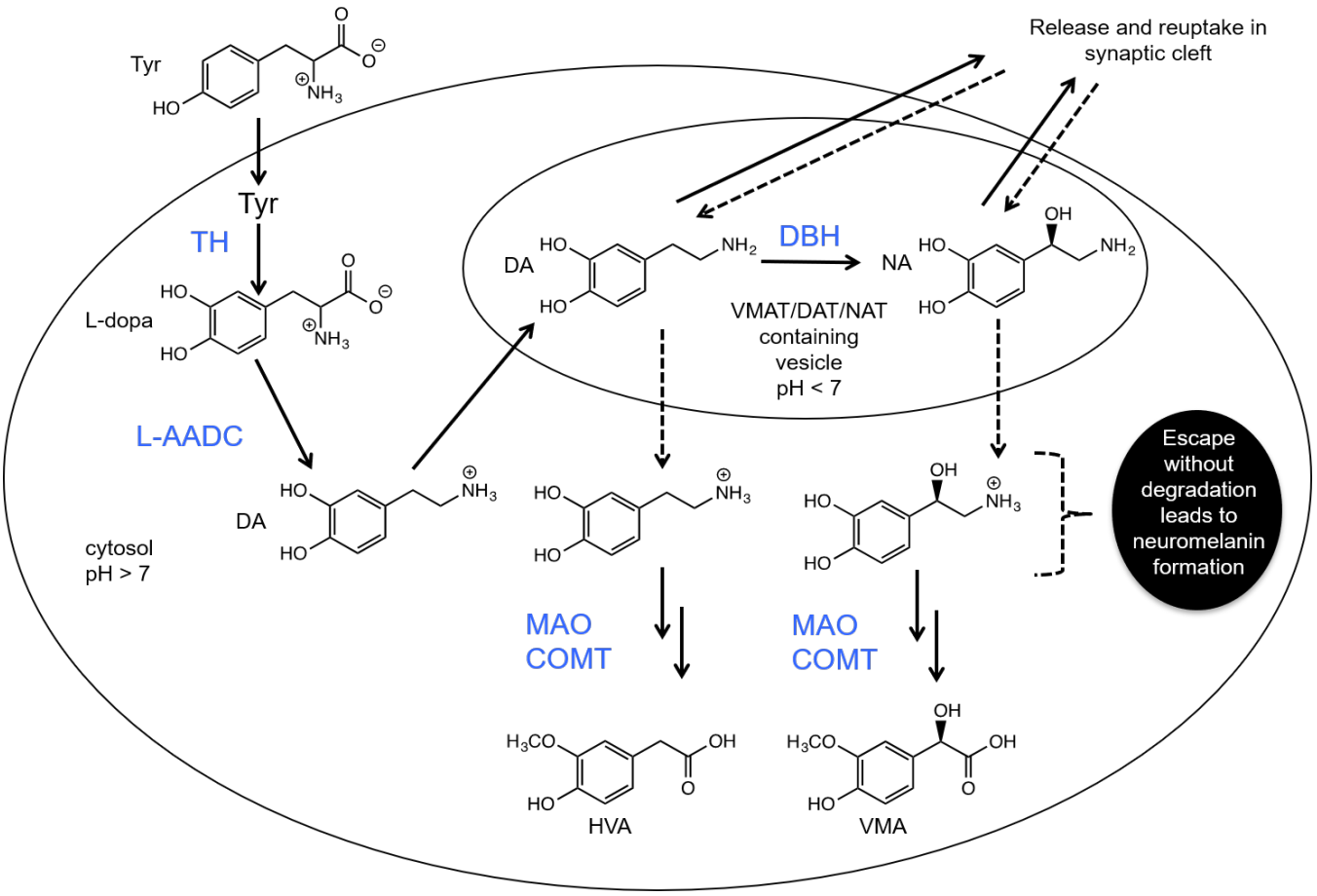

Figure 1.5. Dopamine and noradrenaline synthesis and metabolism
Enzymatic oxidation of tyrosine (Tyr) by tyrosine hydroxylase (TH) produces dopamine (DA) precursor (L-dopa), which is converted to DA by L-aromatic amino acid decarboxylase (L-AADC) and stored in acidic vesicles. Noradrenaline (NA) is produced within the locus coeruleus by DA-β-hydroxylase (DBH). The presence of vesicular monoamine transporter-2 (VMAT2) protein, DA transporter (DAT), or NA transporter (NAT) facilitates release and reuptake of these neurotransmitters into the synapse. A portion of DA and NA is released into the cytosol and is typically metabolized by monoamine oxidase (MAO) and catecholamine-O-methyltransferase (COMT) to homovanilic acid (HVA) and vanillylmandelic acid (VMA), respectively, for excretion in urine. If large stores of DA and NA are released, a portion will escape enzymatic degradation and form neuromelanin. Dashed lines represent less prominent pathways.

Intriguingly, primates are also the only mammals known to produce readily detectable NM and exhibit spontaneous age-related parkinsonian phenotypes.[43] Hirsh et al. in 1988 demonstrated that certain *S. nigra* DA cell types, which produced higher levels of NM, were less vulnerable to degeneration,[80] suggesting that the presence of NM is protective. The mechanism of NM formation (**Fig. 1.6**), as opposed to melanin produced in the epidermis, is still not fully understood but is known to involve the oxidation and sequestration of DA and NA. In melanin-producing cells found in the skin, L-3,4-dihydroxyphenylalanine (L-dopa) is specifically used to produce melanins within tightly confined organelles called melanosomes using glutathione and the enzyme tyrosinase, and the activity of lysosomal-associated membrane proteins (LAMPs)-1 and -2.[79,81,82] It is currently postulated that NM formation is a complex phenomenon that involves a combination of catecholamine autoxidation and autopolymerization[83]; conjugation to biomolecules containing nucleophilic residues such as thiols; as well as, fusion to non-degradative lysosomes and autophagic vacuoles (**Fig. 1.6**).[82,84,85]

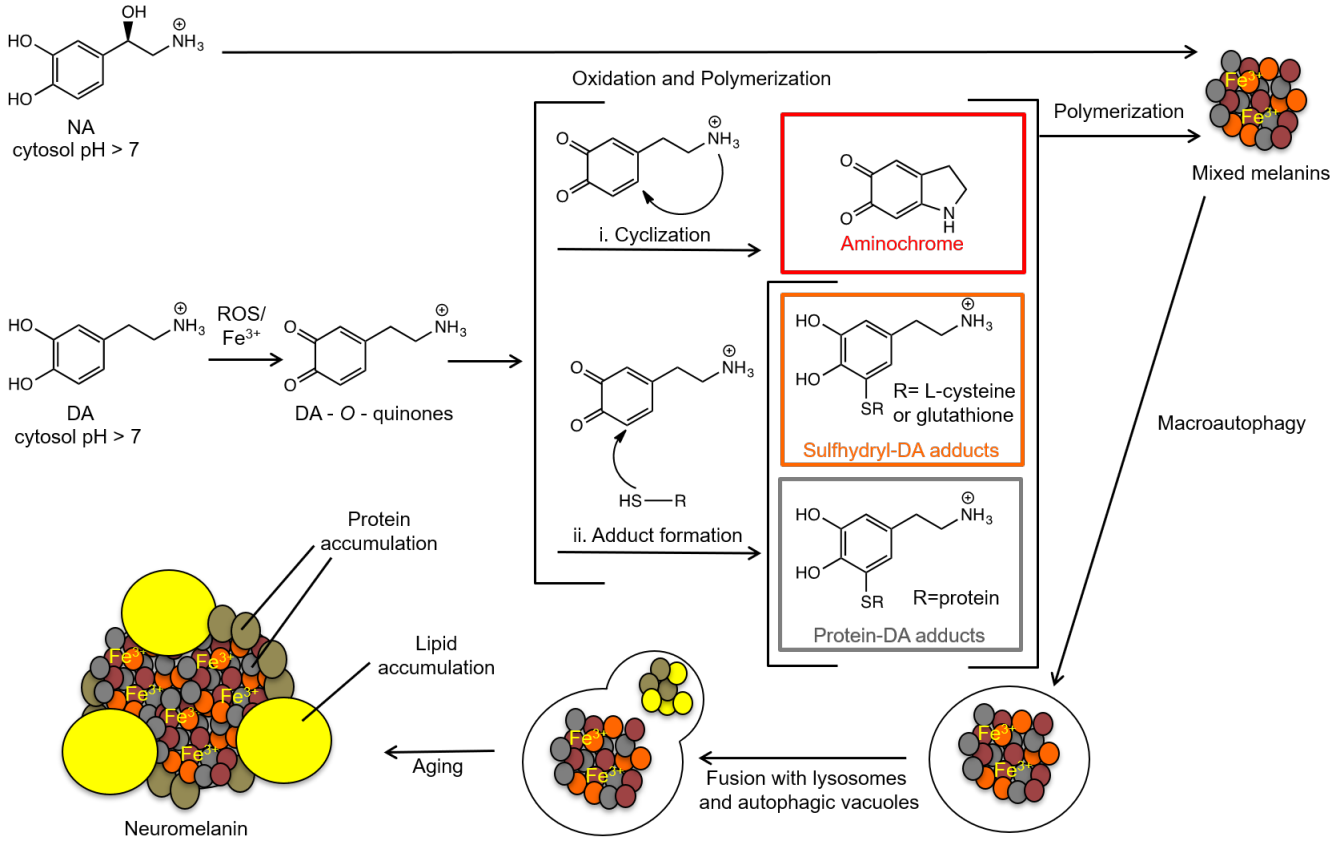

Figure 1.6. Neuromelanin synthesis
Accumulation of dopamine (DA) and noradrenaline (NA) leads to auto- and iron-mediated oxidation or the formation of sulfhydryl-adducts. Further cyclization and polymerization lead to formation of melanins. Those containing only DA polymerized molecules (i) are called eumelanins while melanins containing sulfhydryl adducts (ii) form pheomelanins. Newly formed melanins recruit and fuse to lysosomes and autophagic vacuoles that contain various lipids and proteins in order to sequester it from the cytosol. With aging the size of neuromelanin deposits increase. Modified from Zucca 2014 and Sulzer 2018.[84,86]

1.1.2 Treatments

There currently exists no disease-modifying pharmacological treatment for PD. All PD patients are initially prescribed DRT.[4,87] The most common and gold standard formulation is co-administration of L-dopa (for levodopa) and an inhibitor of peripheral DA breakdown (such as via benserazide or carbidopa), to facilitate effective entry into the CNS.[39,88] Other forms of DRT include DA agonists (DA molecular mimics),[89] and inhibitors of DA-metabolizing enzymes MAO and COMT.[87] Initially, motor symptoms respond very well to DRT, described as the "symptom-control years".[4,87] Unfortunately, with prolonged use (~5 years of DRT), 40% of patients often complain of limited therapeutic efficacy during the interval between dosages (leading to more 'off-time') and can also develop L-dopa-induced dyskinesias (involuntary movements).[90] As DA is involved in activating the mesolimbic pathway, there is also a 40% risk of inadvertently inducing the response-reward pathway, particularly with DA agonist usage.[91] This leads to a pattern of reward-seeking behaviour known as the DA dysregulation syndrome (or impulse control behavioural disorder). Patients with this syndrome are at risk of misusing DA, placing them at risk of engaging in other impulse control disorders. Once diagnosed, DA agonists need to be discontinued gradually (and are often replaced by L-dopa medication) to avoid withdrawal symptoms.[92] Fortunately, newly emerging procedural therapies have shown promise in providing better symptom relief. Today the surgical procedure, known as deep brain stimulation (DBS), is offered to select patients who are experiencing marked reduction in 'on-time', more 'off-time', more severe tremor and L-dopa-induced dyskinesias. As most commonly practiced, the procedure involves the placement of the tip of electrodes into the subthalamic nucleus (STN) within the basal ganglia to regulate its activity[93,94] and it is hypothesized that these electrodes interfere with the normal firing rate of the STN during episodes of increased tremor or dyskinesia.[94] Although this procedure does not completely

eliminate the need for DRT, it substantially improves motor symptom control, in particular the ratio of on- vs. off-time.[93]

The replacement of dopaminergic cells by stem cell implantation for the purpose of neurorestoration has also been extensively explored.[95,96] Initial trials in 1980s, which used undifferentiated fetal stem cells, had variable outcomes[97,98] caused by variability in quantity and quality of the implanted embryonic stem (ES) cells.[96] Surprisingly, many of the cells transplanted remained viable beyond a decade and some developed LB formation, which some authors believe demonstrates a host-to-graft propagation of disease, either by direct transfer of α-synuclein aggregates (such as of oligomers), or by the induction of a yet-to-be determined disease process (or signal thereof) from the host onto the grafted cells.[99] Major side effects, such as dyskinesia, were unfortunately observed in recipients of ES cells, which required further surgical interventions to treat. Improvements in stem cell technology have increased cell graft survival and integration into the striatum of mice, rats and monkeys.[100] The use of induced pluripotent stem cells (iPSC) is potentially ideal for humans as this allows for autologous cell transfer and thus reduces the risk of transplant rejection. The first-in-human trial of iPSCs, recently conducted on a single PD patient at the Massachusetts General Hospital in Boston,[101] showed sustained graft survival and improved clinical symptoms with no adverse reactions at 24 months post implantation.

As non-motor symptoms of PD are quite variable in type and severity, most are treated on a case-by-case basis with symptom-specific medications (e.g. mood enhancers/stabilizers for depression/anxiety, melatonin for sleep disturbances, adrenergic receptor activators for incontinence/blood pressure dysregulation, and laxatives/prokinetics for GI motility issues).[4,87] Despite the known role of NA dysregulation in the genesis of non-motor PD symptoms, there is currently no standard of treatment focused on replacing this neurotransmitter in PD patients.

1.1.3 Etiology

As the success of novel therapeutic avenues rests on a solid understanding of the cause of disease, much of PD research has focused on understanding the genetic and environmental causes of the disease to develop hypotheses regarding its pathogenesis. Generally, PD is diagnosed late in life (≥65 years)[102] and is considered a heterogeneous disease. These vary from mild PD (49-53% of cases) with fewer motor symptoms and a good response with DRT[103,104] to advanced PD (9-16% of cases) with treatment-resistant motor, and non-motor symptoms that progress rapidly.[103,104] The existence of rarer and purely genetic forms of PD, with some presenting before age 20 years ('juvenile-onset') and 40 years ('young-onset'), also suggests that multiple and distinct cellular pathways are involved in PD pathogenesis.[105]

In the majority of PD cases (>80-85%), termed idiopathic or sporadic PD, the exact cause is unknown.[106,107] Environmental factors were initially proposed as the predominant cause of PD. For example, increased prevalence of individuals with postencephalitic PD following the 1918 influenza pandemic suggested that infection-mediated neuroinflammation led to PD.[108] The hypothesis that environmental factors cause PD was further supported by the identification of the toxin named N-methyl-4-phenyl-1,2,3,6-tetrahydropyridine (MPTP), which is a by-product of heroin synthesis that can selectively cause *S. nigra* DA neuron degeneration in rodents, humans and non-human primates.[109-111] Other environmental exposures known to increase the risk of developing PD include: heavy metals (manganese), pesticides (paraquat, rotenone), prolonged use of neuroleptic or antipsychotic medications, rural or farming life, and recurrent head injuries (see **Fig. 1.7**). [106,107]

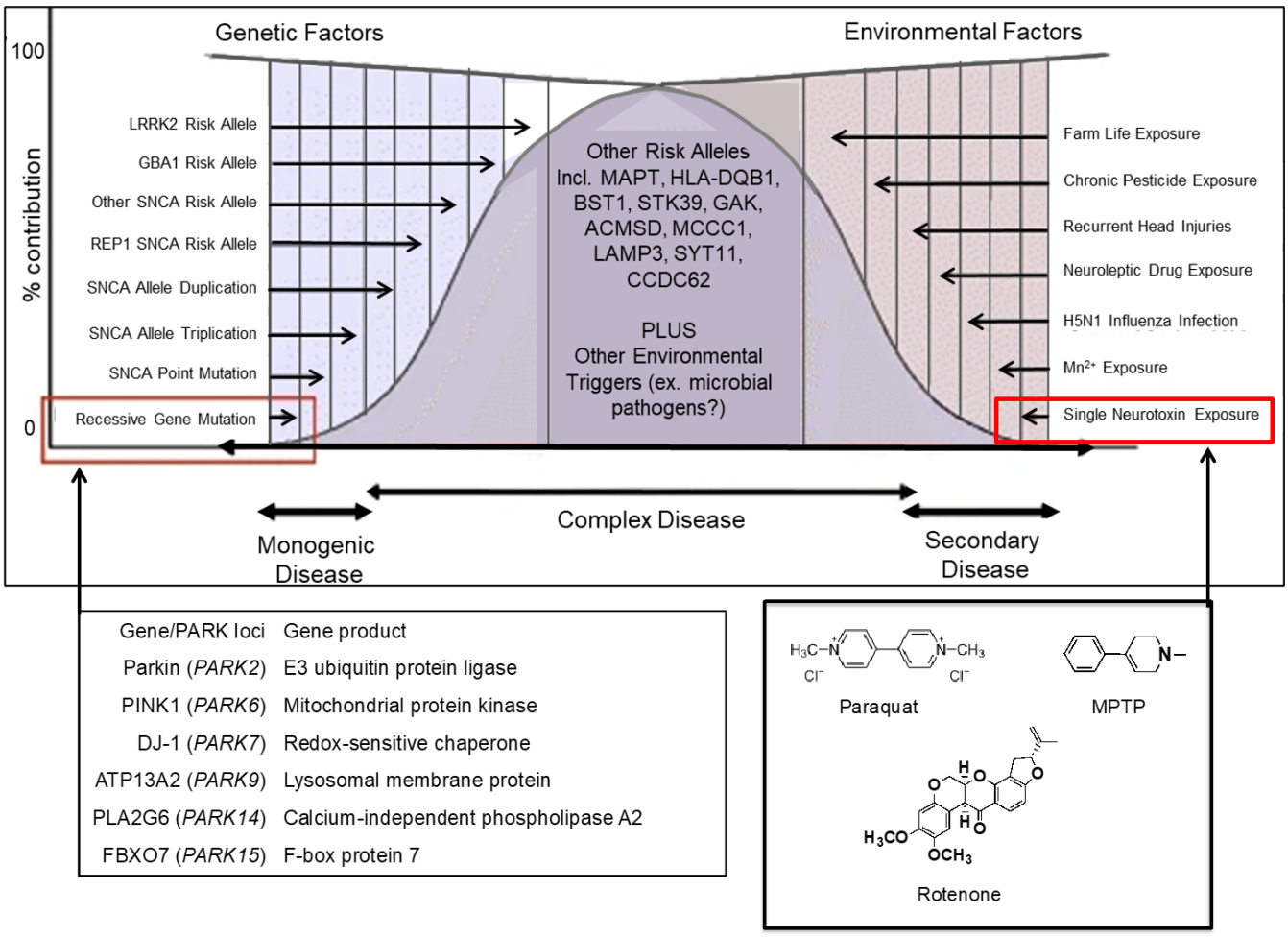

Figure 1.7. Genetic and environmental causes of Parkinson disease

A graphical depiction for the proposed multifactorial etiology of sporadic PD, consisting of an overlap between genetic and environmental factors. The percent contribution refers to the estimated prevalence of each factor found within sporadic PD cases. Rare autosomal familial PD is shown on the bottom left of the graph, with major associated genes listed below. Single toxin exposures are found on the extreme right of the graph, representing rare and purely environmental causes of PD. Modified from Kitada 2012.[106]

The findings that MPTP and rotenone caused oxidative stress (OS) by specifically inhibiting complex I within the mitochondria,[111,112] coupled with the observation that PD patients exhibited complex I dysfunction in *S. nigra*,[113,114] frontal cortex[115,116] and platelets,[117,118] suggested that aberrant mitochondrial activity and OS are involved in PD pathogenesis. PD caused purely by environmental factors are now believed to account for only 5-10% of total prevalence, which has led some researchers to hypothesize that a combination of genetic predisposition and exposure to environmental factors is the major cause of PD.[105,106] Since the discovery that many single nucleotide polymorphisms (SNPs) are linked to PD, probability-based prediction tools were developed to determine the risk of developing PD based on demographic information (e.g. age and sex), the presence of SNPs, and known exposures to environmental risk factors.[119-123] The hope is that these prediction tools will be used to enable closer monitoring of high-risk individuals requiring earlier medical intervention.

1.2 Genetic forms of PD

The finding that certain families have a high incidence of PD led to the discovery of familial forms of PD, thanks to chromosomal mapping of their pedigrees.[124] Disease-causing chromosomal regions were initially given the *PARK* gene loci identification and later replaced by their gene name, once identified.[124] A brief description of the clinical presentation and proposed mechanism of pathogenesis for the major genes responsible for familial PD follows below.

1.2.1 Autosomal dominant PD (ADPD)

α-Synuclein (*SNCA*, aka *PARK1* and *4*)

SNCA was the first gene identified in a large Italian family. Multiplication events as well as missense mutations at the *SNCA* locus cause rare forms of familial PD with a high penetrance rate.[125,126] Clinically, *SNCA*-associated PD patients have broadly varying phenotypes, which includes typical late onset PD (mild form, as in gene duplication events) and earlier onset PD with rapidly progressing motor and non-motor symptoms (including dementia, as in triplication carriers and select point mutation carriers).[127] Given its dominant inheritance, *SNCA* therefore acts through a toxic gain-of-function mechanism, which is supported by the finding that higher gene copy number correlates with increased disease severity.[128-130] The gene encodes a 140 amino-acid protein[131] that is a major component of LB and LN found in synucleinopathies (e.g. PDD and DLB).[31] It contains a highly amyloidogenic domain, and an amphipathic α-helical domain, which helps the protein associate with lipid-rafts and renders it highly susceptible to aggregation.[131,132] Although the exact role of α-synuclein is still unknown, its localization within axon terminals strongly suggests a role in the regulation of synaptic transmission.[133,134] Other suggested roles for α-synuclein include: negatively regulating tyrosine hydroxylase enzymatic activity[135,136] and activating microglia inflammation[137] via Toll-like receptor activation.[138]

Leucine-rich repeat kinase 2 (*LRRK2, aka PARK8*)

The *LRRK2* gene was first identified in a large Japanese family[139]; it is the most prevalent genetic cause of PD, with *LRRK2* mutations found in ~10% of patients with autosomal dominant PD[140] and about 80 variants identified in sporadic PD.[141] Clinically, *LRRK2*-associated PD resembles typical late-onset PD with a mild phenotype that can progress to PDD and demonstrates various degrees of synucleinopathy (or tauopathy) on post-mortem examination.[142-144] The gene encodes a large 2527 amino-acid protein

with multiple domains, including a Ras of complex protein GTPase (Roc) domain, carboxylic acid terminal of Roc (COR) domain and tyrosine kinase-like domain.[145] It is suggested that LRRK2 is capable of undergoing autophosphorylation in addition to phosphorylation of its substrates (mostly Rab protein) and could also serve as a scaffold for multiprotein complex assembly.[105] Seven missense mutations found in the Roc, COR and kinase domains, are considered pathogenic with the most common being G2019S.[146,147] A gain-of-function mechanism for *LRRK2*- associated PD is supported by its dominant inheritance and the fact that its kinase activity is activated by the more common PD-linked mutations. The downstream cellular effect of this toxic gain-of-function in PD pathogenesis is still unknown but may include: aberrant neurite outgrowth, autophagy[148] and an exaggerated inflammatory response to environmental stimuli.[149-152]

1.2.2 Autosomal recessive PD (ARPD)

ARPD usually presents earlier in life (third to fourth decade) and is often called early-onset PD or EOPD.[153,154] *DJ-1*, *PINK1* and *PRKN* all cause ARPD and account for roughly 20% of all people living with EOPD.[155] Disease presents with classic motor symptoms caused by loss of *S. nigra* neurons, however, unlike the other forms of PD, EOPD is slow-evolving with motor symptom-specific progression that responds very well to DRT[156] and rare development of non-motor PD symptoms, such as anxiety, depression, cognitive decline, and sleep disturbances.[156] Post-mortem examination of EOPD cases typically reveals a lack of LB or LN formation in surviving neurons, suggesting that EOPD involves different cellular processes than ADPD or sporadic PD.[157]

Deglycase-1 (*DJ-1*, aka *PARK7*)

Deglycase-1 is a multifunctional cytosolic protein originally found to have a role in oncogenesis[158] and male infertility.[159] Its link to ARPD was discovered in 2003 by the identification of a homozygous deletion and a missense mutation (L166P) in two consanguineous Dutch and Italian families.[160,161] Clinically, patients with *DJ-1* mutations present like *PRKN*-associated EOPD.[162] Many other forms of *DJ-1* mutations cause EOPD including: missense, frame-shift and exonic deletions, however, *DJ-1* is one of the least common genes associated with EOPD, as it accounts for only 1-2% of cases.[105] Therefore, few cases have become available for neuropathological examination; the rare cases autopsied appear similar to *PRKN*-associated PD with specific loss of *S. nigra* and *L. coeruleus*.[163] The L1666P mutation has been shown to cause rapid proteasomal degradation of DJ-1 protein[164,165] and supports a loss-of-function mechanism in PD pathogenesis. It is now accepted that loss of this protein interferes with its role as a redox-sensitive chaperone thanks to the presence of a highly conserved redox-active cysteine residue at amino-acid position 106.[166-168] DJ-1 was also shown to protect cells from various oxidative insults[168-170] and was shown to translocate to the outer mitochondrial membrane in the presence of OS.[171]

Phosphate and tensin homolog (PTEN)-induced kinase 1 (*PINK1*, aka *PARK6*)

PINK1 is a ubiquitously expressed protein that is induced by the tumor suppressor protein called PTEN. It is a positive regulator of cell cycle progression,[172] thanks to its ability to modulate mitochondrial health and quality control.[173] Its protein structure contains a putative transmembrane domain, a serine-threonine kinase domain and an N-terminal mitochondrial-targeting signal (MTS)[174] that enables the protein to accumulate on the outer mitochondrial membrane (OMM) when OS is induced.[173] *PINK1* homozygous or compound heterozygous mutations are the second most frequent cause of ARPD,

accounting for ~1-5% of EOPD.[175,176] Common mutations include point mutations, with the most common being G309D and W437X within its kinase domain. These mutations were found to destabilize the protein and/or reduce its kinase activity (G309D and W437X), supporting a loss-of-function mechanism in PD pathogenesis.[174] Some studies suggest that heterozygote mutations in *PINK1* confer an elevated risk of developing sporadic PD, however, this risk was very low and the relevance of such mutations in sporadic PD is still hotly debated.[175-178]

Clinically, patients carrying homozygous or compound heterozygous *PINK1* mutations present similar to EOPD and tend to have a sustained response to DRT (with less annual dose adjustments than are seen in sporadic PD), suggesting a less severe disease course and, as a result, longer disease duration.[179] Neuropathologically, there is surprisingly exclusive loss of *S. nigra* with some degree of synucleinopathy findings within the *S. nigra* and surrounding brainstem, but no involvement of the *L. coeruleus*.[180] The latter may explain why REM behaviour disorder does not usually occur in these patients.[181] Although its exact role in PD pathogenesis remains unclear, it is believed to function upstream of the *PRKN* gene product (parkin) in promoting mitochondrial turnover mitophagy (discussed in sections 1.3.3 and 1.5.3), and regulate mitochondrial complex 1 function.[182] It is believed that partially linear relationship exists between parkin and PINK1 and is supported by the finding that reduced *pink1* expression in *Drosophila melanogaster* results in mitochondrial disruptions and DA neuron loss, which is partially rescued by *prkn* overexpression.[183]

Parkin (*PRKN*, aka *PARK2*)

Homozygous or compound heterozygous mutations in *PRKN* are the most common cause of ARPD, accounting for ~50% of familial EOPD and 10-20% of EOPD with no previous family history.[154,155] It was first discovered in 1998 in a group of Japanese patients with EOPD.[184] Interestingly, some cases

present later in life[185,186] but these usually occur in compound heterozygous carriers. As with *PINK1* mutations, there is debate regarding the relevance of heterozygote *PRKN* mutations in sporadic PD.[178,186-188] This was initially proposed because occasional *PRKN*-related PD cases displayed autosomal dominant inheritance and an increase in prevalence of *PRKN* gene copy variance has also been observed in sporadic PD.[185,186,189,190] However, a large meta-analysis on sporadic PD patients, who were also carriers of heterozygous *PRKN* mutations suggested that these mutations were likely incidental or at best a risk factor for the disease.[191] Most EOPD-causing mutations represent exonic deletions, insertions, as well as, regional multiplications, but they can also represent missense or nonsense mutations.[141]

Intriguingly, there does not appear to be a specific region targeted by these mutations as they are found to lie indiscriminately within its primary structure. Although not all mutations can currently be explained, it is generally believed that they cause parkin loss-of-function either by: i) reducing its solubility, ii) reducing its function as an E3 ligase enzyme, which would result in accumulation of un-degraded substrates, or, iii) by inhibiting its ability to properly remove damaged mitochondria, which would lead to an increase in OS and/or decline in adenosine triphosphate (ATP) synthesis.[192,193] Clinically, parkin-associated PD is slow progressing and has an excellent response to DRT, much like EOPD caused by *PINK1* and *DJ-1*.[194] It, however, strikingly differs with the presence of lower limb and exercise-induced dystonias, gait and balance issues, early development of L-dopa induced dyskinesias, motor symptom fluctuations and a unique sleep benefit.[185,186,195-197]

Pre-clinical signs of anxiety and panic disorders often present prior to the diagnosis of *PRKN*-PD, however, it is rarely associated with hyposmia and no cognitive decline is observed with disease progress.[185,198-200] The presence of dystonia and sleep benefit in *PRKN*-PD complicates clinical diagnosis since these symptoms overlap with dopa-responsive dystonia (DRD; *aka* Segawa's disease), a disorder caused by DA synthesis deficiency, which exhibits reduced NM but lacks *S. nigra* cell loss on autopsy.

Frequently, but not invariably, DRD can be distinguished from *PRKN*-PD since the former is typically a non-progressive disorder that presents in childhood or adolescence,[201] and is almost exclusively caused by autosomal dominant mutations in GTP cyclohydrolase 1 (*GCH1*), which is an important enzyme required for the synthesis of the tyrosine hydroxylase (TH) cofactor called tetrahydrobiopterin.[202] Interestingly, recessive mutations in *TH* itself can also cause DRD.[203] Although the effect of *GCH1* and *TH* mutations on PD appears to be small,[204] *GCH1* SNPs are linked to sporadic PD risk[120,205] and inversely, several DRD patients have developed PD.[206]

Neuropathologically, *PRKN*-PD specimens show specific cell loss in the *S. nigra* and *L. coeruleus*, and LBs are present in very rare cases of advanced-aged subjects. Given the rarity of LBs and the advanced age of these subjects, they likely represent age-related incidental LBs,[53,195-197,207], however, they may also represent inclusions formed by the enhanced aggregation potential of certain *PRKN* mutations that still result in expression, albeit aberrant forms, of the protein (e.g. point mutations and small deletions).

1.2.3 Autosomal recessive juvenile parkinsonism

Homozygous and compound heterozygous mutations in three genes (*ATP13A2*[208-210], *PLA2G6*[211-214] and *FBOX7*[215,216]) cause parkinsonian-pyramidal (or pallidopyramidal) syndrome. It is a rare genetic neurological disorder that usually manifests in childhood with both parkinsonian (classic motor) and pyramidal or voluntary motor neuron (hyperreflexia, voluntary muscle weakness and spasticity) symptoms[217] Interestingly, when symptoms manifest later in life they are more benign and resemble classic EOPD.[218-220] These genes are involved in cellular processes similar to other familial PD. For example, *ATP13A2 (aka PARK9)* encodes a lysosomal P-type ATPase that regulates lysosomal function.[208,209] *PLA2G6 (aka PARK14)* encodes for a phospholipase A2 believed to be involved in cell

and mitochondrial membrane stability[212] and *FBOX7 (aka PARK15)* encodes an adaptor protein involved in substrate degradation via the ubiquitin proteasomal system (UPS) and believed to participate in mitophagy.[221]

1.2.4 Susceptibility genes in sporadic PD

Glucosylceramidase beta-1 (*GBA1*)

The most common genetic risk factor for sporadic PD is *GBA1 (aka* acid-beta-glucocerebrosidase), with heterozygous mutations in *GBA1* accounting for 7-15% of total cases.[222] The gene encodes for the lysosomal enzyme glucocerebrosidase, which cleaves glucosylceramide intro glucose and ceramide and glucosylsphingosine into glucose and sphingosine. Homozygous and compound heterozygous mutations cause Gaucher disease (GD), which presents as various subtypes of lysosomal storage disease in multiple organs, leading to neurological and non-neurological symptoms.[223] The link between *GBA1* mutations and PD began with the observation that GD patients often developed parkinsonian symptoms.[224-227] Intriguingly, *GBA1*-PD clinically appears similar to *SNCA*-PD, with earlier onset and more prominent non-motor symptoms, such as cognitive decline, REM behaviour disorders and psychiatric disorders like depression and anxiety[222]. It is also the greatest indicator of progression to PDD[228] and is commonly found associated with DLB.[229,230] The exact role of *GBA1* in PD pathogenesis is not fully known but possibly involved in regulating α-synuclein levels, thus explaining its strong link with synucleinopathies (PDD, DLB, *SNCA*-PD).[231-233]

Susceptibility genes identified by genome-wide association studies (GWAS)

Single-environmental exposures and familial PD, each separately, only contribute 5-10% to the total prevalence of PD.[105,106,234] Some groups, including ours, propose that sporadic PD (representing 80-90% of total cases) is multifactorial, caused by the cumulative effect of both genetic predisposition and environmental exposures (as shown in **Fig. 1.7**).[106] Using such a model aids in stratifying pre-diagnosed individuals into those at higher vs. lower risk of developing PD and helps identify appropriate patients for gene-targeted clinical trials. While it is clear that heterozygous mutants and SNPs of *SNCA* or *LRRK2* have a role in causing sporadic PD, there is debate over the role of heterozygous mutations and SNPs of EOPD-associated genes (*PINK1* and *PRKN*) in sporadic PD.[175,177,178,186-188] As sporadic cases are diagnosed at more advanced ages and present clinically much different than EOPD, it is hypothesized that the observed increase in heterozygous *PINK1*/*PRKN* mutations and SNPs in sporadic PD is likely incidental.[191] Two recent large meta-analyses of PD GWAS have identified SNPs in a total of 34 genes on 26 different loci.[119,120] Note that *PINK1*, *DJ-1* and *PRKN* do not appear in this list, which supports different pathogenic pathways in EOPD vs. other forms of PD. Known roles for the genes identified by GWAS span a wide range of functions, including: lysosomal function,[223,235-237] cell structure/signaling/growth/metabolism,[238-261] lipid homeostasis,[223,254,257] DA processing,[82,202,262,263] synaptic transmission[264,265] and immune modulation,[152,236,266] which correlate well with the putative roles for genes involved in familial PD. The fact that some genes are involved in immune or inflammatory modulation could suggest that individuals carrying SNPs of these genes require an environmental trigger, such as microbial infection,[267] to elicit the PD phenotype.

1.3 Cellular pathways involved in PD pathogenesis

The discovery of monogenic and environmental causes has led to various hypotheses regarding the pathogenesis of PD, including: protein aggregate accumulation and propagation, lysosomal dysfunction, aberrant immune activation, mitochondrial dysfunction, and catecholamine misprocessing, which are all believed to cause substantial OS and neuroinflammation (**Fig. 1.8**).

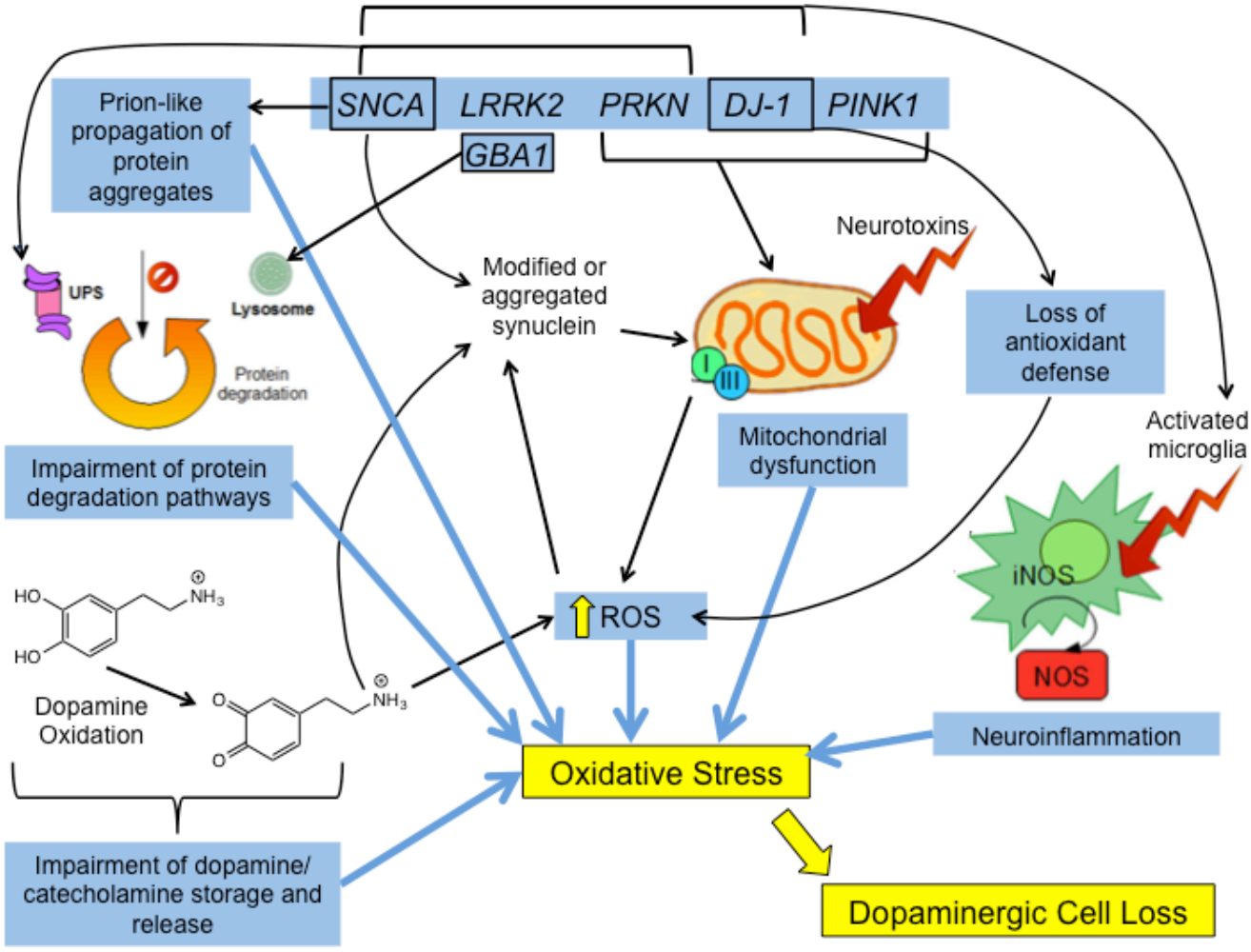

Figure 1.8. Cellular pathways involved in Parkinson disease pathogenesis
The five major cellular pathways involved in Parkinson disease (PD) pathogenesis include: protein aggregate accumulation, protein degradation and lysosomal dysfunction, mitochondrial dysfunction, neuroinflammation and catecholamine autoxidation and misprocessing. As shown, these all converge into downstream oxidative stress, leading to dopaminergic cell loss. PD-associated genes are shown grouped together according to their proposed role in each cellular pathway. *SNCA*, α-synuclein; *LRRK2*, leucine rich repeat kinase 2; *PRKN*, Parkin; *DJ-1*, deglycase-1; *PINK1*, PTEN-inducing kinase 1; *GBA1*, glucosylceramidase beta-1; ROS, reactive oxygen species; iNOS, inducible nitric oxide synthase; UPS, ubiquitin proteasome system. Modified from Blesa 2015.[268]

1.3.1 Protein aggregate accumulation and lysosomal dysfunction

Although it is unclear whether aggregated α-synuclein [269] is a by-product of some unknown physiological function or a marker of its misprocessing, it is generally believed to be a cellular toxin as direct application of α-synuclein aggregates [270-272] or increasing α-synuclein expression[133,273] causes cellular dysfunction and death. The aggregation process of α-synuclein is gradual, beginning with oligomer formation, progressing through protofibrils, and resulting in insoluble amyloid fibrils.[269] Higher α-synuclein aggregation states often require lysosomal-mediated degradation pathways such as macroautophagy[274] or chaperone-mediated autophagy[275-277] Although the protein structure is inherently prone to aggregation, multiple post-translational modifications (PTMs) are known to further enhance this phenomenon[278,279] and include: i) C-terminal truncation; ii) methionine oxidation via iron, nitric oxide (NO), DA or H_2O_2; iii) phosphorylation of serine at position 129; and iv) ubiquitination.[280-288] Although the exact mechanism of α-synuclein-mediated cell death is unclear, aggregate forms have shown to disrupt UPS,[289] autophagic[289] and mitochondrial[290] function, and shown to increase overall levels of reactive oxygen species (ROS) and reactive nitrogen species (RNS) within the cell.[291]

Another PD-associated gene linked to ubiquitin proteasome system (UPS) function is *PRKN*.[292] Parkin is an E3 ligase enzyme that functions to tag specific proteins (including itself) with polyubiquitin chains for degradation via the UPS. While it has been suggested that proteasomal dysfunction causes sporadic PD,[293,294] attempts at using proteasomal inhibitors to generate non-human primate PD models were unreliable[295] and there is a limited number of putative parkin substrates that reliably accumulate in parkin-deficient brains (further discussed in section 1.5.2).[296-299]

Given that mutations in the lysosome-associated enzyme GBA1 are a major risk factor for sporadic PD with synucleinopathy[222], it is hypothesized that this enzyme is involved in regulating α-synuclein aggregate removal.[231-233] Although it is still unknown exactly how GBA1 increases α-

synuclein levels, application of a GBA1 inhibitor (conduritol B epoxide) leads to a moderate accumulation of α-synuclein protein in mice,[300] and over-expression of wild-type GBA1 (but not mutant), as well as, GBA1-specific chaperone treatment of neural cells lowers α-synuclein.[232]

A few studies suggest that LRRK2 is involved in regulating the autophagy-lysosomal pathway. LRRK2 was found to inhibit autophagy in the promotion of neurite outgrowth,[148] and a *LRRK2* knockdown (KD) resulted in increased autophagy in cells.[301] Since, *LRRK2*-PD demonstrates variability in synucleinopathy,[147] it is unlikely causing direct α-synuclein degradation.

1.3.2 Aberrant immune activation

Braak and del Tredici *et. al.*[302-304] proposed that sporadic PD is caused by a prion-like ('prionoid') propagation of α-synuclein aggregates from an initial extra-cranial nucleation site towards the midbrain and frontal cortex. The theory was inspired by the non-motor symptoms of PD and supported by their neuropathological findings, which demonstrated an age-dependent retrograde migration of synucleinopathy along neuronal axons from either the olfactory bulb or the intestine to the brain stem; with further dissemination into the frontal cortex in advanced disease (i.e. PDD). Many researchers accept the hypothesis that synucleinopathy dissemination occurs via cellular transmission of preformed α-synuclein fibrils that form under aggregation-favouring conditions (i.e. high α-synuclein expression level and PTMs) and is supported by findings showing that direct application of preformed α-synuclein fibrils to cells leads to increased formation of α-synuclein aggregates, suggesting that these preformed fibrils act as nucleation triggers (reviewed in [305]).

However, based on their findings, Braak and del Tredici et al. postulated that α-synuclein aggregate nucleation occurs as a result of exposure to infectious agents in environment-exposed locations such as the gut and nasal cavity.[306] Although neither the exact microbial cause nor how these infectious agents

lead to α-synuclein aggregation are known, there is some evidence to suggest that α-synuclein plays a role in the immune response. It was discovered that extracellular α-synuclein functions as a Toll-like receptor 2 agonist to activate microglia inflammatory pathways,[138] which corroborates with signs of microglial activation in *S. nigra* of mice overexpressing α-synuclein.[137] It is plausible that microglial over-activation is an alternate explanation for why α-synuclein aggregation promotes OS, as shown through the activation of ROS/RNS producing enzymes (e.g. nicotinamide adenine dinucleotide phosphate oxidase, NOX),[307] which are highly produced in cytotoxic microglia.[308,309]

Furthermore, LRRK2, parkin and DJ-1 proteins can also regulate inflammatory responses. LRRK2 was shown to increase proinflammatory cytokine release in primary microglial cells[150,151] and is upregulated in mouse brains following lipopolysaccharide (LPS) exposure.[310] More recently, our group has shown in mice that LRRK2 is highly expressed in immune cells (peripheral blood, mesenteric lymph nodes and spleen),[149] and has a role in promoting the innate immune response, such as augmenting macrophage chemotaxis and ROS production.[152] Parkin expression in microglia enhances their ability to protect DA neurons from neurotoxin or LPS-mediated neuroinflammation,[311,312] while DJ-1 is believed to have a direct role in regulating astrocyte inflammatory responses, e.g. reducing NO and cytokine production.[313,314]

Finally, mitochondrial toxins (MPTP and rotenone) and extracellular NM cause microglial activation. MPTP was found to induce glial-mediated inflammatory responses via brain angiotensin and NOX activation,[315,316] while rotenone induces NOX activation and the nuclear factor kappa B (NF-ϰB) inflammation pathway.[317-320] The production of NM is generally believed beneficial for catecholaminergic cells as it functions to sequester various toxins, including: cytosolic catecholamine oxidation by-products, damaged or aggregated proteins and lipids, as well as, iron released from tightly controlled stores (**Fig. 1.6**).[82,321] However, release of NM into the intercellular space from dying

catecholaminergic cells causes OS-mediated cell death via microglia activation and is considered a major contributor to chronic inflammation in PD.[322-324]

1.3.3 Mitochondrial dysfunction

The discovery that exposure to the mitochondrial toxin MPTP[109,110,325] caused a parkinsonian phenotype in young adult humans led to the hypothesis that mitochondrial dysfunction plays a key role in PD pathogenesis.[326] Both familial and sporadic PD exhibit signs of mitochondrial dysfunction.[113,116,327,328] Mitochondria contain five redox-active protein complexes (I-V), which catalyze the production of energy via oxidative phosphorylation (OXPHOS) and are a major source of ROS (such as H_2O_2 and superoxide, $\cdot O_2^-$)[329,330] Leakage of ROS into the cytoplasm can occur at baseline (mostly from complex I and III), but is substantially increased when mitochondria are damaged or inhibited.[329,330] Parkinsonism-associated toxins such as MPTP and rotenone exhibit dopaminergic cytotoxic effects due to their ability to inhibit complex I,[331-333] and deficiencies in the activity of complex I are observed in multiple cell types derived from PD patients (brain, fibroblasts, platelets, skeletal muscle and lymphocytes).[113-118,334] Interestingly, OS itself is known to inhibit complex I function, which highlights the existence of an important feedback loop between ROS generation and mitochondrial function.[335,336] The evidence that certain PD-associated genes (*PINK1*, *PRKN*, *DJ-1* and *SNCA*) affect mitochondrial metabolism (and integrity) further supports the role of mitochondrial dysfunction in PD pathogenesis. Deficiency in PINK1 protein leads to mitochondrial defects in humans,[337,338] while mice and *Drosophila* exhibit aberrant mitochondrial function and morphology.[183,339-341] Although, parkin deficiency was only shown to directly cause aberrant mitochondrial form and function in *Drosophila*,[342-344] but not rodents, parkin-deficient PD patients have impaired complex I activity.[345] Since the deficits observed in *pink1* knockout (KO) *Drosophila* could be partially rescued by *prkn* overexpression, without the inverse occurring for

prkn KO, investigators suggested that parkin functions downstream of PINK1 along a common pathway.[346,347] The current model stipulates that PINK1 and parkin proteins are tightly connected in a process called mitophagy, which promotes the degradation of damaged mitochondria under high stress conditions (see **Fig. 1.9** and section 1.5.3).[348-353]

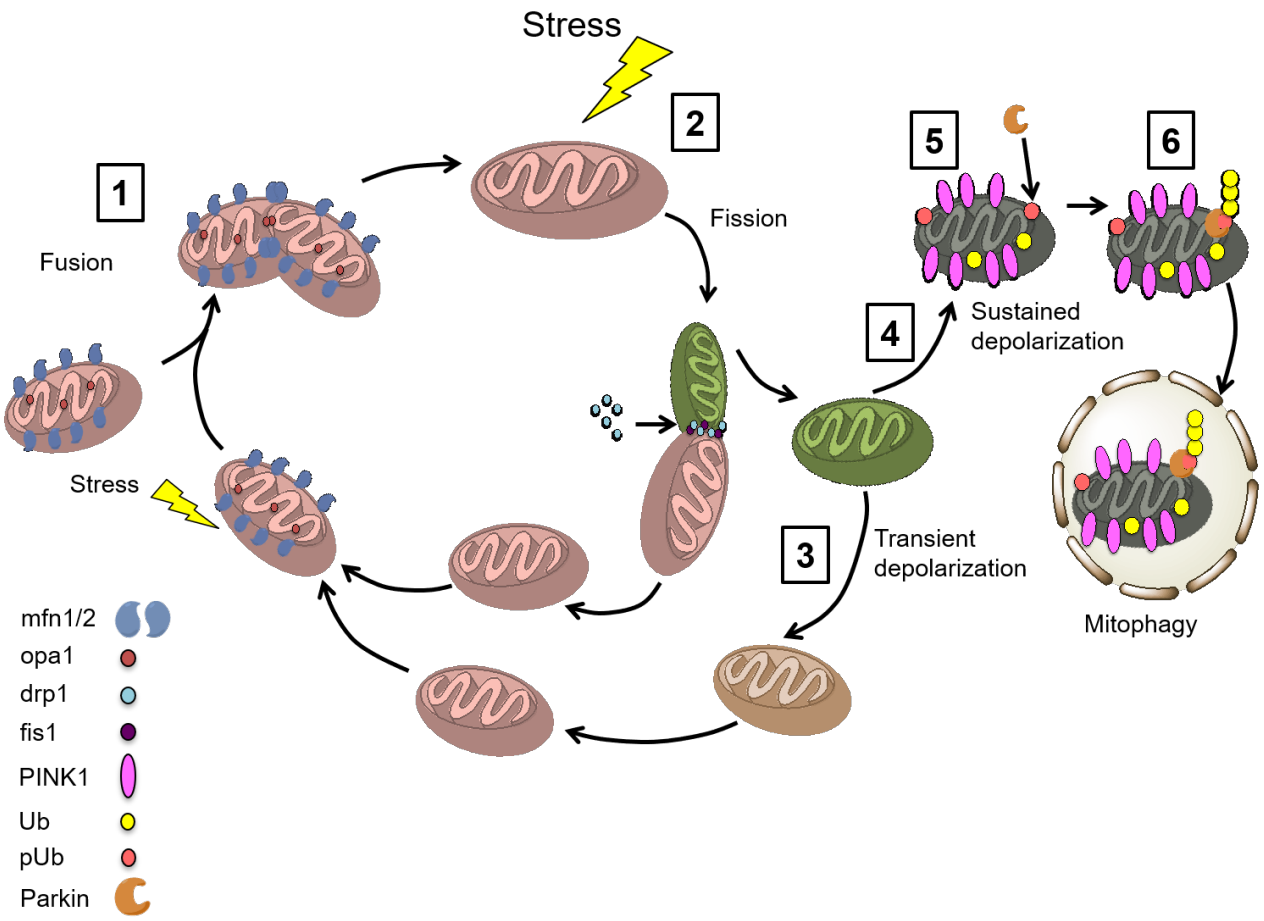

Figure 1.9. Mitochondrial dynamics involved in maintenance and mitophagy
Under low stress conditions (**1**) mitochondria will fuse by aide of mitofusin (mfn1/2) located on the outer mitochondrial membrane (OMM) and opa1 located on the inner mitochondrial membrane. This permits the mitochondrion to repair and remove damaged components via fission (**2**), activated by recruitment of dynamin-related protein 1 (drp1) to fission protein 1 (fis1). Fission can also be triggered under high stress conditions to quickly removed severely damaged mitochondrial components. Following fission, the mitochondrion is either restored with repolarization (**3**) or remains in a depolarized state (**4**). Sustained depolarization (**5**) triggers recruitment of PINK1 to the OMM and phosphorylation of ubiquitinated (pUb) OMM proteins. Parkin is subsequently recruited (**6**) to promote formation of polyubiquitin chains (Ub), which triggers mitophagy. Modified from Twig 2011.[353]

It is postulated that aberrant accumulation of damaged mitochondria results in increased OS and neuronal death, although this theory continues to be hotly debated as will be discussed in section 1.5.3. As *Dj-1* overexpression also partially reverses mitochondrial defects observed in *Pink1* KO *Drosophila*, it was initially proposed that DJ-1 functioned along a similar pathway.[354] However, it is now accepted that DJ-1 directly reduces OS by various mechanisms, including: i) direct binding to mitochondrial subunits to inhibit ROS production,[355] ii) direct lowering of intracellular ROS levels via cysteine oxidation,[168-170] and iii) rescuing proteins from degradation by acting as a redox-sensitive chaperone. [166-168] Finally, the effect of α-synuclein on mitochondrial function is predominantly linked to its aggregation under OS conditions, which is also self-perpetuating since accumulation of α-synuclein aggregates promotes mitochondrial ROS production and complex I dysfunction.[290,356] As certain studies suggested that acquired mitochondrial DNA (mtDNA) mutations[357] and/or SNPs changes in mitochondrial enzymes[242,255] were linked to PD, it was postulated that alterations in mtDNA was involved in PD pathogenesis. However, this hypothesis is less pursued currently, because increasing mtDNA mutations alone failed to cause *S. nigra* degeneration in mice.[358,359]

1.3.4 Catecholamine misprocessing

In addition to baseline metabolic ROS and RNS generation, *S. nigra* and *L. coeruleus* cells are subject to increased OS as a result of DA and NA metabolism.[76,360] Generally, these autoxidation-prone molecules are stored in VMAT (subtype 2)-containing vesicles and, if released into the cytosol, are promptly metabolized by COMT and MAO to homovanilic acid and vanillylmandelic acid for excretion in urine.[78,86] However, if they escape COMT and MAO metabolism, which can occur in cells that produce high levels of catecholamine, these molecules undergo rapid autoxidation and cyclization to form electron-deficient quinones (also termed reactive electrophilic species or RES).[83] Unfortunately, COMT

and MAO can no longer metabolize these RES, which accumulate and cause significant cellular damage. For example, DA-quinone adducts have been found on PD-associated proteins like α-synuclein,[284,361] parkin[362] and DJ-1,[363] and are known to promote α-synuclein aggregation.[284] RES are also shown to inactivate DAT[364] and TH,[365] as well as, promote mitochondrial complex I[366,367] and autophagy dysfunction[368]. Furthermore, DA-quinones can be further oxidized to aminochrome, which is a highly reactive redox-cycling molecule that increases $\cdot O_2^-$ formation and depletes nicotinamide adenine dinucleotide phosphate (NADPH).[83] Along with aminochrome, other DA- and NA-derived RES deplete the cell of electron dense biomolecules, such as sulfur-containing proteins, antioxidants like glutathione, and reducing cofactors like NADPH.[83,360] In fact, NM formation involves the action of electron dense biomolecules in sequestering DA- and NA-derived RES from the cytosol (**Fig. 1.6**).[82,83] Finally, the discovery that the dopamine analogue, 6-hydroxydopamine (6-OHDA) induces specific DA-cell death in mammals[369,370,371] supports the theory that OS from toxic catecholamine accumulation can be directly linked to nigrostriatal degeneration.

While PD pathogenesis appears to encompass divergent cellular processes (shown in **Fig. 1.8**), they converge into common neuroinflammatory- and OS-mediated cell death pathways.[268,372] OS occurs when the balance between ROS/RNS/RES production and antioxidant capacity is disrupted,[373] and leads to further disruption of proteasomal, lysosomal and mitochondrial function since these pathways are redox-sensitive.[374] With the exception of OS caused by toxic catecholamine accumulation, these processes, however, appear to lack a clear explanation for the specific loss of *S. nigra* and *L. coeruleus* cells found in PD, as one would predict that all high-energy demanding cell types would indiscriminately undergo degeneration. Some, however, argue that *S. nigra* are uniquely vulnerable due to DA-neuron physiology.[375] *S. nigra* DA-neurons regulate the release of DA by continuously activating L-type voltage-gated calcium channels,[376-379] which under high DA-output conditions produces a large

increase in intracellular levels of calcium that triggers mitochondrial dysfunction and OS.[380,381] As one of the only sources of DA in the CNS, *S. nigra* DA-neurons typically have a higher number of axonal arborizations and a higher basal metabolic rate compared to other CNS cells,[44] and are, therefore, at higher risk of experiencing OXPHOS-generated ROS.[382] Also, the proportion of support cells (astrocytes) surrounding the *S. nigra* DA-neurons is the lowest for any brain region,[383] leaving DA-neurons in deficit of important toxin-neutralization support, as well as, neurotrophic and antioxidant factors.

1.4 Experimental models of PD

One of the main challenges hindering researchers in their pursuit to understand and treat PD is the lack of appropriate animal models. Although toxin-based models (6-OHDA, MPTP, rotenone and paraquat) are widely used because of their reliability with regards to causing *S. nigra* cell loss and PD-like motor symptoms, their ability to induce synucleinopathy and non-motor symptoms is less consistent.[384] 6-OHDA is a DA analogue that cannot cross the blood brain barrier and thus is typically injected directly into the striatum. It causes specific *S. nigra* and VTA DA neuron degeneration by accumulating in the cytosol via DAT to promote the formation of ROS in a similar fashion as DA.[369,385] Not surprisingly, animals treated with 6-OHDA do not develop LBs.[57] MPTP, on the other hand, is a highly lipophilic molecule, which can be systemically administered, and is easily converted to 1-methyl-4-phenylpyridinium (MPP^+) in glial cells via MAO (subtype B) and autoxidation.[57,109,110] MPP^+ has high affinity for DAT and accumulates rapidly in DA neurons.[386] Once inside, it causes aberrant accumulation of ROS by inhibiting the function of complex I within mitochondria.[331-333] It was also found to cause LBs formation in non-human primates but not rodents.[387,388] Both pesticides rotenone and paraquat (N,N-dimethyl-4,4'-bipyridinium dichloride) can cause LB formation in rodent models,[389-391] however, they

employ different mechanisms to induce *S. nigra* degeneration. Rotenone is lipophilic and passively diffuses into DA neurons to cause ROS by directly inhibiting mitochondrial complex I.[112] Its main advantage is that it can be administered systemically and by stereotaxic injection, however, it is a highly toxic agent that can inadvertently cause premature death.[392,393] Paraquat, on the other hand, enters by aide of the DAT or VMAT (subtype 2) receptors and increases ROS production by inducing mitochondrial dysfunction, via an unknown mechanism other than complex I inhibition.[384] Its ability to consistently target DA neurons is, however, debated given observational inconsistencies between studies and, therefore, is used less often than other neurotoxins.[394]

Another approach to researching PD is via generation of animal genetic models of familial PD (*SNCA*, *LRRK2*, *DJ-1*, *PINK1* and *PRKN,* reviewed in Jagmag 2015[384]). Unfortunately, rodent models of PD poorly recapitulate parkinsonism as they either completely lack overt signs and symptoms of PD, or do so in a subtle, or inconsistent fashion. A summary of these results can be found in **Table 1.1**.[384] Genetic murine models of familial dominant PD (*SNCA* and *LRRK2*) were generated by several methods including: i) overexpression of the full human or mouse homologs, ii) overexpression of certain exonic regions of the human or mouse homolog, or iii) overexpression of the full human or mouse homolog containing a PD-associated point mutation. The overexpression of these genes was regulated using a variety of different human- or mouse-derived gene expression promoters in viral vectors, which allowed for tissue and/or cell specificity. As seen in **Table 1.1**,[384] only a select number of α-synuclein murine models (generated using the human homolog within cytomegalovirus (CMV) promoter-containing viral vectors)[395,396] demonstrate PD phenotype comparable to humans, i.e. *S. nigra* cell loss, synucleinopathy and motor impairment. Along a similar trend, LRRK2 animal models expressing the full human homolog[148] or CMV promoter containing viral vectors[397] demonstrated DA neuron loss. Unfortunately,

the majority of LRRK2 models failed to display a PD phenotype. Similar to mice, rat genetic models over-expressing human homologs of *SNCA*[286,398-404] and *LRRK2*[405] can elicit DA cell loss.

Murine EOPD models (*Dj-1*, *Pink1* and *prkn*) were generated by introducing various exonic deletions in the mouse homolog or, in the case of parkin, overexpression of the full human homolog carrying the PD-causing point mutation Q311X. When analyzing the PD-specific effects in these laboratory models it is not surprising that EOPD models are devoid of α-synuclein-like inclusion bodies, given that LBs and LNs are rarely encountered in human specimens of EOPD. However, it is surprising that EOPD murine models exhibited few signs of DA neuronal loss or motor symptoms. The major exceptions being the model generated using human *PRKN* Q311X overexpression[406] and a *Dj-1* model generated by inserting an exon 1 stop codon in the murine homolog on a pure C57BL/6 background.[407] This is especially important as equivalent *Drosophila* EOPD-gene linked KO models exhibit more severe phenotypes, such as reduced lifespan, aberrant mitochondrial form and function, male sterility, and DA neuron dysfunction and loss.[183,340,342-344,408] In contrast to the rat *pkrn* gene disruption model, both exonic deletions of *Dj-1* and *Pink-1* rat homologs were able to elicit DA cell loss and motor impairment.[409]

Genetic/ Toxin Model	Genetic Variant (full length, point mutation, truncation or exon mutation)	Promoter	SNc neuron loss	Inclusion bodies	Motor impairment
α-synuclein	WT	PDGF-β	-	+	+
	WT/A53T	Thy1	-	+	+
	WT/A53T/A30P	TH	-	-	ND
	WT	Prp	-	-	-
	A53T	Prp	-	+	+
	WT	Prp	-	-	-
	A30P	Prp	-	+	-
	A53T	Prp	-	+	+
	WT	TH	-	-	-
	A53T/A30P	TH	+	-	+
	A30P	PrP	-	+	+
	WT/A53T/A30P	CMV	+	+	+
	WT (1-120)	TH	-	+	+
	WT	CMV	+	-	ND
	WT	CaMKII	+	-	+
	WT (1-130)	TH	+	-	+
	WT (1-119)	ROSA26	-	-	ND
	A53T	ROSA26	-	-	ND
	E46K	ROSA26	-	-	ND
	A53T	Pitx3	+	-	+
	WT/A53T	CMVE-Syn-1	+	+	+
LRRK2	R1441C/G*	mLRRK2	ND	ND	ND
	R1441C*	mLRRK2	-	-	-
	WT#	mLRRK2	-	-	+
	R1441G#	mLRRK2	-	-	+
	WT#	hLRRK2	-	-	-
	G2019S#	hLRRK2	-	-	-
	exon 1*	mLRRK2	-	+	ND
	exon 29,30*	mLRRK2	-	+	ND
	G2019S#	CMV-PDGF-β	+ (DAc loss)	-	-
	R1441C#	CMV-PDGF-β	-	-	+
	WT#	CMV-PDGF-β	-	-	-
	G2019S#	CMV-PDGF-β	+ (DAc loss)	-	+
	R1441C#	ROSA26	-	-	-
PINK1	Exon 4-7 deletion	-	-	-	-
DJ-1	Exon 2 deletion	-	-	-	+
	Exon 2 deletion	-	-	ND	ND
	Exon 3-5 delection	-	-	ND	-
	Exon 7 inactivation	-	-	ND	+
	Exon 2-3 deletion	-	-	ND	-
	Exon 2 deletion	-	-	-	+
	Exon 1 stop	-	+	ND	-
Parkin	Exon 3 deletion	-	-	-	-
	Exon 3 deletion	-	-	-	+
	Exon 2 deletion	-	-	-	-
	Exon 7 deletion	-	-	-	-
	Exon 3 deletion	-	ND	ND	ND
	Truncated, Q311X#	*Slc6a3*	+ (DAc loss)	-	+
	wt	nse	-	ND	ND
6-OHDA	-	-	+ (DAc loss in SNc > VTA)	-	+
MPTP	-	-	+ (DAc loss in SNc > VTA)	-	+
Rotenone	-	-	+ (DAc loss in SNc > VTA)	+	+
Paraquat	-	-	+ (DAc loss in SNc)	+	+

Table 1.1. Summary of parkinsonian phenotypes observed in animal models

WT or #, human gene; wt or *, murine gene; PDGF-β, platelet derived growth factor-β; Thy-1, Thy-1 cell surface antigen; TH, tyrosine hydroxylase; Prp, prion protein promoter; CMV: cytomegalovirus; CaMKII: calcium/calmodulin-dependent protein kinase II; ROSA26: ROSAβgeo26P locus; Pitx3: paired-like homeodomain 3; CMVE-Syn 1: cytomegalovirus enhanced with synapsin 1; mLRRK2: murine LRRK2 promoter; hLRRK2: human LRRK2 promoter; CMVE-PDGF-β: cytomegalovirus enhanced with platelet derived growht factor-β; nse: neuron specific enolase; Slc6a3: bacterial artificial chromosome containing solute-dependent dopamine transporter; 6-OHDA: 6-hydroxydopamine; MPTP: N-methyl-4-phenyl-1,2,3,6-tetrahydropyridine; DAc: dopaminergic cell; SNc: substantia nigra compacta; VTA; ventral tegmental area; ND: No data. Modified from Jagmag 2016.[384]

Given the scarcity of PD phenotype in *prkn* KO mice, they are not considered robust PD models alone. Being an age-associated disease, it is speculated that the shortened lifespan of rodents, halts PD-pathogenesis in its initial and subtle stage. It is, therefore, believed that *S. nigra* degeneration requires increased stress conditions in these models, either by introducing PD toxins or mutations to genes linked to PD pathogenesis. One study attempted to increase endogenous cellular stress by creating a triple recessive PD-gene KO. Kitada et al. in 2009 removed murine homologs of *Dj-1*, *prkn* and *Pink1*; surprisingly, no overt PD phenotype was observed with only subtle signs of DA mishandling, leaving some to suggest that this finding supports the theory that these three genes work within a similar pathway.[410] Given that parkin is thought to be involved in mitochondrial health and turnover, two groups attempted to generate murine PD models by introducing mtDNA defects in *prkn* KO mice. First, Sterky et al. in 2011, found that removing the mitochondrial transcription factor A (*Tfam* KO) caused no changes in *prkn* KO phenotype.[358] However, Pickell et al. in 2015, by introducing a deficiency in the genomic proofreading enzyme DNA polymerase γ (Polg), caused progressive accumulation of mtDNA mutations in *prkn* KO mice ($prkn^{-/-}$;mutator mice), which resulted in L-dopa -responsive motor defects.[359]

Finally, it is important to note that non-human primates are currently the only known animals to sporadically demonstrate a spontaneous and age-dependent development of nigrostriatal pathway dysfunction (at >15 or > 25 years of age, depending on the species[43]). Symptoms caused by this dysfunction are subtle and believed to resemble an early-state PD, which include: slight tremor, stooped posture, and gait disturbances;[411-414] their associated neuropathological findings include: *S. nigra* DA-cell loss, decreased DAT and TH expression, and abnormal neuronal morphology.[413,415-421] Interestingly, no LB- or LN-like inclusions have been observed in these animals and spontaneous mutations of *SNCA* have not been found in non-human primates.[43] Being the only experimental animal models known to

form a small degree of NM in their *S. nigra* and *L. coeruleus*, akin to humans, [43,79] indicates a potential primate-specific association between brain regions that generate NM and susceptibility to degeneration with advanced age.

1.5 Parkin protein structure and function

The *PRKN* or *PARK2* gene is the second largest gene in the human genome, with its exonic length measuring 1.53Mb,[154] and is located on chromosome 6 at position 6q25-27.[422] As shown in **Fig. 1.10a**,[105] it contains twelve exons and a bidirectional promoter, with the neighbouring gene called parkin coregulated gene (*PACRG*). Although it is proximal to *PRKN*, only rare exonic deletions extending into exon 1 of *PACRG* have been associated with PD.[423] However, recent observations have linked *PACRG* with a role in modulating the innate immune system via NF-κB activation in a similar fashion as parkin.[424] As previously mentioned, mutations in *PRKN* account for as many as 50% of EOPD cases, with an average age of onset of 38 years of age.[154,155,194] There are more than 120 known pathogenic mutations, with exon deletions being the most common.[141] In fact, exons 2-4 account for roughly 50% of total deletions, with exon 3 having the highest number of mutations overall[425-430] that result in a complete loss of detectable parkin protein expression in human tissue.[431] Given the prevalence of exon deletions in EOPD, the majority of previously generated *prkn* KO mouse models contain deletions of exon 2 or 3.[432-439] However, a large number of studies, using recombinant human protein or cell expression models, have also focused on understanding the effect of missense and nonsense PD-associated mutations on protein structure and function (further discussed below in section 1.5.2).[105,192,193,440-454]

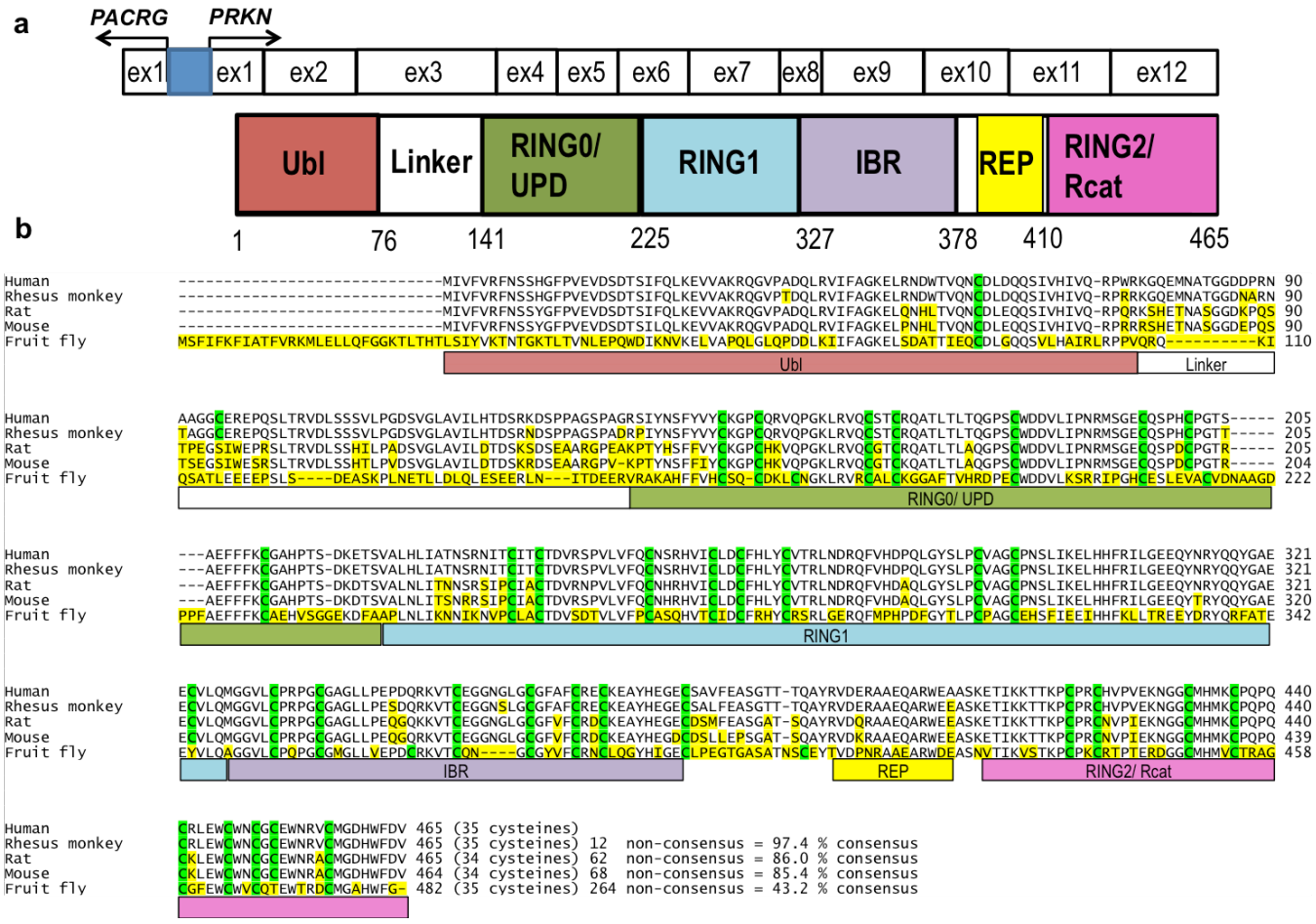

Figure 1.10. Parkin protein primary structure

(**a**) *PRKN* gene mRNA transcript and corresponding primary structure and domains, **a**. Neighbouring parkin coregulated gene (*PARCG*) is shown sharing the promoter region, dark blue box. Modified from Corti 2011.[105] (**b**) Consensus of Parkin protein amino acid (aa) sequence between select species (human, thesus monkey, mouse, rat and fruit fly). Sequences obtained from National Center for Biotechnology Information Database: NM_004562.3; XM_015137330.2; AB019558; AF210434; and AF510072.1. Sites of non-consensus are highlighted in yellow. Cysteine residues are highlighted in green. Location of corresponding protein domains are identified below the aa sequence. Ubl, ubiquitin like domain; RING, really interesting new gene; UPD, unique parkin domain; IBR, in between RING; REP, repressor element of parkin; and Rcat, required for catalysis domain.

1.5.1 Primary and tertiary structures of parkin

As shown in **Fig. 1.10a**,[105] the *PRKN* gene encodes for a highly conserved 465 amino acid (aa) protein with a molecular weight (MW) of ~52 kDa, which is found abundantly expressed in the cytoplasm of tissues experiencing high OS, e.g. heart, muscle and brain. Its structure contains an N-terminal ubiquitin like domain (Ubl), four really interesting new gene, or RING, domains, and two interdomain (or linker) regions. The Ubl domain shares roughly 62% homology with the ubiquitin (Ub) protein and spans residues 1-76.[154] It is separated from RING0 by the first linker region, which contains a poorly conserved peptide sequence and a primate sequence-specific C95 residue.[455] RING0, aa 141-225, is often described as the unique parkin domain (UPD),[455] while RING1, the putative E2 binding domain spans aa 226-326. The third RING structure is described as an in-between RING (or IBR) and spans aa 327-378. It is separated from the final RING domain by the second linker, which contains the repressor element of parkin (REP) with conserved α-helix structure spanning aa 391-403. The final domain, RING2 spans aa 410-465 and contains a catalytic cysteine at position 431, which is important for E3 ligase function.[192,193,448,449] In fact, this domain is often called the required for catalysis, or Rcat, domain.[456] The relationship between exon and primary structure is shown in **Fig. 1.10a**;[105] note that exons 2-4 correspond to Ubl, linker and RING0 domains, respectively.

It is believed that parkin contains a high number of thiols for maintaining proper conformation, as the majority of its cysteines are coordinated to zinc within its RING domains (28/35 or ~80%).[192,193] These domains are comprised of two zinc atoms coordinating to seven cysteines and one histidine residue.[456] Interestingly, there are also non-coordinating cysteine residues within its structure, seven cysteines in primates and six cysteines in rodents (**Fig. 1.10b and 1.11a**), with C95 being a primate-specific cysteine. To date, the role or significance of these unbound cysteines with regards to structure or function is not known, with the exception of cysteine at position 431 as mentioned.[192,193,448-450,452]

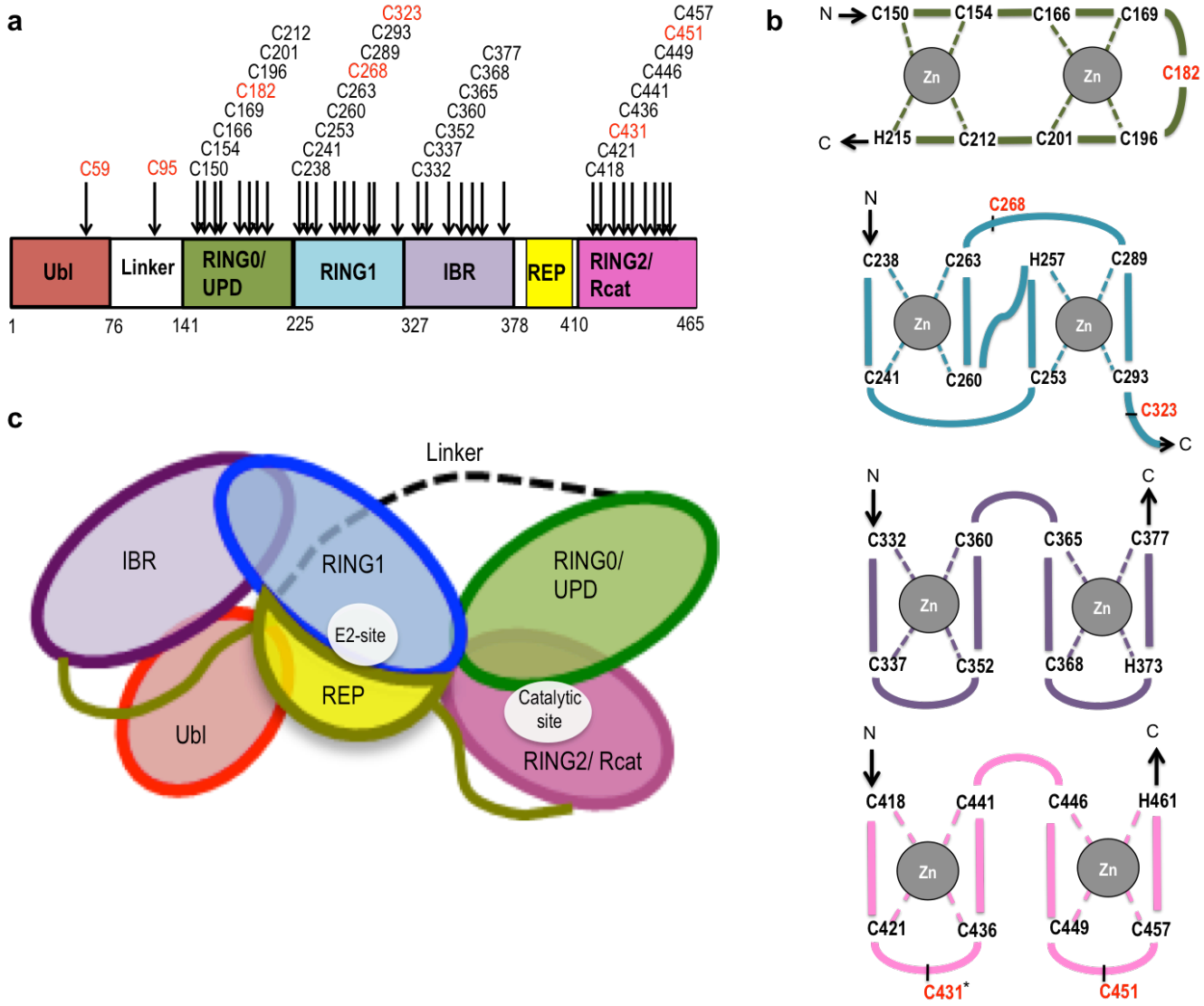

Figure 1.11 RING domain topology and tertiary structure of parkin

(**a**) Location of cysteine residues within primary structure of parkin. (**b**) Proposed topology of the four zinc-coordinating RING structures within parkin, RING0, shown in green, adopts a zinc finger hairpin like structure, while RING1, shown in blue, adopts an E3 ligase canonical cross-brace motif. Both the IBR and RING2 domains have similar sequential zinc finger-like topologies. RING2 contains the catalytic site at position C431, denoted with an asterisk. Non-coordinating cysteines are highlighted in red. (**c**) Overall tertiary structure of parkin. Hydrophobic interactions between Ubl and RING1, as well as, between RING0 and RING2, maintain the protein in an overall coiled position. E2 binding site is located within the RING1 domain and blocked by REP. Modified from Trempe 2013.[448] Ubl, ubiquitin like domain; RING, really interesting new gene; UPD, unique parkin domain; IBR, in between RING; REP, repressor element of parkin; and Rcat, required for catalysis domain.

In the early 2010s, multiple studies were conducted to determine parkin structure, beginning with two groups independently deciphering its X-ray crystal structure. They confirmed the presence of the four RING-like and Ubl domains and identified the novel REP domain.[448,449] Of interest, the linker region was omitted from these early studies due to structural instability. Nonetheless, these studies also revealed that the topology was different among the various RING domains of parkin (**Fig. 1.11b**). For instance, RING0, forms a unique hairpin-like zinc finger, while both IBR and RING2 domains share a similar topology consisting of two zinc-binding regions ordered in a sequential fashion. As only the RING1 domain adopts the canonical cross-brace topology that is found in other RING-containing E3 ligases, it was predicted that RING1 contained an E2 binding site that was later defined to contain an α-helix (aa 263-271) and two loop domains (aa 239-244 and aa 290-292).[192,193] Structural studies also helped decipher the overall tertiary structure of parkin (**Fig. 1.11c**), being a coiled protein that contains multiple interdomain hydrophobic interactions. The first interaction occurs between the Ubl domain and RING1, and is mediated by the isoleucine residue at position 44 within the Ubl domain.[192,193,450,452] The second interdomain interaction is formed between RING0 and RING2 and involves hydrophobic interactions between residues F146, L162, V164, V164, L176, W183 and F208, in RING0, with residues W462 and F463 within RING2.[192,193,450,452] Finally, the binding of REP onto RING1 is proposed to occur via hydrophobic interactions between W403 on REP and a hydrophobic pocket within RING1 formed by residues R234, I236, V250 and R256, which causes the REP to block the E2 binding site within RING1.[450,452] Being a tightly coiled protein, with multiple interdomain interactions that appear to block the E2 binding and RING2 catalytic sites, parkin is considered natively expressed in an auto-inhibited state that must be activated in order to function as E3 ligase.[192,193,450-453,457,458]

1.5.2 Role of parkin in protein turnover as E3 ligase enzyme

Since the RING-like structures in parkin are highly conserved among invertebrate and mammalian species, its proposed to function as a RING-like E3 ligase enzyme,[292,456] with loss of its E3 ligase activity considered crucial in the development of PD, cancer, mitochondrial dysfunction and aberrant cell immunity.[192,193,459,460] Therefore, research on parkin has focused on understanding its E3 ligase mechanism in order to develop methods to enhance it *in vivo*.

E3 ligase proteins are part of the ubiquitination cascade, which functions to tag one or multiple lysine residues on a specific protein with either a single ubiquitin (Ub) molecule (mono-ubiquitination) or a Ub polymeric chain (poly-ubiquitination) in order to regulate various downstream cellular processes, such as protein stability, function, localization and interaction (**Fig. 1.12a**).[459] Ub chains can form using one of seven of its lysine residues (K6, K11, K27, K29, K33, K48 and K63) or its N-terminal methionine residue (M1).[461] The specific type of mono-ubiquitination or poly-ubiquitination chain formed on a particular protein governs its downstream cellular processing, e.g. the canonical K48 poly-ubiquitination causes 26S proteasomal-mediated degradation.[462] The ubiquitination cascade requires the sequential action of three enzymes: the Ub-activating enzyme (E1), the Ub-conjugating enzyme (E2), and the Ub ligase enzyme (E3). There are a little over 600 different E3 ligase proteins[463] expressed in humans, which are grouped into the following three classes: the largest class contains i) the RING/-Ubox-type E3s (600 members),[464] followed by ii) the HECT (Homologous to E6AP C-Terminus)-type E3s (28 members),[465] and finally iii) the RBR (RING- between-RING)-type E3s (14 members).[466] The role of E3 in the ubiquitination process is to confer a high degree of specificity by binding to a select number of substrates and help facilitate the transfer of Ub from E2 onto these targets. The specific method used to transfer Ub defers slightly between the three classes of E3s (**Fig. 1.12b**).[459,462] RING-E3s act as scaffolds to bring both the E2 enzyme and substrate in close proximity, facilitating direct transfer

of Ub from E2 onto the target.[464] HECT E3s, on the other hand, transfer Ub to the target in a two-step process that first requires the formation of an intermediate thioester bond between Ub and a catalytic cysteine residue located within its N-terminal lobe (N-lobe).[465] Ub is then directly transferred from the E3 onto the substrate. RBR E3s are often called RING/HECT hybrids since they contain RING structures, but, function like HECT E3s.[456,459,466,467] They function by binding E2 with their first RING structure, followed by intermediate thioester bond formation on a catalytic cysteine residue located within a second RING structure, and final transfer of Ub to the target substrate.

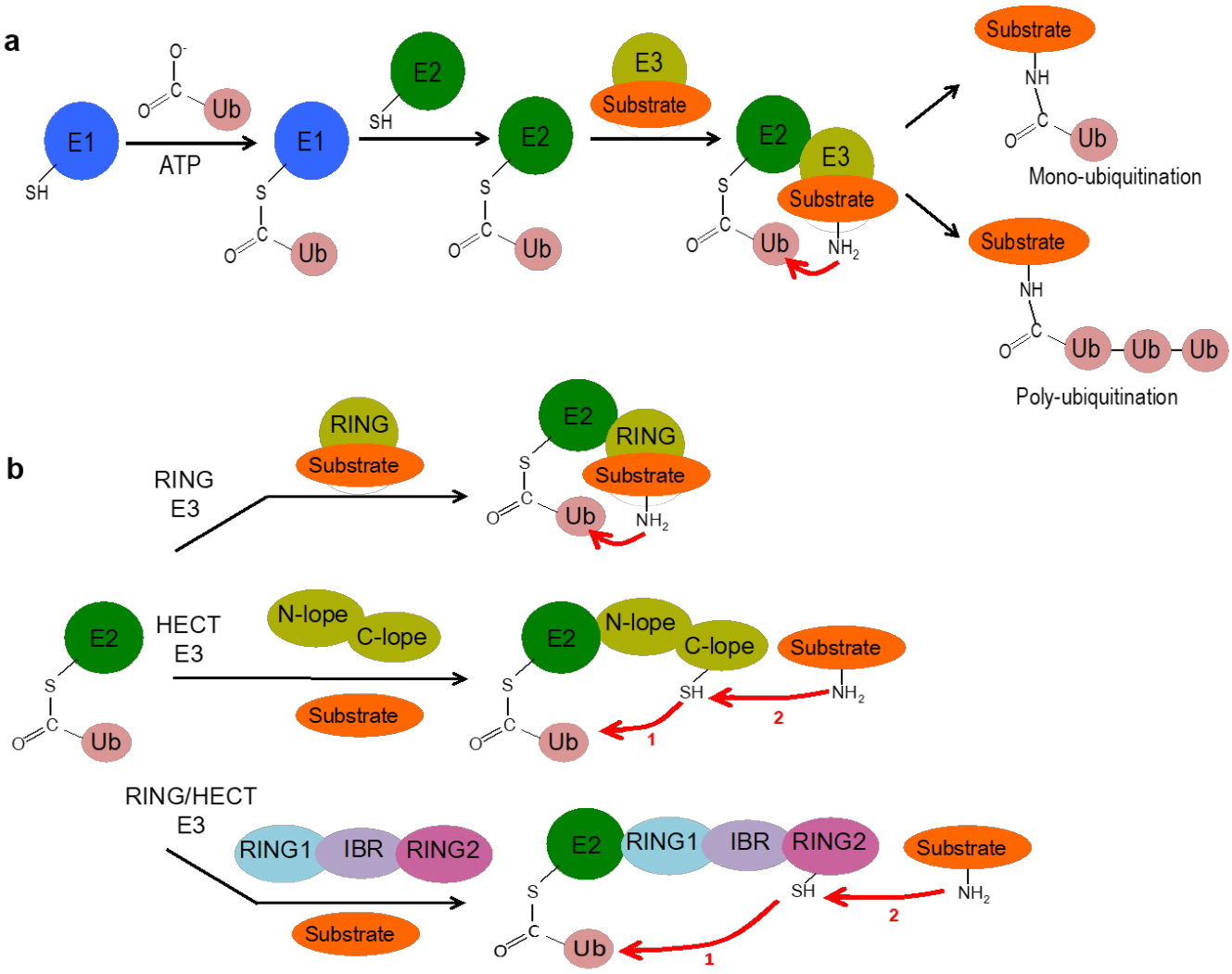

Figure 1.12. Ubiquitination pathway and mechanism of RING E3 ligases
(**a**) Ubiquitination pathway requires the stepwise transfer of ubiquitin across three ubiquitin carrier proteins, E1, E2 and E3, to label a specific protein substrate. (**b**) RING only, HECT and RING/HECT E3 ligase mechanism of action, **b**. HECT: homologous with E6-associated protein C-terminus; RING: really interesting new gene and RBR: RING-Between RING-RING. Modified from Seirafi 2015.[459]

From extensive structural analysis, parkin was determined to function as an RBR E3. Its RING1 contains a well-defined E2-binding site and a catalytic cysteine at position C431 in its RING2 domain capable of forming thioester conjugates with Ub. Interestingly, a neighbouring residue, H433, is believed to further increase the nucleophilic strength of C431 by facilitating thiol deprotonation. Consistent with this hypothesis, point mutations C431A and H433A caused a significant decrease in C431-Ub conjugation.[193] Like other currently known RBR E3s, such as human homolog of Ariadne (HHARI)[468] and heme-oxidized IRP2 ubiquitin ligase 1-interacting protein (HOIP),[469,470] parkin contains auto-inhibitory domains that suppress its E3 activity.[457] In a similar fashion as the RING0 domain of parkin, the Ariadne domain in HHARI[471] and the Ub-associated domain in HOIP[472] occlude their catalytic cysteine sites. Having such highly inhibited structures suggests that dysfunction of RBR E3s leads to significant downstream consequences, as demonstrated by their link to neurodegenerative diseases,[470,473] immunity,[474] inflammation, and cancer.[475]

Several PTMs, molecular activators and domain rearrangements were found to modulate parkin E3 activation. Initial structural work, using domain deletions, suggested that removing Ubl domain inhibition, via PTM or protein-protein interactions, was sufficient to induce activation.[457,458,476] Such activators included various Ubl domain binding partners such as: Src homology 3 (SH3) domain-containing proteins,[477] ubiquitin-interacting motif (UIM)-containing proteins,[478] 26S proteasomal subunits,[479] as well as, putative parkin substrates like ataxin-3.[480] A crucial finding was the discovery that the mitochondria-associated protein PINK1 induced serine phosphorylation, at S65, within the Ubl domain of parkin.[454,481,482] Subsequent modeling studies determined that addition of this negatively charged moiety disrupts the interaction between Ubl and RING1, thus removing Ubl inhibition.[450,452,456,458] Interestingly, this PTM alone is not sufficient to activate parkin, as the mutant S65A did not completely suppress parkin activation.[454] It was later discovered that PINK1 also

phosphorylates Ub at S65, which led to the hypothesis that phosphorylated ubiquitin (pUb) acts as the true activator of parkin, with pUb binding to the RING1 domain of parkin to disrupt its hydrophobic interactions with the Ubl and REP domains.[352,483] A more recent mass spectrometry (MS) study, using hydrogen deuterium exchange, has identified important domain rearrangements, and new interdomain binding, that occur as a result of Ubl S65 phosphorylation and pUb binding to RING1 (**Fig. 1.13**).[448,452] Gladkova et al. found that both the phosphorylated Ubl domain (pUbl) and the binding of pUb to RING1 displaced Ubl from RING1. Unexpectedly, pUbl was predicted to also rebound to the RING0 domain and cause release of the catalytic domain, RING2. Binding of pUb to RING1, in turn, caused additional release of the REP, allowing access to the E2 binding site. Interestingly, they found a novel, highly conversed, activating element (ACT), located within the poorly studied first interdomain linker region (aa 101-110) of parkin. It is postulated that residues L102, V105 and L107 of ACT help facilitate RING2 release by mimicking the RING2-binding motif within RING0.[452] This is an intriguing finding as the first interdomain linker was historically omitted in conformational studies due to its high structural flexibility and was, therefore, deemed unimportant in the E3 activation of parkin.[192,193,448-450]

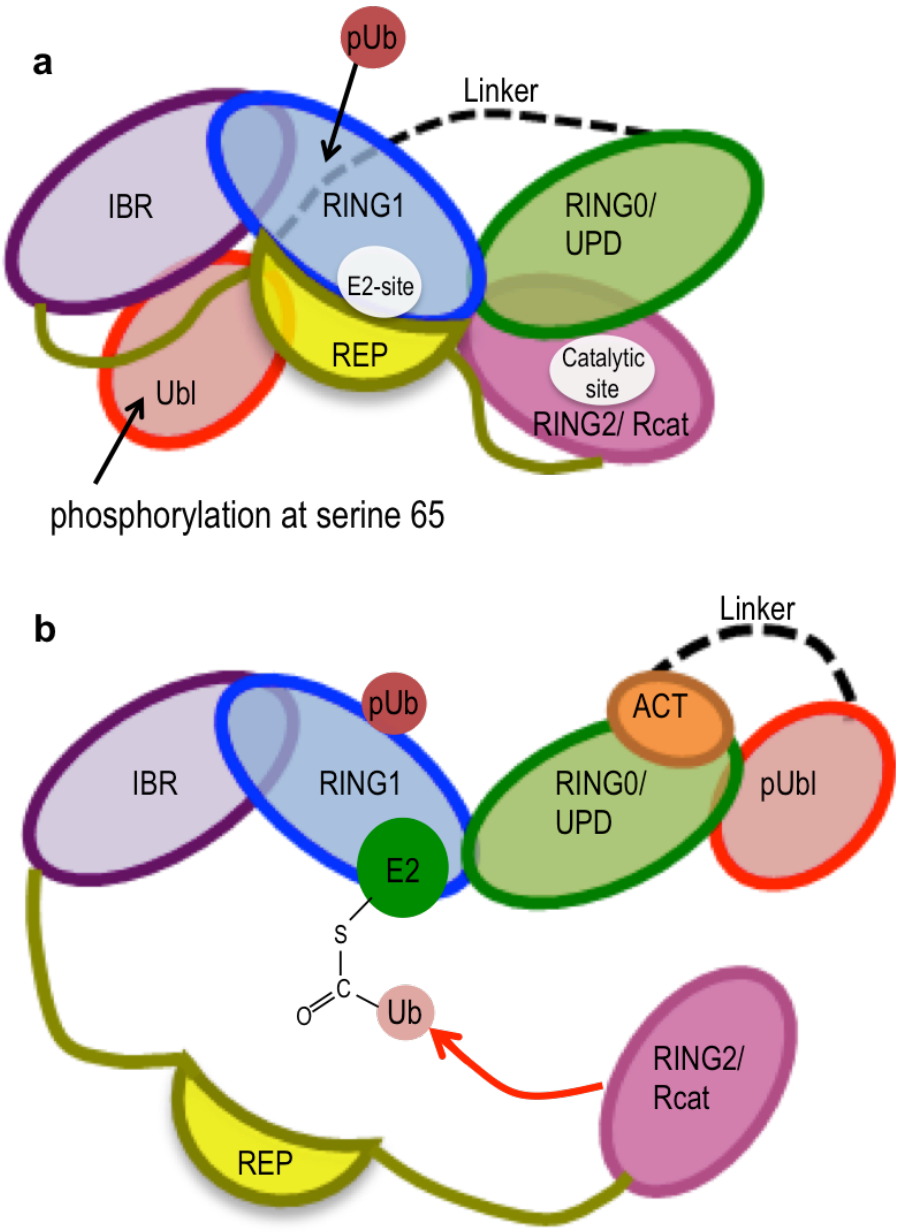

Figure 1.13. Proposed tertiary structure of parkin in autoinhibited and active state
(**a**) In the auto-inhibited state, tight hydrophobic interactions block the E2 binding site and locks it 50 Å away from the catalytic site, thus preventing transfer of ubiquitin from E2. (**b**) Activation is triggered both by S65 phosphorylation and binding of phosphorylated ubiquitin to the RING1 domain. This releases the Ubl and REP domains from RING1, permitting access to the E2 binding site. Binding of Ubl to RING0 is facilitated by the ACT domain, which allows sustained untethering of RING2. Ubl, ubiquitin like domain; RING, really interesting new gene; UPD, unique parkin domain; IBR, in between RING; REP, repressor element of parkin; Rcat, required for catalysis domain, ACT, activating element; Ub, ubiquitin; and pUb, phosphorylated ubiquitin. Modified from Trempe 2013[448] and Gladkova 2018.[452]

Since parkin is found highly expressed in the cytosol, and has many non-mitochondrial E3 ligase substrates, it is not fully understood how its E3 activity is modulated in the absence of PINK1. As shown in **Fig 1.14a**, only a handful of PTMs were found to alter the E3 activity of parkin.[484,485] Generally, the majority of PTMs identified are believed to cause E3 ligase inhibition either by: i) OS modifications from excessive ROS (C212, C253, C268, C289, C431 and C441),[486-488] RNS (C323)[489-492] or DA stress (C268 and C323);[362,493] ii) caspase 1-mediated proteolytic cleavage at D126;[494,495] or by iii) Cdk5 and c-Abl-mediated phosphorylation of S131[496] and Y143,[497,498] respectively. With the exception of low levels of ROS/RNS, and S65 phosphorylation, only three other PTMs are known to increase parkin E3 activity in cellular over-expression paradigms, including: sulfhydration[499], sumoylation[500] and neddylation.[501] Vandiver and colleagues in 2013 demonstrated that cysteine sulfhydration at positions C59, C95 and C182 significantly enhanced E3 ligase activity in HEK-293 cells exposed to the hydrogen sulfide donor GYY4137.[499] Um and Chung in 2006 demonstrated that parkin self-ubiquitination is increased after binding to the small ubiquitin-related modifier (SUMO)-1 protein,[500] and Um et al. in 2012 demonstrated that addition of NEDD8, an ubiquitin-like small molecule, activated parkin E3 activity in cells.[501] As these were single accounts of activation, further studies are required to validate these activating PTMs.

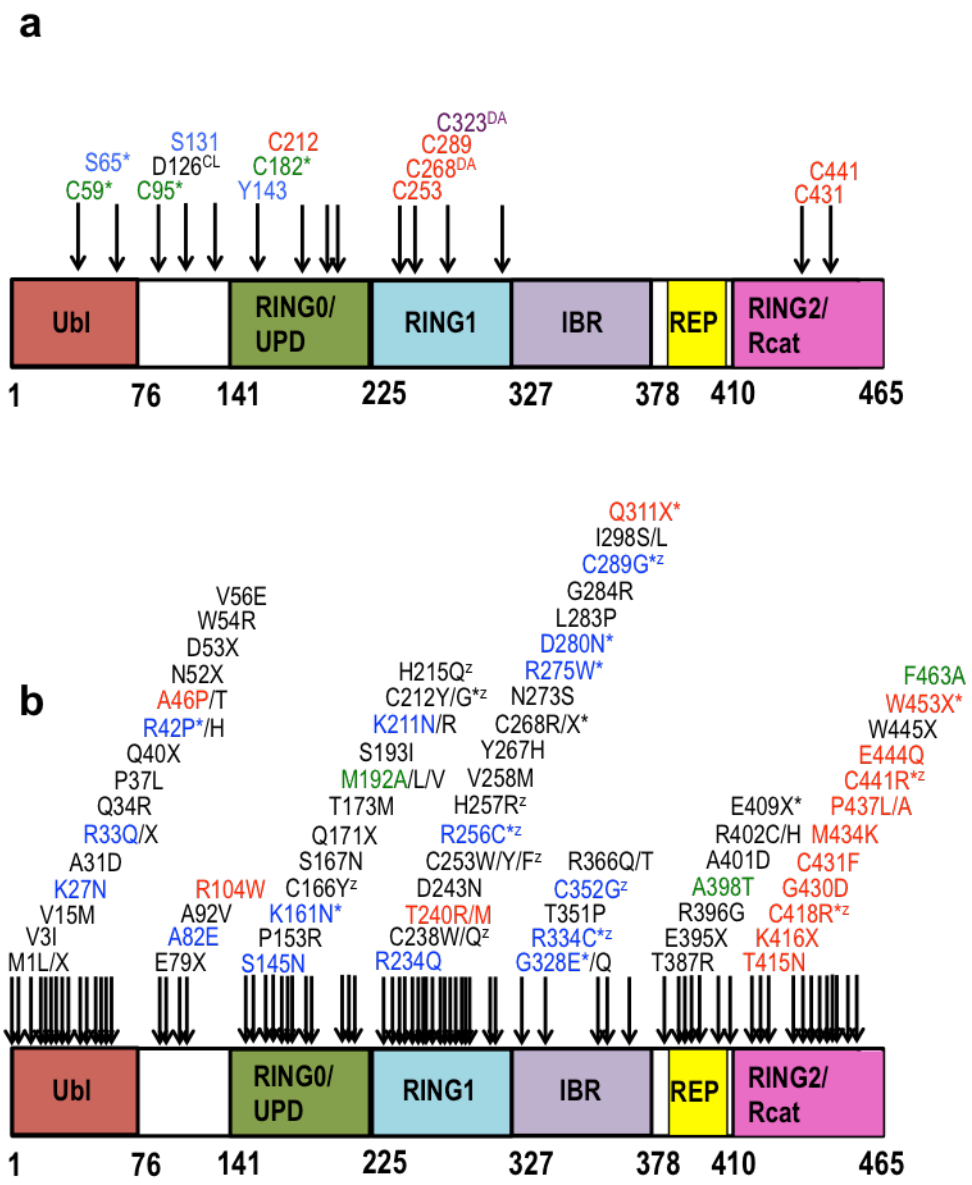

Figure 1.14. Post-translational modifications and Parkinson disease-associated mutations
(**a**) List of various post-translational modifications (PTMs) found to affect parkin E3 ligase activity. Activating PTMs are indicated with an asterisk. Residues highlighted in green indicate sites of sulfhydration; highlighted in blue indicate phosphorylation sites; highlighted in red are sulfonation; highlighted in purple are nitrosylation; identified by "DA" are dopamine-conjugated; and identified with "CL" are cleaved by caspase-1. (**b**) Selection of Parkinson disease-associated mis- and non-sense mutations in parkin. Mutations that retain E3 ligase activity are highlighted in blue; with reduced or loss of activity are highlighted in red; that increase activation are highlighted in green; that reduce solubility or induce aggregate formation are identified with an asterisk; that affect zinc coordination are identified by "z"; and with unknown effect are shown in black. Data compiled from multiple studies and reviews.[105,192,440,441,445,448,449,452,454,484,485]

Despite ongoing efforts to produce small molecular activators of parkin, the link between E3 ligase activity and EOPD pathogenesis is still unclear. The most convincing counterargument to the hypothesis that loss of parkin E3 activity causes PD is that many PD-associated missense mutations in *PRKN* have retained E3 activity (**Fig. 1.14b**).[105,192,440,441,445,448,449,502] In fact, as shown in **Fig. 1.14b**, it appears that the majority of missense and nonsense mutations, which are not found within the catalytic domain, actually retain E3 activity. Some argue that *PRKN* mutations with retained E3 activity affect protein expression/stability, thus, indirectly reducing its E3 activity. As reviewed by Wauer and Komander in 2013,[192] the hypothesized effect of PD-associated *PRKN* mutations is generally separated into three main categories, including: i) protein stability, ii) domain interactions, or iii) catalytic site activity (C431). Protein stability is affected by mutations in zinc coordinating residues (e.g. C253, C289, C418 and C441) or domain core residues, which affect the helical and loop structures within the E2 binding site of RING1 (e.g. T240, Y267 and R275). Enhancement of inhibiting hydrophobic interdomain interactions would render the protein more difficult to activate, while destabilizing domain interactions is predicted to cause aberrant E3 ligase activation, which some believe results in premature degradation of parkin and its substrates. Examples of mutation sites associated with domain interactions include: S145, M192, A230, R234, A398, N273, E310 and G328. Wauer and Komander[192] also suggest that K161N and K211N mutations likely interfere with pUb binding on RING1 and thus hinder parkin activation. There still, however, are some PD-associated mutants (H200Q, V244I, H265R, D280N, L283P, G248R, T415N) within the RING0, RING1 and RING2 domains whose role in parkin structure and function is still unclear.

Parallel to structure and function studies, much effort has gone into identifying potential parkin E3 substrates. Since its discovery in 1998,[184] >60 putative substrates have been identified, as shown in **Appendix Table A1**.[296,299,503-560]

However, having such a large number of E3 substrates appears to contradict its very role as a selective substrate-targeting enzyme. Some propose that only substrates identified for degradation by K48 polyubiquitination, which are also found to accumulate in *prkn* KO mice and in *PRKN*-associated ARPD human brain, are considered true parkin substrates. These include: aminoacyl t-RNA synthetase cofactor, p38/AIMP2[296]; component of SCF-Fbw7 E3 ligase complex, Fbw7β[297]; KRAB and zinc finger protein, PARIS (ZNF746)[298]; and pro-apoptotic negative regulator of mTOR and Akt, RTP801/REDD1.[299] On the other hand, parkin can also facilitate the formation of K6, K11 and K63 polyubiquitination patterns that lead to both non-proteolytic processes and non-proteasomal-mediated protein degradation.[537,561-564] While the role of K6 polyubiquitination is still unclear, it has been associated with the DNA damage response and mitophagy induction.[461] K11 polyubiquitination has been linked to cell cycle regulation and both proteasomal and non-proteasomal degradation of hypoxia-inducible factor 1α (HIF-1α) in response to hypoxia.[565,566] K63 polyubiquitination has been linked to regulation of endocytosis, protein trafficking, innate immunity, and NF-κB signaling.[567] Adding to the complexity of understanding the *in vivo* E3 function of parkin is the fact that parkin can self-ubiquitinate via K6 polyubiquitination chains. Although the full function of K6 linkages in parkin biology remains to be elucidated, they have been linked to inhibition of parkin-mediated mitophagy, which is reversed by USP8, a deubiquitinating enzyme.[568]

1.5.3 Role of parkin in mitochondrial health and mitophagy

As previously mentioned, a prevailing model for the role of parkin in PD pathogenesis is its effect on mitochondrial health via inducing the mitophagy pathway (**Fig. 1.9**) a process that requires the concerted function of both PINK1 and parkin.[349-353] In the absence of parkin-dependent mitophagy, it was proposed that aberrant accumulation of OS from undegraded dysfunctional mitochondria leads to

neurodegeneration. Upon synthesis, PINK1 translocates to the OMM, by aide of its MTS, and several translocase of outer mitochondrial membrane (TOMM) proteins (**Fig. 1.15a**).[569] There PINK1 extends its C-terminus into the inner mitochondrial membrane (IMM) space, while its N-terminus remains in the cytosol. Under basal conditions, it is cleaved by the IMM- and matrix- associated proteases presenilin-associated rhomboid-like protein (PARL)[570] and mitochondrial processing peptidase (MPP), respectively. This causes release of its N-terminal segment into the cytosol, which is further degraded by the proteasome in a process called the N-end rule pathway. However, when mitochondria become depolarized or experience high levels of ROS, cleavage of PINK1 is impaired and results in its accumulation on the OMM. The kinase activity of PINK1 causes phosphorylation of ubiquitin-tagged proteins (and Ub-like proteins) located on the OMM, which, in turn, causes recruitment of parkin from the cytosol.[173,350] The E3 activity of parkin is further activated by PINK1-mediated S65 phosphorylation at its Ub-like domain,[448,571] leading to an increase in OMM protein ubiquitination that triggers the recruitment of autophagy receptors such as optineurin (OPTN) and nuclear dot protein 52 kDa (NDP52) to the mitochondria.[572,573] These, in turn, lead to the recruitment of phagophores containing the microtubule-associated protein 1A/1B-light chain 3 (LC3) that promote lysosomal degradation of the engulfed mitochondria.[350,574]

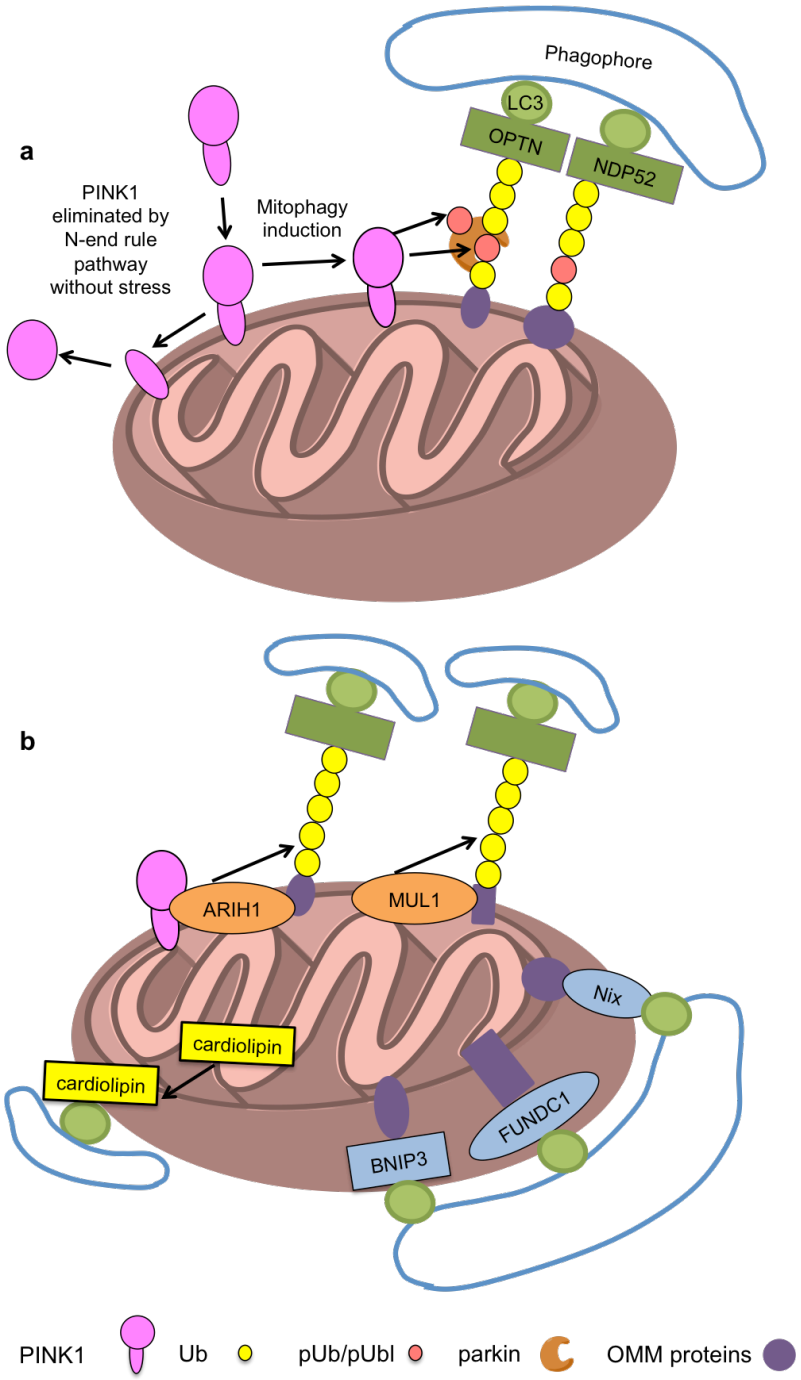

Figure 1.15. Parkin dependent and independent mitophagy pathways
(**a**) Under non-stress conditions, PINK1 locates to the inner mitochondrial membrane and is degraded by the N-end rule pathway. When depolarized, PINK1 accumulates at the outer mitochondrial membrane (OMM) and recruits Parkin, leading to the ubiquitination of substrates and the recruitment of autophagy receptors (OPTN, NDP52 and LC3) to initiate mitophagy. (**b**) Parkin-independent mitophagy includes: i) receptor-mediated by BNIP3, FUNDC1 or Nix, shown in blue; ii) ubiquitin ligase-mediated by ARIHI or MUL1, shown in orange; and iii) cardiolipin-mediated, shown in yellow. BNIP3, BCL2/adenovirus E1B 19 kDa interacting protein 3; FUNDC1, FUN14 domain-containing protein 1; NDP52, nuclear dot protein 52 kDa; ARIH1, ariadne-1 homolog 1; MUL1, mitochondrial E3 ubiquitin protein ligase 1; OPTN, optineurin; LC3, microtubule-associated protein 1A/1B-light chain 3; Ub, ubiquitin; pUB, phosphorylated Ub; pUbl, phosphorylated Ubl domain on parkin. Modified from Liu 2019.[569]

There is evidence demonstrating that high energy-demanding cells like DA-neurons and microglia have higher basal mitophagy, however, its activation occurs independently of the PINK1/parkin pathway.[575] In fact, there are multiple recently-discovered mitophagy pathways that are independent of PINK1 and parkin (**Fig. 1.15b**),[569,576] leading many to question the precise *in vivo* role of PINK1 and parkin in mitophagy regulation; especially, since high, non-physiological, concentrations of the mitochondrial uncoupler carbonyl cyanide m-chlorophenyl hydrazine (CCCP) are required to induce parkin-mediated mitophagy in experimental designs.[349-352] Parkin-independent mitophagy occurs either by receptor-mediated or non-parkin ubiquitin ligase-mediated mechanisms that are induced without the use of uncoupling agents, e.g. elevated hypoxia or ROS.[569] Mitochondrial receptor proteins, including: B-cell lymphoma 2 (BCL2)/adenovirus E1B 19 kDa interacting protein 3 (BNIP3);[577] BCL2/adenovirus E1B 19 kDa interacting protein 3 like (NIX/BNIP3L);[578] and FUN14 domain-containing protein 1 (FUNDC1)[579] are able to induce direct recruitment of LC3-positive phagophores to the mitochondria via their LC3-interacting region (LIR) motifs.[580] In addition, the lipid, cardiolipin can also directly bind LC3 and induce mitophagy, via its stress-induced translocation to the OMM.[581] Intriguingly, parkin is not the only E3 involved in promoting mitophagy. Two other E3s, ariadne-1 homolog 1 (ARIH1)[582] and mitochondrial ubiquitin ligase activator of NF-kB1 (MUL1),[583] were found to induce mitophagy in PINK1- dependent and independent pathways, respectively.

Despite ongoing debate over the role of parkin in mitophagy, there is ample evidence indicating that parkin plays a role in promoting mitochondrial health, including: i) maintaining appropriate mitochondrial function, ii) protecting from mitochondria-specific stressors, and iii) modulating mitochondrial trafficking and dynamics. As mentioned, PD patients demonstrate mitochondrial dysfunction,[345] which is partially recapitulated in *pkrn* KO mice.[435,437] Two independent proteomic studies of *pkrn* KO mice, containing exon 3 deletions, discovered that the absence of parkin caused

structural changes in a large number of mitochondria-associated proteins, which also correlated with reduced OXPHOS capacity (**Appendix Table A2**).[435,437,584-639] It is also well documented, in both animal and cellular models, that parkin protects DA-neurons from damage caused by the mitochondria-specific PD toxins MPTP, rotenone, paraquat and 6-OHDA,[443,640-644] and was also shown to regulate mitochondrial trafficking by binding and ubiquinating important cytoskeleton-associating proteins (**Appendix Table A1**), such as α/β tubulin,[509] Lim kinase 1[518] and mitochondrial Rho GTPase (Miro).[530] The latter being a mitochondria-associated protein that mediates mitochondrial motility, which is removed from damaged mitochondria via parkin-E3-dependent proteasomal degradation. Interestingly, induction of the PINK1/parkin mitophagy pathway was also shown to cause Miro phosphorylation, which causes mitochondrial quarantining prior to mitophagy induction.[530,645] Other putative parkin E3 substrates associated with mitochondrial function are the fusion- and fission- inducing proteins mitofusins (MFNs) 1/2[526] and dynamin-related protein 1 (Drp1),[529] respectively. As shown in **Fig. 1.9**,[353] degradation of MFNs 1/2 leads to reduced fusion, which was observed as fragmented mitochondria in parkin-deficient *Drosophila*.[646] Proteasome-dependent degradation of Drp1, on the other hand, leads to loss of fission, which is required to remove damaged mitochondrial fragments. Similarly, it was reported that PINK1 and parkin promote the budding off of cargo-selective vesicles from the mitochondria (or mitochondrial derived vesicles, MDVs) in a process that is independent of Drp1-mediated fission and mitophagy. Formation of these MDVs, which also co-localize with parkin staining, is initiated by increasing ROS levels and is believed crucial for selectively removing damaged mitochondrial components and transporting them to lysosomes in an effort to preserve mitochondrial integrity, i.e. prevent mitophagy induction.[647,648]

1.5.4 Role of parkin in cancer and immunity

Other intriguing cellular roles for parkin include: promoting neuronal cell survival, acting as tumour suppressor, and regulating both innate immune and inflammatory responses.[649-651] Among its putative E3 targets (see **Appendix Table A1**) include: i) proteins involved in regulating the NF-κB pro-survival pathway (IκκγTRAF2 and 6,[534] FAF1[538], NF-κB essential molecule (NEMO),[537] and RIPK1[557]); and ii) degrading proteins involved in apoptotic processes (PDCD2-1,[522] Fbw7β,[535] Plk1,[545] Sept4_i2,[532] RTP801/REDD1,[299] IPAS,[543] and cyclophilin-D[560]). These pathways appear activated specifically within neuronal cells. In contrast, parkin also functions as a tumour suppressor and induces apoptosis in cancer cells.[650] For instance, there is an intriguingly high risk of melanoma in carriers of *PRKN* gene copy variants or loss of heterozygosity (60% and 74% of primary melanomas, respectively) and its expression gradually diminishes as melanocytes undergo oncogenic transformation.[652] Parkin expression is also shown to suppress other human cancers as it is found mutated in ~1% of breast cancers, 2–5% of colorectal cancers, ~ 5% of lung squamous cell carcinoma, and ~ 5% of gastric cancers; [553,650,651,653-657] with its absence increasing tumourigenesis susceptibility in mice.[658] The proposed mechanism of parkin-mediated tumour suppression is linked to its influence on cell cycle regulation, hypoxia resistance and metabolic reprogramming.[650] Parkin E3 targets known to promote cell cycle progression or mitosis include: cyclin E/D,[510] PDCD2-1,[522] Plk1[545] and p21,[554] and parkin interacts with anaphase-promoting complex/cyclosome (APC/C) co-activators Cdc20 and Cdh1, which help to degrade several key mitotic regulators, including cyclin B1 and Aurora A/B.[659] In contrast to promoting neuronal survival, parkin-mediated degradation of mitochondrial anti-apoptosis proteins Bcl-2[524] and BAX/BAK[531,550,558] appears to promote apoptosis in cancer cells.[660] Its interaction with microtubules[661] and down-regulation of follistatin[662] explains, in part, how parkin increases tumour sensitivity to chemotherapeutic agents such as paclitaxel, cisplatin, doxorubicin and etoposide.[651,663] Furthermore, parkin was shown to play a role in

preventing metastasis in clear-cell renal cell carcinoma,[664] pancreatic cancer, and nasopharyngeal carcinoma,[665,666] by E3-mediated degradation of HIF-1α.[553,667] Finally, loss of parkin promotes the Warburg effect,[668,669] characterized as a metabolic change in cancers that enhances the use of glycolysis over OXPHOS for energy production.[670] Zhang et al. demonstrated that the *PRKN* gene is transcriptionally activated by the tumour suppressor p53 (a well-known suppressor of glycolysis).[669] In opposition, parkin protein was also shown to repress p53 expression in an E3-independent fashion via its function as DNA-binding transcription factor.[668,671,672] These observations suggest that an important feedback loop exists between these two proteins and supports a role for parkin in regulating cellular metabolism as observed in pancreatic,[673] adipose[674] and muscle cells.[675]

The association of parkin with the innate immune response was first observed in 2004, by the Schurr group, which found that polymorphisms in the regulatory region of *PRKN* was associated with increased susceptibility to the intracellular pathogen *Mycobacterium leprae* in Vietnamese subjects. [676] Subsequently, in 2006, another group found that *PRKN* polymorphisms in humans was also associated with susceptibility to *Salmonella typhi and S. paratyphi A*,[677] and Manzanillo et al later demonstrated using *in vivo* and *in vitro* paradigms that parkin expression mediates resistance to *Mycobacterium tuberculosis*, and other similar, intracellular pathogens. They found that parkin induced lysosomal-autophagic encapsulation and degradation of *M. tuberculosis* via K63 polyubiquitination.[649] Parkin is known to enhance NEMO activation via linear ubiquitination to promote neuronal cell survival.[537]. NEMO is, however, also a key transcription regulator of the immune system and ectodermal development, with genetic mutations found to cause X-linked ectodermal dysplasia and immunodeficiency.[678] A more recent study has linked the formation of MDVs to immune activation with the discovery of mitochondrial antigen presentation (MitAP).[679] This process is believed essential for developing immune tolerance and promoting immune responses against infectious disease and cancer.

Its mechanism requires the formation of MDVs that contain organelle-specific antigens, which are presented to major histocompatibility complex class I molecules in both macrophages and dendritic cells to modulate self-identification. As mentioned, the formation of MDVs occurs via PINK1 and parkin-dependent expression in HeLa, U2OS and COS7 cell-lines. Surprisingly, however, *in vivo* and *in vitro* evidence indicated that MitAP was actively inhibited by PINK1 and parkin expression in immune cells. Similarly, recent studies have linked parkin deficiency with enhanced inflammation activation via nod-like receptor family pyrin domain containing 3 (NLRP3) inflammasomes[680,681] and stimulator of interferon genes (STING).[682] The former is part of an immune complex that is stimulated via caspase-1-dependent release of interleukins (ILs) (IL-1beta and IL-18) [683,684], and linked to a lack of induction of A20 (a negative regulator of NF-κB) in blood-derived macrophages from parkin-deficient mice and humans.[680] Intriguingly, Li et al also found that loss of parkin increased NLRP3 inflammasomes following viral infection and that this process was mediated by enhanced mitochondrial-derived ROS production.[681,685] These results indicate an interesting link between parkin-loss and elevated ROS in immune cells. As mentioned, loss of parkin activates STING, a protein residing in the endoplasmic reticulum, which induces an immune response by activating NF-κB and interferon (IFN) regulatory factor 3, causing downstream expression of IFN1 (alpha and beta).[686] Initiation of STING occurs via cyclic GMP-AMP synthase activation by the presence of cytosolic DNA.[687] This pathway was found to mediate IFN1 signaling in parkin-deficient mice subject to acute (excessive exercise) and/or chronic (Mutator mice that accumulate mtDNA mutations over time) mitochondrial stress. The authors reasoned that parkin expression inhibited STING activation because mtDNA was removed via parkin-mediated mitophagy, *i.e.* lowering the level of cytosolic DNA.[682]

With so many diverse and even opposing (depending on cell type) functions proposed for parkin, and limited demonstrations of their validity in mammalian tissues, it is difficult to determine a unifying

mechanism by which parkin is able to execute all these functions. In addition, it is unclear how these lead to PD pathogenesis, notably the highly specific loss of catecholaminergic neurons in the *S. nigra* and *L. coeruleus* seen in parkin-associated EOPD. This dissertation presents a collection of findings related to the proposed unifying role of cell redox-state regulation as a mechanism by which parkin executes its diverse roles and introduces catecholamine sequestration as a cell-specific explanation for how expression of human parkin protein prevents PD.

1.5.5 Current limitations in parkin research

Parkin research is currently limited by the lack of a unifying mechanism of action that is able to explain its diverse cellular roles and tissue-specificity in parkin-associated EOPD, as well as, by the lack of human brain parkin- specific tools amenable to various experimental applications. As discussed in detail above, the large number of E3 ligase substrates and diverse biological roles discovered for parkin are not consistent with the specificity of *S. nigra* and *L. coeruleus* cell loss observed in parkin-associated PD. The fact that certain PD-associated mutations retain E3 ligase activity obscures its role in PD-pathogenesis and its precise role in mitophagy is unclear. Although signs of aberrant mitochondrial form and function occur in the absence of parkin, high concentrations of uncoupling molecules are required to induce PINK1/parkin-dependent mitophagy and while neuronal cells exhibit high basal mitophagy, it appears to occur in a PINK1/parkin-independent fashion. While parkin is recognized as an OS-sensitive protein, its potential as a redox molecule and non-enzymatic antioxidant, akin to DJ-1 and glutathione, has not been previously considered. Nor has the majority of parkin-related research, with the exception of the effect of oxidative PTMs on E3 activity, analyzed their results in the context of parkin redox-biology. Finally, there is a lack of appropriate PD- and parkin-specific tools, as animal parkin models generally do not recapitulate loss of DA-neurons and commonly used commercially available antibodies

do not detect parkin *in situ* using immunohistochemistry (IHC). The former is possibly linked to the uniqueness of DA-processing and NM production in the human brain, while the latter is possibly linked to the fact that these antibodies were generated prior to the knowledge of parkin protein structure. There are very few reports describing *in situ* staining of parkin in human brain, however most (polyclonal) antibodies with positive staining were not made commercially available due to their limited supply.

Initial parkin antibody generation by Shimura et al in 1999, using a parkin fragment containing aa 293-306, found that parkin strongly labeled NM containing cells in the *S.* nigra.[431] Shortly thereafter, in 2001, another group, using a similar protein fragment as antigen (aa 295-311) again observed strong parkin staining in *S. nigra* neuron perikarya and processes, with lesser staining observed in non-striatal neurons, glial cells and blood vessels.[688] An additional study by Schlossmacher et al in 2002 found that an antibody generated against an N-terminal fragment (aa 84-98) showed similar staining as the previous two studies, however, found that an antibody generated from a more C-terminal fragment (342-353) also detected synuclein-containing LB inclusions throughout the midbrain.[689] Unfortunately, these studies were not expanded (e.g. larger sample sizes or epitope mapping) and the antibodies they generated, with the exception of the one generated using aa 295-311, were never made commercially available.

In 2003, Pawlyk et al developed the most widely used monoclonal antibody (Prk8) to parkin using WT recombinant parkin and found no inclusion-like co-labeling but rather diffuse pan-cytosolic staining in mammalian cell lines overexpressing parkin; no specific staining by IHC could be elicited in sections of human brain.[690] Intriguingly, the epitope of this antibody resides in the E3 catalytic domain (RING2), which according to structural studies is now known to be strongly hindered by RING0 via hydrophobic interactions.[192,193,450-453,457,458] Given the differences observed in staining profiles of the above antibodies, it is possible that Prk8, which detects the RING2 domain of the protein, is selective for a

particular cytosolic form of activated or unfolded parkin that non-denaturing conditions or protein cross-linking in IHC are not able to reveal.

1.6 Cellular redox state regulation

The oxidation-reduction (or redox) reaction is defined as the transfer of electrons between two molecules, specifically from an electron-rich reducing agent (or nucleophile) to an electron-poor oxidant (or electrophile). Together, the reducing agent and oxidant form a redox pair.[691] Nature has generated a variety of redox pairs, which function as essential electron carriers involved in various cellular pathways, such as energy production, biomolecule synthesis, antioxidant defenses, and metabolite/xenobiotic detoxification. Such redox pairs include: nicotinamide adenine dinucleotide and its phosphorylated form (redox pairs NAD+/NADH and $NADP^+$/NADPH), glutathione/glutathione disulfide (GSH/GSSG), coenzyme Q (ubiquinone/ubiquinol), and the prosthetic groups flavin mononucleotide or flavin adenine dinucleotide ($FMN/FMNH_2$ or $FAD^+/FADH_2$). These redox pairs rely on the presence of redox-active components, such as metal ions (iron and copper), oxygen or nitrogen atoms and sulfur-containing thiol groups.[691-693] In addition, redox reactions of cysteine residues within general proteins can also occur via their nucleophilic thiol residues (RSHs) and help contribute to redox homeostasis, *i.e.* a balance between intracellular oxidative and reductive agents.[694,695] As oxygen is the most ubiquitous oxidizing agent it contributes to the formation of ROS and RNS, with the most abundant form being O_2^- , which quickly converts to membrane permeable H_2O_2; and NO.[692] These molecules can combine with oxygen again to produce more reactive oxidants, like hydroxyl radical ($^{\bullet}OH$) or peroxynitrite ($ONOO^-$), or cause oxidation of various intracellular molecules, like DNA, proteins and lipids.

The major cellular sources of ROS and RNS include: i) mitochondrial transport chain ROS leakage; ii) iron and copper generation of hydroxyl radicals (via Fenton reaction); iii) lysosomal myeloperoxidase activity within phagocytes; iv) oxidases and flavoproteins within peroxisomes, v) unfolded protein response (UPR) within the endoplasmic reticulum; vi) ROS and RNS synthesis in the cytosol by xanthine oxidase or NADH oxidases; and vii) lipoxygenase and prostaglandin synthesis in the plasma membrane. It is important to note that, at controlled levels, ROS and RNS are typically used as important signaling molecules and cellular pathway effectors, often leading to transient activation or inactivation of select targets via reversible cysteine oxidation.[692,693,696-699] Such processes include: i) UPS-mediated protein turnover;[700,701] ii) autophagy;[274-276,647,648,702-706] iii) mitochondrial function;[692,707] iv) OS regulation via nuclear factor erythroid-derived 2-related factor 2 (Nrf2) and Kelch-like ECH-associated protein 1 (Keap1) activation;[708-715] v) metabolic state regulation via Nrf2 and p53 activation; [716,717] vi) cancer cell antioxidant defenses,[717,718] and vii) NF-ϰB or activator protein 1 (AP1) driven activation of phagocytic ROS/RNS- mediated degradation of pathogens in the innate immune system.[719-724] Intriguingly, these pathways are also regulated by parkin expression.

In addition to ROS and RNS, reactive electrophilic species (RES), which are electrophilic metabolites that accumulate during detoxification processes, also contribute to OS.[725] Examples of RES include xenobiotics (e.g. exogenous chemicals[725{Mitchell, 1973 #3303], including mitochondrial complex 1 uncouplers[726]), by-products of oxidative stress (e.g. lipid peroxidation-derived 4-hydroxynonenal[727]) or endogenous metabolites (e.g. methylglyoxal, prostaglandins and 8-nitroguanosine 3',5'-cyclic monophosphate)[725,728], and of special interest in PD, oxidation by-products of catecholamine synthesis and degradation (e.g. DA-quinones and aminochrome)[360,729]. RES can greatly alter redox balance by irreversibly modifying thiol-containing antioxidants (e.g. GSH, thioredoxins), or other protein-cysteines, thus depleting antioxidant reserve.[373,725] The most abundant, and versatile, antioxidant in the cell is

glutathione (mM range[730]), for which many pathways in the cell, including recycling enzymes (glutathione reductase, GR) and *de novo* synthesis (glutamate cysteine ligase, GCL), are utilized in order to keep the [GSH]: [GSSG] ratio constant. In fact, glutathione can alter protein function by forming reversible disulfide bonds (S-glutathionylation) between itself and target proteins; many of these proteins are involved in cellular pathways regulated by parkin.[373,730]

It is well established that decreased glutathione concentrations leads to OS, and is associated with aging and age-related diseases, including: cancer, ischemic brain disease, cardiovascular disease, cataract genesis, diabetes mellitus, cancer and PD.[693,696] More precisely, both a depletion of total glutathione (GSH + 2GSSG) and a decrease in the [GSH]:[GSSG] ratio are indicators of OS. Thankfully mammals have developed multiple highly complex antioxidant systems, which include both enzymatic and non-enzymatic antioxidants that work synergistically to reduce OS (**Fig. 1.16**).[692] The enzymatic antioxidants include: glutathione peroxidase (GPx)[731], catalase[732] and superoxide dismutase (SOD),[733] while non-enzymatic antioxidants include both thiol-containing glutathione and thioredoxin.[734] and non-thiol containing antioxidants such as vitamins E[735] and C.[736] Catalase and GPx function to remove H_2O_2 from peroxisomes and mitochondria, respectively.[731,732] SOD, on the other hand exists in both a cytosolic form (bound to copper or zinc, CuSOD or ZnSOD, respectively) and a mitochondrial form (bound to manganese, MnSOD), with the important role of scavenging O_2^{-}.[733,737] Besides glutathione, thioredoxin is the most recognized protein-based antioxidant that also functions as a transcription factor regulator of NF-κB and AP1 activation.[723,724] Vitamins E (α-tocopherol) and C (ascorbic acid) are known to work in concert to prevent lipid peroxidation, with ascorbic acid helping to regenerate α-tocopherol radicals in membranes and lipoproteins,[735,736] and as shown in **Fig. 1.16**,[692] glutathione is also used to reduce oxidized forms of vitamin E and C.[738]

Given that cellular pathways affected by parkin expression are also regulated by redox state alterations, it is therefore plausible that parkin has an effect on regulating OS either directly by thiol-redox chemistry or indirectly by E3-mediated degradation of key regulators of cellular redox state.

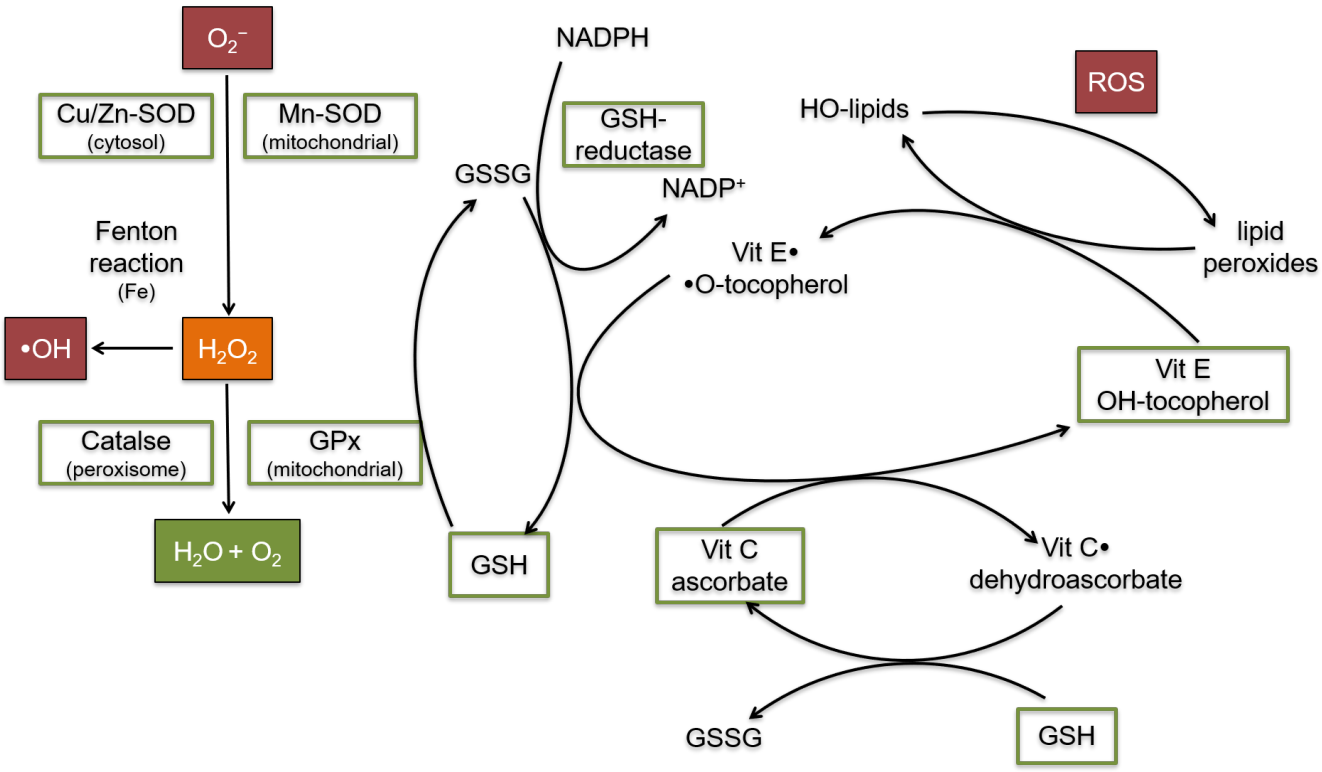

Figure 1.16. Enzymatic and non-enzymatic antioxidant pathways of the cell
·OH, hydroxyl radical; O_2^-, superoxide; H_2O_2, hydrogen peroxide; GSH, reduced glutathione; GSSG, disulfide glutathione; GPx, glutathione peroxidase; GSH-reductase, glutathione reductase; NADP+/ NADPH, nitotinamide adenine dinucleotide phosphate redox pair, Vit E, vitamin E; Vit C, vitamine C; ROS, reactive oxygen species. Modified from Kurutas 2016.[692]

1.7 Evidence supporting parkin as a redox sensitive and OS-regulating protein

The first indication that parkin has a role in OS mitigation and/or redox state regulation is found within its structure. Parkin has high cysteine content compared to most other E3 ligase enzymes and PD-related proteins. (**Table 1.2**) In fact, cysteines comprise 7% of its primary sequence, a value much higher than the redox-sensitive and PD-associated protein DJ-1; and the estimated average cysteine content of 2% found in other general proteins.[373] The only protein listed in **Table 1.2** that has higher cysteine content is the sensitive to apoptosis gene (SAG). This small ~13 kDa protein intriguingly functions both as a RING/-Ubox-type E3 and as non-enzymatic antioxidant. The single RING domain in its structure coordinates 50% of its total cysteine residues (6/12) and facilitates ubiquitination of proteins involved in tumourigenesis, such as apoptosis, DNA repair, embryogenesis and vasculogenesis. It was also found to form oxidation-induced oligomers and protect cells from OS in a thiol-mediated manner.[739] Surprisingly, despite having structural similarities to SAG, parkin is not considered an antioxidant molecule as it is generally presumed that oxidative PTMs lead to loss of its function, either via reduced structural stability or loss of catalytic E3 activity. Although the majority of cysteines in human parkin are zinc-coordinated within RING domains, there are still six unbound cysteines, like the SAG protein, for which no precise role has been identified to date.

	Protein Name	Gene Name	Number of Amino acids	Number of Cysteines	Percent of Cysteines
E3 ligases	E6-AP	*UBE3A*	852	16	1.9
	Chip	*STUB1*	303	8	2.6
	c-Cbl	*Cbl*	472	13	2.8
	Dorfin	*RNF19A*	838	35	4.2
	HHARI	*ARIH1*	557	32	5.7
	HOIL1 (HOIP)	*RBCK1*	510	32	6.3
	RNF43	*RNF43*	783	26	3.3
	SAG	*RNF7*	113	12	10.6
Familial PD genes	α-synuclein	*SNCA/PARK1,4*	140	0	0.0
	Parkin	*PARK2*	465	35	7.5
	Pink1	*PINK1/ PARK6*	581	16	2.8
	DJ-1	*PARK7*	189	3	1.6
	LRRK2	*PARK8*	2527	64	2.5

Table 1.2. Cysteine content of select E3 ligase and Parkinson disease-associated proteins

There are various observations indicating that parkin is influencing cellular redox state. As shown in **Appendix Table A1**, of the many E3 substrates discovered, the majority (86%, 51/59) are found to be either directly susceptible to oxidative modifications, or their activity is altered under OS conditions.[528,555,621,704,740-792] Furthermore, signs of increased OS within the *S. nigra* and mitochondrial dysfunction are found with loss of parkin in both humans and animals (**Table 1.3**).[432-439] These included: altered levels of [GSH]:[GSSG], increased levels of OS markers such as lipid peroxidation and nitrosylation, as well as, reduced metabolic capacity.[116,432,435,793,794] As mentioned earlier, unbiased proteomic screens conducted by two independent groups also found that the majority of proteins altered in *prkn* KO mice involve metabolism and OS regulation (**Appendix Table A2**),[435,437,584-639] and as discussed above, the cellular processes that are regulated by parkin are themselves tightly linked to cellular redox state modulation. Together, these findings suggest that parkin is involved in mitigating OS. However, whether parkin is able to achieve this directly, as a non-enzymatic antioxidant such as the SAG protein, or indirectly, via promoting the regulation of OS mitigation pathways remains to be determined. Most intriguingly, Pawlyk et al. in 2003[690] made the observation, using then two novel antibodies (e.g. Prk8 and Prk109), that parkin natively becomes insoluble with age and does so specifically in humans compared to mice. Using six human frontal cortex control samples (three aged 14-23 and three aged 60-74) and a sequential extraction protocol with gradually increasing detergent strength, they found that parkin specifically and completely transitioned from the saline soluble or cytosolic extract into the SDS- (sodium dodecyl sulfate) soluble or protein-aggregate extract in the older-aged brains (**Fig. 1.17a**). Unfortunately, their antibodies they are not amenable to IHC and thus cannot locate parkin *in situ*. From their observations, and the fact that PD is an age-related disease, they concluded that loss of parkin solubility correlated with inactive protein, however, they did not provide an explanation or mechanism for how this occurs.

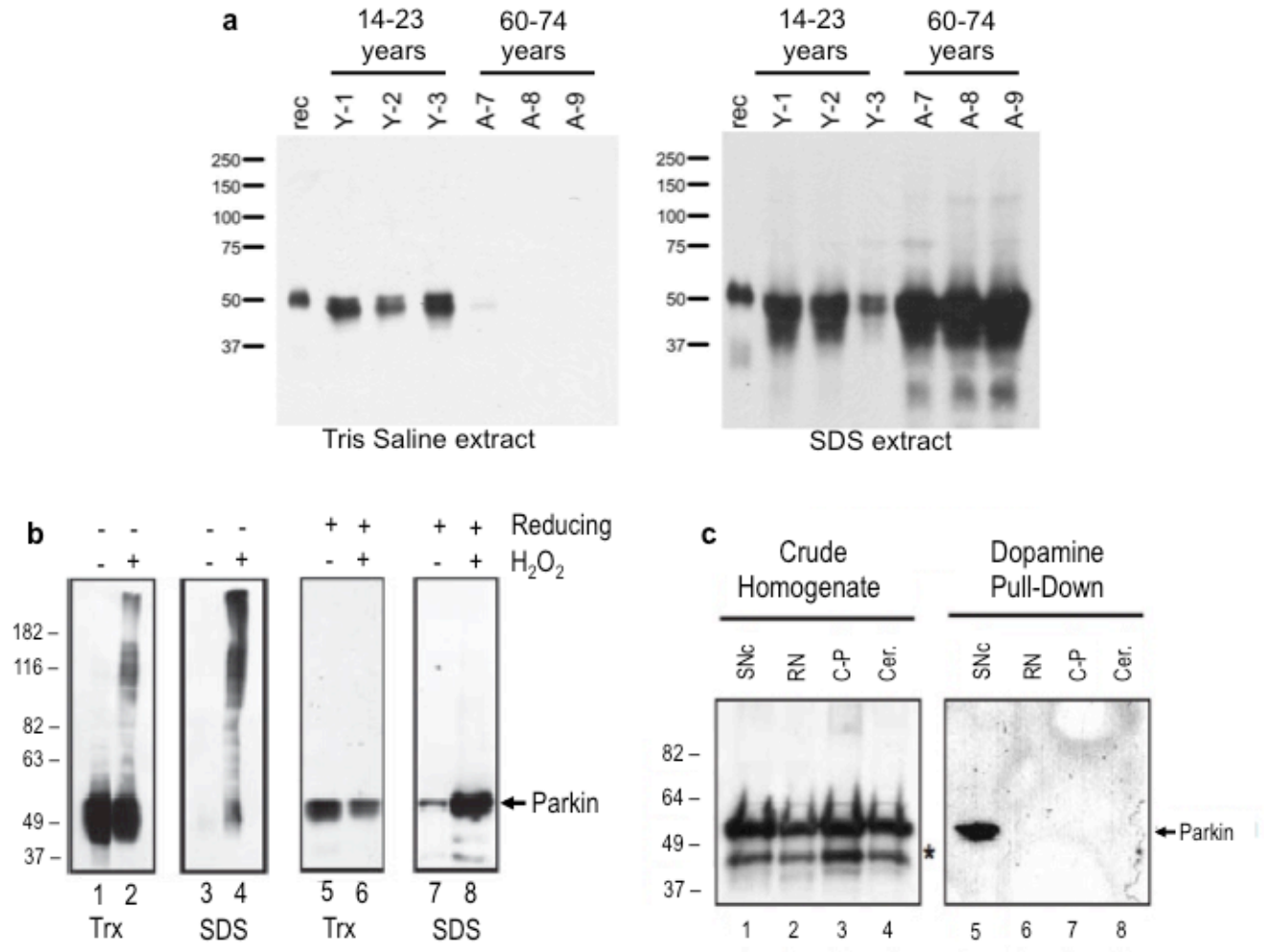

Figure 1.17. Biochemical changes of parkin observed in human tissue

(**a**) Age-dependent loss in parkin solubility in human frontal cortex. Three samples each from young (Y) and aged (A) human brain Tris saline extracts (left panel) and SDS extracts (right panel) run on SDS/PAGE and blotted for parkin using Prk8 antibody. (**b**) Parkin solubility is oxidation-sensitive. Rodent mesencephalic stem cells stably expressing human myc-tagged parkin were treated with either PBS (control) or 10 mM H_2O_2 for 30 min. Cells were extracted using solution containing 0.1% Triton-X-100. Extract and pellet were separated via SDS/PAGE in the presence or absence of reducing agent and blotted for parkin. (**c**) Biochemical isolation of catechol-modified proteins from human brain. Human brain extracts were incubated with an amino-phenyl boronate agarose (PBA), which undergoes selective covalent attachment to catechol *cis*-diols under basic conditions. Following several washes, proteins were eluted under acidic conditions, separated using SDS/PAGE and blotted for parkin. SNc, *substantia nigra*; RN, red nucleus; C-P, caudate putamen; Cer, cerebellum. Taken from Pawlyk et al 2003, LaVoie et al 2005 and LaVoie et al 2007.[362,486,690]

There is evidence linking parkin solubility to its redox state. Lavoie and Schlossmacher were the first to demonstrate this link in 2007.[486] They found that overexpression of myc-tagged human parkin protein in WT mouse embryonic stem cell homogenates was predominantly recovered in the Tris-saline soluble extract, but could be partially partitioned into the SDS-soluble extract with oxidizing (H_2O_2) conditions. They also observed that OS generated high molecular weight (HMW) parkin, which were reversed when a reducing agent (dithiothreitol, DTT) was re-introduced, thus indicating that these HMW species form via intermolecular disulfide bridges (**Fig. 1.17b**). Later in 2011, Meng et. al. also found that parkin E3 activity could be activated with low levels of RNS, but further increasing RNS levels inhibited E3 activity. They concluded that S-nitrosylation was affecting the structural integrity of the protein, leading to loss of solubility and reduced ubiquitination activity.[487]

In humans and non-human primates, in addition to baseline metabolic ROS and RNS generation, catecholaminergic cells are subject to increased OS as a result of their bioenergetics and catecholamine-derived RES.[44]By-products of dopamine metabolism (e.g. DA-quinones) form irreversible adducts with various proteins, causing mitochondrial and autophagic dysfunction.[82,85,360] In melanin-producing cells within the skin L-dopa is used to produce OS-protective melanins in melanosomes by aide of glutathione and the enzyme tyrosinase.[79,82] Only humans and, to a lesser extent, certain non-human primate brains can produce NM via catecholamine oxidation.[43] Interestingly the regions that produce NM (*S. nigra* an *L. coeruleus*) are specifically lost in parkin-associated PD.[53,195-197,207] It was initially believed that NM was made only by catecholamine autoxidation because *S. nigra* and *L. coeruleus* cells lack melanosome-like organelles and tyrosinase. However, autoxidation of DA as the sole mechanism for NM production could not explain why NM is not restored in patients treated with L-dopa.

Further studies have discovered that NM: i) contains more thiols than peripheral melanin, ii) is de-pigmented under high OS, and iii) can act as a metal chelator; suggesting that NM could be acting similarly to peripheral melanins (i.e.. by protecting the cell from OS).[79] Also intriguing is the fact that *PRKN* variants and mutations are risk factors for melanoma, a cancer with aberrant production of melanin.[652] The first indications that parkin may be involved in DA metabolism came from initial work generated by Itier et al. in 2003 who demonstrated that loss of parkin in mice not only increased OS, but also altered catecholamine metabolism.[432] An alteration in DA processing was further confirmed by three other groups using other *prkn* exon deletion mouse models (see **Table 1.3**).[433,438,439]

Genetic Model	Results	Reference
Exon 3 deletion	Motor and cognitive deficits Inhibition of amphetamine-induced dopamine release Inhibition of glutamate neurotransmission Increased dopamine in limbic brain areas Increased dopamine metabolism by MAO No nigrostriatal dopamine neuron degeneration Decreased levels of dopamine transporter and increased levels of glutathione	Itier 2003
Exon 3 deletion	Normal brain morphology Increase in extracellular dopamine in the striatum Reduction in synaptic excitability No changes in the number of dopamine neurons No changes in the levls of CDCrel-1, synphilin-1 and α-synuclein	Goldberg 2003
Exon 3 deletion	Decreased abundance of proteins involved in mitochondrial function and oxidative stress Reduction in respiratory capacity in striatal mitochondria No gross abnormalities in striatal mitochondria Decreased levels of proteins involved in protection against OS	Palacino 2004
Exon 7 deletion	No impairment in the nigrostriatal dopaminergic system Loss of catecholaminergic neurons Reduction in the noradrenaline-dependent startle response	Von Coelln 2004
Exon 3 deletion	No changes in behavior No differences in catecholamine levels	Perez and Palmiter 2005
Exon 3 deletion	Absence of nigral degeneration Upregulation of a number of mitochondrial and other proteins that may be acting as compensatory	Periquet 2005
Exon 2 deletion	Decrease in endogenous dopamine release Upregulation of dopamine receptor binding in the striatum Increased dopamine levels in the midbrain	Sato 2006
Exon 3 deletion	Lower release and uptake od dopamine in young mice Enhanced dopamine overflow by repetitive stimulation in older mice Absence of nigral degeneration	Oyama 2010

Table 1.3. Motor phenotype and signs of oxidative stress observed in *pkrn*-knockout mice
Oxidative stress changes are highlighted in green and dopamine misprocessing highlighted in blue. MAO: monoamine oxidase; and ROS: reactive oxygen species.

LaVoie and Schlossmacher in 2005 also demonstrated that parkin isolated from human *S. nigra* specimens formed covalent adducts with DA-quinones and reduced parkin solubility (**Fig. 1.17c**).[362] Additionally, Wong et al. in 2007 also saw that parkin-DA quinone adduct formation caused loss of parkin solubility and E3 function, which occurred via a thiol-DA quinone conjugation. They found, using cysteine to alanine mutagenesis at residues C268 and C323, that parkin protein fragments overexpressed in dopaminergic cell cultures formed fewer parkin-DA quinone adducts, suggesting these were *bona fide in vitro* sites of DA quinone adduct formation.[493] The fact that these parkin-DA quinone adducts are preferentially formed in *S. nigra* suggests that parkin is a significant target of DA-misprocessing; more recent work by Jiang et al. in 2012 demonstrated that human iPSCs expressing PD-related parkin mutations have increased expression of DA-degrading enzyme MAO, as well as, increased release and reduced uptake of DA by DAT.[795]

In sum, the general conclusion made from previous parkin biochemistry experiments, is that ROS, RNS and RES exposure decreases human parkin solubility and causes E3 inactivation, with E3 loss considered the mechanism for parkin-associated PD pathogenesis. However, based on its structure and reaction with ROS/RNS/RES, parkin is likely a redox-sensitive molecule, which has the capacity to change the redox state of its environment in response to its own oxidation.

1.8 Hypothesis and Aims

Here a more unifying mechanism is proposed for parkin's function within eukaryotic cells, namely that of a redox-state regulating protein (**Fig. 1.18**). This would not only help explain its roles in mitochondrial health, cancer and immune function, but also provide a plausible reason for the selective catecholaminergic cell loss observed in *PRKN*-associated PD. Being a highly thiolated protein, parkin is proposed to function as a redox-state regulator by reacting directly with cysteine-modifying biomolecules, such as ROS, RNS, RES (e.g. DA) and GSSG, and, furthermore, that the absence of these complementary redox activities by parkin in, long-lived, catecholaminergic human neurons leads to EOPD. To investigate this hypothesis, the following aims were developed:

AIM 1- Further characterize how oxidation promotes insolubility of parkin within human brain (Chapter 2). Initial studies were directed towards determining: i) the uniqueness of human brain-derived parkin insolubility compared to other redox-sensitive and PD-associated proteins, ii) whether parkin insolubility is mediated predominantly via cysteine-oxidation, and iii) if these redox-modifications within parkin are natively observed in human brain using mass spectrometry.

AIM-2- Determine the antioxidant potential of parkin and its effect on melanin production (Chapter 2). Biochemical analyses included determining: i) whether parkin is an antioxidant and whether PD-related mutations alter this capacity, ii) which cysteine residues on parkin are most reactive with ROS and RES like DA-quinones, and ii) whether parkin directly alters melanin produced by DA polymerization.

AIM 3- Determine whether parkin alters cellular redox state (Chapter 2 and 3).

The antioxidant ability of parkin was tested at the cellular level using two different readouts: i) intracellular and tissue ROS levels, and ii) the corresponding thiol redox equilibrium (i.e. the oxidation status of glutathione in cells and in tissues).

AIM 4- Generate novel antibodies that detect parkin *in situ* (Chapter 2 and 4).

Parkin isolated from the brain of older human subjects is found in an SDS-soluble extract, yet parkin is predominantly cytosolic in human-derived neuronal cell lines and rodent brain. To further explore this observation, novel antibodies were generated against full-length, untagged, WT recombinant parkin and tested for their ability to detect soluble and aggregated parkin using various experimental applications.

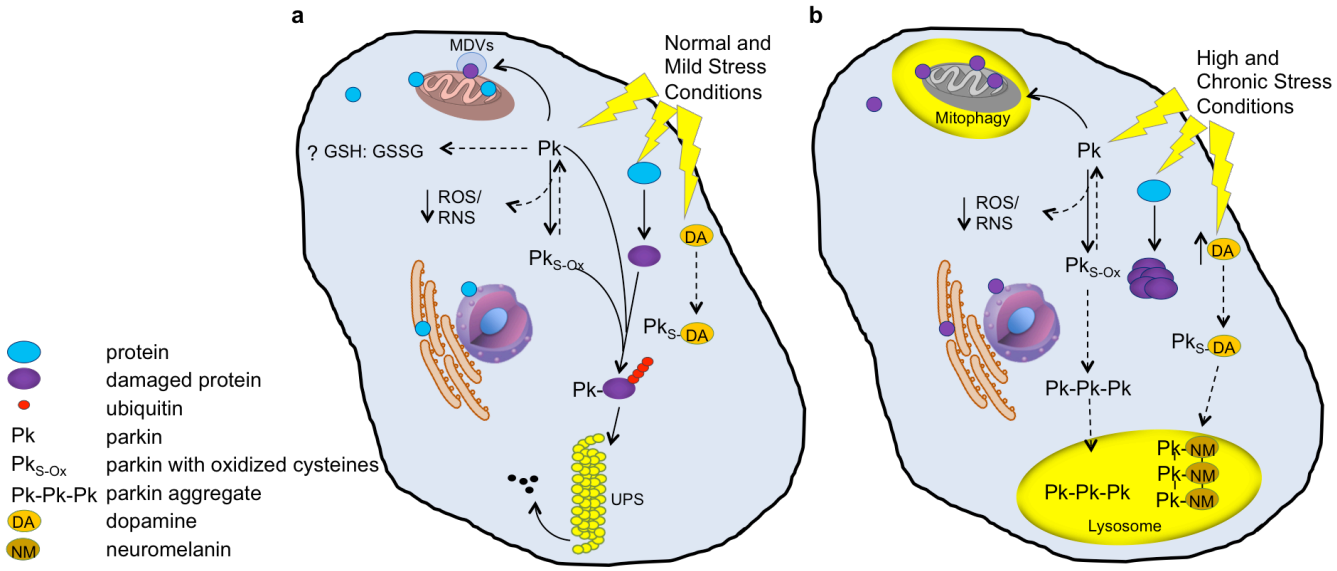

Figure 1.18. Hypothetical working model of parkin function with study aims
Current understanding of parkin function in normal and mild stress conditions, shown as solid arrows in (**a**) vs. high and chronic stress conditions, shown as solid arrows in (**b**). Both native (Pk) and mildly oxidized parkin (PkS-Ox) target damaged proteins for degradation via the ubiquitin proteasome system (UPS). Parkin also mediates the formation of mitochondria-derived vesicles (MDVs) under mild oxidative conditions. High oxidative stress leads to protein aggregation, parkin oxidation, and parkin-mediated mitophagy induction. The current aims of this study focus on the following areas which are depicted above by dashed arrows: Aim 1) further characterizing parkin cysteine oxidative modifications and linking them to the formation of parkin aggregates (Pk-Pk-Pk); Aim 2) determining if parkin functions as a cysteine-dependent antioxidant capable of lowering intracellular reactive oxygen/nitrogen species (ROS/RNS) and promoting melanin formation; Aim 3) determine if and how parkin alters cellular glutathione redox state; and Aim 4) develop novel anti-parkin monoclonal antibodies capable of detecting parkin and parkin aggregates in human tissue.

Chapter 2: Manuscript 1 - Age-Associated Insolubility of Parkin in Human Midbrain is Linked to Redox Balance and Sequestration of Reactive Dopamine Metabolites

Author List:
Jacqueline M. Tokarew*, Daniel N. El-Kodsi*, Nathalie A. Lengacher, Travis K. Fehr, Angela P. Nguyen, Bojan Shutinoski, Brian O'Nuallain, Ming Jin, Jasmine M. Khan, Andy C. H. Ng, Juan Li, Qiubo Jiang, Mei Zhang, Liqun Wang, Rajib Sengupta, Kathryn R. Barber, An Tran, Doo Soon Im, Steve Callaghan, David S. Park, Stephanie Zandee, Xiajun Dong, Clemens R. Scherzer, Alexandre Prat, Eve C. Tsai, Masashi Takanashi, Nobutaka Hattori, Jennifer A. Chan, Luigi Zecca, Andrew B. West, Arne Holmgren, Lawrence Puente, Gary S. Shaw, Gergely Toth, John M. Woulfe, Peggy Taylor, Julianna J. Tomlinson and Michael G. Schlossmacher
*these authors contributed equally to this work

2.1 Preface

This manuscript provides the first evidence that parkin functions as a thiol-mediated anti-oxidant and redox-state regulator. Here, > 60 human brain, spinal cord and muscle specimens were used to validate the unique age-associated and oxidation-mediated aggregation of parkin. Novel findings included the determination that aggregation of parkin begins at 40 years of age and is directly proportional to the level of H_2O_2 measured in cells and tissues. Oxidation of parkin led to a select number of parkin-cysteines being reversibly and irreversibly oxidized, including the primate-specific Cys95. Cysteine-specific oxidation also led to a reciprocal lowering of H_2O_2 levels within its surrounding environment, i.e. shown either directly by anti-oxidant assays or in cells, meeting the criteria for a thiol-dependent anti-oxidant that functions similar to glutathione. In contrast, however, parkin-cysteines enhanced the formation of melanin via dopamine polymerization, in part, via direct dopamine-adduct conjugation to Cys95. This function correlated with staining obtained using novel, human-specific, monoclonal parkin antibodies (also see Chapter 4), which found parkin associated with neuromelanin and LAMP3-positive lysosomal storage vesicles in human *S. nigra*.

2.2 Statement of author contribution

As co-first-author I provided major contributions to: establishing experimental techniques and their optimization, the overall project direction and design, data analysis and interpretation, as well as, initial drafts and edits of the manuscript. Specific protocols I established included: i) recombinant protein production (**Fig. 2.1, 2.3, 2.5-2.7; Supplementary Fig. 2.1-2.5, and 2.7 and Supplementary Table 2.2**), ii) protein oxidation, dopamine-adduct conjugation and staining methods (**Fig. 2.3, 2.5, and 2.6, and Supplementary Fig. 2.3, 2.5 and 2.7),** iii) chemiluminescence anti-oxidant assay (**Fig. 2.5e and Supplementary Fig. 2.5f-m**), iv) thiol quantification assay (**Fig. 2.5f**), v) mass spectrometry sequential cysteine-labeling assay with guidance from L. Puente and completed by D. El-Kodsi, T. Fehr and A. Tran in the G. Shaw group (**Fig. 2.3, 2.4 and 2.6, and Supplementary Fig. 2.7 and Supplementary Table 2.2**), and vi) melanin polymerization assay (**Fig. 2.7**) continued by T. Fehr. I provided supervision of parkin extraction from human frontal cortex and human parkin immunoprecipitation (**Fig. 2.1, 2.3 and 2.4, Supplementary Fig. 2.1, 2.3 and 2.4a-b**) run by N. Lengacher, J. Khan and A. Ng, as well as, initial immunoblotting and immunohistochemistry trials of novel monoclonal parkin antibodies run by A. Nguyen (also while part of J. Chan group), N. Lengacher, Q. Jiang and J. Khan (**Fig. 2.8 and Supplementary Fig. 2.8 and 2.9**). Materials I provided include: i) recombinant parkin used as loading controls in immunoblots (**Fig. 2.1 and Supplementary Fig. 2.1-2.3**), ii) recombinant parkin proteins used for monoclonal antibody production (**Fig. 2.8 and Supplementary Fig. 2.8-2.9**), iii) recombinant parkin, DJ-1 and α-synuclein proteins used in assays (**Fig. 2.3d and 2.5a-c; Supplementary Fig. 2.3e and Supplementary Table 2.2**) and iv) expression vectors for parkin mutants (**Fig. 2.5j-k**). Experiments I independently run are included in **Fig. 2.3c, 2.5e-g and 2.7b; Supplementary Fig. 2.3a, 2.3d, 2.5f-n; Supplementary Table 2.2 and Appendix Figures C1-9, C12-15**. J. Li ran correlation statistics on parkin insolubility in human brain. B. Shutinoski provided help with mutant cloning. B.

O'Nuallain, M. Jin, L. Wang and P. Taylor at BioLegend were involved in antibody production. M. Zhang (J. Woulfe group) ran immunoflurescence-based co-labelling of parkin and LAMP-3 on human samples. G. Toth group ran circular dichroism and dynamic light scattering assays. K. Barber (G. Shaw group) provided wild- type and 321C recombinant parkin constructs and expression protocols. D. S. Im and S. Callaghan (D. Park group) assisted with mouse MPTP injections. S. Zandee (A. Prat group), X. Dong, C. Scherzer provided data for *PRKN* mRNA isolation and quantification. E. Tsai, M. Takanashi, N. Hattori, A. West and J. Woulfe provided fresh-frozen and paraffin-embedded human tissues. R. Sengupta, L. Zecca and A. Holmgren provided feedback.

2.3 Abstract

The mechanisms by which parkin protects the adult human brain from Parkinson disease remain incompletely understood. We hypothesized that parkin cysteines participate in redox reactions, and that these are reflected in its posttranslational modifications. We found that in *post mortem* human brain, including in the *S. nigra*, parkin is largely insoluble after age 40 years; this transition is linked to its oxidation, such as at residues Cys95 and Cys253. In mice, oxidative stress induces posttranslational modifications of parkin cysteines that lower its solubility *in vivo*. Similarly, oxidation of recombinant parkin by H_2O_2 promotes its insolubility and aggregate formation, and in exchange leads to the reduction of H_2O_2. This thiol-based redox activity is diminished by parkin point mutants, e.g., p.C431F and p.G328E. In *prkn*-null mice, H_2O_2 levels are increased under oxidative stress conditions, such as acutely by MPTP toxin exposure or chronically due to a second, genetic hit; H_2O_2 levels are also significantly increased in parkin-deficient human brain. In dopamine toxicity studies, wild-type parkin, but not disease-linked mutants, protects human dopaminergic cells, in part, through lowering H_2O_2. Parkin also neutralizes reactive, electrophilic dopamine metabolites via adduct formation, which occurs foremost at the primate-specific residue Cys95. Further, wild-type but not p.C95A-mutant parkin augments melanin

formation *in vitro*. By probing sections of adult, human midbrain from control individuals with epitope-mapped, monoclonal antibodies, we found specific and robust parkin reactivity that co-localizes with neuromelanin pigment, frequently within LAMP-3/CD63^{+} lysosomes. We conclude that oxidative modifications of parkin cysteines are associated with protective outcomes, which include the reduction of H_2O_2, conjugation of reactive dopamine metabolites, sequestration of radicals within insoluble aggregates, and increased melanin formation. The loss of these complementary redox effects may augment oxidative stress during ageing in dopamine-producing cells of mutant *PRKN* allele carriers, thereby enhancing the risk of Parkinson-linked neurodegeneration.

2.4 Introduction

Bi-allelic mutations in *PRKN*, which encodes parkin, lead to a young-onset, recessive form of Parkinson disease (PD).[184,796] Pathology studies of parkin-deficient brains have demonstrated that neuronal loss is largely restricted to the *S. nigra* and *L. coeruleus*, two brainstem nuclei that synthesize dopamine.(reviewed in Doherty *et al.* [53])

Parkin is a principally cytosolic protein. It has been associated with diverse cellular functions, foremost related to its ubiquitin ligase (E3) activity, the control of inflammation signalling, and maintenance of mitochondrial integrity, as mediated through participation in mitophagy and mitochondrial antigen presentation (MITAP) [350,537,647,679,680,682,797,798] (reviewed in Barodia *et al.* [799]). Although mitophagy has recently been shown to be co-regulated by parkin in the developing heart of mice,[800] the diverse roles ascribed to parkin function have not yet explained its selective neuroprotection. For example, vertebrate models of genomic *prkn* deletion do not reproduce dopamine cell loss; one exception is the parkin-deficient *Polg* mouse, where mitochondrial DNA mutagenic stress had been added as a second, genetic hit.[359] The general lack of dopamine cell loss in genomic parkin

deficiency-based models of vertebrates could be due to compensatory mechanisms,[528] a shorter life span of non-human mammals, and possibly, unique aspects of dopamine metabolism in humans. The latter is exemplified by the generation of cytoplasmic neuromelanin in dopamine synthesizing neurons beginning after childhood.[86] Nevertheless, genomic *prkn*-null models have revealed biochemical and structural changes in high energy-producing cells of flies and murine tissues,[799,801,802] which suggested the presence of elevated oxidative stress.[432,435,437] These observations pointed at a contribution of parkin to redox homeostasis *in vivo.*

Redox equilibrium invariably involves cysteine-based chemistry. There, thiols are subjected to oxidative modifications by reactive oxygen-, reactive nitrogen- and reactive electrophilic species (ROS, RNS, RES),[695,698] some of which are reversible. Proteins irreversibly conjugated by RES, including by electrophilic dopamine radicals, are either degraded or sequestered within inclusions. It is thought that the latter process occurs via lysosomal functions and underlies neuromelanin formation throughout adulthood.[360]

Human parkin contains 35 cysteines,[184] its murine homologue 34. Of these, 28 cysteines are involved in the chelation of eight zinc ions within four RING domains [455]. Although Cys431 has been identified as critical in catalyzing human parkin's E3 ligase activity, 6 other cysteines are structurally unaccounted for, including Cys95 located within parkin's 'linker' domain. Several reports have demonstrated unique sensitivity of parkin to ROS and RES in cells.[486-488] Further, RNS and sulfhydration can also modify its cysteines, and NO-/NO_2-modified parkin variants have been described in cells and brain tissue.[485,489-491,499] Oxidation of parkin has been linked to both activating ('gain-of-function') and detrimental ('loss-of-function') outcomes when tested in the context of parkin's E3 ligase activity *in vitro*.[362,487,489,490]

We found that wild-type parkin is highly oxidized and insoluble in adult human midbrain, leading us to explore non-E3 ligase-mediated, protective functions. Owing to its large number of cysteine-based thiols, we hypothesized: one, that parkin confers neuroprotection by acting as an anti-oxidant molecule *in vivo* and thereby contributes to redox balance; two, specifically, that parkin directly lowers ROS- as well as RNS-linked stressors and promotes the conjugation of dopamine radicals (RES); and three, we posited that selective neurodegeneration in *PRKN*-linked, autosomal-recessive PD (ARPD) could be partially explained by the absence of parkin-mediated sequestration of toxic metabolites during decades of human ageing.

2.5 Results

Parkin solubility declines in the ageing human brain including in the *Substantia nigra*

Parkin's biochemistry in the human brainstem *vs.* other regions of the neuroaxis has remained largely unexplored.[690] We serially fractionated 20 midbrain specimens (ages, 26-82 yrs) and >40 cortices (ages, 5-85 yrs) from human subjects, which had been collected *post mortem* (**Fig. 2.1**, **Supplementary Fig. 2.1**; **Supplementary Table 2.1**). In control brain, we found that before the age of 20 yrs, nearly 50% of cortical parkin was found in soluble fractions generated by salt [Tris-NaCl; TS]- and non-ionic detergent [Triton X-100; TX]-containing buffers (**Fig. 2.1a, b; Supplementary Fig. 2.1a**). In contrast, after age 50 yrs, parkin was predominantly (>90%) found in the 2% SDS-soluble (SDS) fraction and the 30% SDS extract of the final fractionation pellet (P). The same distribution was seen in adult midbrain (e.g., *S. nigra*; red nucleus), the pons (e.g., *L. coeruleus*), and the striatum (**Fig. 2.1a, b; Supplementary Fig. 2.1a-c**).

Intriguingly, in older individuals (ages, ≥50 yrs) approximately half of detectable parkin remained soluble in human spinal cord and skeletal muscle specimens, which had also been collected *post mortem*

(**Fig. 2.1c, d**). We used univariate linear regression analysis to explore a correlation between soluble parkin (of TS- and TX-fractions relative to the total signal for parkin, plotted as %) and age in human control cortices (**Fig. 2.1e**). The regression coefficient of age was -0.54 (at a 95% confidence interval (CI) of -0.79 to -0.29, $P=7.7e^{-05}$), where the multiple R-squared value was 0.302. When defining parkin solubility as a binary variable, *i.e.*, the presence or absence of soluble parkin in TS- and TX-fractions (absent defined as less than 2% of total signal), and using logistic regression analysis, we found that the transition to insoluble parkin occurred between the ages of 28 yrs (with low sensitivity but high specificity values) and 42 yrs (with high sensitivity and low specificity values).

This age-dependent partitioning of parkin was not seen for any other protein examined, including two other PD-linked proteins, i.e., DJ-1 and a-synuclein (**Fig. 2.1a, f**), or for organelle-associated markers, e.g., cytosolic glyoxalase-1, peroxiredoxin-1 and -3; and endoplasmic reticulum-associated calnexin. Notably, mitochondrial markers, e.g., voltage-dependent anion channel (VDAC) and Mn^{2+}-superoxide dismutase (MnSOD), also did not partition with parkin in an age-associated manner (**Fig. 2.1g; Supplementary Fig. 2.1b, c**). In contrast, parkin did co-distribute with LC3B, a marker of protein aggregation, foremost in brain specimens from older individuals (**Fig. 2.1a, h; Supplementary Fig. 2.1c**).

The age-associated loss in parkin solubility appeared unique to human brain in that it remained predominantly soluble in the adult nervous system of other species, e.g., mice and rats, as well as, cynomolgus monkey, which were processed in the same way (**Fig. 2.1i**). Specifically, in brain lysates of two different wild-type strains of mice (C57Bl/6J, and a mixed 129S//FVB/N//C57Bl/6J background) aged to 18 and 22 months respectively, parkin remained present in the soluble fraction throughout their lifespan (**Supplementary Fig. 2.1d**).

In soluble fractions from older humans, we did not detect any truncated species of parkin using several, specific antibodies. Despite the loss of parkin solubility with progression in age, *PRKN* mRNA was detectable in individual neurons isolated from the *S. nigra* and cortex throughout all age groups; there, transcript levels in neurons did not correlate with the subject's age (**Supplementary Fig. 2.1e,f**).

Our analysis comprised samples with *post mortem* intervals (PMI) that spanned from 2 to 74 hrs (**Supplementary Table 2.1**). Using univariate linear regression analysis, we detected no correlation between parkin solubility in human control cortices (n=41) and PMI length, where the regression coefficient for PMI measured -0.15 (95% CI: -0.76 to 0.46, P=0.62), and the multiple R-squared value was 0.0064 (**Fig. 2.1j**). As expected, PMI did not correlate with age of the diseased person (not shown). Likewise, wild-type parkin was found to be largely insoluble in striatal, midbrain and pontine samples isolated from aged subjects with PMIs as short as 2 to 6 hrs (**Fig. 2.1k; Supplementary Fig. 2.2a,b**). We further explored a possible contribution of PMI to parkin solubility by mimicking conditions of some of the human autopsy cases, using adult mice. This included a PMI length of up to 40 hrs, where animals were kept at room temperature for the first 14 hrs, followed by storage over 26 hrs at 4°C before removal of their brain; in these cases, parkin remained in the soluble compartments (**Fig. 2.1l**). While we cannot exclude that PMI length could affect parkin's solubility in some cases, the age dependent loss of parkin solubility observed in human brain samples of our cohort was not due to the PMI.

Further, we determined that the decline in detectable parkin solubility in aged human brain did not differ based on the sex of the deceased person, such as when examined by univariate linear regression analysis or by multivariate analysis; it was also not caused by either tissue freezing prior to protein extraction or the pH value of the buffer (**Supplementary Fig. 2.2c-f**). Moreover, employing the commonly used 'RIPA buffer' instead of our serial extraction buffers resulted in the release of parkin into the supernatant with some reactivity left in the pellet, as expected (**Supplementary Fig. 2.2g**).

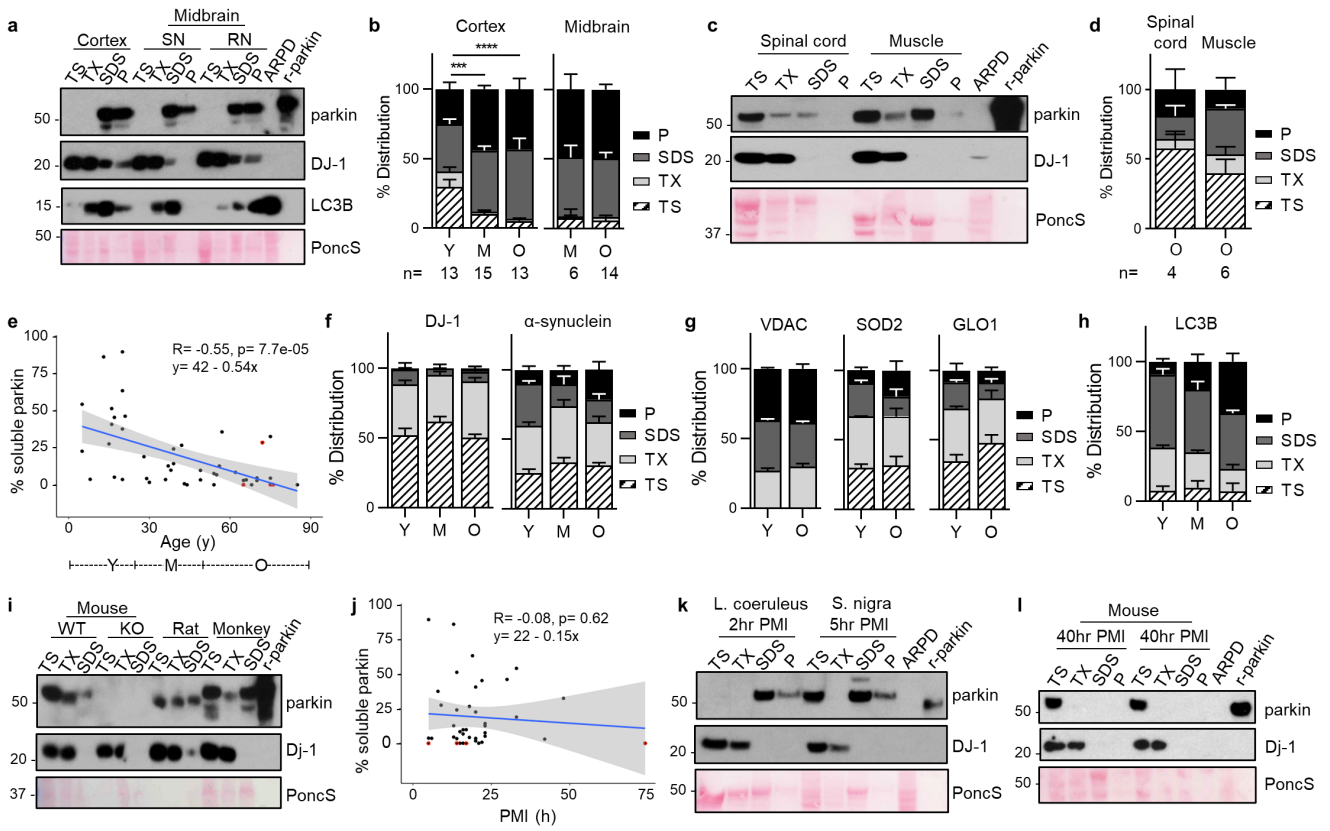

Figure 2.1. Parkin's decline in solubility is specific to adult human brain and correlates with age

(a) Representative Western blots of parkin, DJ-1, and LC3B distribution in human cortex, *S. nigra* (SN) and red nucleus (RN) serially fractionated into Tris-NaCl buffer-soluble (TS), Triton X-100-soluble (TX), 2% SDS-soluble (SDS) extracts and the pellet (P) lysed in 30% SDS-containing buffer. SDS extracts from *PRKN*-linked Parkinson disease (ARPD) brain and recombinant human parkin (r-parkin) are included. Ponceau S is shown as loading control.

(b) Relative distribution of parkin signal within each fraction for cortex and midbrain grouped by age ranges: young (Y, ≤20 yrs; n=13); mid (M, >20 yrs but <50 yrs; n=15 for cortex, and n=6 for midbrain); older (O, ≥50 yrs; n=13 for cortex and n=14 for midbrain). Data shown as mean ± SEM. The significance in protein distribution between soluble (TS+TX) and insoluble (SDS+pellet) fractions was determined using two-way ANOVA [$F(2, 76)=26.21$, $p<0.001$] with Tukey's post hoc test (***$p<0.001$; ****$p<0.0001$). Additional Western blots are shown in **Supplementary Fig. 2.1a-c**. Midbrains include both control and neurological disease cases, as listed in **Supplementary Table 2.1**. **(c)** Western blots of parkin and DJ-1 as well as Ponceau S staining of serial fractions from representative human spinal cord and skeletal muscle tissues from individuals ≥50 yrs. **(d)** Relative distribution of parkin as in (b) for human spinal cord (n=4) and skeletal muscle specimens (n=6) from donors aged 50-71 yrs. **(e)** Univariate linear regression analysis of parkin solubility in cortices as a function of age (n=46). Each brain is represented by an individual dot; red circles denote three cases of late-onset Parkinson disease not linked to *PRKN*; the linear regression line (in blue) and 95% confidence intervals (grey) are shown. Age ranges that correspond to Y-O-M in (b) are shown under the graph. Age coefficient was -0.54 (95% CI: -0.79 to -0.29, $P=7.7e^{-05}$). **(f-h)** Relative distribution of **(f)** DJ-1, α-synuclein and **(g)** VDAC, MnSOD, glyoxalase (GLO1) and **(h)** LC3B in human cortices (n=3-5 per age group), as described in (b). Representative Western blots are shown in **Supplementary Fig. 2.1b, c**.

(i) Western blots of parkin and Dj-1 and Ponceau S staining of serial fractions from whole brains of wild-type (WT; 8 mths of age) and *prkn* knock-out (KO) mice, WT rat (WT; 14 mths) and from frontal cortex of a cynomolgus monkey (60 mths).

(j) Univariate linear regression analysis of parkin solubility in human brain as a function of length for *post mortem* interval (PMI; in hrs); the linear regression line (in blue) and 95% confidence intervals (grey) are shown (n=41 cortices).

(k) Western blots of parkin and DJ-1 distribution in two human brainstem nuclei, *L. coeruleus* and *S. nigra*, which were collected within 2-5 hrs after death prior to freezing and processed as in (a, c). **(l)** Immunoblots for endogenous parkin and DJ-1 as well as Ponceau S staining from serially extracted WT mouse brains (n=3) dissected after a 40 hr *post mortem* interval at 4°C. Note, Western blots followed SDS/PAGE under reducing conditions.

Decline in parkin solubility correlates with rising hydrogen peroxide levels in mammalian brain

We next explored a possible association between parkin distribution, age and oxidative changes. Using sister aliquots from the brain specimens examined above, we found that hydrogen peroxide (H_2O_2) concentrations positively correlated with age (**Fig. 2.2a, b;** see also **Supplementary Table 2.1**), as expected from the literature.[803] Using univariate linear regression analysis, we determined that the coefficient of age was 0.067 (95% CI: 0.035 to 0.098, $P=3e^{-04}$; multiple R-squared value, 0.4877).

In three brains from subjects with non-*PRKN*-linked parkinsonism, the levels of H_2O_2 were similar to those measured in age-matched controls (**Fig. 2.2b**). When analyzing parkin distribution *vs.* H_2O_2 concentrations in human cortices, we found that parkin solubility in human brain negatively correlated with H_2O_2, where the coefficient of the latter was -4.2 (95% CI: -7.92 to -0.48, P=0.029; multiple R-squared value, 0.2174) (**Fig. 2.2c**).

We next sought to dynamically model the observed correlation between higher ROS levels in the nervous system and reduced parkin solubility. We first used an *ex vivo* approach, whereby wild-type mouse brains were exposed to either saline or H_2O_2 during tissue homogenization. There, we saw a significant reduction in soluble parkin and an increase in insoluble parkin in the H_2O_2-exposed lysates (**Fig. 2.2d, e**). We next examined two *in vivo* models. In the first, wild-type mice were intraperitoneally injected with 40 mg/kg of MPTP toxin one hour before sacrificing them in order to induce acute oxidative stress, but no cell death.[804] Brains were serially fractionated, and parkin distribution was quantified across soluble and insoluble compartments. There, we measured a decrease of murine parkin in the soluble fraction and a corresponding rise in the insoluble fractions of MPTP- *vs.* saline-injected littermates (**Fig. 2.2f, g**).

In the second *in vivo* model, we observed a similar, significant shift in parkin distribution toward insolubility in adult mice that were haploinsufficient for the *Sod2* gene, which encodes mitochondrial

MnSOD, and which occurred in the absence of an exogenous toxin (**Fig. 2.2h, i**). Of note, in both models we confirmed the expected rise in H_2O_2 levels (see Chapter 3). Moreover, in contrast to murine parkin, the solubility of endogenous Dj-1, which is encoded by a second, ARPD-linked gene, was not visibly altered under these elevated oxidative stress conditions, as monitored by SDS/PAGE/Western blotting (**Fig. 2.2h**).

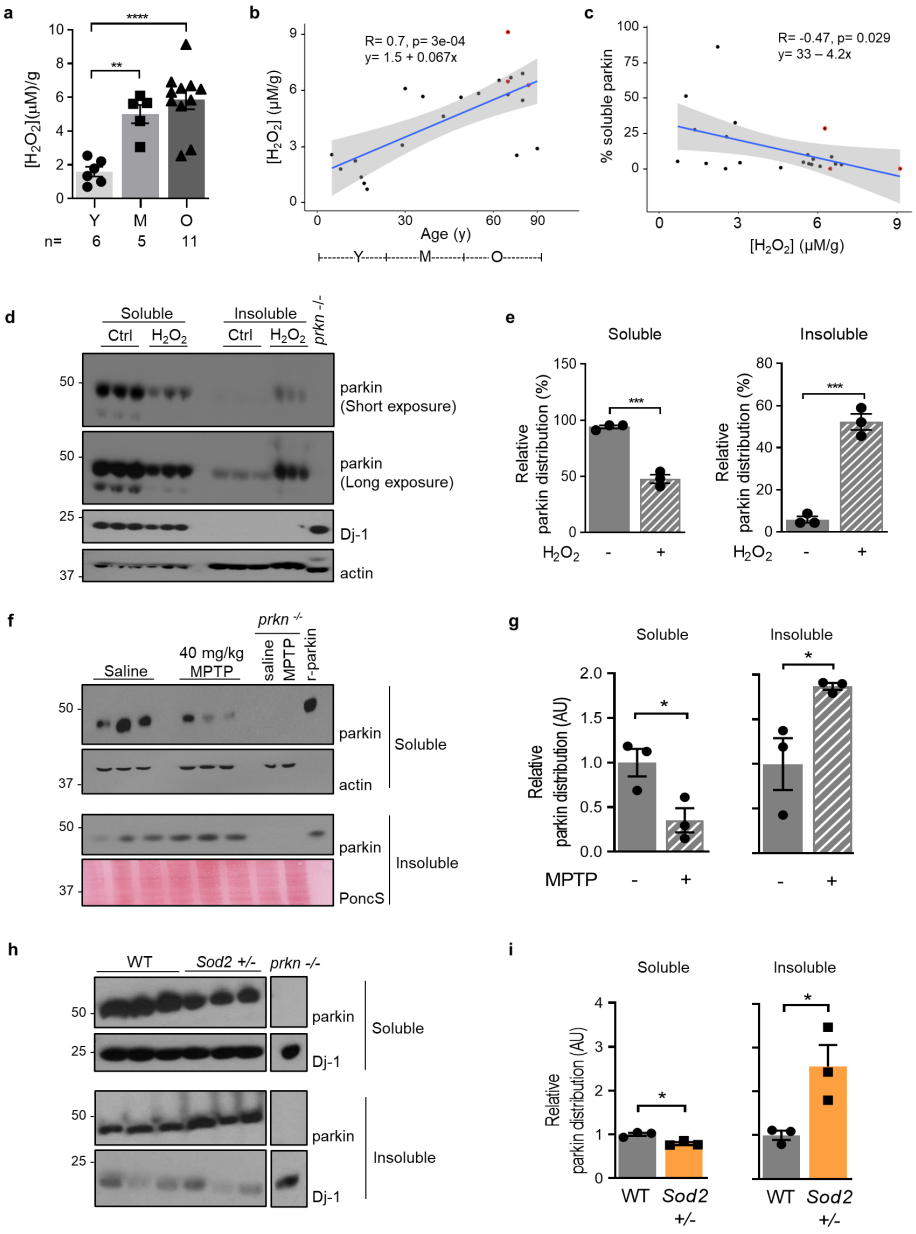

Figure 2.2. Decline in parkin solubility correlates with a rise of oxidative stress in mammalian brain

(a) Mean concentrations of H_2O_2 in human brain cortices grouped by age range, as described in Figure 2.1. Individual data points represent separate brains, as reported in **Supplementary Table 2.1**. Results are plotted as mean ± SEM; significance was determined using one-way ANOVA [$F(2, 76)=26.21$, $p<0.001$] with Tukey's post hoc test (**p<0.01; ***p<0.001).

(b-c) Linear regression analysis of H_2O_2 concentrations in control cortices (mM/g tissue) as a function of age **(b)**, and **(c)** linear regression analysis of parkin solubility as a function of H_2O_2 levels in the same specimens (n=22). Red circles denote three disease cortices (non-*PRKN*-linked parkinsonism). H_2O_2 concentration coefficient (in (c)) was -4.2 (95% CI: -7.92 to -0.48, P=0.0287).**(d-e)** Western blots **(d)** of parkin distribution in brain lysates of 2-4 month-old wild-type C57Bl/6J mice containing either saline or 1% H_2O_2; **(e)** parkin signal distribution was quantified using ImageJ, as controlled for respective loading controls, in both soluble and insoluble fractions. A Student T-test was used for statistical analysis (* p< 0.05).

(f-g) Western blots **(f)** of parkin distribution in brains of wild-type C57Bl/6J mice 1 hour following intraperitoneal administration of either saline or MPTP neurotoxin (40mg/kg); **(g)** parkin signals were quantified as in (e). **(h-i)** Western blots **(h)** of fractionated brain homogenates from C57Bl/6J wild-type and *Sod2*$^{+/-}$ mice; **(i)** parkin signals were quantified and statistically analyzed as in (e) (* p< 0.05). Note, Western blots followed SDS/PAGE under reducing conditions.

Parkin is reversibly oxidized in adult human brain

The correlation between parkin insolubility and H_2O_2 levels in human brain suggested to us that the relation could be due to posttranslational, oxidative modifications. Indeed, in contrast to SDS-containing brain fractions carried out under reducing conditions (+DTT), when gel electrophoresis was performed under non-reducing (-DTT) conditions, we detected parkin proteins ranging in M_r from >52 to 270 kDa, invariably in the form of redox-sensitive, high molecular weight (HMW) smears (right *vs.* left panel; **Fig. 2.3a**). We saw the same pattern in fractions prepared from control midbrains; no such reactivity was seen in SDS-extracts of parkin-deficient ARPD brains, thus demonstrating specificity of protein detection.

We confirmed that reversible oxidation of brain parkin was also present in soluble (TS-, TX-) fractions, albeit at lesser intensities (**Fig. 2.3b**). Of note, the formation of high M_r parkin was not due to secondary oxidation *in vitro,* because specimens had been processed and fractionated in the presence of iodoacetamide (IAA) prior to SDS/PAGE in order to protect unmodified thiols. These HMW parkin smears also did not arise from covalent ubiquitin-conjugation, such as due to auto-ubiquitylation of parkin, owing to the fact that such adducts cannot be reversed by reducing agents (e.g., DTT).

Because we predicted that the loss of parkin solubility was due to thiol-based, posttranslational oxidation events,[486] we first sought to test this *in vitro* using purified, tag-less, full-length, recombinant (r-) parkin. There, we observed the H_2O_2 dose-dependent formation of HMW smears and loss of parkin solubility; however, r-parkin protein solubility was greatly recovered by adding DTT (**Fig. 2.3c**; **Supplementary Fig. 2.3a**) or β–mercaptoethanol (not shown). Demonstrating its sensitivity to bi-directional redox forces, the exposure of naïve r-parkin to excess DTT also rendered it increasingly insoluble (**Supplementary Fig. 2.3b**), likely due to loss of zinc-sulfur chelation in its four RING domains.[455,805] Unlike r-parkin, the addition of up to 1M DTT in the extraction buffer did not alter

parkin's extraction into a soluble phase (i.e., TS- or TX-fractions) in aged human brain tissue (**Supplementary Fig. 2.3c**).

We confirmed by mass spectrometry (MS) of the holoprotein carried out without any trypsin digestion that all 35 cysteine-based thiol groups of human r-parkin are principally accessible to alkylation by IAA (right *vs.* left panel; **Supplementary Fig. 2.3d**). These results unequivocally demonstrated that each parkin cysteine theoretically possesses the capacity to function as a reducing thiol. Nevertheless, in these *in vitro* experiments we consistently observed a concentration-dependent change in r-parkin solubility, thereby suggesting that some thiols were more amenable than others to modification by reactive species (see below and summary in **Supplementary Table 2.2**).

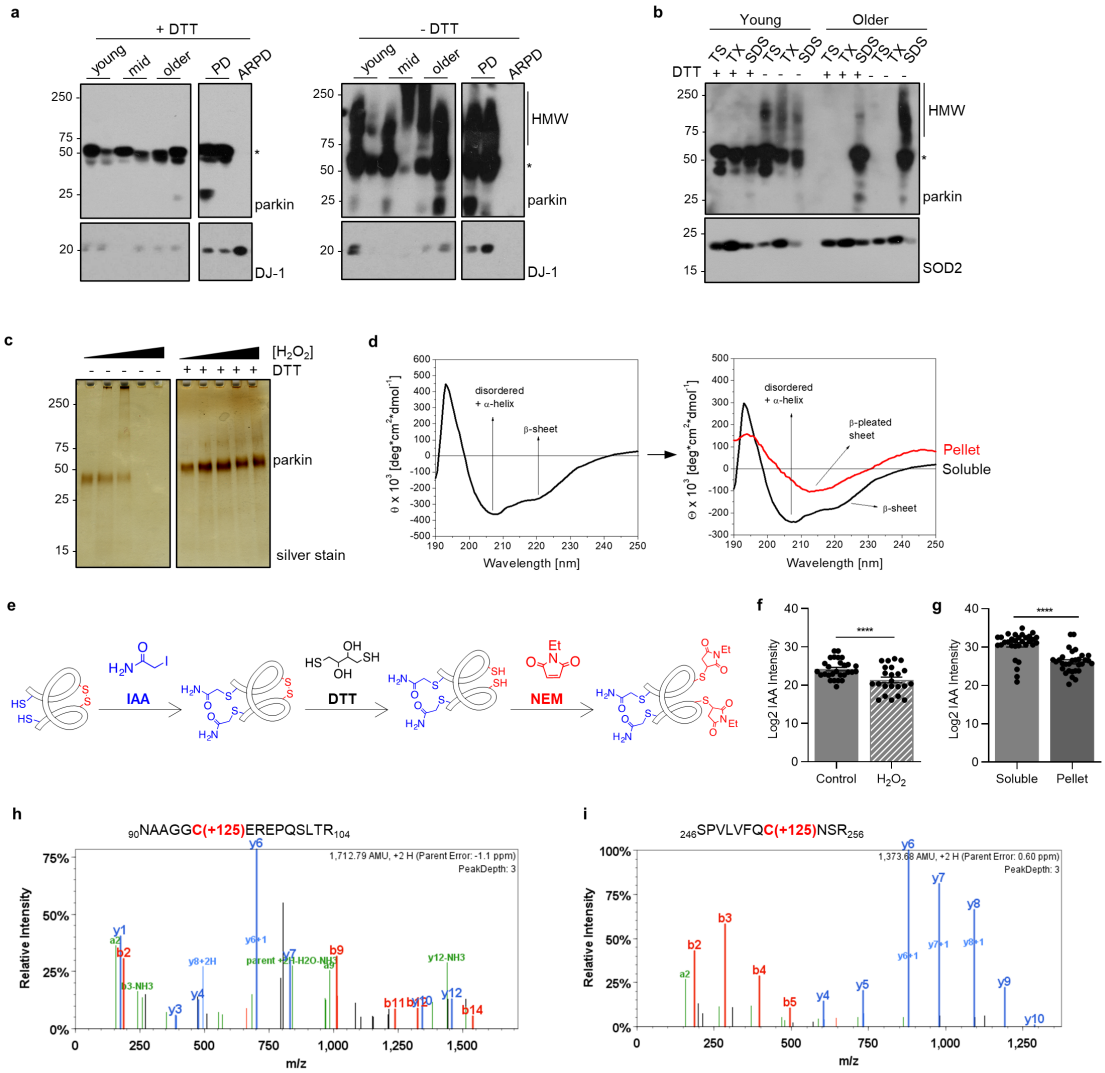

Figure 2.3. Parkin's solubility and structure are altered by oxidative modifications

(a) Western blots of parkin and DJ-1 in SDS fractions from normal cortices (3 age groups are shown) and two age-matched patients, i.e., idiopathic Parkinson disease (PD) and parkin-deficient ARPD. Sister aliquots of the same lysates were processed in parallel by SDS-PAGE either under reducing (+DTT) or non-reducing (-DTT) conditions.

(b) Western blots of parkin and SOD2 distribution in serially fractionated human cortices from a young individual (age, 5 yrs) and an adult (62 yrs) subject, and separated by SDS-PAGE under reducing (+DTT) and non-reducing (-DTT) conditions.

(c) Silver staining of the supernatant of sister aliquots of r-parkin (10 ng) following initial exposure to increasing concentrations of H_2O_2 (0, 1.0, 2.5, 5.0, 7.5 and 10 mM) followed by the addition (or absence of) DTT (100mM) prior to centrifugation as indicated. **(d)** Circular dichroism spectra of soluble, untreated, wild-type r-parkin at the start of experiment (T=0; left panel), and spectra of soluble (black line) and aggregated (red line) states following incubation at 37°C for T=5 days (right panel). **(e)** Graphic depiction of strategy for LC-MS/MS-based analysis to identify cysteine oxidation state for untreated and H_2O_2-treated, parkin species, by using IAA-DTT-NEM fingerprinting to identify reduced cysteines with an iodacetamide (IAA) tag or reversibly-oxidized residues with a N-ethylmaleimide (NEM) tag. **(f-g)** Quantitative analyses of IAA-modified cysteines captured by LC-MS/MS for **(f)** untreated *vs.* H_2O_2-exposed, wild-type, human r-parkin, and **(g)** soluble compared to insoluble (pellet) fractions. Each dot represents the log2-transformed total IAA-signal intensities of individual cysteines (n=3 runs for each). The cysteine pool is shown with the mean ± SEM; significance **p<0.01, as determined using Student T-test. **(h-i)** LC-MS/MS-generated spectra following trypsin digestion of labelled, oxidized r-parkin indicating NEM adducts (+125 mass gain) at Cys95 and Cys253; r-parkin was exposed to H_2O_2, and cysteines labelled as in (e). See **Supplementary Table 2.2**, for a complete list of modified cysteines and oxidizing conditions.

Oxidative conditions alter parkin structure

The progressive insolubility of brain parkin and r-parkin due to redox stress suggested that the protein had undergone structural changes. Indeed, when we analyzed the effects of spontaneous oxidation using naïve r-parkin by far-UV-circular dichroism (**Fig. 2.3d**), soluble fractions initially contained both α-helically ordered, as well as, unstructured r-parkin proteins. Five days later, r-parkin preparations were separated by centrifugation and fractions re-analyzed. There, we found a marked shift to increased β-pleated sheet-positive r-parkin in insoluble fractions (**Fig. 2.3d**). Similarly, when we monitored r-parkin during spontaneous oxidization using dynamic-light scattering (**Supplementary Fig. 2.3e**), we observed a gradual shift in the hydrodynamic diameter from 5.1 nm, representing a folded monomer, to multiple peaks with larger diameters 5 hrs later. The latter indicated spontaneous multimer formation, which was partially reversed by the addition of DTT (right panel; **Supplementary Fig. 2.3e**). Thus, these structural and solubility changes of r-parkin were congruent with our immunoblot results for human brain parkin (**Fig. 2.3a**).

Hydrogen peroxide modifies parkin at multiple cysteines

To determine whether oxidation of cysteines and/or methionine residues caused parkin insolubility, we analysed r-parkin that was treated with and without H_2O_2 and/or thiol-alkylating agents using liquid chromatography-based MS (LC-MS/MS). To differentiate reduced from oxidized cysteines we used a serial thiol-fingerprinting approach, which labelled reduced thiols with IAA, and tagged reversibly oxidized thiols with N-ethylmaleimide (NEM) after their prior reduction with DTT (**Fig. 2.3e**). The first test was to determine how progressive oxidation affected thiol accessibility. As expected, using the strong alkylating agent IAA on the nascent protein (and trypsin digestion to map individually modified peptides), we confirmed that the majority of parkin cysteines were reactive (**Supplementary Fig. 2.3d;**

Supplementary Table 2.2). Intriguingly, when treating naïve r-parkin with lower H_2O_2 concentrations, we identified an average of 19 cysteines (54.3%) to be modified; in contrast, higher H_2O_2 concentrations increased this number to 32 cysteines (91.4%). These results suggested progressive unfolding of r-parkin with increasing oxidation (**Supplementary Table 2.2**).

Next, we sought to precisely identify the location of oxidized cysteine residues. Using Scaffold PTM-software, we found a rise in the number of oxidized residues (NEM-Cys, range of 3-26), which was proportional to the increase in H_2O_2 concentrations and appeared to begin in parkin's RING1 domain at three residues, i.e., Cys238, Cys241 and Cys253 (**Supplementary Table 2.2**, **Fig. 2.3i**), but also involved Cys95 in its linker domain (**Fig. 2.3h**). Furthermore, when quantifying thiol modifications by MaxQuant software [806], we found a significant drop for the number of cysteines in the reduced state (IAA-cysteines) within the H_2O_2-treated samples (P=0.0016; **Fig. 2.3f**), as expected.

In accordance, when comparing cysteine oxidation events in soluble and insoluble fractions of untreated *vs.* oxidized r-parkin preparations, the number of IAA-Cys was significantly decreased in the pellets (P<0.0001; **Fig. 2.3g**). Of note, modifications at methionine residues did not correlate with r-parkin solubility. These collective results unequivocally demonstrated that H_2O_2-induced oxidation events at cysteine-based thiols are linked to both progressive, structural change and lesser solubility of human r-parkin.

Parkin is also irreversibly oxidized in adult human and mouse brains

We next sought to identify oxidation events at parkin cysteines *in vivo* by LC-MS/MS. To this end, we examined both cortex-derived, human parkin and brain parkin isolated from intraperitoneally, MPTP toxin- (*vs.* saline-) treated mice (**Fig. 2.4**). Specimens were processed with IAA during homogenization and fractionation to prevent any oxidation artefacts *in vitro*. Following immunoprecipitation and gel

excision of endogenous parkin at the 50-53 kDa range (an example is shown in **Supplementary Fig. 2.4a, b**), we focused on cysteine mapping and the identification of thiol redox states (**Fig. 2.4a**). A graphic representation of theoretically possible, thiol-based redox modifications is provided in **Supplementary Fig. 2.4c**).

In human control cortices (n=12 runs; summarized in **Fig 2.4a**), we mapped a mean of 46.8 and 19.4% of parkin's wild-type sequence in the soluble and insoluble fractions, respectively. There, we found cysteines in either a redox reduced state (IAA-alkylated Cys+57; examples shown in **Fig. 2.4b, d**) or in oxidized states (e.g., to sulfonic acid Cys+48). Irreversible oxidation events in human cortices occurred, for example, at Cys95 (**Fig. 2.4c**) and Cys253 **(Fig. 2.4e**). The relative frequencies of detection for parkin thiols that were found in a reduced state *in vivo* (and thus, were alkylated by IAA *in vitro*) in the soluble *vs.* insoluble fractions of human brain were 67.3 *vs.* 38.1%, respectively (**Fig. 2.4a**).

Likewise, in saline- and MPTP-treated mouse brains (n=6 runs), we mapped 25.0 and 51.5% of wild-type parkin, respectively (summarized in **Fig. 2.4a**). Interestingly, akin to the findings in human brain, we identified the murine sequence-corresponding residue Cys252 in either a reduced or in irreversibly oxidized states (**Fig. 2.4f, g**; also found in a reversibly oxidized state, see **Appendix Fig. C13**). As mentioned, mice do not carry a cysteine at residue 95 (for sequence comparison, see below). The relative frequencies of detection for thiols that were in a reduced state *in vivo* (and thus, alkylated by IAA *in vitro*) in parkin from saline- *vs.* MPTP toxin-treated mouse brains were 92.9 *vs.* 68.2%, respectively (**Fig. 2.4a**). These collective results demonstrate that H_2O_2-induced oxidation of cysteine-based thiols confers structural changes and insolubility of r-parkin.

a

	Human Brain		Mouse Brain	
Mean (range)	**TSS-extractable (IP, n=4)**	**SDS-extractable (IP, n=8)**	**Saline (IP, n=3)**	**MPTP (IP, n=3)**
% Parkin protein coverage	46.8 (35-72)	19.4 (2-58)	25.0 (23-27)	51.5 (33-70)
# Peptides identified	15.0 (10-23)	6.4 (1-17)	11.0	22.5 (18-27)
# Cysteines identified	17.5 (13-26)	6.1 (1-16)	6.5 (6-7)	18.0 (10-26)
# Reduced residues (=IAA-Cys)	17.5 (13-26)	6.1 (1-16)	6.5 (6-7)	15.0 (8-22)
IAA / total # Cys identified	17.5/26	6.1/16	6.5/7	15.0/22
% of above	67.3	38.1	92.9	68.2

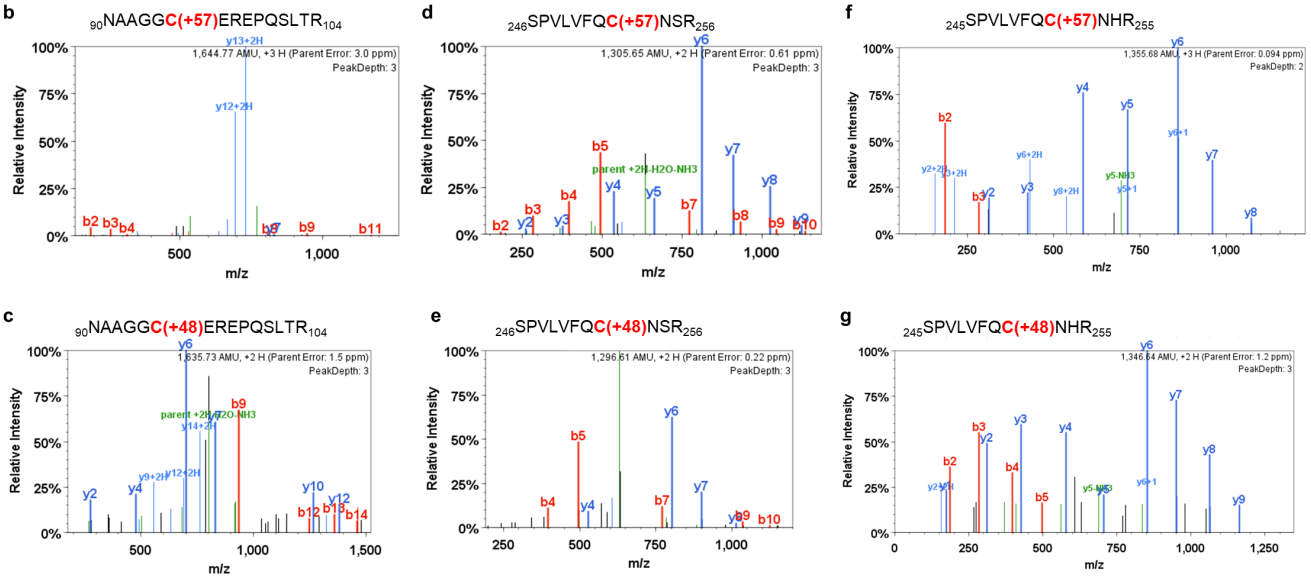

Figure 2.4. Select parkin cysteine residues are oxidized in human and mouse brain
(a) Summary of results for 12 immunoprecipitation (IP) runs (TS extracts; n=4; SDS extracts, n=8) from human cortices and either saline- or acute (1hr) MPTP toxin-treated murine brain (as described in **Fig. 2.2d,e**) for endogenous parkin enrichment to identify the redox state of its cysteine residues (see also b-g). All specimens were fractionated in the presence of IAA.
(b-g) Among the redox active residues identified, Cys95 and Cys253 in human brain parkin were found in either a reduced redox state **(b,d)** (i.e., IAA-labelled; +57 mass gain), or **(c,e)** in irreversibly oxidized states, e.g., to sulfonic acid (trioxidation; +48 mass). In mouse brain parkin **(f,g)**, Cys252 was found either reduced or oxidized as well.

Parkin thiols reduce hydrogen peroxide *in vitro*

A typical redox reaction involves the reduction of an oxidized molecule in exchange for oxidation of the reducing agent (examples are shown in **Supplementary Fig. 2.4c**). We therefore asked whether parkin oxidation resulted in reciprocal reduction of its environment (**Fig. 2.5; Supplementary Fig. 2.5**). Using r-parkin, we established that parkin could reduce H_2O_2 levels in a concentration-dependent manner *in vitro* (**Fig. 2.5a; Supplementary Fig. 2.5h**). This reducing activity was not enzymatic, in that it did not mirror the dynamics of catalase, and r-parkin did not possess peroxidase activity (**Fig. 2.5a; Supplementary Fig. 2.5a**). Rather, the reaction was dependent on parkin's thiol integrity, because pre-treatment with NEM (or IAA) and pre-oxidation of the protein with H_2O_2 abrogated the ROS-reducing activity of r-parkin (**Fig. 2.5b; Supplementary Fig. 2.5b, g**). It thus appeared similar to the effect of glutathione (**Fig. 2.5a; Supplementary Fig. 2.5a, e, f**).

The anti-oxidant effect by r-parkin was also dependent on its intact Zn^{2+} coordination, because increasing concentrations of the divalent ion chelator, EDTA, abrogated the activity; the latter could be ameliorated by supplementing the reaction buffer with zinc (**Supplementary Fig. 2.5c**). As expected, the exposure of r-parkin to excess H_2O_2 (or excess DTT) led to the release of zinc ions from the nascent recombinant protein, as measured *in vitro* (**Supplementary Fig. 2.5d**).

Interestingly, RNF43 (a distinct E3 ligase that contains a zinc-finger domain), HOIP (an E3 ligase containing a RING domain) and bovine serum albumin (BSA, which akin to parkin has 35 cysteines), did not show any H_2O_2-lowering capacity (**Fig. 2.5c, d; Supplementary Fig. 2.5e**). Further, Parkinson-linked a-synuclein, which has no cysteines, also had no reducing effect (**Fig. 2.5c, d**). These results suggested that the cysteine-rich, primary sequence and the tertiary structure of r-parkin conferred anti-oxidant activity.

We next examined additional, cysteine-containing, ARPD-linked proteins, e.g., r-DJ-1 and two disease-linked variants of full-length r-parkin, p.G328E and p.C431F, as well as a C-terminal RING2-peptide of parkin (r-parkin$_{321C}$). We also used a second ROS quantification assay for further validation and to expand our dose dependency studies (**Fig. 2.5e, Supplementary Fig. 2.5f-m**). There, r-DJ-1 and r-parkin$_{321C}$ showed negligible H_2O_2-lowering capacity, and the two point-mutants conferred less activity than did wild-type, human r-parkin (**Fig. 2.5e**). As expected from typical redox reactions (**Supplementary Fig. 2.4c**), the lowering of ROS *in vitro* correlated with reciprocal r-parkin oxidation, as revealed by SDS/PAGE, which was performed under non-reducing conditions immediately after the reaction with H_2O_2 (**Supplementary Fig. 2.5n**).

These results suggested that the anti-oxidant activity by r-parkin was dependent on its reactive thiol content, which we examined next using the Ellman's reagent. There, full-length r-parkin, r-parkin$_{321C}$ and r-DJ-1 showed the predicted number of reactive thiols, whereas the single point-mutant variants of r-parkin revealed fewer accessible thiols (**Fig. 2.5f**). From these results, we observed a linear correlation between thiol equivalencies and the degree of ROS reduction *in vitro*, demonstrating that a greater number of readily reactive and/or a greater number of accessible thiols in human parkin proteins corresponded with more effective lowering of H_2O_2 (**Fig. 2.5g**).

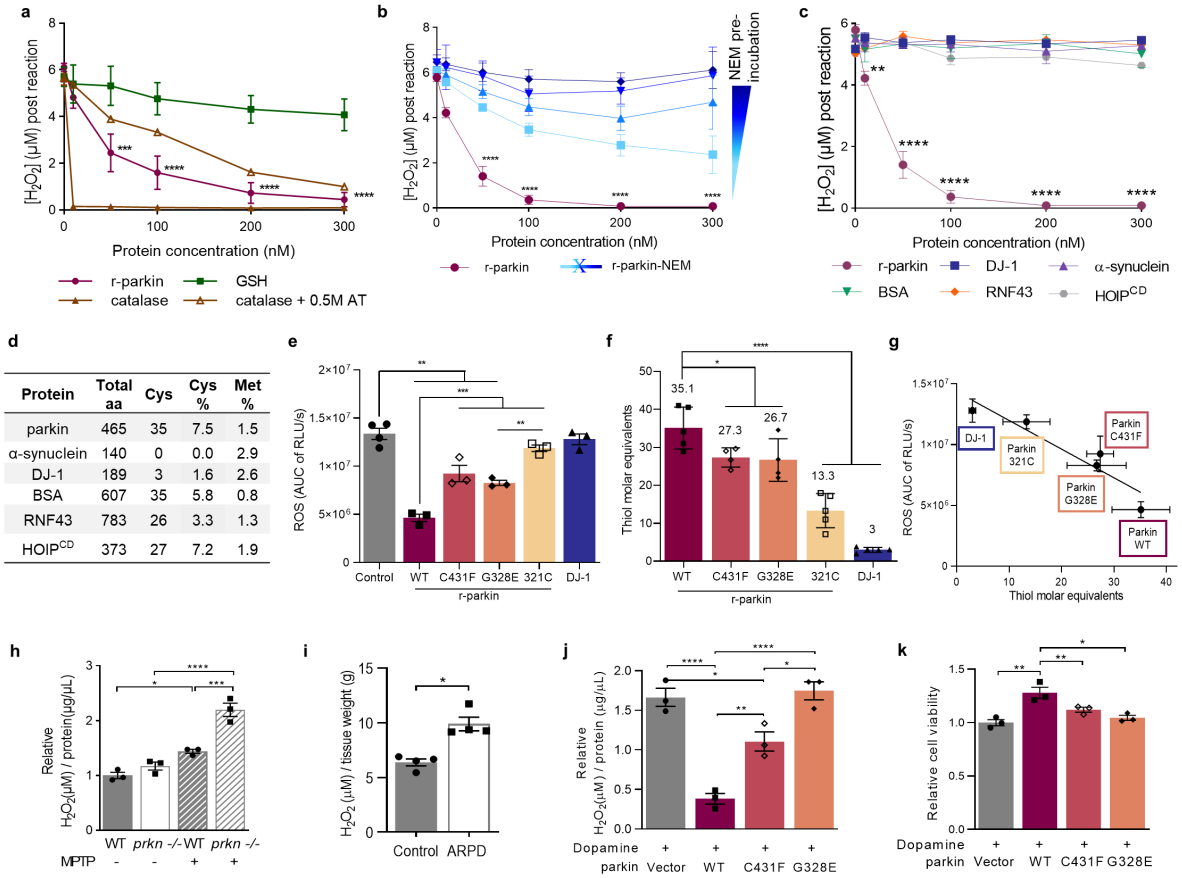

Protein	Total aa	Cys	Cys %	Met %
parkin	465	35	7.5	1.5
α-synuclein	140	0	0.0	2.9
DJ-1	189	3	1.6	2.6
BSA	607	35	5.8	0.8
RNF43	783	26	3.3	1.3
HOIP^{CD}	373	27	7.2	1.9

Figure 2.5. Wild-type parkin lowers hydrogen peroxide *in vitro*, in cells and the brain

(**a-c**) Quantification of H_2O_2 concentration using AmplexRed, demonstrating **(a)** full-length, human, recombinant (r-) parkin when incubated with H_2O_2 is able to reduce it to water in a r-parkin concentration-dependent manner. Effects of r-Parkin were compared to catalase and GSH at equimolar concentrations as well as following partial inhibition of catalase by amino-triazole (AT), as indicated. **(b)** Pre-incubation of r-parkin with a thiol-conjugating compound (NEM) inhibits parkin-dependent H_2O_2 reduction in a NEM-concentration-dependent manner. **(c)** Reducing capacity of wild-type r-parkin compared to two other, PD-linked proteins (DJ-1; α-synuclein), bovine serum albumin (BSA) and two RING-carrying ubiquitin ligases (RNF43; HOIP^{cd}; cd = catalytic domain). Their respective cysteine and methionine contents are summarized in **(d)**. Two-way ANOVA with Tukey's post hoc test (**p < 0.01,***p < 0.001, and ****p < 0.0001) was used for statistical analysis in a,[F (15, 48) = 5.069, p< 0.0001]; b, [F (20, 60) = 3.966, p< 0.0001]; and c, [F (25, 72) = 22.91, p< 0.0001].

(e) Area under the curve (AUC) plots for results from *in vitro* colorimetric assays, where AUC integrates total H_2O_2 levels measured over the time course of the assay (see also **Supplementary Fig. 2.5f**). Comparison of WT r-parkin with DJ-1, two r-parkin point mutants, and r-parkin$_{321-465}$ (321C). Results represent n=3 ± SD using one-way ANOVA [F (7, 17) = 99.87, p< 0.0001] with Tukey's post hoc test *p < 0.05, **p < 0.01,***p < 0.001, and ****p < 0.0001.

(f) Quantification of reactive thiol content (in molar equivalents) for r-parkin (WT; two point mutants; 321C) and full-length r-DJ-1 using the Ellman's reagent assay. Results analyzed by one-way ANOVA [F (4, 18) = 45.11, p< 0.0001].

(g) Correlation curve between number of free thiols **(f)** *vs.* the H_2O_2-reducing capacity **(e)** for indicated proteins with R^2= 0.8789.**(h-i)** Quantification of H_2O_2 levels in **(h)** saline *vs.* MPTP toxin-treated *prkn* wild-type (WT) and *prkn*$^{-/-}$ mouse brain (n=3/genotype/condition), and **(i)** in human brain from parkin-deficient ARPD cortices compared to age- and *post-mortem* interval-matched controls (n=4/group) collected at the same institution. Results are represented as the mean concentration of H_2O_2 (μM) per total protein concentration (μg/μL) or tissue weight (g) analyzed ± SEM; *p<0.05, ***p < 0.001, and ****p < 0.0001 determined using a Student T-test or one-way ANOVA with Tukey's post hoc test; [F (3, 8) = 45.41, p< 0.0001].

(j-k) H_2O_2 quantification **(j)** and cell viability assay **(k)** for dopamine-treated, human M17 cells expressing either WT or two ARPD-linked parkin point mutants, as indicated relative to treatment with vehicle alone. Cells were exposed to 200 μM dopamine or vehicle for 20h, as indicated. Data points represent the mean of duplicates ± SEM (n=3 experiments); *p<0.05 and **p < 0.01, and ****p < 0.0001 by one-way ANOVA with Tukey's post hoc test: j, [F (3, 8) = 35.34, p< 0.0001]; and k, [F (3, 8) = 12.92, p= 0.0020].

Hydrogen peroxide levels are increased in parkin-deficient brain

To explore whether parkin oxidation conferred ROS reduction *in vivo*, we first quantified H_2O_2 concentrations in the brains of wild-type and *prkn*$^{-/-}$ mice. A trend, but no significant difference, was measured under normal redox equilibrium conditions. However, when analyzing brain homogenates from mice treated with MPTP-toxin *vs.* saline, carried out as above (**Fig. 2.2**), we found significantly higher H_2O_2 levels in the brains of adult *prkn*$^{-/-}$ mice compared to wild-type littermates ($p<0.001$; **Fig. 2.5h**). Similarly, in adult humans H_2O_2 levels were significantly increased in the cortex of *PRKN*-linked ARPD patients *vs.* age-, PMI-, ethnicity- and brain region-matched controls.[184] ($p<0.05$; **Fig. 2.5i**) Specimens of three non-*PRKN*-linked patients with parkinsonism showed H_2O_2 levels comparable to those from age-matched normal cortices (**Fig. 2.2b**, red circles). We concluded that the expression of wild-type *PRKN* alleles contributes to the lowering of ROS concentrations in adult, mammalian brain.

Parkin prevents dopamine toxicity in cells in part by lowering hydrogen peroxide

To address the question of selective neuroprotection, we revisited the role of parkin in cellular dopamine toxicity studies.[362,493] We first tested parkin's effect on ROS concentrations in dopamine-synthesizing, human M17 neuroblastoma cells. There, dopamine exposure of up to 24 hrs caused a significant rise in endogenous H_2O_2 ($p<0.05$; **Fig. 2.5j**), as expected. Wild-type *PRKN* cDNA expression effectively protected M17 cells against the dopamine stress-related rise in H_2O_2 levels ($p<0.0001$; **Fig. 2.5j)**. By comparing sister cultures that expressed similar amounts of exogenous parkin proteins, the E3 ligase-inactive p.C431F mutant had a partial rescue effect, whereas p.G328E, which we confirmed to retain its E3 ligase activity *in vitro*, showed no H_2O_2-lowering capacity in these cells (**Fig. 2.5j**).

Moreover, only wild-type parkin, but none of the mutant variants tested, increased the viability of M17 cells under rising dopamine stress conditions ($p<0.01$; **Fig. 2.5k**). This protective effect also correlated with parkin insolubility and its HMW smear formation, as expected from previous studies.[362]

These posttranslational changes in M17-expressed parkin were not reversible by DTT or SDS (**Supplementary Fig. 2.6a, b**), thereby suggesting irreversible dopamine-adduct formation. Notably, the protection from dopamine toxicity positively correlated with the level of *PRKN* cDNA transcribed, as confirmed in sister lines of M17 cells that stably express human, wild-type parkin. There, we estimated that ~4 ng of parkin protein expressed in healthy, neural cultures neutralized each mM of dopamine added during up to 24 hrs (**Supplementary Fig. 2.6c, d**).

Parkin binds dopamine radicals predominantly at primate-specific cysteine 95

We next explored which thiols of parkin were involved in the neutralization of dopamine radicals. Covalent conjugation of RES metabolites at parkin residues had been previously suggested,[362,493] but not yet mapped by LC-MS/MS examining the whole protein. Aliquots of r-parkin were exposed to increasing levels of the relatively stable dopamine metabolite aminochrome. As expected, this led to the loss of protein solubility and HMW species formation at the highest dose tested (**Fig. 2.6a, b**). These reaction products were then used to map modified residues by LC-MS/MS. Specifically, proteins corresponding to r-parkin monomer (51-53 kDa) and two HMW bands, one at ~100 kDa, the other near the loading well, were gel-excised (**Fig. 2.6a**), trypsin digested and structurally analyzed.

There, we made the following four related observations: i) Increasing aminochrome concentrations led to a significant decline in the total number of spectra readily identified by LC-MS/MS as parkin-derived peptides, both in the monomeric and HMW bands ($p<0.001$ and $P<0.0001$), respectively (**Fig. 2.6c**). This indicated to us either a marked loss in solubility (and thus, lesser accessibility by trypsin) or a rise in heterogenous, complex modifications, which rendered the analyte undetectable by LC-MS/MS, or both; ii) Despite fewer spectra recorded, we identified a significant increase in the number of oxidized cysteines (such as irreversibly modified to sulfonic acid) following aminochrome exposure, in particular

within the HMW bands of r-parkin ($p<0.0001$; **Fig. 2.6d**); iii) Under these conditions, four distinct forms of dopamine metabolites were found conjugated to parkin cysteines. Mass shifts of +145, +147, +149 and +151 were identified, which represented covalent attachment by indole-5,6-quinone, two variants of aminochrome (O=; HO-), and dopamine quinone itself, respectively (**Fig. 2.6e; Supplementary Fig. 2.7a**); and iv) Unexpectedly, we identified in Cys95 the most frequently dopamine-conjugated parkin residue ($p<0.0001$; n=98 spectra; **Fig. 2.6e-g; Supplementary Fig. 2.7b-g**). Other residues of r-parkin, which we identified to carry any one of the dopamine metabolites we tracked, included Cys166, Cys169, Cys182, Cys212, Cys238, Cys 293, Cys360 and Cys365, but at a much lesser frequency (**Fig. 2.6e,f; Supplementary Fig. 2.7h-o**). No dopamine metabolite-related mass shifts were detected in the control samples that had not been exposed to aminochrome, as expected. We noted with interest that residue Cys95 of wild-type parkin, as the most frequently catalogued one to be modified by dopamine metabolites, is also primate sequence-specific (**Fig. 2.6g, h**).

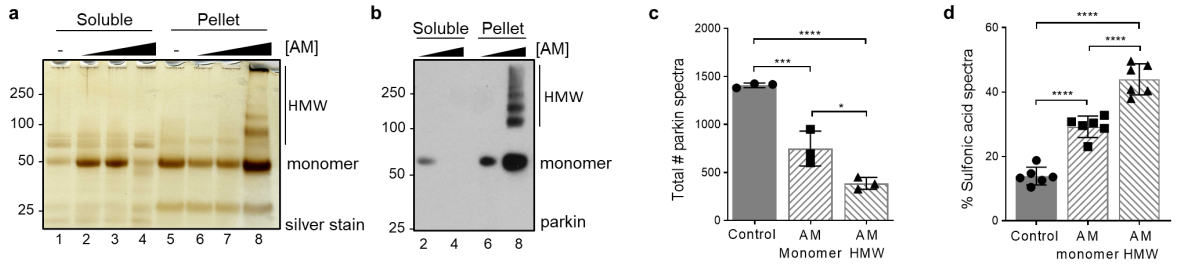

e

Peptide Sequence	Variable Modifications	Observed m/z	Spectrum Charge	Actual Peptide Mass (AMU)	Peptide Identification Probability	Mascot Ion Score	Scaffold Peptide Score	Quantity
76 KGQEmNATGGDDPRNAAGGcEREPQSLTR 104	M80 Oxidation (+16), C95 Indolequinone (+145)	802.3541	4	3,205.39	99.40%	28.2	29.55	1
76 KGQEmNATGGDDPRNAAGGcEREPQSLTR 104	M80 Oxidation (+16), C95 Aminochrome (+147)	802.8554	4	3,207.39	99.70%	33.3	41.69	5
76 KGQEmNATGGDDPRNAAGGcEREPQSLTR 104	M80 Oxidation (+16), C95 Aminochrome (+149)	642.8917	5	3,209.42	97.40%	27.7	18.71	1
76 KGQEmNATGGDDPRNAAGGcEREPQSLTR 104	M80 Oxidation (+16), C95 Dopamine Quinone (+151)	803.8625	4	3,211.42	97.80%	28.4	64.11	1
90 NAAGGcEREPQSLTR 104	C95 Indolequinone (+145)	867.388	2	1,732.76	99.70%	59.5	130.03	57
90 NAAGGcEREPQSLTR 104	C95 Aminochrome (+147)	579.2650	3	1,734.77	99.70%	37.3	87.17	29
90 NAAGGcEREPQSLTR 104	C95 Dopamine Quinone (+151)	580.6098	3	1,738.81	99.50%	27.7	72.14	4
162 LRVQcSTcRQATLTLTQGPSCWDDVLIPNR 191	C166 Aminochrome (+149), C169 Cys->Dha (-34)	1164.2490	3	3,489.73	99.30%	83.9	42.91	3
162 LRVQcSTcRQATLTLTQGPScWDDVLIPNR 191	C166 Aminochrome (+149), C169 Dopamine Quinone (+151), C182 Cys->Dha (-34)	1214.6033	3	3,640.79	99.20%	31.4	25.73	1
164 VQcSTcRQATLTLTQGPScWDDVLIPNR 191	C166 Aminochrome (+149), C169 Dopamine Quinone (+151), C182 Indolequinone (+145)	888.4120	4	3,549.62	99.50%	32	11.71	1
212 cGAHPTSDKETSVALHLIATNSRNITcITCTDVR 245	C212 Dopamine Quinone (+151), C238 Dopamine Quinone (+151)	1310.9731	3	3,929.90	99.10%	27.8	19.84	2
235 NITcITcTDVRSPVLVFQcNSR 256	C238 Indolequinone (+145), C241 Cys->Dha (-34), C253 Trioxidation (+48)	1314.6143	2	2,627.21	99.20%	26.3	38.93	1
276 QFVHDPQLGYSLPcVAGcPNSLIK 299	C289 Cys->Dha (-34), C293 Indolequinone (+145)	899.7746	3	2,696.30	99.70%	38.1	45.87	1
350 VTcEGGNGLGcGFAFcREcKEAYHEGEcSAVFEA SGTTTQAYR 392	C352 Cys->Dha (-34), C360 Aminochrome (+147), C365 Cys->Dha (-34), C368 Trioxidation (+48), C377 Trioxidation (+48)	1179.4941	4	4,713.95	98.40%	27.2	14.08	1
350 VTcEGGNGLGcGFAFcREcKEAYHEGEcSAVFEA SGTTTQAYR 392	352 Cys->Dha (-34), C360 Cys->Dha (-34), C365 Indolequinone (+145), C368 Trioxidation (+48), C377 Trioxidation (+48)	1178.9937	4	4,711.95	96.10%	29.3	11.1	1

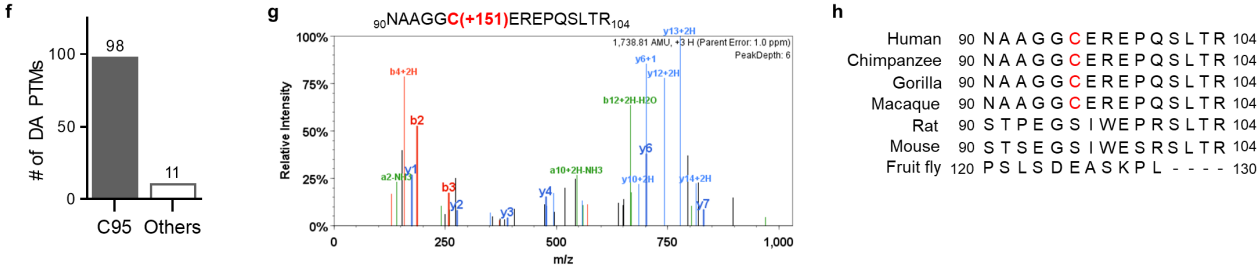

Figure 2.6. Human parkin conjugates dopamine radicals foremost at residue Cys95

(a-b) Silver staining **(a)** and Western blot **(b)** of r-parkin in soluble (supernatant) and insoluble (pellet) phases following exposure to increasing concentrations of aminochrome (AM; 0-200 μM) and analyzed under non-reducing conditions. See lane number for corresponding samples. **(c)** Mean total number of parkin spectra, as identified by LC-MS/MS following trypsin digestion, of control *vs.* monomeric *vs.* high molecular weight (HMW), AM-modified r-parkin. Data represent the mean of n=3 runs ± SEM. *p<0.05; ***p<0.001; ****p<0.0001 by one-way ANOVA with Tukey's post-hoc test [$F(2,6) = 64.73$, $p < 0.0001$]. **(d)** Percentage of peptides carrying a sulfonic acid modification in control *vs.* monomeric and HMW, AM-modified r-parkin. Each point represents one gel specimen submitted to MS. The percentage was calculated using only the subset of peptides that were ever detected as carrying a sulfonic acid modification. Statistics were done as in (c) [$F(2,15) = 96.87$, $p < 0.0001$]. **(e)** Table summarizing LC-MS/MS-based detection of adducts representing dopamine metabolites conjugated to cysteines identified in human r-parkin following exposure to aminochrome *in vitro*. Chemical structures for identified cysteine-conjugated adducts are shown in **Supplementary Fig. 2.7b**. Individual quantification of each peptide with adduct listed is shown on the right side of the table. **(f)** Frequency of occurrences for dopamine-metabolite adducts being detected on Cys95 *vs.* all other cysteine residues, as detected by LC-MS/MS and individually shown in (e).

(g) LC-MS/MS-generated spectrum following trypsin digestion of AM-exposed r-parkin highlighting a dopamine (+151 mass gain) adduct covalently bound to Cys95. See also **Supplementary Fig. 2.7c-p** for additional spectra.

(h) Species comparison for wild-type parkin proteins covering sequence alignment of aa90-104, with primate-specific residue Cys95 highlighted in red.

Parkin augments melanin formation *in vitro*, which involves residue cysteine 95

The oxidation of dopamine in the presence of cysteine-containing proteins, which generates covalent adduct-carrying proteins, underlies structural characteristics during the formation of neuromelanin pigment in the human midbrain (and pons), of which biochemical aspects have been modeled *ex vivo*.[807,808] Given the observed relations between r-parkin, dopamine radical conjugation, aggregate formation and protein insolubility, we next examined whether melanin formation was altered by the presence of parkin. Indeed, wild-type r-parkin augmented total melanin formation in a protein concentration- and time-dependent manner *in vitro* (**Fig. 2.7a**). Like the wild-type protein, two ARPD-linked, full-length r-parkin variants, p.C431F and p.G328E, also augmented melanin formation *in vitro*, when monitored over 60 mins, whereas r-DJ-1 and BSA showed no effect under these conditions (**Fig. 2.7b**).

Interestingly, mutagenesis of residue Cys95 to alanine (p.C95A; **Fig. 2.7c**), which was confirmed by nucleotide- and protein sequencing (by LC-MS/MS), completely abrogated the enhancing effect by r-parkin on the polymerization rate of dopamine to melanin (**Fig. 2.7d, e**). Of note, in our study all the recombinant proteins heretofore analyzed were used after their N-terminal His-SUMO-tag had been removed; however, the p.C95A-mutant was resistant to enzymatic digestion of the tag from the parkin holoprotein. Therefore, both His-SUMO-r-parkin and His-SUMO-p.C95A were utilized (**Fig. 2.7c-e**). Importantly, in parallel experiments we saw no difference in the kinetics of melanin formation between wild-type r-parkin proteins that either carried a His-SUMO-tag or were tag-less. We concluded that under these *in vitro* conditions, residue Cys95 was highly relevant to enhanced melanin polymerization by human parkin.

Furthermore, when the p.C95A-variant of parkin was expressed in M17 cells and examined in our dopamine toxicity assay, the mutant protein showed only a partial effect in H_2O_2 lowering capacity

when compared to wild-type parkin, even when p.C95A was expressed at much higher levels (**Fig. 2.7f, g**). These results were consistent with our collective LC-MS/MS results of oxidative modifications of parkin at Cys95 (shown in: **Figs. 2.3h; 2.4c; Supplementary Table 2.2**). We reasoned from these complementary, *ex vivo,* results that wild-type parkin could be associated with the synthesis of neuromelanin *in vivo*. Therefore, we sought to explore this further in dopamine neurons of human midbrain.

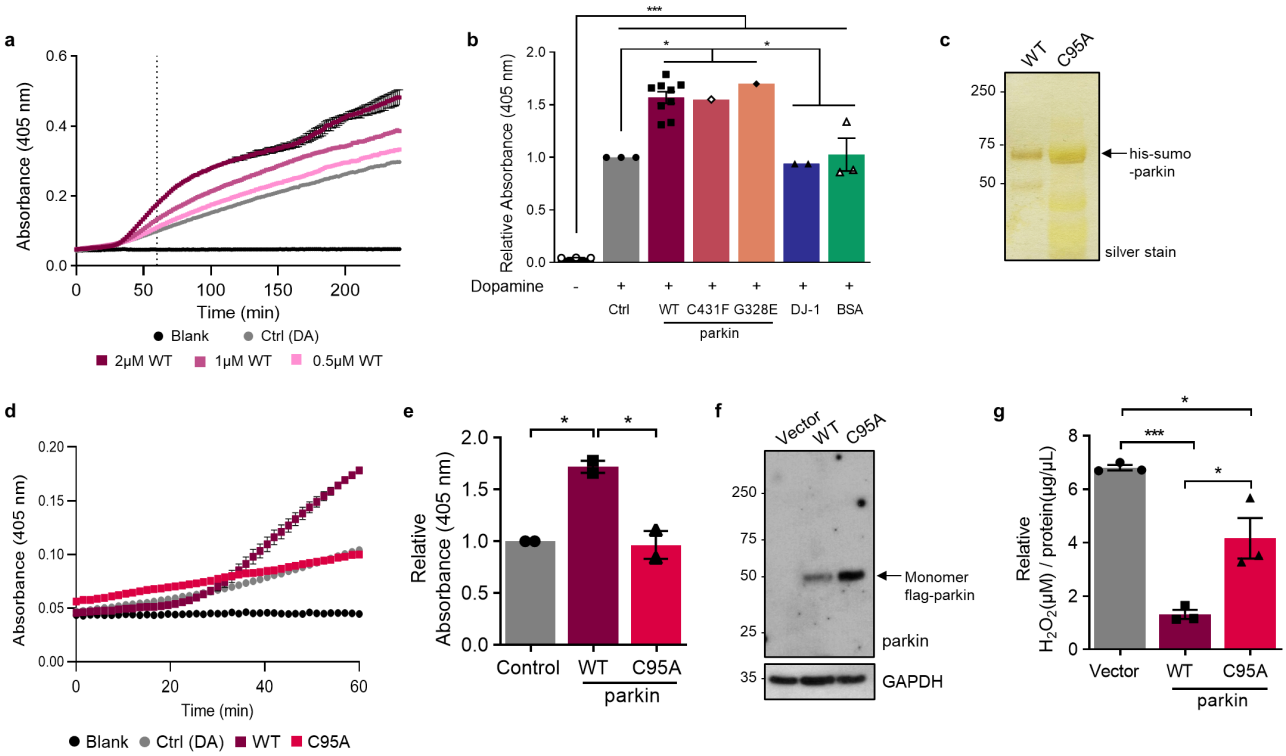

Figure 2.7. Parkin-dependent increase in melanin formation involves residue cysteine 95

(a) Kinetic curve of melanin production (read at absorbance 405nm) over time in the absence of exogenous protein (dopamine (DA Ctrl) alone) *vs.* increasing molar concentrations of wild-type (WT), full-length human r-parkin shown for three concentrations (0.5, 1, 2μm). Each condition was performed in triplicate. **(b)** Total melanin formation for indicated recombinant proteins at 60 mins, as expressed relative to its production under dopamine only control (Ctrl) condition. Data represent the mean of triplicates ± SEM. ***$p<0.05$ by one-way ANOVA with Tukey's post-hoc test [$F(6,15)=40.05$, $p<0.0001$]. **(c)** Silver gel for the analysis of His-SUMO-tagged, full-length, human r-parkin proteins of wild-type sequence and its variant carrying a p.C95A mutation. SDS/PAGE was performed under reducing conditions. **(d-e)** Representative kinetic curve for melanin production **(d)** and relative total melanin formation at 60 mins **(e)**, where production in the presence of wild-type (WT) or p.C95A mutant r-parkin (each, 2 μM) is shown relative to dopamine (DA) (Ctrl) alone. Data represent mean of n=2, each performed in triplicate ± SEM. ***$p<0.05$ by one-way ANOVA with Tukey's post-hoc test [$F(2,3) = 24.96$, $p = 0.0135$]. **(f-g)** Protein expression, as shown by Western blotting **(f)**, and fold change in H_2O_2 levels **(g)** for dopamine-treated M17 cells -relative to vehicle treated sister wells- that transiently express either FLAG-control, or WT *vs.* p.C95A-mutant human parkin-encoding cDNA plasmids. Results are shown as mean ± SEM (n=3) and all dopamine-treated samples (200μM dopamine) were normalized to their respective untreated samples. Anti-GAPDH immunoblotting served as loading control (in f). A one-way ANOVA with Tukey's post hoc test (*$p<0.05$ and ***$p<0.001$) was used for statistical analysis; [$F(2, 6) = 36.86$, $p= 0.0004$].

Anti-parkin reactivity localizes to neuromelanin in the *Substantia nigra* of adult control brain

Subcellular localization studies of parkin in human brains had previously been hindered by the lack of renewable antibodies (Abs) that reliably detect the protein *in situ*.[207,431,689,690] We therefore developed and extensively characterized several, monoclonal Abs of the IgG_2b-subtype using preparations of untagged, full-length, human r-parkin as immunogen. To this end, we generated four stable, epitope-mapped clones, i.e., A15165B, A15165D, A15165G, and A15165E. The performance and specificity of these clones had been confirmed by ELISA, dot blot analyses, SDS/PAGE/Western blotting under reducing conditions, which included the usage of ARPD brain extracts, immunoprecipitation from human brain and indirect immunofluorescence in cellular studies (**Supplementary Fig. 2.8a-c**, and Chapter 4). Importantly, clones A15165D, A15165G, and A15165E were able to specifically detect human parkin in human brain sections by immunohistological methods (see below).

Serial sections of adult, human midbrain from control subjects were developed by traditional immunohistochemistry (IHC) using metal-enhanced 3-3'-diaminobenzadine (eDAB), which generates a black signal for positive immunoreactivity. There, anti-parkin clones A15165D, A15165G and A15165E revealed dark, granular staining throughout the cytoplasm of pigmented cells (ages, ≥55 yrs) (**Fig. 2.8a, b, d**). Using sections of anterior midbrains from nine adult control subjects, ≥83% of the anti-tyrosine hydroxylase (TH)-positive neurons were also positive for parkin, as quantified by double labelling (**Fig. 2.8c**). Under these conditions and Ab concentrations, no anti-parkin signal was generated by clone A15165B, which had been successfully used in IP experiments above (**Fig. 2.4a**). Further, in brainstem nuclei outside the *S. nigra*, for example in neurons of cranial nerve III (CNIII) and the periaquaductal grey, as well as in sections of control cortices anti-parkin clones A15165D, -G and -E also stained vesicular-like structures adjacent to the nucleus, albeit at a much lesser intensity than pigmented neurons (Tokarew et al., manuscript in preparation).

Intriguingly, sections from younger control subjects (ages, ≤33 yrs) that were processed in parallel revealed less intense, anti-parkin reactivity in *S. nigra* neurons, which matched the paucity of their intracellular pigment (**Fig. 2.8e**); of note, mature neuromelanin consistently generates a brown color in sections developed without any primary Ab. The different immunoreactivities seen between younger *vs.* older midbrains suggested that the three anti-parkin clones (A15165D, -G and -E) likely reacted with an age-related, modified form of parkin *in situ,* because the *PRKN* gene is already expressed in dopamine cells at a young age (**Fig. 2.1b; Supplementary Fig. 2.1a-d**).

To confirm the specificity of the new anti-parkin clones, we serially stained midbrain sections from a 71 yr-old, male ARPD patient, who was entirely deficient in parkin protein due to compound heterozygous deletions of *PRKN* exons 2 and 3 (**Fig. 2.8f; Supplementary Fig. 2.9a-c**).[809] Development of serial sections with anti-parkin clones A15165E, -D and -G revealed no immunoreactivity in surviving midbrain neurons of the *S. nigra* from this ARPD subject. In the absence of parkin, there was no signal overlap between eDAB reactivity (black color) and either intracellular neuromelanin granules in surviving dopamine cells or with extracellular pigment (brown; **Fig. 2.8f; Supplementary Fig. 2.9c**). In parallel, development of midbrain sections from individuals with the diagnoses of dementia with Lewy bodies, of non-*PRKN*-linked, sporadic PD, as well as, of cases with incidental Lewy bodies readily demonstrated eDAB reactivity overlapping with neuromelanin for all three anti-parkin clones (**Supplementary Fig. 2.9d-g**). These results demonstrated that the staining by the three anti-parkin clones in our microscopy studies of *post mortem* human brain was specific.

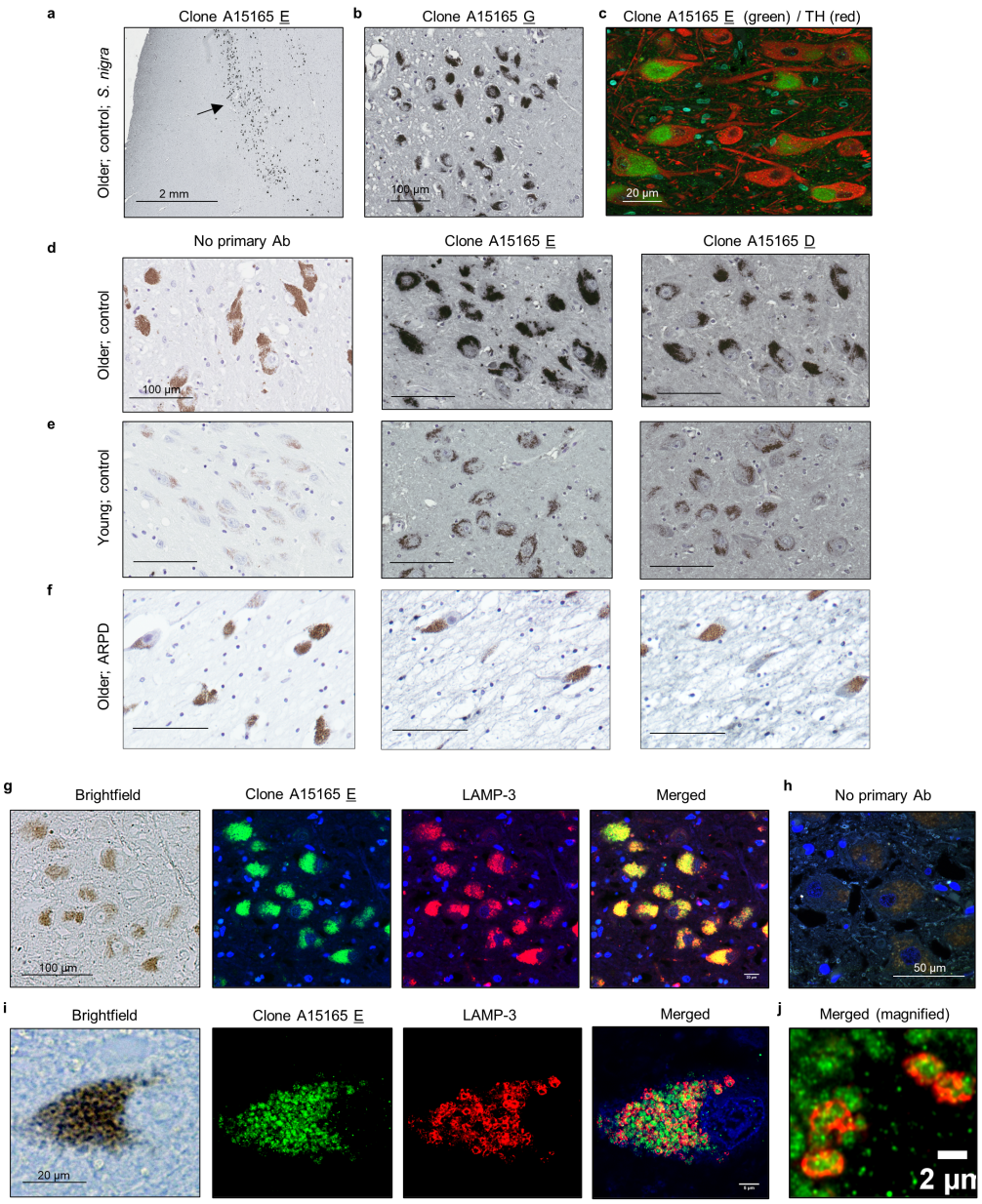

Figure 2.8. Parkin localizes to neuromelanin pigment in *S. nigra* neurons of normal human midbrain
(a-b) Immunohistochemical detection of parkin in adult human brain including dopamine neurons of the *S. nigra* using anti-parkin monoclonal antibody clones A15165 E **(a)** and -G (**b**). **(c)** Double labelling for tyrosine hydroxylase (TH) and parkin (clone A15165 E) in the *S. nigra* from an adult control subject using indirect immunofluorescence microscopy. **(d-f)** Immunohistochemical reactivities generated by no primary antibody *vs.* two anti-parkin (Clones A15165 E, D) antibodies on sections of the *S. nigra* from two control subjects, aged **(d)** 66 yrs and **(e)** 24 yrs, as well as **(f)** from a parkin-deficient ARPD case, aged 71 years. In the indicated panels, immunoreactivity was detected by metal-enhanced DAB (eDAB; generating black colour) and hematoxyline as a counterstain (blue). No primary antibody added generates a pigment-induced signal for neuromelanin (brown). Scale bars represent 100µm, or as indicated. **(g-j)** Immunofluorescent signals, as generated by double-labelling of human *S. nigra* sections containing dopamine neurons, using anti-parkin (clone-E; green colour) and anti-LAMP-3/CD63 (red colour) antibodies; (blue colour, Hoechst stain). Brightfield microscopy image in the same field (neuromelanin pigment is visible; left panel) and a no primary antibody **(h)** run in parallel are shown. **(i)** Higher magnification of a single dopamine neuron and **(j)** further magnification for visualization of subcellular signals within a neighbouring dopamine neuron is shown, as indicated.

Parkin frequently localizes to LAMP-3^{+}-lysosomes within *Substantia nigra* neurons

Neuromelanin granules have been shown to occur in specialized autolysosomes.[82] When screening for co-localization of parkin reactivity with a variety of markers for subcellular organelles in sections of adult control brain, we detected that immunofluorescent signals by anti-parkin (green) and anti-CD63/LAMP-3 (red) antibodies strongly overlapped with pigmented granules of nigral neurons (**Fig. 2.8g-I**; see also **Supplementary Fig. 2.9h**).

Using confocal microscopy, we demonstrated that in adult midbrain anti-parkin signals, as generated by clone A15165E, and neuromelanin granules were frequently surrounded by circular, ~2 μM (in diameter)-sized rings of anti-LAMP-3 reactivity (**Fig. 2.8i, j**). A z-stack video for the parkin and LAMP-3 co-labelling studies is appended (**Supplemental File 2,** online resource, https://doi.org/10.1007/s00401-021-02285-4). We concluded that in the adult, human midbrain from neurologically healthy controls and in surviving neurons of subjects, who suffer from parkinsonism that is not linked to bi-allelic *PRKN* deletion, a pool of parkin appears physically associated with neuromelanin pigment in close association with juxtanuclear, lysosomal structures.

2.6 Discussion

Here, we demonstrate that posttranslational modifications of parkin contribute to its age-related decline in solubility, and in exchange, to redox homeostasis in human brain. Our study also provides insights into the native processing of the PD-linked parkin protein in adult midbrain. Parkin's progressive insolubility in the ageing human brain is relatively unique when compared to other PD-linked proteins and several other cellular constituents, which include mitochondrial proteins. It is also tissue and species-specific. Unlike in the brain, approximately 50% of detectable parkin remain soluble in the spinal cord and in skeletal muscle from aged human subjects, and a comparable loss of parkin solubility is not observed in aged rodent brain and adult monkey cortex (**Fig. 2.1a-d,i; Supplementary Fig. 2.1d**).

In human control brain, the loss of parkin solubility in *post mortem* tissue correlates with a rise in H_2O_2 concentrations and with age, but not with the subject's sex or the length of PMI (**Fig. 2.1e, j, Fig. 2.2a-c**). Although we have analyzed autopsy material with a PMI as short as 2 hrs (**Supplementary Table 2.1**), in future work we will also extend our efforts to the analysis of specimens removed from living subjects during neurosurgical procedures. Using our cohort of specimens, we found that the transition to parkin insolubility in frontal lobe cortices occurs between the ages of 28 and 42 yrs (**Fig. 2.1b; Supplementary Fig. 2.1a-b; Supplementary Table 2.1**). The age at which parkin transitions in the *S. nigra* will require a larger number of midbrain specimens from young, neurologically normal subjects. While we were unable to assess its solubility in midbrains from subjects younger than 20 yrs, parkin's relative distribution in adult midbrain specimens matched the results of control cortices (**Fig. 2.1b**). Of note, in the brainstem nuclei that we examined (i.e*., S. nigra; L. coeruleus;* red nucleus; CN III nucleus; periaqueductal grey), we found that parkin's distribution was not visibly affected by disease state *per se* (11 control cases *vs.* 9 neuropathological cases; **Fig. 2.1b**; **Supplementary Table 2.1**). However, parkin's total abundance was lower in the *S. nigra* of cases from subjects with various forms of neurodegenerative illnesses, as expected. In mice, brain parkin showed partial partitioning when oxidative stress had been induced systemically, either acutely or chronically (**Fig. 2.2c-i**). In future work, we will examine parkin distribution in larger numbers of brainstem specimens of autopsy material from different neuropathological diagnoses.

In accordance, we demonstrate that a key contributor to parkin insolubility is based on thiol-oxidation and that the resulting, post-translational modifications are linked to three protective outcomes: i) the neutralization of a range of potentially toxic, pro-oxidant radicals (ROS, RES); ii) the effective lowering of H_2O_2 concentrations, including its direct reduction *in vitro;* and iii) the apparent effect that parkin has on dopamine metabolism through Cys95-mediated conjugation of its radicals and enhanced

melanin formation. We have modeled parkin's redox chemistry-based function *in vitro*, in cells and in mice, and provide evidence that these outcomes are physiologically relevant to human brain. From these observations we propose that insoluble parkin represents a functionally important protein of the ageing human brain including the *S. nigra*. Further, our findings integrate the early literature related to parkin mutations and stress-induced modifications *vis a vis* its insolubility, which included a wide range of complementary investigations,[442-444,485,487,488,493,502,810] such as findings from induced pluripotent stem cell-derived, human dopamine neurons.[795,811,812] Our discovery of a function for parkin in redox homeostasis also helps explain seemingly disparate evidence of previous observations made in studies of flies, mice [435,437] and humans.[690]

The reactivity of cysteine thiols is governed by their own redox state, as well as, by the surrounding electrostatic environment, which includes the charges of neighbouring residues.[813] Unlike parkin, 34 out of 35 cysteines found in BSA are engaged in disulphide bonds.[814,815] BSA was not able to reduce H_2O_2, nor did it enhance the formation of insoluble melanin polymers *in vitro*. Two other Zn^{2+}-coordinating, cysteine-containing proteins that we tested, RNF43 and $HOIP^{CD}$ (**Fig. 2.5c**), also did not lower H_2O_2, thus suggesting that select cysteines in parkin have a high affinity for ROS and, as discussed below, RES molecules. When mapping the redox state of parkin cysteines under progressively pro-oxidant conditions *in vitro*, we found that Zn^{2+}-coordinating residues at its RING domains are not protected from modifications by ROS[816] (**Supplementary Table 2.2**). This observation suggests that oxidative changes of parkin *in vivo* could occur continuously in the form of a gradient, rather than representing a binary event.

Based on our results, we also estimated the levels of pro- *vs.* anti-oxidant forces. There, the ratio of H_2O_2-to-r-parkin (0.1-1.0 mM of H_2O_2 per 1 ng of r-parkin) was within the physiological range of what we had measured for human control brain extracts (i.e., 0.4-6.0 mM of H_2O_2 per 1 ng of parkin). In the

latter, H_2O_2 concentrations were calculated to lie between 0.7-9.1 mM/mg of tissue (see **Supplementary Table 2.1**). Using semiquantitative Western blotting with aliquots of the same Ab lot (Prk8), parkin concentrations were estimated to be ~1.42 ng/mg brain tissue using r-parkin dilutions as standards; these had been run in parallel with brain lysates of ARPD cortices to demonstrate specificity for the detection of the ~51-53 kDa holoprotein. Although these estimates represent a first approximation of the concentration of wild-type parkin in adult human brain, they may need to be revised in the future based on controlling for potentially confounding variables, such as the presence of truncated species and modified forms (not detected by our antibodies), and/or due to marked variability in parkin's turnover rate in different regions of the cortex and between subjects.

As was observed for r-parkin, we also found cysteine residues that were oxidized in parkin proteins after their affinity isolation from human control cortices and mouse brains, including of Zn^{2+}-binding ones. For example, Cys253 (Cys252 in mice), which helps coordinate Zn^{2+} within parkin's RING1 domain, was frequently identified by us as being oxidized (**Fig. 2.3i; Fig. 2.4e, g**). We predict that variable modifications of non-Zn^{2+}-coordinating residues in human parkin could induce early, conformational changes in parkin's tertiary structure, such as at Cys95, which is located in the - heretofore structurally understudied - linker region, or Cys59, as positioned in its ubiquitin-like (UbL) domain (see **Fig. 2.6e-h**; **Fig. 2.7c-g,** and Chapter 3). Such N-terminally located changes could profoundly affect both the structure and function of other domains in wild-type parkin, as has been convincingly delineated in studies of parkin's E3 ligase activity as a readout following modifications at its UbL domain[192,362,484,487,489-493] (and reviewed by Yi e*t al.* [817]). Our results do not exclude the possibility that other non-thiol-based, posttranslational modifications alter parkin's solubility, such as phosphorylation at Ser65,[483] or at Ser77, which we also found in the brains of MPTP-treated mice. Currently ongoing experiments seek to answer the question as to how structural changes caused by

select ARPD-linked parkin mutants, e.g., p.C431F and p.G328E, as determined by far-UV-circular dichroism, dynamic-light scattering and NMR techniques, could alter redox functions *in vitro*. Their completion will add to our understanding as to how these mutants alter solubility and half-life of nascent parkin proteins in cell-based studies.[442,502]

As mentioned above, *PRKN*-linked ARPD is thought to be pathologically restricted to catecholamine producing cells of the brainstem.[53,185,194,818,819] Dopamine neurons of the *S. nigra* have unique biophysical properties that lead to high bioenergetic demands and the related rise in oxidative stress.[375] Further, unlike in other animals, dopamine is not completely catabolized in human brain, and neuromelanin is thought to be essential for the sequestration and long-term storage of its otherwise toxic metabolites.[86] We found parkin to be involved in mitigating two well-established, PD-linked stressors (i.e., ROS; dopamine radicals), which is indirectly supported by our findings in human brain.

We show that parkin functions as a classic redox molecule that is able to lower H_2O_2 in a thiol-dependent manner. In the absence of wild-type parkin, H_2O_2 concentrations are elevated in human brain (**Fig. 2.5i**), in dopaminergic cells (**Fig. 2.5j, k**) and in brains from mice exposed to MPTP-toxin (**Fig. 2.5h**). There, acute MPTP exposure not only correlated with the loss of parkin solubility but also with oxidation of select cysteines (**Fig. 2.4a**). Hence, *PRKN* expression contributes to anti-oxidant activity *in vivo* through a net reduction in H_2O_2 levels, which can occur in part through its direct reduction, as shown by us *in vitro* (**Fig. 2.5; Supplementary Fig. 2.5**).

Because both MPTP toxin exposure and *Sod2* gene function affect mitochondrial integrity,[57,820] we reason that redox homeostasis in the cytosol, as coregulated by parkin oxidation, could also indirectly influence the health of mitochondria, in addition to E3 ligase-associated mitophagy (and MITAP). Such a cross-talk between cytosol and mitochondria likely includes glutathione metabolism-linked pathways, in which we and others found parkin cysteines to be involved in as well (Chapter 3 and [312,432,433,821,822]).

A role for *PRKN* expression in the neutralization and sequestration of dopamine metabolites may explain why dopamine synthesizing neurons are at greater risk in humans born with parkin deficiency. Previously, parkin has been shown to be uniquely sensitive to dopamine stress leading to aggregate formation[362,493] (**Supplementary Fig. 2.6a, b**). In both cells and mice, *prkn* gene expression has been indirectly implicated in the metabolism of this neurotransmitter, in particular under *ex vivo* conditions, such as induced by high dopamine level-induced stress[362,432,433,641,795,823] (see also **Supplementary Fig. 2.6c, d**).

Our results, and those by others, suggest that dopamine-mediated stress in neural cells is ameliorated when parkin undergoes irreversible modifications by dopamine metabolites. However, in contrast to current interpretations, which stipulate oxidation by quinones is equal to a loss of parkin activity, we posit that such oxidation is part of parkin's physiological role within post-mitotic cells of the adult brain based on two principal findings. First, we demonstrate that wild-type parkin directly interacts with highly electrophilic dopamine metabolites at specific residues, foremost Cys95 (**Fig. 2.6e-h**). This primate-specific cysteine is located within the linker region next to charged residues that impact its electrostatic properties and likely its redox reactivity.[452,813] In support, we found that in addition to dopamine adduct conjugation, Cys95 is vulnerable to ROS attacks (**Fig. 2.3h; Fig. 2.4b, c**), and in parallel studies, is S-glutathionylated when exposed to rising concentrations of oxidized glutathione (Chapter 3). Strikingly, we found that Cys95 is not only required for parkin-dependent enhanced melanin formation, but also for participation in effective H_2O_2 reduction in M17 cells during dopamine stress-mediated toxicity (**Fig. 2.6e-g; Fig. 2.7f-g**).

Second, our finding that parkin augments melanin formation *in vitro*, together with our finding that the protein is closely associated with neuromelanin granules within LAMP-3^+- lysosomes of human brain (**Fig. 2.8g-j; Supplementary Fig. 2.9h**), suggest a role for parkin in dopamine metabolism-linked

neuroprotection (**Supplementary Fig. 2.10**). We have noted with interest that several autopsy reports have described lesser neuromelanin content in surviving neurons of the *S. nigra* in *PRKN*-linked ARPD[195,197,430,824-826] (**Fig. 2.8f**). Intriguingly, variants at the *LAMP3/CD63* locus, as well as, of other dopamine metabolism-related genes, e.g., *GCH-1,* have been recently identified as modifiers of susceptibility to late-onset, typical PD.[119,120,827] However, proof of concept that parkin plays an important, contributing role in the formation of neuromelanin in human brain awaits a suitable animal model.

To date, parkin is best known for its function as an E3 ligase, and the ubiquitin ligation-dependent involvement in mitophagy. Because ubiquitin-ligating activity occurs via cysteine-mediated trans-thiolation, controlling the cellular redox state and functioning as an E3 ligase may not be mutually exclusive. For example, low concentrations of pro-oxidants, as well as sulfhydration, can activate parkin's E3 activity *in vitro*.[484,489,499] A similar duality in functions, i.e., regulating ubiquitylation and redox state in cells, has been previously described for the sensitive-to-apoptosis gene (SAG) product, also known as RBX2 / ROC2 / RNF7.[739,828] It contains a RING finger, and similar to parkin, was found to form HMW oligomers through oxidation of its cysteines.[739,828] SAG protein protects cells from oxidative stress in a thiol-mediated manner in addition to functioning as an E3 ligase.

From this analogy, we postulate that parkin's cytoprotective E3 function and its role in mitophagy are possibly linked to its soluble form within the cytosol, which could be most important during early developmental stages, such as during organ development,[800] in dividing striated muscle cells,[829] and in relatively younger, neural cells including glia.[312] In support, Yi et al. recently described a strong correlation between parkin point mutants, their impact on structure and protein stability *vs.* ubiquitin ligase activity and the degree of mitophagy efficiency.[817] Conversely, other parkin functions, such as

those related to MITAP,[679] inflammation signaling,[680,682] and redox-based neutralization of radicals could be more essential to the sustained health of long-lived, postmitotic cells, e.g., *S. nigra* neurons.

In summary, we have shown that parkin fulfils criteria of a typical redox molecule: the sensing of oxidative (and reducing) stress via its thiols; and the direct, reciprocal redox regulation of its environment, thus conferring protective outcomes. If confirmed by future work, this redox chemistry-based expansion of parkin functions in the ageing human midbrain (**Supplementary Fig. 2.10**) may open the door to test its anti-oxidant role in related neurodegenerative conditions, such as late-onset, non-*PRKN*-linked PD.[830] Most important, our findings emphasize the need for early identification of persons afflicted by bi-allelic *PRKN* gene mutations for the prioritization of appropriate interventions in the future, such as via gene therapy[106] and polyvalent, anti-oxidant therapy.[831]

2.7 Materials and methods

Tissue collection

All tissues were collected in accordance with Institutional Review Board-approved guidelines. Fresh frozen samples of cortical human brain from subjects under 50 years of age were acquired through the University of Alabama and the Autism Tissue Program. *Post mortem*, frozen brain samples from frontal cortices were also obtained from the NICHD Brain and Tissue Bank at the University of Maryland. Brain tissues, including midbrain specimens, with short *post mortem* interval (PMI) were also obtained from patients diagnosed clinically and neuropathologically with multiple sclerosis (MS) according to the revised 2010 McDonald's criteria.[832] There, tissue samples were collected from MS patients, as approved by the Montreal-based CRCHUM research ethics committee. Autopsy samples were preserved and lesions classified using Luxol Fast Blue / Haematoxylin & Eosin staining and Oil Red-O staining, as previously published.[833,834] No inflamed tissue areas were used in the current study. Additional, fresh-

frozen and paraffin-embedded human samples were obtained from the Neuropathology Service at Brigham and Women's Hospital in Boston, MA. and from archived autopsy specimens in the Department of Pathology and Laboratory Medicine of The Ottawa Hospital, Ottawa, ON. Post-mortem, frozen and paraffin embeded brain samples from the cerebral cortex and midbrain of ARPD and their age matched control samples were obtained from the Department of Neurology, Juntendo University School of Medicine. Human spinal cord and muscle tissues were collected *post mortem* from organ donors at The Ottawa Hospital with approval from the Ottawa Health Science Network Research Ethics Board.

Animal tissues

All animal protocols were approved by the review board of the Animal Care and Veterinary Services at the University of Ottawa. Brains and hearts were collected from wild-type C57Bl/6J mice from Jackson laboratories (Bar Harbor, ME); *prkn*-null mice were from Dr. Brice's laboratory[432] and back-crossed onto a pure C57Bl/6J background; *Sod2* +/- mice were from Jackson laboratories (pure C57Bl/6J background), and the bi-genic mouse ($prkn^{-/-}$//$Sod2^{+/-}$) was created by crossing *prkn*-null mice with *Sod2*-haploinsufficient mice, and the interbreeding of heterozygous offspring. These bi-genic mice have been characterized elsewhere (Chapter 3). Following euthanasia by Euthanyl (65mg/mL) intraperitoneal injection, mouse brains were collected and processed on ice in a Dounce glass homogenizer by 20 passes in Tris salt buffer with *vs.* without the addition of 1% hydrogen peroxide (H_2O_2 - Sigma), or 0.1-1 M dithiothreitol (DTT - Sigma), transferred to ultracentrifuge tubes and spun during 30 mins at 163,202.1 x g and 4°C to extract the soluble fraction. The resulting pellets were further homogenized in the tris-salt buffer with the addition of 2-10% SDS, transferred to ultracentrifuge tubes and spun at 163,202.1 x g and 10°C for 30 mins to extract the insoluble fraction. Wild-type mice (of C57Bl/6J or

mixed background, as indicated) were used for analysis of the effects of PMI on murine parkin distribution in the brain. Mice ranging from 4 to 22 mths in age were perfused with PBS, their brains collected and processed, as above. Wild-type SAS Sprague Dawley rats were obtained from Charles River Laboratories; frozen frontal lobe specimens of a cynomolgus monkey were provided by the New England Primate Research Center.

Sequential extraction of parkin from neural tissue

Approximately 1 cm^3 of human frontal cortex and midbrain specimens (age range, 5-85 years) were weighed and placed in 3x volume/weight of Tris-salt buffer (TS; 5 mM Tris, 140 mM NaCl, pH 7.5) containing complete EDTA-free protease inhibitor cocktail, and 10 mM iodoacetamide (IAA, Bio-Rad). The samples were homogenized on ice in a Dounce glass homogenizer by 50 passes, transferred to ultracentrifuge tubes and spun at 163202.1 x g and 4°C for 30 mins. The TS supernatant was transferred to a fresh tube and the pellet was extracted further with addition of 3x volume/weight of Triton X-100 buffer (TX, TS + 2 % Triton X-100). The samples were mixed by vortexing, incubated on ice for 10 min and centrifuged again using the same setting. The TX supernatant was transferred to a fresh tube and the pellet was extracted further with addition of 3x volume/weight of SDS buffer (SDS, TS + 2 % SDS). The samples were mixed by vortexing, incubated at room temperature for 10 min and centrifuged again at 163202.1 x g and 12°C for 30 mins. The SDS supernatant was transferred to a fresh tube and the pellet was either stored at -80°C or extracted further with the addition of 3x volume/weight of 6x non-reducing Laemmli buffer (LB, 30 % SDS, 60 % glycerol, 375 mM Tris; pH 6.8), mixed by vortex and incubated at room temperature for 10 min. Samples were centrifuged again at 163,202.1 x g and 12°C for 30 mins and the LB supernatant was transferred to a fresh tube. Extracted proteins from TS, TXS and SDS buffers including pellet (20-30 μg) and 10-20 μL of LB extracts were run on SDS-PAGE using

reducing (100 mM DTT) and/or non-reducing (0 mM DTT) LB. Following transfer to membranes, Ponceaus S staining (Sigma) was used to probe for equal loading; following washing, membranes were immunoblotted for the detection of parkin (Biolegend 808503, 1: 5,000), DJ-1 (Ab18257, 1: 2,000), α-synuclein (syn-1, 1:1,000 or MJFR-1, 1:2,000), LC3B (3868, 1:2,000), VDAC (MSA03, 1:5,000), MnSOD and GLO1 (each at 1:1,000), calnexin (MAB3126, 1:1,000), cathepsin D (sc-6486, 1:1,000), GRP75 (sc-1058, 1:1,000). ImageJ software (version 1.52 k; National Institutes of Health, USA) was used for signal quantification purposes.

mRNA analyses

PRKN mRNA isolated from individual *S. nigra* dopamine neurons, cortical pyramidal neurons and non-neuronal, mononuclear cells from venous blood were processed, as described[835] and annotated in the Human BRAINcode database (www.humanbraincode.org).

1-methyl-4-phenyl-1,2,3,6-tetrahydropyridine (MPTP) treatment

Eight to 12 mths-old wild-type and *prkn*-null mice were injected intraperitoneally with 40mg/kg of saline or MPTP and sacrificed an hour later.[804] Brains were harvested for ROS measurement, protein analysis by Western blotting and immunoprecipitation of parkin followed by MS analysis. For LC-MS/MS, murine brains were first incubated in IAA prior to homogenization and fractionation, as described above. Brain homogenates were then incubated with anti-parkin conjugated to magnetic beads (Dynabeads Coupling Kit; Invitrogen), as below. A magnet was used to enrich mouse parkin bound to Prk8 conjugated to beads, and several washes were used to remove non-specific proteins. Eluted fractions (IP elute) along with controls (input, unbound, wash and recombinant parkin protein standards) were run on SDS/PAGE under reducing conditions and blotted with anti-parkin. A sister gel was stained

with Coomassie, as described above, and gel slices corresponding to band sizes at 50-75 kDa were excised and analyzed by LC-MS/MS, as described below.

Recombinant protein expression using a pET-SUMO vector

Plasmid cDNA encoding for wild-type and truncated (amino acid 321-465) human parkin proteins were expressed as 6His-Smt3 fusion proteins in *Escherichia coli* BL21 (DE3) Codon-Plus RIL-competent cells (C2527, New England Biolabs), as previous described.[193,458,571] Plasmids encoding for human parkin with p. C95A, p.G328E and p.C431F substitutions were generated with the use of a restriction-free cloning strategy[836] using the following primers:

p.C95A *PRKN* F: 5' CAGAAACGCGGCGGGAGGCgcTGAGCGGGAGCCCCAGAGCT 3'

p.C95A *PRKN* R: 5' CATCCCAGCAAGATGGACCC 3'

p.G328E *PRKN* F: 5' TCCAAACCGGATGAGTGGTG 3'

p.G328E *PRKN* R: 5' CGGGGGCATAACACGCCCcCCATCTGCAGGACACACTC 3'

p.C431F *PRKN* F: 5' CTACTCCCTGCCTTGTGTGG 3'

p.C431F *PRKN* R: 5' GCGGACACTTCATGTGCATaaaGCCTCCATTTTTTTCCACTGG 3'

DJ-1 and *SNCA* coding regions were cloned from pcDNA3.1 into the pET-SUMO vector using PCR and restriction enzymes. A new restriction site for NotI was inserted between SUMO cleavage site and protein start codon in pET-SUMO using the following primers:

pET-SUMO F: 5' GTGATGCCGGCCACGATGCGTCCGGC 3'

pET-SUMO R: 5' TTTTAAGCTTCCgcggccgcCACCACCAATCTGTTC 3'

The inserts containing wild-type *DJ-1* and *SNCA* sequences with 5' NotI and 3' HindIII restriction sites were generated using the following primers and inserted into pET-SUMO using standard conditions:

DJ-1, F: 5' agggcggccgcATGGCTTCCAAA 3'

DJ-1, R: 5’ cctaagcttCTAGTCTTTAAGAACAAGTGGAGCCTTC 3’

SNCA, F: 5’ agggcggccgcATGGATGTATTCATGAAAGG 3’

SNCA, R: 5’ ctTTAAGCTTCAGGTTCGTAGTCTTGATACCCTTCAGA 3’

Quality control steps were performed at the Sequencing Core Facility of the Ottawa Hospital Research Institute (OHRI) to confirm the correct sequences (see **Appendix Fig. C1-5 and C8-10** for schematic of cloning strategies and complete sequencing results).

Transformed bacteria were grown at 37 °C in 2 % Luria Broth containing 30 mg/L kanamycin. All parkin protein-expressing cultures were supplemented with 0.5 mM $ZnCl_2$. Protein expression was induced at 16 °C with isopropyl β-D-1-thiogalactopyranoside (Sigma) using 25 μM for wild-type parkin, and 0.75 mM for truncated parkin, DJ-1 and ulp1 protease. Bacteria were harvested after 16-20 hrs by centrifugation and resuspended in isolation buffer, T500i (50 mM Tris, 500 mM NaCl, 250 μM TCEP, 25 mM imidazole, pH 7.5). Lysozyme (0.1 mg/mL, except for ulp1 protease) treatment and sonication steps (Sonics Vibra Cell) were used to lyse cells. Proteins were collected after 1 hr incubation at 4°C with Ni-NTA agarose and washed several times with buffers T500i and T200i (50 mM Tris, 200 mM NaCl, 250 μM TCEP, 25 mM imidazole, pH 7.5). Fractions of elution buffer T200e (50 mM Tris, 200 mM NaCl, 250 μM TCEP, 250 mM imidazole, pH 7.5) were combined with 2-2.5 mg of 6xHis-tagged ulp1 protease and subsequently dialyzed (6-8 kDa cut-off,) against T200 (50 mM Tris, 200 mM NaCl, 250 μM TCEP, pH 7.5) for 24 hrs at 4°C. Remaining proteins were incubated with Ni-NTA agarose for 1 hr at 4°C. Fractions were collected until no protein was detectable, pooled and concentrated to 1 mg/mL using 10 kDa cut-off centrifugation filters (Millipore). The purity and correct masses of isolated proteins were assessed using electron spray ionization mass spectrometry (Agilent 6538 Q-TOF).

Protein staining methods

All proteins were separated on pre-cast 4-12 % Bis-Tris SDS-PAGE gels (NPO321BOX, NPO322BOX, NPO336BOX) from Invitrogen using MES running buffer (50mM MES, 50mM Tris, 1mM EDTA and 0.1 % SDS, pH 7.3) and Laemmli loading buffer (10% SDS, 20% glycerol, 0.1% bromophenol blue, 0.125M Tris HCl, 200mM DTT or β-mercaptoethanol). Proteins were stained in gel using SilverQuest™ Silver Staining Kit (LC6070) from Invitrogen or Coomassie brilliant blue R-250 dye (20278) from Thermo Scientific using the following protocol: The gel was transferred to a plastic container and rocked for 30 min in Fix Solution (10% acetic acid, 50% methanol), followed by staining for 2-24 h (0.25% Coomassie R250) until the gel turned a uniform blue. The stain was replaced with Destain Solution (7.5% acetic acid and 5% methanol) and the gel was rocked until crisp blue bands appeared. Following a wash with water the gel was stored in 7 % acetic acid. Proteins transferred to PVDF (1620177, Bio-Rad) membranes were stained with Ponceau S solution (Sigma) for 20 min, washed three times with water, imaged and then destained with 0.1M NaOH prior to Western blotting.

Dynamic light scattering assay

For each recombinant protein preparation tested, the buffer (50mM Tris, 200mM NaCl and 250μM TCEP, pH 7.5) was exchanged for a 20mM phosphate buffer with 10mM NaCl (pH 7.4). 20 μM full-length wild-type recombinant parkin was centrifuged at 21,000 x g for 60 min at 4°C and light scattering intensity of the supernatant was collected 30 times at an angle of 90° using a 10 sec acquisition time. Measurements were taken at 37 °C using a Malvern Zetasizer Nano ZS instrument equipped with a thermostat cell. The correlation data was exported and analyzed using the nanoDTS software (Malvern Instruments). The samples were measured at 0, 1, 3 and 5 hours. Following 24 hr incubation, 2 mM DTT was added to the sample and the light scattering intensity of the supernatant was measured again.

Far UV circular dichroism spectroscopy

Fifteen μM of reduced and partially oxidized full-length wild-type, recombinant (r-) parkin was measured at t = 0 and t = 5 days of incubation under native conditions in 20 mM phosphate, 10 mM NaCl buffer. The aggregate-rich phase and the monomer-rich phase in the samples were separated with ultracentrifugation (100,000 x g for 2 hours). Far UV circular dichroism (CD) spectra were recorded for the monomer- and aggregate-rich phase of protein samples using a JASCO J-720 spectrometer. The final spectrum was taken as a background-corrected average of 5 scans carried out under the following conditions: wavelength range 250–190 nm at 25 °C; bandwidth was 1 nm; acquisition time was 1 sec and intervals was 0.2 nm. Measurements were performed in a 0.01 cm cell. CD spectra were plotted in mean residue molar ellipticity units (deg cm^2 $dmol^{-1}$) calculated by the following equation: $[\Theta] = \Theta_{obs}/(10ncl)$, where $[\Theta]$ is the mean residue molar ellipticity as a function of wavelength, Θ_{obs} is the measured ellipticity as a function of wavelength (nm), *n* is the number of residues in the protein, *c* is the concentration of the protein (M), and *l* is the optical path length (cm). Secondary structure analysis of proteins using CD spectroscopic data was carried out using the BeStSel (Beta Structure Selection) software.[837-840]

Cysteine labeling for mass spectrometry

Recombinant protein samples were first prepared by exchanging the T200 buffer for PBS. The protein concentrations were measured and adjusted to 10 μM using PBS. Stock solutions of 500 mM DTT, 100 mM IAA, 100 mM H_2O_2 and 250 mM EDTA were prepared in PBS. A stock of 500 mM NEM was prepared in ethanol immediately before use. For the first optimization and comparison of IAA and NEM labelling (i.e., **Supplementary Table 2.2**), r-parkin was treated with 2 mM DTT for 30 min at 37°C followed by incubation with 5 mM IAA or 85 mM NEM for 2 hr at 37°C. The stepwise Cys labeling

procedure was as follows: A 10 μL aliquot of protein (at 10 μM) was reacted with hydrogen peroxide at various concentrations, as indicated (**Supplementary Table 2.2**) for 30 min (and up to 60 min) at 37°C as indicated. Any unreacted cysteines were alkylated with incubation with 5 mM IAA (either with or, in some runs, without 10 mM EDTA) for 2 hr at 37°C. Previously oxidized cysteines were then reduced by treatment with 40 mM DTT for 30 min at 37°C. Newly reduced cysteines were alkylated by incubation with 85 mM N-ethyl maleimide (NEM) for 2 hr at 37°C. The samples were separated on SDS-PAGE using Laemmli buffer containing 100 mM DTT and proteins visualized using Coomassie staining. Appropriate bands were excised and analyzed by liquid chromatography mass spectrometry (LC-MS/MS).

Protein identification by LC-MS/MS

Proteomic analyses were performed at the OHRI Proteomics Core Facility (Ottawa, Canada). Proteins were digested in-gel using trypsin (Promega) according to the method of Shevchenko.[841] Peptide extracts were concentrated by Vacufuge (Eppendorf). LC-MS/MS was performed using a Dionex Ultimate 3000 RLSC nano HPLC (Thermo Scientific) and Orbitrap Fusion Lumos mass spectrometer (Thermo Scientific). MASCOT software version 2.6.2 (Matrix Science, UK) was used to infer peptide and protein identities from the mass spectra. For detection of dopamine metabolites on parkin, the following variable modifications were included: 5,6-indolequinone ($+C_8O_2NH_3$, m/z shift +145), aminochrome ($+C_8O_2NH_5$, +147), aminochrome +2H ($+C_8O_2NH_7$, +149), and dopamine quinone ($+C_8O_2NH_9$, +151). These samples were prepared for analysis without any use of DTT or IAA. The observed spectra were matched against human sequences from SwissProt (version 2018-05) and also against an in-house database of common contaminants. The results were exported to Scaffold (Proteome Software, USA) for further validation and viewing.

Analysis of the r-parkin holoprotein and of three runs of H_2O_2-exposed r-parkin (**Supplemental Table 2.2**) were also performed at the University of Western Ontario. There, samples were run on a QToF Ultima mass spectrometer (Waters) equipped with a Z-spray source and run on positive ion mode with an Agilent 1100 HPLC used for LC gradient delivery (University of Western Proteomics Facility).

MaxQuant analysis of mass spectrometry data

For select experiments, the raw MS data files were further processed with MaxQuant software version 1.6.5 and searched with the Andromeda search engine[806]. The reference fastas were set to uniprot-human (version 2019-02-12) and uniprot-ecoli. The *E. coli* proteome was included to account for bacterial proteins present in the recombinant protein samples. The 'second peptides' and 'match between runs' settings were enabled. All other settings were left as default. Selected variable modifications included oxidation (Met), acetylation (protein N-terminus), and carbamidomethyl (Cys), as well as custom modifications for pyro-carbamidomethyl (N-terminal Cys), N-ethylmaleimide (Cys), and NEM+water (Cys). For data analyses, site-level intensity values were obtained from the MaxQuant-generated "CarbamidomethylSites" table which combines the intensity of MS1 signals from all peptides covering a particular cysteine residue.

Immunoprecipitation (IP) of brain parkin

Conjugation of anti-parkin antibody (Prk8, 808503, lot B209868) and clone A15165-B (this report: **Supplementary Fig. 2.8c**) to magnetic beads at a final concentration of 10 mg of antibody / mL of beads was carried out following the Magnetic Dynabeads Antibody Coupling Kit from Invitrogen (14311D). Human tissue lysates were also prepared using the Sequential Extraction of Proteins from Neural Tissue protocol, as described above, with addition of 10 mM IAA prior to homogenization.

Equal amounts of protein from TS tissue extracts (n=4) and SDS tissue extracts (n=8) were diluted in TS buffer, resulting in final SDS concentrations of 0.0175- 0.05 % in the SDS extracts. For the IP, anti-parkin primary antibody-conjugated agarose beads were first prepared by multiple washes with 1 mL of TS buffer using centrifugation (1000 x g at 4°C for 3 min) and adhesion to a strong magnet. Amounts of Prk8 conjugated agarose beads used for each experiment were approximated based on the amount of parkin (μg) / sample calculated by densitometry when the sample was compared to recombinant parkin protein standards using Western blotting with Prk8 as primary antibody. The mixture was incubated for 16 hrs at 4°C with slow rotation. Unbound proteins, were separated from the beads by centrifugation (1,000 x g at 4°C for 3 min) followed by adhesion to a strong magnet and saved as the IP "unbound" fraction.

Beads were washed three times with 1 mL of ice-cold RIPA buffer (1 % nonionic polyoxyethylene-40, 0.1 % SDS, 50 mM Tris, 150 mM NaCl, 0.5 % sodium deoxycholate, 1 mM EDTA) using centrifugation (1000 x g at 4°C for 3 min) and adhesion to a strong magnet. Approximately 5-10 μL of each wash was combined and saved as the IP "wash" fraction. To elute antibody-bound proteins, 35 uL of 6X reducing Laemmli buffer (30 % SDS, 60 % glycerol, 0.3 % bromophenol blue, 0.375 M Tris, 100 mM DTT, pH 6.8) was added to the beads and the samples were boiled for 5 min. Following centrifugation (1000 x g at 4°C for 3 min), the supernatant was transferred to a fresh tube labeled "IP elute" and the beads were discarded. To assess IP efficiency, eluted fractions (IP elute), along with controls (input, unbound, wash and recombinant parkin protein standards) were run on SDS/PAGE and blotted with anti-parkin antibody (Prk8, MAB5512 Millipore or 2132S Cell Signaling). Human IP elutes used for mass spectrometry (MS) analysis were incubated with 500 mM NEM (as indicated for select runs) for 16 hr at 4°C prior to SDS-PAGE and further processed for MS, as described above. Gel slices corresponding to band sizes at 50-75 kDa were excised and analyzed by LC-MS/MS.

Reactive oxygen species (H_2O_2) measurements in recombinant protein preparations, cell lysates and tissue homogenates

An Amplex® Red hydrogen peroxide/peroxidase assay kit (Invitrogen A22188) was used to monitor endogenous levels of H_2O_2 in aliquots of tissues and cells, and in test tubes following either exposure to increasing concentrations of H_2O_2, n-ethylmaleidmide (NEM), and ethylenediaminetetraacetic acid (EDTA), or after incubation with either select, recombinant parkin proteins, or DJ-1, α-synuclein, bovine serum albumin (Thermo Scientific), ring finger protein 43 (RNF43 - BioLegend, MA.), HOIL-1-interacting protein (HOIP - Boston Biochem, MA.), glutathione (Sigma), or catalase (Sigma) for 30 mins at room temperature. Pre-weighed cortex pieces from human brain and pelleted cells were homogenized on ice in the 1x reaction buffer provided (Invitrogen A22188) using a Dounce homogenizer (3x volume to weight ratio). Homogenates were diluted in the same 1x reaction buffer (5- to 10-fold). A serial dilution of the H_2O_2 standard provided was prepared (20, 10, 2 and 0 μM). Fifty μL of standards and samples were plated in a 96-well black plate with clear flat bottom (Thermo Fisher Scientific). The reaction was started by the addition of 50 μL reaction buffer, Amplex® Red and horseradish peroxidase (HRP) (10 mM Amplex® Red and 10 U/mL HRP). Plates were incubated at room temperature for 30 mins protected from light. A microplate reader was used to measure either fluorescence with excitation at 560 nm and emission at 590 nm, or absorbance at 560 nm. The obtained H_2O_2 levels (μM) were normalized to the tissue weight (g) or protein concentration (μg/μL). The same assay was also used to measure parkin and glutathione's peroxidase activity compared to horseradish peroxidase.

Chemiluminescence-based, direct reactive oxygen species assay

The assay was modified from Muller et al. 2013[842] to measure the ROS-quenching ability of parkin proteins, DJ-1, GSH, and catalase. Protein concentrations were quantified using Bradford assay and adjusted to 5, 10, 15 and 30 μM in buffer not containing TCEP. Bovine serum albumin (BSA; 10 and 20 μM; Thermo Scientific), glutathione (15, 20, 200, 400, 800 and 2000 μM; Sigma), and catalase (0.015, 0.15, 0.25 and 15 μM, Sigma) were prepared. Stock solutions of H_2O_2 for standard curve were prepared at 5, 10, 20, 40 and 50 mM in 0.1 M Tris HCl pH 8.0 using 30 % H_2O_2. Stock solutions of 300 mM luminol and 40 mM 4-iodophenol were prepared in DMSO and protected from light. Signal reagent, containing 1.94 mM luminol (Sigma) and 0.026 mM 4-iodophenol (Sigma), was prepared in 0.1 M Tris HCl pH 8.0 and protected from light. A 0.4 % horseradish peroxidase solution was prepared using HRP-linked anti-rabbit secondary antibody diluted in Stabilizyme solution (SurModics SZ02). Each read was set up in triplicate on a white polystyrene 96-well plate (Thermo Scientific 236105) and to each well was added 80 μL Stabilizyme, 15 μL of 0.4 % horseradish peroxidase (HRP) and 25 μL of sample or controls. One of the injectors in a Synergy H1Multi-Mode Plate Reader (Bio Tek) was primed and set to inject 15 μL of signal reagent and 15 μL of each H_2O_2 stock solution was manually added to corresponding controls and samples just prior to reading. Final concentrations of reagents were 0.04 % HRP, 500, 1,000, 2,000, 4,000 and 5,000 μM H_2O_2, 194 μM luminol, 2.6 μM 4-iodophenol and 0.8, 1.7, 2.5 or 5 μM of protein. The plate reader was set to measure luminescence every 1 min for a total of 10 min.

The resulting kinetic data were converted to area under the curve (AUC) using Prism softaware version 6. For samples pre-incubated with 20 mM iodoacetamide (Bio-Rad), a stock solution of 1 M iodoacetamide was prepared. To each well containing 25 μL of sample, 0.52 μL of 1 M iodoacetamide

and 0.48 µL of buffer not containing TCEP was added and the samples were incubated for 2 h at 37°C. Following incubation, the reagents for chemiluminescence were added as above except 79 µL of Stabilizyme was used instead of 80 µL and the samples were analyzed as above.

Thiol quantification in recombinant proteins

Recombinant protein samples were first prepared by exchanging the T200 protein buffer (50 mM Tris, 200 mM NaCl and 250 µM TCEP, pH 7.5) for T200-TCEP using repeat centrifugations (8 times 4000 x g at 4°C for 10 min) in Amicon Ultra 10 kDa MWCO filters (Millipore). The protein concentrations were measured and recorded. A glutathione stock solution of 32,539 µM was prepared by dissolving 1 mg glutathione (GSH) in 1 mL of T200 and the standards 0, 50, 101, 203, 406, 813 and 1000 µM were prepared by serial dilution in T200. The reaction buffer (0.1 M sodium phosphate, pH 8.0) was prepared by adding 93.2 mL 1M Na_2HPO_4 and 6.8 mL of NaH_2PO_4 in 1 L of water. Thiol detecting reagent (Ellman's reagent) was prepared by dissolving 2 mg of 5,5'-dithio-bis-[2-nitrobenzoic acid] (DNTB; Sigma) in 1 mL of reaction buffer. The assay was performed in 96-well clear round bottom plates (Corning) by adding 50 µL of thiol detecting reagent to 50 µL of sample or standard and incubating for 15 min at room temperature.

The resulting 5-thio-2-nitrobenzoic-acid (TNB) produced was measured by absorbance at 412 nm using a Synergy H1Multi-Mode Plate Reader (Bio Tek). The amount of free thiols detected in each sample was calculated using the regression curve obtained from the glutathione standards and dividing by the concentration of the sample.

Zinc ion release assay

A zinc quantification kit (Abcam – ab102507) was used to assay zinc ion (Zn^{2+}) release from proteins. Recombinant human proteins (wild-type r-parkin and r-DJ-1) were spun in 10 or 30 kDa cut-off centrifugation filters (Millipore) to remove residual TCEP. Increasing concentrations of protein (0 to 2.5 μM) were incubated under basal conditions or with the addition of H_2O_2 (2 mM) or DTT (100mM) for 30 mins at 37°C. A standard curve was prepared using a zinc standard (stock, 50 mM) provided by the manufacturer. Two hundred μL of reaction mixture was added to 50 μL standards and samples on 96 well pates (Thermo Fisher Scientific) followed by incubation at room temperature for 10 mins. A microplate reader was used to measure the absorbance at OD560 nm. The background was corrected by subtracting the value derived from wells of zero zinc standard from all readings.

Cell cytotoxicity assay

Human neuroblastoma cell lines (M17) without transduction (controls), or transduced by vector-only plasmid (Myc-tag), or those with low levels of stable expression of Myc-parkin cDNA (P5) and high levels of stable expression of Myc-parkin (P17), or sister lines transiently over-expressing FLAG-parkin (wild-type), FLAG-vector and FLAG-parkin carrying one, of three, point mutations (p.C431F; p.G3289E; p.C95A) were grown in 6-well culture plates at $0.3x10^6$ cell density (80% confluence). There, Opti-MEM media (Gibco 11052-021) contained heat inactivated fetal bovine serum (Gibco 10082-147), Pen/strep/Neo (5mg/5mg/10mg; Gibco 15640-055), MEM-non-essential amino acids (10mM; Gibco 11140-050) and sodium pyruvate (100mM). For rescue experiments, M17 cells transiently expressing cDNA for FLAG-vector, FLAG-parkin wild-type, and variants carrying p.G328E, p.C431F, or p.C95A-encoding parkin protein were used. There, 4 μg of cDNA was transfected using a 1:1 ratio of cDNA to Lipofectamine 2000 (52887, Invitrogen) in OPTI-MEM transfection medium.

Lipofectamine 2000 and cDNA were first incubated for 20 min at room temperature before being applied directly to the cells for 1 hr at 37°C with 5 % CO_2 followed by direct addition of fresh growth medium. The cells were incubated another 20-24 hrs at 37°C with 5 % CO_2.

Dopamine hydrochloride (Sigma) 200 mM stock was prepared. Cells were washed with fresh media once and then incubated with media alone or supplemented with dopamine at final concentrations of 20 μM and 200 μM for 18-20 hr. Post dopamine exposure, conditioned media were collected for cytotoxicity assays and cells were harvested for lysis in TS buffer, vortexed and centrifuged. Supernatants were collected and saved for Western blot analyses and to be assessed for cytotoxicity. Cell pellets were suspended in 2-10% SDS buffer and centrifuged to collect the 'insoluble fraction'.

Vybrant ^{TM} cytotoxicity assay kit (Molecular Probes V-23111) was used to monitor cell death through the release of the cytosolic enzyme glucose 6-phosphate dehydrogenase (G6PD) by damaged cells into the surrounding medium. Fifty μl of fresh media (without any exposure to cells) as well as conditioned media from control and stressed cells, in addition to lysates of M17 cells (as positive control for maximum G6PD), were added to a 96-well microplate. Fifty μl of reaction mixture containing buffer (as per manufacturer) and resazurin, which reacts with G6PD generating fluorescently detectable resorufin, were added to each well, and the mircroplate was incubated at 37°C for 30 mins. A microplate reader was used to measure either fluorescence with excitation at 560 nm and emission at 590 nm, where the rise in fluoresence indicates a rise in G6PD levels as a surrogate marker of cell death.

Aminochrome synthesis

A solution of 0.1 M sodium phosphate buffer pH 6.0 was prepared from a mixture of 12 mL of 1M NaH_2PO_4 and 88.0 mL of 1M Na_2HPO_4. The reaction buffer (0.067 M sodium phosphate, pH 6.0) was prepared by adding 33 mL of 0.1 M sodium phosphate buffer to 17 mL water. A solution of 10mM

dopamine in reaction buffer was prepared by adding 19 mg of dopamine hydrochloride (Sigma) to 1 mL of reaction buffer. Oxidation was activated by adding 5 µL of tyrosinase (25,000 U/mL; Sigma) and the mixture was incubated at room temperature for 5 min. Tyrosinase was separated from the oxidized dopamine using a 50 kDa cut-off Amicon Ultra centrifugation filter (Millipore) by centrifuging at 21,000 x g for 10 min. The absorbance of the filtrate was measured at a wavelength of 475 nm (Ultrospec 2100 pro spectrophotometer, Biochrom) and the concentration of aminochrome was determined using the Beer-Lambert equation and extinction coefficient of 3058 L x mol^{-1} x cm^{-1}.

Redox chemistry reactions including oxidation of cysteine-containing proteins in vitro

Purified, recombinant proteins were prepared by removing excess TCEP, present in the elution buffer, by using repeat centrifugations (8 times 4000 x g at 4°C for 10 min) in Amicon Ultra 10kDa MWCO filters (Millipore). Protein concentrations were measured and adjusted to 20 µM. Stock solutions of hydrogen peroxide (H_2O_2, 9.8 mM) were prepared. An aliquot of 10 µL of each protein sample (at 20 µM) was reacted with oxidants at the following concentrations: 0, 1.0, 2.5, 5.0, 7.5 and 10 mM for H_2O_2, and 0, 10 µM, 100 µM, 1 mM, 10 mM, 100 mM, 1000 mM for DTT. Samples were treated for 30 min at 37°C and centrifuged at 21,000 x g for 15 min. The supernatant was transferred to a fresh tube and the remaining pellet was extracted with 10 µL of T200 containing either 10 % SDS or 100 mM DTT. The pellets were incubated again for 30 min at 37°C and centrifuged at 21,000 x g for 15 min. Laemmli buffer (10 µL, containing 100 mM mercaptoethanol) was added to both the pellet and supernatant fractions and samples were separated by SDS-PAGE and visualized by silver staining. Specific bands of aminochrome-treated wild-type, full length r-parkin were excised and analyzed by LC-MS/MS, as described above.

In vitro melanin formation assay

Recombinant protein samples were first prepared by exchanging the T200e protein buffer (50 mM Tris, 200 mM NaCl and 250 μM TCEP, pH 7.5) for T200 (50 mM Tris and 200 mM NaCl, pH 7.5) using repeat centrifugations (8 times 4,000 x g at 4°C for 10 min) in Amicon Ultra 10 kDa MWCO filters (Millipore). The protein concentrations were measured and adjusted to 20 μM using T200. A 0.067 M sodium phosphate buffer, pH 6.0, was prepared by adding 33 mL of 0.1 M sodium phosphate buffer to 17 mL water and adjusting the pH using HCl. A stock solution of 100 mM dopamine hydrochloride was prepared in 0.067 M sodium phosphate buffer and stock solutions of 100 mM reduced glutathione and H_2O_2 were prepared in T200.

Samples and controls were prepared in 100 μL total volume that contained 10 μL of protein sample or T200, 10 μL of 100 mM dopamine or 0.067 M sodium phosphate buffer, 10 μL of 100 mM glutathione or T200 buffer, and 70 μL T200. Unless otherwise indicated, the final concentration of protein was 2 μM and the final concentration of reagents was 10 mM. The samples and controls were plated in triplicate, and absorbance read at 405 and 475 nm every 90 sec for 1 hr and up to 4 hr (Synergy H1Multi-Mode Plate Reader; Bio Tek).

Immunohistochemistry

Immunohistochemistry (IHC) was performed on paraffin-embedded sections, as previously described.[152,689,843] Briefly, prior to antibody incubation, sections were deparaffinized in xylene and successively rehydrated through a series of decreasing ethanol concentration solutions. Endogenous peroxidase activity was quenched with 3% hydrogen peroxide in methanol, followed by a standard citric acid-based antigen retrieval protocol (CitriSolv, Decon Labs) to unmask epitopes. Sections were blocked in 10-20% goat serum in PBS-Tween (Tween 20 0.075%) to reduce non-specific signal. Sections were

incubated overnight at 4°C in primary antibodies diluted in 1-5% goat serum in PBS-T according to the following concentrations: novel anti-parkin mAbs from Biolegend clones D (BioLegend, A15165-D; 1:250), clone E (BioLegend, A15165E; 1:2,000), and clone G (1:250), Prk8 (BioLegend, MAB5512; 1:500) as well as anti-LAMP-3/CD63 (Santa Cruz, SC5275; 1:100), anti-LC3B (Sigma, L7543-200uL; 1:100), anti-VDAC (MitoScience, MSA03; 1:100). Biotinylated, secondary antibodies (anti mouse IgG (H+L), Vector Labs, BA-9200, and biotinylated anti-rabbit IgG (H+L), both made in goat; Vector Labs, BA-1,000) were diluted to 1:225, and sections were incubated for 2 hr at room temperature. The signal was amplified with VECTASTAIN® Elite® ABC HRP Kit (Vector Labs, PK-6100), and visualized via standard diaminobenzidine solution (DAB, 55 mM), or Vina green (Biocare Medical, BRR807AH), or most frequently by using 'metal enhanced DAB' (Sigma, SIGMAFAST™ DAB with Metal Enhancer D0426). Samples were counterstained with Harris Modified Hematoxylin stain and dehydrated through a series of increasing ethanol concentration solutions and xylene. Permount (Fisher Scientific, SP15-100) was used for mounting and slides processed for IHC were visualized and processed using a Quorum Slide Scanner at the OHRI Imaging Core Facility.

Immunofluorescence and confocal microscopy

Paraffin-embedded human midbrain sections were stained by routine indirect immunofluorescence (IIF) with the following details. Antigen retrieval was performed in Tris-EDTA buffer pH 9.0 for 10 min. Primary antibodies were incubated overnight at 4^{o}C. Details for primary antibodies anti-parkin clone E (1:500), anti-LAMP-3 (1:250) are described above. Fourty min-long incubations with the following secondary antibodies were performed: goat anti-mouse alexa fluor 488 (1:200), goat anti-rabbit alexa fluor 594 (1:500). Slides were mounted with fluorescence mounting medium using DAPI. Sections

stained for IIF were imaged using a Zeiss LSM 880 AxioObserver Z1 with an Airyscan Confocal Microscope, and then processed for further analysis using Zeiss Zen and Fiji software.

Statistical analyses

Statistical analyses were performed using GraphPad Prism version 6 (GraphPad Software, San Diego, CA, USA, www.graphpad.com). Differences between two groups were assessed using an unpaired Student T-test. Differences among 3 or more groups were assessed using a one-way or two-way ANOVA followed by Tukey's post hoc corrections to identify statistical significance. Select post hoc tests are depicted graphically to visualize significance. For all statistical analyses, a cut-off for significance was set at 0.05. Data are displayed with p values represented as *$p < 0.05$, **$p < 0.01$, ***$p < 0.001$, and ****$p < 0.0001$. Linear regression (for continuous dependent variable, e.g., % soluble parkin and H_2O_2 concentration) was performed using R version 3.6.0. Furthermore, to address the effect of age on parkin solubility (defined as a dichotomous variable using criteria below), logistic regression and receiver operating characteristic (ROC) curves and area under the ROC curve (AUC) values were calculated using R, as reported.[152]

2.8 Acknowledgements

We are grateful for the commitment of patients and their families to participate in autopsy studies. We thank Dr. J. Palacino for creating stable M17 cell lines, Drs. A. Brice and E. Fon for sharing *prkn*-null mice, Dr. B. Madras for providing specimens of cynomolgus brain, Drs. R. Tam, L. Dong, and Ms. K. Solti for technical support, Dr. D. Gibbings for antibodies, Dr. D. Gray for assistance with confocal imaging, Drs. M. Medina and R. R. Ratan for encouragement, Drs. S. Bennett, D. Pratt for discussions, and Drs. H. Lochmueller, M. Rousseaux and past members of the Schlossmacher lab for their

suggestions. **Funding:** This work was supported by the: Parkinson Research Consortium of Ottawa (J.M.T., D.N.E.K., J.J.T.); Queen Elizabeth II Graduate Scholarship Fund (J.M.T.); Government of Canada [Natural Sciences and Engineering Research Council of Canada (J.K.); Canadian Institutes of Health Research (CIHR) MD/PhD Program (J.M.T., A.C.N.); CIHR Research Grant (G.S.S., A.P.); CIHR Canada Research Chair Program (M.G.S., A.P.)]; Michael J. Fox Foundation for Parkinson's Research (P.T., J.J.T., L.Z., M.G.S.); The Research Foundation of the Multiple Sclerosis Society of Canada; Progressive Multiple Sclerosis Alliance (A.P.); Hungarian Brain Research Program (G.T.); Uttra and Sam Bhargava Family (E.T., M.G.S.); and The Ottawa Hospital (E.T., M.G.S.).

2.9 Supplementary figures and tables

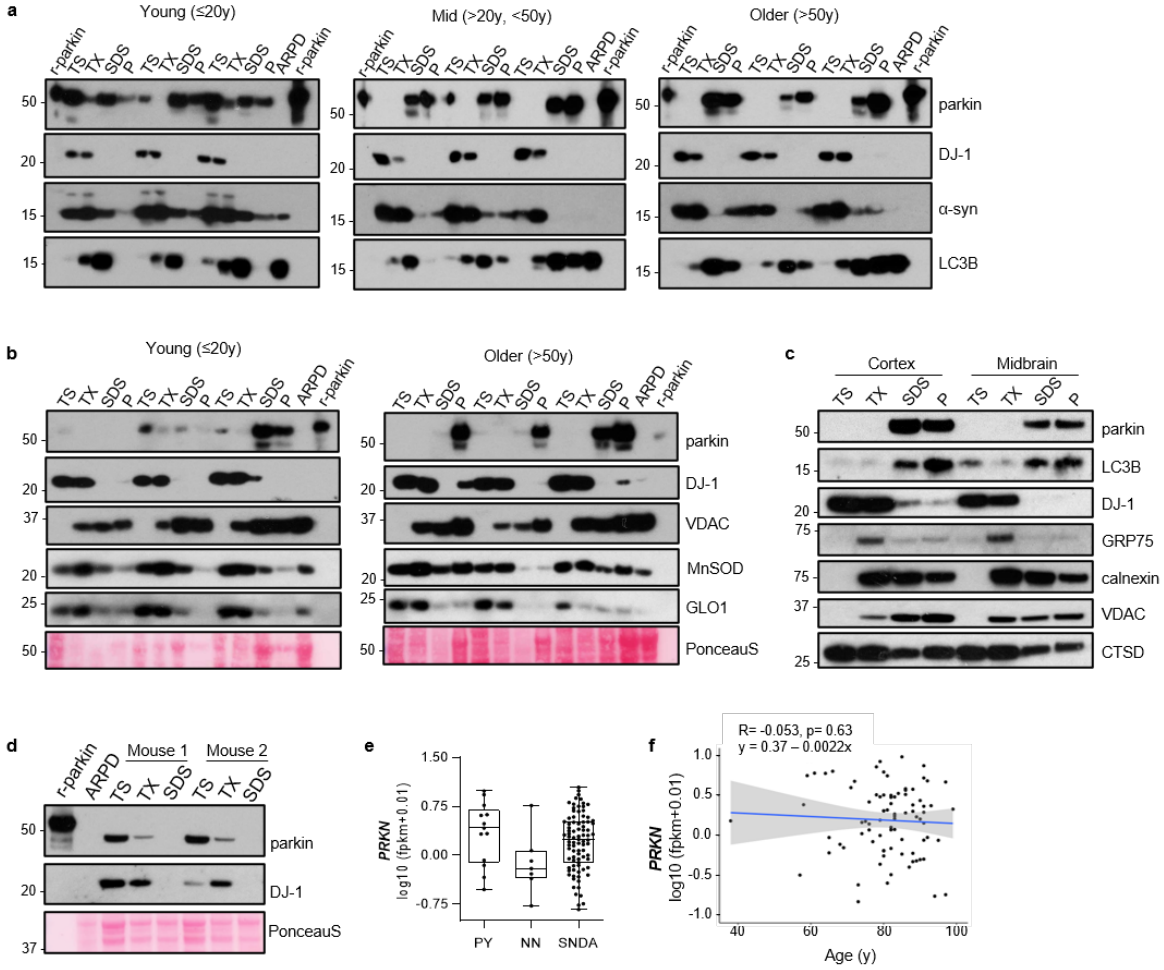

Supplementary Figure 2.1. Parkin becomes largely insoluble with progression in age in post mortem human brain
(**a**) Western blots of parkin, DJ-1, a-synuclein and LC3B distribution in 9 representative human cortices (see **Supplementary Table 2.1**). Tissue fractionation and age ranges were as described in **Fig. 2.1**; SDS/PAGE experiments run under reducing conditions; SDS-extracted fractions of parkin-deficient PD cortices (ARPD) and r-parkin are included as controls.
(**b**) Western blots of parkin, DJ-1, VDAC, MnSOD and glyoxalase-1 proteins, and Ponceau S staining in serially fractionated human cortices from younger (n=3) and older (n=3) individuals. Quantification of relative protein distribution is shown in **Fig. 2.1g**. **(c)** Western blot of indicated proteins from serially fractionated cortex and midbrain from a single donor as described in (**a**). (**d**) Quantification of log-transformed *PRKN* mRNA signals from individual pyramidal neurons (PY), leukocytes (non-neuronal cells; NN) and *S. nigra* dopamine neurons (SNDA) isolated from post mortem control brains (age range, 38 to 99 yrs). (**e**) Linear regression analysis of log-transformed PRKN transcripts as a function of age in human control *S. nigra* dopamine neurons where each dot represents values for a single neuron, as shown in (**d**).

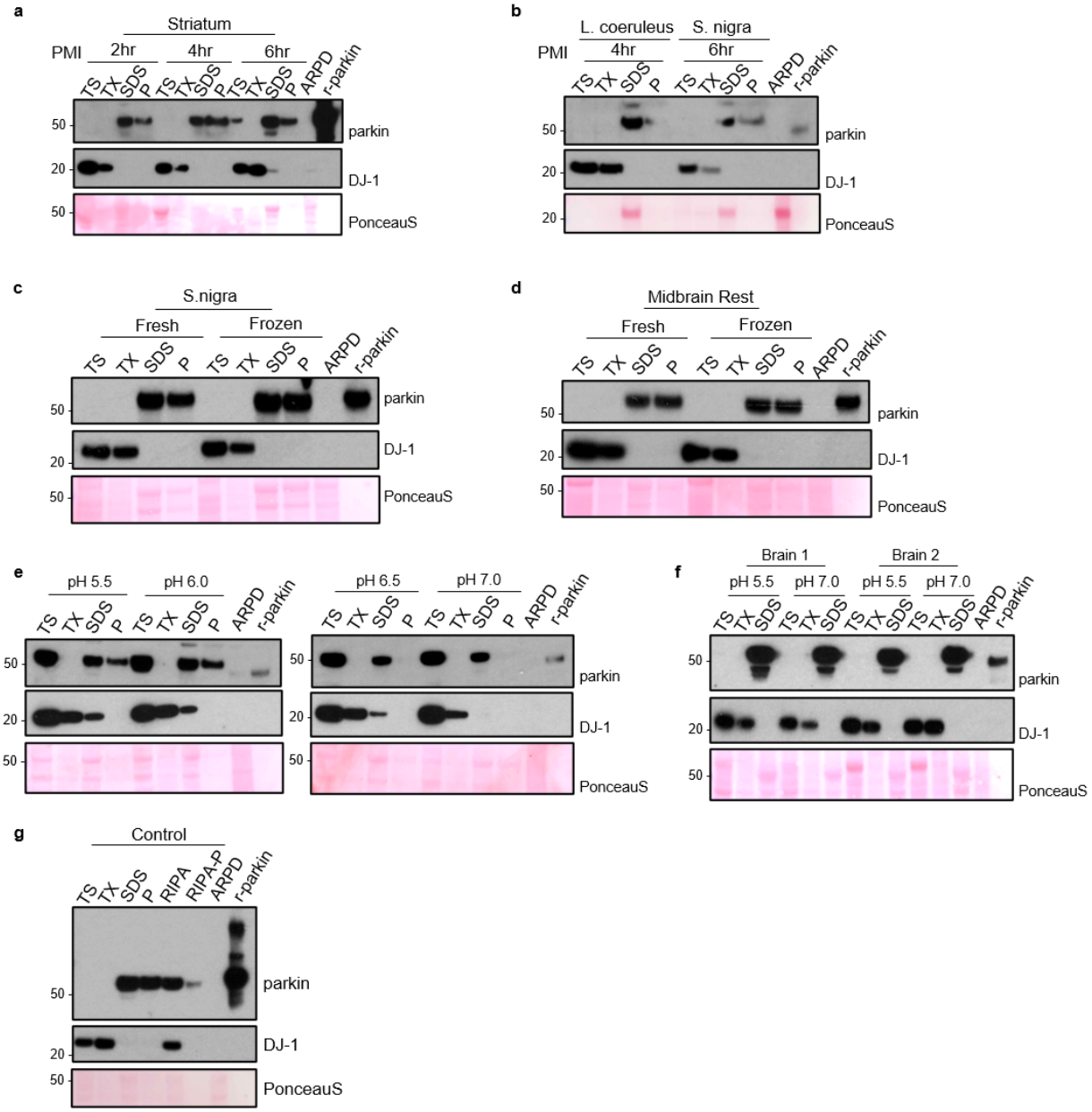

Supplementary Figure 2.2. Parkin solubility in human brain is not detectably altered by length of *post mortem* interval, tissue freezing, or pH levels of the buffer

(**a-b**) Western blots of parkin and DJ-1 distribution as well as Ponceau S staining for fractions of human brain tissue from striatum (**a**), *L. coeruleus* and *S. nigra* (**b**) with short *post mortem* interval (2-6 hrs, as indicated). (**c-d**) Western blots, as described in (a), from dissected *S. nigra* (**c**) and posterior midbrain structures comprising nucleus of cranial nerve-III and the periaqueductal grey (**d;** rest). Tissues were collected *post mortem* and parkin distribution visualized in aliquots of the same specimens processed in parallel after being kept at 4^{o}C or processed via one-time freezing to -80^{o}C and subsequent thawing prior to serial fractionation. (**e-f**) Western blots of parkin and DJ-1 distribution as well as Ponceau S staining in fractions of human cortex (**e**), single brain; (**f**), two different brains) serially extracted in parallel using standard buffers with varying pH, as indicated.(**g**) Western blots of parkin and DJ-1 distribution in a human cortex sample following serial fractionation with TS- TX-, SDS- and Pellet buffers compared to processing by standard RIPA buffer, where the pellet after RIPA extraction is denoted as RIPA-P.

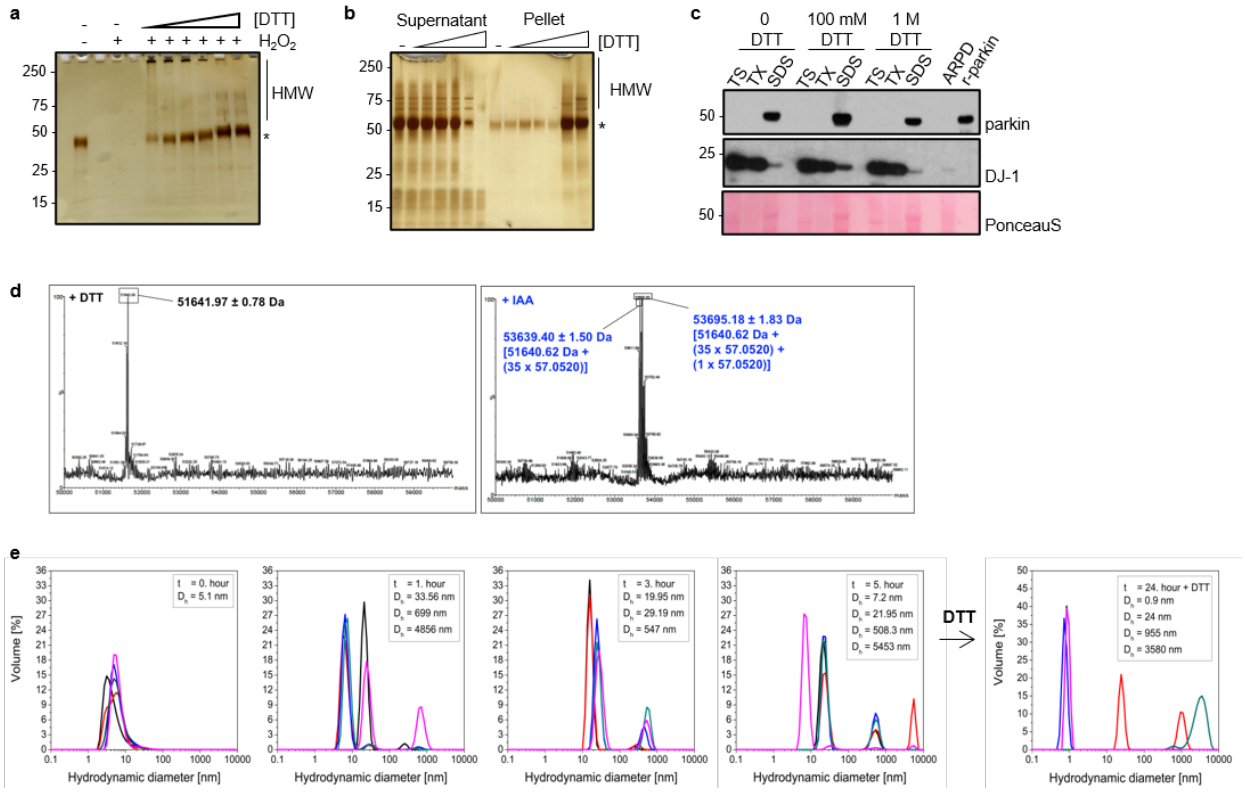

Supplementary Figure 2.3. Oxidation of human parkin thiols promotes insolubility

(**a**) Silver stained gel of wild-type, human r-parkin exposed to H_2O_2 (10 mM), followed by treatment with increasing concentrations of DTT (0-100 mM) prior to centrifugation and loading of the supernatant onto SDS/PAGE, run under non-reducing conditions. (**b**) Detection of r-parkin in soluble (supernatant) and insoluble phases (pellet; recovered by 10% SDS-containing buffer) following exposure to increasing concentrations of DTT (0-1M), run under non-reducing conditions.
(**c**) Western blot analyses with anti-parkin and anti-DJ-1 as well as Ponceau S staining of three dissected pieces from a single human cortex specimen serially extracted in parallel by TS-, TX- and SDS-buffer without (0 mM DTT) or including either 100 mM or 1M DTT in the extraction buffers, as indicated, run under reducing conditions. (**d**) Spectra from LC-MS/MS analyses of recombinant (r-), human, wild-type parkin holoprotein (without any trypsin digestion) without pre-labelling (panel on the left) and after tagging of 35 *vs.* 36 thiol-carrying residues by iodoacetamide (IAA; right panel), corresponding to the three main peaks (one in left panel; two in right panel), as indicated. The 51,641.97 Da peak closely matches its calculated mass of 51,640.62 Da; 53,639.40 Da corresponds to the conjugation of 35 IAA adducts; 53,695.18 Da corresponds to 36 IAA adducts, indicating that all 35 cysteine residues and either the N-terminal amino group or a single methionine residue was IAA-modified. (**e**) Dynamic light scattering analysis showing progressive size changes, as measured in hydrodynamic diameters (nm), as monitored during 0, 1, 3 and 5 hrs at room temperature. The structural state for wild-type, human r-parkin under non-reducing, native conditions showed increased aggregate formation over time, which was partially reversed by DTT.

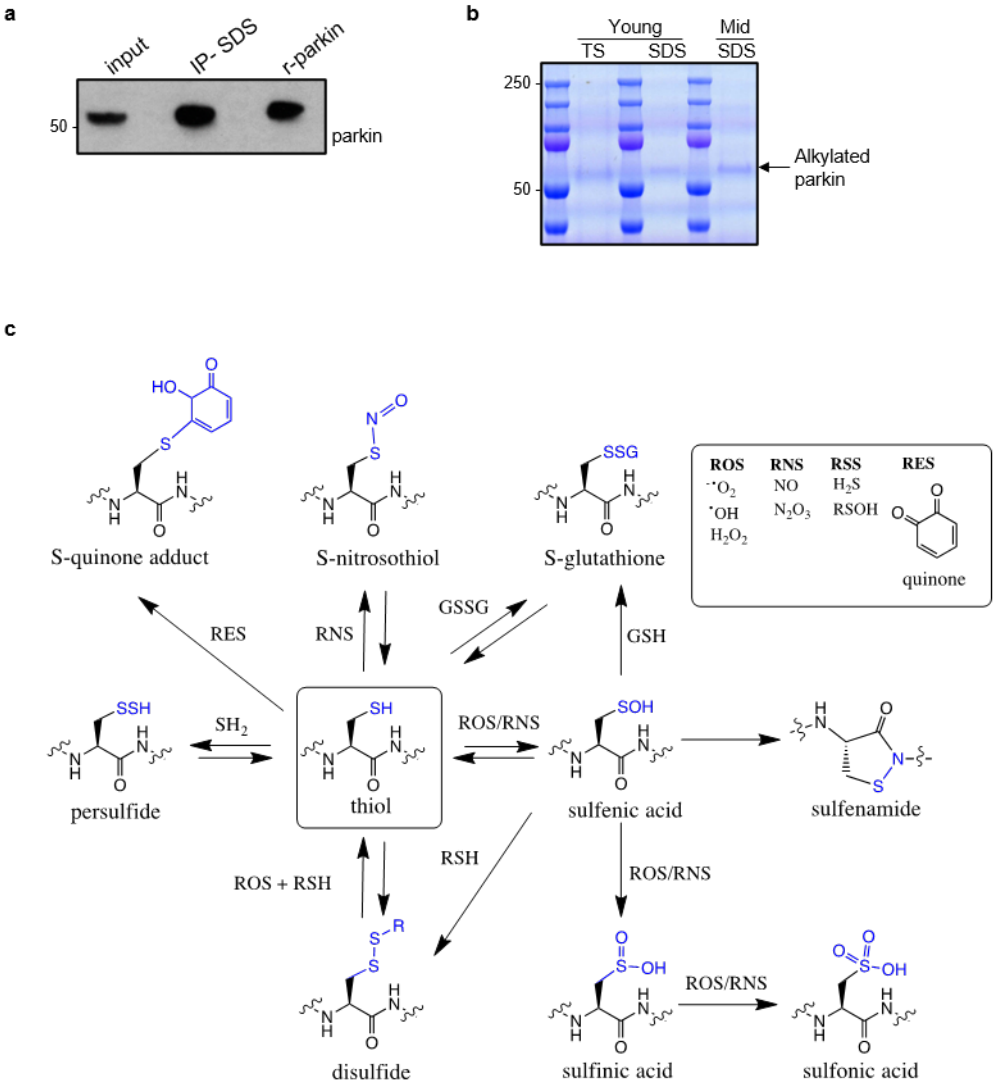

Supplementary Figure 2.4. Immunoprecipitation of parkin from human brain and summary of redox-related thiol chemistry

(**a-b**) Representative Western blot (**a**) and Coomassie blue-stained **(b)** visualization of parkin immunoprecipitated from human frontal lobe cortex, as described [Shimura and Schlossmacher, Methods Enzymol 2005] by monoclonal anti-parkin A15165-B and visualized by polyclonal anti-parkin 2132, in preparation for LC-MS/MS (see also **Fig. 2.4**). Brain tissue was homogenized in the presence of IAA to prevent the oxidation of reduced thiols during processing, thereby generating alkylated-parkin monomers at the 51-54 kDa position. (**c**) Schema of select, reversible and irreversible cysteine modifications that can occur on thiols (-SH) due to attacks by reactive oxygen species (ROS), reactive nitrogen species (RNS), reactive sulfur species (RSS) and reactive electrophilic species (RES), which include dopamine quinones. Graphic summary was modified from Alcock *et al.,* 2018.[695]

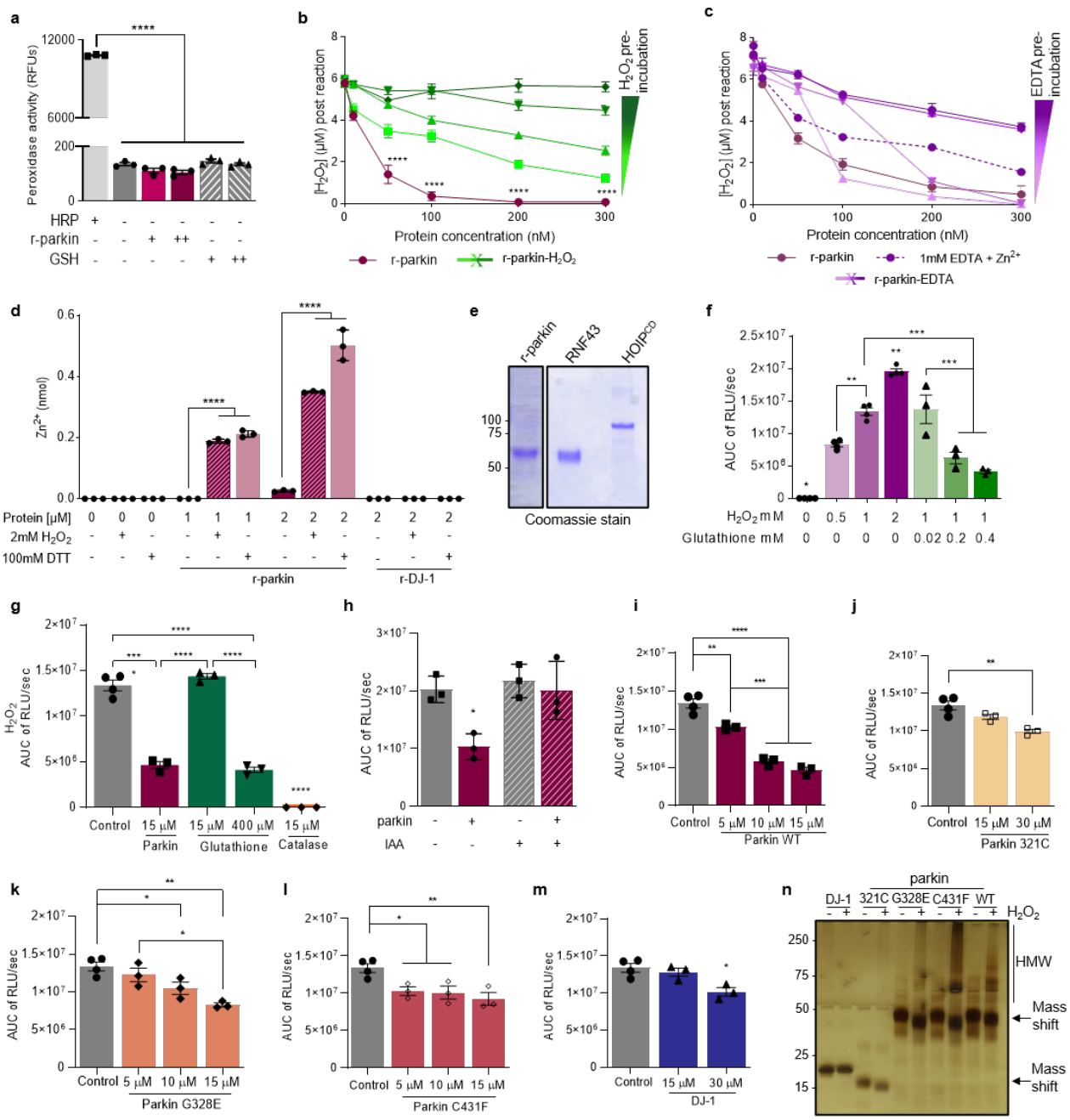

Supplementary Figure 2.5. Parkin directly reduces hydrogen peroxide in a concentration- and thiol integrity-dependent but non-enzymatic manner (legend on following page)

Supplementary Figure 2.5. Parkin directly reduces hydrogen peroxide in a concentration- and thiol integrity-dependent but non-enzymatic manner

(**a**) Peroxidase enzymatic activity for r-parkin and glutathione (GSH; +, 0.5μM; ++, 1μM), as tested *in vitro* in comparison to horseradish peroxidase (HRP, 1mU/mL). Mean peroxidase activity ± SEM. ****p<0.0001 by one-way ANOVA with Tukey's post hoc test; [F (5, 12) = 81945, p< 0.0001]. (**b-c**) Quantification of H_2O_2 concentrations by AmplexRed following incubation of increasing levels of r-parkin (**b**) pre-oxidized with increasing concentrations of H_2O_2, or (**c**) treated with increasing concentrations of EDTA or EDTA with excess zinc ions, as indicated. A two-way ANOVA with Tukey's post hoc test (****p<0.0001) was used for statistical analysis; b, [F (20, 60) = 24.37, p< 0.0001]; and c, [F (25, 12) = 6.438, p= 0.0008]. (**d**) Quantification of unbound zinc (Zn^{2+}) ions quantified using an *in vitro* assay. Increasing concentrations of recombinant, wild-type parkin and DJ-1 (as control) proteins were assayed under basal conditions or under oxidizing (2 mM H_2O_2) *vs.* reducing (100 mM DTT) conditions. Free Zn^{2+} release was measured colorimetrically at OD560 nm. A two-way ANOVA with Tukey's post hoc test (****p<0.0001) was used for statistical analysis; b, [F (4, 18) = 151.1, p< 0.0001].

(**e**) Coomassie Blue-stained visualization of r-parkin, RNF43 and $HOIP^{cd}$ proteins, used in the AmplexRed assay shown in **Fig. 2.5c**. (**f**) Area under the curve (AUC) plots from kinetic readings of an *in vitro* colorimetric H_2O_2 assay comparing increasing concentrations of ROS input (shades of green) and the effect of rising concentrations of GSH (shades of purple). AUC integrated the total value of H_2O_2 signals generated over a 10 min-long time course in the assay. Results analyzed by one-way ANOVA [F (6, 18) = 73.02, p< 0.0001] (**g-m**) AUC graphs for results from *in vitro* H_2O_2 assays for various concentrations of recombinant proteins, as indicated. Statistical analysis was performed as in **Fig. 2.5e**. Results analyzed by one-way ANOVA, (**f**) [F (4, 11) = 229.6, p< 0.0001], (**g**) [F (3, 8) = 7.415, p= 0.0107], (**h**) [F (3, 9) = 87.58, p< 0.0001], (**i**) [F (2, 7) = 13.45, p=0.0040], (**j**) [F (3, 9) = 11.23, p= 0.0021], (**k**) [F (3, 9) = 7.263, p= 0.0089] and (**l**) [F (2, 7) = 8.536, p= 0.0133] (**n**) Visualization of recombinant PD proteins post H_2O_2 exposure by silver staining where SDS/PAGE gel was run under non-reducing conditions.

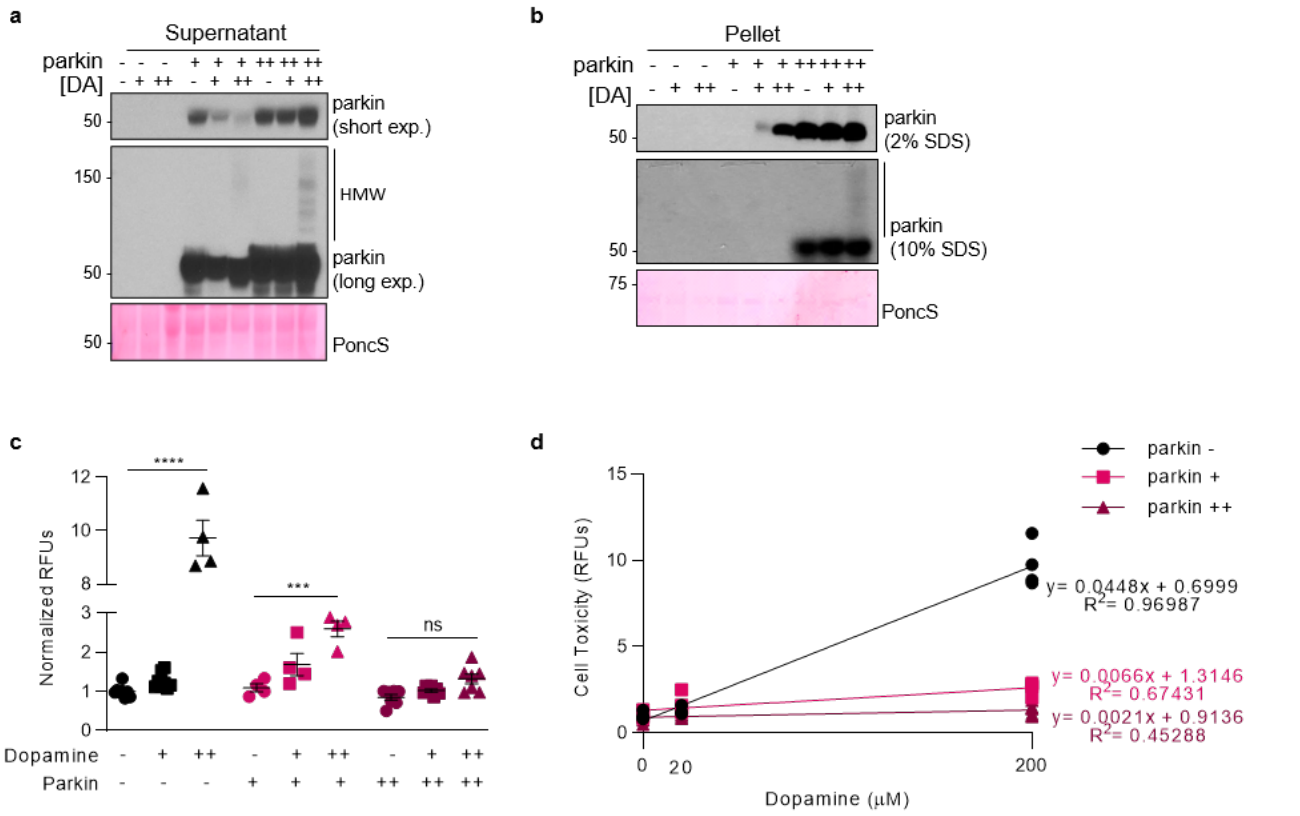

Supplementary Figure 2.6. Wild-type, human parkin protects neural cells from dopamine toxicity in a protein concentration-dependent manner

(**a-b**) Western blots of parkin in the soluble supernatant (**a**) and insoluble, serial pellet (**b**) fractions of lysates from dopamine-treated human M17 neuroblastoma cells, which stably express vector-control plasmid (parkin -) or myc-tagged, human *PRKN* cDNA at mid- (+) or high (++) levels. Cells were exposed to 20 μM (+) and 200 μM (++) dopamine for 20 hrs, as indicated. SDS/PAGE gels were run under reducing conditions. (**c**) Cell viability assay of cells highlighted in (a, b). Representative data are shown for the mean of duplicates ± SEM from n=4-8 independent experiments; *$p<0.05$ by two-way ANOVA with Tukey's post hoc test; [$F(4, 44) = 189.2$, $p< 0.0001$]. (**d**) Correlation studies of experiments, as conducted in (**a**, **b**), to monitor parkin expression levels *vs*. cell survival.

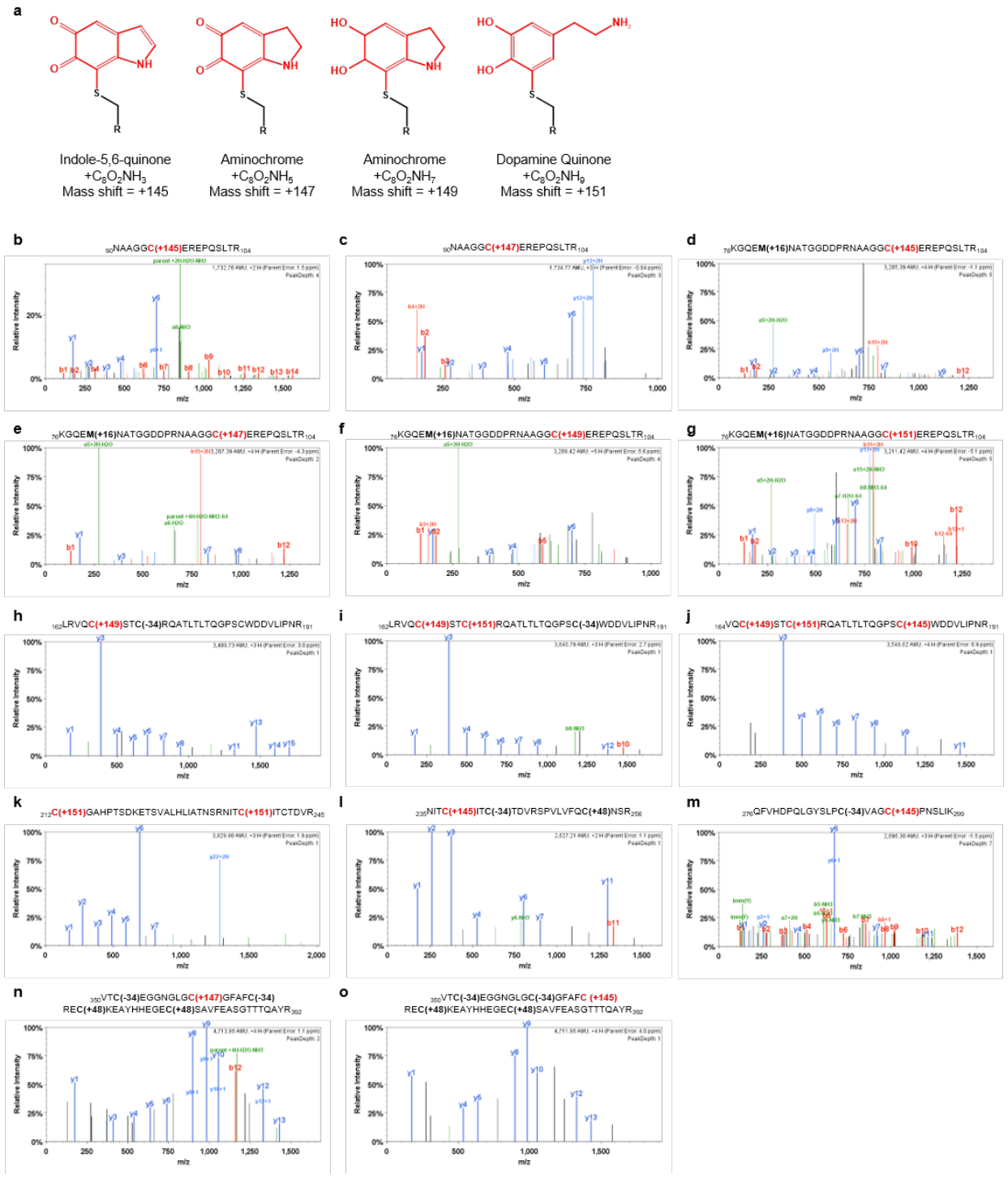

Supplementary Figure 2.7. Human parkin conjugates dopamine metabolites at cysteine 95 and other cysteine residues (**a**) Chemical structures of 4 dopamine metabolites (red) conjugated to a thiol group (black) that were screened for in LC-MS/MS experiments, with their corresponding mass shift added. (**b-o**) LC-MS/MS-generated spectra following trypsin digestion of aminochrome-treated, human r-parkin protein highlighting representative adduct conjugation events, which were identified by mass shift gains as shown in (**a**), at the following residues: Cys95 (**b-g**), Cys166, Cys169 and Cys182 (**h-j**), Cys212 (**k**), Cys238 (**l**), Cys293 (**m**), Cys360 (**n**), and Cys365 (**o**). See also **Fig. 2.6e, g**.

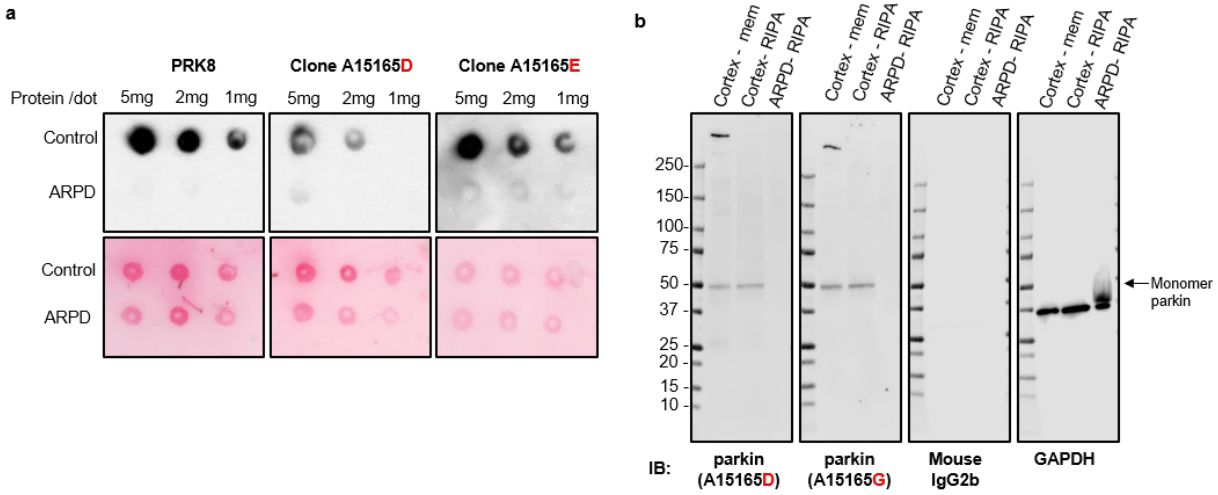

c

Clone	Epitope	Domain
A15165B	aa 89-93	Linker
A15165D	aa 397-404	REP
A15165G	aa 398-404	REP
A15165E	aa 177-184; aa 443-453; aa 459-464	RING0; RING2 [conformational]

Supplementary Figure 2.8. Characterization of four, new monoclonal antibodies raised in mice against human parkin (**a**-**b**) Characterization of four murine, monoclonal antibodies (of IgG_2 isotype; clone-B, -E, -D, and -G) by (**a**) non-denaturing dot blots against human brain lysates (SDS fractions from cortices of control individuals and *PRKN*-linked ARPD patients); and (**b**) by denaturing SDS/PAGE under reducing conditions and Western blotting of extracts from cortical specimens of a control brain and a parkin-deficient ARPD case. Screening by these three methods as well as by cell-based microscopy using indirect immunofluorescence (not shown) revealed specific staining for four anti-parkin clones (-B, -E, -D and -G), which was conformation-dependent for clone-E. (**c**) Select list of epitopes within the sequence of human parkin, as recognized by clones -B, -E, -D, and -G and identified by screening with overlapping 7-12 amino acid-long peptides covering full-length, human parkin (see also Chapter 4).

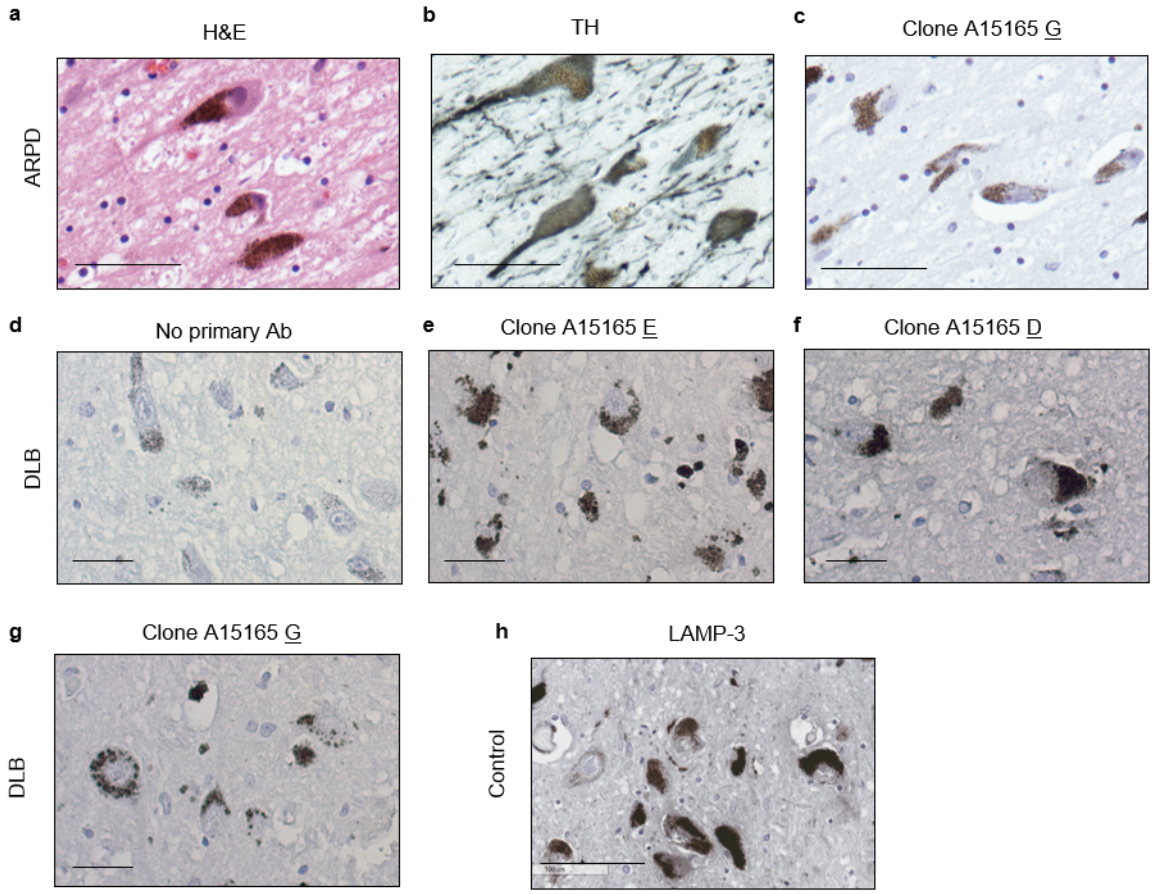

Supplementary Figure 2.9. Parkin is specifically detected in human midbrain sections by routine immunohistochemistry

(**a-c**) H&E (**a**), anti-tyrosine hydroxylase (TH) (**b**) and anti-parkin (clone A15165-G) (**c**) staining of dopamine neurons in the *S. nigra* of midbrain sections from a parkin-deficient ARPD case [Kano et al., npj Parkinson's Disease 2020].

(**d-g**) Immunohistochemical detection of parkin in the *S. nigra* of an individual with dementia with Lewy bodies. Both intra- and extracellular anti-parkin-reactive neuromelanin granules are visible. (**b**) No primary antibody control and staining with anti-parkin monoclonal antibodies **(e)** A15165-E, (**f**) -D and (**g**) -G are shown. (**h**) Immunohistochemical detection of LAMP-3 protein in dopamine neurons of the *S. nigra* from an adult control brain. Scale bars represent 100 μm.

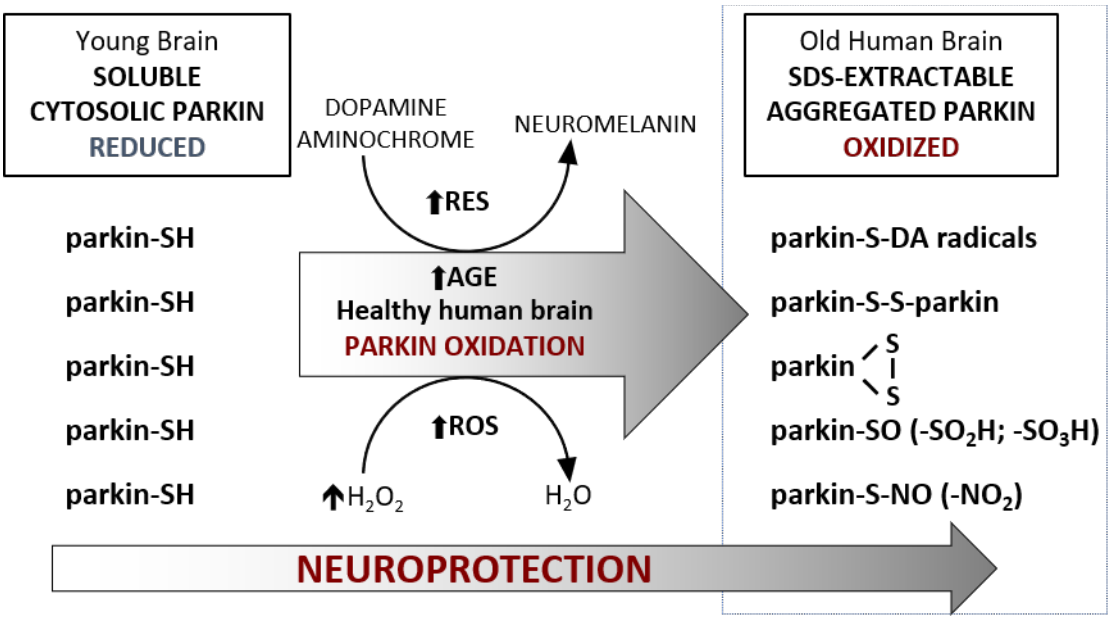

Supplementary Figure 2.10. Graphic summary of a working model for parkin's redox functions in adult, human dopamine neurons

In human brain, parkin thiol (-SH) oxidation neutralizes cellular reactive oxygen species (ROS; H_2O_2) and potentially toxic dopamine (DA) radicals (e.g., DA quinones; RES) during normal ageing. In human brain, both reversible and irreversible oxidation events occur gradually, which promote parkin's transition into a less soluble state by the beginning of the 4th decade. In adult dopamine neurons of the *S. nigra*, post-translational modifications lead to the accumulation of a pool of parkin within LAMP-3-positive lysosomes. This multimodal oxidation of parkin confers neuroprotection. In *PRKN*-linked ARPD, the absence of parkin's redox effects contributes to a rise in ROS (and RNS) levels, reduced sequestration of dopamine radicals (RES), and possibly, less neuromelanin formation.

Sample ID	Brain region	Age	Sex	PMI (hrs)	Diagnosis	% soluble parkin	H_2O_2/ Tissue ratio	Appears in figures
1	FC	5	F	33	Healthy control	54.1		2.2.1b, 2.2.1e, 2.2.1f, 2.2.1g, 2.2.1h, 2.2.1k, S2.2.1a, S2.2.1b
2	FC	5	F	20	Healthy control	22.6	2.551	2.2.1b, 2.2.1e, 2.2.1f, 2.2.1g, 2.2.1h, 2.2.1k, 2.2.2a, 2.2.2b, 2.2.2c, S2.2.1a, S2.2.1b
3	FC	8	M	5	Healthy control	3.7	1.780	2.1b, 2.1e, 2.1k, 2.2a, 2.2b, 2.2c
4	FC	13	M	13	Healthy control	86.0	2.217	2.1b, 2.1e, 2.1f, 2.1k, 2.2a, 2.2b, 2.2c
5	FC	15	F	9	Healthy control	27.5	1.349	2.1b, 2.1e, 2.1f, 2.1k, 2.2a, 2.2b, 2.2c
6	FC	16	F	20	Healthy control	40.6		2.1b, 2.1e, 2.1f, 2.1g, 2.1h, S2.1b
7	FC	16	F	14	Healthy control	51.3	1.016	2.1b, 2.1e, 2.1f, 2.1k, 2.2a, 2.2b, 2.2c, S2.1a
8	FC	17	M	23	Healthy control	5.1	0.701	2.1b, 2.1e, 2.1k, 2.2a, 2.2b, 2.2c
9	FC	17	M	22	Healthy control	45.3		2.1b, 2.1e, 2.1k
10	FC	20	F	19	Healthy control	63.3		2.1b, 2.1e, 2.1f, 2.1k
11	FC	20	M	8	Healthy control	37.5		2.1b, 2.1e, 2.1f, 2.1k
12	FC	20	M	6	Healthy control	3.6		2.1b, 2.1e, 2.1f, 2.1k
13	FC	20	M	5	Healthy control	89.4		2.1b, 2.1e, 2.1f, 2.1k
14	FC	21	M	30	Healthy control	46.1		2.1b, 2.1e, 2.1f, 2.1k
15	FC	28	M	33	Epilepsy *	18.9		2.1b, 2.1e, 2.1f, 2.1k
16	FC	29	F	18	Epilepsy *	4.2	3.061	2.1b, 2.1e, 2.1f, 2.1k, 2.2a, 2.2b, 2.2c, S2.1a
17	FC	30	M	20	Healthy control	1.6	6.089	2.1b, 2.1e, 2.1f, 2.1k, 2.2a, 2.2b, 2.2c
18	FC	36	M	20	Healthy control	3.5	5.665	2.1b, 2.1e, 2.1f, 2.1k, 2.2a, 2.2b, 2.2c
19	FC	37	F	13	Healthy control	12.7		2.1b, 2.1e,2.1f, 2.1k
20	FC	38	M	17	Healthy control	9.8		2.1b, 2.1e, 2.1f, 2.1k
21	FC	39	M	23	Healthy control	14.3		2.1b, 2.1e, 2.1f, 2.1k
22	FC	39	M	14	Healthy control	24.1		2.1b, 2.1e, 2.1f, 2.1k, S2.1a
23	FC	42	M	18	Healthy control	26.6		2.1b, 2.1e, 2.1f, 2.1k
24	FC	43	F	22	Healthy control	0.7	4.601	2.1b, 2.1e, 2.1f, 2.1k, 2.2a, 2.2b, 2.2c, S2.1a
25	FC	44	F	21	Spina bifida *	0.0		2.1b, 2.1e, 2.1k, S2.1c
26	FC	49	F	16	Healthy control	9.8	5.622	2.1b, 2.1e, 2.1f, 2.1k, 2.2a, 2.2b, 2.2c, S3c
27	FC	49	F	14	Healthy control	3.3		2.1b, 2.1e, 2.1k
28	FC	54	M	16	Alzheimer disease	0.0		2.1b, 2.1e, 2.1f, 2.1k
29	FC	54	F	23	Huntington disease	7.6		2.1b, 2.1e, 2.1k
30	FC	55	F	16	Healthy control	6.7	5.829	2.1b, 2.1e, 2.1f, 2.1k, 2.2a, 2.2b, 2.2c
31	FC	56	M	23	Healthy control	12.6		2.1b, 2.1e, 2.1f, 2.1g, 2.1h, 2.1k, S2.1b
32	FC	57	M	n.d.	Healthy control	35.6		2.1e
33	FC	62	M	15	Brain hemorrhage *	8.4	6.525	2.1b, 2.1e, 2.1f, 2.1k, 2.2a, 2.2b, 2.2c, S2.1a
34	FC	65	M	5	Lewy body dementia	0.0	6.473	2.1e, 2.1j, 2.1k, 2.1l, 2.1m, 2.2a, 2.2b, 2.2c
35	FC	65	M	14	Sporadic Parkinson's	0.0	9.112	2.1e, 2.1k, 2.2a, 2.2b, 2.2c
36	FC	65	F	42	Healthy control	3.0	5.768	2.1a, 2.1b, 2.1e, 2.1k, 2.2a, 2.2b, 2.2c, S2.2e
37	FC	66	M	n.d.	Healthy control	3.3	6.674	2.1b, 2.1e, 2.1f, 2.2a, 2.2b, 2.2c, S2.1a
38	FC	68	M	17	Healthy control	0.0	2.514	2.1b, 2.1e, 2.1f, 2.1g, 2.1h, 2.1k, 2.2a, 2.2b, 2.2c, S2.1b
39	FC	70	F	n.d.	Healthy control	2.9	6.897	2.1b, 2.1e, 2.1f, 2.2a, 2.2b, 2.2c, S2.1a
40	FC	70	M	n.d.	Healthy control	4.6	5.459	2.1b, 2.1e, 2.1f, 2.1g, 2.1h, 2.2a, 2.2b, 2.2c, S2.1b
41	FC	72	M	n.d.	Lewy body dementia	28.4	6.274	2.1e, 2.2a, 2.2b, 2.2c
42	FC	75	M	48	Healthy control	32.5	2.878	2.1b, 2.1e, 2.1k, 2.2a, 2.2b, 2.2c
43	FC	75	F	13	Ischaemic stroke *	4.4		2.1b, 2.1e, 2.1f, 2.1k
44	FC	75	M	17	Lewy body dementia	0.0		2.1e, 2.1j, 2.1k
45	FC	76	M	74	Pick's disease	0.0		2.1e, 2.1k
46	FC	85	F	15	Alzheimer disease	0.0		2.1b, 2.1e, 2.1f, 2.1j, 2.1k
ARPD1	FC	66	M	17	*PRKN*-linked Parkinson's	n/a		
ARPD2	FC	57	M	31	*PRKN*-linked Parkinson's	n/a		
ARPD3	FC	70	F	42	*PRKN*-linked Parkinson's	n/a		
ARPD4	FC	70	M	13	*PRKN*-linked Parkinson's	n/a		
47	MB	26	M	2	Multiple sclerosis *			2.1b, S2.2b
65	MB	34	M	n.d.	Encephalitis*			2.1b
25	MB	44	F	21	Healthy control			2.1b
48	MB	44	F	5	Multiple sclerosis *			2.1c, S2.2b
49	MB	45	M	13	Ischaemic stroke *			2.1b
50	MB	47	F	20	Brain hemorrhage *			2.1b
51	MB	56	M	44	Multiple system atrophy			2.1b
52	MB	60	M	16	Progressive supranuclear palsy			2.1b
53	MB	61	M	20	Healthy control			2.1b
54	MB	61	M	3.5	Multiple sclerosis *			2.1b
36	MB	65	F	42	Healthy control			2.1b, S2.2a
55	MB	65	M	6	Multiple sclerosis *			2.1b
64	MB	71	M	n.d.	Lewy body dementia			2.1b
41	MB	72	M	n.d.	Lewy body dementia			2.1b
56	MB	74	F	n.d.	Amyotrophic lateral sclerosis			2.1b
42	MB	75	M	48	Healthy control			2.1b
57	MB	75	M	70	Sporadic Parkinson's			2.1b
45	MB	76	M	74	Pick's disease			2.1b
58	MB	79	M	n.d.	Progressive supranuclear palsy			2.1b
59	MB	82	M	48	Lewy body dementia			2.1b
60	SC/Muscle	68	F	2.5	Ischaemic stroke *			2.1c, 2.1d
61	SC/Muscle	64	F	2	Subarachnoid hemorrhage*			2.1d
62	SC/Muscle	74	M	2	Cerebellar hemorrhage *			2.1d
63	SC/Muscle	50	M	4	Subarachnoid hemorrhage *			2.1d

Supplementary Table 2.1. List of human tissue specimens examined in this study

Characteristics listed include brain regions of frontal cortex (F ctx), midbrain, thoracic spinal cord (harvested with skeletal muscle); age (in years); sex (F, female; M, male); PMI, *post mortem* interval recorded in hours (hrs); n.d., not determined with accuracy (i.e., inconsistent PMI information); brain diagnosis, where * indicates that the tissue examined was not affected by a detectable disease process; % parkin solubility (TS+TX/total signal); and the corresponding figure(s); S, supplementary data.

	Treatment	Control	Control	H_2O_2	H_2O_2	H_2O_2	H_2O_2	H_2O_2
	Run	IAA+NEM	IAA	20µM	1mM	4.5mM	4.5mM	4.5mM
Region	**Cysteine Residue**							
UBL	59		•	n/d	•	• +	•	•
Linker	95	•	•	•	•	• +	• +	• +
RING0	150	•	•	•	•	• +	• +	•
	154	•	•	n/d	•	• +	• +	•
	166	n/d	n/d	•	• +	n/d	•	•
	169	n/d	•	•	• +	n/d	•	•
	182	•	•	•	n/d	• +	• +	•
	196	•	•	•	•	• +	• +	• +
	201	•	•	•	•	• +	• +	• +
	212	•	•	•	n/d	• +	• +	• +
RING1	238	•	•	• +	•	• +	•	• +
	241	•	•	• +	•	• +	•	•
	253	•	•	• +	•	• +	•	•
	260	•	•	n/d	n/d	• +	•	•
	263	•	•	n/d	n/d	• +	•	•
	268	•	•	n/d	n/d	• +	•	•
	289	•	•	n/d	n/d	• +	• +	• +
	293	•	•	n/d	•	•	• +	• +
	323	•	•	n/d	n/d	• +	• +	• +
IBR	332	•	•	n/d	n/d	• +	•	•
	337	•	•	n/d	•	• +	•	• +
	352	•	•	•	•	•	• +	• +
	360	•	•	•	•	• +	•	•
	365	•	•	•	n/d	• +	•	•
	368	•	•	n/d	n/d	• +	• +	•
	377	•	•	•	n/d	• +	• +	• +
RING2	418	n/d	n/d	n/d	•	n/d	n/d	n/d
	421	n/d	n/d	n/d	• +	n/d	• +	• +
	431	n/d	•	n/d	•	n/d	•	•
	436	n/d	n/d	n/d	• +	n/d	•	•
	441	n/d	n/d	n/d	• +	n/d	•	•
	446	•	•	n/d	n/d	• +	• +	• +
	449	•	•	n/d	n/d	• +	• +	•
	451	•	•	n/d	n/d	• +	•	•
	457	•	•	•	•	• +	•	• +
	% Parkin protein coverage	83	89	57	60	86	98	97
	# peptides identified	40	35	22	33	38	51	47
	# Cysteines identified	27	31	16	21	28	34	34
	# IAA-cysteines	27	30	16	21	28	34	34
	IAA-cys/identified-cys	27/27	30/31	16/16	21/21	28/28	34/34	34/34
	%	100	97	100	100	100	100	100
	# NEM-cysteines	0	n/a	3	5	26	16	14
	NEM-cys/identified-cys	0/27	n/a	3/16	5/21	26/28	16/34	14/34
	%	0	n/a	19	24	93	47	41

• IAA + NEM

Supplementary Table 2.2. Cysteine residues in recombinant human parkin are redox active

Aliquots of human recombinant (r-) parkin (10 µM) that were oxidized by variable concentrations of H_2O_2 *vs.* control preparations were differentially labelled with iodoacetamide (IAA) and/or N-ethylmaleimide (NEM; as in **Fig. 2.3e**) to identify reduced cysteines (IAA) or reversibly-oxidized residues (NEM). Proteins were subjected to LC-MS/MS and analyzed using Mascot Scaffold PTM to identify IAA (•) or NEM (+) adducts indicating when these were detectable on individual residues. Cysteines that were not detected as modified in individual runs are also listed (n/d). Note that cysteines within all four RING domains of human parkin as well as in the linker and UbL domains could be variably modified.

Chapter 3: Manuscript 2 - *PRKN* Gene Expression in the Brain Lowers Chronic Oxidative Stress in the Cytosol by Altering Glutathione Homeostasis

Author list:
Daniel N. El-Kodsi*, **Jacqueline M. Tokarew***, Rajib Sengupta, Nathalie A. Lengacher, Angela P. Nguyen, Heather Boston, Qiubo Jiang, Carina Palmberg, Chantal Pileggi, Chet E. Holterman, Bojan Shutinoski, Juan Li, Travis K. Fehr, Amanda Hadwen, Sarah Kealey, Mirela Barclay, Kerstin Ure, Matthew J. LaVoie, Rajiv R. Ratan, Masashi Takanashi, Nobutaka Hattori, Christopher R. Kennedy, Mary-Ellen Harper, Arne Holmgren, Julianna J. Tomlinson, and Michael G. Schlossmacher
*these authors contributed equally to this work.

3.1 Preface

This manuscript provides further evidence that parkin functions as a thiol-mediated redox-state regulator. Here, lower parkin expression correlated with increased levels of H_2O_2 and oxidative stress markers (i.e. protein nitrotyrosination and carbonylation) in human brain, in a bi-genic mouse model with parkin-deficiency combined with MnSOD haploinsufficiency, and in cell models, and led to altered enzymatic activity of mitochondria-associated enzymes aconitase-2 and mitochondrial creatine kinase in mouse brain. Although, the endogenous stress applied recapitulated the oxidation-mediated aggregation of human brain parkin in the bi-genic mouse brain (Chapter 2), it was not sufficient to cause a parkinsonian phenotype or dopaminergic cell loss in the *S. nigra*. In cell models, overexpression of human parkin increased cell viability and lowered intracellular levels of H_2O_2 under oxidative stress conditions, which, in exchange, led to the formation of aggregated and insoluble parkin in a thiol-dependent manner. Supporting evidence for a direct link between parkin and intracellular glutathione was demonstrated by the dynamic shift in glutathione redox profile caused by reduced parkin expression; compensation was mediated by increased glutathione reductase activity. Additionally, recombinant parkin was found to directly reduce GSSG to GSH and, in exchange, undergo reversible cysteine S-glutathionylation at Cys59, Cys377 and primate sequence-specific Cys95.

3.2 Statement of author contribution

As co-first-author I provided major contributions to: establishing experimental techniques and their optimization, the overall project direction and design, data analysis and interpretation, as well as, initial drafts and edits of the manuscript. Specifically, I had made initial attempts at investigating the effect of parkin expression on intracellular ROS levels in live cells and tissues, as well as, the dynamic relationship between parkin and intracellular glutathione using various techniques, including: ROS-, GSH- and viability-detecting fluorophores, as well as, enzymatic- and HPLC-based measurements of glutathione (**Fig. 3.3a-c, 3.5, 3.6d, 3.6g-h, 3.7e; Supplementary Fig. 3.2e, and Appendix Fig. C16-17**) These experiments were later optimized and completed by D. El-Kodsi and C. Pileggi (M-E. Harper group). Specific protocols I helped establish included: i) thiol-dependent and oxidation-induced insolubility of parkin in cells (**Supplementary Fig. 3.2a-d**), ii) concentrations of exogenous oxidative stress agents used in cellular ROS experiments (**Fig. 3.3a-b, and Supplementary Fig. 3.2),** iii) live cell ROS measurements using flow cytometry (**Supplementary Figure 3.2e; Appendix Fig. C17**), and iv) glutathione measurement assays in tissues, cells and in presence of recombinant protein (**Fig. 3.5c, 3.6d and 3.7e, and Appendix Fig. C16-17**). I also provided supervision and optimization help for sequential protein extraction from human frontal cortex (**Supplementary Fig. 1a**) run by N. Lengacher. The experiments that I ran independently are included in **Fig. 3.5c, 3.6d and 3.7e; Supplementary Fig. 3.2e and Appendix Fig. C16-19**. D. El-Kodsi ran ROS and chronic oxidative stress measurements in cells and tissues. He also maintained mice colonies, performed genotyping, analyzed behavioural assays and also ran glutathione reductase activity measurements. R. Sengupta and C. Palmberg (A. Holmgren group) ran parkin labeling with eosin-GSSG and GSH-MS experiments. H. Boston performed mitchondrial enzyme activity assays and measured expression levels. A. Nguyen performed stereological quantification of TH-positive neurons. Q. Jiang and T. Fehr provided general technical

support with genotyping and assays. C. Holterman (C. Kennedy group) provided guidance on superoxide measurements. B. Shutinoski performed mRNA expression measurements of glutathione enzymes. J. Li performed correlation statistics. A. Hadwen, S. Kealey, M. Barclay and K. Ure provided technical help with mice colony maintenance and behavioural testing. M. Takanashi, N. Hattori, A. West and J. Woulfe provided fresh-frozen human tissues. M. LaVoie provided CHO and CHOmP cell cultures. R. Ratan and A. Holmgren provided feedback.

3.3 Abstract

We recently discovered a new role for Parkinson disease (PD)-linked parkin as a thiol-dependent antioxidant. We hypothesized that *PRKN* expression prevents degeneration of human dopamine cells during ageing by reducing reactive oxidative, reactive nitrosylating and reactive electrophilic species (ROS; RNS; RES). To further increase redox stress in *prkn*$^{-/-}$ mice, we combined the genomic loss of *prkn* with *Sod2* haploinsufficiency. Heart and brain tissue derived from this bi-genic model show evidence of elevated hydrogen peroxide and oxidative stress markers (i.e. protein nitrotyrosination and carbonylation). Similar findings were also observed in parkin-deficient PD brain. Although these changes occurred exclusively in the cytosol, the activity (but not levels) of redox-active mitochondrial enzymes was altered in the absence of parkin. Despite displaying the highest signs of oxidative stress, 12-month-old *prkn*$^{-/-}$//*Sod2*$^{+/-}$ mice show no loss of *S. nigra* neurons and no motoric deficits. Intriguingly, in parkin's absence the concentrations of reduced glutathione (GSH) increased and oxidized glutathione (GSSG) decreased in human cortex and murine brain. This response to parkin's absence was not based on new synthesis but the recycling of GSSG to GSH through upregulated glutathione reductase activity. Parkin was also found to interact directly with GSSG dipeptide and regenerate GSH, resulting in S-glutathionylation of parkin at cysteine residues 59, 95 and 377. Our

results demonstrate that, in mammalian brain, parkin confers antioxidant activities in the cytosol through mechanisms that alter glutathione recycling. Parkin's redox contributions reduce hydrogen peroxide, lower nitrotyrosination-, as well as, carbonylation-linked damage, and in turn, affect mitochondrial enzyme activities. However, in parkin's absence these changes were not damaging enough to induce nigral cell loss in the bi-genic mouse. We propose that modeling of *prkn*-linked parkinsonism requires increased oxidative stress, accomplished, in part, by hindering glutathione recycling.

3.4 Introduction

Parkinson disease (PD) is a progressive, heterogeneous disorder of the human brain that remains incurable. Parkin-linked, young-onset, autosomal-recessive PD (ARPD) is characterized by the degeneration of dopamine producing neurons in the *S. nigra* and *L. coeruleus*.[844] In the ageing human brain, these neurons are thought to be particularly vulnerable due to their high oxidative demands, which are a result of their unique cellular characteristics. These include: extensive arborization; a high number of axonal mitochondria; the presence of metals in redox-reactive forms;[86] ongoing generation of toxic dopamine metabolites in the cytosol; and a greater need to buffer Ca^{2+} ions.[44-46]

Oxidative stress and mitochondrial damage have been implicated in the pathogenesis of several brain disorders including PD.[327] Mitochondrial dysfunction, as induced by the neurotoxicants MPTP and rotenone, augments oxidative stress.[845] The integrity of the cellular thiol pool, a network formed by glutathione and the cysteine proteome, is essential in maintaining redox homeostasis in long-lived neurons. The reduced form of glutathione (GSH) serves a critical role as an antioxidant. Accordingly, a decline in GSH has been implicated in many human disorders, including neurodegenerative diseases.[696]

The genomic loss of parkin in mice does not induce loss of *S. nigra* neurons, and *prkn*$^{-/-}$ animals do not develop parkinsonism; several models have been created and characterized to study early onset

parkinsonism.[432-439] Most failed to recapitulate the disease as seen in humans, including a triple knockout mouse that is deficient in three recessively inherited PD genes *prkn*, *Dj-1* and *Pink1*.[410] However, unbiased studies have revealed proteomic changes in *prkn*$^{-/-}$ brains. These consist of alterations in the isoelectric focusing point rather than total abundance of various proteins.[435,437] There, we noted that a majority of dysregulated proteins had been previously identified as enzymes (55/92; 59.8%), and known to be redox-sensitive (72/92; 78.2%), *e.g.,* glyoxalase and aconitase-2.[435,437]

In addition to its known role as an E3-type ubiquitin ligase and regulation of mitophagy with PINK1,[292,349,798]we recently demonstrated that parkin acts as a redox regulator. In this context, it functions to maintain redox homeostasis and mediate redox reactions that lower chronic oxidative stress in mammalian tissues in a cysteine-dependent manner.[846] We propose that this function contributes to the proteomic changes observed in parkin-deificient mice and also contributes to the neuroprotection conferred by *PRKN* gene expression in human brain. We sought to test this concept further in rodent models and explore the sequelae of parkin deficiency in the context of increasing endogenous oxidative stress.

Sod2 encodes manganese superoxide dismutase (MnSOD), an enzyme that is the first line of defense against the rise of reactive oxygen species (ROS) within mitochondria, *i.e.,* superoxide anion (O_2^-). A loss of *SOD*-mediated activities has been implicated in cellular dysfunction and the pathogenesis of several neurodegenerative disease, including PD.[820] *Sod2*-null mouse models are neonatally lethal and feature markedly elevated, oxidative stress in their mitochondria, motor deficits and neurodegeneration.[847,848] Although analysis, including behavioural and redox chemistry changes, of *Sod2*$^{+/-}$ mice has not been completed, mice carrying haploinsufficiency for *Sod2* on a double *Dj-1* and *prkn* knockout background display behavioural and neurotransmitter abnormalities.[849]

Therefore, combined with our previous findings that parkin mediates redox homeostasis in mammalian tissues, including the midbrain,[846] we hypothesized that genomic *prkn* deficiency, when combined with *Sod2* haploinsufficiency and increased age, would exacerbate redox imbalance, and thus, potentially induce motoric deficits. Here, in studying *Sod2*$^{+/-}$ mouse brains, we found increased levels of endogenous H_2O_2 and elevated markers of irreversible oxidative stress, such as protein nitrotyrosination and carbonyl formation. This biochemical phenotype was further exacerbated in bi-genic mice that also lack parkin. However, by twelve months of age, we detected no dopamine cell loss and no motor deficits. In exploring potentially compensatory mechanisms, we also investigated parkin's effects on the thiol network. In doing so, we identified several elements of a heretofore unknown feedback loop between expression of endogenous parkin and glutathione metabolism in cells, murine brain and human cortices.

3.5 Results

Generation of bi-genic *prkn*$^{-/-}$//*Sod2*$^{+/-}$ mutant mice

The bi-genic mouse was generated by first crossing *prkn*$^{-/-}$ animals[432] with *Sod2*$^{+/-}$ mice[847] (**Fig. 3.1a**); the new line was maintained on a pure C57Bl/6J background. Because both *prkn* and *Sod2* loci are located on mouse chromosome 17, separated only by 1 centimorgan (cM), the physical proximity predicted a 1% recombination rate (**Fig. 3.1a**) in a single generation.[850] Heterozygous offspring at both the *prkn* and *Sod2* loci were bred over 10 generations to allow for recombination and to produce the desired genotype of *prkn*$^{-/-}$//*Sod2*$^{+/-}$ (**Fig. 3.1b**). The bi-genic model has no detectable parkin protein and shows significantly reduced MnSOD levels and activity (**Fig. 3.1c, d**). Several cohorts of WT, *prkn*$^{-/-}$, *Sod2*$^{+/-}$, and *prkn*$^{-/-}$//*Sod2*$^{+/-}$ genotypes were bred and aged to 2-4, 6 and 12 months for biochemical and behavioural analyses, respectively (**Supplementary Table 3.1**). Group sizes and equal sex ratios within

genotypes were comparable within and across all cohorts (**Supplementary Table 3.1**). Of note, fully MnSOD-deficient mice were not viable, as described.[847]

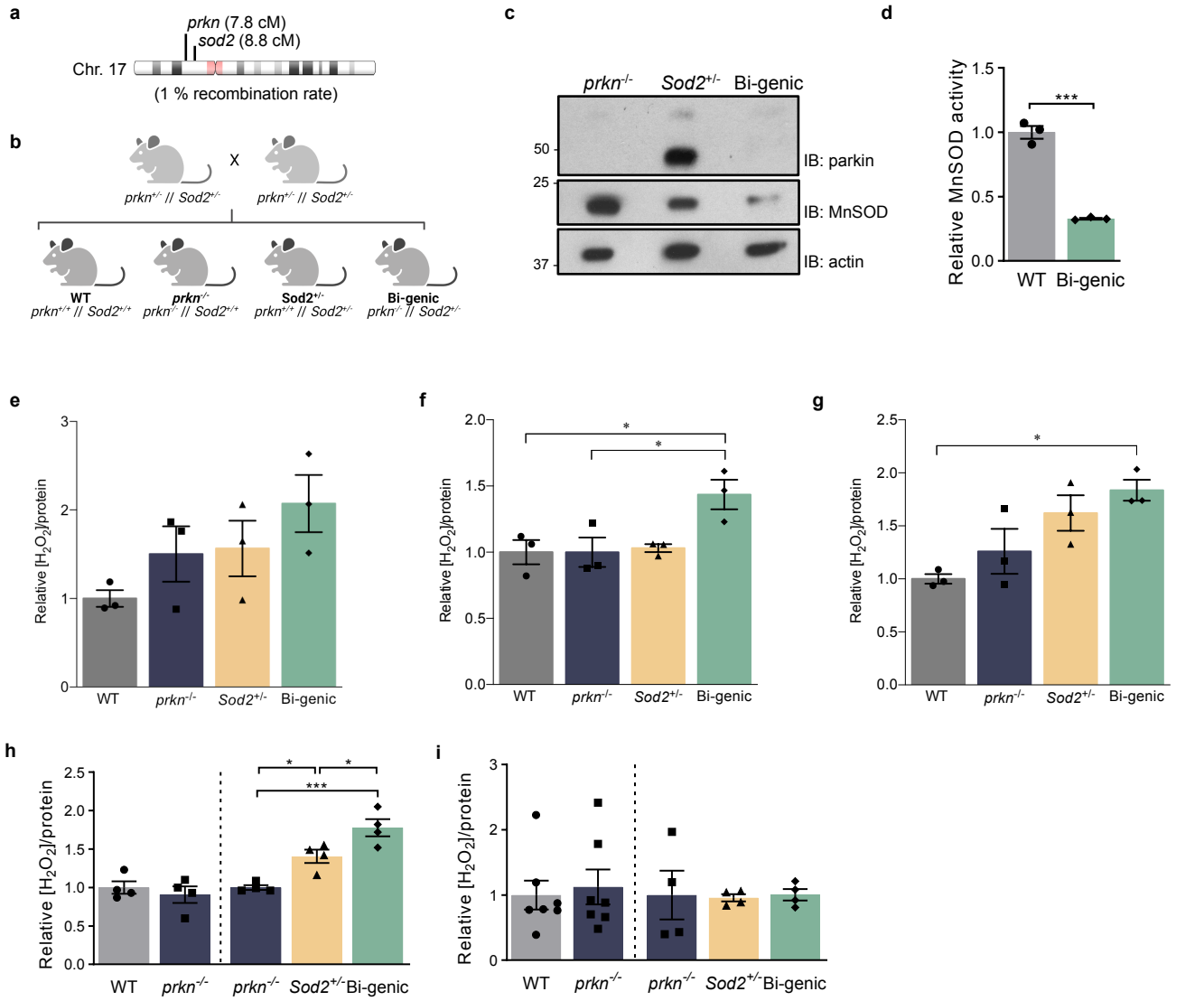

Figure 3.1. Parkin deficiency increases hydrogen peroxide levels in murine brain when MnSOD activity is reduced. (**a**)**,** Schemas of mouse chromosome 17, with *prkn* and *Sod2* loci separated by 1 centimorgan (cM) and (**b**)**,** the breeding strategy used to generate bi-genic *prkn*$^{-/-}$*//Sod2*$^{+/-}$ and littermate control mice. (**c**)**,** Representative Western blot of parkin, MnSOD and actin expression in brains of 2-4 months-old *prkn*$^{-/-}$, *Sod2*$^{+/-}$ and bi-genic (*prkn*$^{-/-}$*//Sod2*$^{+/-}$) mice. (**d**)**,** Relative MnSOD activity in whole brain homogenates of 2-4 months-old WT and bi-genic littermates. (**e-g**)**,** Ratio of endogenous levels of H_2O_2 (µM) to total protein concentration (µg/µL) in homogenates of heart (**e**), cortex (**f**) and midbrain (**g**) from 6-month-old mice. (**h-i**)**,** Ratio of endogenous levels of H_2O_2 (µM) to total protein concentration (µg/µL) in cytosolic-dominant (**h**) and mitochondria-enriched fractions of the brain (**i**) from 6–8-month-old WT and *prkn*$^{-/-}$ (left panel), and 2-4 month-old *prkn*$^{-/-}$*//Sod2*$^{+/-}$ as well as bi-genic mice (right panel). Data represent the mean normalized to WT using n=3/genotype (**d-g**) or n=4-7/genotype (**h-i**) ± SEM. Significance was determined using unpaired Student T-test (p =0.0002) in (**d**), for the left panel in (**h**) (p= 0.5166) and for the left panel in (**i**) (p= 0.7327); a 1-way ANOVA with Tukey's post-hoc-analysis was used in (**e**) [F(3,8) = 2.480, p=0.1354], in (**f**) [F(3,8) = 5.361, p=0.0257], in (**g**) [F(3,8) = 6.512, p=0.0154], for the right panel in (**h**) [F(2,9)= 22.17, p=0.0003], and for the right panel in (**i**) [F(2, 9)=0.01367, p=0.9864].

Bi-genic mice show elevated hydrogen peroxide levels in high-energy generating tissues

No differences were observed in endogenous H_2O_2 levels of heart homogenates when comparing bi-genic to WT littermates ($p=0.13$; **Fig. 3.1e**). In cortices, the bi-genic mouse showed higher H_2O_2 levels when compared to WT and *prkn*$^{-/-}$ mice ($p<0.05$; **Fig. 3.1f**). Similar differences were found in dissected midbrains ($p<0.05$; **Fig. 3.1g**). We also quantified levels of the highly reactive superoxide anion (O_2-) in the brains from the 6 months-old cohort by HPLC. There, bi-genic mice showed significantly altered levels compared to their age-matched WT littermates, as expected ($p<0.01$).

When testing parkin's direct effects on H_2O_2 concentrations in mouse brain, we found that basal ROS levels did not differ significantly in adult *prkn*$^{-/-}$ versus WT mice (**Fig. 3.1e-g**), which we had anticipated based on our results obtained in homogenates from ARPD cortices.[846] Moreover, no difference was seen for ROS levels in the cytosol or in isolated mitochondria of *prkn*$^{-/-}$ versus WT mice under basal conditions (**Fig. 3.1h,i**). However, H_2O_2 concentrations were higher in the cytosol of total brain homogenates from *Sod2*$^{+/-}$ mutant and bi-genic animals (*prkn*$^{-/-}$*//Sod2*$^{+/-}$) when compared to age-matched *prkn*$^{-/-}$ mice ($p<0.05$ to $p<0.001$; **Fig. 3.1h**). Unexpectedly, in isolated mitochondria from *Sod2*$^{+/-}$ and *prkn*$^{-/-}$*//Sod2*$^{+/-}$ brains, ROS levels remained the same (**Fig. 3.1i**). Together, these results established that WT parkin contributed to a net lowering of H_2O_2 levels in the brain during rising oxidative stress caused by reduced MnSOD activity.

***Prkn* gene expression lowers nitrotyrosination-related stress in mammalian brain**

Given the relevance of superoxide anion levels on cellular peroxynitrite concentrations, we next examined the degree of nitrotyrosination in tissues as a marker of chronic, irreversible stress-induced protein modification (**Fig. 3.2a-e**). When quantifying nitrotyrosination profiles in 6 months-old cohorts from the four genotypes, we found that *prkn*$^{-/-}$ mice displayed significantly higher levels in dissected

midbrains when compared to WT and *Sod2*$^{+/-}$ littermates, with the bi-genic animals showing a related trend. As was seen for H_2O_2 levels (**Fig. 3.1h**), the rise in nitrotyrosination was seen foremost in the cytosol, but not in isolated mitochondria, including from murine midbrain (**Fig. 3.2c**). Of note, nitrotyrosination levels were also significantly higher in heart lysates from 6 months-old *prkn*$^{-/-}$ and bi-genic animals (**Fig. 3.2d, e**).

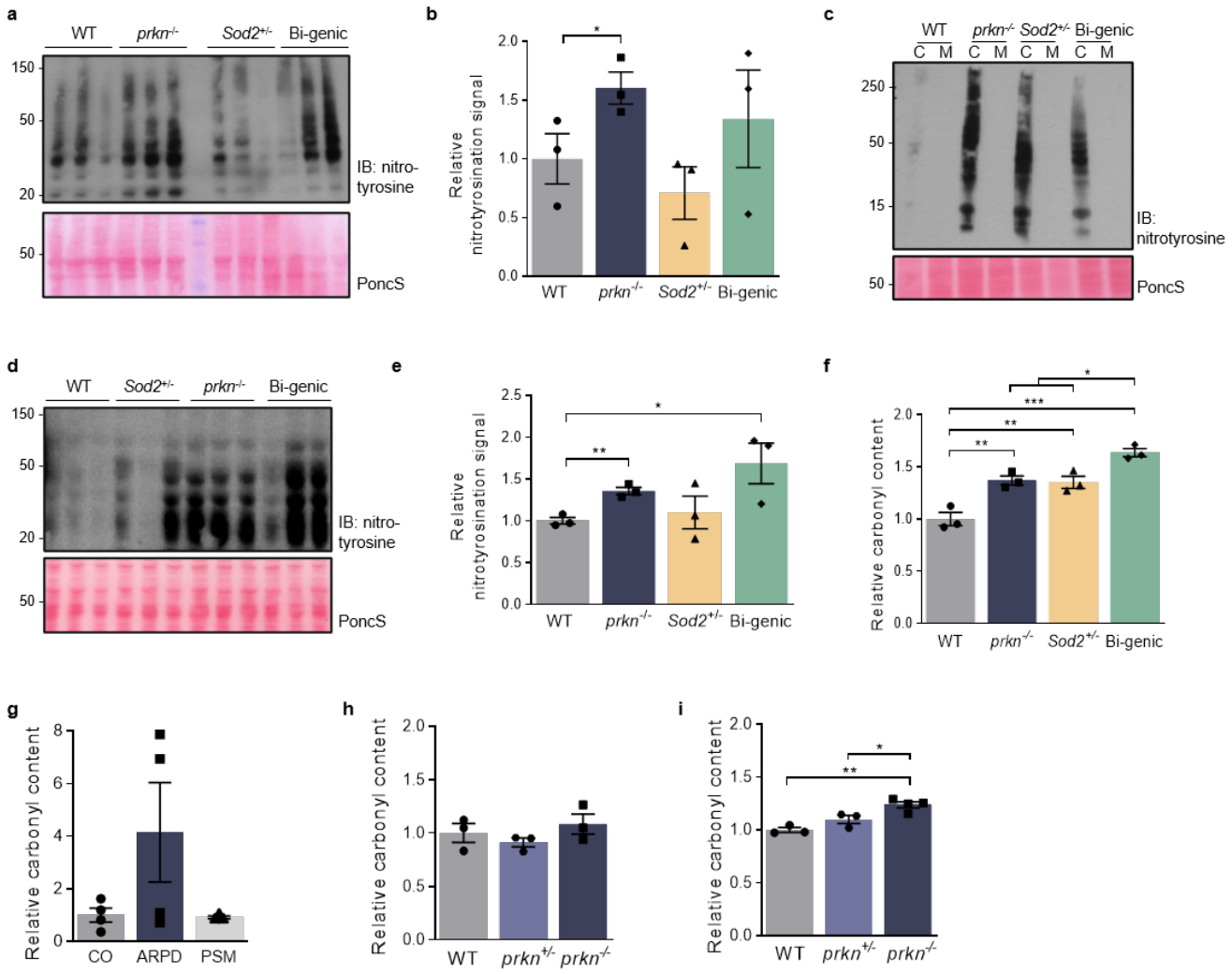

Figure 3.2. Parkin significantly lowers chronic oxidative stress-induced damage in the cytosol of mammalian brain. (**a**) Total protein nitrotyrosination in midbrain homogenates of 6-month-old mice of 4 genotypes (as in **Figure 3.1**); each lane is a separate mouse. Ponceau S was used as loading control and used to quantify total signal as shown in (**b**).
(**c**) Representative blot of total protein nitrotyrosination in cytoplasmic versus mitochondrial fractions from midbrains of 6-month-old mice (n=1/genotype). (**d**) Western blot, and (**e**) quantification of nitrotyrosination signal in heart homogenates from 6-month-old mice, as described in (**a,b**). (**f**) Relative mean protein carbonyl content in brain homogenates from 6-month-old mice, (**g**) human cortices from age- and ethnicity-matched controls and parkin-deficient autosomal recessive Parkinson disease (ARPD), as well as, age-matched cases of non-*PRKN*-linked parkinsonism (PSM). (**h**) Relative mean protein carbonyl content in mitochondria, and (**i**) cytosolic fractions of 6-month-old WT, *prkn*$^{+/-}$ and *prkn*$^{-/-}$ mice. Data in (**b,d-i**) represent n=3-4/genotype ± SEM. Significance was determined using Student T-test between each genotype in (**b**) and (**e**) with p=0.0379 found between WT and *prkn*-/- in (**b**), p=0.0038 found between WT and *prkn*-/-; and p= 0.0495 found between WT and bi-genic in (**e**). A one-way ANOVA with Tukey's post-hoc analysis in (**f**) [F(3, 8)= 25.13, p=0.0002], in (**g**) [F(2, 8)=2.362, p=0.1563], in (**h**) [F(2, 6)= 1.227, p=0.3574]**,** and in (**i**) [F(2, 7)= 15.56, p=0.0027].

***Prkn* gene expression lowers carbonyl content-related stress in mammalian brain**

We next examined the degree of protein carbonylation, a second irreversible outcome of chronically elevated H_2O_2, in the same mouse tissues (**Fig. 3.2f, h-i**). Carbonyl content was increased in *prkn*-deficient brain, even under basal conditions (**Fig. 3.2f**), consistent with a previous report by Palacino et al., who had employed a different mouse model.[435] As expected, the carbonyl content was further increased in the bi-genic mice ($p<0.05$; **Fig. 3.2f**). We also examined protein carbonyl content in patients with *PRKN*-linked ARPD *vs.* control subjects (each, n=4; **Fig. 3.2g**). These had been matched for age, *post mortem* interval and ethnicity (**Supplementary Fig. 3.1a**)[506,846] In the absence of human parkin, protein carbonyl levels also appeared to rise, although not significantly. Cortices from three, non-*PRKN*-linked parkinsonism cases revealed the same degree of carbonyl content as age-matched controls (**Fig. 3.2g**) and using a linear regression model with the protein carbonyl content of all brains (mouse and human) as the dependent variable, we found that this marker correlated with parkin deficiency (co-efficient of -0.3754, 95% CI, -0.6611–0.0053; p=0.05). Intriguingly, in murine brain the carbonyl content remained normal in isolated mitochondria (**Fig. 3.2h**), but was again elevated in the brain cytosol (**Fig. 3.2i**) from 6 months-old animals. Moreover, we also observed a *prkn*-null allele dosage effect (**Fig. 3.2i**). Together, these results indicated that WT parkin contributed significantly to the net lowering of protein carbonyl concentrations in adult brain.

***PRKN* expression lowers hydrogen peroxide in cells in exchange for parkin's own oxidation**

We next explored parkin-dependent redox changes to investigate potential mechanisms to explain its effect on oxidation state. We began this search using non-neural cell culture models (**Fig. 3.3; Supplementary Fig. 3.2**). Under basal conditions, HEK293-parkin cell lysates showed a trend toward lower H_2O_2 concentrations when compared to controls (**Fig. 3.3a**); this difference was significant when

measured by flow-cytometry in live cells ($p<0.05$; **Supplementary Fig. 3.2e**). When HEK293 cultures were exposed to rising oxidative stress, *e.g.,* after uncoupling treatment with CCCP, or exposure to exogenously added H_2O_2, or treatment with aminotriazole (a catalase inhibitor[846]), parkin-expressing cells consistently showed a significant reduction in ROS levels ($p<0.05$ to $p<0.0001$; **Fig. 3.3a; Supplementary Fig. 3.2e**). Additionally, in stress-exposed HEK293 cells transiently over-expressing WT *PRKN*, parkin became progressively aggregated and insoluble when exposed to increasing H_2O_2 concentrations (**Supplementary Fig. 3.2a**). Because the majority of aggregated parkin species collapsed following dithiothreitol treatment (**Supplementary Fig. 3.2b,c**), we postulated that these modifications had occurred via cysteine oxidation,[486] which we demonstrated in parallel using recombinant parkin and murine brain.[846] We confirmed this in HEK293 cell cultures using N-ethylmaleimide (NEM) and iodoacetamide (IAA), which irreversibly alkylate free thiols, and thus precluded post-translational modifications of cellular parkin (**Supplementary Fig. 3.2a,d**). Similar results were obtained in CHO-cells stably expressing WT human *PRKN* cDNA. Thus, our cell culture-based models provided us with suitable platforms to investigate the interactions between oxidative stress, as induced by exogenous and endogenous sources, versus thiol network responses in the context of defined parkin expression levels.

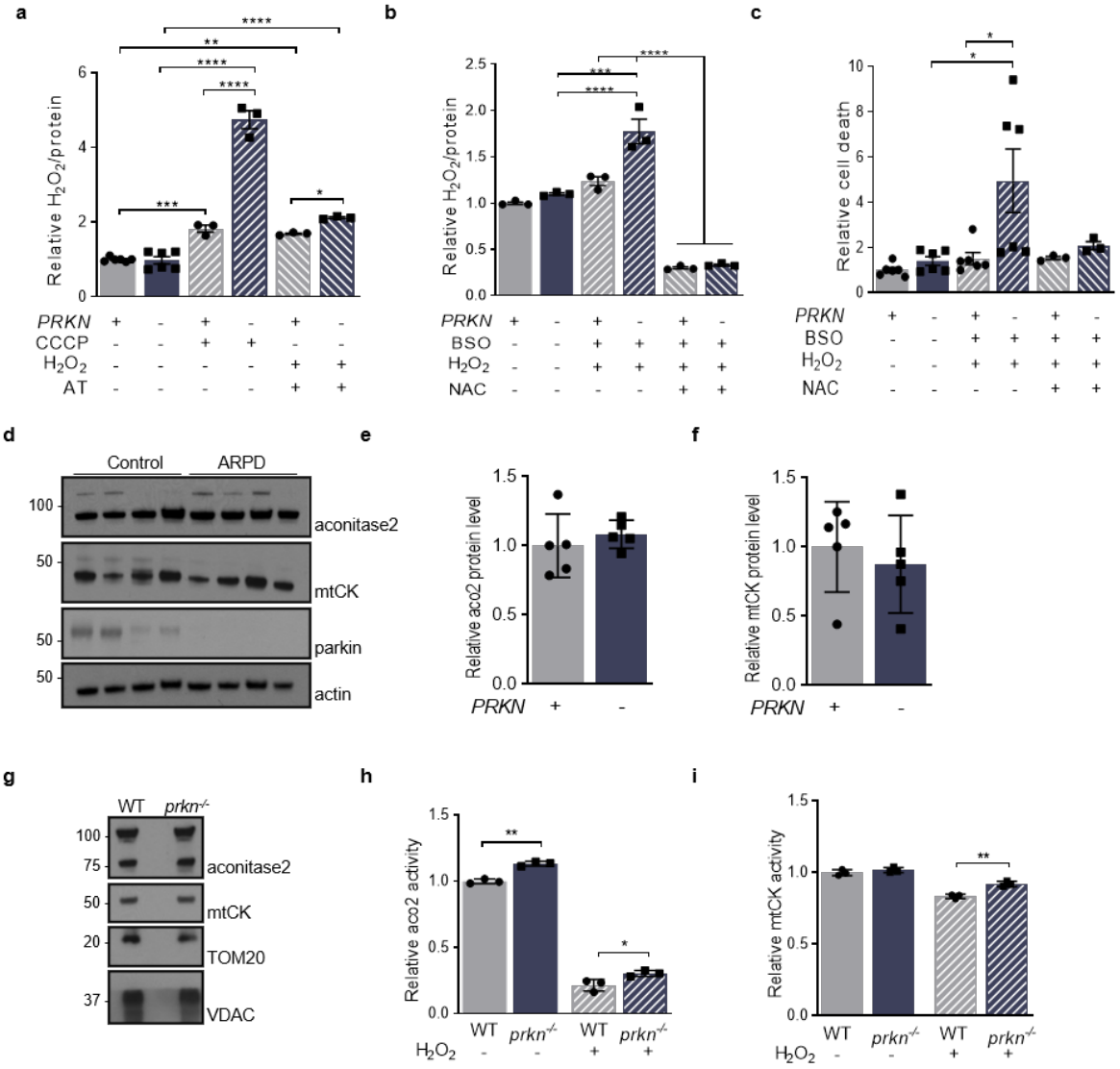

Figure 3.3. ***PRKN*** **expression alters cellular redox state and affects redox-dependent enzymatic activity in mice.** (**a**) Endogenous H_2O_2 levels in HEK293 cells overexpressing FLAG-parkin (denoted as *PRKN* +) or FLAG-control vector alone (denoted as *PRKN* -), following treatment with vehicle, 10μM CCCP-incubation for 1 hour, or the combination of 2mM H_2O_2 and 0.5M aminotriazole (AT) for 30mins, as indicated. (**b**) Endogenous H_2O_2 levels, and (**c**) cellular toxicity in CHO cells stably expressing myc-parkin (denoted as *PRKN* +) or myc-control vectors (denoted as *PRKN* -) with or without exposure to 2 mM H_2O_2, 2mM BSO, or 20mM NAC, as indicated. (**d**) Western blot of aconitase-2, mitochondrial creatine kinase (mtCK), and parkin expression in four control and four *PRKN*-deficient ARPD cases. (**e**) Quantification of relative expression levels of aconitase-2 (Aco-2), and (**f**) mtCK from Western blots shown in (**d**). (**g**) Protein expression of Aconitase-2, mtCK, Tom20 and VDAC in mitochondrial extracts from WT and *prkn*$^{-/-}$ mouse brains of 12 months of age. (**h**) Aconitase-2, and (**i**) mtCK activity in mitochondrial extracts from WT and *prkn*$^{-/-}$ brains with or without exogenous treatment of 4 μM H_2O_2. Data in (**a-c**) are shown as mean normalized to untreated *PRKN* + and in (**e,f, h** and **i**) are shown as mean normalized to untreated control (CO or WT). Results are plotted as n=3-6 (**a-c**) biological replicates or n=3/genotype (**h-i**) ± SEM. Significance was determined using a one-way ANOVA with Tukey's post-hoc analysis in (**a**) [$F(3, 14)= 54.86$, $p< 0.0001$], in (**b**) [$F(5, 12)= 92.38$, $p< 0.0001$], in (**c**) [$F(5, 24)= 4.683$, $p= 0.0040$], in (**h**) $F(3, 8)= 836.5$, $p<0.0001$] and in (**i**) $F(3, 8)= 60.19$, $p< 0.0001$]; an unpaired Student T-test was used in (**e** and **f**) ($p>0.05$).

Parkin contributes to the thiol network during oxidative stress

To explore how parkin contributed to the thiol network, we first compared survival rates of CHO-parkin cells following exposure to H_2O_2 after depletion of GSH with buthionine sulfoximine (BSO). We chose CHO cells because of their known efficiency in antioxidant responses.[851] Treatment with either H_2O_2 or BSO alone did not cause parkin-dependent changes in cell death (**Supplementary Fig. 3.2f**), as expected. However, under combined stress conditions, *PRKN* expression was cytoprotective: it normalized ROS levels ($p<0.001$; **Fig. 3.3b**) and led to a significant abrogation of cell death ($p<0.05$; **Fig. 3.3c**); it also resulted in parkin's own oxidation. Treatment with excess N-acetylcysteine, an abundant source of thiols, resulted in similarly protective effects as did *PRKN* over-expression (**Fig. 3.3b, c**). We concluded from these results that parkin supplemented the cellular thiol network by neutralizing ROS through mechanisms that lead to the oxidation of parkin's own cysteines (of which the human holoprotein has 35, the murine 34).[846]

Parkin deficiency alters activity of select redox-dependent, mitochondrial enzymes

To link our redox chemistry findings back to previously identified changes from proteomic screens of parkin-deficient mouse brain,[435,437] we explored redox-sensitive enzymatic activities. Although our collective findings point at excess oxidative stress in the cytosol of parkin-deficient neural systems, these previously conducted, unbiased proteomic screens had identified both cytosolic and mitochondrial enzymes as dysregulated in their 2D-electrophoretic migration pattern on SDS/PAGE. Given that the cellular thiol network involves crosstalk between the cytosol and organelles, we selected two enzymes with principal roles in mitochondrial function, i.e., aconitase-2 (Aco2) and mitochondrial creatine kinase (mtCK) (**Fig. 3.3d-i**). When screening homogenates of cortices from ARPD versus control subjects and brains from *prkn* $^{-/-}$ mice versus WT littermates by Western blotting (**Fig. 3.3d-g; Supplementary Fig.**

3.1a, b), we found no detectable differences in either Aco2 or mtCK protein concentrations or of several other mitochondrial constituents examined, such as VDAC and MnSOD. However, we recorded a significant increase in the activity of Aco2, a $NADP^+$-associated enzyme, even under basal conditions when compared to littermate controls ($p<0.01$; **Fig. 3.3h**). Following exposure of isolated brain mitochondria to H_2O_2 *in vitro*, both Aco2 and mtCK activities were generally decreased, as expected; however, their residual activities remained consistently higher in mitochondria isolated from *prkn*$^{-/-}$ brains ($p<0.05$ and $p<0.01$, respectively; **Fig. 3.3h.i**). We suspect that cytosolic redox effects in *prkn*$^{-/-}$ mice, such as changes in the thiol network and / or changes in the redox state of co-factors (such as $NADP^+$ or $NADPH/H^+$) may contribute to the observed differences in the activities of these two mitochondrial enzymes.

Bi-genic mice show no deficit in general locomotion tests

We sought to test whether the documented increase of chronic oxidative stress in bi-genic mice, including in the midbrain (**Fig. 3.1-3.2**), was associated with any altered behavioural outcome (**Fig. 3.4a**). Prior to tissue collections for biochemical readouts (above), mice were evaluated by several behavioural tests previously validated to be sensitive to changes observed in diverse models of parkinsonism. Of note, each cohort contained an equal distribution of both sexes (**Supplementary Table 3.1**).

When placed in a novel cage and monitored for 4 hours in 5-minute-long bins, using infrared light beams and sensors that monitor the animal's ambulatory activity, a two-way ANOVA analysis revealed no differences at 12 months between the bi-genic mice versus their littermates (WT; *prkn*$^{-/-}$; *Sod2*$^{+/-}$) in general locomotion. This activity was observed during exploration of the novel cage during the first hour (**Fig. 3.4b**). Additionally, the animals habituated normally to their new environment, with

no genotypic differences seen at 12 months of age (two-way ANOVA analysis). This was monitored as a decrease in their activity over the last 3 hours of testing (**Fig. 3.4b**). The result was similar when assessing each hour of the 4 hours testing time separately (**Supplementary Fig. 3.3b**). The same outcomes were obtained with the 6 months old cohort (**Supplementary Fig. 3.3a, c**), and together, these results indicated no baseline deficits in locomotion during ambulatory and exploratory activities across the 4 genotypes tested and during aging between 6 and 12 months.

Prkn$^{-/-}$*//Sod2*$^{+/-}$ mice display no motor deficits on the rotarod

To evaluate task-related motor coordination, balance and learning,[852] littermates were tested on the rotarod over four trials a day for three days. By utilizing an accelerating rod protocol (4-40 revolution per minute (rpm) over 5 minutes, as opposed to a constant speed protocol, we minimized testing fatigue, thus providing a more challenging test paradigm; this, to detect more subtle coordination deficits, as has been described.[853] As expected, WT mice displayed normal motor task learning, which was observed by the increasing latencies to fall over the 3 days of testing (**Fig. 3.4c; Supplementary Fig. 3.3d**), as well as, across the 4 trials per day, both at 6 and 12 months of age. However, when testing the 4 genotypes at both 6 and 12 months of age, and when analyzing the results by two-way ANOVA tests, we saw no difference in motor coordination, measured as latencies to fall off the accelerating rod (**Fig. 3.4c; Supplementary Fig. 3.3d)**. Further, *prkn*$^{-/-}$, *Sod2*$^{+/-}$, and bi-genic mice showed task learning capacities that were comparable to WT animals. As expected, across the 4 genotypes the latencies to fall decreased with age.

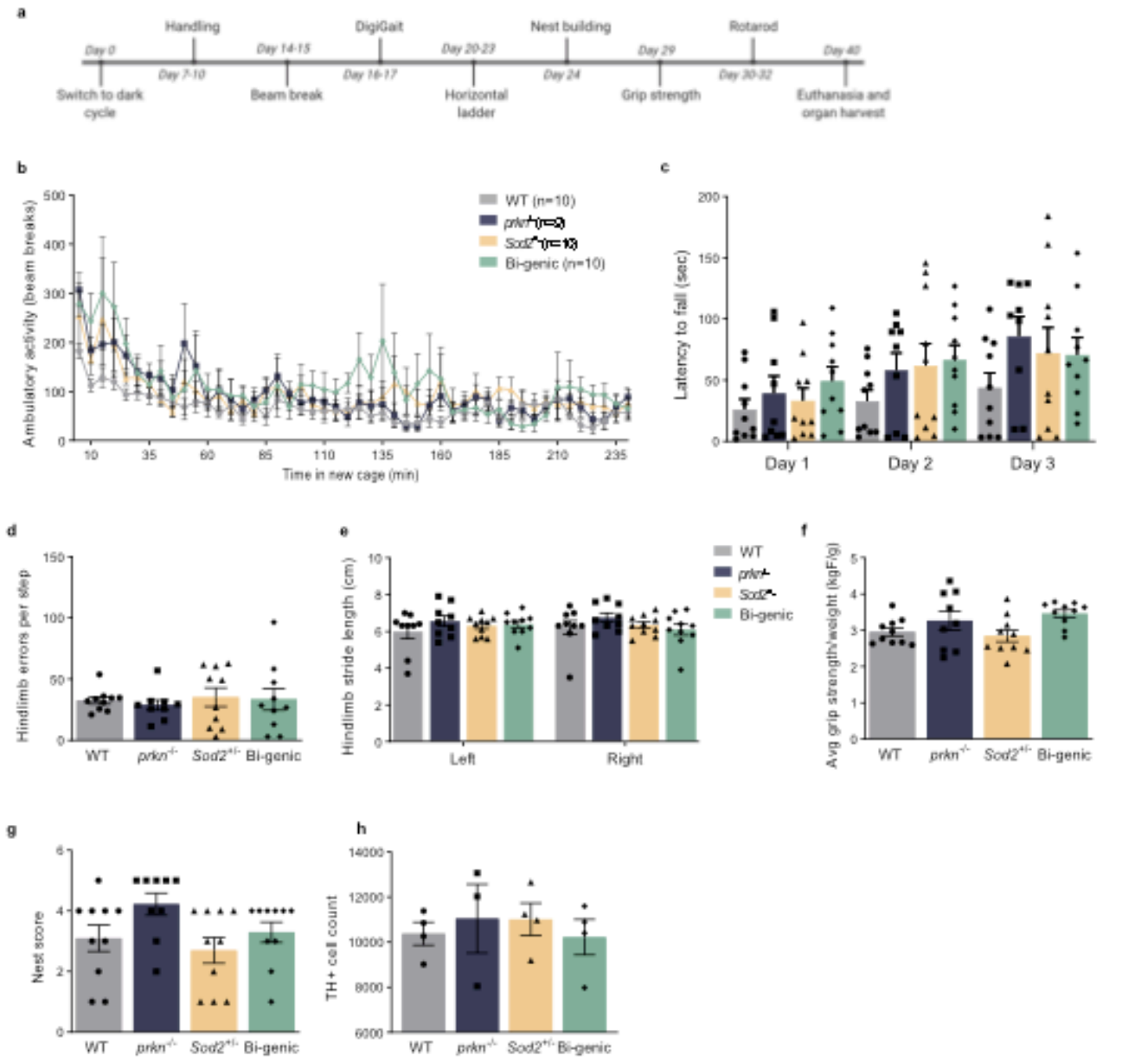

Figure 3.4. Chronically elevated oxidative stress in adult bi-genic mouse brain does not result in parkinsonism.
(**a**) Timeline of behavioural studies in 12-month-old cohort (shown in **b-g**). (**b**) Ambulatory activity of individual mice measured as beam breaks over 4 hours, when placed in a novel cage. (**c**) Average latency to fall in seconds (sec) of 4 trials/day, over 3 consecutive days using the Rotarod test. (**d**) Number of hindlimb errors per step/genotype determined using the horizontal ladder test. (**e**) DigiGait analysis of left and right hindlimb stride length (in cm). (**f**) Average grip strength per animal weight (kilogram-force, kgF). (**g**) Nest building scores based on a qualitative scale of 1-5. (**h**) Stereological quantification of TH-positive neurons in the *S. nigra* of the 12 months of age cohort. Data are shown as mean values/genotype with number of animals/genotype indicated in (**b**) except for (**h**) (n=4/genotype) ± SEM. Significance was determined using a two-way ANOVA with Tukey's post-hoc analysis comparing time and genotype in (**b**) [$F(141, 1680) = 0.6079$, $p = 0.9999$], in (**c**) [$F(6, 105) = 0.3214$, $p = 0.9245$], and in (**e**) [$F(3, 68) = 0.4018$, $p = 0.7522$], with no significance found between genotypes within individual time points or limbs; a one-way ANOVA with Tukey's post-hoc analysis in (**d**) [$F(3, 35) = 0.1666$, $p = 0.9182$], in (**f**) [$F(3, 35) = 2.816$, $p = 0.0533$], in (**g**) [$F(3, 35) = 2.582$, $p = 0.0690$], and in (**h**) [$F(3, 11) = 0.2452$, $p = 0.8631$].

The bi-genic mice exhibit no deficits in horizontal ladder testing

To further evaluate gait and coordination, a second skill-based locomotion test was used. The mice were first trained to cross a horizontal ladder with uneven rungs and encased in two plexiglass walls on each side, with their home cage placed on one end, as an incentive to cross. On testing day, all animals were recorded crossing the ladder over 4-5 trials. The number of correct steps and errors (scored as 'missing' a rung or 'cheating' by placing the paw on the plexiglass wall) were quantified,[854] and analyzed by one-way ANOVA. When assessing hindlimb errors per step, the bi-genic mouse displayed no deficits at 12 months of age, when compared to WT, *prkn*$^{-/-}$, and *Sod2*$^{+/-}$ mice (**Fig. 3.4d**). As a more general assessment of gait and to evaluate whether the bi-genic mouse took more or fewer steps to cross the ladder, the average hindlimb step count was quantified. There, we saw no genotypic differences at 12 months of age (**Supplementary Fig. 3.4c**). Similar outcomes were observed in 6 months-old mice (**Supplementary Fig. 3.4a, b**). Overall, and as expected, the percent number of hindlimb errors increased with age across all genotypes, while the average step count remained the same. Additionally, observing no differences in the average hindlimb step count determined that *prkn*$^{-/-}$, *Sod2*$^{+/-}$, and bi-genic mice were able to perform the task in a comparable manner to age-matched WT animals.

***Prkn*$^{-/-}$*//Sod2*$^{+/-}$ mice display no gait or posture deficits by DigiGait analysis**

The DigiGait imaging system represents a ventral plane videography instrument that allows for gait and posture analyses by continuously imaging the underside of mice while they walk on a treadmill with speed varying from 10 to 18 cm/s. Built-in algorithms quantify several readouts to assess dynamic gait signals. This technique has been used in recent studies to better evaluate subtle changes in gait and locomotion of rodents (as observed in PD patients), separate from other behavioural tests, and has been applied to several animal models of PD.[855-857] Confirming the validity of the test, WT animals behaved

and scored as expected, and as previously published.[855-857] A two-way ANOVA analysis conducted at 6 and 12 months of age, showed no quantifiable differences in the stride lengths of forelimbs and hindlimbs (in cm) across the four genotypes (**Fig. 3.4e; Supplementary Fig. 3.4d,e,g**). When evaluating stance widths (cm), there were also no genotypic differences between the cohorts tested (**Supplementary Fig. 3.4f, h**; two-way ANOVA analysis). Of note, these latter measures of gait were not altered by age across the four genotypes.

Bi-genic animals display normal grip strength

When behaviourally evaluating animal models of PD, grip strength is not routinely used, because loss of power is not one of the cardinal motor signs seen in patients. Nevertheless, in a recent report, it is suggested that early-onset, reduced grip strength, observed as low muscle strength in late adolescence, could predict the development of PD.[858] Additionally, parkin has been previously observed to be highly expressed in skeletal muscle.[184,829,846] Therefore, we analyzed grip strength in WT, *prkn*$^{-/-}$, *Sod2*$^{+/-}$ and bi-genic mice. The forelimb grip strength was measured (in kg-force units), using a force transducer that recorded the maximum force generated by the animal as it was pulled off of a grate. There were no genotypic differences in the average forelimb grip strength across 5 trials at 6 and 12 months of age (**Supplementary Fig. 3.5a, c**), when analyzed by one-way ANOVA. To determine whether body weight was a contributing factor in the outcome, the average forelimb grip strength data were normalized to body weight. After normalization, no differences between the bi-genic mice versus their littermates were seen at either 6 months or 12 months of age (**Fig. 3.4f; Supplementary Fig. 3.5b**). It is worth noting that grip strength measures did not measurably decrease with advanced age across the four genotypes.

Prkn$^{-/-}$*//Sod2*$^{+/-}$ mice show no deficits in nest building

Nest building assesses a complex and innate activity in mice, including motivation, planning and usage of fine motor skills. It can be qualitatively analyzed[859] and has been shown to be altered in select PD models.[860] The bi-genic mice did not score significantly lower than WT, *prkn*$^{-/-}$, and *Sod2*$^{+/-}$ mice at 6 and 12 months of age, when the scoring (1-5) was averaged, and analyzed by one-way ANOVA on ranks with a non-parametric Kruskal-Wallis test (**Fig. 3.4g; Supplementary Fig. 3.5d**). When assessing the frequencies of each score, a two-way ANOVA analysis showed that the bi-genic mice did not significantly score lower (scores 1-3) at either 6 or 12 months of age, when compared to their WT, *prkn*$^{-/-}$, and *Sod2*$^{+/-}$ littermates (**Supplementary Fig. 3.5e, f**).

Prkn$^{-/-}$*//Sod2*$^{+/-}$ mice show no evidence of nigral degeneration

Given the cumulative evidence of irreversible signs of oxidative stress and redox dysregulation in the brain of bi-genic mice when compared to WT, *prkn*$^{-/-}$ and *Sod2*$^{+/-}$ mice, we sought to investigate whether these changes, when combined with advanced age, generated any midbrain-specific cell loss. We used stereological methods to quantify the relative and absolute numbers of dopaminergic cells in the *S. nigra* by counting tyrosine hydroxylase (TH)-positive neurons detected by immunohistochemistry-based microscopy. Consistent with our behavioural results, no genotypic differences in the total number of detectable, TH-positive neurons were observed in 12-month-old bi-genic animals versus their control groups (**Fig. 3.4h**).

Of note, when analyzing the data sets for behavioural tests, as well as, microscopic outcomes, no sex effects were observed, akin to what has been reported in the literature for subjects with *PRKN*-linked PD. Additionally, each animal's body weight had been recorded and analyzed as a variable. However,

weight was also not a contributing factor in the outcomes recorded across all behavioural tests and genotypes.

***PRKN* over-expression alters the redox state of glutathione in eukaryotic cells**

Although *prkn*$^{-/-}$ and bi-genic mice lacked measurable motor and behavioral deficits, their tissues demonstrated signs of increased oxidation state. We, therefore, returned to cell models to examine the thiol network further by directly measuring the levels of GSH (reduced form) and GSSG (oxidized form) by HPLC. There, CHO-control cells showed high concentrations of GSH, as expected, and low amounts of GSSG with an elevated [GSH]: [GSSG] ratio (**Fig. 3.5a**). Stable over-expression of human parkin significantly reversed these redox indices ($p<0.01$, and $p<0.001$); in contrast, no change was found in total concentrations of GSH and GSSG in CHO-parkin versus CHO-control cells (**Fig. 3.5b**). Exogenous parkin-dependent changes in GSH levels were also observed in human, dopaminergic SH-SY5Y cells (**Fig. 3.5c**).

Consistent with published reports of the high stress tolerance by CHO cells,[851] exogenously added H_2O_2 did not dramatically change the redox indices between CHO-control and CHO-parkin cells with the notable exception of -now equalized- GSSG levels between the two sister cultures (**Fig. 3.5d**). When using a linear regression model with GSH levels as the dependent variable, we found that a lower expression of endogenous parkin (such as in CHO-control cells) was consistently associated with higher GSH levels in both control and H_2O_2-stressed cells ($p=0.043$ and $p=0.0071$, respectively) and vice versa. This inverse relation between GSH concentrations and parkin protein levels in healthy cells suggested the existence of a feedback loop.

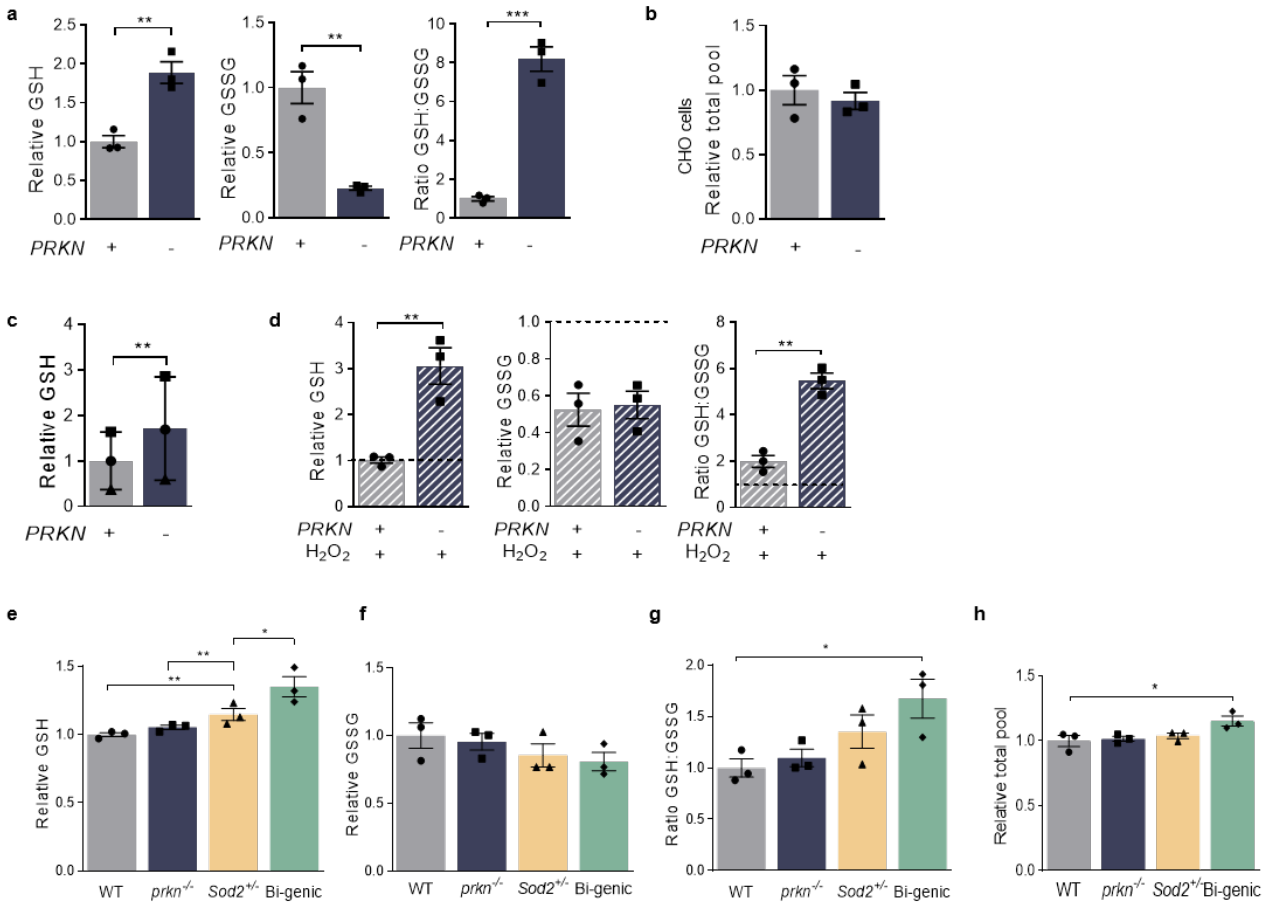

Figure 3.5. *PRKN* expression alters glutathione metabolism in cells and murine brain.
(**a-d**) HPLC-based quantification of reduced glutathione (GSH), oxidized glutathione (GSSG), the ratio of GSH:GSSG and the total glutathione pool (GSH+GSSG) in CHO cells under control conditions (**a,b**), and following H_2O_2 stress (**d**).
(**c**) Quantification of GSH by monochlorobimane assay in SH-SY5Y neural cells over-expressing FLAG-parkin or FLAG-control vector alone. (**e-h**) HPLC-based quantification of (**e**) reduced glutathione (GSH), **f** oxidized glutathione (GSSG), **g** the ratio of GSH:GSSG, and **h,** total glutathione pool (GSH+GSSG) in the brains of 6-month-old mice, as indicated. Data in (**a-d**) are plotted as mean values/ total protein (nmol/µg) normalized to WT or *PRKN* +, with n=3 biological replicates in (**a-d**) and n=3/genotype in (**e-h**) ± SEM or SD (**c** only). Significance was determined using an unpaired Student T-test in (**a**) (p= 0.0052 for GSH, p=0.0033 for GSSG, p=0.0004 for ratio), (**b**) (p=0.5564) and (**d**) (p=0.0071 for GSH, p=0.8352 for GSSG, p=0.0013 for ratio); a paired Student T-test was used in (**c**) (p= 0.0024) with paired replicates identified with identical symbols; a one-way ANOVA with Tukey's post-hoc analysis in (**e**) [F(3, 8)= 12.02, p=0.0025], in (**f**) [F(3, 8)= 1.266, p=0.3495] in (**g**) [F(3, 8)= 4.667, p=0.0362], and in (**h**) [F(3, 8)= 4.583, p=0.0378].

***Prkn* gene expression alters glutathione redox state in bi-genic mice**

The possible impact of parkin expression on GSH metabolism was further investigated in mouse brains. Two groups previously reported elevated GSH levels in *prk* $^{-/-}$ brain and glial cultures.[312,432] When examining the same mutant line as Itier et al., but using our HPLC-based quantification method instead of their protocol (see below), parkin-deficient brains showed a trend, but no significant difference, in thiol changes, *i.e.*, for the subtle rise in GSH concentrations, a trend toward lower levels of GSSG, and a subtle rise in the [GSH]:[GSSG] ratio (**Fig. 3.5e-h**). In parallel, the brains from *Sod2*$^{+/-}$ haploinsufficient animals showed similar changes, as seen for *prkn*$^{-/-}$ mice, with a rise in GSH level reaching significance ($p<0.05$; **Fig. 3.5e**). Moreover, in the *prkn* $^{-/-}$*//Sod2*$^{+/-}$ animals, three of the changes in redox indices were significantly altered, i.e., the GSH concentration ($p<0.05$; **Fig. 3.5e**), the [GSH]:[GSSG] ratio ($p<0.05$; **Fig. 3.5g**), and the total level of detectable glutathione [GSH and GSSG], when using the HPLC method ($p<0.05$; **Fig. 3.5h**).

Transcription for new glutathione synthesis is not altered in parkin-deficient and bi-genic brains

To elucidate the apparent rise in GSH concentrations in the mutant mice, we examined its *de novo* synthesis (**Fig. 3.6a, b**). Among the four genotypic groups, we found no difference in transcript numbers for the rate-limiting enzymes in glutathione synthesis isolated from brain homogenates of age-matched (6-month-old) mice, *i.e.,* the glutamate-cysteine-ligase-catalytic (*GCLC*) and glutamate-cysteine-ligase-modifier (*GCLM*) subunits,[861] or for *Dj-1,* which we investigated as a second, ARPD-linked gene (**Fig. 3.6b**). Unexpectedly, in the bi-genic mice, where we had recorded a significant rise in the total glutathione (GSH and GSSG) levels (**Fig. 3.5h**), we also found no change in copy numbers for *GCLC* or *GCLM* mRNA (**Fig. 3.6b**). Thus, *de novo* synthesis from transcription did not explain the glutathione redox changes seen in bi-genic mice.

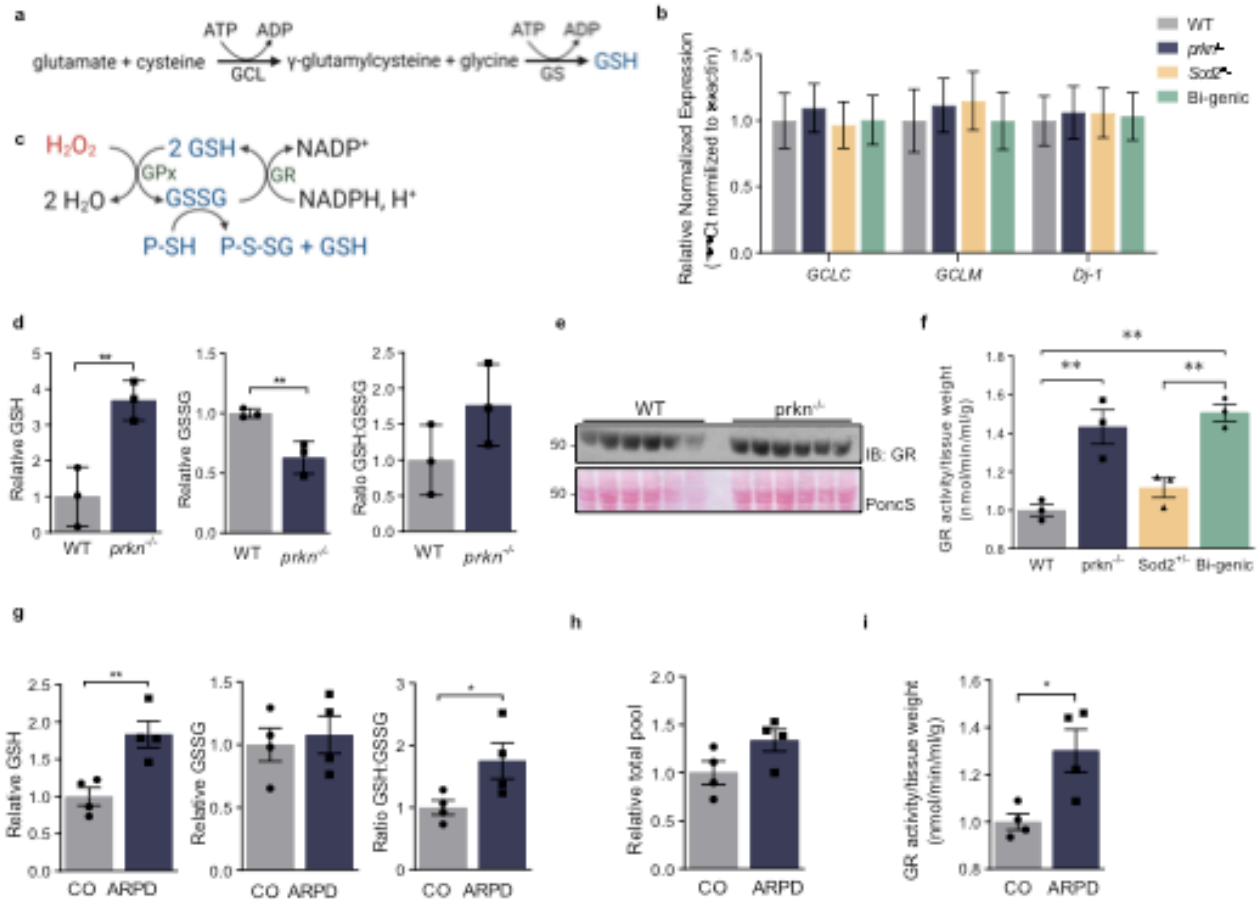

Figure 3.6. Parkin contributes to glutathione recycling in the brain independent of *de novo* synthesis.
(**a**) Schema of GSH synthesis pathway, where GCL is the rate-limiting enzyme. (**b**) *Dj-1*, *GCLC* and *GCLM* mRNA levels in brains of 6-month-old mice, as indicated. (**c**) Schema highlighting glutathione-peroxidase (GPx)- and glutathione-reductase (GR)-dependent recycling of GSH and GSSG. (**d**) Quantification of reduced glutathione (GSH), oxidized glutathione (GSSG), the ratio of [GSH]:[GSSG] in the brains in 8-12-month-old WT and *prkn*$^{-/-}$ mouse brains, as measured using the GR-dependent Tietze method. (**e**) Western blot analysis of GR expression levels in 6-month-old WT and *prkn*$^{-/-}$ brains. Each lane is an individual mouse. (**f**) GR activity in 6-month-old genotyped mice, as indicated. (**g**) HPLC-based quantification of [GSH], [GSSG], [GSH]:[GSSG], (**h**) total glutathione (GSH+GSSG), and (**i**) relative GR activity in brain cortices from age-matched human controls and *PRKN*-deficient autosomal recessive PD (ARPD) cases. Data in (**b,f** and **i**) are shown as mean normalized to untreated control (CO; WT) ± SEM**.** Data in (**d, g-h**) are plotted as mean values/protein (nmol/mg) normalized to WT or CO ± SEM or SD (**d** only). Results were obtained using n=3/genotype (**b, d** and **f**) or n=4/genotype (**g,h**). Significance was determined using a two-way ANOVA with Tukey's post-hoc test in (**b**) [F(6, 24)= 0.1748, p=0.9811], with no significance found within individual genes (*e.g. GCLC* expression level alone between genotypes); a one-way ANOVA with Tukey's post-hoc analysis was used in (**f**) [F(3, 8)= 17.80, p=0.0007]; an unpaired Student T-test was used in (**d**) (p=0.0094 for GSH, p=0.0099 for GSSG, p=0.1522 for ratio), in (**g**) (p=0.0080 for GSH, p=0.7085 for GSSG, p=0.0536 for ratio), in (**h**) (p= 0.0891), and in (**i**) (p=0.0200).

Glutathione recycling is upregulated in *prkn*-deficient mouse brain

We then used a second protocol (the Tietze method) to quantify glutathione metabolites in murine brain. This assay is based on the enzyme glutathione reductase (GR), which, *in vivo*, is activated by rising levels of ROS and/or its substrate, i.e., GSSG, and is inhibited by excess product level, i.e., GSH, and excess $NADP^+$ (**Fig. 3.6c**).[862-864] When using the Tietze method, which utilizes exogenously added GR to indirectly measure GSH and GSSG levels, we reproduced the same -but now significant- changes in *prkn*$^{-/-}$ mice (**Fig. 3.6d**), *i.e.,* [GSH] elevation ($p<0.01$), [GSSG] lowering ($p<0.01$) and a trend for a rise in the [GSH]:[GSSG] ratio (**Fig. 3.5e-h**). These results suggested that the two protocols employed to quantify glutathione metabolites (using HPLC versus the Tietze method) may have had different degrees of sensitivity. Importantly, they pointed at GR activity as a potential mechanism to explain the relation between parkin protein expression levels, glutathione redox state, and the relative protection of parkin-deficient mice from chronic oxidative stress.

Glutathione reductase activity is upregulated in prkn-deficient mouse brain

To assess GR activity in the brain, we first optimized its quantification in frozen versus fresh homogenates, which revealed comparable results after a single freeze / thaw step (**Supplementary Fig. 3.6a-b**). When further examining our mouse lines (with the operator blinded to their genotype), we found no significant change in its total protein concentration by immunoblotting (**Fig. 3.6e**), but detected higher GR activity levels (by approximately >40%) in *prkn*$^{-/-}$ and bi-genic mouse brains when compared with age-matched (6 -month-old) WT and *Sod2*$^{+/-}$ animals ($p<0.01$; **Fig. 3.6f**). Under these conditions, MnSOD reduction alone seemed to have no impact on GR activity.

Parkin deficiency in human cortex reveals compensatory changes in glutathione metabolism

The interplay between parkin and glutathione metabolism was further examined in human brain using cortex specimens collected at autopsy from patients with *PRKN*-linked ARPD and age- and *post mortem* interval-matched healthy controls (**Fig. 3.6g-i; Supplementary Fig. 3.1a**).[506,846] In the absence of detectable parkin, reduced GSH levels, as well as, the ratio of [GSH]:[GSSG] were significantly increased, as measured by HPLC ($p<0.01$ and $p<0.05$, respectively; **Fig. 3.6g**). No differences were seen for GSSG concentrations (2nd panel in **Fig. 3.6g**) or the total concentrations of GSH and GSSG in these brains (**Fig. 3.6h**). Therefore, the redox changes recorded in human brain closely mirrored those in CHO cells monitored under oxidative stress conditions and in adult mouse brain (**Fig. 3.4 and 3.6**). Using a linear regression model with GSH concentrations as the dependent variable, we found that deficiency in WT parkin protein was associated with higher GSH levels in both human cortices and mouse brains ($p= 0.008$ and $p= 0.044$, respectively).

When examining the GR activity in these human frontal cortex specimens (and with the operator blinded to the genotype), we detected an ~30% significant rise in its activity in ARPD samples when compared to the controls ($p<0.05$; **Fig. 3.6i**). We conclude from these complementary results that in mammalian brain a bidirectional feedback loop exists between parkin protein expression and glutathione metabolism.

Through its own oxidation parkin directly contributes to the pool of recycled glutathione

We next explored whether parkin had a direct effect on thiol network changes, e.g. through GSH recycling. We first tested this using recombinant proteins, both MBP-tagged and untagged, and eosin-labelled GSSG (*i.e.,* E-GSSG-E, referred to as Di-E-GSSG) (**Fig. 3.7a-c; Supplementary Fig. 3.7**). We

discovered that full-length, human parkin had concentration-dependent activity in reducing Di-E-GSSG to the fluorescence emitting E-GSH (at 545 nm) (**Fig. 3.7a**). Of note, Di-E-GSSG itself is not fluorescent.[865] N-terminally truncated parkin comprising the IBR-RING2 domains (aa 327-465) and an untagged, C-terminal RING2 peptide (aa 425-465) also showed E-GSH-regenerating activity (**Fig. 3.7b**). Moreover, using a different source of Di-E-GSSG and untagged, full-length, human WT parkin (r-parkin)[846] we confirmed the parkin-dose dependent conversion of Di-E-GSSG to E-GSH *in vitro* (**Fig. 3.7c**).

From these results, we suspected a redox reaction during which one half of GSSG is reduced to GSH and the other engaged in S-glutathionylation (*i.e.,* parkin; **Fig. 3.7d**). To test this, we next incubated r-parkin (1uM) with eosin-free ratios of [GSH]:[GSSG] at a total concentration of 10μM per well (**Fig. 3.7e**). Following its incubation with GSSG, we determined that, under these conditions, parkin was able to generate up to 5 equivalents of GSH (*i.e.,* 6.8μM GSH minus a baseline signal of 1.3μM for r-parkin alone; **Fig. 3.7e**). Therefore, for every recycled GSSG molecule one reduced GSH and one S-glutathionylated cysteine on parkin had been generated. These *in vitro* findings demonstrated a direct biochemical effect by parkin on its surrounding thiol network. Together with our biochemical findings of parkin modifications in living cells exposed to pro-oxidants (**Supplementary Fig. 3.2a-d**) [846], our findings support a role for parkin as a redox state effector on the thiol network of eukaryotic cells.

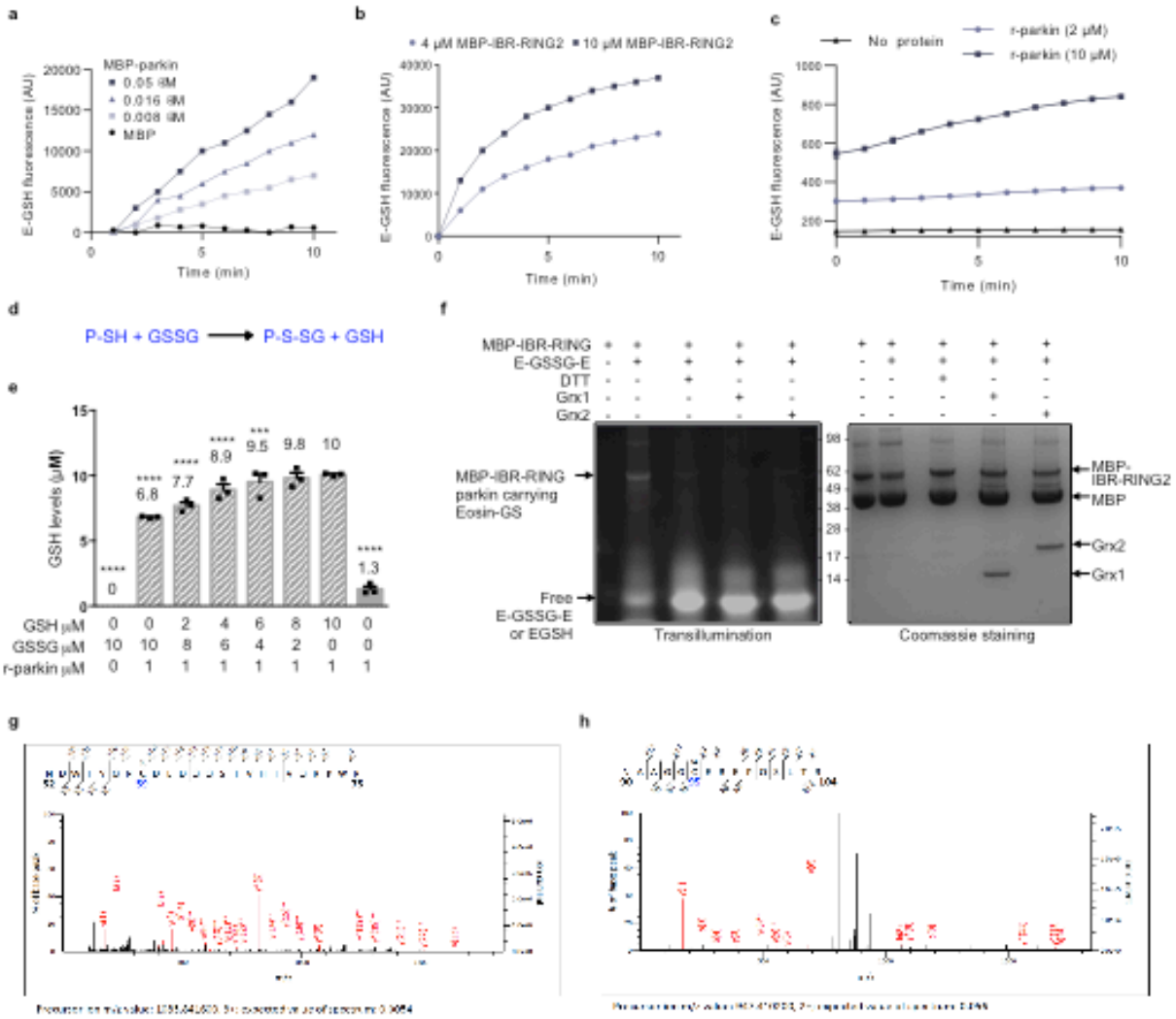

Figure 3.7. Parkin contributes to recycling of oxidized glutathione by directly reducing GSSG to GSH, resulting in parkin's own glutathionylation at Cys59 and Cys95.

(**a-c**) Fluorescence-based quantification of eosin (E)-labelled GSH following incubation of recombinant, full-length, MBP-parkin (**a**), MBP-IBR-RING2 parkin (**b**) or untagged, human full-length parkin (**c**) with 20 μM Di-E-GSSG over 10 minutes. The fluorescence increase of Di-E-GSSG (black circles) was used as background (n=2 runs (**a**, **b**, **c**) with triplicate wells) (**d**) Schematic of reversible S-glutathionylation reaction of parkin cysteine residues. (**e**) Quantification of free GSH levels measured using the monochlorobimane assay, following incubation of indicated levels of untagged glutathione preparations (μM) at various [GSH]:[GSSG] ratios with 1 μM of tag-less, full-length r-parkin (n=3 ± SEM). A one-way ANOVA with Dunnett's post-hoc test was used to compare all values to r-parkin incubated with 10 μM GSH, [F (7, 16) = 154.9, p< 0.0001]. (**f**) In vitro glutathionylation studies of MBP-IBR-RING2 parkin, where redox reduced preparations of 10 μM MBP-IBR-RING2 parkin were treated with 20 μM Di-E-GSSG in the absence or presence of 5 mM DTT or 1 mM NADPH, 5 mM GSH, and 0.1 μM glutathione reductase (GR) in the presence of either 1 μM glutaredoxin 1 (Grx1) or Grx2, as indicated. Results are representative of three independent experiments. (**g,h**) Examples of LC-MS/MS-generated spectra following trypsin digestion of MBP-parkin proteins incubated with Di-E-GSSG showing S-glutathionylation: (**g**) Cys59 within human parkin peptide aa 52-75, and (**h**) S-glutathionylation of Cys95 within human parkin peptide aa 90-104.

S-glutathionylated parkin occurs at cysteines 59, 95 and 377

The formation of E-S-glutathionylated parkin (referred to as parkin-SG-E) was confirmed by using MBP-parkin proteins, non-reducing SDS/PAGE analyses and UV light. We found that SG-E-parkin proteins were only visible under UV light after the incubation of nascent preparations with Di-E-GSSG (*e.g.,* **Fig. 3.7f**, lane 2 of left panel). Furthermore, the incubation of MBP-IBR-RING2-SG-E and MBP-parkin-SG-E with either DTT (as a positive control) or with activated glutaredoxin-1 or -2 (Grx1, Grx2)[865] reversed the S-glutathionylation of parkin and confirmed that parkin-SG-E S-glutathionylation occurred via cysteine-mediated disulphide-bond formation (**Fig. 3.7a-f**). Parkin proteins without an -SG-E modification did not interact with Grx1 or Grx2; moreover, thioredoxin-1 (Trx1; tested as a negative control)[866] did not react with parkin-SG-E. We concluded that parkin's ability to interact with GSSG is able to raise the net concentration of GSH, which in the process leads to reversible S-glutathionylation of WT parkin.

Finally, using a redox-controlled mass spectrometry (MS) technique we successfully mapped several S-glutathionylation sites on parkin. MBP-parkin-SG-E was subjected to trypsin digestion followed by LC-MS/MS and MALDI analyses. There we detected two residues that were consistently S-glutathionylated, namely the conserved residue cysteine 59 and primate sequence-specific cysteine 95,[846] each carrying an extra mass of 305.0682 (**Fig. 3.7g,h**). This mass adduct corresponds to a S-linked glutathionylated oxidation event. A third, less frequently identified residue to be S-glutathionylated in human parkin was cysteine 377 within its IBR domain. We concluded from these results that S-glutathionylation represents a *bona fide* oxidative modification of human parkin, which arises from its direct interaction with GSSG.

3.6 Discussion

The goal of our study was to build on our previous work on parkin redox function,[846] and to generate a model for oxidative stress-induced, recessive parkinsonism (**Fig. 3.1-3.3**). Further, we sought to examine redox mechanisms by which the mammalian brain responds to parkin deficiency. To this end, we generated a bi-genic mouse model of chronic oxidative stress by combining the *Sod2* locus haploinsufficiency onto the established background of systemic parkin deficiency. Age-dependent analysis revealed that oxidative stress did indeed increase in the brain, including midbrain of bi-genic mice (**Fig. 3.1-3.2**). Loss of parkin also altered the activity of redox-sensitive mitochondria-associated enzymes (Aco2 and mtCK, **Fig. 3.3**). However, by 12 months of age, our bi-genic animals did not exhibit any motor deficits and showed no evidence for degeneration of dopamine neurons in the midbrain (**Fig. 3.4**). Nevertheless, our work revealed a heretofore unknown, bidirectional feedback loop between parkin expression and glutathione metabolism, whereby in the absence of parkin a compensatory upregulation of recycled GSH is observed in cells, in human cortex and in mouse brain (**Fig. 3.5-3.7**).

Reduced glutathione is the most abundant cytosolic, low molecular weight thiol involved in antioxidant defenses and in regulating metabolism.[867] By extension, GSH deficiency contributes to oxidative stress and plays a role in aging and the pathogenesis of many diseases, including PD.[696] In the absence of parkin, murine and human brains upregulate recycling of GSH, presumably as a compensatory mechanism to keep ROS levels controlled and maintain redox homeostasis. If done efficiently, this could be consistent with the lack of a robust increase in baseline endogenous H_2O_2 levels in *prkn*$^{-/-}$ brains when compared to WT (**Fig. 3.1**).[846] The lack of a neurodegenerative phenotype in our bi-genic mice may also relate to mitochondria-generated compensatory mechanisms associated with the decrease in MnSOD activity. In response to increasing levels of superoxide, a more efficient VDAC-

mediated shuttling of this radical into the cytosol could occur, with subsequent neutralization by SOD1 (and/or -3).[868]

In addition, we speculate that the limited lifespan of mice, the nature of oxidative radicals generated, and the degree of stress, or any combination thereof, may have been insufficient to lead to nigral cell loss in our bi-genic mice. This was partially demonstrated by Hennis et al, whose similar mouse model demonstrated behavioural and neurotransmitter alterations when additional stress was applied with systemic loss of *Dj-1* expression.[849] Nevertheless, in parallel work, we recently found that parkin-dopamine conjugate formation leads to the enhancement of melanin polymer formation and prevented dopamine-mediated rise in oxidative stress and cell death.[846] Neuromelanin-rich pigment formation is markedly enriched in aged primates, and generally not observed in aged mouse brain, which could, yet again, explain the lack of PD-like pathogenesis in many rodent models. Therefore, a possible avenue to induce neurodegeneration in the midbrain of adult mice could also include increasing dopamine toxicity through exogenous L-dopa treatment, monoamine oxidase (MAO)-B inhibition,[869,870] elevated cytosolic concentrations of dopamine due to dysfunction of VMAT,[871] or increased neuromelanin production by inducing the expression of human tyrosinase-encoding cDNA in the *S. nigra*.[872]

Here, we uncovered a reciprocal relationship between *PRKN* expression and glutathione metabolism *in vivo*. The thiol network, to which we propose parkin contributes, is critical in the maintenance of overall redox balance, and thus, to cellular and organ health.[873] In parkin's absence: [GSH] is elevated; [GSSG] is diminished; the ratio of [GSH]:[GSSG] is increased; and total glutathione levels [GSH and GSSG] are unchanged, except in bi-genic mice (**Fig. 3.5-3.6**). We propose that parkin's presence reduces cellular needs for higher levels of free GSH. We first explored *de novo* synthesis of GSH but found no increase in *GCLM* or *GCLC* mRNA levels (**Fig. 3.6**). As for the rise in total

glutathione in bi-genic mice, and pending further investigations, we posit that higher GSH levels may still have resulted from *de novo* synthesis but via more effective translation of existing *GCLM* mRNA.[861,864]

Nevertheless, in parkin's absence, we attributed the upregulation of GSH to an increase in GR activity, which is the cognate enzyme for recycling GSH from GSSG, rather than through *de novo* synthesis (**Fig. 3.6-3.7**). Parkin caused direct recycling of GSSG, resulting in one molecule of GSH and parkin S-glutathionylation at residues 59, 95 and 377 (**Fig. 3.7**). We noted with interest that primate-specific cysteine 95 is targeted for oxidation by both S-glutathionylation and dopamine radical adduct formation.[846] Thus, we question whether this specific residue, which is located in the linker region of human parkin, could have an effect on parkin activation akin to serine 65 phosphorylation during PINK1 and parkin-dependent mitophagy.[571] We anticipate that the many posttranslational modifications of parkin that we have identified[846](**Fig. 3.7**), will inform structural studies and cell biology research in the future. We propose that these should be pursued in the context of parkin's redox chemistry.

Future studies will also explore which region and which cell type in the nervous system[312] contribute most significantly to the parkin-dependent glutathione redox changes we have observed. The lack of significantly elevated GSH levels in *prkn*$^{-/-}$ mouse brain by HPLC suggests that this animal can also compensate for increased cytosolic ROS via other redox state-regulating mechanisms, such as via glutathione peroxidase (GPx) activity (**Fig. 3.8**). High tolerance to ROS and the unique elevated oxidation state observed in human nigral neurons (discussed above) may help explain the lack of dopamine cell loss in *prkn*-deficient mice.[82,85,432,433,823] Therefore, in aged mouse brain, one or more additional stressors could be required. Based on our observations, the reduction of cytosolic GSH levels, such as through the disruption of *GCLM*-mediated GSH biosynthesis,[874] treatment with BSO,[875] or pharmacological inhibition of GR[876] could facilitate a parkin-associated neurodegenerative phenotype.

Additionally, due to the transient nature of S-glutathionylation (as well as of S-nitrosylation,[489] we have not yet validated parkin's S-glutathionylation *in vivo*. Furthermore, we wish to study a greater number of *PRKN*-genotyped, age-matched, human brain tissue specimens to quantify protein carbonylation and nitrotyrosination, as well as, to explore human brain-specific changes in redox state-related transcriptomes. This to validate mechanistic pathways that parkin is likely involved in (**Fig. 3.8**).

Building mouse models focusing on increasingly impaired redox homeostasis, in addition to parkin deficiency, should better recapitulate ARPD, as informed by human studies. Our discovery that parkin's seemingly diverse activities are anchored in traditional redox chemistry provides a biochemical and unifying explanation for its role in neuroprotection. It may help answer the two decades-old question: "What function of parkin is essential in conferring the selective protection of dopamine neurons in the human brainstem?"[106,846] Further exploration of parkin's redox biology should create new opportunities to develop urgently needed therapies for patients with young-onset parkinsonism.[801,877,878]

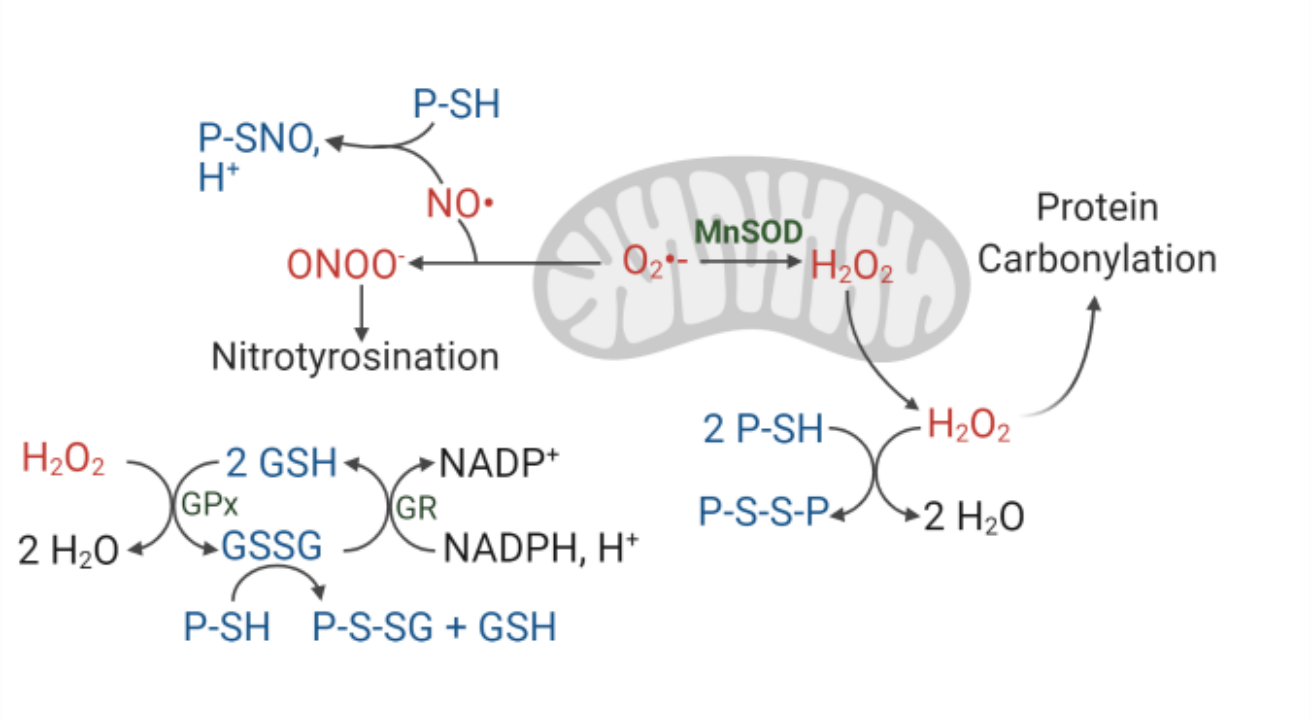

Figure 3.8. Summary of parkin-dependent changes to redox state in the cytosol of mammalian brain.
Graphical depiction of redox changes identified in murine parkin-deficient brain and human cortex from ARPD patients. Highlighted are: GSH recycling; generation of ROS levels (*i.e.,* H_2O_2; superoxide) leading to carbonylation; metabolism of nitric oxide (NO) leading to nitrotyrosination; and function of select enzymes identified in WT *vs.* parkin-deficient (*prkn*-/-) mammalian brain. P, parkin; MnSOD, Mn2+-dependent superoxide dismutase; GPx, glutathione peroxidase; GR, glutathione reductase. Note, interactions of parkin with dopamine metabolites are shown elsewhere [846].

3.7 Materials and Methods

Mouse lines and tissues

Wild-type C57BL/6J mice were purchased from the Jackson laboratory. The *prkn*$^{-/-}$ mice (C57BL/6J background) were obtained from Dr. A. Brice's lab[432]. The *Sod2*$^{+/-}$ mice (C57BL/6J) were generated by Dr. R. Lebovitz[847], and purchased from the Jackson laboratory; *prkn*$^{-/-}$ //*Sod2*$^{+/+}$ and *Sod2*$^{+/-}$ //*prkn*$^{+/+}$ mice were crossed to generate *prkn*$^{+/-}$ //*Sod2*$^{+/-}$ offspring, that was then interbred to produced the desired *prkn*$^{-/-}$ //*Sod2*$^{+/-}$ bi-genic mouse. All animal-related experiments were conducted in accordance with the Canadian Council on Animal Care Standards and the Animals for Research Act and were approved by the University of Ottawa Animal Care Council. The mice were bred in parallel (wild-type (WT), and *Sod2*$^{+/-}$ animals from a *prkn*$^{+/+}$ //*Sod2*$^{+/+}$ x *prkn*$^{+/+}$ //*Sod2*$^{+/-}$ crossing; and *prkn*$^{-/-}$ and bi-genic from a *prkn*$^{-/-}$ //*Sod2*$^{+/+}$ x *prkn*$^{-/-}$ //*Sod2*$^{+/-}$ crossing). Mice were group housed (3-5 mice per cage) on a reversed 12h dark:12h light cycle with food and water available *ad libitum*. Room temperature was maintained at 23°C and humidity at 30-40%. All behaviour testing was performed in the Behavioural Core Facility at the University of Ottawa. Mice were minimally disturbed during behavioural testing. Body weights were measured before testing began and after its completion. Behaviour testing was conducted with the operator blinded to the genotype of the mice. Behaviour tests were separated by 2-4 days and all mice were brought into the dark testing room with red light to habituate for 30-60 min prior to testing. Mice were handled once per day for four days before testing began. Brains and hearts were collected for the four genotypes of interest: WT; *prkn*$^{-/-}$; *Sod2*$^{+/-}$; and *prkn*$^{-/-}$ //*Sod2*$^{+/-}$.

Genotyping

Ear tissue was collected for genotyping. DNA was extracted from the tissue by incubating the ear sample in 1X solution A (Solution A (10X): 250mM NaOH, 2mM EDTA, in water) at 95°C for 30

minutes, followed by neutralizing the reaction with 1X solution B (Solution B (10X): 400mM Tris-HCl, in water). Standard polymerase chain reaction (PCR) was used to amplify the *prkn* and *sod2* loci. The following primers were used:

$prkn^{+/+}$	F: 5' TGCTCTGGGGTTCGTC 3'	R: 5' TCCACTGGCAGAGTAAATGT 3'
$prkn^{-/-}$	F: 5' TTGTTTTGCCAAGTTCTAAT 3'	R: 5' TCCACTGGCAGAGTAAATGT 3'
$sod2^{+/+}$	F: 5' TGAACCAGTTGTGTTGTCAGG 3'	R: 5'TCCATCACTGGTCACTAGCC 3'
$sod2^{-/-}$	F: 5' TGTTCTCCTCTTCCTCATCTCC 3'	R: 5' ACCCTTTCCAAATCCTCAGC 3'

Amplifications products were electrophoresed on a 1% agarose gel and stained with ethidium bromide. A band at 300 base pairs (bp) represented $prkn^{+/+}$ or $prkn^{-/-}$ (ran separately; a sample with 300bp bands for both $prkn^{+/+}$ and $prkn^{-/-}$ is a $prkn^{+/-}$ mouse). A band at 123bp represented $Sod2^{+/+}$ and a band at 240bp represented $Sod2^{-/-}$.

Locomotion activity (beam break) test

To measure general locomotion and habituation, Micromax analyzer software and frames (Omnitech Electronics; Columbus, OH, USA) were used. Mice were single housed in new clean cages containing only a thin layer of bedding, food and water, and were loaded into the Micromax frames, following 1 hour of habituation in then dark. Testing was conducted for 4 hours. Infrared beam emitters and receptors were utilized to monitor the mice ambulatory activity, and beam breaks in 5 min sampling bins were analyzed.

Nest building score

Nest building was qualitatively analysed as per Deacon et al., 2012.[859] Mice were single house in a new clean cage with food, water and a single pressed cotton square 'nestlet'. No habituation was needed.

Mice were left in the new cage with the nestlet for 12 hours. Thereafter, mice were removed from the testing cages. Videos were taken of the nests from the top and both sides, and scoring by an operator blinded to the genotype for nest quality on a scale of 1 to 5 based on the percentage of intact material remaining, cage floor area covered by the nesting material, and the height of the nest.[859]

Grip strength test

To measure forelimb grip strength independent of body weight, a grip strength meter (Columbus Instruments; Columbus, OH, USA) was used.[879] Mouse were held by the tail and lowered until they grab the grate of the meter with both forepaws. The mouse was then pulled horizontally gently but firmly until the mouse released the grate. The force reading in kilogram-force (kgF) was recorded. This was repeated until five successful pulls were recorded. Some examples of unsuccessful trials include: hindlimb contact with the grate, the mouse prematurely loosening its grip on the grate, or the body was not straight and horizontal to the table.

Rotarod test

To monitor motor function, coordination and balance, the rotarod (IITC Life Sciences; Woodland Hills, CA, USA) was used as described previously.[880,881] Mice were habituated to the rod by being placed on a rod rotating at 5rpm for 2 minutes, with the mice being replaced on the rod each time they fall off. Latency to fall, in seconds, was recorded after placing the mice on the rod accelerating from 4 rpm to 40 rpm for 5 minutes with a 10 minutes inter-trial time (ITI). The time was stopped when the mouse fell from the rod or when the mouse rotated around with the bar. Mice were tested for four trials per day for 3 days to assess learning.

Horizontal ladder test

To assess gait and coordination, we used the horizontal ladder, with irregularly spaced rungs, and measured the steps taken by an animal as it crossed it.[854] The horizontal ladder is flanked by two plexiglass sidewalls. The ladder is 50 cm long and the rungs are spaced 0.5-2 cm apart. On day 1 (training day), each mouse was trained to walk across the ladder for 5 trials or until they walked across without stopping. On day 2 (testing day), the mice were filmed walking across the ladder for 4-5 trials. They mice were placed at the start end of the ladder and guided (if required), and the end of the ladder was their home cage to serve as an incentive to cross the ladder. The trials were videotaped and then analyzed, blindly, for correct stepping or errors (misses or cheats) for both forelimbs and hindlimbs.

DigiGait

To measure gait dynamics and posture we used the DigiGait™ imaging system (Mouse Specifics, Inc., Boston, MA, USA).[855-857] Mice were first habituated to the room for 30 minutes before testing, then placed on a transparent treadmill equipped with an under-mounted camera, with the following conditions set; belt speed: 10-18cm/s, incline: 8 degrees, shutter speed: 22-24 for black mice. Approximately three seconds of video was recorded for each mouse. Built in algorithms analyzed the videos and quantified many gait and posture characteristics of which we chose to present stride length in centimeters (cm), stance width (cm), and step angle in degrees (°).

MnSOD activity assay

Superoxide dismutase assay kit (Cayman chemical 706002) was used to assay MnSOD activity in mouse brains. Pre-weighed perfused mouse brain pieces were homogenized in 5 mL cold 20 mM HEPES buffer, pH 7.2, supplemented with EGTA, mannitol and sucrose, with a Dounce homogenizer on ice.

The homogenates were centrifuged at 1,500 x g 5 minutes at 4 °C. The SOD standards were prepared by adding 200 µL of the radical detector and 10 µL of the provided standards, in duplicates in a 96-well plate. The same was repeated for the samples. The reaction was initiated by adding 20 µL of xanthine oxidase to all the wells. Background absorbance was assayed by adding 20 µL xanthine oxidase to sample buffer (optional). The plate was incubated on a shaker for 30 minutes at room temperature. The absorbance was measure at 450 nm. The linearized SOD standard curve was plotted and used to calculate the MnSOD activity (U/mL) from the averaged sample absorbances.

Human tissue collection

All tissue was collected in accordance with Institutional Review Board-approved guidelines. Post-mortem, frozen brain samples from the cerebral cortex of ARPD and their age matched control samples were obtained from the Department of Neurology, Juntendo University School of Medicine. Detailed characteristics of these samples are found in **Supplementary Table 2.1** and correspond to sample ID numbers 32, 34, 37, 39, 40 and ARPD1-4.

ROS (H_2O_2) measurements in tissues

Amplex® Red hydrogen peroxide/peroxidase assay kit (Invitrogen A22188) was used to monitor endogenous levels of H_2O_2 in mouse tissues and cells. Pre-weighed hearts, cortex and midbrain pieces from mouse and human brains (or pelleted cells) were homogenized on ice in the 1x reaction buffer provided, using a Dounce homogenizer (3 times volume to weight ratio). Homogenates were diluted in the same 1x reaction buffer (10x and 5x). A serial dilution of the H_2O_2 standard provided was prepared (20, 10, 2 and 0 µM). 50 µL of standards and samples were plated in a 96 well black plate with clear flat bottom. The reaction was started by the addition of 50µL working solution which consisted of 1x

reaction buffer, Amplex® red and horseradish peroxidase. The plate was incubated at room temperature for 30 minutes protected from light. A microplate reader was used to measure either fluorescence with excitation at 560 nm and emission at 590 nm, or absorbance at 560 nm. The obtained H_2O_2 levels (μM) were normalized to the tissue weight (g) or protein concentration (μg/μL).

ROS measurements in intact cells

HEK293 cells were transfected with FLAG-parkin or control vector (pcDNA) as described above. After 24 h the cells were lifted using trypsin and re-seeded in a 12-well dish at a density of 0.3 x 10^6 cells/mL. After 48 h the cells were treated with 0 mM or 2 mM H_2O_2 in OPTI-MEM medium at 37°C and 5 % CO_2. After 1 h the cells were washed with OPTI-MEM and incubated with 20 μM of dichlorofluorescin diacetate (DCFH-DA, Sigma) for 30 min at 37°C and 5 % CO_2. Cells were collected using a cell lifter and treated with ethidium-1 dead stain (Invitrogen) for 15 min at room temperature. Samples were analyzed using a BD Fortessa flow cytometer set to measure the ROS-sensitive (DCFH-DA, ex. 488 nm - em. 527 nm) and viability (ethidium-1, ex. 528 nm - em. 617 nm) stains. The results were reported as the average mean fluorescence intensity (MFI) of ROS in live cells. Each separate transfection was considered one biological replicate.

Western blot and densitometry

Brain and heart homogenates were run on 4-12 % Bis-Tris SDS-PAGE gels using MES running buffer. Proteins were transferred to PVDF membranes using transfer buffer, and parkin, DJ-1, MnSOD, aconitase-2, creatine kinase, VDAC, TOM20, nitrotyrosine, glutathione reductase, and FLAG-epitopes. Actin and Ponceau S staining were used as loading controls. For densitometry quantification, the signal

intensity of protein nitrotyrosination from each sample was measured as pixel using Image J Software, and controlled for loading.

Protein carbonyl assay

Protein carbonyl colorimetric assay kit (Cayman chemical 10005020) was used to assay the carbonyl content in human and mouse brains or hearts. Pre-weighed tissues were rinsed in PBS and then homogenized in 1 mL cold PBS at pH 6.7 supplemented with 1 mM EDTA, using a Dounce homogenizer on ice. Homogenates were centrifuged at 10,000 x g for 15 minutes at 4 °C. 200 µL of the supernatant was added to a tube with 800 µL 2,4-Dinitrophenylhydrazine (DNPH; sample tube) and 200 µL of the supernatant was added to a tube with 800 µL 2.5 M HCl (control tube), both tubes were incubated in the dark for 1 hour with occasional vortex. 1 mL 20 % TCA followed by 1 mL 10% TCA solutions were added to the centrifuged (10,000 x g 10 minutes at 4 °C) pellet after discarding the supernatant. The resulting pellet was resuspended in1 mL of 1:1 ethanol: ethyl acetate mixture and centrifuged 3 times to extract protein pellets. The final pellets were suspended in 500 µL guanidine hydrochloride and centrifuged. A total of 220 µL per sample and control supernatants were added to two wells of a 96-well plate, and the absorbance was measure at 360 nm. The corrected absorbance (CA, sample – control) was used in the following equation to obtain the protein carbonyl concentration: Protein Carbonyl (nmol/mL) = $[(CA)/(0.011\ \mu M^{-1})](500\ \mu L/200\ \mu L)$. Total protein concentration from the sample tissues were measured to obtain the carbonyl content: protein carbonyl/total protein concentration.

Superoxide (O_2^-) measurements in tissue

To measure endogenous superoxide anion levels in mouse brains, we used high-performance liquid chromatography (HPLC), with the fluorescent probe dihydroethidium (DHE)[882]. Upon oxidation, DHE becomes positively charged and emits fluorescence. Two products emerge, ethidium from reaction with H_2O_2, and 2-hydroxyethidium (2OHE) from the specific reaction with O_2^-. Using HPLC enables the separation and quantification of the two reaction products. Hemibrains pieces were cut, pre-weighed, and their weights equalized to 1-5mg. The pieces were incubated in 500µl PBS/diethylenetriaminepentaacetic acid (DPTA) containing 50µM DHE for 30 minute at 37°C. After incubation, the brains tissues were washed with PBS, dried, snap frozen in liquid nitrogen, homogenized and resuspended in 500µl acetonitrile, sonicated and centrifuged at 12,000g fro 10 minutes at 4°C. The supernatants were transferred to a fresh tube and vacuum dried at low setting without heat. The pellets were resuspended in 120µl 20% methanol, 79.9% water and 0.1% trifluoroacetic acid, and a volume of 100µl was injected into the column. DHE was detected via UV (9.8-9.9 minutes), ethidium was detected via fluor (12.7-12.8 minutes) and 2OHE was detected via fluor (13.2 minutes).

Tissue processing, immunohistochemistry, and stereological cell counts

Mice were euthanized with a lethal injection of sodium pentobarbital. For immunohistochemistry, mice were transcardially perfused with 1x PBS followed by 4% paraformaldehyde (PFA). Brains were removed, post-fixed overnight in 4% PFA, and cryoprotected in 20% sucrose. Serial free-floating coronal sections were collected throughout the forebrain and midbrain. For estimates of dopaminergic neurons of the substantia nigra pars compacta (SNc), every 6th midbrain (Bregma -2.78 mm to -3.88mm Paxinos and Franklin, 2001) section (40µm) was collected and stained for tyrosine hydroxylase (TH-1) for stereological counts. All steps were done on a rotating shaker. Briefly, sections were washed in PBS,

and endogenous peroxidase activity was quenched with 0.9% hydrogen peroxide in PBS. Sections were washed in PBS and blocked in 10% normal serum in PBS to reduce non-specific signal. Sections were incubated overnight at 4°C in primary TH-1 antibody (1:10,000; Millipore, AB152) diluted in 1% normal serum in PBS-T. Sections were washed in PBS, and subsequently incubated for 2 hours in biotinylated rabbit secondary antibody (1:225) in 10% normal serum in PBS-T. Sections were then washed in PBS, and the signal was amplified with VECTASTAIN® Elite® ABC HRP Kit (Vector Labs, PK-6100), and visualized via standard DAB solution, 55mM DAB. Sections were washed with PBS, and mounted on charged slides, counterstained with Harris Modified Hematoxylin nuclei stain and dehydrated through a series of increasing ethanol concentration solutions and xylene, and coverslipped using Permount. A total of seven to eight 40μm sections were examined within the rostral and caudal limits of the SNc. The number of dopaminergic neurons in the SNc were obtained via an unbiased stereological estimate with a 100x lens using Stereo Investigator (MicroBrightField). The total number of TH-1 positive neurons was determined by applying optical fractionation.[883]

Cell culture, transfection and oxidation

Human embryonic kidney (HEK293) were grown in Dulbecco's Modified Eagle Medium (DMEM) supplemented with 1 % penicillin/streptomycin and 10 % heat-inactivated fetal bovine serum (FBS) at 37°C with 5 % CO_2. Four to 15 μg of cDNA coding for N-terminally FLAG-tagged parkin or empty FLAG control vector (pcDNA3.1) using a 1:1 ratio of cDNA:Lipofectamine 2000, was used for ectopic overexpression. The cDNA and Lipofectamine 2000 were incubated for 20 min at room temperature before being applied directly to the cells for 1 hour at 37°C with 5 % CO_2 followed by direct addition of fresh growth medium. Cells were incubated another 24 hours before treatment, harvesting and analysis.

Control Chinese hamster ovary cells, stably expressing the myc-vector (CHO), or expressing myc-parkin (CHO-parkin) were also used.

All chemicals (H_2O_2, CCCP, NEM, IAA, DTT, AT, BSO and NAC) were added directly to cells at ~75% confluence in growth or OPTI-MEM media. Cells were manually scrapped, spun at a 100 x g for 5 minutes, the pellets washed with PBS and then homogenized in a Tris salt buffer, transferred to ultracentrifuge tubes and spun at 163,202.1 x g and 4°C for 30 minutes to extract the soluble fraction. The resulting pellets were further homogenized in the Tris salt buffer with the addition of 2-10% SDS, transferred to ultracentrifuge tubes and spun at 163,202.1 x g and 10°C for 30 minutes to extract the insoluble fraction. SH-SY5Y cells were seeded at a density of 0.5-1 x 10^6 cells/mL. Once cells reached 70-80 % confluency they were transfected with cDNA coding for C-terminally FLAG-tagged Parkin or empty FLAG control vector (pcDNA3) by electroporation using the nucleofector method described by Hu and Li, 2015. A total of 2 million cells were resuspended in 100 µL of OPTI-MEM containing cDNA (2 µg) and 1 % polyoxamer 188. The cells were electroporated using the X Unit and pulse code "CA-137" on a Lonza 4D-Nucleofector. Following electroporation, cells were seeded at a concentration of 0.8-1 x 10^6 cells/mL.[884]

Recombinant, tag-less protein expression in pET-SUMO vector

Wild-type and truncated (residues 321-465) human parkin were expressed as 6His-Smt3 fusion proteins in *Escherichia coli* BL21 (DE3) Codon-Plus RIL competent cells (New England Biolabs) as previous described.[193,458,571,846] Proteins were overexpressed in *E. coli* BL21 Codon-Plus competent cells and grown at 37 °C in 2 % Luria Broth containing 30 mg/L kanamycin until OD600 reached 0.6, at which point the temperature was reduced to 16°C. Parkin protein-expressing cultures were also supplemented

with 0.5 mM $ZnCl_2$. Once OD600 reached 0.8, protein expression was induced with isopropyl β-D-1-thiogalactopyranoside, except ulp1 protease, which was induced once OD600 had reached 1.2. The concentration of IPTG used for each construct is as follows: 25 μM for wild-type and point mutants of parkin, and 0.75 mM for truncated parkin, DJ-1, α-synuclein, SAG, and ulp1 protease. Cultures were left to express protein for 16-20 h. Cells were then harvested, centrifuged, lysed and processed via Ni-NTA agarose beads in elution columns.

Recombinant maltose-binding protein-tagged fusion proteins expressed in pMAL-2T vector

Wild-type and truncated (residues 327-465) human parkin proteins were expressed in the pMAL-2T vector (a gift from Dr. Keiji Tanaka), as previously described.[445] Parkin produced in this vector contained an N-terminal maltose-binding protein (MBP) and thrombin cleavage site (LVPRGS). All proteins were overexpressed in *E. coli* BL21 Codon-Plus competent cells (New England Biolabs) and grown at 37 °C in 2 % Luria Broth containing 0.2 % glucose and 100 mg/L ampicillin until OD600 reached 0.3-0.37, at which point protein expression was induced with addition of 0.4 mM isopropyl β-D-1-thiogalactopyranoside. Cultures were left to express protein at 37 °C until OD600 reached 0.9-1.0. Harvested protein isolates were purified using amylose resin in buffers containing 100 μM zinc sulfate and 10 mM maltose.

Cell cytotoxicity assay

Vybrant ™ cytotoxicity assay kit (Molecular Probes V-23111) was used to monitor cell death through the release of the cytosolic enzyme glucose 6-phosphate dehydrogenase (G6PD) from damaged cells into the surrounding medium. 50 μl of media alone (no cells), media from control and stressed CHO-parkin and control cells and cell lysates were added to a 96-well microplate. 50 μl of reaction mixture,

containing reaction buffer, reaction mixture and resazurin, was added to all wells, and the microplate was incubated at 37°C for 30 mins. A microplate reader was used to measure either fluorescence with excitation at 560 nm and emission at 590 nm. A rise in fluorescence indicates a rise in G6PD levels i.e. a rise in cell death.

Mitochondria isolation

Fresh tissue was cut with scissors into smaller pieces, rinsed in cold PBS, then homogenized using either a Dounce homogenizer or Warning blender in the presence of twice the tissue volume of buffer A (20mM Hepes pH 7.4, 220mM mannitol, 68mM sucrose, 80mM KCl, 0,5mM EGTA, 2mM $Mg(Ac)_2$, 1mM DTT, 1X protease inhibitor (Roche)). The sample was centrifuged at 4070 x g in a tabletop centrifuge for 20 minutes at 4^oC. The supernatant was collected and spun again as above. The resulting supernatant was spun at 10 000 x g for 20 minutes at 4^oC and the pellet was then washed in the above buffer and spun again at 10 000 x g for 20 minutes. The resulting mitochondrial pellet was carefully resuspended in buffer B (20mM Hepes pH 7.4, 220mM mannitol, 68mM sucrose, 80mM KCl, 0,5mM EGTA, 2mM $Mg(Ac)_2$, 10% glycerol), aliquoted, and snap frozen.

Aconitase assay

The Aconitase Enzyme Activity Microplate Assay Kit (MitoSciences) was used to measure aconitase activity in mitochondria isolated from wild type and parkin knock-out mouse brains as per manufacturer's instructions. Two brains each from 12 months old mice were pooled to provide the mitochondria samples and normalized for total protein concentration. These were treated with 0 or 4 μM H_2O_2 just prior to assay. The catalytic conversion of isocitrate to cis-aconitate by aconitase was

measured by quantifying the amount of cis-aconitate in the reaction by reading the samples at 240nm. Rates in μM/min were determined from 3 independent experiments performed in triplicate.

Creatine kinase assay

The EnzyChrom Creatine Kinase Assay Kit (BioAssay Systems) was applied to measure creatine kinase activity in mitochondria purified from wild type and parkin knock-out mouse brains following the manufacturer's instructions. Two brains were pooled each from 12 months old mice to provide the mitochondrial samples and normalized for total protein concentration. Mitochondria were incubated with 0 or 0.5mM H_2O_2 at room temperature for 20 minutes prior to assay. The creatine kinase-dependent catalytic conversion of creatine phosphate and ADP to creatine and ATP, was quantified indirectly by measuring NADPH at 340nm. The ATP produced by the reaction phosphorylates glucose to glucose-6-phosphate by hexokinase, which is then oxidized by NADP in the presence of glucose-6-phosphate dehydrogenase, yielding NADPH. Rates in uM/min were calculated for 3 independent experiments done in triplicate.

Glutathione (GSH; GSSG) quantification by HPLC

Human and mouse brain pieces, and CHO cell pellets were homogenized in buffer containing 125 mM sucrose, 5 mM TRIS, 1.5 mM EDTA, 0.5%TFA and 0.5%MPA in mobile phase. Then samples were spun at 14000 x g at 4 °C for 20 mins. Supernatants were collected and analyzed using an Agilent HPLC system equipped with a Pursuit C_{18} column (150 ×4.6 mm, 5 μm; Agilent Technologies) operating at a flow rate of 1 ml/min. The mobile phase consisted of 0.09% trifluoroacetic acid diluted in ddH2O and mixed with HPLC-grade methanol in a 90:10 ratio. Standard solutions were used to estimate the retention times for GSH and GSSG. Using Agilent Chemstation software, absolute amounts of GSH and

GSSG were acquired by integrating the area under the corresponding peaks, and values were calculated from standard curves.

Glutathione concentration determined by monochlorobimane assay

Stock solutions of assay dye (monochlorobimane (MCB), 22 mM) and glutathione-S-transferase (50 units/mL) were prepared in PBS and stored protected from light at -20°C. The working solution was prepared using 12.8 µL of stock MCB and 80 µL of stock glutathione-S-transferase in 4 mL PBS and stored on ice. Samples were prepared as follows: cells were lifted mechanically using cell-lifters, washed twice and re-suspended in ice-cold PBS, mixed by vortex and incubated on ice for 30 min. Following two freeze thaw cycles using solid CO_2, the samples were sonicated 1 min on wet ice (S220 Ultra-sonicator from Covaris) and spun at 3000 x g, 4°C, for 5 min. Total protein concentration of supernatants was determined using Bradford assay. Samples and glutathione (GSH) standards (0- 13 µM) were plated in 25 µL aliquots in a 96-well plate with clear bottom and black sides. Twenty five µL of working solution was added to all experimental wells and protected from light for 15 min at room temperature. Fluorescence (ex 380 nm, em 461 nm) was measured using a Synergy H1Multi-Mode Plate Reader (Bio Tek). The amount of GSH detected in each sample was calculated using the regression curve obtained from the glutathione standards.

Tietze's enzymatic recycling determination of glutathione (GSH; GSSG)

The enzymatic recycling method described by Rahman et al.[885] was used to determine reduced glutathione (GSH) and oxidized glutathione (GSSG) levels in mouse brain lysates. Hemi-brains of wild type (n=3) and parkin KO (n=3) mice, at 13 and 11 months of age respectively, were collected, weighed and homogenized in 3X volume/weight of KPEX (0.1 M potassium phosphate, 5 mM EDTA, 0.1 %

Triton X-100, 0.6 % sulfosalicylic acid, pH 7.5) using a glass Dounce homogenizer (50 passes). Samples were spun at 8000 x g, 4°C, for 5 min and the supernatant protein concentration was determined using Bradford assay. To determine the total glutathione (GSH + GSSG) concentration, the following stock solutions were freshly prepared in KPE (0.1 M potassium phosphate, 5 mM EDTA, pH 7.5): 5,5'-dithio-bis-[2-nitrobenzoic acid] (DNTB) at 0.6 mg/mL, nicotinamide adenine dinucleotide phosphate (NADPH) at 0.6 mg/mL and glutathione reductase at 3 units/mL. GSH standards were prepared in KPE at concentrations of 0-26 nM/mL. 20 µL of diluted sample or GSH standard was added per well and 120 µL of a 1:1 mixture of the DNTB and glutathione reductase stocks solutions was added to each assayed well. After 30 sec incubation, 60 µL of the NADPH was added and absorbance was immediately measured at 412 nm in 30 sec intervals for a total of 2 min. To determine the concentration of oxidized glutathione (GSSG), the samples were first diluted (1 in 4) in KPE and treated with 0.2 % 2-vinylpyridine for 1 h at room temperature. Excess vinyl-pyridine was quenched with 1 % triethanolamine and GSSG was measured using the same method as total glutathione except GSH standards were replaced with GSSG (0-26.24 nM/mL) treated with vinyl-pyridine and triethanolamine. The absolute values of total glutathione (GSH + GSSG) and oxidized glutathione (GSSG) per sample were calculated using the linear regression obtained from the change in absorbance/min plotted against the GSH or GSSG standard concentrations, respectively, and dividing by the total protein concentration. Absolute values for GSH were determined using the following equation: GSH= [GSH + GSSG] – 2[GSSG].

Total RNA isolation, cDNA synthesis and PCR-based amplification

Pre-weighed cortex pieces from mouse brains were homogenized in QIAzol (Qiagen), at 1ml volume per 100mg of tissue, and incubated at room temperature for 5 minutes. 0.2mL of chloroform (per 1mL

QIAzol) was added and the homogenates were shaken vigorously for 15 seconds, followed by a 2-3 minutes incubation at room temperature, the tubes were centrifuged at 12,000 x g for 15 minutes at 4°C. The upper clear aqueous layer was transferred to a new tube and 1 volume of 70% ethanol was added, and mixed by vortexing. The solution was then added to an RNAeasy Mini spin column (Qiagen) placed in a 2mL collection tube and centrifuged for 15 sec at 8000 x g at room temperature. The flow-through was discarded and 700 µL Buffer RW1 was added to the spin column and spun for 15 sec at 8,000 x g. The same step was repeated with 500 µL Buffer RPE, one spin for 15 sec and a second spin for 2 min. An optional spin in a new collection tube at full speed for 1 min to remove excess buffer was added. The RNAeasy Mini spin column was placed in a new collection tube, 50 µL RNase-free water was added directly to the membrane and centrifuged for 1 minute at 8000 x g. A NanoDrop machine was used to measure the amount of total RNA obtained from the cortices. Turbo DNA-free™ (Life Technologies) was used to remove trace to moderate amounts of contaminating DNA. SuperScrpit™ IV First-Strand Synthesis System (Invitrogen) was used for cDNA synthesis reaction. iTaq™ Universal SYBR® Green Supermix (BIO-RAD) and select primer sets were used for PCR amplification of the newly synthesized cDNA templates, and controls, and analyzed by agarose gel electrophoresis and ethidium bromide staining. The following primers[886,887] were used:

Dj-1, F: ATCTGAGTCGCCTATGGTGAAG; R: ACCTACTTCGTGAGCCAACAG

GCLC, F: ATGTGGACACCCGATGCAGTATT; R: TGTCTTGCTTGTAGTCAGGATGGTTT

GCLM, F: GCCACCAGATTTGACTGCCTTT; R: CAGGGATGCTTTCTTGAAGAGCTT

Actin, F: CTTCCTCCCTGGAGAAGAGC; R: AAGGAAGGCTGGAAAAGAGC

Glutathione reductase activity assay

A glutathione-reductase (GR) assay kit (Cayman Chemical – 703202) was used to measure its activity in tissues. Human and mouse brains were either perfused or rinsed with PBS (pH7.4). Tissues were homogenized in 5-10 mL of cold buffer (50 mM potassium phosphate, pH 7.5, 1mM EDTA) per gram of tissue, followed by centrifugation at 10,000g for 15 mins at 4°C. In a 96 well clear plates, three wells were loaded with 120 µl assay buffer (provided) and 20 µl GSSG (provided) as background control; and three wells were loaded with 100 µl assay buffer, 20 µl GSSG and 20 µl diluted GR (provided) as positive control. Twenty µl of samples supernatant were loaded in triplicates, with 100 µl assay buffer and 20 µl GSSG. Reactions were initiated by adding 50 µl NADPH (provided) to each well. The 96-well plate was gently shaken for a few seconds and absorbance was read at 340 nm once every minute for 10 mins, or to obtain readings at a minimum of 5 time points. The oxidation of NADPH to $NADP^+$ is accompanied by a decrease in absorbance at 340 nm and is directly proportional to the GR activity in the sample.

Parkin-mediated redox recycling of glutathione

Parkin protein buffer exchange to T200 protein buffer (50 mM Tris, 200 mM NaCl, pH 7.5) was first performed using repeat centrifugations (8 times 4000 x g at 4°C for 10 min) in Amicon Ultra 10 kDa MWCO filters. Protein concentration was adjusted to 10 µM using T200. Both reduced (GSH) and oxidized (GSSG) glutathione stocks were prepared in phosphate buffered saline at concentrations of 1 mg/mL (3250 µM) and 2.01 mg/mL (6560 µM) respectively. Glutathione standards of 0, 2.5, 5, 10 µM and 100 µM of both GSH and GSSG were prepared and combined in the following ratios to a final volume of 90 µL: (10 µM GSH: 0 µM GSSG), (9 µM GSH: 1 µM GSSG), (8 µM GSH: 2 µM GSSG), (6 µM GSH: 4 µM GSSG), (4 µM GSH: 6 µM GSSG), (2 µM GSH: 8 µM GSSG), (1 µM GSH: 9 µM

GSSG), and (0 μM GSH: 10 μM GSSG). Recombinant-parkin (1 μL of a 10 μM solution) was added to the prepared mixtures and allowed to incubate at room temperature for 15 min. Samples were analyzed for GSH concentration using the monochlorobimane assay described above.

Glutathionylation assay

Glutathionylation of tagged and untagged parkin proteins was performed, as described previously [888]. MBP-tagged parkin proteins were eluted from columns with excess maltose. Concentrated eluates were supplemented with 0.1% DMSO (10 μl DMSO in 10 ml PBS), and excess DTT and maltose were removed by several cycles of centrifugation with 30 kDa cut-off filters. Proteins/peptides (14 μM) were incubated with 3 mM GSH for 1 h and then with 5 mM GSSG for 2 h at room temperature. Trypsin digestion was performed (Peptide: Trypsin = 20: 1) overnight at 4 °C. Trypsin-digested fragments were run through MALDI analysis. To monitor S-glutathionylation, eosin-labeled GSSG (Di-E-GSSG) was used to glutathionylate proteins, as described[865]. Di-E-GSSG has quenched fluorescence in the disulphide form, which increases ~20-fold upon reduction of its disulphide bond and following the formation of E-GSH. Blackened 96-well-plates were used in a PerkinElmer Victor3 multilabel counter containing a final well volume of 200 μl in 0.1 M potassium phosphate buffer (pH 7.5), 1 mM EDTA. The reaction was started by addition of 20 μM Di-E-GSSG to parkin proteins, followed by recording the fluorescence emission at 545 nm after excitation at 520 nm. Controls with no peptide added were used as fluorescent background. To confirm S-glutathionylation, reaction products were incubated with Di-E-GSSG. Aliquots of S-glutathionylated proteins were further treated with 10 mM DTT or with the complete GSH-glutaredoxin (Grx) system. All samples were run on a non-reducing SDS-PAGE 4–12% acrylamide. The gel was exposed to UV transilluminator to visualize eosin-tagged glutathionylated protein. The same gels were later stained with Coomassie Blue staining. Di-Eosin-GSSG was purchased

form IMCO, Sweden. Human Grx-1, and Grx-2 were prepared, as described.[865] Rat recombinant thioredoxin was a kind gift from Prof. Elias Arner.

Mass spectrometry analysis of glutathionylated parkin

The protein was treated with trypsin, and the resulting peptides were separated using one dimension of liquid chromatography (LC). The LC eluent was interfaced to a mass spectrometer using electrospray ionization and the peptides were analyzed by MS. LC−MS/MS analyses were performed using an Easy-nLC chromatography system directly coupled online to a Thermo Scientific Q Exactive hybrid quadrupole-Orbitrap mass spectrometer with a Thermo Scientific™ Nanospray Flex™ ion source. The sample was injected from a cooled autosampler onto a 10 cm long fused silica tip column (SilicaTips, New Objective, USA) packed in-house with 1.9 μm C18-AQ ReproSil-Pur (Dr. Maisch, Germany). The chromatographic separation was achieved using an acetonitrile (ACN)/ water solvent system containing 0,1% formic acid and a gradient of 60 min from 5 to 35% of ACN. The flow rate during the gradient was 300 nL/ min.

MS/MS data were extracted and searched against in-house Mascot Server, (Revision 2.5.0)**,** search engine that uses mass spectrometry data to identify and characterize proteins from sequence databases. The following parameters were used: trypsin digestion with a maximum of two missed cleavages; Carbamidomethyl (C), Oxidation (M), Deamidated (NQ) and Glutathione (G) as variable modifications; and a precursor mass tolerance of 10 ppm and a fragment mass tolerance of 0.02 Da. The identified protein was filtered using 1% false discovery rate and at least two peptides per protein as limiting parameters.

Statistical analyses

All statistical analyses were performed using GraphPad Prism version 8 (GraphPad Software, San Diego, CA, USA, www.graphpad.com). Differences between two groups were assessed using a Student T-test. Differences among 3 or more groups were assessed using a 1way or two-way ANOVA followed by Tukey, Dunnett or Bonferroni post hoc corrections (as indicated) to identify statistical significance. Subsequent post hoc tests are depicted graphically and show significance between treatments. For all statistical analyses, a cut-off for significance was set at 0.05. Data are displayed with p values represented as *$p < 0.05$, **$p < 0.01$, ***$p < 0.001$, and ****$p < 0.0001$. Linear regression (for continuous dependent variable, e.g., GSH level) or logistic regression (for binary dependent variable, *e.g.,* parkin presence or absence) modelling were performed.

3.8 Acknowledgements

We wish to thank Dr. G. S. Shaw (University of Western Ontario) for his gift of the recombinant parkin construct. This work was supported by the: Parkinson Research Consortium of Ottawa (D.N.E.K., J.M.T., J.J.T.); Queen Elizabeth II Graduate Scholarship Fund (J.M.T.); Government of Canada [CIHR MD/PhD Program (J.M.T.); NINDS/NIH (to M.J.L.); CIHR Research Grants (M.E.H.); CIHR Canada Research Chair Program (M.G.S.)]; Michael J. Fox Foundation for Parkinson's Research (J.J.T., M.G.S.); Uttra and Sam Bhargava Family (M.G.S.); and The Ottawa Hospital (M.G.S.).

3.9 Supplementary figures and tables

6 months old cohort			
	M	F	Total
WT	4	5	9
prkn$^{-/-}$	7	5	12
Sod2$^{+/-}$	5	5	10
Bigenic	8	4	12
Total	24	19	43
6 months old repeat cohort			
	M	F	Total
WT	5	5	10
prkn$^{-/-}$	5	5	10
Sod2$^{+/-}$	5	6	11
Bigenic	7	5	12
Total	22	21	43
12 months old cohort			
	M	F	Total
WT	5	5	10
prkn$^{-/-}$	4	5	9
Sod2$^{+/-}$	4	6	10
Bigenic	5	5	10
Total	18	21	39

Supplementary Table 3.1. Behaviour mouse cohorts.
Summary of 6-month-old and 12-month-old behaviour cohorts. Mouse numbers per genotype, wild-type (*WT*); prkn-null (*prkn*$^{-/-}$); *Sod2* haploinsufficient (*Sod2*$^{+/-}$); and bi-genic (*prkn*$^{-/-}$ //*Sod2*$^{+/-}$) are displayed, along with the female to male ratios.

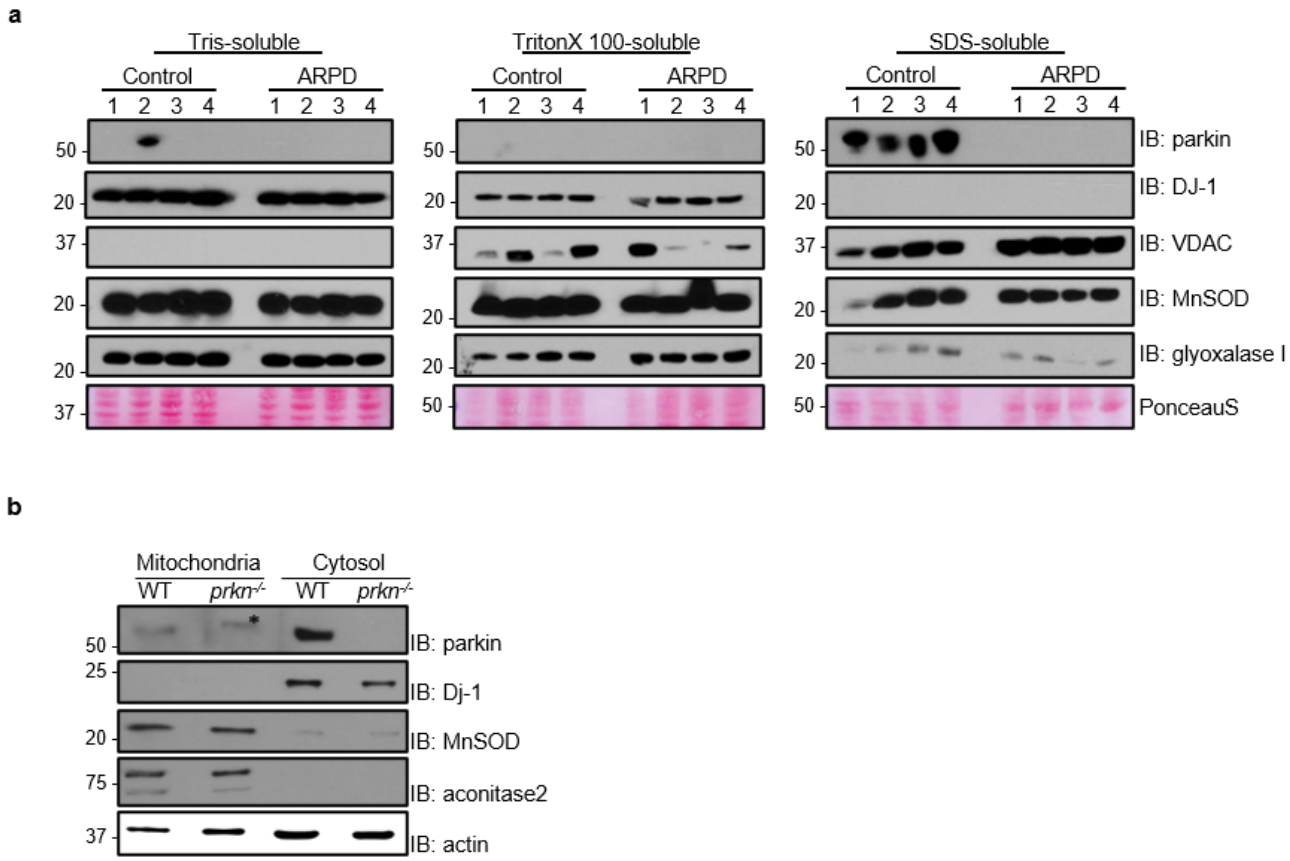

Supplementary Figure 3.1. Western blots of human cortex and mouse brain extracts.
(**a**) Aged-matched control and human ARPD (*PRKN* mutant) cortices, described in [506,846] were serially fractioned using increasing concentrations of detergent to extract soluble (TS), lipid-bound (TX) and insoluble (SDS) fractions, as described in Tokarew et al. 2021. Fractions were immunoblotted for parkin, DJ-1 and three other proteins, voltage-dependent anion channel (VDAC), manganese superoxide dismutase (MnSOD) and glyoxalase-1. (**b**) Western blot analysis of mitochondria-enriched and cytosolic fractions from *WT* and *prkn*-/- mouse brains, using parkin, Dj-1, MnSOD, aconitase-2 and actin as markers (* indicates non-specific band).

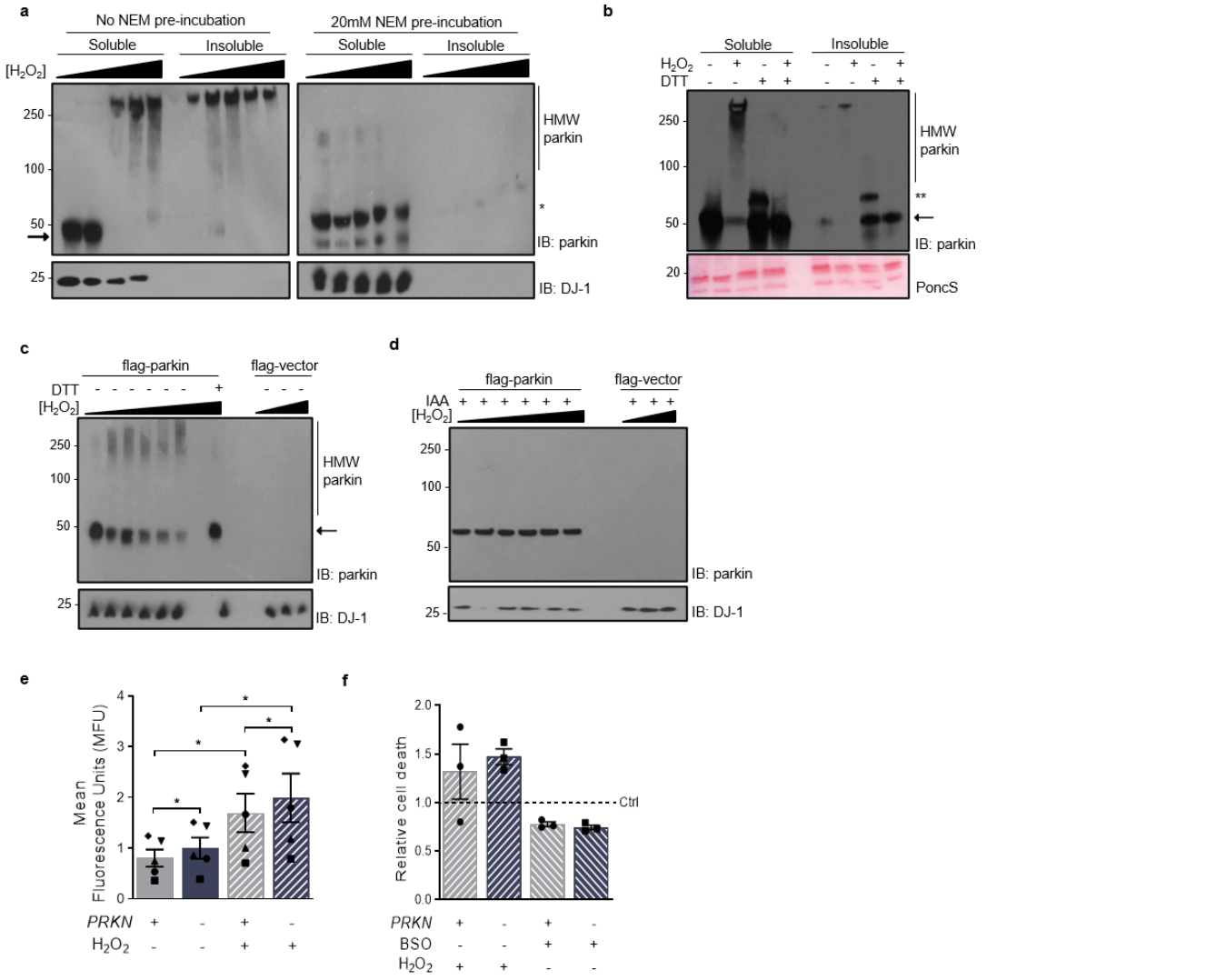

Supplementary Figure 3.2. Effect of *PRKN* cDNA expression on cellular redox state and viability under oxidative stress.

(**a**) Representative Western blot of parkin oxidation and solubility across soluble (salt-extracted) and insoluble (2-10% SDS-extracted) fractions of human embryonic kidney cells (HEK293) ectopically expressing FLAG-parkin, following incubation with increasing concentrations of H_2O_2 (2µM to 2M) for 30 minutes with or without a 15 minutes 20mM N-ethylmaleimide (NEM) pre-incubation. (*) Alkylated-parkin. (**b**) Parkin's HMW formation and shift in solubility was visualized by immunoblotting for parkin in lysates from HEK293 cells ectopically overexpressing FLAG-parkin under oxidizing and/or reducing conditions. Monomeric (arrow), DTT-modified (**) and high molecular weight (HMW) parkin are highlighted.

(**c**) Western blot analysis of parkin oxidation and solubility in HEK293 cells ectopically expressing FLAG-parkin or FLAG-control vector that were incubated with increasing concentrations of H_2O_2 (2µM to 20mM) in the presence of a reducing agent DTT for 30 minutes or (**d**) pre-incubating with 100mM iodoacetamide (IAA) for 15 minutes to block free available cysteines. (**e**) Level of ROS measured by flow cytometry in living HEK293 cells treated with 0 or 2 mM H_2O_2 and exposed to dichlorofluorescin diacetate, DCFH-DA. Paired data are represented by identical symbols. (**f**) Cell cytotoxicity assayed in CHO cells stably expressing myc-parkin (denoted as *PRKN* +) or myc-control vectors (denoted as *PRKN* -) under normal conditions with or without the addition of 2mM H_2O_2 or 20mM BSO. Data in (**e-f**) are plotted as mean normalized to untreated control. Results were obtained using n=5 (**e**) or n=3 (**f**) ± SEM. Significance in (**e**) was determined using a paired two-way ANOVA with Bonferroni's post-hoc test [F (1,4 = 11.00, p=0.0295 found for *PRKN* expression, F (1,4)= 13.03, p=0.0226 found for treatment, and F(1,4)= 1.767, p=0.2545 for interaction ; an unpaired two-way ANOVA with Bonferroni's post-hoc test was used to determine significance in (**f**) [F(1,8)= 0.1654, p=0.6949 found for *PRKN* expression, F(1.8)= 18.23, p=0.0027 found for treatment, and F(1, 8)=0.3960, p=0.5467 found for interaction].

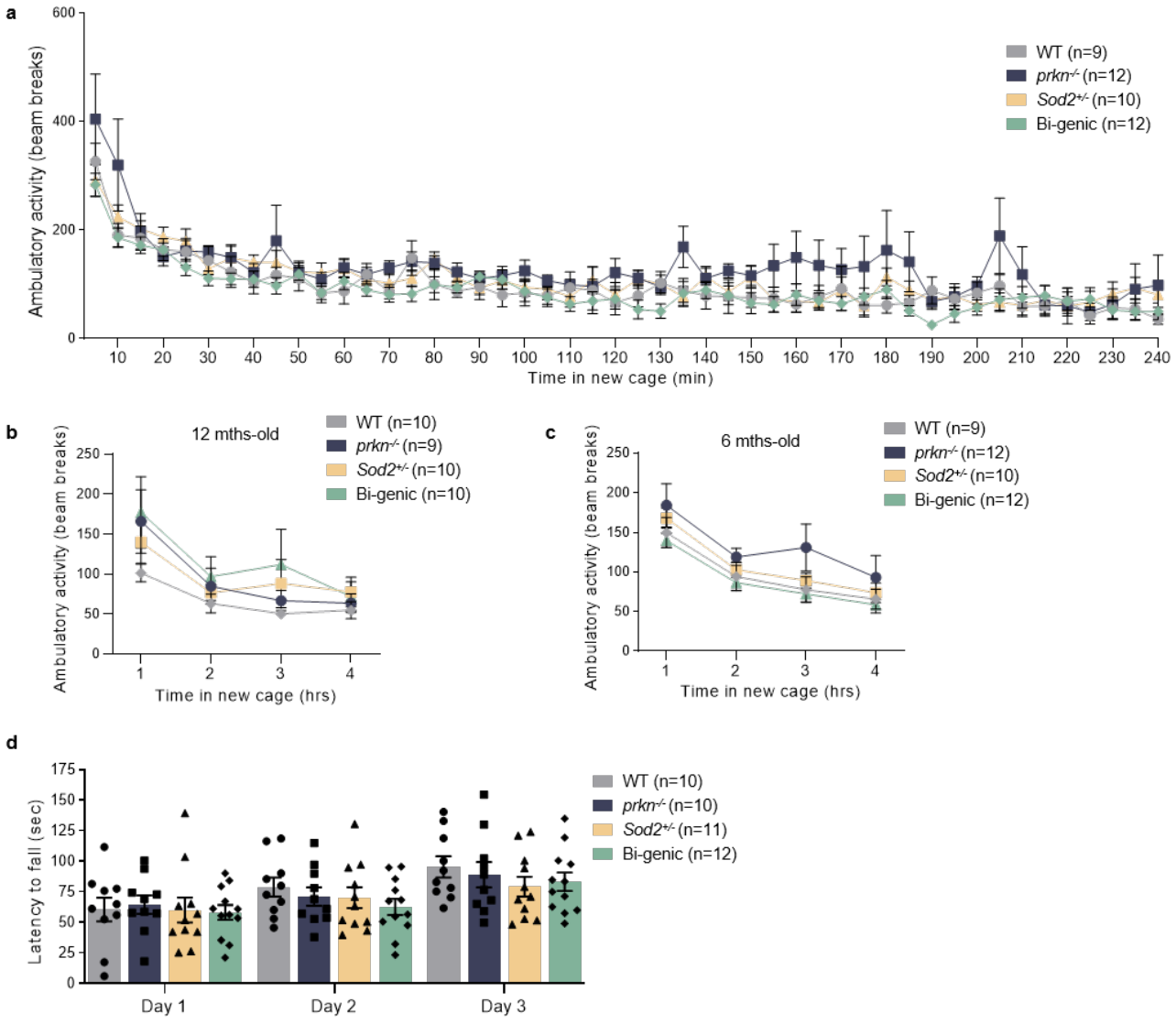

Supplementary Figure 3.3. Additional ambulatory activity and latency to fall results in 6-12-month-old mice.
(**a-c**) Ambulatory activity measured as beam breaks over 4 hours in 5 mins bins (**a**) or 1 hr bins (**b**) in a novel cage at 12 months of age and at 6 months of age (**c**). (**d**) Average latency to fall in seconds (sec) over 4 trials/day observed in the 6-month-old cohort. The 3 days of trial are represented. Data are shown as mean values/genotype with number of animals/genotype indicated in (**a**) for the 6-month and in (**c**) for the 12-month-old cohorts ± SEM. Significance was determined using a two-way ANOVA with Tukey's post-hoc analysis comparing genotype and time in (**a**) [$F(141, 1872)= 0.6478$, $p= 0.9995$], in (**b**) [$F(9, 140)= 0.3488$, $p= 0.9567$], in (**c**)[$F(9, 156)= 0.1497$, $p= 0.9980$], and in (**d**) [$F(6, 117)= 0.2475$, $p=0.9594$]. Note, no significance was found between genotypes within individual time points.

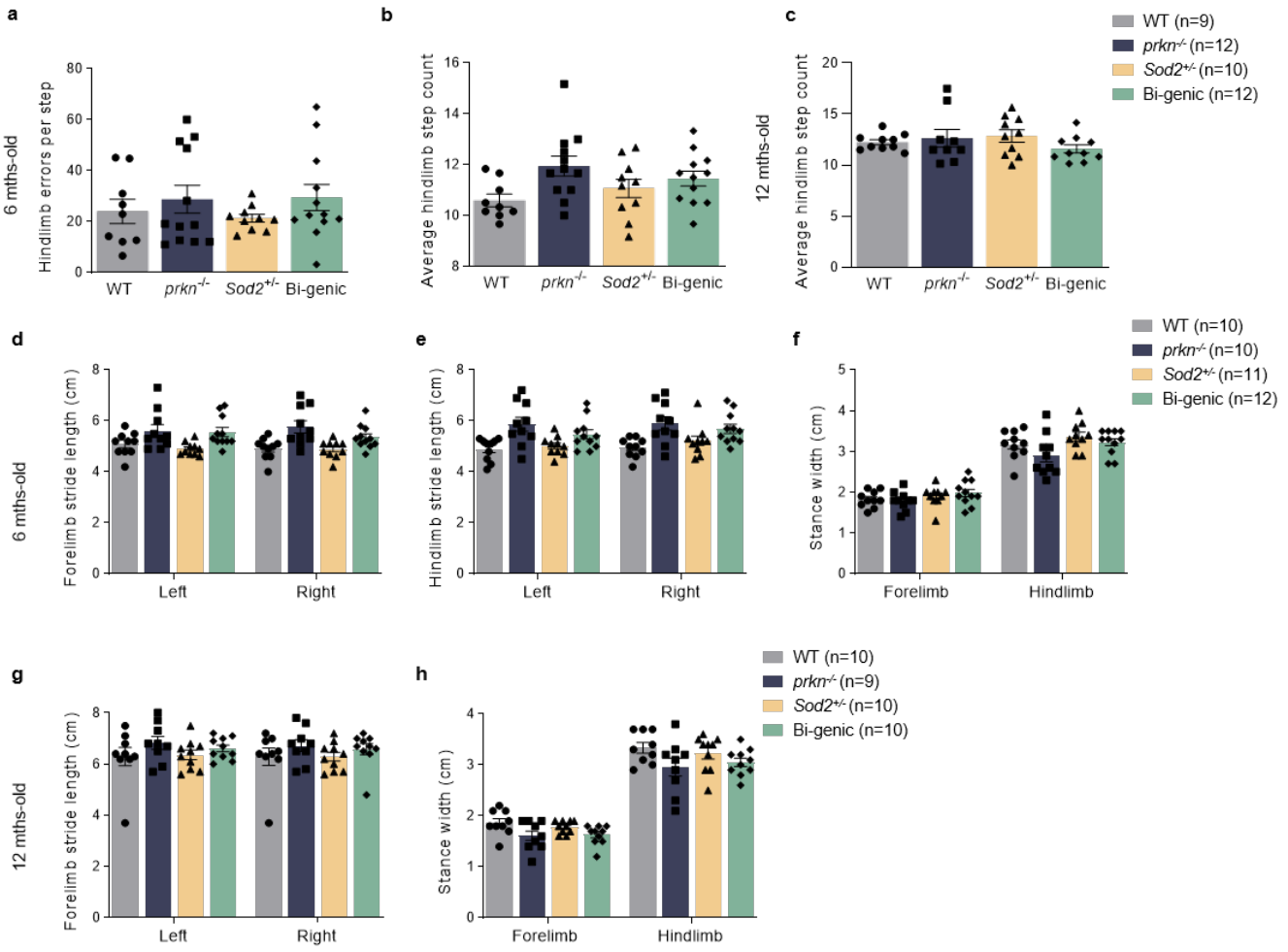

Supplementary Figure 3.4. Additional gait, posture and coordination assessments in 6 to 12-month-old mice.
(**a**) Number of hindlimb errors per step observed in the 6-month-old cohort. The average hindlimb step count observed in the 6-month-old (**b**) and the 12-mont-old (**c**) cohorts. Forelimb (**d**), and hindlimb (**e**) stride length in centimeters (cm) observed in the 6-month-old cohort. Stance width in centimeters (cm) observed in the 6-month-old (**f**) and the 12-mont-old (**h**) cohorts. (**g**) Forelimb stride length in centimeters (cm) observed in the 12-month-old cohort. Data are shown as mean values/genotype with number of animals/genotype indicated in (**b**, horizontal ladder data, **a-b**) and (**f,** DigiGait data, **d-f**) for the 6-month and in (**h**) for the 12-month-old cohorts (**c, g-h**) ± SEM. Significance was determined using a one-way ANOVA with Tukey's post-hoc analysis in (**a**) [$F(3, 39)= 0.6841$, $p= 0.5672$], in (**b**) [$F(3, 39)= 2.756$, $p= 0.0552$], and in (**c**) [$F(3, 35)= 1.010$, $p= 0.3998$]; a two-way ANOVA with Tukey's post-hoc analysis was used in (**d**) [$F(3,74)= 0.4810$, $p= 0.6965$], in (**e**) [$F(3, 74)= 0.1266$, $p= 0.9441$], in (**f**) [$F(3, 74)= 1.111$, $p= 0.3500$ found for interaction between limb and genotype, with $F(1, 74)= 327.6$, $p<0.0001$ found between limbs], in (**e**) [$F(3, 68)= 0.01592$, $p= 0.9972$] and, in (**h**) [$F(3, 68)= 0.1435$, $p= 0.9335$ found for interaction between limb and genotype, with $F(1, 68)= 411.6$, $p<0.0001$ found between limbs].

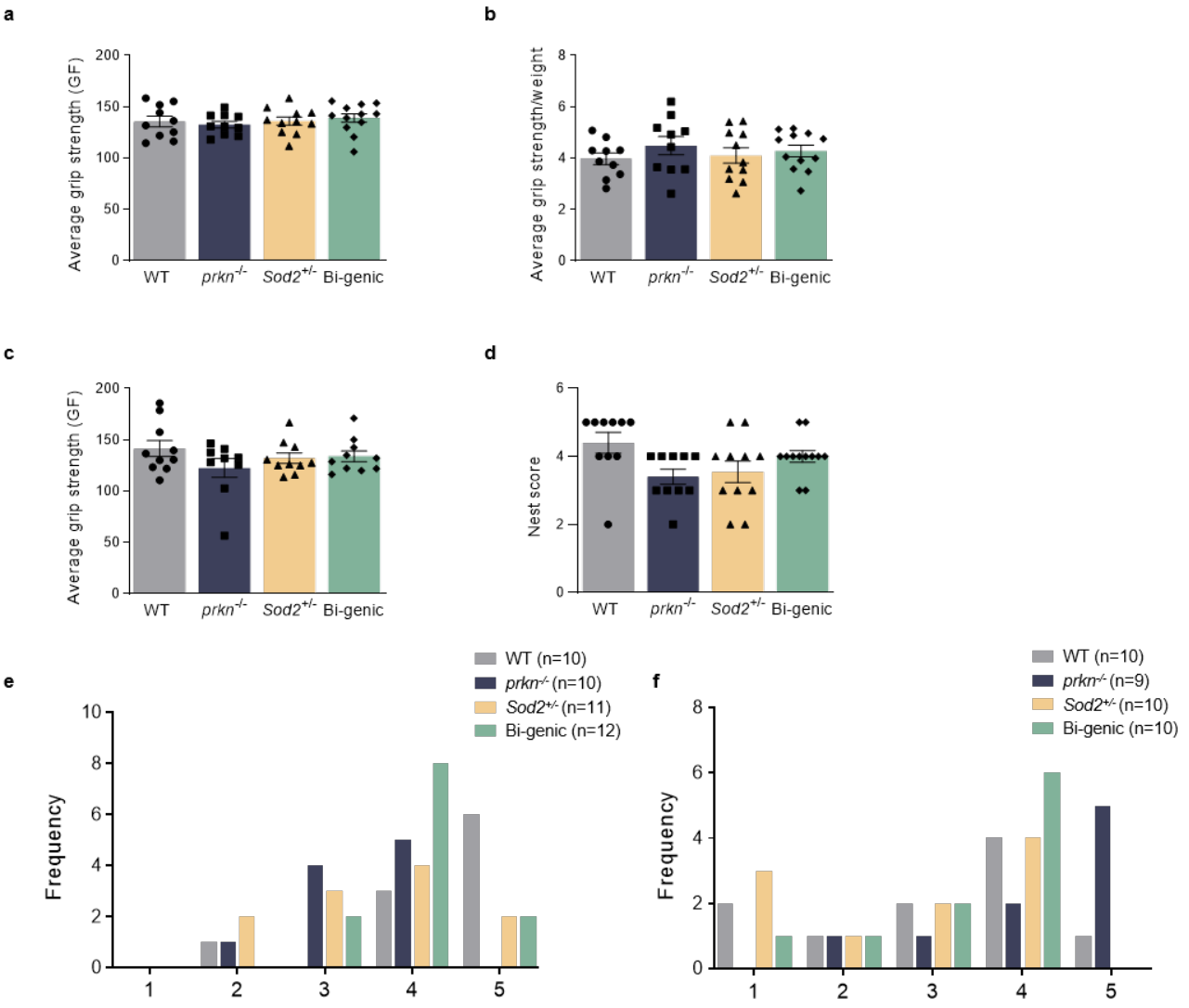

Supplementary Figure 3.5. Additional grip strength and nest score assessments in 6 to 12-month-old mice. (**a**) Average grip strength measured in kilogram-force (kgF) observed in the 6-month-old cohort. (**b**) Average grip strength per weight measured in kilogram-force (kgF) observed in the 6-month-old cohort. (**c**) Average grip strength measured in kilogram-force (kgF) observed in the 12-month-old cohort. (**d**) Nest building scores of the 6-month-old cohort. Scoring frequencies of the 6-month (**e**) and the 12-month-old (**f**) cohorts. Data in (**a-d**) are shown as mean values/genotype with number of animals/genotype indicated in (**e**) for the 6-month and in (**f**) for the 12-month-old cohorts ± SEM. Significance was determined using a one-way ANOVA with Tukey's post-hoc analysis in (**a**) [$F(3, 39)= 0.4002$, $p= 0.7536$], in (**b**) [$F(3, 39)= 0.5987$, $p= 0.6197$], and in (**c**) [$F(3, 35)= 1.209$, $p= 0.3209$] and in (**d**) [$F(3, 35)= 2.582$, $p= 0.0690$].

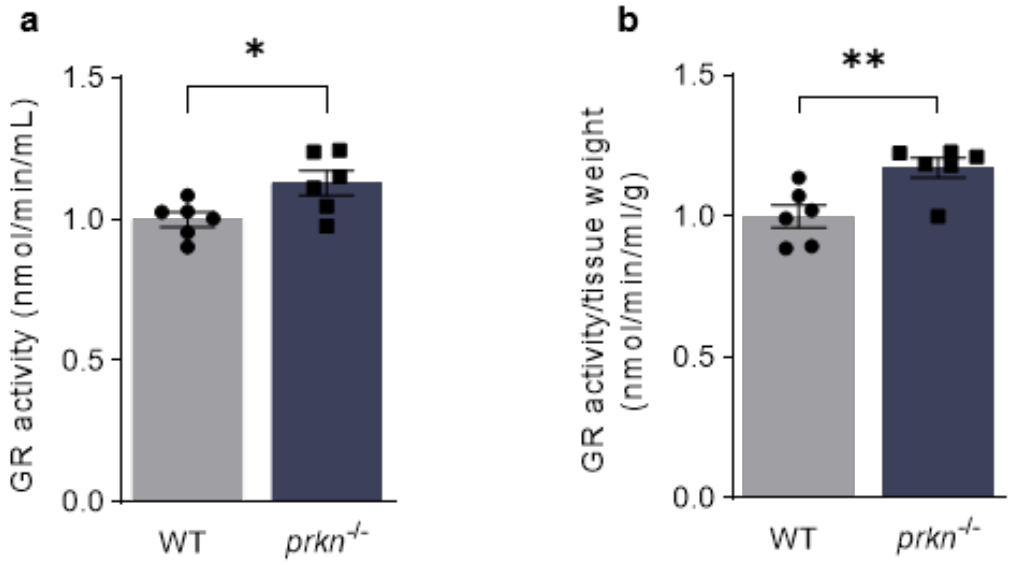

Supplementary Figure 3.6. Glutathione reductase activities in fresh vs. frozen tissues.
Glutathione reductase (GR) activity in fresh (**a**) vs. frozen (**b**) brain tissue from 7-8-month-old *WT* and *prkn*-/- mice. Data were obtained using n=6 and are plotted as mean normalized to *WT* ± SEM. Significance was determined using an unpaired Student T-test with p= 0.0291 for (**a**) and p= 0.0096 for (**b**).

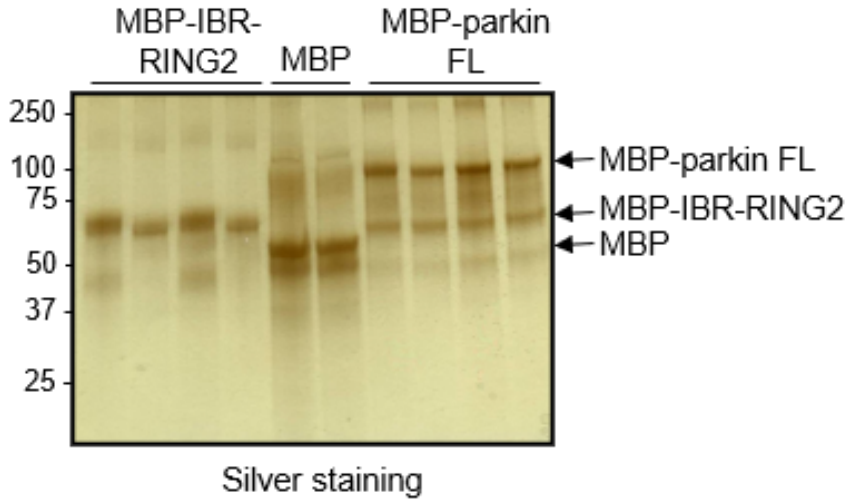

Supplementary Figure 3.7. MBP-parkin proteins used in in vitro glutathione regeneration studies.
Silver staining of recombinantly expressed maltose binding protein (MBP)-tag and MBP-tagged parkin proteins that were run on SDS-PAGE under reducing conditions. Lanes 1-4 contain MBP-IBR-RING2 parkin (aa 327-465; ~60-65 kDa), lanes 5-6 contain MBP alone (~45-50 kDa) and lanes 7-10 contain MBP-full length (FL)-parkin (aa1-465, ~95 kDa).

Chapter 4: Manuscript 3 - Characterization of second generation, parkin monoclonal antibodies to explore its metabolism in human brain

Author list:
Jacqueline M. Tokarew, Daniel N. El-Kodsi, Angela P. Nguyen, Nathalie A. Lengacher, Brian O'Nuallain, Ming Jin, Jasmine M. Khan, Andy C. H. Ng, Kelsey Grimes, Qiubo Jiang, Mei Zhang, Liqun Wang, Masashi Takanashi, Daisuke Tanigu, Nobutaka Hattori, Jennifer A. Chan, John M. Woulfe, Peggy Taylor, Julianna J. Tomlinson and Michael G. Schlossmacher

4.1 Preface

This manuscript describes the characterization of novel, human-specific, anti-parkin monoclonal antibodies (mAbs) using multiple experimental modalities. The goal being the generation of stable mAbs amenable to immunohistochemistry and standard microscopic techniques, which also possessed higher affinity for oxidized and aggregated parkin. The novelty of using untagged recombinant holoprotein as antigen resulted in the production of multiple human-specific mAbs that also preferentially detected oxidized and aggregated parkin. This was demonstrated by immunoblotting and immunofluorescence techniques using recombinant protein, several cell-lines, as well as, human and mouse brain lysates. Antibody clones A15165-B and -E possessed interesting characteristics, such as having highest affinity for oxidized and non-denatured parkin, respectively. Ultimately, three clones (A15165-D, -E and -G) demonstrated parkin-specific staining associated with neuromelanin and/or lysosomal storage vesicles in dopaminergic cells of human midbrain (see Chapter 2). The epitopes of these three mAbs, along with A15165-B, were subsequently mapped, with A15165-E having a conformational epitope. Clones A15165-E and -D were further developed and are now commercially available through BioLegend Inc.

4.2 Statement of author contribution

As first-author I provided major contributions to: establishing experimental techniques and their optimization, the overall project direction and design, data analysis and interpretation, as well as, initial drafts and edits of the manuscript. Specifically, I designed and drafted the initial proposal for antibody production sent to BioLegend Inc. (B. O'Nuallain, M. Jin, L. Wang and P. Taylor), participated in initial meetings and produced all antigens used for antibody production. I also independently performed initial immunoblotting and immunofluorescence characterization of mAbs (**Fig. 4.1a-c, 4.2 and Appendix Fig. C10-11**) and supervised immunoblotting and immunohistochemical characterizations performed by K. Grimes, Q. Jiang, N. Lengacher and Jasmine M. Khan (**Fig. 4.4 and Supplementary Fig. 4.2**). D. El-Kodsi and A. Ng helped characterize WB and immunofluorescence staining in CHO and M17 cell models. M. Zhang (J. Woulfe group) ran immunoflurescence-based co-labelling of parkin and LAMP-3 on human brain slices. A. Nguyen (also while part of J. Chan group) optimized the eDAB-staining protocol. M. Takanashi, D. Tanigu, N. Hattori, A. West and J. Woulfe provided fresh-frozen and paraffin-embedded human tissues.

4.3 Abstract

Mutations in the *PRKN* gene are linked to multiple disease processes including Parkinson disease (PD), cancer and changes in innate immunity. Deciphering the precise role of its gene product, parkin, in PD pathogenesis remains elusive and has been hindered by the lack of parkin-specific antibodies (Abs) capable of detecting brain parkin *in situ*. Here, we sought to develop monoclonal Abs (mAb) specific to the predominant, insoluble and aggregated form of parkin found in aged human brain. Using full-length and truncated (aa 321-465), recombinant human proteins as antigens, we generated a total of 16 clones, i.e., ten (A15165A-J) using wild-type parkin and six (I6004a'-f') using truncated parkin. Clones

A15165A-J provided the strongest signal against their antigen and its aggregated form, and were thus prioritized. Clone A15165B performed best to monitor parkin in CHO and M17 cell lines that stably express *PRKN* cDNA, including following mitochondrial toxin exposure; it also specifically detected parkin at its predicted molecular weight (52 kDa) in human brain. Intriguingly, despite their sequence homologies, clones A15165D, -E and -G could not detected parkin in mouse brain lysates, but a few reacted with rat parkin on immunoblots. In a previous report, clones A15165D, -E and -G produced parkin-specific immunohistochemical reactivities that localized within lysosomal vesicles in routine microscopy sections of human midbrains. The corresponding epitopes of clones A15165B, -D and -G lie within regulatory domains of parkin (i.e., linker region; REP domain), while the one for clone A15165E is conformational; it binds to peptides within the RING0 and RING2 domains, which are in proximity to each other within parkin's tertiary structure. We conclude that aspects of parkin's unique metabolism in adult human brain, which involves gradual insolubility and association with lysosomal structures, can now be monitored *in situ* through the usage of renewable, monoclonal antibodies.

4.4 Introduction

The exact role of parkin in Parkinson disease (PD) pathogenesis remains to be determined. Motor symptoms of this disease arise from neurodegeneration of dopamine-producing cells in the *substantia nigra* (*S. nigra*) *pars compacta*.[156,194] It is well established that parkin (containing 465 amino acids, aa) functions as a structurally-dependent E3 ubiquitin ligase enzyme; a large number of PD-linked *PRKN* point mutations cause protein misfolding. Its various domains include: the ubiquitin-like domain (Ubl, aa 1-75), a poorly conserved linker region (aa 76-140), four really interesting new gene (RING) type domains [(RING0, aa 141-225), (RING1, aa 226-326), (in-between RING or IBR, aa 327-378), and (RING2, aa 410-465)], and a second linker region between IBR and RING2 containing the repressor

element of parkin (REP, aa 391-403).[192,193,448-453,455,457,458] It is currently postulated that E3 loss-of-function leads to neuronal death due to: i) toxic accumulation of damaged proteins,[192,193,448,449,458]and/or ii) aberrant mitochondrial function from lack of proper mitochondrial turnover[349,351,889](*i.e.* mitophagy).[460] However, these current models have yet to explain the cell-specific loss of dopaminergic neurons in the *S. nigra*. For example, > 60 proteins, which affect vastly different cellular pathways, have been identified as parkin E3 ligase targets, and mitophagy occurs in both parkin-dependent and independent processes, depending on cell type examined or stressor(s) applied;[569,576] one study demonstrated that basal mitophagy in neuronal cells is independent of parkin.[575] As PD is a human-specific central nervous system disease, human brain tissue is the ideal research medium, yet detecting brain parkin *in situ* remains a challenge.

Unfortunately, there are no commercially available antibodies (Abs) that reliably detect human brain parkin by immunohistochemistry (IHC). Only one published study described the production of monoclonal antibodies (mAb), including clone Prk8 and 109, which are commonly used in research.[690] Initially produced by Pawlyk et al in 2003, these mAbs are experimentally versatile, because they robustly label overexpressed parkin in the cytosol of human and animal-derived cell-lines, and detect endogenous parkin in mammalian brain lysates; unfortunately, they are not amenable to IHC. Pawlyk and colleagues also discovered that ionic detergent (SDS) was required to extract parkin from aged human cortex. This suggested to us that, with age, parkin accumulates in a non-cytosolic compartment, and/or adopts a highly aggregated state.[690] Many studies have shown that parkin forms similar SDS-soluble aggregates when exposed to oxidants[486-492] and electrophiles (*e.g.* dopamine quinones)[362,493] that are highly produced in dopaminergic neurons. Interestingly, Prk8 detects an epitope spanning the RING2 domain of parkin (aa 399-465). This domain contains the E3 ligase catalytic site, which is inaccessible when parkin adopts its native E3 ligase-inactive state in solution;[192,193,448-453,458]; therefore,

it is possible that Prk8 detects an activated or unfolded form of parkin. Since SDS is required to extract parkin from aged human cortices, it is also likely that Prk8 cannot detect parkin by IHC as this technique utilizes non-denaturing conditions.

There, however, are reports of parkin-specific staining within human brain by IHC, which describe the use of non-renewable polyclonal Abs raised against various parkin protein fragments, including: regions corresponding to the RING1 domain (aa 293-306[431] and aa 295-311[688]) and the linker region found between the Ubl and RING0 domains (aa 84-98).[689] The antibodies were found to label perikarya and processes of neuromelanin (NM)-containing neurons in the *S. nigra* with lesser staining observed in non-striatal neurons, glial cells and blood vessels. Unfortunately, these studies were not further expanded upon and although the antibody generated against fragment aa 295-311 is commercially available, its production as a polyclonal antibody renders it susceptible to issues with reproducibility.

Here, we sought out to fill a critical void in parkin research by developing renewable antibodies. We hypothesized that using untagged, recombinant immunogens of the full-length protein, as well as, of a C-terminal (also untagged) peptide of human parkin (aa 321-465) may be suitable to adopt a native state-like structure and confer robust antigenicity. Here, we describe the production of four mAbs (clones A15165B, -D, -E and -G) that are specific to human parkin based on their characterization under *in vitro, ex vivo* and *in situ* conditions; three of them (clones A15165D, -E and -G) were previously found[846] amenable to routine microscopy that generated lysosome-associated staining within neurons in *S. nigra* of the adult human brain.

4.5 Results

Oxidation-induced aggregation of parkin and ELISA screening of initial hybridomas

The goal of producing additional anti-parkin monoclonal antibodies (mAbs) was to detect oxidized and aggregated forms of parkin *in situ*. As shown in **Fig. 4.1a-b** and in previous work [362,486,690,846] oxidative and dopamine stress cause parkin insolubility in cells and tissues, and is the predominant form found in adult human brain over the age of 40. Additionally, shown in **Fig. 4.1c**, the commercially available Prk8 mAb clone readily labels reduced forms of full-length parkin (WT) and truncated parkin (321C, aa 321-465, corresponding to Prk8 epitope), but has lower avidity for high molecular weight (HMW) oxidized forms of the protein. Therefore, the initial experimental design included non-modified, as well as, oxidized and dopamine-conjugated antigens containing the full and truncated (aa 321-465) protein sequences of parkin. In contrast to Pawlyk et al.,[690] recombinant protein tags were removed as more recent structural work had revealed that N-terminal modifications alter the protein's native folding.[192,193,448-453,458] Unfortunately, the modified antigens failed to produce satisfactory binding avidities, as measured by ELISA, and, therefore, were not further developed. Nonetheless, a total of sixteen hybridoma clones were generated from the remaining antigens, and the binding avidity of their supernatants was measured; ten from WT parkin (A15165A-J, **Fig. 1d-e**) and six from 321C parkin (I6004a'-f', **Fig. 4.1f-g**). When comparing their effective concentrations, (see **Fig. 1h**), clones I6004a'-f', with the exception of I6004e'-f', were specific to their antigen, *i.e.* 321C parkin, while clones, A15165A-J, with the exception of A15165B, detected both WT and 321C with similar avidities. Of note, clone A15165E, which was later revealed to specifically detect parkin *in situ*, had the lowest overall binding avidity for both WT and 321C parkin.

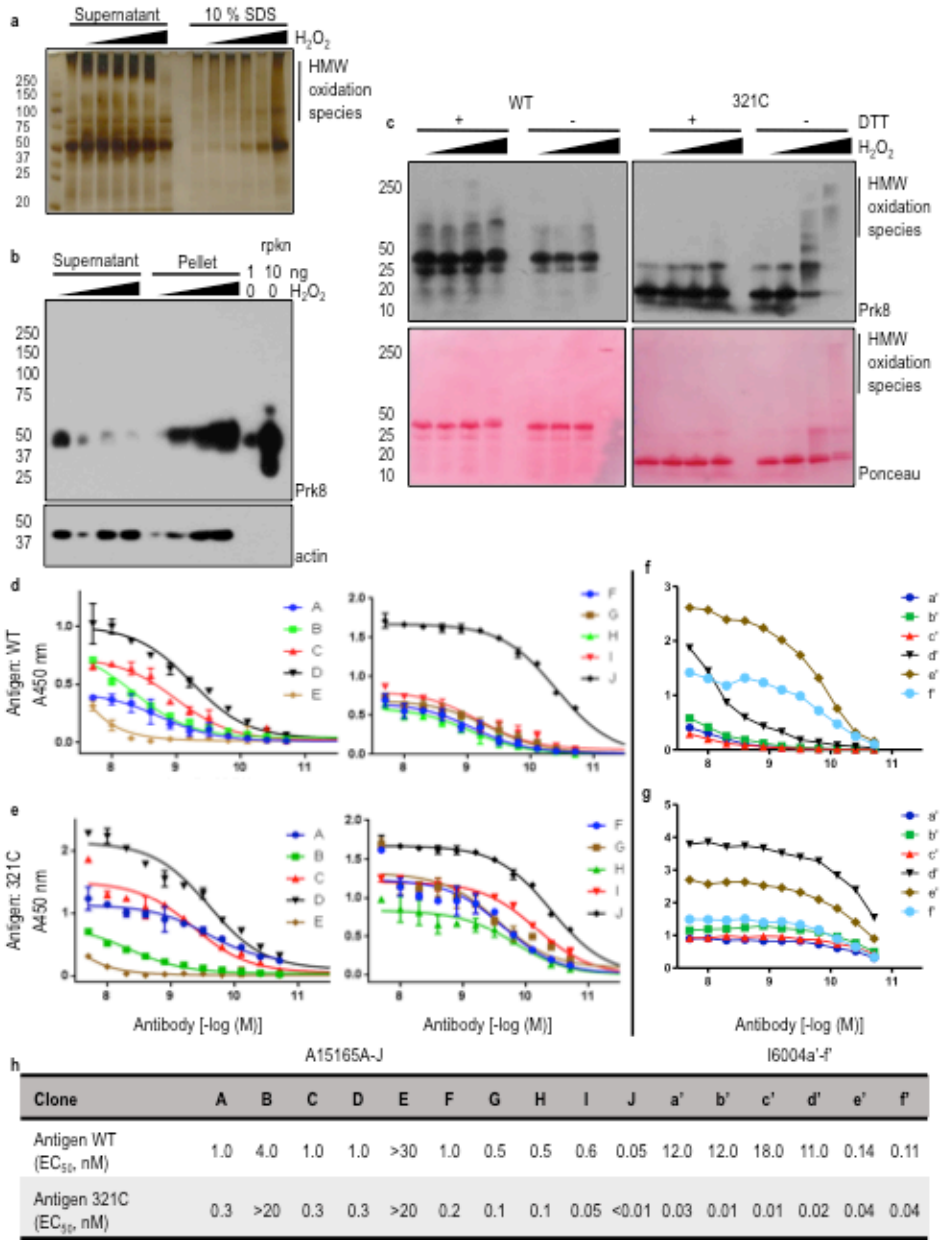

Clone	A	B	C	D	E	F	G	H	I	J	a'	b'	c'	d'	e'	f'
Antigen WT (EC_{50}, nM)	1.0	4.0	1.0	1.0	>30	1.0	0.5	0.5	0.6	0.05	12.0	12.0	18.0	11.0	0.14	0.11
Antigen 321C (EC_{50}, nM)	0.3	>20	0.3	0.3	>20	0.2	0.1	0.1	0.05	<0.01	0.03	0.01	0.01	0.02	0.04	0.04

Figure 4.1. Oxidation-induced aggregation of parkin and ELISA screening of select hybridomas
(**a-b**) Example of oxidation-induced aggregation of parkin *in vitro*. (**a**) Recombinant tagless WT parkin (0.02 mM or 10 µg) treated with increasing concentrations of H_2O_2 (0, 0.02, 0.2, 0.5, 0.75, 1 and 2 mM) and extracted using salt buffer with and without 10 % SDS. (**b**) HEK-293 cells treated with increasing concentrations of H_2O_2 (0, 0.2, 2 and 5 mM) and extracted using RIPA buffer. Resulting supernatant and pellet, along with recombinant parkin (rprn), were blotted for parkin (Prk8, 1: 2000) and actin (1: 1000). (**c**) SDS-PAGE of recombinant tagless WT parkin and C-terminal parkin (321C, containing aa 321-465). Proteins were treated with 0,0.1,1 and 10 mM H_2O_2 with or without 50 mM DTT as indicated and loaded at 10 µg per lane. Membranes were stained with Ponceau S and blotted for parkin (Prk8, 1: 40K); HMW: high molecular weight. (**d-e**) ELISA screening of 10 subcloned hybridomas (A15165A-J, 0.02-20 nM) produced from immunizing mice with WT parkin and tested against (**d**) WT parkin and against (**e**) 321C (f-g) ELISA screening of 6 subcloned hybridomas (I6004a'-f', 0.02-20 nM) produced from immunizing mice with 321C and tested against (**f**) WT parkin and against (**g**) 321C. Proteins were loaded at 50 ng/well. Antibody concentrations (mol·L-1) converted on logarithmic scale and plotted against absorbance at 450 nm (A450 nm). (**h**) Summary table of calculated EC50 (nM) for mAbs A15165A-J and I6004a'-f' screened using ELISA.

Clones A15165A-J, except E, detect denatured and aggregated parkin.

To validate the initial ELISA results clones A15165A-J and I6004a'-f' were screened using a slot immunoblot technique to determine their specificity for non-denatured WT and 321C parkin antigens. The cysteine-containing protein, DJ-1, was also used as a negative control. Examples of the strongest signals obtained are shown in **Fig. 4.2a**, with the full summary of screening for all clones tested below in **Fig. 4.2c**. The results confirmed the specificity of clones A15165B and I6004a'-d' towards their respective antigens. The mAbs were further screened against denatured and oxidized recombinant WT and 321C parkin protein using the Western blotting (WB) technique (see **Fig. 4.2b**). Here, tagless recombinant parkin (50 ng) was treated with increasing concentrations of H_2O_2 (0-500 nM) and run on non-reducing SDS-PAGE. Again, A15165B demonstrated specificity for WT parkin, suggesting its epitope was closer to the N-terminus of WT parkin. The loss of signal from clone A15165E in **Fig. 4.2b** suggests that its epitope was conformational as it only recognized a non-denatured form of parkin. While Prk8 had poorer detection of HMW species formed by oxidation of both WT and 321C parkin, all A15165A-J clones, except for A15165E, detected HMW species at a similar intensity as the reduced, monomeric form. Surprisingly, clones I6004a'-f' had the poorest detection of HMW species, suggesting that their epitopes become oxidized or hidden within oxidized parkin multimers. Since epitopes that recognized non-denatured and oxidized forms of parkin were desired, only clones A15165A-J were further characterized.

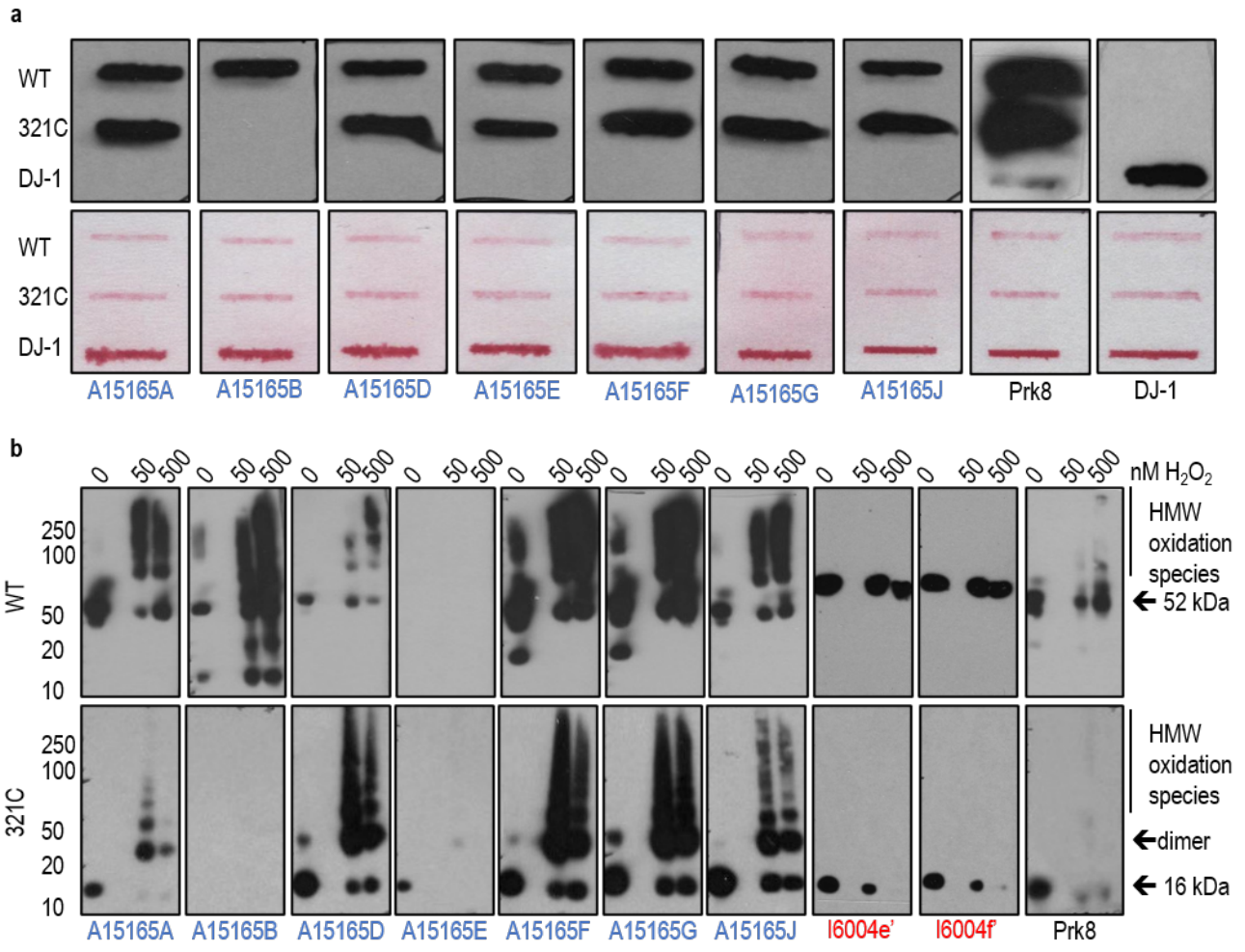

c

Clone	A	B	C	D	E	F	G	H	I	J	a'	b'	c'	d'	e'	f'
non-denatured WT	+	+	+	+	+	+	+	+	+	+	-	-	-	-	+	+
non-denatured 321C	+	-	+	+	+	+	+	+	+	+	+	-	+	+	+	+
oxidized WT	+	+	+	+	-	+	+	+	+	+	-	-	-	-	-	-
oxidized 321C	+	-	+	+	-	+	+	+	+	+	-	-	-	-	-	-

Figure 4.2. Clones A15165A-J, except E, detect denatured and aggregated parkin.
(**a**) Non-denaturing slot-blotting of select anti-parkin mAb clones on recombinant WT parkin (5 µg/slot), C-terminal parkin (321C, 5 µg/slot) and DJ-1 (20 µg/slot) as negative control. Corresponding Ponceau S staining is below each blot. Dilutions of antibodies were as follows: A15165E (1:500); A15165A, -B, -D, -F, -G and J (1:1000); Prk8 (1:20K); and DJ-1 (1:2000). (**b**) Non-reducing SDS-PAGE (0 mM DTT) Western blotting of select anti-parkin mAb clones on progressively oxidized recombinant WT and 321C parkin. Dilutions of antibodies were as follows: A15165A (1:5000); A15165E and I6004f'(1:500); A15165B, D, F, G , J and I6004e'(1:1000); and Prk8 (1:20K); HMW: high molecular weight. (**c**) Summary table of performance of all clones (A15165A-J and I6004a'-f') tested in experiments shown in (**a**) and (**b**) above.
;-, poor or negative signal; +, positive signal.

Clones A15165B, -D, -F and -G detect oxidized and aggregated parkin *in vitro*.

Clones A15165A-J were further screened against human embryonic kidney cells (HEK-293) ectopically expressing FLAG-tagged human parkin using WB and immunofluorescence (IF) techniques (summarized in **Fig. 4.3a**). Here the clones performed similarly to Prk8, except A15165E, which demonstrated no signal against parkin using both techniques. To further validate these results, IF was performed on Chinese hamster ovary (CHO) and human neuroblastoma (M17) cell lines engineered to stably express myc-tagged parkin, denoted CHOmP and M17/P17, or myc control vectors (**Fig. 4.3** and **Supplementary Fig. 4.1**). Only clones A15165B, -D, -F and -G produced parkin-specific fluorescence within the cytosol, with A15165B demonstrating the highest signal: noise ratio among clones tested (**Fig. 4.3a**). By visual comparison, it also appeared that parkin expression was higher in CHOmP vs. M17/P17. As previously described using Prk8,[349] the signal obtained by clone A15165B also co-localized with the mitochondrial-marker, translocase complex of the outer mitochondrial membrane 20 (TOM20), following treatment with carbonyl cyanide-m-chlorophenylhydrazone (CCCP), see **Fig. 4.3b**. Consistent with the WB analysis of oxidized recombinant parkin (see **Fig. 4.2b**), clones A15165B, -D, -F and -G detected oxidized parkin, as diffusely distributed puncta, in cells treated with 200 μM H_2O_2. Surprisingly, as shown in **Supplementary Fig. 4.1**, it appeared that clones A15165D, -F and –G had a particular preference for oxidized parkin, as the intensity of their staining increased following H_2O_2 treatment. Complementary non-reducing WB (see **Fig 4.3c**) was performed on lysates obtained from CHO and CHOmP cells treated as described in **Fig. 4.3b**. Here treatments of CCCP and H_2O_2 both resulted in the formation of HMW parkin species that were more readily detectable using clone A15165B vs. Prk8; similar results were also obtained for clone A15165F. This suggested that parkin undergoes oligomerization post CCCP treatment.

a

Clone	A	B	C	D	E	F	G	H	I	J
HEK WB	+	+	+	+	-	+	+	+	+	+
HEK IF	+	+	+	+	-	+	+	+	+	+
CHO IF	-	++	-	+	-	+	+	-	-	-
M17 IF	-	++	-	+	-	+	+	-	-	-

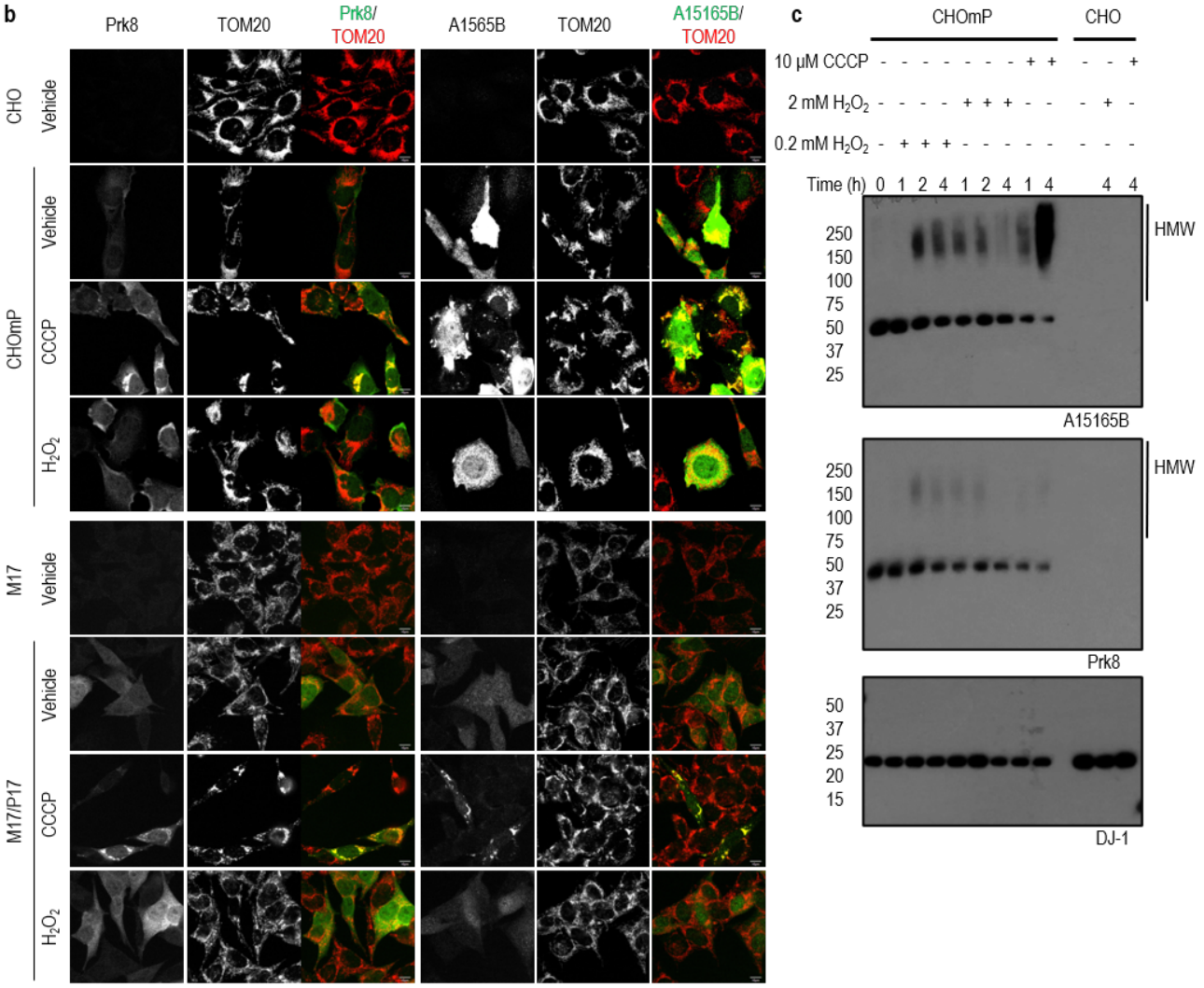

Figure 4.3. Clone A15165B detects oxidized and aggregated parkin *in vitro*.
(**a**) Summary table of performance of all mAbs (A15165A-J) tested in cell immunofluorescence (IF) and Western blotting (WB) experiments.;-, negative signal; +, positive signal; ++, strong signal, CHO, Chinese hamster ovary; M17, human neuroblastoma cell line ; HEK, human embryonic kidney cell line. (**b**) Mitochondrial recruitment of parkin immunofluorescence experiments in CHO and M17 cells using CCCP (10 µM) and H_2O_2 (200 µM) as stressors. Cells were imaged 4 hours after stressor was applied. All mAbs (A15165A-J) were used at 1:200 dilution; Prk8 (1:250) served as positive control and anti-TOM20 served as mitochondrial marker. Shown is Prk8 and clone A15165B, which demonstrated the strongest positive signal. see **Supplementary Fig. 4.1** for A15165D, -F and -G; TOM20, Mitochondrial import receptor subunit TOM20 homolog. (**c**) SDS-PAGE of sister experiment shown in (**b**) using CHO cells and blotting with A15165B (1:1000) and Prk8 (1:5000); DJ-1 (1:1000) served as loading control.

Clones A15165D, -E and -G detect parkin specifically in human brain

To compare parkin detection in human brain lysates by WB, clones A15165A-J were tested against Tris saline-soluble and SDS-soluble cortical brain extracts derived from control subjects of various ages and subjects presenting with *PRKN*-associated autosomal recessive Parkinson disease, which lack complete expression of parkin protein (see Tokarew et al. 2021[846]). The summary of these experiments is shown in **Fig. 4.4a** along with results of WB analyses of clones A15165A-J against whole brain Tris saline-soluble extracts of wildtype mice and brain membrane-associated extracts of wildtype rats. Note that clones A15165F, -H, -I and –J had significant non-specific staining and were not further characterized. An example of the staining obtained from clones A15165B, -D and –G is shown in **Fig. 4.4b**, along with Prk109 mAb (also recognizes rat parkin homolog[690]) and mouse immunoglobulin isotype 2b (mIgG2b) as positive and negative controls, respectively. In parallel work, immunohistochemistry (IHC) analyses of human *Substantia nigra* (*S. nigra*) sections using clones A15165D, -E and –G, found parkin-specific staining within LAMP3+ vesicles that also associated with neuromelanin.[846] Surprisingly, clone A15165B did not detect parkin using IHC technique, despite its strong signal observed for oxidized and aggregated parkin in human cells and tissues by IF and WB techniques.

a

Clone	A	B	C	D	E	F	G	H	I	J
Hu WB	-	+	+	+	-	+*	+	+*	+*	+*
Ms WB	-	-	-	-	-	-	-	-	-	-
Rt WB	nd	-	nd	+	nd	nd	+	nd	nd	nd
Hu IHC	-	-	-	+	+	-	+	-	-	-

b

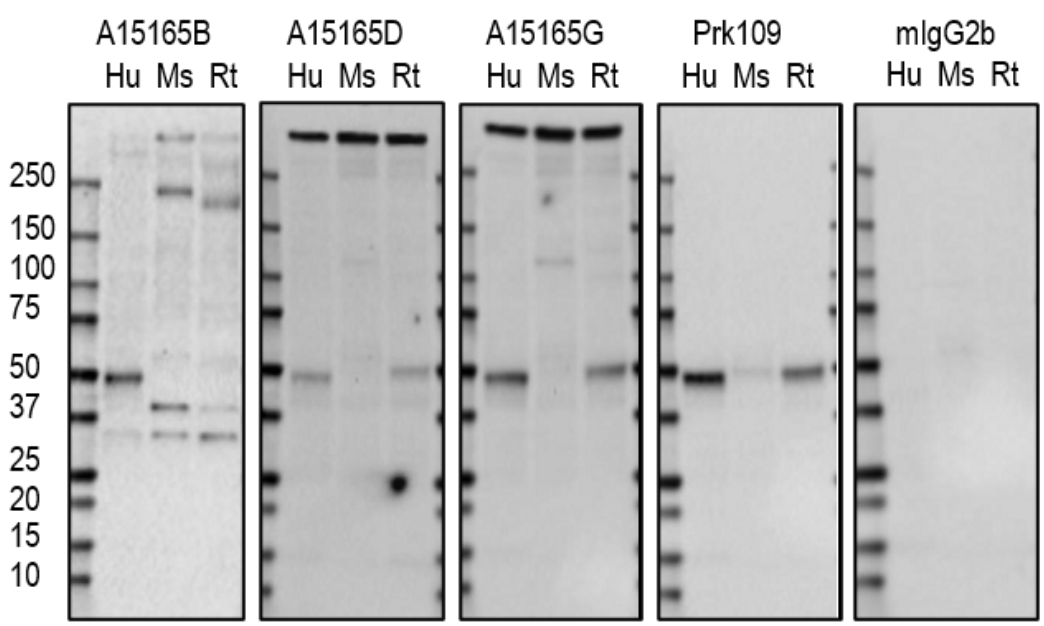

Figure 4.4. Clones A15165D, E and G specifically detect human brain parkin
(a) Summary of detection of parkin in mammalian brain using mAbs A15165A-J; Hu, human; Ms, mouse; Rt, rat; IHC, immunohistochemistry; WB, Western blot; -, negative signal; +, positive signal; +* positive non-specific signal; nd, not determined. (**b**) SDS-PAGE of human, mouse and rat brain membrane lysates (20 µg/well) blotted for parkin with mAbs A15165B, -D and -G (5.0 µg/mL) , positive control antibody Prk109 (1.0 µg/mL) and mouse IgGs subtype 2b (mIgG2b, 10.0 µg/mL) as negative control.

Epitope mapping of clones A15165B, -D, -E and -G

Although clone A15165B was not amenable to IHC, its higher selectivity towards oxidized and aggregated parkin made it an interesting candidate to pursue further development and was therefore included along with A15165D, -E and –G for epitope mapping. This was performed using an ELISA-based conformational parkin peptide microarray (see **Fig.** 4.**5a** and **Supplementary Fig. 4.2)**. Here an array of cyclized parkin peptides with 6-12 amino acid overlapping residues was adhered to assay plates and probed against clones A15165B, -D, -E and –G using fluorescently labeled anti-mouse secondary antibody. Epitope affinity was determined by comparing individual fluorescence intensities obtained from each cyclized parkin peptide, shown plotted in **Fig. 4.5a**. Therefore, highest fluorescence intensities identified highest binding affinity, with the corresponding peptide sequence being the likely epitope. It was determined that clones A15165D and –G (shown in purple and green, respectively) recognized an identical epitope located within the repressor element of parkin (REP) domain of parkin (see **Fig. 4.5b**). While it appeared that clone B (shown in light blue) might have two epitopes, the sequence homology between GVLCPRPGCG and its main epitope RNAAG, suggested that this might rather be a cross-reaction. Consistent with its inability to detect the more C-terminal residues of 321C parkin, the main epitope of A15165B lies within the linker domain of parkin. Also consistent with data presented above, clone A15165E (shown in orange) appeared to recognize a particular conformation of parkin, since the epitopes identified for A15165E are in spatial proximity within parkin's tertiary structure. Finally, it was interesting to note that while most clones were human-specific, only clone A15165B retains a human-specific epitope sequence (see **Fig. 4.5c**).

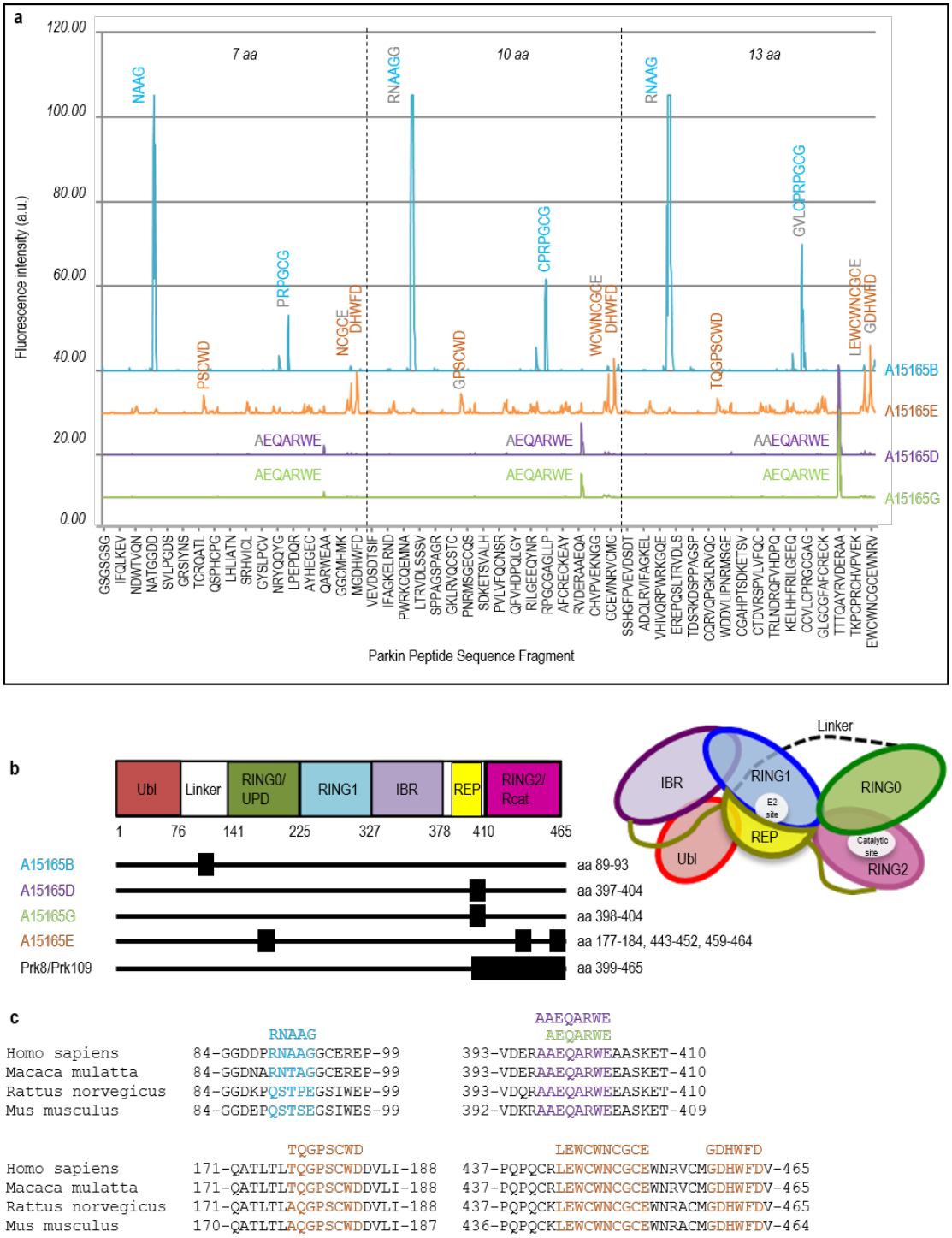

Figure 4.5. Epitope mapping of clones A15165B, D, E and G.
(**a**) Results of epitope mapping performed on mAbs A15165B, D, E and G using conformational parkin peptide microarrays plotted as fluorescence intensities against corresponding parkin peptide sequences. Peaks of higher fluorescence intensities indicate peptide regions (*ie* epitope) with highest mAb affinity. In case it was not clear if a certain amino acid contributed to antibody binding, the corresponding letters were written in gray. (**b**) Location of mapped epitopes within the primary structure of parkin. Tertiary structure (far right) is shown to demonstrate conformational nature of clone A15165E epitope. (**c**) Epitope alignment with amino acid sequences for parkin in human (UniProt ID: O60260), Rhesus monkey (UniProt ID: F6U1L3), rat (UniProt ID: Q9JK66) and mouse (UniProt ID: Q9WVS6).

4.6 Discussion

This study describes the production and characterization of human-specific anti-parkin mAbs that are amenable to standard microscopic techniques, *i.e.* IF and IHC. To our knowledge this is the first study that used untagged parkin protein as antigen, and selected mAbs for further production based on their ability to detect aggregated and oxidized forms of parkin protein. This strategy proved successful as a total of four mAbs (A15165B, -D, -E, and -G) retained the desired qualities, with three (A15165D, -E, and –G) generating positive staining predominantly within vesicle-like structures of human neurons.[846] Removing the tag likely permitted refolding of the protein, which may have better recapitulated its native form; possibly distinguishing it from the murine tertiary conformation. Although it was initially surprising that unmodified parkin antigens generated mAbs with sensitivity towards oxidized forms of parkin, this was likely the result of inadvertent antigen oxidation during shipment, processing and/or inoculation. Also, the oxidation of parkin antigens may have contributed to the fact that clones A15165D, -E, and –G are able to distinguish human from murine parkin as our parallel studies have discovered that human brain parkin is natively more oxidized than its murine homolog (see Chapter 3 and[846]).

While clone A15165E had the poorest performance in laboratory analyses that denatured proteins, it provided the best parkin signal when used in IHC (**Fig 4.4a**). In fact, in our parallel study,[846] A15165E produced a strong, age- and neuromelanin-associated, signal for parkin in the *S. nigra*, and was also amenable to indirect immunofluorescence, where it co-labeled parkin within lysosomal-associated membrane protein -3 (LAMP3) positive vesicles. Consistent with its localization within lysosomes, parkin was also found to co-distribute with light chain 3-B (LC3B) when extracted with progressively increasing concentrations of detergent, *i.e.* Triton-X and SDS. Thus, it is possible that A15165E detects the non-denatured form of parkin that is predominantly recovered within the SDS-

soluble extract of older human brain.[690,846] This may also be true for clones A15165D and –G, which have a similar staining profile as clone A15165E, albeit with lesser intensity. Additionally, all three clones (A15165D, -E and -G) appeared to prefer a non-denatured form of human brain parkin since their detection of parkin in human brain lysates by WB technique was less favourable (**Fig. 4.4b**).

In contrast, clone A15165B was amenable to WB and IF in cells and tissues, but lacked signal when tested against human brain sections using IHC. The location of its epitope (aa 89-93) within the primate-specific linker domain of parkin easily explains its preference for the human homolog. However, the close-proximity of its epitope to the redox-sensitive residue, Cys95, may also explain its preference for oxidized and HMW parkin species. Again, in our parallel study, using clone A15165B to isolate parkin from human brain lysates, we uncovered native Cys95 cysteine-oxidation events. There, we also determined that Cys95 is the predominant site that undergoes dopamine conjugation, and is, in part, responsible for promoting dopamine polymerization; a preliminary step in neuromelanin formation.[846] Pending further validation, it is possible that native posttranslational modifications of residue Cys95, *e.g.* oxidation of direct binding to neuromelanin, alters or blocks the epitope of A15165B, resulting in the loss of signal.

Furthermore, it was interesting to note that Prk8[690] and clones I6004a'-f', which were generated from a C-terminal parkin protein fragment (aa 399-465 and 321-365, respectively), demonstrated the weakest signal for oxidized and HMW parkin species (**Fig. 4.2a**). Not only does this finding suggest that the C-terminal fragment of parkin contains an important site through which dimer and multimer formation occur, it also indicates that the widely used Prk8 mAb lacks the ability to detect an important parkin conformer, which appeared to increase post-CCCP treatment when blotted using A15165B (**Fig 4.3b**). In light of these findings, we caution that parkin resides in different redox-states *in vivo*, which

are currently under-investigated, since they are not easily detected using Prk8 and conventional laboratory conditions.

In sum, we have generated and fully characterized four novel anti-parkin mAbs, which detect various forms of native, oxidized and HMW parkin (of note, clones A15165D and –E have now been made commercially available) and we believe that their addition to the parkin research toolkit will further enhance our understanding of parkin biochemistry within human cells and tissues.

4.7 Materials and Methods

Tissue Collection

All tissue was collected in accordance with Institutional Review Board-approved guidelines. Post-mortem, frozen brain samples from the cerebral cortex were obtained from the NICHD Brain and Tissue Bank at the University of Maryland, as well as, the University of Alabama and the Autism Tissue Program. Paraffin embedded human brain samples were obtained from the Harvard Brain Tissue Resource Center at Harvard University, the Neuropathology Service at Brigham and Women's Hospital and from archived autopsy specimens in the Department of Pathology and Laboratory Medicine of The Ottawa Hospital. ARPD and their age matched control samples were obtained from the Department of Neurology, Juntendo University School of Medicine. Mouse tissue was collected from WT (C57BL/6 background, Jackson Laboratories) and parkin KO mice (C57BL/6 background back crossed, originally developed by Alexis Brice Laboratory)[432] in accordance with protocols approved by the University of Ottawa Animal Care and Veterinary Services Committee.

Western Blotting

All proteins were separated on pre-cast 4-12 % Bis-Tris SDS-PAGE gels (Invitrogen) using MES running buffer (50 mM MES, 50 mM Tris, 1 mM EDTA and 0.1 % SDS, pH 7.3) and Laemmli loading buffer [10% SDS, 20% glycerol, 0.1% bromophenol blue, 0.125 M Tris HCl with either (0-200 mM) DTT or 200 mM β-mercaptoethanol]. Proteins were transferred to PVDF (Bio-Rad) membranes using Transfer Buffer (25 mM Tris base, 200 mM glycine, 20 % methanol). Completion of transfer was verified by incubating membranes with Ponceau S solution, followed by 1 h blocking (5 % milk in PBST, 0.075 % Tween 20, 1.4 mM NaCl, 27 mM KCl, 100 mM Na_2HPO_4, 18 mM KH_2PO_4, pH 7.5). Primary antibodies were diluted in blocking solution and incubated at 4°C for 16 h. Following a wash with PBST the membranes were incubated for 1 h with horseradish peroxidase (HRP)-conjugated secondary antibody diluted 1:10,000 in blocking solution. Signal was detected using Pierce™ ECL Western Blotting Substrate and CL-XPosure Film (ThermoFisher Scientific). Membranes were incubated with ReBlot 1X solution (Millipore) for 15 min before repeating the blotting procedure.

Parkin in vitro Aggregation

Recombinant tagless WT parkin (10 µL of 20 µM, or 10 µg) was incubated with H_2O_2 (0, 20, 200, 500, 750, 1000 and 2000 µM) in protein buffer (50 mM Tris, 200 mM NaCl, pH 7.5) for 30 min at 37°C and centrifuged at 21,000 x g for 15 min. The supernatant was separated and the pellet was incubated with 10 µL of 10 % SDS in protein buffer for 30 min at 37°C followed by repeat centrifugation. Both supernatant fractions (with and without 10 % SDS) were separated on reducing SDS-PAGE (100 mM mercaptoethanol) and visualized with silver staining (SilverQuest^{TM} Staining Kit, Invitrogen).

HEK-293 cells were grown in Dulbecco's Modified Eagle Medium (DMEM, Sigma) supplemented with 1 % penicillin/streptomycin and 10 % fetal bovine serum (lot AAA198121, Hyclone)] at 37°C with 5 %

CO_2 and seeded on 75 cm^2 cell culture flasks (Corning) at a density of 1-3 x 10^5 cells/mL. Once cells reached 70-80 % confluency they were transfected with cDNA coding for FLAG-tagged parkin or empty FLAG control vector (pcDNA3.1) using a 1:1 ratio of cDNA: Lipofectamine 2000 (Invitrogen) in a minimum of OPTI-MEM transfection medium (Gibco). After 24 h the cells were lifted using trypsin and plated at a density of 2 million cells/ well in a 12-well dish. After 48 h, the cells were treated with 0, 0.2, 2 and 5 mM H_2O_2 for 30 min at 37°C and 5 % CO_2. Cells were lifted using a cell scraper and spun at 21 000 x g for 10 min. Following one wash with PBS (1.4 mM NaCl, 27 mM KCl, 100 mM Na_2HPO_4, 18 mM KH_2PO_4, pH 7.5) cells were lysed in 20 µL of RIPA (1 % nonionic polyoxyethylene-40, 0.1 % SDS, 50 mM Tris, 150 mM NaCl, 0.5 % sodium deoxycholate, 1 mM EDTA) buffer and spun at 21,000 x g for 10 min. The supernatant was separated and the pellet was resuspended in 20 µL of non-reducing Laemmli buffer. Supernatant containing 10 µg of total protein (approx. 10 µL) and 10 µL of resuspended pellet were run on SDS-PAGE along with 1 and 10 ng of recombinant WT parkin and blotted for parkin (Prk8, 1: 2,000; MAB5512, Millipore,) and actin (1: 1000; A3853, Sigma).

Antibody Production and Clone Selection

All recombinant proteins were expressed as 6His-Smt3 fusion proteins using pET-SUMO expression vector, as previously described.[193,458,571,846] The tag was removed by overnight incubation with ulp1 protease (2 mg). A total of 15-20 mg each of tagless WT and truncated (aa 321-465, 321C) recombinant parkin was shipped to BioLegend Inc., thawed on ice, and centrifuged prior to inoculation. Each antigen was used to immunize 5 mice multiple times. Initial sera were screened for presence of immunoglobulins (IgGs) using the SureBlue Reserve TMB (KPL Inc.) enzyme-linked immunosorbent assay (ELISA). Murine sera IgGs were immobilized using anti-mouse IgG and tested against HRP-conjugated parkin antibodies (BioLegend Inc.). Spleen B cells from immunized mice whose sera gave a

positive response on initial screening were collected and fused with myeloma cells to produce stable hybridoma cell lines. Individual clones were selected and the purified IgGs were tested for immunoreactivity to recombinant parkin again using the SureBlue Reserve TMB ELISA detection system. Both recombinant WT and 321C parkin were absorbed onto an assay plate at a concentration of 50 ng/well. Isolated anti-parkin monoclonal antibodies (mAbs) A15165A-J and I6004a'-f' were added at a concentration of 0.02-20 nM and incubated for 45 min at 37°C. After several wash steps, and incubation with HRP-conjugated goat anti-mouse (1: 2000; 405306, BioLegend Inc.), the binding capacity of each mAb was determined by measuring the optical density at 450 nm. The absorbance at 450 nm was plotted against the IgG concentrations ($mol \cdot L^{-1}$) converted on a logarithmic scale and the EC_{50}, expressed as nM, was calculated using nonlinear regression on Prism software (range of R^2 values obtained: 0.9734-0.9989).

Immunoblotting of Novel Anti-Parkin Monoclonal Antibodies

Anti-parkin mAbs were screened for their ability to detect non-denatured antigens using a slot-blot technique. A nitrocellulose membrane (Bio-Rad) was pre-moistened in TBS buffer (10 mM Tris, 150 mM NaCl, pH 7.4) and secured in a Bio-Dot SF Microfiltration Apparatus (Bio-Rad). Wild type parkin (5 µg), truncated parkin (321C, 5 µg) and DJ-1 (20 µg) recombinant proteins were adhered to the membrane under light vacuum. After several washes the membrane was stained with Ponceau S, cut into individual strips and blocked in 5 % milk (in TBS buffer containing 0.1 % Tween). Individual strips were blotted using novel anti-parkin mAbs A15165A-J and I6004a'-f' at dilutions of 1:500-1:5000, corresponding to the following concentrations: A (0.11 µg/mL), B (0.18 µg/mL), C (0.24 µg/mL), D (0.76 µg/mL), E (0.49 µg/mL), F (0.77 µg/mL), G (0.40 µg/mL), H (0.37 µg/mL), I (0.85 µg/mL), J (0.81 µg/mL), a' (0.88-4.42 µg/mL), b' (0.70 µg/mL), c' (1.01-2.03 µg/mL), d' (0.56 µg/mL), e' (0.47

μg/mL) and f' (0.34-0.67 μg/mL), along with Prk8 (1: 20,000; MAB5512, Millipore) and DJ-1 (1:2000; A3853, Sigma) as positive and negative controls, respectively. All blots were developed together.

Detection of denatured and oxidized parkin antigens was tested using 50 ng of recombinant WT or 321C parkin treated with 0, 50 and 500 nM H_2O_2 for 30 min at 37°C. Samples were run on non-reducing SDS-PAGE (0 mM DTT). Membranes were cut into individual strips and blotted using novel anti-parkin mAbs A15165A-J and I6004a'-f'at dilutions of 1:500-1:5000 as above, along with Prk8 (1: 20,000; MAB5512, Millipore) as positive control. All blots were developed together.

Detection of denatured antigens in cells and tissue lysates was tested using Chinese hamster ovary (CHO) cells, human embryonic kidney (HEK-293) cells, as well as, human, mouse and rat brain lysates. CHO and CHOmP cells, stably expressing myc-tag alone or myc-tagged parkin expression vectors, respectively, were grown in Dulbecco's Modified Eagle Medium (DMEM, 11960-044, Gibco) supplemented with 1 % penicillin/streptomycin, 2 mM glutamine (Gibco), 10 μg/mL gentamicine (Gibco), 0.1 mM geneticin (Gibco) and 10 % heat-inactivated fetal bovine serum (FBS, Hyclone) at 37°C with 5 % CO_2, and seeded on 6 well culture dishes (Corning). Once cells reached 70-80 % confluency they were treated with either 10 μM CCCP, 200 or 2000 μM H_2O_2, with DMSO alone serving as vehicle control. Following incubations of 0-4 h at 37°C the cells were sequentially homogenized in Tris salt (TS) buffer (50 mM Tris, 40 mM NaCl pH 7.5) and in TS buffer containing 2% SDS (SDS buffer) as previously described.[846] Samples (30 μg total protein) from both TS and SDS buffer extracts were run on non-reducing SDS-PAGE (0 mM DTT) and blotted for parkin using A15165B (1:1000, 0.18 μg/mL), Prk8 (1:5000, 0.10 μg/mL, 808503, BioLegend Inc.) and DJ-1 (1:1000; A3853, Sigma).

HEK-293 cells were grown in Dulbecco's Modified Eagle Medium (DMEM, Sigma) supplemented with 1 % penicillin/streptomycin and heat inactivated 10 % fetal bovine serum (FBS,

Hyclone) at 37°C with 5 % CO_2 and seeded on 75 cm^2 cell culture flasks (Corning) at a density of 1-3 x 10^5 cells/mL. Once cells reached 70-80 % confluency they were transfected with FLAG-tagged parkin or empty FLAG control vectors (pcDNA3) using a 1:1 ratio of cDNA: Lipofectamine 2000 (Invitrogen) in a minimum of Opti-MEM transfection medium (Gibco). After 24 h the cells were lysed with RIPA buffer (1 % nonionic polyoxyethylene-40, 0.1 % SDS, 50 mM Tris, 150 mM NaCl, 0.5 % sodium deoxycholate, 1 mM EDTA) and run on reducing SDS-PAGE (100 mM DTT) using 15 μg total protein. PVDF membranes were cut into individual strips and blotted using anti-parkin mAbs A15165A-J and I6004a'-f' at dilutions of 1:500-1:5000 as above along with Prk8 (1: 20,000; MAB5512, Millipore) as positive control.

Brain lysates of 7-month-old WT and parkin KO mice were obtained by homogenizing hemibrains in TS buffer, as previously described,[846] and run on reducing SDS-PAGE (100 mM DTT) using 20 μg of total protein. PVDF membranes were cut into individual strips and blotted using anti-parkin mAbs A15165A-J and I6004a'-f' at the same dilutions as above along with Prk8 (1: 20,000; MAB5512, Millipore) as positive control. Blots were developed together.

Human frontal cortex lysates from control and autosomal recessive Parkinson disease (ARPD) subjects were processed as previously described[846] and 20 μg total protein was run on reducing and non-reducing (0 or 100 mM DTT) SDS-PAGE along with 0.5 ng of recombinant WT parkin. The membranes were blotted using novel anti-parkin mAbs A15165A-J at dilutions 1:50-1:5000, corresponding to the following concentrations: A (5.31 μg/mL), B (1.85 and 3.70 μg/mL), C (2.39 and 4.78 μg/mL), D (7.64 and 15.28 μg/mL), E (2.50 μg/mL), F (7.70 μg/mL), G (3.98 and 7.96 μg/mL), H (3.71 μg/mL), I (8.50 μg/mL) and J (8.13 μg/mL) along with Prk8 (0.10 μg/mL, 808503, BioLegend Inc.) as positive control. Human cortex, mouse and rat brain membrane-associated tissue lysates were also prepared in HEPES buffer (pH 7.9) by BioLegend Inc. and 20 μg of total protein was run on reducing SDS-PAGE and

blotted with anti-parkin mAbs A15165B, -D and -G at 5.0 μg/mL along with Prk109 (BioLegend Inc.)[690] at 1.0 μg/mL as positive control and mouse IgG subtype 2b at 10.0 μg/mL as negative control.

Mitochondrial Recruitment and Immunofluorescence

Human neuroblastoma cell line expressing Myc vector (M17) and stably expressing high levels of Myc-parkin (M17/P17) were grown in 6 well culture dishes (Corning) at 0.3 x 10^6 density in Opti-MEM (Gibco) containing 10% heat-inactivated FBS (Gibco), penicillin/streptomycin/neomycin (25mg/25mg/50mg, Gibco), Minimum Essential Medium (MEM) non-essential amino acids (1X, Gibco) sodium pyruvate (1mM, Sigma) and geneticin (0.1 mM, Gibco). CHO and CHOmP were grown as described above. Cells were seeded at a density of 2000 cells /well in 384-well imaging plates and treated with either 10 μM CCCP, 200 μM H_2O_2 or DMSO alone as vehicle. Following a 4 h incubation at 37°C the cells were fixed for 1 h with 3.7 % formaldehyde and nuclei counterstained with Hoeschst 33342 (2 μg/mL, ThermoFisher). Samples were washed with 0.75% glycine in PBS (1.37 M NaCl, 27 mM KCl, 100 mM Na_2HPO_4, 18 mM KH_2PO_4, pH 7.4) and incubated for 1hr at room temperature with 0.1% Triton X-100 in PBS. The samples were incubated for 1 h at room temperature in blocking solution (3 % bovine serum albumin, BSA in PBS). The following primary antibodies were diluted in blocking solution and applied to the samples for 16 h at 4°C: novel anti-parkin mAbs A15165A-J diluted to 1:200, corresponding to the following concentrations: A (2.66 μg/mL), B (0.92 μg/mL), C (1.20 μg/mL), D (3.82 μg/mL), E (1.23 μg/mL), F (3.85 μg/mL), G (1.99 μg/mL), H (1.86 μg/mL), I (4.24 μg/mL), J (4.06 μg/mL), Prk8 (1:250, 2.00 μg/mL, 808503, BioLegend Inc.) and anti-TOM20 (0.40 μg/mL, FL-145, Santa Cruz). Alexa fluor 488 and 594 conjugated goat anti-mouse IgG antibodies (Invitrogen) were diluted to 1:1000 in blocking solution and incubated on samples for 1 h at room temperature. Co-localization imaging of anti-parkin and anti-TOM20 signals was performed as

previously described[890] using Cellomics ArrayScan V^{TI} HCS Reader (Thermo Scientific) with 40 X objective.

HEK-293 cells transfected with FLAG-tag alone and FLAG-tagged parkin expression vectors were grown as described above and seeded on 24-well culture dishes (Corning) at a density of 1 x 10^5 cells/well. After 24 h the cells were washed with PBS (pH 7.4), fixed for 10 min in 4 % formaldehyde, permeabilized with 0.5 % saponin in PBS for 15 min at room temperature and blocked (2 % BSA in 0.1 % Tween 20 in PBS) for 90 min at room temperature. Primary mAbs were diluted 1:100 in blocking solution, corresponding to the following concentrations: and applied to cells for 16 h at 4°C. Following several washes (0.075 % Tween in PBS), Alexa fluor 594 -conjugated secondary antibody [goat anti-mouse IgG (H+L), Invitrogen] was diluted 1:200 and incubated on cells for 1 h at room temperature. Following repeat washes nuclei were counterstained with Hoeschst 33342 (2 µg/mL, ThermoFisher) and cells imaged using ZOE^{TM} Fluorescent Cell Imager (Bio-Rad).

Immunohistochemistry

Immunohistochemistry was performed on paraffin-embedded sections using a standard citric acid-based antigen retrieval as previously described.[689,843] [152,846] Primary antibodies were diluted in 1-5 % goat serum in PBST at the following concentrations: novel anti-parkin mAbs A15165A-J with dilutions of 1:100-1:2000: A (5.31 µg/mL), B (1.85 µg/mL), C (2.39 µg/mL), D (0.76, 1.53 and 7.64 µg/mL), E (0.12 and 4.92 µg/mL), F (7.70 µg/mL), G (0.40, 0.80 and 3.98 µg/mL), H (3.71 µg/mL), I (8.49 µg/mL), J (8.13 µg/mL), and Prk8 (1:2000, MAB5512, Millipore); and incubated on samples for 16 h at 4°C. Biotinylated secondary antibodies [goat anti-mouse IgG (H+L, BA-9200, Vector Labs), goat anti-rabbit IgG (H+L, BA-1000, Vector Labs)] were diluted to 1:225 in 1-5 % goat serum in PBST and incubated on samples for 2 h at room temperature. Signal amplification was performed using

VECTASTAIN® Elite ® ABC HRP Kit (PK-6100, Vector Labs). Development proceeded with either standard 3,3-Diaminobenzidine (DAB, 55 mM, Sigma) solution, Vina green (BRR807AH, Biocare Medical) or metal enhanced DAB (SIGMAFAST™ DAB with Metal Enhancer, D0426, Sigma). Samples were counterstained with Harris Modified Hematoxylin nuclei stain and dehydrated using increasing ethanol concentrations. Specimens were mounted with coverslips using Permount (SP15-100, Fisher Scientific).

Epitope Mapping

Microarray-based conformational epitope mapping was performed by PEPperPRINT GmbH (Heidelberg, Germany). The *PRKN* sequence (UniProt ID: O60260) was elongated by neutral GSGSGSG linkers at the C- and N-termini and translated into 7, 10 and 13 amino acid peptides containing overlaps of 6, 9 and 12 amino acids. Each peptide was cyclized by creating a thioether linkage between a C-terminal cysteine and appropriately modified N-terminus. The resulting conformational microarrays contained 1,410 different parkin peptides printed in duplicate (2,820 peptide spots) and were framed by additional HA (YPYDVPDYAG, 116 spots) control peptides. The assay plate was incubated 30 min in Rockland™ blocking buffer (MB-070, Rockland) and washed with 0.005% Tween 20 in PBS (pH 7.4). Mouse monoclonal anti-parkin antibodies A15165B, A15165D, A15165E and A15165G were diluted in incubation buffer (10 % blocking buffer in washing buffer) at a concentration of 1 µg/mL and incubated for 16 h at 4°C with shaking (140 rpm). DyLight680 conjugated goat anti-mouse IgG (H+L) secondary antibody (0.2 µg/mL) and control DyLight800 conjugated monoclonal anti-HA (12CA5, Invitrogen) primary antibody (0.5 µg/mL) were incubated for 45 min at room temperature. Images were taken using LI-COR Odyssey Imaging System (scanning offset 0.65 mm, resolution 21 µm, scanning intensities of 7/7 with red = 680 nm/green = 800 nm), converted to 16-

bit gray scale and quantified using PepSlide® Analyzer. No background subtraction was required as no signal was detected using secondary antibody alone (see **Supplementary Fig. 4.2**). Fluorescence intensities were plotted against the conformational parkin peptide sequences, with highest signals corresponding to antibody epitopes.

4.8 Acknowledgments

We wish to thank Dr A. B. West (Departments of Neurobiology and Pharmacology & Cancer Biology, Durham, NC, USA) for his gift of young human brain samples used in immunoblotting experiments. We wish to thank Dr. G. S. Shaw (University of Western Ontario) for his gift of the recombinant parkin construct. Thanks also to Dr R.Y. Tam (Health Canada, Ottawa, Ontario, Canada) for help with manuscript editing. Funding: This work was supported by the: Parkinson Research Consortium of Ottawa (J.M.T., D.N.E.K., J.J.T.); Queen Elizabeth II Graduate Scholarship Fund (J.M.T.); Government of Canada [NSERC (J.M.K.); CIHR MD/PhD Program (J.M.T., A.C.N.); CIHR Canada Research Chair Program (M.G.S.)]; Michael J. Fox Foundation for Parkinson's Research (P.T., J.J.T., M.G.S.); Uttra and Sam Bhargava Family (M.G.S.); and The Ottawa Hospital (M.G.S.).

4.9 Supplementary figures

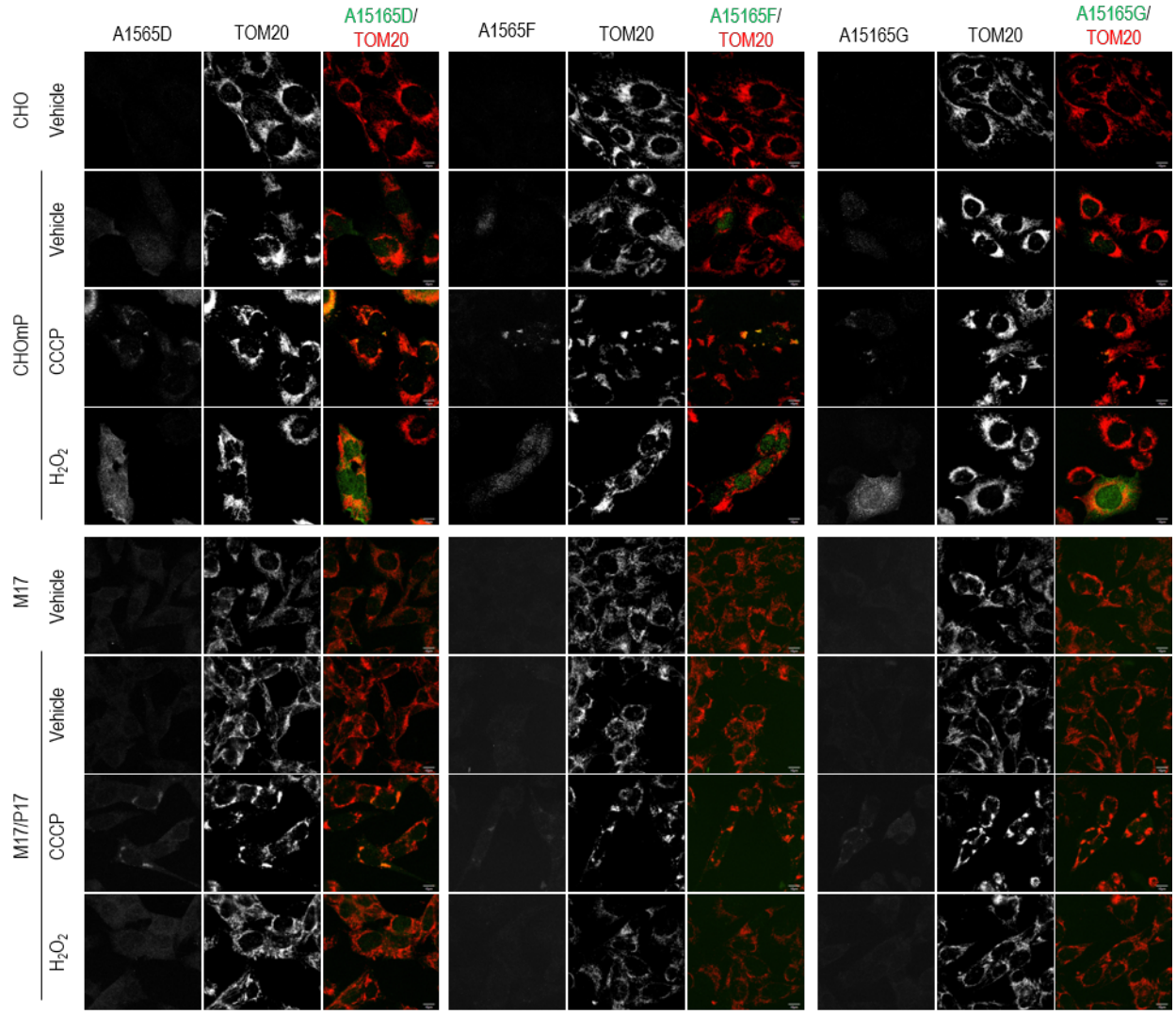

Supplementary Figure 4.1. Immunofluorescence detection of parkin *in vitro* by clones A15165D, -F and –G.
Mitochondrial recruitment of parkin immunofluorescence experiments in CHO and M17 cells using CCCP (10 µM) and H_2O_2 (200 µM) as stressors. Cells were imaged 4 hours after stressor was applied. Shown are clones A15165D, -F and -G, which also demonstrated positive signal.

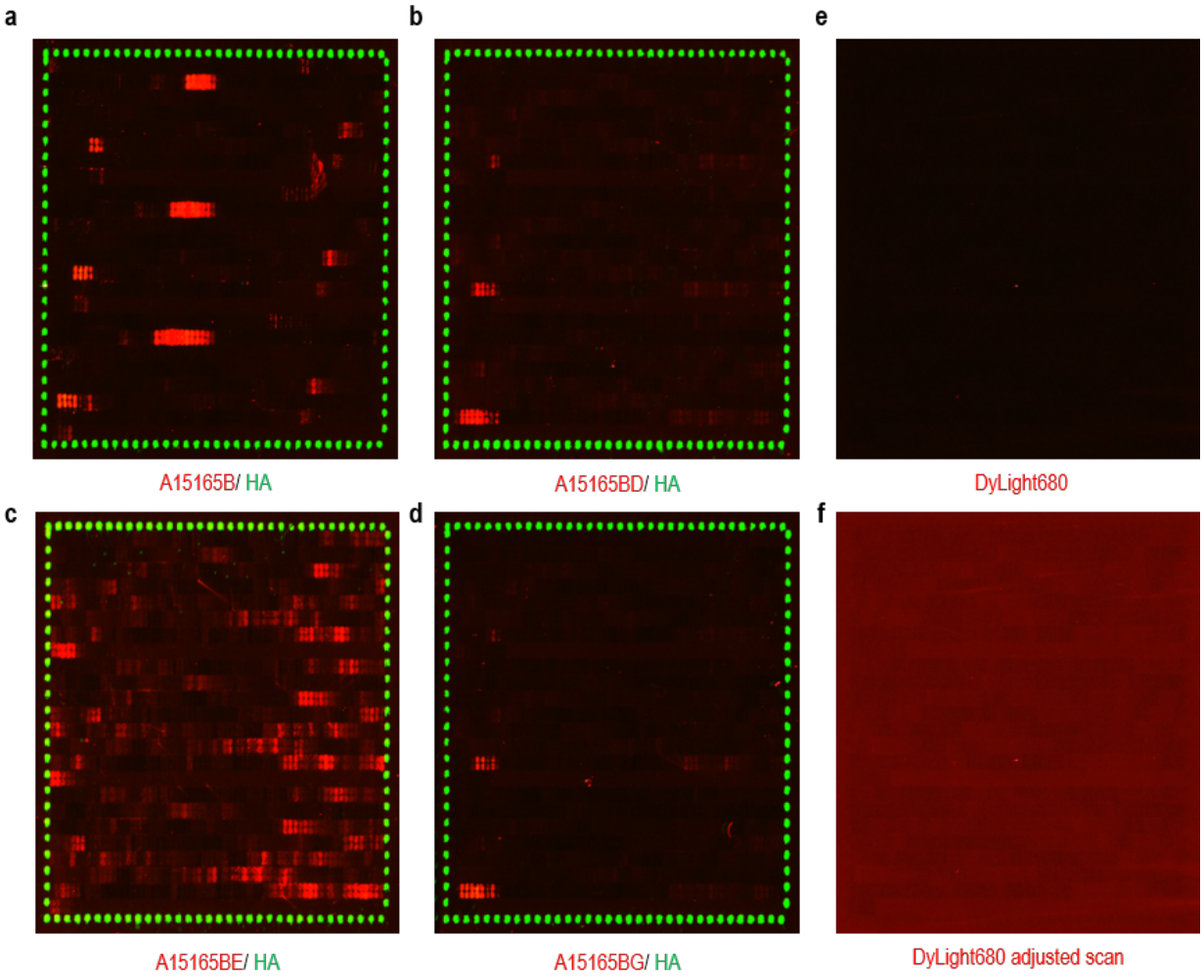

Supplementary Figure 4.2. Raw data of epitope mapping of clones A15165B, -D, -E and -G.
Raw data of epitope mapping performed on (**a-d**) mAbs A15165B, -D, -E and -G using conformational parkin peptide microarrays compared to DyLight680 conjugated secondary antibody alone using matched (**e**) vs. increased (**f**) image brightness intensity. Control peptides containing HA-tag were plated on the border of each plate and served as internal control.

Chapter 5: General discussion

5.1 Summary of principle findings

Homozygous and compound heterozygous mutations in the *PRKN* gene cause a rare, and purely genetic, form of early-onset PD (EOPD), [154,155] which has an intriguing motor-specific phenotype compared to sporadic and other genetic (autosomal-dominant) forms of PD. Its impressive (and sustained) treatment response to dopamine-replacement therapy (DRT) and its highly selective vulnerability of neurons in the *Substantia nigra* (*S. nigra)* and *Locus coeruleus* (*L. coeruleus*) suggest that dopamine (DA) neuron loss and DA processing by wild-type parkin are closely intertwined in its pathogenesis.[185,186,194-197,207] Since its gene product (parkin) has been found to possess the structure and function of an E3 (ubiquitin ligase) enzyme,[192,193,448,449] the prevailing model for *PRKN*-associated PD is linked to the accumulation of specific E3 targets, including damaged proteins and mitochondria, which cause oxidative degeneration.[192,193,459,460] Shortcomings of this model include the following: i) the lack of consensus and reproducibility regarding the *bona fide* E3 targets of parkin that accumulate in parkin-deficient brain (**Appendix Table A1**), ii) the presence of PD-associated *PRKN* mutations that retain and even increase E3 function,[105,192,440,441,445,448,449,502] iii) the presence of baseline parkin-independent mitophagy in neurons,[569,575,576] with non-physiological conditions required to induce parkin-dependent mitophagy in cell culture models, and iv) the unclear link between loss of E3 function and cell-specific neurodegeneration of the *S. nigra* and *L. coeruleus*. In addition to causing PD, parkin loss affects other high-energy demanding cell types, e.g. heart[800] and skeletal muscle[829], and is involved in several other pathways including: the regulation of glycolysis, the activation of the innate immune system and the prevention of tumorigenesis. [649-651,668,669] Therefore, a major aim of this study has been to develop a model for parkin function that unifies its various cellular roles. Review of its protein structure revealed a high number of oxidation-sensitive cysteines (**Table 1.2**), which were previously found involved in the

formation of oxidation- and dopamine stress- mediated insoluble species. Currently, these insoluble species are believed to contain E3-inactive parkin and accumulate naturally with advanced aging.[192,362,486-488,493,502,690] However, it became intriguing to envision that evolution, which had produced a human protein with such a high number of oxidation-sensitive cysteines, may have also endowed it with a function that involves regulating redox chemistry. Therefore, the framework of this thesis was based on answering five main questions about parkin redox chemistry and its effect on the regulation of redox state in neural tissues.

The **first** question posed was how sensitive parkin was to oxidation-induced insolubility compared to other cysteine-rich proteins, mitochondrial-associated proteins, and PD-associated proteins. Strikingly, as shown in Chapter 2, of the proteins analyzed, only parkin demonstrated an age-associated loss in solubility, which appeared to accumulate in a fraction associated with the microtubule-associated protein 1A/1B-light chain 3 (LC3) B subtype. As LC3 is an important structural component of autophagosomes, its co-distribution with parkin supports a role for parkin in autophagy.[350,574] Although analysis of PINK1 is lacking, it was interesting to note that the mitochondria-associated proteins, *i.e*. MnSOD and VDAC (the latter being a putative E3 target of parkin), did not also co-distribute with parkin in an age-dependent manner, as would be expected during mitophagy upregulation.[350,353] Another striking observation in specimens derived from neurologically healthy adult brains was that complete loss of Tris saline-soluble with subsequent increase in SDS-soluble parkin occurred at an earlier age than previously reported, which also intriguingly coincides with the age of onset of most parkin-associated PD patients (21-40 years of age).[194] This suggests, that contrary to previous interpretations, SDS-soluble parkin potentially holds a physiologically relevant role, which has greater importance with aging. Otherwise,

one would reason that all middle-aged individuals with predominantly insoluble parkin would develop PD.

While analyzing structural changes in parkin under pro-oxidant conditions, it was determined that parkin oxidation occurs via two main mechanisms: one, being the formation of reversible high molecular weight (HMW) species, and, two, the formation of irreversible SDS-soluble species; each potentially possessing a distinct function.

The formation of reversible HMW species occurred in both the Tris saline- and SDS-soluble fractions of young and aged human brain, and did not represent lysine-conjugated polyubiquitin chains, as these latter covalent modifications would not be reversed under reducing conditions.[459] These large shifts in molecular weight could rather represent intermolecular disulfide bond formation between several parkin proteins or between parkin and other cysteine-containing binding partners of unknown identity. It is important to note that the identity of proteins present in these parkin-positive HMW species could only be revealed in experiments run under controlled redox conditions, which is not common practice in parkin research.[460]

The formation of SDS-soluble parkin species also occurred in both young and aged human brain, and likely represent various oxidation and aggregation states of parkin, as modeled using SDS-PAGE, circular dichroism and dynamic light scattering (Chapter 2). The composition of native parkin aggregates, however, is yet-to-be determined as these may represent homogeneous mixtures of parkin alone or heterogeneous mixtures of parkin with other proteins. Its co-distribution with LC3B and localization within lysosomal-associated membrane protein 3 (LAMP3)-positive vesicles (Chapters 2) suggests that SDS-soluble parkin species likely represent parkin proteins accumulated in lysosomes that are destined for sequestration or degradation.[79,81,82] However, further investigations are required to determine how parkin came to accumulate within lysosomes; possibly via direct macroautophagy of

auto-ubiquitinated parkin-protein aggregates or during the autophagosome-engulfment of ubiquitinated protein-aggregates and mitochondria that are also bound to parkin.[274]

In addition, parkin-oxidation may also promote the formation of intramolecular disulfide bonds (Chapter 2). As shown in **Supplementary Fig. 2.5n**, when recombinant parkin protein was subjected to oxidizing SDS-PAGE, it formed HMW species as expected but a portion also appeared more compact in globular size, which disappeared upon treatment with dithiothreitol. The identity of these potential cysteine-disulfide amino acid residue binding partners remains to-be-determined but appeared retained in the PD-associated point mutations C431F and G328E (of which the latter is adjacent to cysteine residue C332). Interestingly, the formation of HMW species, post oxidation, was more prominent than wild type in the C431F mutant (also see **Appendix Fig. C12f** for immunoblot). This result indicates that C431 is not involved in cysteine-based HMW species formation. However, the introduction of phenylalanine could potentially unfold the parkin structure through hydrophobic interactions or steric hinderance. This could result in exposure of cysteines involved in HMW species formation. Conversely, introduction of the G328E glutamic acid mutation caused less HMW species than wild type. It is possible that the glutamic acid residue is acting as a zinc-coordinating ligand and disrupting structural integrity, possibly leading to premature oxidation of cysteine residues that are normally involved in HMW species formation.[891-893]

Analysis of parkin immunoprecipitated from both the Tris saline- and SDS- soluble fractions of human and mouse brain (Chapter 2) revealed intriguing parkin cysteine-oxidation events - notably, the irreversible oxidation of C95 and C253 (or equivalent murine amino acid, C252). The physiologically-occurring oxidation of C95 is an intriguing discovery that beckons further query as this residue is primate-specific and located within the poorly studied linker region of parkin, which only recently was found to include an E3 activating element, ACT.[450,452] Despite not being identified as a PD-associated

PRKN mutation, sulfhydration at C95 has also been linked to activation of parkin E3 activity in cells[499], and as mentioned in Chapter 1, only humans and other primates to a lesser degree, develop spontaneous age-associated loss of *S. nigra* neurons.[43]

It was surprising that C253, a zinc-coordinating cysteine residue predicted to be important for structural integrity,[192,193,448,449] was found oxidized in samples that were not treated with oxidizing agents (**Fig. 2.4**), and was one of the first cysteines found oxidized in human recombinant parkin treated with mild oxidizing conditions (**Supplementary Table 2.2**). It was also surprising to find that nearly all cysteines in recombinant parkin underwent oxidation and alkylation despite several structural studies predicting that the majority of parkin-cysteines serve as ligands for zinc coordination.[192,193,448,449,894] A similar observation is noted in other zinc finger protein structures, where zinc-cysteine coordination sites are often misinterpreted as static in nature, given their role in maintaining protein tertiary structure and generally high zinc-binding affinity.[894-896] However, local molecular environment factors, such as zinc concentration, the presence of other zinc-bound ligands, solvent pH, and most importantly, the acidity of the cysteinyl thiol (see **Fig. 5.1**) can affect zinc-sulfur coordination strength, or susceptibility to oxidation and alkylation.[892,894,897-899] In addition to the published data in Chapter 2, as shown in **Appendix Fig. C13**, C253 was also found in a reversibly oxidized state in the SDS-soluble extract of an older human frontal cortex specimen. As HMW species are likely formed via reversible disulfide bridging, C253 may represent a potential site through which parkin natively forms HMW species.

Although the use of thiol-specific labeling techniques with LC-MS/MS confirmed the presence of many physiologically-occurring irreversible oxidation sites, some of which were previously reported in literature, it was surprising to find so few reversibly oxidized parkin cysteines; especially since SDS-PAGE indicated the presence of reversibly oxidized residues. This may have been caused by several factors. It is known that initial cysteine oxidation generates a reversible oxidation product, sulfenic acid,

which is susceptible to subsequent attacks by thiols, nitrogen nucleophiles, and/or hyperoxidation to form disulfides, sulfenamides or sulfonic acid, respectively (see **Supplementary Fig. 2.4c**, Chapter 2).[900] Since there are limits on the complete prevention of thiol-oxidation during sample preparation, this may have falsely increased the level of irreversibly oxidized cysteines. Also, sulfenic acids are reported to react with thiol-labeling agents such as iodoacetamide (IAA).[901] This may have led to the erroneous identification of sulfenic acids as unmodified thiol residues, although, its impact may have been minimal as the complete reduction of sulfenic acid-IAA conjugates to thiols nears ~90% with the use of dithiothreitol as reducing agent.[901] Nevertheless, the collective biochemical results from human and murine brain have delineated -for the first time- a comprehensive inventory of physiological oxidation events that affect parkin in normal brain, which informed subsequent investigations.

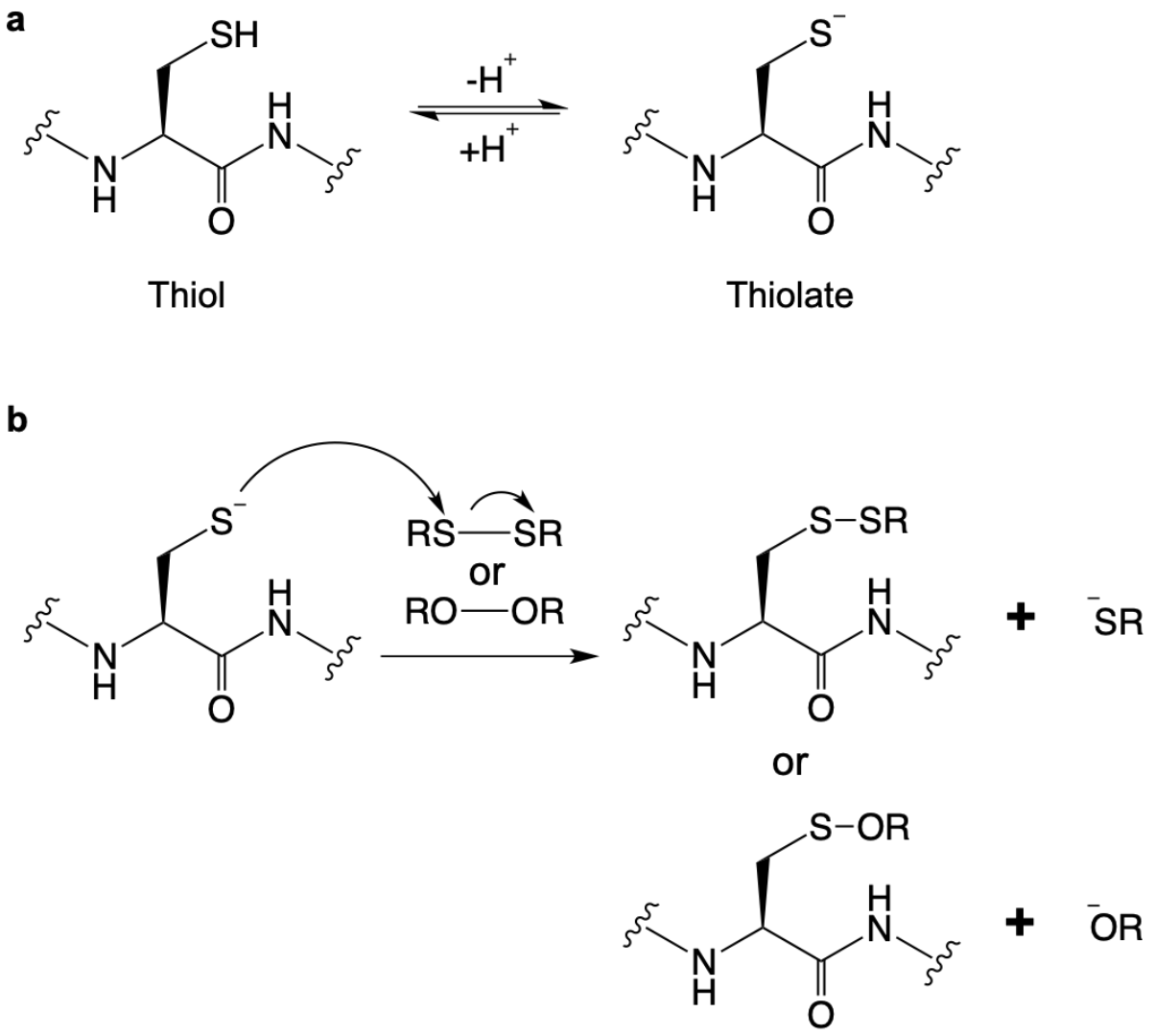

Figure 5.1. Thiol acidity and nucleophilicity.
(**a**) Thiol deprotonation is dependent on environmental factors such as solvent polarity, pH and hydrogen bonding with adjacent basic amino acids, which stabilize the resulting thiolate, **a**. Negatively charged sulfur atoms on thiolates act as nucleophilic centers. (**b**) Shown are two examples of biologically relevant nucleophilic reactions occurring between thiolates and disulfides (RS-SR) or peroxides (RO-OR).

The **second** question posed was whether parkin could benefit its environment by acting as an antioxidant or reactive oxygen species (ROS) scavenger. As shown, in multiple experimental models, including human cell lines and murine models treated with endogenous and exogenous oxidative stress (see Chapters 2 and 3), the oxidation state of parkin was found to be inversely proportional to the oxidation state of its environment. Higher oxidation state corresponded with the following: an increase in the number of parkin-cysteine oxidative modifications, an increase in parkin-aggregate formation, and a decrease in intracellular ROS. By approximation, the ratio of measured H_2O_2 to parkin concentrations in this tissue was between 0.4-6.0 mM H_2O_2 per 1 ng of parkin. Intriguingly, these values were above the minimal ratio required to induce insolubility of recombinant parkin protein (0.25 mM H_2O_2 per 1 ng of parkin, see lane 3 in **Fig. 2.3c**, Chapter 2). Along with the observation that parkin mRNA expression level remained unchanged in human cortical and nigral specimens of various ages, these observations demonstrate that intracellular concentrations of ROS affect the distribution of parkin within the soluble (Tris-saline) and insoluble (SDS) fractions of cells and tissues.

Although the transient nature of H_2O_2 renders its exact measurement difficult[902], other more stable markers of oxidative stress, protein nitrotyrosination and carbonylation[903] were also elevated in the absence of parkin (Chapter 3), and while there are limits to the complete control of oxidation in brain tissue post-mortem, the data presented in Chapter 2 do not indicate a positive correlation between post-mortem interval and H_2O_2 concentrations. Therefore, despite these limitations, the overall conclusion that parkin is involved in mitigating oxidative stress still holds and, as presented in Chapter 2, may be linked to its antioxidant potential.

Compared to other known antioxidants, RING-containing structures, catalase and glutathione, parkin appeared to function similarly to glutathione, with an approximate 25-fold increase in effectiveness when compared stoichiometrically (15 μM parkin vs. 400 μM glutathione, see

Supplementary Fig. 2.5g, Chapter 2). While the sensitive to apoptosis gene (SAG) protein provides the ideal comparison for parkin, as it contains the highest percentage of cysteine residues (**Table 1.3**) and functions both as an E3 enzyme and antioxidant,[739] attempts at its synthesis were unsuccessful. As shown in **Appendix Fig. C6**, cloning the DNA sequence (*RNF7*) of SAG into the pET-SUMO expression vector was successful, however, protein isolation from bacteria occurred in low yields, and analysis of its protein mass by electron-spray ionization-MS did not match its predicted size (11261.5 vs. 12953.7 Da). It is possible that its high cysteine content rendered it susceptible to the formation of insoluble inclusion bodies. Attempts at improving its isolation by replacing the *E.coli* stain B21 for Rosetta, which is designed to reduce the formation of inclusion bodies caused by the presence of rarely expressed eukaryotic codons[904-906], were also unsuccessful.

The ROS-lowering effect of parkin was also confirmed to depend on its total number of reactive thiols, with both PD-linked point mutations (C431F and G328E) causing a reduction in the total number of reactive thiols. As mentioned above, the addition of phenylalanine could lead to steric hindrance that destabilizes zinc-cysteine coordination within a surrounding RING domain and leads to increased thiol exposure and premature thiol oxidation. [892,894,897-899] In addition, zinc ions in RING zinc fingers are sometimes found in nature coordinated to aspartic acid or glutamic acid instead of cysteine.[891,893] With G328E being only four amino acids away from the zinc-coordinating C332, it may disrupt this coordination site and cause premature oxidation of C332 and the six other cysteines located within the IBR RING-domain, lowering the total number of available thiols from 35 to just 28 (thiol reactivity measured for G328E was 26.7, see **Fig. 1.11 and 2.5f**, Chapters 1 and 2). As analysis of PD-associated *PRKN* mutations will help to validate its potential as an antioxidant, other mutants were also produced (C289G and W453X, see **Appendix Fig. C14**). Unfortunately, their isolation was unsuccessful to date,

and akin to C95A (as described in Chapter 2), isolation of C289G may improve with the presence of the histidine-SUMO tag.

While the above findings support a role for parkin as an antioxidant, its biological relevance also requires further validation. Changes in cellular oxidation state can arise by a myriad of pathways including proteasomal and mitochondrial dysfunction[268,907]. Therefore, validation of a potential antioxidant requires determining its true intracellular concentration, calculating its ROS-reducing rate or redox constant and comparing its location within the cell to other known antioxidants to determine the likelihood that this potential antioxidant is interacting with oxidants at a sufficient rate and concentration compared to other intracellular antioxidants.[692,693] For example, catalase is considered highly specific to H_2O_2, as it holds one of the highest rate constants for reducing H_2O_2 and is able to efficiently degrade this oxidant while residing in ROS-producing peroxisomes.[732,908] In contrast, glutathione holds a low rate constant for reducing H_2O_2 but resides in very high concentrations (1-10 mM range[909]) within the cytosol and, in part, helps to scavenge ROS and other reactive species by action of the enzymes glutathione-*S*-peroxidase (Gpx) and glutathione-*S*-transferase (GST).[730,907] Because parkin has a similar distribution and antioxidant profile as glutathione, it therefore potentially has a similar ROS scavenging role. However, further investigations are required to determine the true cellular beneficiaries of parkin oxidation.

The **third** question posed was whether parkin had a direct role in modulating dopamine metabolism or neuromelanin (NM) pigment formation. As discussed in Chapter 1, dopamine metabolite dysregulation and is observed in *prkn*$^{-/-}$ mice,[432,433,438,439] and specific loss of NM-containing cells is found in *PRKN*-associated PD[53,195-197,207] Although thiol-containing antioxidants, like glutathione, are relatively slow in their ability to reduce ROS directly, their electron-rich thiols also conjugate reactive electrophilic

species, or RES. [83,360,910] These toxic molecules are derived from either catabolic degradation of various endogenous metabolites, e.g., dopamine, or from introduction of xenobiotics, such as MPP^+, and they cause significant damage to biomolecules via electron abstraction and/or direct conjugation.[83,360] Both glutathione and parkin are known to conjugate dopamine metabolites *in vivo*, with the former occurring via GST activity and found to decrease the rate of dopamine-associated melanin (DAM) formation[322], which accumulates as pheomelanin within NM (see **Fig. 1.6**, Chapter 1).[83,360,362,910]

As parkin performed similarly to glutathione in antioxidant assays *in vitro*, the related hypothesis was that parkin would also decrease the rate of melanin polymerization *in vitro*. Strikingly, however, the opposite was observed, with parkin enhancing DAM formation compared to control proteins, and due to the presence of the primate-specific cysteine, C95. In additional data (see **Appendix Fig. C12g**), parkin increased DAM formation at a higher rate than α-synuclein. Since α-synuclein is highly prone to aggregate formation, it is possible that DA-bound α-synuclein aggregates are reciprocally enhancing DAM polymerization.[284] While α-synuclein did demonstrate antioxidant-like activity in the chemiluminescence assay (**Appendix Fig. C12a,d**), it was not via cysteine-mediated activity since treatment with iodoacetamide did not reverse this effect and the Ellman's assay confirmed the absence of any reactive thiols within its cysteine-less protein structure (**Appendix Fig. C12b,c,e**). According to a previous report, α-synuclein is found to form complexes with the peroxidase-active protein, cytochrome *c*.[911] It is plausible that the α-synuclein-mediated reduction of ROS, as measured using the chemiluminescence assay, may rather have been due to its complexation to horseradish peroxidase. Having a similar DAM-enhancing profile as α-synuclein, it is therefore possible that parkin aggregation is enhancing DAM formation and may represent an important role for insoluble parkin, namely to facilitate sequestration of toxic RES. As seen in Chapter 2 (**Fig. 2.8**), parkin colocalized with NM pigment, which accumulates in lysosomal storage vesicles with progression in age and is formed, in part,

via dopamine-derived RES.[83,360] Parkin aggregation also occurred with exposure to PD-associated and mitophagy-inducing toxins, such as MPP^+, rotenone and CCCP. In Chapter 2, brain lysates of wildtype mice exposed to intraperitoneal injection of MPTP (MPP^+ precursor) saw an increase in insoluble parkin species (**Fig. 2.2f-g**, Chapter 2). Also seen in **Supplementary Fig. 2.6a-b** and **Fig. 4.3c** (Chapters 2 and 4), cells stably overexpressing parkin that were exposed to excess dopamine or CCCP (at a concentration used to induce mitophagy) caused the formation of insoluble parkin, and, shown in **Appendix Fig. C15**, recombinant human parkin became increasingly insoluble when incubated directly with increasing concentrations of aminochrome, MPP^+, rotenone and CCCP. As these toxins demonstrate electrophilic properties[726,912-914]. The effect of these toxins on parkin aggregation state may be linked to their potential to either directly conjugate parkin thiols or change the oxidation state of their environment. However, while the exact mechanism by which these compounds induce parkin-aggregation remains to be determined, these preliminary data (**Fig. 2.2f-g, Supplementary Fig. 2.6a-b**, **Fig. 4.3c** and **Appendix Fig. C15**) highlight the need to interpret cell culture-based experiments using these toxins with caution, as these molecules hold the potential to alter oxidation state and possibly conjugate other thiol-containing proteins. Should it be determined that parkin directly conjugates RES derived from sources other than dopamine auto-oxidation, an intriguing question that emerges is whether RES-conjugation to parkin, preferentially at residue C95, represents an important activation site that is relatively unique to primate brain. Also, as parkin is known to act as its own E3 target[500,568], along with the fact that ubiquitination also signals lysosomal degradation pathways[562,563], the question arises whether RES-modified parkin could represent a specific trigger for either proteasomal degradation or non-degradative lysosomal sequestration to ensue. In summary, oxidative PTMs at C95 within the context of mammalian parkin processing may be of similar (or even greater) importance to its

cytoprotective functions as was the discovery of its phosphorylation at S65 during the induction of mitophagy.

The **fourth** question posed was if parkin cysteines could directly alter glutathione redox state. The role of glutathione in the cell is to regulate cellular redox state, which is accomplished by several mechanisms, including: i) recycling of antioxidants such as thioredoxin, vitamins C and E, and itself, via glutathione reductase (GR); ii) scavenging ROS, RNS and RES with aid from GPx and GST activation; and iii) altering the activity of proteins by causing reversible S-glutathionylation of their cysteines (PSSG) via GR.[692,693,696,730,907,915] The redox status of a cell is often described in terms of the ratio between the reduced state of glutathione (GSH) over the oxidized state (or disulfide form) of glutathione (GSSG), with ratios exceeding 100:1 occurring in normal conditions and decreasing to 10:1, or even as low as 1:1, under stress conditions.[907] However, redox state is also governed by the thiol oxidation state of cysteine-containing proteins within the cell.[694,873,916] Curiously, across several cellular, murine and human experimental models and tissues (Chapter 3), expression of both physiological and excess levels of parkin correlated with a reduction in [GSH] and the [GSH]:[GSSG] ratio, and an increase in GR activity.

It did appear, however, that these parkin-dependent changes were cell-specific. As shown in **Fig. 3.5** and **3.6d,g**, human and mouse neuronal tissue, Chinese hamster ovary cells (CHO) and human neuroblastoma cells (SH-SY5Y) all demonstrated a decrease in GSH with increased parkin expression. However, the relative decrease in GSH levels measured between low (or absent) expression of parkin vs. increased expression of parkin varied between ~1.6 and 3.5, with the lowest shift observed in SH-SY5Y cells and the highest in mouse brain lysates (as measured by the Tietze GR recycling assay, **Fig 3.6d**. Also, as shown in **Appendix Fig. C16a-e**, the measurement of glutathione in human embryonic kidney

cells (HEK-293, using the Tietze GR recycling assay) revealed no significant differences in glutathione redox state between low vs. high expression of parkin. While these observed differences may indicate veritable cell-specific variations, they may also be the result of genomic changes that occurred either due to the effects of transient and stable vector transfections or as a result of tumorigenic transformation in the CHO, SH-SY5Y and HEK-293 cell lines.[917] As reviewed by Stepanenko and Heng, common transfection methods, including the DNA vector, the transfection agent, the use of antibiotic resistance or reporter transgenes, the selection antibiotic, as well as, the culture conditions can cause significant genomic, transcriptomic and phenotypic changes in tumorigenic cell lines.[917] Therefore, while the use of the stably-transfected CHO cells eliminated issues related to inconsistent transcriptome expression (as seen with HEK-293 and SH-SY5Y cells, **Appendix Fig. C11** and **C17**) and structural changes caused by the acute stress associated with transient transfections (as seen in differences observed in flow cytometry plots of untransfected vs. vector control transfected HEK-293, **Appendix Fig. C18a-d**), the persistent use of selection antibiotic may have also contributed to genomic, transcriptomic and/or phenotypic changes that led to altered glutathione state regulation in CHO cells.

In contrast to findings that demonstrated that parkin expression reduces biochemical signs of oxidative stress (see Chapter 3 and [432,435,437,846]), it was peculiar to find that its expression also caused a decrease in the [GSH]:[GSSG] ratio, since this would indicate a rise in oxidative stress.[907] Again, this may be due to inadvertent GSH oxidation during processing.[695,918,919] Importantly, and as supported by the observation that the total pool of glutathione was unchanged (see **Fig. 3.5b,h** and **3.6h**), it may be possible that the overall cellular redox state, i.e. combined glutathione and protein-cysteine redox states, was altered, given the connection that exists between protein-cysteine and glutathione redox states.[694,873,916] Therefore, this data may rather indicate that parkin thiols contribute, in part, to maintaining the overall cellular redox state, with higher thiol equivalents required, in the form of recycled GSH, when

parkin is absent. Such a theory may explain why several redox sensitive proteins were found structurally altered in *prkn*$^{-/-}$ murine brain[435,437] (some of which were recently found to undergo S-glutathionylation,[920] see **Appendix Table A2**), and also invites further investigation into whether parkin helps to directly recycle GSSG or glutathionylated proteins (PSSG). Some preliminary evidence of a role for parkin in direct modulation of glutathione redox state was presented in Chapter 3. As shown in **Fig. 3.7**, direct incubation of recombinant human parkin with oxidized GSSG induced S-glutathionylation at three sites (i.e. C59, C95 and C377). However, in **Fig. 3.7e**, while measuring the direct recycling of GSSG to GSH in the presence of parkin, it was determined that one mole of parkin was able to convert 5 equivalents of GSSG back to GSH. This indicates that there are two unidentified S-glutathionylation sites residing in the parkin protein, warranting further investigation. Also, parkin alone appeared to react with one molar equivalent of the monochlorobimane (mcB) probe, which was used to measure the levels of recycled GSH (**Fig. 3.7e**). With mcB functioning as an electrophile in the GSH-measuring assay (see **Appendix Fig. C16f**),[921] its interaction with parkin supports the hypothesis that parkin has the potential to react with non-dopaminergic RES. Furthermore, additional data in **Appendix Fig. C19** provides initial *in vitro* evidence of parkin S-glutathionylation. Both HEK-293 and SH-SY5Y cells lines were incubated with biotin-tagged GSSG[922,923] and the resulting glutathionylated proteins were retrieved using streptavidin-conjugated agarose and separated on SDS-PAGE. Endogenous and ectopically expressed parkin were precipitated from cells under both normal and oxidative stress conditions. Whether direct S-glutathionylation of parkin (PkSSG) is responsible for causing glutathione redox-state changes will still need further investigation; however, it does open the field to new questions about the structure and function of parkin, including whether parkin S-glutathionylation, notably at residue C95, alters E3 activity. Nevertheless, the exploration of oxidative

PTMs occurring on parkin uncovered its contribution to the maintenance of cellular redox equilibrium in a close feedback loop with glutathione redox state.

The **final** question posed was whether oxidized and aggregated parkin could be visualized *in situ*. The presumption that E3-active parkin predominantly resides in the cytosol is based on data derived mostly from cellular models and mouse tissue. As discussed above, and shown in Chapter 2, parkin predominantly resides in an insoluble compartment of the human brain (but not of the spinal cord or skeletal muscle) starting at age 40 years, which likely represents an important secondary role for parkin, possibly associated with its redox-sensitivity. Therefore, a series of human recombinant parkin proteins were selected as antigens for the production of novel monoclonal antibodies (Chapter 4). This set included both a full-length and a truncated form of parkin (aa 321-465), which included the amino acid sequence recognized by the commercial antibody Prk8, aa 399-465.[690] Several samples were also treated with H_2O_2 (10 mM) or oxidized dopamine (aminochrome, 200 μM) to induce the formation of HMW species and oxidation-induced aggregates. Although it was initially surprising that the oxidized and dopamine-modified antigens failed to produce strong antibody titres, in retrospect, this is likely due to the fact that the levels of oxidative and dopamine stress applied to the parkin antigens caused a significant loss in solubility, thus reducing their immunogenicity. Unfortunately, this was only realized once monoclonal clone production and their comprehensive characterization had begun.

Despite this shortcoming, most of the antibodies derived from untreated, full-length parkin antigens (A15165A-J series) had observable reactivity towards oxidized forms of parkin, with clone A15165B retaining higher affinity than Prk8 in CHO cells. This may be due to partial oxidation of the untreated parkin antigens during freeze-thaw cycles prior to inoculation, or during antigen presentation *in vivo*, and may indicate that these antibodies recognize a partially oxidized form of parkin. This may

also help explain the species-specificity of the antibodies produced, as the amino acid sequences of the majority of their epitopes do not differ between species. Native oxidation of parkin, as seen in Chapter 2, occurs more readily in human brain tissue than in mouse tissue. Akin to the oxidation-induced activation of parkin E3, such PTMs likely result in partial protein unfolding and expose regions hidden within the inactive state. For example, clones A15165D and -G recognize an epitope located in the repressor element of parkin (REP), which requires displacement to allow access to the E2 binding site in RING1 (see **Fig 1.13**).[448,449,452] It is possible that parkin oxidation causes REP displacement and exposes select residues that were recognized during inoculation. Furthermore, the epitope of clone A15165E was determined to be conformational, as it could not recognize denatured protein and contained residues located in both the RING0 and RING2 regions, which only interact when parkin adopts an E3-inactive state (see **Fig. 1.13**).[448,452] Conformational changes post-oxidation alter antigen exposure. However, it remains to be determined what PTM(s), if any, cause(s) the conformer identified by clone A15165E and will have to be addressed in future investigations. In addition the species-specificity of clone A15165B may also be explained by its epitope location (aa 89-93), which could involve, or be influenced by, the oxidation-state of residue C95. Although further work is currently ongoing, the strong detection of oxidized parkin by clone A15165B in cells treated with CCCP and H_2O_2 (**Fig. 4.3b**) suggests that its epitope recognizes an oxidized form of parkin, which likely involves oxidation of C95.

The major, and surprising, outcome of our novel, monoclonal parkin antibody work was the protein-specific labeling observed in human brain. Not only was it detectable in human *S. nigra* using IHC technique, it was found associated with NM pigment, which cannot be degraded in human brain (Chapter 2). The vesicular-granular staining pattern of parkin that colocalized within lysosomal storage vesicles in neurons also correlates with its co-extraction with LC3B in the SDS-soluble human cortical extracts (Chapter 2), and, possibly represents the insoluble form of parkin first identified by Pawlyk et al

2003.[690] The question now is whether this represents aggregated parkin formed as a by-product during ROS/RES scavenging, or whether parkin is actively serving a different role within non-degradative, LAMP3-positive lysosomes?

5.2 Model for the function of parkin

The data presented in this thesis indicate the presence of a direct relationship between parkin and cellular redox states. Although more research is required to decipher the mechanism(s) governing this relationship, the proposed model for parkin function, as will be further discussed, is two-fold: i) When exposed to lower concentrations of ROS/RNS/RES/GSSG, parkin locates predominantly in the cytosol and functions as a redox-selective E3 ligase; and ii) when exposed to higher concentrations of ROS/RNS/RES, parkin acts to sequester to neutralize these damaging species. It was previously determined that parkin-oxidation had a biphasic effect on parkin E3 activity. Cells exposed to 200 μM H_2O_2 saw an increase in parkin E3 activity at 2 hours post exposure that later decreased at 6 hours, and was accompanied by the accumulation of parkin-positive aggregates.[487] Given that increased oxidation state correlates with increased parkin aggregation, it was largely assumed that SDS-soluble parkin aggregates do not retain E3 activity.[460,486-492,502,690] Although our analyses of recombinant and immunoprecipitated human parkin confirmed that SDS-soluble parkin possesses higher cysteine-oxidation states than Tris saline-soluble parkin, the presence of reversible HMW species and the identification of reversibly-oxidized C253 in SDS-soluble cortical extracts suggest that native parkin aggregates are only partially oxidized. In addition, data presented in **Appendix Fig. C20** (performed by Daniel El-Kodsi) demonstrate that parkin self-ubiquitination is activated when exposed to a concentration of H_2O_2 that induces insolubility (~2-200 μM H_2O_2 per 1 μM parkin, see lane 3 and 4 in **Appendix Fig. C20** of the ubiquitination experiment vs. ~125- 250 μM H_2O_2 per 1 μM parkin, lane 3

and 4 in **Fig. 2.3c** of the insolubility experiment). It is therefore plausible that some parkin aggregates represent a form of E3-activated parkin. This is supported by the observation that parkin aggregates associate with lysosomal proteins, which may represent the lysosomal degradation of parkin-bound ubiquitinated targets. Therefore, further characterization of *in situ* SDS-soluble parkin aggregates is warranted as this may help identify *bona fide* parkin E3 targets.

Given the lack of consensus regarding the identity of parkin E3 targets, an attractive theory is that parkin self-ubiquitination represents the major mechanism by which parkin co-regulates cellular redox state.[568] Controlling its own expression within the cell could lead to alterations in glutathione redox state, which may explain the alterations observed in the expression and activity of numerous redox-sensitive proteins in the absence of parkin. However, how parkin selectively self-identifies modified species *in vivo* is still unclear,[568] although one could envision that select PTMs could either serve as E3-activators or as targets for degradation. With the presently accepted activators of parkin E3 activity being the PINK1-mediated phosphorylation of serine residue 65 in the UbL parkin domain (pUbL) and the binding of RING1 parkin domain to phosphorylated ubiquitin (pUb),[352,454,481-483] it was surprising that S65 ubiquitination was not found in immunoprecipitated parkin from both human and mouse brain lysates; rather, serine 77 was found to be phosphorylated in mice brain lysates in this presented work. As nascent parkin is predominantly cytosolic and has numerous, soluble proteins as putative E3 targets (as deduced from cell culture-based experiments), it may indicate that other PTMs cause cytosolic parkin E3 activation. However, due to the transient nature of phosphorylation, the lack of evidence does not exclude their potential presence *in situ*. Regardless, oxidized C253 and C95 were recurrently found in human and mouse brain lysates. These residues are located within the RING1 domain, and adjacent to the ACT region within the linker domain, respectively. As discussed in Chapter 1, these regions are now recognized as important E3-activating sites, which promote protein

unfolding.[352,448,450,452,483] While sulfonation of C253 was previously found in aggregated and oxidized GST-tagged recombinant parkin, its effect on E3 ligase activity was assumed by inference, as cells treated with similar oxidizing conditions had an increase in cysteine-sulfonation, accompanied with a loss in parkin self-ubiquitination. Given that C253 oxidation occurred in recombinant parkin at a H_2O_2 concentration that induces E3 activation (2 μM H_2O_2, per 1 μM parkin see **Supplementary Table 2.2**), it may rather represent an E3-activating PTM. Akin to pUb binding to RING1,[352,448,452,483] addition of a negatively charged sulfonic acid at C253 likely induces protein unfolding. Alternatively, a sulfenic acid present on C253 may form intramolecular or intermolecular disulfide bonds with other parkin molecules or cysteine-containing proteins, which also create unfolding of the RING1 domain.

Both the conjugation of C95 to dopamine and the association of parkin with NM in lysosomal storage vesicles may indicate that C95 oxidation and DA-conjugation activates E3 activity. This is supported by the finding that C95 sulfhydration causes parkin E3 activation.[499] While a previous study determined that DA-conjugated parkin loses E3 activity, dopamine was used in large excess and likely caused rapid parkin aggregation and may not truly represent *in vivo* concentrations since dopamine is largely contained within VMAT-2-positive vesicles.[78,86,362] Therefore, low levels of cytosolic dopamine may conjugate parkin C95 and lead to its selective self-ubiquitination, aggregate-induced autophagy or sequestration.[487] Similarly, S-glutathionylation of C95 may also alter E3 activity. High concentrations of GSSG could lead to parkin S-glutathionylation,[907,915] which in turn could cause direct recycling of GSSG to GSH or lead to parkin E3-mediated degradation. Alternatively, other S-glutathionylated proteins may form disulfide bridging with parkin cysteines, which could potentially lead to the regeneration of GSH and the degradation of parkin-bound proteins. While the exact role of these newly discovered parkin PTMs remain to-be-determined, it is surprising that mutations in C95 have not been linked to *PRKN*-associated PD. As parkin E3 activity is tightly regulated by its structure,[192,193,450-453,457,458]

it may be that PD-associated mutations at other sites lead to C95 exposure, with subsequent C95 PTMs activating parkin self-ubiquitination.

While there is still much more investigation required to uncover the precise role of parkin in PD pathogenesis, a working model for the function of parkin can be hypothesized based on data presented in this study (**Fig 5.2**). Here, parkin is proposed to function similar to the SAG protein, exhibiting both E3 function and redox-state regulation. When cells are exposed to low levels of ROS, RNS, RES and GSSG, modified parkin or parkin bound to damaged proteins is ubiquitinated and undergoes ubiquitin-proteasome system (UPS) degradation. However, under high stress conditions, parkin undergoes rapid ROS,RNS and RES-mediated aggregation in an attempt to scavenge such damaging species. The resulting aggregates cannot be degraded by the UPS and are therefore sequestered within lysosomal vesicles, along with other aggregated proteins, for autophagic degradation and/or non-degradative storage (depending on the cell-type). Therefore, the persistent stress of dopamine autooxidation in long-lived neurons of the *S. nigra* and *L. coeruleus* over time depletes glutathione-based and parkin-associated neutralization at a faster rate than occurs in other cells and may help explain the neuronal selectivity of degeneration observed in *PRKN*-associated PD.

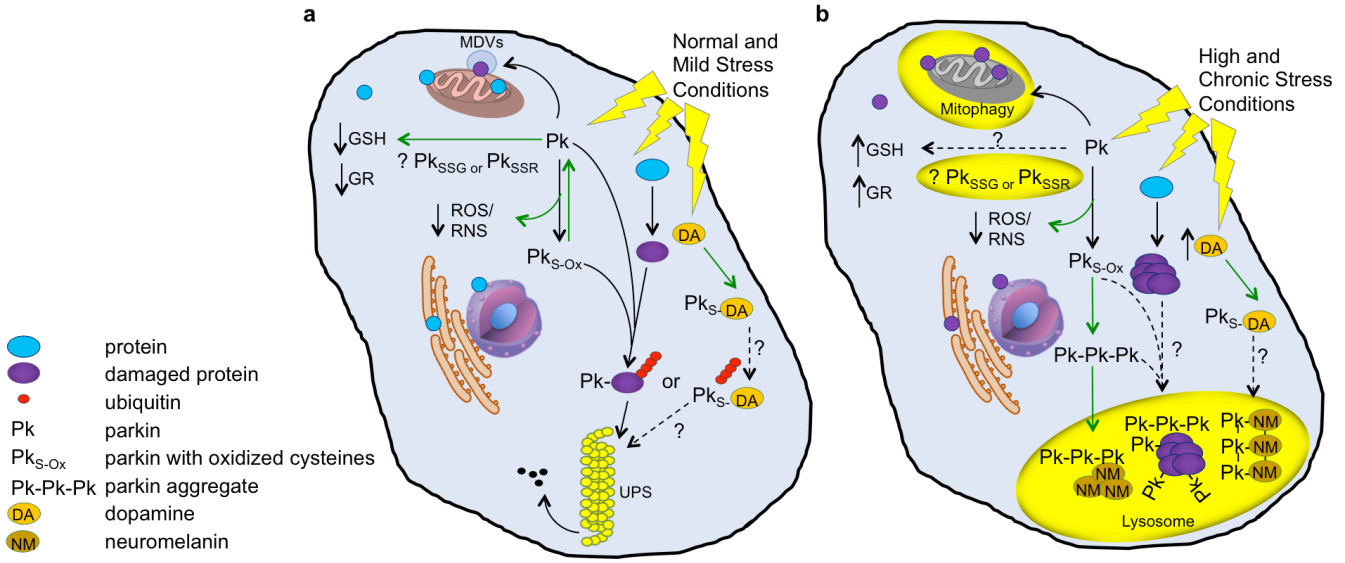

Figure 5.2. Proposed working model for the function of parkin in cells based on study findings
Summary of findings, shown by green coloured arrowsr, found under normal and mild stress conditions (**a**) vs. high and chronic stress conditions (**b**). Dashed arrows and question marks potential further investigations. These include: 1) determining whether parkin S-glutathionylation (PkSSG) and parkin S-protein (PkSSR) degradation modify glutathione levels and/or glutathione reductase (GR) activity; 2) determining whether low levels of parkin-DA (PkS-DA) and parkin-RES conjugation activates its E3 activity, causing degradation by ubiquitin-proteasome system (UPS); 3) determining if parkin mediates neuromelanin formation; and 4) determining whether oxidized (PkS-Ox) and/or aggregated parkin (Pk-Pk-Pk) signals autophagy and lysosomal-mediated protein/organelle degradation.

5.3 Future directions

Based on the observations and interpretations presented above, the following is a list of potential future experiments that will help validate the proposed model for the function of parkin in dopaminergic cells.

Following repeat experiments to confirm the identity of parkin-cysteine PTMs identified *in vivo*, their effect(s) on parkin E3 activity should be undertaken. This could include: i) repeat LC-MS/MS of parkin immunoprecipitated from a larger sample size of mid-age human cortical and *S. nigra* specimens; ii) LC-MS/MS of wild-type and/or C95A mutant parkin immunoprecipitated from dopaminergic cell lines or iPSCs from control and PD patients[101,326] (subjected to normal and dopamine stress conditions) in order to identify *in vivo* cysteine oxidation and dopamine-conjugation sites; iii) 3-D modeling[924] of parkin holoprotein containing cysteines carrying dopamine conjugates, S-glutathionylation and sulfenic/sulfonic acid PTMs, such as at residues C95 and C253; and iv) comparing HMW formation and E3 activity of wild-type recombinant parkin and mutants, C95A and C253A, treated with low levels of H_2O_2 and dopamine. These techniques could later be extended to include other non-dopamine derived RES and radicals, such as MPP^+, rotenone and CCCP, in order to determine if these compounds directly bind and alter the structure of parkin.

A similar sequential thiol-fingerprinting technique, as utilized in Chapter 2, could be used on parkin retrieved from cells treated with biotinylated GSSG[922] followed by LC-MS/MS analysis in order to identify *in vitro* cysteine-S-glutathionylation sites. Furthermore, treatment with non-lethal doses of buthionine sulfoximine[925]and 2-acetylamino-3-[4-(2-acetylamino-2-carboxy-ethylsulfanylthio-carbonylamino)-phenylthiocarbamoylsulfanyl]-propionic acid (2-AAPA),[876] as gamma-glutamyl cysteine synthetase and glutathione reductase inhibitors, respectively, in cell and mouse models could be used to determine whether these enzymes contribute to the glutathione redox states changes observed with parkin loss. Additionally, employing both commercially available Prk8 and the novel mAbs

developed in Chapter 4 to retrieve parkin from cells, under redox-controlled conditions, could help identify disulfide-linked, heteromer-forming binding partners of parkin; some of which may represent *bona fide* E3 targets.

Finally, a combination of parkin-specific antibodies, biorthogonal unnatural amino acid labelling techniques[926] and dopamine-derived probes (6-OHDA-PEG3-yne)[927] could help track parkin localization and aggregation in dopaminergic cells at specific time points following oxidative and dopaminergic insults. These experiments, combined with monitoring the effects of wild-type and C95A mutant human parkin expression on pigment formation in cells and transgenic mice designed to overexpress mammalian tyrosinase in the brainstem,[872] could help validate a role for human parkin in NM production.

Appendix A-Supplementary tables

Table A1. Putative E3 ligase substrates of parkin

Cellular Function	*Substrate*	*Function*	*Ub Type*	*Degrade*	*Accumulate*	*Oxidation*
Protein Homeostasis and Proteasome Regulation	α-Sp22	Glycosylated form of alpha-synuclein	Poly [506]	Yes	Yes in Lewy Body positive PD	Sensitive [740]
	Ataxin-3	deubiquitinating enzyme	Poly [511]	Yes	n.d.	Promoting [741]
	DJ-1 (misfolded state)$^{+}$	Redox-sensitive chaperone (PD linked gene)	Poly [519]	No	n.d.	Sensitive [704]
	Hsp70^{+}	Molecular chaperone	Mono [520]	No	n.d.	Sensitive [742]
	ubiquitin C-terminal hydrolase L1 (UCH-L1)$^{\#}$	neuronal deubiquitinating enzyme (PD linked gene)	Poly [546]	Yes	Yes in parkin KD mice	Sensitive [743]
	p62^{+}	Shuttle polyubiquitylated proteins to proteasomal and/or autophagy/lysosomal degradation	Poly [548]	Yes	Yes in parkin KO mice	Sensitive [744]
Endo-lysosomal Pathway and Lipid homeostasis	PLCγ1$^{\#}$	Hydrolyzes lipids	Poly*[521]	Yes	n.d.	Sensitive [621]
	class B scavenger receptor (CD36)	multivalent transmembrane receptor for lipid ligands	Mono [527]	No	n.d.	Possible sensitivity [745]
	glucocerebrosidase (GBA)-mutant form L444P	Lysosomal β-glucocerebrosidase	Poly [539]	Yes	n.d.	Possible sensitivity [746]
	Rab7^{+}	late-endosomal GTPase in endo-lysosomal pathway	n.d. [549]	No	n.d.	Sensitive [747]
	ER regulatory C/EBP homologous protein (CHOP)	CCAAT/enhancer binding protein involved in gene regulation during ER stress	Poly [551]	Yes	Yes in parkin KO mice	Promoting [748]
	nucleotide-oligomerization domain receptor 2 (NOD2)	cytosolic receptor integrating ER stress and inflammation	Poly* [556]	Yes	n.d.	Promoting [749]
Stability of Cytosqueletal Components	α/β-tubulin^{+}	Cytosqueletal components	Poly* [509]	Yes	Yes in Lewy Body positive PD	Sensitive [750]
	Lim Kinase 1	Phosphorylation of cofilin that binds to actin filaments, causing reorganization.	Poly [518]	Yes	n.d.	Possible sensitivity [751]

Table A1 continued

Cellular Function	*Substrate*	*Function*	*Ub Type*	*Degrade*	*Accumulate*	*Oxidation*
Cell Signaling, Vesicular Dynamics and Synaptic Proteins	CDCrel-1/SEPT5	Synaptic vesicle associated GTPase involved in dopamine release	Poly [503]	Yes	Yes in ARPD	Promoting [752]
	Synphilin-1	Interact with α-synuclein and promotes inclusion bodies	Poly [504]	No	n.d.	n.d.
	Pael-R	G-protein coupled receptor	Poly [505]	Yes	Yes in ARPD and Lewy Body positive PD	Promoting [753]
	CDCrel-2a/SEPT4	Synaptic vesicle associated GTPase involved in dopamine release	Poly [507]	Yes	Yes in ARPD	n.d.
	Synaptotagmin XI#	Calcium-independent membrane trafficking protein, involved in phagocytosis	Poly [508]	Yes	n.d.	Possible sensitivity [754]
	PICK1	Synaptic scaffolding protein	Mono [517]	No	n.d.	Sensitive [755]
	Ataxin-2	RNA-binding protein localizing to endoplasmic reticulum and plasma membrane involved in endocytosis, mTOR signaling and ribosomal translation	Poly [516]	Yes	n.d.	Sensitive [756]
	STEP61	tyrosine dephosphorylation of ERK1/2, pCREB causing reduced synaptic strengthening	Poly [544]	Yes	Yes in parkin KO and PD	Sensitive [757]
	Caveolin-1	Lipid raft constituent	Poly* [541]	Yes	n.d.	Sensitive [758]
	Synaptotagmin IV#	Calcium-independent membrane trafficking protein, modulates exocytosis	Poly [552]	Yes	Yes in parkin KO mice	n.d

Table A1 continued

Cellular Function	*Substrate*	*Function*	*Ub Type*	*Degrade*	*Accumulate*	*Oxidation*
Regulation of Genomic Translation, DNA Repair and Cell Cycle	p38/AIMP2	Aminoacyl t-RNA synthetase cofactor, activator of p53	Poly [296]	Yes	Yes in parkin KO mice, ARPD, PD	Possible sensitivity [759]
	Cyclin E#	Cell cycle regulating protein (G1-S transition)	Poly [510]	Yes	Yes in ARPD	Possible sensitivity [760]
	FUSE-binding protein 1 (FBP1)	Regulates c-myc mRNA	Poly [513]	Yes	Yes in parkin KO mice	Possible sensitivity [761]
	RanBP2+	Interact with nuclear pore complex, involved in stress response	Poly [514]	Yes	n.d.	Sensitive [762]
	PDCD2-1	Involved in apoptosis, inflammation and proliferation	Poly [522]	Yes	Yes in ARPD	Sensitive [763]
	β-catenin#	Component in Wnt signaling	Poly* [523]	Yes	Yes in parkin KO mice	Sensitive [764]
	TDP-43+	Transactivation response DNA-binding protein (ALS linked gene)	Poly [536]	No	abnormal cytosolic TDP-43 accumulate in PD	Sensitive [765]
	Fbw7β	Part of SCF-Fbw7 E3 ligase complex. Regulates cellular apoptosis via Mcl-1	Poly [535]	Yes	Yes in parkin KO mice and ARPD	Possible sensitivity [766]
	Plk1	serine/threonine kinase, role in promoting mitosis and inhibiting apoptosis	Poly [545]	Yes	Yes in parkin KO mice	Sensitive [767]
	p21	inhibitor of cyclin-dependent kinases	Poly* [554]	Yes	Yes in parkin KO mice	Sensitive [768]
	Apurinic/apyrimidinic endonuclease 1 (APE1)	Endonuclease that generates single strand breaks for repair	Poly and Mono [555]	Yes	n.d.	Sensitive [555]

Table A1 continued

Cellular Function	*Substrate*	*Function*	*Ub Type*	*Degrade*	*Accumulate*	*Oxidation*
Cell Survival and Stress Regulation	lκκγ	Component in NFκB signaling	Poly [515]	No	n.d.	Sensitive [769]
	TRAF2	Component in TNF and NFκB signaling	Poly [515]	Yes/No [Chung 2013]	n.d.	Sensitive [770]
	PARIS (ZNF746) #	KRAB and zinc finger protein. repression of PGC-1α and NRF-1	Poly [528]	Yes	Yes in parkin KO mice, ARPD, PD	Possible sensitivity [528][771]
	ARTS (Sept4_i2)	mitochondrial pro-apoptotic protein, binds and inhibits XIAP	Poly* [532]	Yes	Yes in Lewy Body positive PD	Sensitive [772]
	BCL-2 associated protein (BAX)	Inducer of apoptosis	Poly [531,550]	Yes, dysregulated or mutant form	n.d.	Sensitive [773,774]
	FAF1	member of the death-inducing complex, NFκB suppression	Poly [538]	Yes	Yes in MPTP treated mice	Sensitive [775]
	NEMO	NFκB essential modulator, part of IκB kinase complex	Poly (Linear) [537]	No	n.d.	Sensitive [776]
	TRAF6	Component in TNF and NFκB signaling	Poly [534]	Yes	Yes in PD	Sensitive [777]
	RTP801/REDD1	Pro-apoptotic negative regulator of mTOR and Akt	Poly [299]	Yes	Yes parkin KO mice and ARPD	Sensitive [778]
	Inhibitory PAS domain protein (IPAS)	potent negative transcriptional regulator of hypoxia-inducible factor-1 (HIF-1) and proapoptotic factor	Poly [543]	Yes	Yes in PD and MPTP treated mice	Sensitive [779]
	hypoxia-inducible factor 1α (HIF-1α)	Oxygen-dependent heterodimeric transcription factor	Poly* [553]	Yes	Parkin downregulation and HIF-1α upregulation in breast cancers	Sensitive [780]

Table A1 continued

Cellular Function	*Substrate*	*Function*	*Ub Type*	*Degrade*	*Accumulate*	*Oxidation*
Cell Survival and Stress Regulation	RIPK1[#]	TNFR1 activation and NFκB signaling	Poly [557]	No	n.d.	Sensitive [781]
	BCL□2 Antagonist/Killer□1 (BAK)[+]	Inducer of apoptosis	Poly and Mono [558]	No		Sensitive [773,774]
	cyclophilin-D	receptor protein in necrosis signaling pathway	Poly [560]	No		Sensitive [782]
Mitochondrial Form/Function and Metabolism	VDAC[+]	Mitochondrial ion channel	Poly [525]	No		Sensitive [783]
	Bcl-2	Anti-apoptotic protein	Mono [524]	No		Sensitive [774,784]
Mitochondrial Form/Function and Metabolism	Mitofusin-1/-2	Mitochondrial fusion protein	Poly [526]	Yes		Sensitive [785]
	Drp1	Mitochondrial fission protein	Poly [529]	Yes		Sensitive [786]
	Miro (Mitochondrial Rho GTPase)	Mitochondrial anchor protein	Poly* [530]	Yes		Possible sensitivity [787]
	hexokinase HK1[+]	phosphorylation of glucose, first step in glycolysis	Poly* [533]	Yes		Sensitive [788]
	HSD10 (17-beta hydroxysteroid dehydrogenase type 10)	ubiquitous NADH-dependent multifunctional enzyme	Mono [540]	No		Possible sensitivity [789]
	BNIP3L/Nix	outer mitochondrial membrane protein required for mitophagy	n.d. [542]	Yes, indirectly		Possible sensitivity [790]
	pyruvate kinase M2[+]	Aerobic glycolysis	Mono [547]	No		Sensitive [791]
	MITOL/March5	mitochondrial E3 ubiquitin ligase	n.d. [559]	No		Sensitive [792]

Table A1. Putative E3 ligase substrates of parkin
Comprehensive list of parkin substrates grouped according to cellular function along with the ubiquitination type afforded by parkin; its degradation profile post-ubiquitination; its accumulation within cellular tissue; and whether it exhibits redox sensitivity. Glutathionylated proteins are denoted by +, or a related subtype of the same protein family by #, found Su et al 2014[920] are also included. * denotes studies that did not indicate ubiquitination type, but the downstream effect of ubiquitination was degradation by the proteasome, here, the ubiquitination type is presumed polyubiquitination. Mono: monoubiquination; poly: polyubiquitination; PD: Parkinson disease; KO; knockout; ARPD: autosomal recessive PD; MPTP: 1-methyl-4-phenyl-1,2,3,6-tetrahydropyridine; and n.d. not determined. References are in brackets.

Table A2. Proteins structurally changed in *prkn*$^{-/-}$ mice

a *Name*	*Protein or Enzyme*	*Redox Sensitivity*
Pyruvate dehydrogenase E1$^{\#}$	Enzyme	Yes [584
NADH-ubiquinone oxidoreductase 24-kDa subunit$^{\#}$	Enzyme	Yes [584]
NADH-ubiquinone oxidoreductase 30-kDa subunit$^{\#}$	Enzyme	Yes [584]
Cytochrome c oxidase, subunit Vb$^{\#}$	Enzyme	Yes [584]
Peroxiredoxin 2	Enzyme	Yes [584]
Peroxiredoxin 6^{+}	Enzyme	Yes [584]
Peroxiredoxin 1	Enzyme	Yes [584]
Lactoylglutathione lyase (glyoxalase I)	Enzyme	Yes [585]
Profilin II	Protein	Yes [586]
Hypothetical Protein dJ37E16.5- similar to nitrophenylphosphatases	Enzyme	Yes [587]
Vacuolar protein sorting-29	Protein	n.d.
α-Crystallin, chain B	Protein	Yes [588]
Heterogeneous nuclear ribonucleoprotein A1$^{\#}$	Protein	Yes [589]
Lasp-1	Protein	n.d.
Ratio of redox sensitive : Not redox sensitive	12:2	

b *Name*	*Protein or Enzyme*	*Redox Sensitivity*
Fructose-bisphosphate aldolase C$^{\#}$	Enzyme	Yes [584]
ATP synthase α chain, mitochondrial$^{\#}$	Enzyme	Yes [590]
Citrate synthase^{+}	Enzyme	No [591]
Dihydrolipoamide dehydrogenase (E3)$^{+}$	Enzyme	Yes [592,593]
Succinate dehydrogenase flavoprotein subunit^{+}	Enzyme	Yes [584]
Glyceraldehyde-3-phosphate dehydrogenase^{+}	Enzyme	Yes [584]
GTP:AMP phosphotransferase mitochondrial^{+}	Enzyme	n.d.
Pyruvate kinase, M2 isozyme^{+}	Enzyme	Yes [594]
L-Lactate dehydrogenase A chain^{+}	Enzyme	Yes [595]
Malate dehydrogenase, cytoplasmic^{+}	Enzyme	Yes [584]
NADH-ubiquinone oxidoreductase 51-kDa subunit (complex 1) $^{\#}$	Enzyme	Yes [596]
Pyruvate dehydrogenase E1 component β subunit$^{\#}$	Enzyme	Yes [584,597]
Phosphoglycerate kinase 1^{+}	Enzyme	Yes [598,599]
Succinyl-CoA ligase β-chain, mitochondrial$^{\#}$	Enzyme	Yes [584]
Acetyl-CoA acetyltransferase, mitochondrial (thiolase)	Enzyme	Yes [600]
Ubiquinol-cytochrome c reductase complex core protein I (complex III) $^{+}$	Enzyme	Yes [584]
β-Adrenergic receptor kinase 1	Enzyme	n.d.
Proto-oncogene C-crk (adapter molecule crk, member of adapter protein family)	Protein	Yes [601]
Dihydropyrimidinase-related protein-2 (CRMP-2)	Enzyme	Yes [602]
Ser/Thr protein phosphatase 2B catalytic subunit, α isoform (PP2B) $^{\#}$	Enzyme	Yes [603]

b continued *Name*	*Protein or Enzyme*	*Redox Sensitivity*
Ser/Thr protein phosphatase PP1-β catalytic subunit[#]	Enzyme	Yes [603]
Protein tyrosine phosphatase, non receptor type 1-1[#]	Enzyme	Yes [584,604]
14-3-3 prot[+]	Protein	n.d.
MAGUK p55 subfamily member 3	Protein	n.d.
rho GDP-dissociation inhibitor 1[#]	Protein	n.d.
N-ethylmaleimide-sensitive fusion protein (NSF)	Enzyme	Yes [605,606]
Syntaxin 1B	Protein	Yes [607]
Syntaxin-binding protein 1	Protein	Yes [608]
Septin 5	Protein	Yes [609]
Septin 7	Protein	Yes [609]
Septin-like protein KIAA0202 (Septin 8)	Protein	Yes [609]
Hypothetical protein FLJ10849 (Septin 2 or 6 homologue)	Protein	Yes [609]
Stress-70 protein (mortalin) [+]	Protein	Yes [610]
Heat-shock cognate 71-kDa protein[+]	Protein	Yes [589]
Carbonyl reductase [NADPH] 1	Enzyme	Yes [595]
Glutathione S-transferase P 2[#]	Enzyme	Yes [595]
Glyoxalase I	Enzyme	Yes [585]
Thioredoxin reductase	Enzyme	Yes [611,612]
ARP2/3 complex 20-kDa subunit[#]	Protein	n.d.
Adenyl cyclase-associated protein 1[+]	Protein	No [613]
Dynamin-1	Protein	Yes [614]
Tubulin α1 chain[+]	Protein	Yes [615]
Proteasome subunit beta type 5[#]	Protein	Yes [589]
Ubiquitin carboxyterminal hydrolase L1[#]	Enzyme	Yes [616,617]
Deubiquitinating enzyme (Ubiquitin thioesterase) OTUB1[+]	Enzyme	Yes [618]
Acyl-CoA dehydrogenase, very-long chain specific[+]	Enzyme	Yes [584]
Propionyl CoA carboxylase α chain[+]	Enzyme	Yes [619]
Lysophospholipase 1 (phospholipase B)[#]	Enzyme	Yes [620,621]
Tyrosyl tRNA synthetase	Enzyme	Yes [622]
Threonyl tRNA synthetase[+]	Enzyme	Yes [623]
Glutamine synthetase	Enzyme	Yes [624]
Serine racemase	Enzyme	Yes [604]
Probable ATP-dependent RNA helicase p47[#]	Enzyme	No [625,626]
Poly(rC)binding protein[+]	Protein	n.d.
4-Aminobutyrate aminotransferase, mitochondrial (GABA transaminase)	Enzyme	Yes [627]
Tyrosine 3-hydroxylase	Enzyme	Yes [628]
Serum albumin	Protein	Yes [629]
ADP-ribosylarginine hydrolase[+]	Enzyme	n.d.
Carbonic anhydrase II	Enzyme	Yes [599]

b continued *Name*	*Protein or Enzyme*	*Redox Sensitivity*
Low-affinity immunoglobulin epsilon FC receptor	Protein	n.d.
Ribose-phosphate pyrophosphokinase I	Enzyme	n.d.
Voltage-dependent anion-selective channel protein 1^{+}	Protein	Yes [584]
Spermidine synthase	Enzyme	n.d.
γ Enolase$^{\#}$	Enzyme	Yes [630]
NADH-ubiquinone oxidoreductase PDSW subunit HS homolog$^{\#}$	Enzyme	Yes [596]
MAGUK p55 subfamily member 6	Protein	Yes [631]
Sumo-1 activating enzyme subunit 2 (Ubiquitin-like 1-activating enzyme) $^{+}$	Enzyme	Yes [632]
MAGUK p55 subfamily member 2	Protein	n.d.
Sorting nexin 5	Protein	n.d.
78-kDa glucose-regulated protein (heat shock 70 kDa protein 5)$^{\#}$	Protein	Yes [589,633]
Heat-shock-related 70 kDa protein 2$^{\#}$	Protein	Yes [589,633]
Heat-shock 70-related protein APG-1	Protein	Yes [589,633]
T-complex protein 1, α subunit B^{+}	Protein	Yes [634]
Aconitate hydratase, mitochondrial (aconitase) $^{+}$	Enzyme	Yes [584]
γ-Actin^{+}	Protein	Yes [635]
Spectrin α chain, brain	Protein	Yes [636]
Ubiquitin-activating enzyme E1 type 1	Enzyme	Yes [637]
Acyl-coenzyme A oxidase 1, peroxisomal	Enzyme	n.d.
Acyl CoA thioester hydrolase^{+}	Enzyme	Yes [638]
Sodium/potassium-transporting ATPase α-3 chain$^{\#}$	Enzyme	Yes [584]
Calretinin	Protein	Yes [639]
ATP-dependent RNA helicase DDX19, dead box protein$^{\#}$	Protein	n.d.
Ratio of redox sensitive: Not redox sensitive	64:18	

Table A2. Proteins structural changes in *prkn*$^{-/-}$ mice
Summary of proteins altered in *prkn*$^{-/-}$ mice observed in unbiased proteomic analyses by Palacino et al 2004,[435] shown in (**a**), and by Periquet et al 2005,[437] in (**b**). Proteins were also identified by their redox sensitivity and of the combined total of 92 proteins observed, 72 were identified as redox-sensitive. n.d., not determined. References for redox sensitivity are in brackets. Glutathionylated proteins are denoted by +, or a related subtype of the same protein family by #, found Su et al 2014[920] are also included; n.d., not documented.

Appendix B-References

1 Beitz, J. M. Parkinson's disease: a review. *Frontiers in bioscience (Scholar edition)* **6**, 65-74, doi:10.2741/s415 (2014).

2 Pringsheim, T., Jette, N., Frolkis, A. & Steeves, T. D. The prevalence of Parkinson's disease: a systematic review and meta-analysis. *Mov Disord* **29**, 1583-1590, doi:10.1002/mds.25945 (2014).

3 Dorsey, E. R. *et al.* Projected number of people with Parkinson disease in the most populous nations, 2005 through 2030. *Neurology* **68**, 384-386 (2007).

4 Grimes, D. *et al.* Canadian guideline for Parkinson disease. *CMAJ* **191**, E989-E1004, doi:10.1503/cmaj.181504 (2019).

5 Moscovich, M. *et al.* Death certificate data and causes of death in patients with parkinsonism. *Parkinsonism Relat Disord* **41**, 99-103, doi:10.1016/j.parkreldis.2017.05.022 (2017).

6 Pennington, S., Snell, K., Lee, M. & Walker, R. The cause of death in idiopathic Parkinson's disease. *Parkinsonism Relat Disord* **16**, 434-437, doi:10.1016/j.parkreldis.2010.04.010 (2010).

7 Macleod, A. D., Taylor, K. S. & Counsell, C. E. Mortality in Parkinson's disease: a systematic review and meta-analysis. *Mov Disord* **29**, 1615-1622, doi:10.1002/mds.25898 (2014).

8 Parkinson, J. An essay on the shaking palsy. 1817. *J Neuropsychiatry Clin Neurosci* **14**, 223-236; discussion 222, doi:10.1176/jnp.14.2.223 (2002).

9 Kempster, P. A., Hurwitz, B. & Lees, A. J. A new look at James Parkinson's Essay on the Shaking Palsy. *Neurology* **69**, 482-485, doi:10.1212/01.wnl.0000266639.50620.d1 (2007).

10 Postuma, R. B. *et al.* MDS clinical diagnostic criteria for Parkinson's disease. *Mov Disord* **30**, 1591-1601, doi:10.1002/mds.26424 (2015).

11 Koga, S. *et al.* When DLB, PD, and PSP masquerade as MSA: an autopsy study of 134 patients. *Neurology* **85**, 404-412, doi:10.1212/wnl.0000000000001807 (2015).

12 Kanazawa, M. *et al.* Early clinical features of patients with progressive supranuclear palsy with predominant cerebellar ataxia. *Parkinsonism Relat Disord* **19**, 1149-1151, doi:10.1016/j.parkreldis.2013.07.019 (2013).

13 Fanciulli, A. & Wenning, G. K. Multiple-system atrophy. *N Engl J Med* **372**, 249-263, doi:10.1056/NEJMra1311488 (2015).

14 Schrag, A., Ben-Shlomo, Y. & Quinn, N. How valid is the clinical diagnosis of Parkinson's disease in the community? *Journal of neurology, neurosurgery, and psychiatry* **73**, 529-534, doi:10.1136/jnnp.73.5.529 (2002).

15 Hughes, A. J., Ben-Shlomo, Y., Daniel, S. E. & Lees, A. J. What features improve the accuracy of clinical diagnosis in Parkinson's disease: a clinicopathologic study. *Neurology* **42**, 1142-1146 (1992).

16 Liu, Z. Y., Liu, F. T., Zuo, C. T., Koprich, J. B. & Wang, J. Update on Molecular Imaging in Parkinson's Disease. *Neuroscience bulletin* **34**, 330-340, doi:10.1007/s12264-017-0202-6 (2018).

17 Badoud, S. *et al.* Discriminating among degenerative parkinsonisms using advanced (123)I-ioflupane SPECT analyses. *NeuroImage. Clinical* **12**, 234-240, doi:10.1016/j.nicl.2016.07.004 (2016).

18 Palermo, G. & Ceravolo, R. Molecular Imaging of the Dopamine Transporter. *Cells* **8**, doi:10.3390/cells8080872 (2019).

19 Maass, F., Schulz, I., Lingor, P., Mollenhauer, B. & Bähr, M. Cerebrospinal fluid biomarker for Parkinson's disease: An overview. *Molecular and cellular neurosciences* **97**, 60-66, doi:10.1016/j.mcn.2018.12.005 (2019).

20 El-Agnaf, O. M. *et al.* Detection of oligomeric forms of alpha-synuclein protein in human plasma as a potential biomarker for Parkinson's disease. *Faseb j* **20**, 419-425, doi:10.1096/fj.03-1449com (2006).

21 Hong, Z. *et al.* DJ-1 and alpha-synuclein in human cerebrospinal fluid as biomarkers of Parkinson's disease. *Brain* **133**, 713-726, doi:10.1093/brain/awq008 (2010).

22 Mollenhauer, B. *et al.* alpha-Synuclein and tau concentrations in cerebrospinal fluid of patients presenting with parkinsonism: a cohort study. *Lancet Neurol* **10**, 230-240, doi:10.1016/S1474-4422(11)70014-X (2011).

23 Simonsen, A. H. *et al.* The utility of α-synuclein as biofluid marker in neurodegenerative diseases: a systematic review of the literature. *Biomarkers in medicine* **10**, 19-34, doi:10.2217/bmm.14.105 (2016).

24 Tokuda, T. *et al.* Decreased alpha-synuclein in cerebrospinal fluid of aged individuals and subjects with Parkinson's disease. *Biochem Biophys Res Commun* **349**, 162-166 (2006).

25 Mollenhauer, B. *et al.* Baseline predictors for progression 4 years after Parkinson's disease diagnosis in the De Novo Parkinson Cohort (DeNoPa). *Mov Disord* **34**, 67-77, doi:10.1002/mds.27492 (2019).

26 Sawada, H. *et al.* Baseline C-Reactive Protein Levels and Life Prognosis in Parkinson Disease. *PLOS ONE* **10**, e0134118, doi:10.1371/journal.pone.0134118 (2015).

27 Holmberg, B., Rosengren, L., Karlsson, J. E. & Johnels, B. Increased cerebrospinal fluid levels of neurofilament protein in progressive supranuclear palsy and multiple-system atrophy compared with Parkinson's disease. *Mov Disord* **13**, 70-77, doi:10.1002/mds.870130116 (1998).
28 Hansson, O. *et al.* Blood-based NfL: A biomarker for differential diagnosis of parkinsonian disorder. *Neurology* **88**, 930-937, doi:10.1212/wnl.0000000000003680 (2017).
29 Dickson, D. W. *et al.* Neuropathological assessment of Parkinson's disease: refining the diagnostic criteria. *Lancet Neurol* **8**, 1150-1157, doi:10.1016/S1474-4422(09)70238-8 (2009).
30 Agamanolis, D. P. *Neuropathology an Illustrated Interactive Course for Medical Students and Residents*, <https://neuropathology-web.org/agamanolis.html> (2020).
31 Spillantini, M. G. *et al.* Alpha-synuclein in Lewy bodies. *Nature* **388**, 839-840 (1997).
32 Harding, A. J. & Halliday, G. M. Cortical Lewy body pathology in the diagnosis of dementia. *Acta Neuropathol* **102**, 355-363, doi:10.1007/s004010100390 (2001).
33 Forno, L. S. Concentric hyalin intraneuronal inclusions of Lewy type in the brains of elderly persons (50 incidental cases): relationship to parkinsonism. *Journal of the American Geriatrics Society* **17**, 557-575, doi:10.1111/j.1532-5415.1969.tb01316.x (1969).
34 Gibb, W. R. & Lees, A. J. The relevance of the Lewy body to the pathogenesis of idiopathic Parkinson's disease. *J Neurol Neurosurg Psychiatry* **51**, 745-752, doi:10.1136/jnnp.51.6.745 (1988).
35 Bennett, D. A. *et al.* Neuropathology of older persons without cognitive impairment from two community-based studies. *Neurology* **66**, 1837-1844, doi:10.1212/01.wnl.0000219668.47116.e6 (2006).
36 Ehringer, H. & Hornykiewicz, O. [Distribution of noradrenaline and dopamine (3-hydroxytyramine) in the human brain and their behavior in diseases of the extrapyramidal system]. *Klin Wochenschr* **38**, 1236-1239, doi:10.1007/BF01485901 (1960).
37 Birkmayer, W. & Hornykiewicz, O. [The L-3,4-dioxyphenylalanine (DOPA)-effect in Parkinson-akinesia]. *Wien Klin Wochenschr* **73**, 787-788 (1961).
38 Fehling, C. Treatment of Parkinson's syndrome with L-dopa. A double blind study. *Acta Neurol Scand* **42**, 367-372, doi:10.1111/j.1600-0404.1966.tb01188.x (1966).
39 Cotzias, G. C. L-Dopa for Parkinsonism. *N Engl J Med* **278**, 630, doi:10.1056/nejm196803142781127 (1968).
40 Bernheimer, H., Birkmayer, W., Hornykiewicz, O., Jellinger, K. & Seitelberger, F. Brain dopamine and the syndromes of Parkinson and Huntington. Clinical, morphological and neurochemical correlations. *J Neurol Sci* **20**, 415-455, doi:10.1016/0022-510x(73)90175-5 (1973).
41 Lees, A. J., Tolosa, E. & Olanow, C. W. Four pioneers of L-dopa treatment: Arvid Carlsson, Oleh Hornykiewicz, George Cotzias, and Melvin Yahr. *Mov Disord* **30**, 19-36, doi:10.1002/mds.26120 (2015).
42 Lanciego, J. L., Luquin, N. & Obeso, J. A. Functional neuroanatomy of the basal ganglia. *Cold Spring Harb Perspect Med* **2**, a009621, doi:10.1101/cshperspect.a009621 (2012).
43 Emborg, M. E. Nonhuman primate models of Parkinson's disease. *ILAR J* **48**, 339-355, doi:10.1093/ilar.48.4.339 (2007).
44 Pacelli, C. *et al.* Elevated Mitochondrial Bioenergetics and Axonal Arborization Size Are Key Contributors to the Vulnerability of Dopamine Neurons. *Curr Biol* **25**, 2349-2360, doi:10.1016/j.cub.2015.07.050 (2015).
45 Giguere, N. *et al.* Comparative analysis of Parkinson's disease-associated genes in mice reveals altered survival and bioenergetics of Parkin-deficient dopamine neurons. *J Biol Chem* **293**, 9580-9593, doi:10.1074/jbc.RA117.000499 (2018).
46 Burbulla, L. F. *et al.* Dopamine oxidation mediates mitochondrial and lysosomal dysfunction in Parkinson's disease. *Science* **357**, 1255-1261, doi:10.1126/science.aam9080 (2017).
47 Blandini, F., Nappi, G., Tassorelli, C. & Martignoni, E. Functional changes of the basal ganglia circuitry in Parkinson's disease. *Prog Neurobiol* **62**, 63-88, doi:10.1016/s0301-0082(99)00067-2 (2000).
48 Cheng, H. C., Ulane, C. M. & Burke, R. E. Clinical progression in Parkinson disease and the neurobiology of axons. *Ann Neurol* **67**, 715-725, doi:10.1002/ana.21995 (2010).
49 Alberico, S. L., Cassell, M. D. & Narayanan, N. S. The Vulnerable Ventral Tegmental Area in Parkinson's Disease. *Basal Ganglia* **5**, 51-55, doi:10.1016/j.baga.2015.06.001 (2015).
50 Aarsland, D. *et al.* Risk of dementia in Parkinson's disease: a community-based, prospective study. *Neurology* **56**, 730-736, doi:10.1212/wnl.56.6.730 (2001).
51 McKeith, I. G. *et al.* Diagnosis and management of dementia with Lewy bodies: Fourth consensus report of the DLB Consortium. *Neurology* **89**, 88-100, doi:10.1212/wnl.0000000000004058 (2017).
52 Jellinger, K. A. & Korczyn, A. D. Are dementia with Lewy bodies and Parkinson's disease dementia the same disease? *BMC Medicine* **16**, 34, doi:10.1186/s12916-018-1016-8 (2018).

53 Doherty, K. M. & Hardy, J. Parkin disease and the Lewy body conundrum. *Mov Disord* **28**, 702-704, doi:10.1002/mds.25486 (2013).
54 Marsden, C. D. Parkinson's disease. *Lancet* **335**, 948-952, doi:10.1016/0140-6736(90)91006-v (1990).
55 Ross, G. W. *et al.* Parkinsonian signs and substantia nigra neuron density in decendents elders without PD. *Ann Neurol* **56**, 532-539, doi:10.1002/ana.20226 (2004).
56 Lang, A. E. & Lozano, A. M. Parkinson's disease. First of two parts. *N Engl J Med* **339**, 1044-1053, doi:10.1056/NEJM199810083391506 (1998).
57 Dauer, W. & Przedborski, S. Parkinson's disease: mechanisms and models. *Neuron* **39**, 889-909, doi:10.1016/s0896-6273(03)00568-3 (2003).
58 Albin, R. L., Young, A. B. & Penney, J. B. The functional anatomy of basal ganglia disorders. *Trends Neurosci* **12**, 366-375, doi:10.1016/0166-2236(89)90074-x (1989).
59 Bolam, J. P., Hanley, J. J., Booth, P. A. & Bevan, M. D. Synaptic organisation of the basal ganglia. *Journal of anatomy* **196 (Pt 4)**, 527-542, doi:10.1046/j.1469-7580.2000.19640527.x (2000).
60 Knierim, J. *Section 3: Motor Systems- Chapter 4: Basal Ganglia*, <https://nba.uth.tmc.edu/neuroscience/index.htm> (2020).
61 Gerfen, C. R. *et al.* D1 and D2 dopamine receptor-regulated gene expression of striatonigral and striatopallidal neurons. *Science* **250**, 1429-1432, doi:10.1126/science.2147780 (1990).
62 DeLong, M. R. Primate models of movement disorders of basal ganglia origin. *Trends Neurosci* **13**, 281-285, doi:10.1016/0166-2236(90)90110-v (1990).
63 Kalia, L. V. & Lang, A. E. Parkinson's disease. *Lancet* **386**, 896-912, doi:10.1016/S0140-6736(14)61393-3 (2015).
64 Klein, C. & Schlossmacher, M. G. Parkinson disease, 10 years after its genetic revolution: multiple clues to a complex disorder. *Neurology* **69**, 2093-2104, doi:10.1212/01.wnl.0000271880.27321.a7 (2007).
65 Frisina, P. G., Borod, J. C., Foldi, N. S. & Tenenbaum, H. R. Depression in Parkinson's disease: health risks, etiology, and treatment options. *Neuropsychiatr Dis Treat* **4**, 81-91, doi:10.2147/ndt.s1453 (2008).
66 Barone, P. *et al.* The PRIAMO study: A multicenter assessment of nonmotor symptoms and their impact on quality of life in Parkinson's disease. *Mov Disord* **24**, 1641-1649, doi:10.1002/mds.22643 (2009).
67 Schenck, C. H. *et al.* Rapid eye movement sleep behavior disorder: devising controlled active treatment studies for symptomatic and neuroprotective therapy--a consensus statement from the International Rapid Eye Movement Sleep Behavior Disorder Study Group. *Sleep Med* **14**, 795-806, doi:10.1016/j.sleep.2013.02.016 (2013).
68 Iranzo, A. *et al.* Neurodegenerative disease status and post-mortem pathology in idiopathic rapid-eye-movement sleep behaviour disorder: an observational cohort study. *Lancet Neurol* **12**, 443-453, doi:10.1016/s1474-4422(13)70056-5 (2013).
69 Postuma, R. B., Gagnon, J. F., Bertrand, J. A., Génier Marchand, D. & Montplaisir, J. Y. Parkinson risk in idiopathic REM sleep behavior disorder: preparing for neuroprotective trials. *Neurology* **84**, 1104-1113, doi:10.1212/wnl.0000000000001364 (2015).
70 Doty, R. L. Olfactory dysfunction in Parkinson disease. *Nat Rev Neurol* **8**, 329-339, doi:10.1038/nrneurol.2012.80 (2012).
71 Agid, Y. Biochemistry of neurotransmitters in Parkinson's disease. *Movement disorders 2* (1987).
72 Gesi, M. *et al.* The role of the locus coeruleus in the development of Parkinson's disease. *Neurosci Biobehav Rev* **24**, 655-668, doi:10.1016/s0149-7634(00)00028-2 (2000).
73 Dickson, D. W. Parkinson's disease and parkinsonism: neuropathology. *Cold Spring Harb Perspect Med* **2**, doi:10.1101/cshperspect.a009258 (2012).
74 Schwarz, L. A. & Luo, L. Organization of the locus coeruleus-norepinephrine system. *Curr Biol* **25**, R1051-r1056, doi:10.1016/j.cub.2015.09.039 (2015).
75 Bari, B. A., Chokshi, V. & Schmidt, K. Locus coeruleus-norepinephrine: basic functions and insights into Parkinson's disease. *Neural Regen Res* **15**, 1006-1013, doi:10.4103/1673-5374.270297 (2020).
76 Fernstrom, J. D. & Fernstrom, M. H. Tyrosine, phenylalanine, and catecholamine synthesis and function in the brain. *J Nutr* **137**, 1539S-1547S; discussion 1548S, doi:10.1093/jn/137.6.1539S (2007).
77 Yaffe, D., Forrest, L. R. & Schuldiner, S. The ins and outs of vesicular monoamine transporters. *J Gen Physiol* **150**, 671-682, doi:10.1085/jgp.201711980 (2018).
78 Meiser, J., Weindl, D. & Hiller, K. Complexity of dopamine metabolism. *Cell Communication and Signaling* **11**, 34, doi:10.1186/1478-811X-11-34 (2013).
79 Fedorow, H. *et al.* Neuromelanin in human dopamine neurons: comparison with peripheral melanins and relevance to Parkinson's disease. *Prog Neurobiol* **75**, 109-124, doi:10.1016/j.pneurobio.2005.02.001 (2005).
80 Hirsch, E., Graybiel, A. M. & Agid, Y. A. Melanized dopaminergic neurons are differentially susceptible to degeneration in Parkinson's disease. *Nature* **334**, 345-348, doi:10.1038/334345a0 (1988).

81 Correia, M. S. *et al.* Melanin Transferred to Keratinocytes Resides in Nondegradative Endocytic Compartments. *J Invest Dermatol* **138**, 637-646, doi:10.1016/j.jid.2017.09.042 (2018).
82 Zucca, F. A. *et al.* Neuromelanin organelles are specialized autolysosomes that accumulate undegraded proteins and lipids in aging human brain and are likely involved in Parkinson's disease. *NPJ Parkinsons Dis* **4**, 17, doi:10.1038/s41531-018-0050-8 (2018).
83 Sulzer, D. *et al.* Neuromelanin biosynthesis is driven by excess cytosolic catecholamines not accumulated by synaptic vesicles. *Proc Natl Acad Sci U S A* **97**, 11869-11874, doi:10.1073/pnas.97.22.11869 (2000).
84 Sulzer, D. *et al.* Neuromelanin detection by magnetic resonance imaging (MRI) and its promise as a biomarker for Parkinson's disease. *NPJ Parkinsons Dis* **4**, 11, doi:10.1038/s41531-018-0047-3 (2018).
85 Zucca, F. A. *et al.* Interactions of iron, dopamine and neuromelanin pathways in brain aging and Parkinson's disease. *Prog Neurobiol* **155**, 96-119, doi:10.1016/j.pneurobio.2015.09.012 (2017).
86 Zucca, F. A. *et al.* Neuromelanin of the human substantia nigra: an update. *Neurotox Res* **25**, 13-23, doi:10.1007/s12640-013-9435-y (2014).
87 Armstrong, M. J. & Okun, M. S. Diagnosis and Treatment of Parkinson Disease: A Review. *JAMA* **323**, 548-560, doi:10.1001/jama.2019.22360 (2020).
88 Birkmayer, W. & Hornykiewicz, O. [Additional Experimental Studies on L-Dopa in Parkinson's Syndrome and Reserpine Parkinsonism]. *Arch Psychiatr Nervenkr* **206**, 367-381, doi:10.1007/BF00341704 (1964).
89 Sit, S. Y. Dopamine agonists in the treatment of Parkinson s disease past, present and future. *Curr Pharm Des* **6**, 1211-1248, doi:10.2174/1381612003399581 (2000).
90 Ahlskog, J. E. & Muenter, M. D. Frequency of levodopa-related dyskinesias and motor fluctuations as estimated from the cumulative literature. *Mov Disord* **16**, 448-458, doi:10.1002/mds.1090 (2001).
91 O'Sullivan, S. S., Evans, A. H. & Lees, A. J. Dopamine dysregulation syndrome: an overview of its epidemiology, mechanisms and management. *CNS Drugs* **23**, 157-170, doi:10.2165/00023210-200923020-00005 (2009).
92 Rabinak, C. A. & Nirenberg, M. J. Dopamine agonist withdrawal syndrome in Parkinson disease. *Arch Neurol* **67**, 58-63, doi:10.1001/archneurol.2009.294 (2010).
93 Lozano, A. M., Dostrovsky, J., Chen, R. & Ashby, P. Deep brain stimulation for Parkinson's disease: disrupting the disruption. *Lancet Neurol* **1**, 225-231, doi:10.1016/s1474-4422(02)00101-1 (2002).
94 McIntyre, C. C. & Anderson, R. W. Deep brain stimulation mechanisms: the control of network activity via neurochemistry modulation. *J Neurochem* **139 Suppl 1**, 338-345, doi:10.1111/jnc.13649 (2016).
95 Boronat-García, A., Guerra-Crespo, M. & Drucker-Colín, R. Historical perspective of cell transplantation in Parkinson's disease. *World J Transplant* **7**, 179-192, doi:10.5500/wjt.v7.i3.179 (2017).
96 Fan, Y., Winanto & Ng, S. Y. Replacing what's lost: a new era of stem cell therapy for Parkinson's disease. *Transl Neurodegener* **9**, 2, doi:10.1186/s40035-019-0180-x (2020).
97 Freed, C. R. *et al.* Transplantation of embryonic dopamine neurons for severe Parkinson's disease. *N Engl J Med* **344**, 710-719, doi:10.1056/nejm200103083441002 (2001).
98 Olanow, C. W. *et al.* A double-blind controlled trial of bilateral fetal nigral transplantation in Parkinson's disease. *Ann Neurol* **54**, 403-414, doi:10.1002/ana.10720 (2003).
99 Hallett, P. J. *et al.* Long-term health of dopaminergic neuron transplants in Parkinson's disease patients. *Cell Rep* **7**, 1755-1761, doi:10.1016/j.celrep.2014.05.027 (2014).
100 Kriks, S. *et al.* Dopamine neurons derived from human ES cells efficiently engraft in animal models of Parkinson's disease. *Nature* **480**, 547-551, doi:10.1038/nature10648 (2011).
101 Schweitzer, J. S. *et al.* Personalized iPSC-Derived Dopamine Progenitor Cells for Parkinson's Disease. *N Engl J Med* **382**, 1926-1932, doi:10.1056/NEJMoa1915872 (2020).
102 Lees, A. J., Hardy, J. & Revesz, T. Parkinson's disease. *Lancet* **373**, 2055-2066, doi:10.1016/s0140-6736(09)60492-x (2009).
103 Fereshtehnejad, S. M., Zeighami, Y., Dagher, A. & Postuma, R. B. Clinical criteria for subtyping Parkinson's disease: biomarkers and longitudinal progression. *Brain* **140**, 1959-1976, doi:10.1093/brain/awx118 (2017).
104 De Pablo-Fernández, E., Lees, A. J., Holton, J. L. & Warner, T. T. Prognosis and Neuropathologic Correlation of Clinical Subtypes of Parkinson Disease. *JAMA Neurol* **76**, 470-479, doi:10.1001/jamaneurol.2018.4377 (2019).
105 Corti, O., Lesage, S. & Brice, A. What genetics tells us about the causes and mechanisms of Parkinson's disease. *Physiol Rev* **91**, 1161-1218, doi:10.1152/physrev.00022.2010 (2011).
106 Kitada, T., Tomlinson, J. J., Ao, H. S., Grimes, D. A. & Schlossmacher, M. G. Considerations regarding the etiology and future treatment of autosomal recessive versus idiopathic Parkinson disease. *Current treatment options in neurology* **14**, 230-240, doi:10.1007/s11940-012-0175-8 (2012).
107 Kouli, A., Torsney, K. M. & Kuan, W. L. in *Parkinson's Disease: Pathogenesis and Clinical Aspects* (eds T. B. Stoker & J. C. Greenland) (Codon Publications Copyright: The Authors., 2018).

108 Poskanzer, D. C. & Schwab, R. S. COHORT ANALYSIS OF PARKINSON'S SYNDROME: EVIDENCE FOR A SINGLE ETIOLOGY RELATED TO SUBCLINICAL INFECTION ABOUT 1920. *Journal of chronic diseases* **16**, 961-973, doi:10.1016/0021-9681(63)90098-5 (1963).

109 Langston, J. W., Ballard, P., Tetrud, J. W. & Irwin, I. Chronic Parkinsonism in humans due to a product of meperidine-analog synthesis. *Science* **219**, 979-980 (1983).

110 Langston, J. W., Irwin, I., Langston, E. B. & Forno, L. S. 1-Methyl-4-phenylpyridinium ion (MPP+): identification of a metabolite of MPTP, a toxin selective to the substantia nigra. *Neurosci Lett* **48**, 87-92, doi:10.1016/0304-3940(84)90293-3 (1984).

111 Singer, T. P. & Ramsay, R. R. Mechanism of the neurotoxicity of MPTP. An update. *FEBS Lett* **274**, 1-8, doi:10.1016/0014-5793(90)81315-f (1990).

112 Heinz, S. *et al.* Mechanistic Investigations of the Mitochondrial Complex I Inhibitor Rotenone in the Context of Pharmacological and Safety Evaluation. *Scientific Reports* **7**, 45465, doi:10.1038/srep45465 (2017).

113 Janetzky, B. *et al.* Unaltered aconitase activity, but decreased complex I activity in substantia nigra pars compacta of patients with Parkinson's disease. *Neurosci Lett* **169**, 126-128, doi:10.1016/0304-3940(94)90372-7 (1994).

114 Mann, V. M. *et al.* Brain, skeletal muscle and platelet homogenate mitochondrial function in Parkinson's disease. *Brain* **115 (Pt 2)**, 333-342, doi:10.1093/brain/115.2.333 (1992).

115 Keeney, P. M., Xie, J., Capaldi, R. A. & Bennett, J. P., Jr. Parkinson's disease brain mitochondrial complex I has oxidatively damaged subunits and is functionally impaired and misassembled. *J Neurosci* **26**, 5256-5264, doi:10.1523/jneurosci.0984-06.2006 (2006).

116 Parker, W. D., Jr., Parks, J. K. & Swerdlow, R. H. Complex I deficiency in Parkinson's disease frontal cortex. *Brain Res* **1189**, 215-218, doi:10.1016/j.brainres.2007.10.061 (2008).

117 Haas, R. H. *et al.* Low platelet mitochondrial complex I and complex II/III activity in early untreated Parkinson's disease. *Ann Neurol* **37**, 714-722, doi:10.1002/ana.410370604 (1995).

118 Krige, D., Carroll, M. T., Cooper, J. M., Marsden, C. D. & Schapira, A. H. Platelet mitochondrial function in Parkinson's disease. The Royal Kings and Queens Parkinson Disease Research Group. *Ann Neurol* **32**, 782-788, doi:10.1002/ana.410320612 (1992).

119 International Parkinson Disease Genomics, C. *et al.* Imputation of sequence variants for identification of genetic risks for Parkinson's disease: a meta-analysis of genome-wide association studies. *Lancet* **377**, 641-649, doi:10.1016/S0140-6736(10)62345-8 (2011).

120 Nalls, M. A. *et al.* Large-scale meta-analysis of genome-wide association data identifies six new risk loci for Parkinson's disease. *Nat Genet* **46**, 989-993, doi:10.1038/ng.3043 (2014).

121 Schrag, A., Anastasiou, Z., Ambler, G., Noyce, A. & Walters, K. Predicting diagnosis of Parkinson's disease: A risk algorithm based on primary care presentations. *Mov Disord* **34**, 480-486, doi:10.1002/mds.27616 (2019).

122 Ahmadi Rastegar, D., Ho, N., Halliday, G. M. & Dzamko, N. Parkinson's progression prediction using machine learning and serum cytokines. *npj Parkinson's Disease* **5**, 14, doi:10.1038/s41531-019-0086-4 (2019).

123 Schlossmacher, M. G. *et al.* Modelling idiopathic Parkinson disease as a complex illness can inform incidence rate in healthy adults: the PR EDIGT score. *Eur J Neurosci* **45**, 175-191, doi:10.1111/ejn.13476 (2017).

124 Marras, C. *et al.* Nomenclature of genetic movement disorders: Recommendations of the International Parkinson and Movement Disorder Society task force. *Mov Disord* **32**, 724-725, doi:10.1002/mds.27045 (2017).

125 Polymeropoulos, M. H. *et al.* Mutation in the alpha-synuclein gene identified in families with Parkinson's disease. *Science* **276**, 2045-2047 (1997).

126 Polymeropoulos, M. H. *et al.* Mapping of a gene for Parkinson's disease to chromosome 4q21-q23. *Science* **274**, 1197-1199, doi:10.1126/science.274.5290.1197 (1996).

127 Krüger, R. *et al.* Familial parkinsonism with synuclein pathology: clinical and PET studies of A30P mutation carriers. *Neurology* **56**, 1355-1362, doi:10.1212/wnl.56.10.1355 (2001).

128 Ibáñez, P. *et al.* Alpha-synuclein gene rearrangements in dominantly inherited parkinsonism: frequency, phenotype, and mechanisms. *Arch Neurol* **66**, 102-108, doi:10.1001/archneurol.2008.555 (2009).

129 Ikeuchi, T. *et al.* Patients homozygous and heterozygous for SNCA duplication in a family with parkinsonism and dementia. *Arch Neurol* **65**, 514-519 (2008).

130 Ross, O. A. *et al.* Genomic investigation of alpha-synuclein multiplication and parkinsonism. *Ann Neurol* **63**, 743-750 (2008).

131 Fortin, D. L. *et al.* Lipid rafts mediate the synaptic localization of alpha-synuclein. *J Neurosci* **24**, 6715-6723, doi:10.1523/jneurosci.1594-04.2004 (2004).

132 Giasson, B. I., Murray, I. V., Trojanowski, J. Q. & Lee, V. M. A hydrophobic stretch of 12 amino acid residues in the middle of alpha-synuclein is essential for filament assembly. *J Biol Chem* **276**, 2380-2386, doi:10.1074/jbc.M008919200 (2001).

133 Nemani, V. M. *et al.* Increased expression of alpha-synuclein reduces neurotransmitter release by inhibiting synaptic vesicle reclustering after endocytosis. *Neuron* **65**, 66-79, doi:10.1016/j.neuron.2009.12.023 (2010).
134 Larsen, K. E. *et al.* Alpha-synuclein overexpression in PC12 and chromaffin cells impairs catecholamine release by interfering with a late step in exocytosis. *J Neurosci* **26**, 11915-11922, doi:10.1523/jneurosci.3821-06.2006 (2006).
135 Perez, R. G. *et al.* A role for alpha-synuclein in the regulation of dopamine biosynthesis. *J Neurosci* **22**, 3090-3099, doi:20026307 (2002).
136 Peng, X., Tehranian, R., Dietrich, P., Stefanis, L. & Perez, R. G. Alpha-synuclein activation of protein phosphatase 2A reduces tyrosine hydroxylase phosphorylation in dopaminergic cells. *J Cell Sci* **118**, 3523-3530, doi:10.1242/jcs.02481 (2005).
137 Watson, M. B. *et al.* Regionally-specific microglial activation in young mice over-expressing human wildtype alpha-synuclein. *Exp Neurol* **237**, 318-334, doi:10.1016/j.expneurol.2012.06.025 (2012).
138 Kim, C. *et al.* Neuron-released oligomeric alpha-synuclein is an endogenous agonist of TLR2 for paracrine activation of microglia. *Nat Commun* **4**, 1562, doi:10.1038/ncomms2534 (2013).
139 Funayama, M. *et al.* A new locus for Parkinson's disease (PARK8) maps to chromosome 12p11.2-q13.1. *Ann Neurol* **51**, 296-301, doi:10.1002/ana.10113 (2002).
140 Lesage, S. *et al.* Molecular analyses of the LRRK2 gene in European and North African autosomal dominant Parkinson's disease. *Journal of medical genetics* **46**, 458-464, doi:10.1136/jmg.2008.062612 (2009).
141 Nuytemans, K., Theuns, J., Cruts, M. & Van Broeckhoven, C. Genetic etiology of Parkinson disease associated with mutations in the SNCA, PARK2, PINK1, PARK7, and LRRK2 genes: a mutation update. *Human mutation* **31**, 763-780, doi:10.1002/humu.21277 (2010).
142 Zimprich, A. *et al.* Mutations in LRRK2 cause autosomal-dominant parkinsonism with pleomorphic pathology. *Neuron* **44**, 601-607 (2004).
143 Rajput, A. *et al.* Parkinsonism, Lrrk2 G2019S, and tau neuropathology. *Neurology* **67**, 1506-1508, doi:10.1212/01.wnl.0000240220.33950.0c (2006).
144 Kalia, L. V. *et al.* Clinical correlations with Lewy body pathology in LRRK2-related Parkinson disease. *JAMA Neurol* **72**, 100-105, doi:10.1001/jamaneurol.2014.2704 (2015).
145 Mata, I. F., Wedemeyer, W. J., Farrer, M. J., Taylor, J. P. & Gallo, K. A. LRRK2 in Parkinson's disease: protein domains and functional insights. *Trends Neurosci* **29**, 286-293, doi:10.1016/j.tins.2006.03.006 (2006).
146 Aasly, J. O. *et al.* Novel pathogenic LRRK2 p.Asn1437His substitution in familial Parkinson's disease. *Movement disorders : official journal of the Movement Disorder Society* **25**, 2156-2163, doi:10.1002/mds.23265 (2010).
147 Healy, D. G. *et al.* Phenotype, genotype, and worldwide genetic penetrance of LRRK2-associated Parkinson's disease: a case-control study. *Lancet Neurol* **7**, 583-590, doi:10.1016/s1474-4422(08)70117-0 (2008).
148 Ramonet, D. *et al.* Dopaminergic neuronal loss, reduced neurite complexity and autophagic abnormalities in transgenic mice expressing G2019S mutant LRRK2. *PLoS One* **6**, e18568, doi:10.1371/journal.pone.0018568 (2011).
149 Hakimi, M. *et al.* Parkinson's disease-linked LRRK2 is expressed in circulating and tissue immune cells and upregulated following recognition of microbial structures. *J Neural Transm* **118**, 795-808, doi:10.1007/s00702-011-0653-2 (2011).
150 Moehle, M. S. *et al.* LRRK2 inhibition attenuates microglial inflammatory responses. *J Neurosci* **32**, 1602-1611, doi:10.1523/JNEUROSCI.5601-11.2012 (2012).
151 Gillardon, F., Schmid, R. & Draheim, H. Parkinson's disease-linked leucine-rich repeat kinase 2(R1441G) mutation increases proinflammatory cytokine release from activated primary microglial cells and resultant neurotoxicity. *Neuroscience* **208**, 41-48, doi:10.1016/j.neuroscience.2012.02.001 (2012).
152 Shutinoski, B. *et al.* Lrrk2 alleles modulate inflammation during microbial infection of mice in a sex-dependent manner. *Sci Transl Med* **11**, doi:10.1126/scitranslmed.aas9292 (2019).
153 Lücking, C. B. *et al.* Association between early-onset Parkinson's disease and mutations in the parkin gene. *N Engl J Med* **342**, 1560-1567, doi:10.1056/nejm200005253422103 (2000).
154 Klein, C. & Westenberger, A. Genetics of Parkinson's disease. *Cold Spring Harb Perspect Med* **2**, a008888, doi:10.1101/cshperspect.a008888 (2012).
155 Hernandez, D. G., Reed, X. & Singleton, A. B. Genetics in Parkinson disease: Mendelian versus non-Mendelian inheritance. *J Neurochem* **139 Suppl 1**, 59-74, doi:10.1111/jnc.13593 (2016).
156 Koros, C., Simitsi, A. & Stefanis, L. Genetics of Parkinson's Disease: Genotype-Phenotype Correlations. *Int Rev Neurobiol* **132**, 197-231, doi:10.1016/bs.irn.2017.01.009 (2017).
157 Ahlskog, J. E. Parkin and PINK1 parkinsonism may represent nigral mitochondrial cytopathies distinct from Lewy body Parkinson's disease. *Parkinsonism & related disorders* **15**, 721-727, doi:10.1016/j.parkreldis.2009.09.010 (2009).

158 McNally, R. S. *et al.* DJ-1 enhances cell survival through the binding of Cezanne, a negative regulator of NF-kappaB. *J Biol Chem* **286**, 4098-4106, doi:10.1074/jbc.M110.147371 (2011).
159 Niki, T., Takahashi-Niki, K., Taira, T., Iguchi-Ariga, S. M. & Ariga, H. DJBP: a novel DJ-1-binding protein, negatively regulates the androgen receptor by recruiting histone deacetylase complex, and DJ-1 antagonizes this inhibition by abrogation of this complex. *Molecular cancer research : MCR* **1**, 247-261 (2003).
160 Bonifati, V. *et al.* Mutations in the DJ-1 gene associated with autosomal recessive early-onset parkinsonism. *Science* **299**, 256-259, doi:10.1126/science.1077209 (2003).
161 van Duijn, C. M. *et al.* Park7, a novel locus for autosomal recessive early-onset parkinsonism, on chromosome 1p36. *American journal of human genetics* **69**, 629-634, doi:10.1086/322996 (2001).
162 Abou-Sleiman, P. M., Healy, D. G., Quinn, N., Lees, A. J. & Wood, N. W. The role of pathogenic DJ-1 mutations in Parkinson's disease. *Ann Neurol* **54**, 283-286, doi:10.1002/ana.10675 (2003).
163 Taipa, R. *et al.* DJ-1 linked parkinsonism (PARK7) is associated with Lewy body pathology. *Brain* **139**, 1680-1687, doi:10.1093/brain/aww080 (2016).
164 Miller, D. W. *et al.* L166P mutant DJ-1, causative for recessive Parkinson's disease, is degraded through the ubiquitin-proteasome system. *J Biol Chem* **278**, 36588-36595 (2003).
165 Moore, D. J., Zhang, L., Dawson, T. M. & Dawson, V. L. A missense mutation (L166P) in DJ-1, linked to familial Parkinson's disease, confers reduced protein stability and impairs homo-oligomerization. *J Neurochem* **87**, 1558-1567, doi:10.1111/j.1471-4159.2003.02265.x (2003).
166 Taira, T. *et al.* DJ-1 has a role in antioxidative stress to prevent cell death. *EMBO Rep* **5**, 213-218, doi:10.1038/sj.embor.7400074 (2004).
167 Clements, C. M., McNally, R. S., Conti, B. J., Mak, T. W. & Ting, J. P. DJ-1, a cancer- and Parkinson's disease-associated protein, stabilizes the antioxidant transcriptional master regulator Nrf2. *Proc Natl Acad Sci U S A* **103**, 15091-15096, doi:10.1073/pnas.0607260103 (2006).
168 Andres-Mateos, E. *et al.* DJ-1 gene deletion reveals that DJ-1 is an atypical peroxiredoxin-like peroxidase. *Proc Natl Acad Sci U S A* **104**, 14807-14812, doi:10.1073/pnas.0703219104 (2007).
169 Mitsumoto, A. *et al.* Oxidized forms of peroxiredoxins and DJ-1 on two-dimensional gels increased in response to sublethal levels of paraquat. *Free radical research* **35**, 301-310, doi:10.1080/10715760100300831 (2001).
170 Miyama, A. *et al.* Oxidation of DJ-1 Induced by 6-Hydroxydopamine Decreasing Intracellular Glutathione. *PLOS ONE* **6**, e27883, doi:10.1371/journal.pone.0027883 (2011).
171 Canet-Aviles, R. M. *et al.* The Parkinson's disease protein DJ-1 is neuroprotective due to cysteine-sulfinic acid-driven mitochondrial localization. *Proc Natl Acad Sci U S A* **101**, 9103-9108, doi:10.1073/pnas.0402959101 (2004).
172 O'Flanagan, C. H., Morais, V. A., Wurst, W., De Strooper, B. & O'Neill, C. The Parkinson's gene PINK1 regulates cell cycle progression and promotes cancer-associated phenotypes. *Oncogene* **34**, 1363-1374, doi:10.1038/onc.2014.81 (2015).
173 Yamano, K. & Youle, R. J. PINK1 is degraded through the N-end rule pathway. *Autophagy* **9**, 1758-1769, doi:10.4161/auto.24633 (2013).
174 Beilina, A. *et al.* Mutations in PTEN-induced putative kinase 1 associated with recessive parkinsonism have differential effects on protein stability. *Proc Natl Acad Sci U S A* **102**, 5703-5708, doi:10.1073/pnas.0500617102 (2005).
175 Marongiu, R. *et al.* PINK1 heterozygous rare variants: prevalence, significance and phenotypic spectrum. *Hum Mutat* **29**, 565, doi:10.1002/humu.20719 (2008).
176 Valente, E. M. *et al.* Hereditary early-onset Parkinson's disease caused by mutations in PINK1. *Science* **304**, 1158-1160, doi:10.1126/science.1096284 (2004).
177 Abou-Sleiman, P. M. *et al.* A heterozygous effect for PINK1 mutations in Parkinson's disease? *Ann Neurol* **60**, 414-419, doi:10.1002/ana.20960 (2006).
178 Klein, C., Lohmann-Hedrich, K., Rogaeva, E., Schlossmacher, M. G. & Lang, A. E. Deciphering the role of heterozygous mutations in genes associated with parkinsonism. *Lancet Neurol* **6**, 652-662 (2007).
179 Ibáñez, P. *et al.* Mutational analysis of the PINK1 gene in early-onset parkinsonism in Europe and North Africa. *Brain* **129**, 686-694, doi:10.1093/brain/awl005 (2006).
180 Samaranch, L. *et al.* PINK1-linked parkinsonism is associated with Lewy body pathology. *Brain* **133**, 1128-1142, doi:10.1093/brain/awq051 (2010).
181 Tuin, I. *et al.* Sleep quality in a family with hereditary parkinsonism (PARK6). *Sleep Med* **9**, 684-688, doi:10.1016/j.sleep.2007.07.004 (2008).
182 Voigt, A., Berlemann, L. A. & Winklhofer, K. F. The mitochondrial kinase PINK1: functions beyond mitophagy. *J Neurochem* **139 Suppl 1**, 232-239, doi:10.1111/jnc.13655 (2016).

183 Park, J. *et al.* Mitochondrial dysfunction in Drosophila PINK1 mutants is complemented by parkin. *Nature* **441**, 1157-1161, doi:10.1038/nature04788 (2006).
184 Kitada, T. *et al.* Mutations in the parkin gene cause autosomal recessive juvenile parkinsonism. *Nature* **392**, 605-608, doi:10.1038/33416 (1998).
185 Khan, N. L. *et al.* Parkin disease: a phenotypic study of a large case series. *Brain* **126**, 1279-1292, doi:10.1093/brain/awg142 (2003).
186 Kubo, S.-I., Hattori, N. & Mizuno, Y. Recessive Parkinson's disease. *Movement Disorders* **21**, 885-893, doi:10.1002/mds.20841 (2006).
187 Lincoln, S. J. *et al.* Parkin variants in North American Parkinson's disease: cases and controls. *Mov Disord* **18**, 1306-1311, doi:10.1002/mds.10601 (2003).
188 Valente, E. M. & Ferraris, A. Heterozygous mutations in genes causing parkinsonism: monogenic disorders go complex. *Lancet Neurol* **6**, 576-578, doi:10.1016/s1474-4422(07)70158-8 (2007).
189 Klein, C. *et al.* Frequency of parkin mutations in late-onset Parkinson's disease. *Annals of Neurology* **54**, 415-416, doi:10.1002/ana.10737 (2003).
190 West, A. B. *et al.* Functional association of the parkin gene promoter with idiopathic Parkinson's disease. *Hum Mol Genet* **11**, 2787-2792, doi:10.1093/hmg/11.22.2787 (2002).
191 Huttenlocher, J. *et al.* Heterozygote carriers for CNVs in PARK2 are at increased risk of Parkinson's disease. *Hum Mol Genet* **24**, 5637-5643, doi:10.1093/hmg/ddv277 (2015).
192 Wauer, T. & Komander, D. Structure of the human Parkin ligase domain in an autoinhibited state. *EMBO J* **32**, 2099-2112, doi:10.1038/emboj.2013.125 (2013).
193 Spratt, D. E. *et al.* A molecular explanation for the recessive nature of parkin-linked Parkinson's disease. *Nat Commun* **4**, 1983, doi:10.1038/ncomms2983 (2013).
194 Lucking, C. B. *et al.* Association between early-onset Parkinson's disease and mutations in the parkin gene. *N Engl J Med* **342**, 1560-1567, doi:10.1056/NEJM200005253422103 (2000).
195 Takahashi, H. *et al.* Familial juvenile parkinsonism: clinical and pathologic study in a family. *Neurology* **44**, 437-441, doi:10.1212/wnl.44.3_part_1.437 (1994).
196 Farrer, M. *et al.* Lewy bodies and parkinsonism in families with parkin mutations. *Ann Neurol* **50**, 293-300 (2001).
197 Yokochi, M., Narabayashi, H., Iizuka, R. & Nagatsu, T. Juvenile parkinsonism--some clinical, pharmacological, and neuropathological aspects. *Adv Neurol* **40**, 407-413 (1984).
198 Khan, N. L. *et al.* Olfaction differentiates parkin disease from early-onset parkinsonism and Parkinson disease. *Neurology* **62**, 1224-1226, doi:10.1212/01.wnl.0000118281.66802.81 (2004).
199 Alcalay, R. N. *et al.* Olfaction in Parkin heterozygotes and compound heterozygotes: the CORE-PD study. *Neurology* **76**, 319-326, doi:10.1212/WNL.0b013e31820882aa (2011).
200 Malek, N. *et al.* Olfaction in Parkin single and compound heterozygotes in a cohort of young onset Parkinson's disease patients. *Acta neurologica Scandinavica* **134**, 271-276, doi:10.1111/ane.12538 (2016).
201 Lee, W. W. & Jeon, B. S. Clinical spectrum of dopa-responsive dystonia and related disorders. *Curr Neurol Neurosci Rep* **14**, 461, doi:10.1007/s11910-014-0461-9 (2014).
202 Thöny, B., Auerbach, G. & Blau, N. Tetrahydrobiopterin biosynthesis, regeneration and functions. *Biochem J* **347 Pt 1**, 1-16 (2000).
203 van den Heuvel, L. P. *et al.* A common point mutation in the tyrosine hydroxylase gene in autosomal recessive L-DOPA-responsive dystonia in the Dutch population. *Human genetics* **102**, 644-646, doi:10.1007/s004390050756 (1998).
204 Rengmark, A., Pihlstrøm, L., Linder, J., Forsgren, L. & Toft, M. Low frequency of GCH1 and TH mutations in Parkinson's disease. *Parkinsonism Relat Disord* **29**, 109-111, doi:10.1016/j.parkreldis.2016.05.010 (2016).
205 Mencacci, N. E. *et al.* Parkinson's disease in GTP cyclohydrolase 1 mutation carriers. *Brain* **137**, 2480-2492, doi:10.1093/brain/awu179 (2014).
206 Eggers, C. *et al.* Are Dopa-responsive dystonia and Parkinson's disease related disorders? A case report. *Parkinsonism Relat Disord* **18**, 666-668, doi:10.1016/j.parkreldis.2011.10.003 (2012).
207 Pramstaller, P. P. *et al.* Lewy body Parkinson's disease in a large pedigree with 77 Parkin mutation carriers. *Ann Neurol* **58**, 411-422, doi:10.1002/ana.20587 (2005).
208 Ramirez, A. *et al.* Hereditary parkinsonism with dementia is caused by mutations in ATP13A2, encoding a lysosomal type 5 P-type ATPase. *Nat Genet* **38**, 1184-1191, doi:10.1038/ng1884 (2006).
209 Santoro, L. *et al.* Novel ATP13A2 (PARK9) homozygous mutation in a family with marked phenotype variability. *Neurogenetics* **12**, 33-39, doi:10.1007/s10048-010-0259-0 (2011).
210 Di Fonzo, A. *et al.* ATP13A2 missense mutations in juvenile parkinsonism and young onset Parkinson disease. *Neurology* **68**, 1557-1562, doi:10.1212/01.wnl.0000260963.08711.08 (2007).

211 Khateeb, S. *et al.* PLA2G6 mutation underlies infantile neuroaxonal dystrophy. *Am J Hum Genet* **79**, 942-948, doi:10.1086/508572 (2006).
212 Morgan, N. V. *et al.* PLA2G6, encoding a phospholipase A2, is mutated in neurodegenerative disorders with high brain iron. *Nat Genet* **38**, 752-754, doi:10.1038/ng1826 (2006).
213 Paisán-Ruiz, C. *et al.* Widespread Lewy body and tau accumulation in childhood and adult onset dystonia-parkinsonism cases with PLA2G6 mutations. *Neurobiology of aging* **33**, 814-823, doi:10.1016/j.neurobiolaging.2010.05.009 (2012).
214 Yoshino, H. *et al.* Phenotypic spectrum of patients with PLA2G6 mutation and PARK14-linked parkinsonism. *Neurology* **75**, 1356-1361, doi:10.1212/WNL.0b013e3181f73649 (2010).
215 Di Fonzo, A. *et al.* FBXO7 mutations cause autosomal recessive, early-onset parkinsonian-pyramidal syndrome. *Neurology* **72**, 240-245, doi:10.1212/01.wnl.0000338144.10967.2b (2009).
216 Shojaee, S. *et al.* Genome-wide linkage analysis of a Parkinsonian-pyramidal syndrome pedigree by 500 K SNP arrays. *Am J Hum Genet* **82**, 1375-1384, doi:10.1016/j.ajhg.2008.05.005 (2008).
217 Davison, C. Pallido-pyramidal disease. *J Neuropathol Exp Neurol* **13**, 50-59, doi:10.1097/00005072-195401000-00007 (1954).
218 Malakouti-Nejad, M. *et al.* Identification of p.Gln858* in ATP13A2 in two EOPD patients and presentation of their clinical features. *Neurosci Lett* **577**, 106-111, doi:10.1016/j.neulet.2014.06.023 (2014).
219 Paisán-Ruiz, C. *et al.* Early-onset L-dopa-responsive parkinsonism with pyramidal signs due to ATP13A2, PLA2G6, FBXO7 and spatacsin mutations. *Movement disorders : official journal of the Movement Disorder Society* **25**, 1791-1800, doi:10.1002/mds.23221 (2010).
220 Shi, C. H. *et al.* PLA2G6 gene mutation in autosomal recessive early-onset parkinsonism in a Chinese cohort. *Neurology* **77**, 75-81, doi:10.1212/WNL.0b013e318221acd3 (2011).
221 Zhao, T. *et al.* Loss of nuclear activity of the FBXO7 protein in patients with parkinsonian-pyramidal syndrome (PARK15). *PLoS One* **6**, e16983, doi:10.1371/journal.pone.0016983 (2011).
222 Sidransky, E. *et al.* Multicenter analysis of glucocerebrosidase mutations in Parkinson's disease. *N Engl J Med* **361**, 1651-1661, doi:10.1056/NEJMoa0901281 (2009).
223 Grabowski, G. A. Phenotype, diagnosis, and treatment of Gaucher's disease. *Lancet* **372**, 1263-1271, doi:10.1016/s0140-6736(08)61522-6 (2008).
224 Goker-Alpan, O. *et al.* The spectrum of parkinsonian manifestations associated with glucocerebrosidase mutations. *Arch Neurol* **65**, 1353-1357, doi:10.1001/archneur.65.10.1353 (2008).
225 Machaczka, M., Rucinska, M., Skotnicki, A. B. & Jurczak, W. Parkinson's syndrome preceding clinical manifestation of Gaucher's disease. *American journal of hematology* **61**, 216-217, doi:10.1002/(sici)1096-8652(199907)61:3<216::aid-ajh12>3.0.co;2-b (1999).
226 Tayebi, N. *et al.* Gaucher Disease and Parkinsonism: A Phenotypic and Genotypic Characterization. *Molecular Genetics and Metabolism* **73**, 313-321, doi:10.1006/mgme.2001.3201 (2001).
227 Tayebi, N. *et al.* Gaucher disease with parkinsonian manifestations: does glucocerebrosidase deficiency contribute to a vulnerability to parkinsonism? *Molecular genetics and metabolism* **79**, 104-109 (2003).
228 Liu, G. *et al.* Prediction of cognition in Parkinson's disease with a clinical-genetic score: a longitudinal analysis of nine cohorts. *Lancet Neurol* **16**, 620-629, doi:10.1016/s1474-4422(17)30122-9 (2017).
229 Geiger, J. T. *et al.* Next-generation sequencing reveals substantial genetic contribution to dementia with Lewy bodies. *Neurobiology of disease* **94**, 55-62, doi:10.1016/j.nbd.2016.06.004 (2016).
230 Shiner, T. *et al.* High Frequency of GBA Gene Mutations in Dementia With Lewy Bodies Among Ashkenazi Jews. *JAMA Neurol* **73**, 1448-1453, doi:10.1001/jamaneurol.2016.1593 (2016).
231 Sardi, S. P., Singh, P., Cheng, S. H., Shihabuddin, L. S. & Schlossmacher, M. G. Mutant GBA1 expression and synucleinopathy risk: first insights from cellular and mouse models. *Neurodegener Dis* **10**, 195-202, doi:10.1159/000335038 (2012).
232 Cullen, V. *et al.* Acid beta-glucosidase mutants linked to Gaucher disease, Parkinson disease, and Lewy body dementia alter alpha-synuclein processing. *Ann Neurol* **69**, 940-953 (2011).
233 Mazzulli, J. R. *et al.* Gaucher disease glucocerebrosidase and alpha-synuclein form a bidirectional pathogenic loop in synucleinopathies. *Cell* **146**, 37-52, doi:10.1016/j.cell.2011.06.001 (2011).
234 Bonifati, V. Genetics of Parkinson's disease--state of the art, 2013. *Parkinsonism Relat Disord* **20 Suppl 1**, S23-28, doi:10.1016/s1353-8020(13)70009-9 (2014).
235 Bento, C. F., Ashkenazi, A., Jimenez-Sanchez, M. & Rubinsztein, D. C. The Parkinson's disease-associated genes ATP13A2 and SYT11 regulate autophagy via a common pathway. *Nature Communications* **7**, 11803, doi:10.1038/ncomms11803 (2016).

236 Burton, T. D., Fedele, A. O., Xie, J., Sandeman, L. Y. & Proud, C. G. The gene for the lysosomal protein LAMP3 is a direct target of the transcription factor ATF4. *J Biol Chem* **295**, 7418-7430, doi:10.1074/jbc.RA119.011864 (2020).
237 Reczek, D. *et al.* LIMP-2 is a receptor for lysosomal mannose-6-phosphate-independent targeting of beta-glucocerebrosidase. *Cell* **131**, 770-783, doi:10.1016/j.cell.2007.10.018 (2007).
238 Wang, S. *et al.* A Role of Rab29 in the Integrity of the Trans-Golgi Network and Retrograde Trafficking of Mannose-6-Phosphate Receptor. *PLOS ONE* **9**, e96242, doi:10.1371/journal.pone.0096242 (2014).
239 Parplys, A. C. *et al.* NUCKS1 is a novel RAD51AP1 paralog important for homologous recombination and genome stability. *Nucleic acids research* **43**, 9817-9834, doi:10.1093/nar/gkv859 (2015).
240 Sanchez, V. B., Ali, S., Escobar, A. & Cuajungco, M. P. Transmembrane 163 (TMEM163) protein effluxes zinc. *Arch Biochem Biophys* **677**, 108166, doi:10.1016/j.abb.2019.108166 (2019).
241 Johnston, A. M. *et al.* SPAK, a STE20/SPS1-related kinase that activates the p38 pathway. *Oncogene* **19**, 4290-4297, doi:10.1038/sj.onc.1203784 (2000).
242 Chu, C. H. & Cheng, D. Expression, purification, characterization of human 3-methylcrotonyl-CoA carboxylase (MCCC). *Protein expression and purification* **53**, 421-427, doi:10.1016/j.pep.2007.01.012 (2007).
243 Cang, C., Aranda, K., Seo, Y. J., Gasnier, B. & Ren, D. TMEM175 Is an Organelle K(+) Channel Regulating Lysosomal Function. *Cell* **162**, 1101-1112, doi:10.1016/j.cell.2015.08.002 (2015).
244 Zhang, L., Gjoerup, O. & Roberts, T. M. The serine/threonine kinase cyclin G-associated kinase regulates epidermal growth factor receptor signaling. *Proc Natl Acad Sci U S A* **101**, 10296-10301, doi:10.1073/pnas.0403175101 (2004).
245 Zhang, W., Swanson, R., Xiong, Y., Richard, B. & Olson, S. T. Antiangiogenic antithrombin blocks the heparan sulfate-dependent binding of proangiogenic growth factors to their endothelial cell receptors: evidence for differential binding of antiangiogenic and anticoagulant forms of antithrombin to proangiogenic heparan sulfate domains. *J Biol Chem* **281**, 37302-37310, doi:10.1074/jbc.M604905200 (2006).
246 Yamamoto-Katayama, S. *et al.* Crystallographic studies on human BST-1/CD157 with ADP-ribosyl cyclase and NAD glycohydrolase activities. *J Mol Biol* **316**, 711-723, doi:10.1006/jmbi.2001.5386 (2002).
247 Li, D. *et al.* Cyclic AMP-stimulated interaction between steroidogenic factor 1 and diacylglycerol kinase theta facilitates induction of CYP17. *Mol Cell Biol* **27**, 6669-6685, doi:10.1128/mcb.00355-07 (2007).
248 Hsu, F., Hu, F. & Mao, Y. Spatiotemporal control of phosphatidylinositol 4-phosphate by Sac2 regulates endocytic recycling. *J Cell Biol* **209**, 97-110, doi:10.1083/jcb.201408027 (2015).
249 Kim, H. S., Li, A., Ahn, S., Song, H. & Zhang, W. Inositol Polyphosphate-5-Phosphatase F (INPP5F) inhibits STAT3 activity and suppresses gliomas tumorigenicity. *Sci Rep* **4**, 7330, doi:10.1038/srep07330 (2014).
250 Chen, C. M. *et al.* Association of GCH1 and MIR4697, but not SIPA1L2 and VPS13C polymorphisms, with Parkinson's disease in Taiwan. *Neurobiol Aging* **39**, 221.e221-225, doi:10.1016/j.neurobiolaging.2015.12.016 (2016).
251 Wallings, R., Manzoni, C. & Bandopadhyay, R. Cellular processes associated with LRRK2 function and dysfunction. *Febs j* **282**, 2806-2826, doi:10.1111/febs.13305 (2015).
252 Chen, M. *et al.* CCDC62/ERAP75 functions as a coactivator to enhance estrogen receptor beta-mediated transactivation and target gene expression in prostate cancer cells. *Carcinogenesis* **30**, 841-850, doi:10.1093/carcin/bgn288 (2009).
253 Hyun, T. S. *et al.* HIP1 and HIP1r stabilize receptor tyrosine kinases and bind 3-phosphoinositides via epsin N-terminal homology domains. *J Biol Chem* **279**, 14294-14306, doi:10.1074/jbc.M312645200 (2004).
254 Kumar, N. *et al.* VPS13A and VPS13C are lipid transport proteins differentially localized at ER contact sites. *J Cell Biol* **217**, 3625-3639, doi:10.1083/jcb.201807019 (2018).
255 García-Cazorla, A. *et al.* Two novel mutations in the BCKDK (branched-chain keto-acid dehydrogenase kinase) gene are responsible for a neurobehavioral deficit in two pediatric unrelated patients. *Hum Mutat* **35**, 470-477, doi:10.1002/humu.22513 (2014).
256 Mishima, T. *et al.* Syntaxin 1B, but not syntaxin 1A, is necessary for the regulation of synaptic vesicle exocytosis and of the readily releasable pool at central synapses. *PLoS One* **9**, e90004, doi:10.1371/journal.pone.0090004 (2014).
257 Bertolio, R. *et al.* Sterol regulatory element binding protein 1 couples mechanical cues and lipid metabolism. *Nat Commun* **10**, 1326, doi:10.1038/s41467-019-09152-7 (2019).
258 Williams, S. R., Zies, D., Mullegama, S. V., Grotewiel, M. S. & Elsea, S. H. Smith-Magenis syndrome results in disruption of CLOCK gene transcription and reveals an integral role for RAI1 in the maintenance of circadian rhythmicity. *Am J Hum Genet* **90**, 941-949, doi:10.1016/j.ajhg.2012.04.013 (2012).

259 Yoshida, H. & Goedert, M. Phosphorylation of microtubule-associated protein tau by AMPK-related kinases. *J Neurochem* **120**, 165-176, doi:10.1111/j.1471-4159.2011.07523.x (2012).
260 Calissano, M. & Latchman, D. S. Functional interaction between the small GTP-binding protein Rin and the N-terminal of Brn-3a transcription factor. *Oncogene* **22**, 5408-5414, doi:10.1038/sj.onc.1206635 (2003).
261 Egunsola, A. T. *et al.* Loss of DDRGK1 modulates SOX9 ubiquitination in spondyloepimetaphyseal dysplasia. *J Clin Invest* **127**, 1475-1484, doi:10.1172/jci90193 (2017).
262 Hoashi, T. *et al.* Glycoprotein nonmetastatic melanoma protein b, a melanocytic cell marker, is a melanosome-specific and proteolytically released protein. *Faseb j* **24**, 1616-1629, doi:10.1096/fj.09-151019 (2010).
263 Martí-Massó, J. F. *et al.* The ACMSD gene, involved in tryptophan metabolism, is mutated in a family with cortical myoclonus, epilepsy, and parkinsonism. *J Mol Med (Berl)* **91**, 1399-1406, doi:10.1007/s00109-013-1075-4 (2013).
264 Andres-Alonso, M. *et al.* SIPA1L2 controls trafficking and local signaling of TrkB-containing amphisomes at presynaptic terminals. *Nat Commun* **10**, 5448, doi:10.1038/s41467-019-13224-z (2019).
265 Huang, C. C. *et al.* Soluble α-synuclein facilitates priming and fusion by releasing Ca(2+) from the thapsigargin-sensitive Ca(2+) pool in PC12 cells. *J Cell Sci* **131**, doi:10.1242/jcs.213017 (2018).
266 Henderson, K. N. *et al.* A structural and immunological basis for the role of human leukocyte antigen DQ8 in celiac disease. *Immunity* **27**, 23-34, doi:10.1016/j.immuni.2007.05.015 (2007).
267 Matheoud, D. *et al.* Parkinson's disease related proteins PINK1 and Parkin are major regulators of the immune system. *The Journal of Immunology* **202**, 177.127-177.127 (2019).
268 Blesa, J., Trigo-Damas, I., Quiroga-Varela, A. & Jackson-Lewis, V. R. Oxidative stress and Parkinson's disease. *Front Neuroanat* **9**, 91, doi:10.3389/fnana.2015.00091 (2015).
269 Horvath, I. *et al.* Mechanisms of protein oligomerization: inhibitor of functional amyloids templates α-synuclein fibrillation. *Journal of the American Chemical Society* **134**, 3439-3444, doi:10.1021/ja209829m (2012).
270 Conway, K. A., Harper, J. D. & Lansbury, P. T., Jr. Fibrils formed in vitro from alpha-synuclein and two mutant forms linked to Parkinson's disease are typical amyloid. *Biochemistry* **39**, 2552-2563 (2000).
271 Sacino, A. N. *et al.* Intramuscular injection of α-synuclein induces CNS α-synuclein pathology and a rapid-onset motor phenotype in transgenic mice. *Proc Natl Acad Sci U S A* **111**, 10732-10737, doi:10.1073/pnas.1321785111 (2014).
272 Winner, B. *et al.* In vivo demonstration that alpha-synuclein oligomers are toxic. *Proc Natl Acad Sci U S A* **108**, 4194-4199, doi:10.1073/pnas.1100976108 (2011).
273 Lundblad, M., Decressac, M., Mattsson, B. & Björklund, A. Impaired neurotransmission caused by overexpression of α-synuclein in nigral dopamine neurons. *Proc Natl Acad Sci U S A* **109**, 3213-3219, doi:10.1073/pnas.1200575109 (2012).
274 Klionsky, D. J. & Emr, S. D. Autophagy as a regulated pathway of cellular degradation. *Science (New York, N.Y.)* **290**, 1717-1721, doi:10.1126/science.290.5497.1717 (2000).
275 Cuervo, A. M., Stefanis, L., Fredenburg, R., Lansbury, P. T. & Sulzer, D. Impaired degradation of mutant alpha-synuclein by chaperone-mediated autophagy. *Science* **305**, 1292-1295, doi:10.1126/science.1101738 (2004).
276 Arias, E. & Cuervo, A. M. Chaperone-mediated autophagy in protein quality control. *Current opinion in cell biology* **23**, 184-189, doi:10.1016/j.ceb.2010.10.009 (2011).
277 Webb, J. L., Ravikumar, B., Atkins, J., Skepper, J. N. & Rubinsztein, D. C. Alpha-Synuclein is degraded by both autophagy and the proteasome. *J Biol Chem* **278**, 25009-25013 (2003).
278 Oueslati, A., Fournier, M. & Lashuel, H. A. Role of post-translational modifications in modulating the structure, function and toxicity of alpha-synuclein: implications for Parkinson's disease pathogenesis and therapies. *Prog Brain Res* **183**, 115-145, doi:10.1016/s0079-6123(10)83007-9 (2010).
279 Zhang, J., Li, X. & Li, J.-D. The Roles of Post-translational Modifications on α-Synuclein in the Pathogenesis of Parkinson's Diseases. *Frontiers in neuroscience* **13**, 381-381, doi:10.3389/fnins.2019.00381 (2019).
280 Tofaris, G. K., Razzaq, A., Ghetti, B., Lilley, K. S. & Spillantini, M. G. Ubiquitination of alpha-synuclein in Lewy bodies is a pathological event not associated with impairment of proteasome function. *J Biol Chem* **278**, 44405-44411, doi:10.1074/jbc.M308041200 (2003).
281 Hashimoto, M. *et al.* Oxidative stress induces amyloid-like aggregate formation of NACP/alpha-synuclein in vitro. *Neuroreport* **10**, 717-721, doi:10.1097/00001756-199903170-00011 (1999).
282 Uversky, V. N., Li, J. & Fink, A. L. Metal-triggered structural transformations, aggregation, and fibrillation of human alpha-synuclein. A possible molecular NK between Parkinson's disease and heavy metal exposure. *J Biol Chem* **276**, 44284-44296, doi:10.1074/jbc.M105343200 (2001).
283 Danielson, S. R. *et al.* Preferentially increased nitration of alpha-synuclein at tyrosine-39 in a cellular oxidative model of Parkinson's disease. *Analytical chemistry* **81**, 7823-7828, doi:10.1021/ac901176t (2009).

284 Lee, H.-J. *et al.* Dopamine promotes formation and secretion of non-fibrillar alpha-synuclein oligomers. *Experimental & molecular medicine* **43**, 216-222, doi:10.3858/emm.2011.43.4.026 (2011).
285 Hokenson, M. J. *et al.* Role of individual methionines in the fibrillation of methionine-oxidized alpha-synuclein. *Biochemistry* **43**, 4621-4633, doi:10.1021/bi049979h (2004).
286 Oueslati, A., Paleologou, K. E., Schneider, B. L., Aebischer, P. & Lashuel, H. A. Mimicking phosphorylation at serine 87 inhibits the aggregation of human α-synuclein and protects against its toxicity in a rat model of Parkinson's disease. *J Neurosci* **32**, 1536-1544, doi:10.1523/jneurosci.3784-11.2012 (2012).
287 Hasegawa, M. *et al.* Phosphorylated alpha-synuclein is ubiquitinated in alpha-synucleinopathy lesions. *J Biol Chem* **277**, 49071-49076, doi:10.1074/jbc.M208046200 (2002).
288 Rott, R. *et al.* SUMOylation and ubiquitination reciprocally regulate α-synuclein degradation and pathological aggregation. *Proc Natl Acad Sci U S A* **114**, 13176-13181, doi:10.1073/pnas.1704351114 (2017).
289 Stefanis, L., Larsen, K. E., Rideout, H. J., Sulzer, D. & Greene, L. A. Expression of A53T mutant but not wild-type alpha-synuclein in PC12 cells induces alterations of the ubiquitin-dependent degradation system, loss of dopamine release, and autophagic cell death. *J Neurosci* **21**, 9549-9560 (2001).
290 Martin, L. J. *et al.* Parkinson's disease alpha-synuclein transgenic mice develop neuronal mitochondrial degeneration and cell death. *J Neurosci* **26**, 41-50, doi:10.1523/JNEUROSCI.4308-05.2006 (2006).
291 Dryanovski, D. I. *et al.* Calcium entry and α-synuclein inclusions elevate dendritic mitochondrial oxidant stress in dopaminergic neurons. *J Neurosci* **33**, 10154-10164, doi:10.1523/jneurosci.5311-12.2013 (2013).
292 Shimura, H. *et al.* Familial Parkinson disease gene product, parkin, is a ubiquitin-protein ligase. *Nat Genet* **25**, 302-305, doi:10.1038/77060 (2000).
293 Bentea, E., Verbruggen, L. & Massie, A. The Proteasome Inhibition Model of Parkinson's Disease. *Journal of Parkinson's disease* **7**, 31-63, doi:10.3233/JPD-160921 (2017).
294 Chung, K. K., Dawson, V. L. & Dawson, T. M. The role of the ubiquitin-proteasomal pathway in Parkinson's disease and other neurodegenerative disorders. *Trends Neurosci* **24**, S7-14, doi:10.1016/s0166-2236(00)01998-6 (2001).
295 Kordower, J. H. *et al.* Failure of proteasome inhibitor administration to provide a model of Parkinson's disease in rats and monkeys. *Ann Neurol* **60**, 264-268, doi:10.1002/ana.20935 (2006).
296 Corti, O. *et al.* The p38 subunit of the aminoacyl-tRNA synthetase complex is a Parkin substrate: linking protein biosynthesis and neurodegeneration. *Hum Mol Genet* **12**, 1427-1437, doi:10.1093/hmg/ddg159 (2003).
297 Ekholm-Reed, S., Goldberg, M. S., Schlossmacher, M. G. & Reed, S. I. Parkin-dependent degradation of the F-box protein Fbw7β promotes neuronal survival in response to oxidative stress by stabilizing Mcl-1. *Molecular and cellular biology* **33**, 3627-3643, doi:10.1128/MCB.00535-13 (2013).
298 Shin, J.-H. *et al.* PARIS (ZNF746) repression of PGC-1α contributes to neurodegeneration in Parkinson's disease. *Cell* **144**, 689-702, doi:10.1016/j.cell.2011.02.010 (2011).
299 Romaní-Aumedes, J. *et al.* Parkin loss of function contributes to RTP801 elevation and neurodegeneration in Parkinson's disease. *Cell death & disease* **5**, e1364, doi:10.1038/cddis.2014.333 (2014).
300 Rocha, E. M. *et al.* Sustained Systemic Glucocerebrosidase Inhibition Induces Brain α-Synuclein Aggregation, Microglia and Complement C1q Activation in Mice. *Antioxidants & redox signaling* **23**, 550-564, doi:10.1089/ars.2015.6307 (2015).
301 Tong, Y. *et al.* Loss of leucine-rich repeat kinase 2 causes impairment of protein degradation pathways, accumulation of alpha-synuclein, and apoptotic cell death in aged mice. *Proc Natl Acad Sci U S A* **107**, 9879-9884 (2010).
302 Braak, H. *et al.* Staging of the intracerebral inclusion body pathology associated with idiopathic Parkinson's disease (preclinical and clinical stages). *J Neurol* **249 Suppl 3**, III/1-5 (2002).
303 Braak, H. *et al.* Staging of brain pathology related to sporadic Parkinson's disease. *Neurobiol Aging* **24**, 197-211, doi:10.1016/s0197-4580(02)00065-9 (2003).
304 Braak, H. & Del Tredici, K. Potential Pathways of Abnormal Tau and alpha-Synuclein Dissemination in Sporadic Alzheimer's and Parkinson's Diseases. *Cold Spring Harb Perspect Biol* **8**, doi:10.1101/cshperspect.a023630 (2016).
305 Uemura, N., Uemura, M. T., Luk, K. C., Lee, V. M. & Trojanowski, J. Q. Cell-to-Cell Transmission of Tau and α-Synuclein. *Trends in molecular medicine* **26**, 936-952, doi:10.1016/j.molmed.2020.03.012 (2020).
306 Braak, H., de Vos, R. A., Bohl, J. & Del Tredici, K. Gastric alpha-synuclein immunoreactive inclusions in Meissner's and Auerbach's plexuses in cases staged for Parkinson's disease-related brain pathology. *Neurosci Lett* **396**, 67-72 (2006).
307 Cristóvão, A. C. *et al.* NADPH oxidase 1 mediates α-synucleinopathy in Parkinson's disease. *J Neurosci* **32**, 14465-14477, doi:10.1523/jneurosci.2246-12.2012 (2012).

308 Banati, R. B., Gehrmann, J., Schubert, P. & Kreutzberg, G. W. Cytotoxicity of microglia. *Glia* **7**, 111-118, doi:10.1002/glia.440070117 (1993).
309 Mander, P. & Brown, G. C. Activation of microglial NADPH oxidase is synergistic with glial iNOS expression in inducing neuronal death: a dual-key mechanism of inflammatory neurodegeneration. *Journal of neuroinflammation* **2**, 20, doi:10.1186/1742-2094-2-20 (2005).
310 Li, T. *et al.* Novel LRRK2 GTP-binding inhibitors reduced degeneration in Parkinson's disease cell and mouse models. *Hum Mol Genet* **23**, 6212-6222, doi:10.1093/hmg/ddu341 (2014).
311 Frank-Cannon, T. C. *et al.* Parkin deficiency increases vulnerability to inflammation-related nigral degeneration. *The Journal of neuroscience : the official journal of the Society for Neuroscience* **28**, 10825-10834, doi:10.1523/JNEUROSCI.3001-08.2008 (2008).
312 Solano, R. M. *et al.* Glial dysfunction in parkin null mice: effects of aging. *J Neurosci* **28**, 598-611, doi:10.1523/JNEUROSCI.4609-07.2008 (2008).
313 Kim, J. H. *et al.* DJ-1 facilitates the interaction between STAT1 and its phosphatase, SHP-1, in brain microglia and astrocytes: A novel anti-inflammatory function of DJ-1. *Neurobiol Dis* **60**, 1-10, doi:10.1016/j.nbd.2013.08.007 (2013).
314 Waak, J. *et al.* Regulation of astrocyte inflammatory responses by the Parkinson's disease-associated gene DJ-1. *Faseb j* **23**, 2478-2489, doi:10.1096/fj.08-125153 (2009).
315 Philippens, I. H., Wubben, J. A., Finsen, B. & t Hart, B. A. Oral treatment with the NADPH oxidase antagonist apocynin mitigates clinical and pathological features of parkinsonism in the MPTP marmoset model. *J Neuroimmune Pharmacol* **8**, 715-726, doi:10.1007/s11481-013-9450-z (2013).
316 Joglar, B. *et al.* The inflammatory response in the MPTP model of Parkinson's disease is mediated by brain angiotensin: relevance to progression of the disease. *J Neurochem* **109**, 656-669, doi:10.1111/j.1471-4159.2009.05999.x (2009).
317 Gao, H. M., Liu, B. & Hong, J. S. Critical role for microglial NADPH oxidase in rotenone-induced degeneration of dopaminergic neurons. *J Neurosci* **23**, 6181-6187, doi:10.1523/jneurosci.23-15-06181.2003 (2003).
318 Pal, R., Monroe, T. O., Palmieri, M., Sardiello, M. & Rodney, G. G. Rotenone induces neurotoxicity through Rac1-dependent activation of NADPH oxidase in SHSY-5Y cells. *FEBS letters* **588**, 472-481, doi:10.1016/j.febslet.2013.12.011 (2014).
319 Jiang, X. *et al.* The effects of rotenone-induced toxicity via the NF-κB-iNOS pathway in rat liver. *Toxicology mechanisms and methods* **27**, 318-325, doi:10.1080/15376516.2017.1285972 (2017).
320 Yuan, Y. H. *et al.* Rotenone could activate microglia through NFκB associated pathway. *Neurochem Res* **38**, 1553-1560, doi:10.1007/s11064-013-1055-7 (2013).
321 Halliday, G. M. *et al.* Alpha-synuclein redistributes to neuromelanin lipid in the substantia nigra early in Parkinson's disease. *Brain* **128**, 2654-2664, doi:10.1093/brain/awh584 (2005).
322 Li, J. *et al.* Differential effects of human neuromelanin and synthetic dopamine melanin on neuronal and glial cells. *J Neurochem* **95**, 599-608, doi:10.1111/j.1471-4159.2005.03404.x (2005).
323 Beach, T. G. *et al.* Marked microglial reaction in normal aging human substantia nigra: correlation with extraneuronal neuromelanin pigment deposits. *Acta Neuropathol* **114**, 419-424, doi:10.1007/s00401-007-0250-5 (2007).
324 Zhang, W. *et al.* Neuromelanin activates microglia and induces degeneration of dopaminergic neurons: implications for progression of Parkinson's disease. *Neurotox Res* **19**, 63-72, doi:10.1007/s12640-009-9140-z (2011).
325 Forno, L. S., Langston, J. W., DeLanney, L. E., Irwin, I. & Ricaurte, G. A. Locus ceruleus lesions and eosinophilic inclusions in MPTP-treated monkeys. *Ann Neurol* **20**, 449-455, doi:10.1002/ana.410200403 (1986).
326 Zuo, L. & Motherwell, M. S. The impact of reactive oxygen species and genetic mitochondrial mutations in Parkinson's disease. *Gene* **532**, 18-23, doi:10.1016/j.gene.2013.07.085 (2013).
327 Schapira, A. H. & Gegg, M. Mitochondrial contribution to Parkinson's disease pathogenesis. *Parkinsons Dis* **2011**, 159160, doi:10.4061/2011/159160 (2011).
328 Parker Jr, W. D., Boyson, S. J. & Parks, J. K. Abnormalities of the electron transport chain in idiopathic parkinson's disease. *Annals of Neurology* **26**, 719-723, doi:10.1002/ana.410260606 (1989).
329 Andreyev, A. Y., Kushnareva, Y. E. & Starkov, A. A. Mitochondrial metabolism of reactive oxygen species. *Biochemistry. Biokhimiia* **70**, 200-214, doi:10.1007/s10541-005-0102-7 (2005).
330 Murphy, M. P. How mitochondria produce reactive oxygen species. *The Biochemical journal* **417**, 1-13, doi:10.1042/BJ20081386 (2009).
331 Mizuno, Y., Sone, N. & Saitoh, T. Effects of 1-Methyl-4-Phenyl-1,2,3,6-Tetrahydropyridine and 1-Methyl-4-Phenylpyridinium Ion on Activities of the Enzymes in the Electron Transport System in Mouse Brain. *Journal of Neurochemistry* **48**, 1787-1793, doi:10.1111/j.1471-4159.1987.tb05737.x (1987).

332 Betarbet, R. *et al.* Chronic systemic pesticide exposure reproduces features of Parkinson's disease. *Nat Neurosci* **3**, 1301-1306, doi:10.1038/81834 (2000).

333 Greenamyre, J. T., Cannon, J. R., Drolet, R. & Mastroberardino, P. G. Lessons from the rotenone model of Parkinson's disease. *Trends in pharmacological sciences* **31**, 141-142; author reply 142-143, doi:10.1016/j.tips.2009.12.006 (2010).

334 Annesley, S. J. *et al.* Immortalized Parkinson's disease lymphocytes have enhanced mitochondrial respiratory activity. *Dis Model Mech* **9**, 1295-1305, doi:10.1242/dmm.025684 (2016).

335 Dan Dunn, J., Alvarez, L. A., Zhang, X. & Soldati, T. Reactive oxygen species and mitochondria: A nexus of cellular homeostasis. *Redox Biol* **6**, 472-485, doi:10.1016/j.redox.2015.09.005 (2015).

336 Babot, M., Birch, A., Labarbuta, P. & Galkin, A. Characterisation of the active/de-active transition of mitochondrial complex I. *Biochimica et biophysica acta* **1837**, 1083-1092, doi:10.1016/j.bbabio.2014.02.018 (2014).

337 Piccoli, C. *et al.* Mitochondrial respiratory dysfunction in familiar parkinsonism associated with PINK1 mutation. *Neurochem Res* **33**, 2565-2574, doi:10.1007/s11064-008-9729-2 (2008).

338 Hoepken, H. H. *et al.* Mitochondrial dysfunction, peroxidation damage and changes in glutathione metabolism in PARK6. *Neurobiol Dis* **25**, 401-411, doi:10.1016/j.nbd.2006.10.007 (2007).

339 Kitada, T. *et al.* Impaired dopamine release and synaptic plasticity in the striatum of PINK1-deficient mice. *Proc Natl Acad Sci U S A* **104**, 11441-11446 (2007).

340 Clark, I. E. *et al.* Drosophila pink1 is required for mitochondrial function and interacts genetically with parkin. *Nature* **441**, 1162-1166, doi:10.1038/nature04779 (2006).

341 Gautier, C. A., Kitada, T. & Shen, J. Loss of PINK1 causes mitochondrial functional defects and increased sensitivity to oxidative stress. *Proc Natl Acad Sci U S A* **105**, 11364-11369, doi:10.1073/pnas.0802076105 (2008).

342 Saini, N. *et al.* Extended lifespan of Drosophila parkin mutants through sequestration of redox-active metals and enhancement of anti-oxidative pathways. *Neurobiol Dis* **40**, 82-92, doi:10.1016/j.nbd.2010.05.011 (2010).

343 Greene, J. C. *et al.* Mitochondrial pathology and apoptotic muscle degeneration in Drosophila parkin mutants. *Proceedings of the National Academy of Sciences* **100**, 4078-4083, doi:10.1073/pnas.0737556100 (2003).

344 Pesah, Y. *et al.* Drosophila parkin mutants have decreased mass and cell size and increased sensitivity to oxygen radical stress. *Development* **131**, 2183-2194, doi:10.1242/dev.01095 (2004).

345 Müftüoglu, M. *et al.* Mitochondrial complex I and IV activities in leukocytes from patients with parkin mutations. *Mov Disord* **19**, 544-548, doi:10.1002/mds.10695 (2004).

346 Yang, Y. *et al.* Mitochondrial pathology and muscle and dopaminergic neuron degeneration caused by inactivation of Drosophila Pink1 is rescued by Parkin. *Proc Natl Acad Sci U S A* **103**, 10793-10798, doi:10.1073/pnas.0602493103 (2006).

347 Exner, N. *et al.* Loss-of-function of human PINK1 results in mitochondrial pathology and can be rescued by parkin. *J Neurosci* **27**, 12413-12418, doi:10.1523/jneurosci.0719-07.2007 (2007).

348 Palikaras, K., Lionaki, E. & Tavernarakis, N. Mechanisms of mitophagy in cellular homeostasis, physiology and pathology. *Nat Cell Biol* **20**, 1013-1022, doi:10.1038/s41556-018-0176-2 (2018).

349 Narendra, D., Tanaka, A., Suen, D. F. & Youle, R. J. Parkin is recruited selectively to impaired mitochondria and promotes their autophagy. *J Cell Biol* **183**, 795-803, doi:10.1083/jcb.200809125 (2008).

350 Narendra, D. P. *et al.* PINK1 is selectively stabilized on impaired mitochondria to activate Parkin. *PLoS Biol* **8**, e1000298, doi:10.1371/journal.pbio.1000298 (2010).

351 Narendra, D., Walker, J. E. & Youle, R. Mitochondrial quality control mediated by PINK1 and Parkin: links to parkinsonism. *Cold Spring Harb Perspect Biol* **4**, doi:10.1101/cshperspect.a011338 (2012).

352 Kane, L. A. *et al.* PINK1 phosphorylates ubiquitin to activate Parkin E3 ubiquitin ligase activity. *J Cell Biol* **205**, 143-153, doi:10.1083/jcb.201402104 (2014).

353 Twig, G. & Shirihai, O. S. The interplay between mitochondrial dynamics and mitophagy. *Antioxid Redox Signal* **14**, 1939-1951, doi:10.1089/ars.2010.3779 (2011).

354 Hao, L. Y., Giasson, B. I. & Bonini, N. M. DJ-1 is critical for mitochondrial function and rescues PINK1 loss of function. *Proc Natl Acad Sci U S A* **107**, 9747-9752, doi:10.1073/pnas.0911175107 (2010).

355 Hayashi, T. *et al.* DJ-1 binds to mitochondrial complex I and maintains its activity. *Biochem Biophys Res Commun* **390**, 667-672, doi:10.1016/j.bbrc.2009.10.025 (2009).

356 Nakamura, K. *et al.* Direct membrane association drives mitochondrial fission by the Parkinson disease-associated protein alpha-synuclein. *J Biol Chem* **286**, 20710-20726, doi:10.1074/jbc.M110.213538 (2011).

357 Lin, M. T. *et al.* Somatic mitochondrial DNA mutations in early Parkinson and incidental Lewy body disease. *Annals of neurology* **71**, 850-854, doi:10.1002/ana.23568 (2012).

358 Sterky, F. H., Lee, S., Wibom, R., Olson, L. & Larsson, N. G. Impaired mitochondrial transport and Parkin-independent degeneration of respiratory chain-deficient dopamine neurons in vivo. *Proc Natl Acad Sci U S A* **108**, 12937-12942, doi:10.1073/pnas.1103295108 (2011).
359 Pickrell, A. M. *et al.* Endogenous Parkin Preserves Dopaminergic Substantia Nigral Neurons following Mitochondrial DNA Mutagenic Stress. *Neuron* **87**, 371-381, doi:10.1016/j.neuron.2015.06.034 (2015).
360 Segura-Aguilar, J. *et al.* Protective and toxic roles of dopamine in Parkinson's disease. *J Neurochem* **129**, 898-915, doi:10.1111/jnc.12686 (2014).
361 Conway, K. A., Rochet, J. C., Bieganski, R. M. & Lansbury, P. T., Jr. Kinetic stabilization of the alpha-synuclein protofibril by a dopamine-alpha-synuclein adduct. *Science* **294**, 1346-1349, doi:10.1126/science.1063522 (2001).
362 LaVoie, M. J., Ostaszewski, B. L., Weihofen, A., Schlossmacher, M. G. & Selkoe, D. J. Dopamine covalently modifies and functionally inactivates parkin. *Nat Med* **11**, 1214-1221, doi:10.1038/nm1314 (2005).
363 Girotto, S. *et al.* Dopamine-derived quinones affect the structure of the redox sensor DJ-1 through modifications at Cys-106 and Cys-53. *The Journal of biological chemistry* **287**, 18738-18749, doi:10.1074/jbc.M111.311589 (2012).
364 Whitehead, R. E., Ferrer, J. V., Javitch, J. A. & Justice, J. B. Reaction of oxidized dopamine with endogenous cysteine residues in the human dopamine transporter. *J Neurochem* **76**, 1242-1251, doi:10.1046/j.1471-4159.2001.00125.x (2001).
365 Kuhn, D. M., Arthur, R. E., Jr., Thomas, D. M. & Elferink, L. A. Tyrosine hydroxylase is inactivated by catechol-quinones and converted to a redox-cycling quinoprotein: possible relevance to Parkinson's disease. *J Neurochem* **73**, 1309-1317, doi:10.1046/j.1471-4159.1999.0731309.x (1999).
366 Jana, S. *et al.* Mitochondrial dysfunction mediated by quinone oxidation products of dopamine: Implications in dopamine cytotoxicity and pathogenesis of Parkinson's disease. *Biochim Biophys Acta* **1812**, 663-673, doi:10.1016/j.bbadis.2011.02.013 (2011).
367 Van Laar, V. S., Mishizen, A. J., Cascio, M. & Hastings, T. G. Proteomic identification of dopamine-conjugated proteins from isolated rat brain mitochondria and SH-SY5Y cells. *Neurobiol Dis* **34**, 487-500, doi:10.1016/j.nbd.2009.03.004 (2009).
368 Muñoz, P., Huenchuguala, S., Paris, I. & Segura-Aguilar, J. Dopamine oxidation and autophagy. *Parkinson's disease* **2012**, 920953-920953, doi:10.1155/2012/920953 (2012).
369 Simola, N., Morelli, M. & Carta, A. R. The 6-hydroxydopamine model of Parkinson's disease. *Neurotox Res* **11**, 151-167, doi:10.1007/BF03033565 (2007).
370 Stott, S. R. & Barker, R. A. Time course of dopamine neuron loss and glial response in the 6-OHDA striatal mouse model of Parkinson's disease. *Eur J Neurosci* **39**, 1042-1056, doi:10.1111/ejn.12459 (2014).
371 Penttinen, A. M. *et al.* Characterization of a new low-dose 6-hydroxydopamine model of Parkinson's disease in rat. *J Neurosci Res* **94**, 318-328, doi:10.1002/jnr.23708 (2016).
372 Park, J. T., Lee, Y. S., Cho, K. A. & Park, S. C. Adjustment of the lysosomal-mitochondrial axis for control of cellular senescence. *Ageing Res Rev* **47**, 176-182, doi:10.1016/j.arr.2018.08.003 (2018).
373 Jones, D. P. Radical-free biology of oxidative stress. *Am J Physiol Cell Physiol* **295**, C849-868, doi:10.1152/ajpcell.00283.2008 (2008).
374 Cook, C., Stetler, C. & Petrucelli, L. Disruption of protein quality control in Parkinson's disease. *Cold Spring Harb Perspect Med* **2**, a009423, doi:10.1101/cshperspect.a009423 (2012).
375 Giguere, N., Burke Nanni, S. & Trudeau, L. E. On Cell Loss and Selective Vulnerability of Neuronal Populations in Parkinson's Disease. *Front Neurol* **9**, 455, doi:10.3389/fneur.2018.00455 (2018).
376 Branch, S. Y., Sharma, R. & Beckstead, M. J. Aging decreases L-type calcium channel currents and pacemaker firing fidelity in substantia nigra dopamine neurons. *The Journal of neuroscience : the official journal of the Society for Neuroscience* **34**, 9310-9318, doi:10.1523/JNEUROSCI.4228-13.2014 (2014).
377 Putzier, I., Kullmann, P. H., Horn, J. P. & Levitan, E. S. Cav1.3 channel voltage dependence, not Ca2+ selectivity, drives pacemaker activity and amplifies bursts in nigral dopamine neurons. *J Neurosci* **29**, 15414-15419, doi:10.1523/jneurosci.4742-09.2009 (2009).
378 Puopolo, M., Raviola, E. & Bean, B. P. Roles of subthreshold calcium current and sodium current in spontaneous firing of mouse midbrain dopamine neurons. *J Neurosci* **27**, 645-656, doi:10.1523/jneurosci.4341-06.2007 (2007).
379 Neuhoff, H., Neu, A., Liss, B. & Roeper, J. I(h) channels contribute to the different functional properties of identified dopaminergic subpopulations in the midbrain. *J Neurosci* **22**, 1290-1302, doi:10.1523/jneurosci.22-04-01290.2002 (2002).
380 Chan, C. S. *et al.* 'Rejuvenation' protects neurons in mouse models of Parkinson's disease. *Nature* **447**, 1081-1086, doi:10.1038/nature05865 (2007).
381 Guzman, J. N. *et al.* Oxidant stress evoked by pacemaking in dopaminergic neurons is attenuated by DJ-1. *Nature* **468**, 696-700, doi:10.1038/nature09536 (2010).

382 Monzani, E. *et al.* Dopamine, Oxidative Stress and Protein-Quinone Modifications in Parkinson's and Other Neurodegenerative Diseases. *Angew Chem Int Ed Engl* **58**, 6512-6527, doi:10.1002/anie.201811122 (2019).
383 Mena, M. A. & García de Yébenes, J. Glial cells as players in parkinsonism: the "good," the "bad," and the "mysterious" glia. *Neuroscientist* **14**, 544-560, doi:10.1177/1073858408322839 (2008).
384 Jagmag, S. A., Tripathi, N., Shukla, S. D., Maiti, S. & Khurana, S. Evaluation of Models of Parkinson's Disease. *Front Neurosci* **9**, 503, doi:10.3389/fnins.2015.00503 (2015).
385 Cohen, G. Oxy-radical toxicity in catecholamine neurons. *Neurotoxicology* **5**, 77-82 (1984).
386 Javitch, J. A., D'Amato, R. J., Strittmatter, S. M. & Snyder, S. H. Parkinsonism-inducing neurotoxin, N-methyl-4-phenyl-1,2,3,6 -tetrahydropyridine: uptake of the metabolite N-methyl-4-phenylpyridine by dopamine neurons explains selective toxicity. *Proc Natl Acad Sci U S A* **82**, 2173-2177, doi:10.1073/pnas.82.7.2173 (1985).
387 Kowall, N. W. *et al.* MPTP induces alpha-synuclein aggregation in the substantia nigra of baboons. *Neuroreport* **11**, 211-213, doi:10.1097/00001756-200001170-00041 (2000).
388 Jackson-Lewis, V. & Przedborski, S. Protocol for the MPTP mouse model of Parkinson's disease. *Nat Protoc* **2**, 141-151, doi:10.1038/nprot.2006.342 (2007).
389 Sherer, T. B. *et al.* Mechanism of toxicity in rotenone models of Parkinson's disease. *J Neurosci* **23**, 10756-10764, doi:10.1523/jneurosci.23-34-10756.2003 (2003).
390 McCormack, A. L. *et al.* Environmental risk factors and Parkinson's disease: selective degeneration of nigral dopaminergic neurons caused by the herbicide paraquat. *Neurobiol Dis* **10**, 119-127, doi:10.1006/nbdi.2002.0507 (2002).
391 Cicchetti, F. *et al.* Systemic exposure to paraquat and maneb models early Parkinson's disease in young adult rats. *Neurobiol Dis* **20**, 360-371, doi:10.1016/j.nbd.2005.03.018 (2005).
392 Xiong, N. *et al.* Stereotaxical infusion of rotenone: a reliable rodent model for Parkinson's disease. *PLoS One* **4**, e7878, doi:10.1371/journal.pone.0007878 (2009).
393 Fleming, S. M. *et al.* Behavioral and immunohistochemical effects of chronic intravenous and subcutaneous infusions of varying doses of rotenone. *Exp Neurol* **187**, 418-429, doi:10.1016/j.expneurol.2004.01.023 (2004).
394 Miller, G. W. Paraquat: the red herring of Parkinson's disease research. *Toxicol Sci* **100**, 1-2, doi:10.1093/toxsci/kfm223 (2007).
395 Lauwers, E. *et al.* Neuropathology and Neurodegeneration in Rodent Brain Induced by Lentiviral Vectormediated Overexpression of α-Synuclein. *Brain Pathology* **13**, 364-372, doi:10.1111/j.1750-3639.2003.tb00035.x (2003).
396 Oliveras-Salvá, M. *et al.* rAAV2/7 vector-mediated overexpression of alpha-synuclein in mouse substantia nigra induces protein aggregation and progressive dose-dependent neurodegeneration. *Mol Neurodegener* **8**, 44, doi:10.1186/1750-1326-8-44 (2013).
397 Chen, C. Y. *et al.* (G2019S) LRRK2 activates MKK4-JNK pathway and causes degeneration of SN dopaminergic neurons in a transgenic mouse model of PD. *Cell Death Differ* **19**, 1623-1633, doi:10.1038/cdd.2012.42 (2012).
398 Klein, R. L., King, M. A., Hamby, M. E. & Meyer, E. M. Dopaminergic cell loss induced by human A30P alpha-synuclein gene transfer to the rat substantia nigra. *Hum Gene Ther* **13**, 605-612, doi:10.1089/10430340252837206 (2002).
399 Koprich, J. B., Johnston, T. H., Reyes, M. G., Sun, X. & Brotchie, J. M. Expression of human A53T alpha-synuclein in the rat substantia nigra using a novel AAV1/2 vector produces a rapidly evolving pathology with protein aggregation, dystrophic neurite architecture and nigrostriatal degeneration with potential to model the pathology of Parkinson's disease. *Mol Neurodegener* **5**, 43, doi:10.1186/1750-1326-5-43 (2010).
400 Kirik, D. *et al.* Parkinson-like neurodegeneration induced by targeted overexpression of alpha-synuclein in the nigrostriatal system. *J Neurosci* **22**, 2780-2791, doi:10.1523/jneurosci.22-07-02780.2002 (2002).
401 Engeln, M. *et al.* Levodopa gains psychostimulant-like properties after nigral dopaminergic loss. *Ann Neurol* **74**, 140-144, doi:10.1002/ana.23881 (2013).
402 Lo Bianco, C., Ridet, J. L., Schneider, B. L., Deglon, N. & Aebischer, P. alpha -Synucleinopathy and selective dopaminergic neuron loss in a rat lentiviral-based model of Parkinson's disease. *Proc Natl Acad Sci U S A* **99**, 10813-10818, doi:10.1073/pnas.152339799 (2002).
403 McFarland, N. R. *et al.* Alpha-synuclein S129 phosphorylation mutants do not alter nigrostriatal toxicity in a rat model of Parkinson disease. *J Neuropathol Exp Neurol* **68**, 515-524, doi:10.1097/NEN.0b013e3181a24b53 (2009).
404 Yamada, M., Iwatsubo, T., Mizuno, Y. & Mochizuki, H. Overexpression of α-synuclein in rat substantia nigra results in loss of dopaminergic neurons, phosphorylation of α-synuclein and activation of caspase-9: resemblance to pathogenetic changes in Parkinson's disease. *Journal of Neurochemistry* **91**, 451-461, doi:10.1111/j.1471-4159.2004.02728.x (2004).
405 Dusonchet, J. *et al.* A rat model of progressive nigral neurodegeneration induced by the Parkinson's disease-associated G2019S mutation in LRRK2. *J Neurosci* **31**, 907-912, doi:10.1523/jneurosci.5092-10.2011 (2011).

406 Lu, X. H. *et al.* Bacterial artificial chromosome transgenic mice expressing a truncated mutant parkin exhibit age-dependent hypokinetic motor deficits, dopaminergic neuron degeneration, and accumulation of proteinase K-resistant alpha-synuclein. *J Neurosci* **29**, 1962-1976, doi:10.1523/JNEUROSCI.5351-08.2009 (2009).
407 Rousseaux, M. W. *et al.* Progressive dopaminergic cell loss with unilateral-to-bilateral progression in a genetic model of Parkinson disease. *Proc Natl Acad Sci U S A* **109**, 15918-15923, doi:10.1073/pnas.1205102109 (2012).
408 Park, J. *et al.* Drosophila DJ-1 mutants show oxidative stress-sensitive locomotive dysfunction. *Gene* **361**, 133-139, doi:10.1016/j.gene.2005.06.040 (2005).
409 Dave, K. D. *et al.* Phenotypic characterization of recessive gene knockout rat models of Parkinson's disease. *Neurobiol Dis* **70**, 190-203, doi:10.1016/j.nbd.2014.06.009 (2014).
410 Kitada, T., Tong, Y., Gautier, C. A. & Shen, J. Absence of nigral degeneration in aged parkin/DJ-1/PINK1 triple knockout mice. *J Neurochem* **111**, 696-702 (2009).
411 Bachevalier, J. *et al.* Aged monkeys exhibit behavioral deficits indicative of widespread cerebral dysfunction. *Neurobiol Aging* **12**, 99-111, doi:10.1016/0197-4580(91)90048-o (1991).
412 Emborg, M. E. *et al.* Age-related declines in nigral neuronal function correlate with motor impairments in rhesus monkeys. *The Journal of comparative neurology* **401**, 253-265 (1998).
413 Irwin, I. *et al.* Aging and the nigrostriatal dopamine system: a non-human primate study. *Neurodegeneration : a journal for neurodegenerative disorders, neuroprotection, and neuroregeneration* **3**, 251-265 (1994).
414 Zhang, Z. *et al.* Motor slowing and parkinsonian signs in aging rhesus monkeys mirror human aging. *The journals of gerontology. Series A, Biological sciences and medical sciences* **55**, B473-480, doi:10.1093/gerona/55.10.b473 (2000).
415 Arnsten, A. F., Cai, J. X., Steere, J. C. & Goldman-Rakic, P. S. Dopamine D2 receptor mechanisms contribute to age-related cognitive decline: the effects of quinpirole on memory and motor performance in monkeys. *The Journal of neuroscience : the official journal of the Society for Neuroscience* **15**, 3429-3439, doi:10.1523/JNEUROSCI.15-05-03429.1995 (1995).
416 Collier, T. J. *et al.* Aging-related changes in the nigrostriatal dopamine system and the response to MPTP in nonhuman primates: diminished compensatory mechanisms as a prelude to parkinsonism. *Neurobiol Dis* **26**, 56-65, doi:10.1016/j.nbd.2006.11.013 (2007).
417 Gerhardt, G. A. *et al.* Age-related changes in potassium-evoked overflow of dopamine in the striatum of the rhesus monkey. *Neurobiol Aging* **16**, 939-946, doi:10.1016/0197-4580(95)02013-6 (1995).
418 Goldman-Rakic, P. S. & Brown, R. M. Regional changes of monoamines in cerebral cortex and subcortical structures of aging rhesus monkeys. *Neuroscience* **6**, 177-187, doi:10.1016/0306-4522(81)90053-1 (1981).
419 Morris, E. D. *et al.* Loss of D2 receptor binding with age in rhesus monkeys: importance of correction for differences in striatal size. *J Cereb Blood Flow Metab* **19**, 218-229, doi:10.1097/00004647-199902000-00013 (1999).
420 Siddiqi, Z. A. & Peters, A. The Effect of Aging on Pars Compacta of the Substantia Nigra in Rhesus Monkey. *Journal of Neuropathology & Experimental Neurology* **58**, 903-920, doi:10.1097/00005072-199909000-00002 (1999).
421 Wenk, G. L., Pierce, D. J., Struble, R. G., Price, D. L. & Cork, L. C. Age-related changes in multiple neurotransmitter systems in the monkey brain. *Neurobiol Aging* **10**, 11-19, doi:10.1016/s0197-4580(89)80005-3 (1989).
422 Matsumine, H. *et al.* Localization of a gene for an autosomal recessive form of juvenile Parkinsonism to chromosome 6q25.2-27. *Am J Hum Genet* **60**, 588-596 (1997).
423 Lesage, S. *et al.* Deletion of the parkin and PACRG gene promoter in early-onset parkinsonism. *Hum Mutat* **28**, 27-32, doi:10.1002/humu.20436 (2007).
424 Meschede, J. *et al.* The parkin-coregulated gene product PACRG promotes TNF signaling by stabilizing LUBAC. *Sci Signal* **13**, doi:10.1126/scisignal.aav1256 (2020).
425 Hedrich, K. *et al.* The importance of gene dosage studies: mutational analysis of the parkin gene in early-onset parkinsonism. *Hum Mol Genet* **10**, 1649-1656, doi:10.1093/hmg/10.16.1649 (2001).
426 Choi, J. M. *et al.* Analysis of PARK genes in a Korean cohort of early-onset Parkinson disease. *Neurogenetics* **9**, 263-269, doi:10.1007/s10048-008-0138-0 (2008).
427 Guo, J. F. *et al.* Mutation analysis of Parkin, PINK1 and DJ-1 genes in Chinese patients with sporadic early onset parkinsonism. *J Neurol* **257**, 1170-1175, doi:10.1007/s00415-010-5485-8 (2010).
428 Macedo, M. G. *et al.* Genotypic and phenotypic characteristics of Dutch patients with early onset Parkinson's disease. *Mov Disord* **24**, 196-203, doi:10.1002/mds.22287 (2009).
429 Pankratz, N. *et al.* Parkin dosage mutations have greater pathogenicity in familial PD than simple sequence mutations. *Neurology* **73**, 279-286, doi:10.1212/WNL.0b013e3181af7a33 (2009).

430 Hayashi, S. *et al.* An autopsy case of autosomal-recessive juvenile parkinsonism with a homozygous exon 4 deletion in the parkin gene. *Mov Disord* **15**, 884-888 (2000).
431 Shimura, H. *et al.* Immunohistochemical and subcellular localization of Parkin protein: absence of protein in autosomal recessive juvenile parkinsonism patients. *Ann Neurol* **45**, 668-672, doi:10.1002/1531-8249(199905)45:5<668::aid-ana19>3.0.co;2-z (1999).
432 Itier, J. M. *et al.* Parkin gene inactivation alters behaviour and dopamine neurotransmission in the mouse. *Hum Mol Genet* **12**, 2277-2291, doi:10.1093/hmg/ddg239 (2003).
433 Goldberg, M. S. *et al.* Parkin-deficient mice exhibit nigrostriatal deficits but not loss of dopaminergic neurons. *J Biol Chem* **278**, 43628-43635, doi:10.1074/jbc.M308947200 (2003).
434 Von Coelln, R. *et al.* Loss of locus coeruleus neurons and reduced startle in parkin null mice. *Proc Natl Acad Sci U S A* **101**, 10744-10749, doi:10.1073/pnas.0401297101 (2004).
435 Palacino, J. J. *et al.* Mitochondrial dysfunction and oxidative damage in parkin-deficient mice. *J Biol Chem* **279**, 18614-18622, doi:10.1074/jbc.M401135200 (2004).
436 Perez, F. A. & Palmiter, R. D. Parkin-deficient mice are not a robust model of parkinsonism. *Proc Natl Acad Sci U S A* **102**, 2174-2179, doi:10.1073/pnas.0409598102 (2005).
437 Periquet, M., Corti, O., Jacquier, S. & Brice, A. Proteomic analysis of parkin knockout mice: alterations in energy metabolism, protein handling and synaptic function. *J Neurochem* **95**, 1259-1276, doi:10.1111/j.1471-4159.2005.03442.x (2005).
438 Sato, S. *et al.* Decline of striatal dopamine release in parkin-deficient mice shown by ex vivo autoradiography. *J Neurosci Res* **84**, 1350-1357, doi:10.1002/jnr.21032 (2006).
439 Oyama, G. *et al.* Impaired in vivo dopamine release in parkin knockout mice. *Brain Res* **1352**, 214-222, doi:10.1016/j.brainres.2010.06.065 (2010).
440 Mata, I. F., Lockhart, P. J. & Farrer, M. J. Parkin genetics: one model for Parkinson's disease. *Hum Mol Genet* **13 Spec No 1**, R127-133, doi:10.1093/hmg/ddh089 (2004).
441 Kahle, P. J. & Haass, C. How does parkin ligate ubiquitin to Parkinson's disease? *EMBO reports* **5**, 681-685, doi:10.1038/sj.embor.7400188 (2004).
442 Sriram, S. R. *et al.* Familial-associated mutations differentially disrupt the solubility, localization, binding and ubiquitination properties of parkin. *Hum Mol Genet* **14**, 2571-2586, doi:10.1093/hmg/ddi292 (2005).
443 Wang, C. *et al.* Alterations in the solubility and intracellular localization of parkin by several familial Parkinson's disease-linked point mutations. *J Neurochem* **93**, 422-431, doi:10.1111/j.1471-4159.2005.03023.x (2005).
444 Hampe, C., Ardila-Osorio, H., Fournier, M., Brice, A. & Corti, O. Biochemical analysis of Parkinson's disease-causing variants of Parkin, an E3 ubiquitin-protein ligase with monoubiquitylation capacity. *Hum Mol Genet* **15**, 2059-2075, doi:10.1093/hmg/ddl131 (2006).
445 Matsuda, N. *et al.* Diverse effects of pathogenic mutations of Parkin that catalyze multiple monoubiquitylation in vitro. *J Biol Chem* **281**, 3204-3209, doi:10.1074/jbc.M510393200 (2006).
446 Geisler, S. *et al.* The PINK1/Parkin-mediated mitophagy is compromised by PD-associated mutations. *Autophagy* **6**, 871-878, doi:10.4161/auto.6.7.13286 (2010).
447 Safadi, S. S., Barber, K. R. & Shaw, G. S. Impact of autosomal recessive juvenile Parkinson's disease mutations on the structure and interactions of the parkin ubiquitin-like domain. *Biochemistry* **50**, 2603-2610, doi:10.1021/bi200065g (2011).
448 Trempe, J. F. *et al.* Structure of parkin reveals mechanisms for ubiquitin ligase activation. *Science* **340**, 1451-1455, doi:10.1126/science.1237908 (2013).
449 Riley, B. E. *et al.* Structure and function of Parkin E3 ubiquitin ligase reveals aspects of RING and HECT ligases. *Nat Commun* **4**, 1982, doi:10.1038/ncomms2982 (2013).
450 Tang, M. Y. *et al.* Structure-guided mutagenesis reveals a hierarchical mechanism of Parkin activation. *Nat Commun* **8**, 14697, doi:10.1038/ncomms14697 (2017).
451 Biswas, R. & Bagchi, A. A comprehensive computational study on pathogenic mis-sense mutations spanning the RING2 and REP domains of Parkin protein. *Gene* **610**, 49-58, doi:10.1016/j.gene.2017.02.008 (2017).
452 Gladkova, C., Maslen, S. L., Skehel, J. M. & Komander, D. Mechanism of parkin activation by PINK1. *Nature* **559**, 410-414, doi:10.1038/s41586-018-0224-x (2018).
453 Biswas, S., Roy, R., Biswas, R. & Bagchi, A. Structural analysis of the effects of mutations in Ubl domain of Parkin leading to Parkinson's disease. *Gene* **726**, 144186, doi:10.1016/j.gene.2019.144186 (2020).
454 Kazlauskaite, A. *et al.* Phosphorylation of Parkin at Serine65 is essential for activation: elaboration of a Miro1 substrate-based assay of Parkin E3 ligase activity. *Open Biol* **4**, 130213, doi:10.1098/rsob.130213 (2014).

455 Hristova, V. A., Beasley, S. A., Rylett, R. J. & Shaw, G. S. Identification of a novel Zn2+-binding domain in the autosomal recessive juvenile Parkinson-related E3 ligase parkin. *J Biol Chem* **284**, 14978-14986, doi:10.1074/jbc.M808700200 (2009).
456 Spratt, D. E., Walden, H. & Shaw, G. S. RBR E3 ubiquitin ligases: new structures, new insights, new questions. *Biochem J* **458**, 421-437, doi:10.1042/BJ20140006 (2014).
457 Chaugule, V. K. *et al.* Autoregulation of Parkin activity through its ubiquitin-like domain. *Embo J* **30**, 2853-2867, doi:10.1038/emboj.2011.204 (2011).
458 Kumar, A. *et al.* Disruption of the autoinhibited state primes the E3 ligase parkin for activation and catalysis. *EMBO J* **34**, 2506-2521, doi:10.15252/embj.201592337 (2015).
459 Seirafi, M., Kozlov, G. & Gehring, K. Parkin structure and function. *FEBS J* **282**, 2076-2088, doi:10.1111/febs.13249 (2015).
460 Hattori, N. & Mizuno, Y. Twenty years since the discovery of the parkin gene. *J Neural Transm (Vienna)* **124**, 1037-1054, doi:10.1007/s00702-017-1742-7 (2017).
461 Akutsu, M., Dikic, I. & Bremm, A. Ubiquitin chain diversity at a glance. *J Cell Sci* **129**, 875-880, doi:10.1242/jcs.183954 (2016).
462 Hershko, A. & Ciechanover, A. The ubiquitin system. *Annu Rev Biochem* **67**, 425-479, doi:10.1146/annurev.biochem.67.1.425 (1998).
463 Berndsen, C. E. & Wolberger, C. New insights into ubiquitin E3 ligase mechanism. *Nat Struct Mol Biol* **21**, 301-307, doi:10.1038/nsmb.2780 (2014).
464 Metzger, M. B., Pruneda, J. N., Klevit, R. E. & Weissman, A. M. RING-type E3 ligases: master manipulators of E2 ubiquitin-conjugating enzymes and ubiquitination. *Biochim Biophys Acta* **1843**, 47-60, doi:10.1016/j.bbamcr.2013.05.026 (2014).
465 Weber, J., Polo, S. & Maspero, E. HECT E3 Ligases: A Tale With Multiple Facets. *Front Physiol* **10**, 370-370, doi:10.3389/fphys.2019.00370 (2019).
466 Dove, K. K. & Klevit, R. E. RING-Between-RING E3 Ligases: Emerging Themes amid the Variations. *J Mol Biol* **429**, 3363-3375, doi:10.1016/j.jmb.2017.08.008 (2017).
467 van der Reijden, B. A., Erpelinck-Verschueren, C. A., Lowenberg, B. & Jansen, J. H. TRIADs: a new class of proteins with a novel cysteine-rich signature. *Protein Sci* **8**, 1557-1561, doi:10.1110/ps.8.7.1557 (1999).
468 Capili, A. D., Edghill, E. L., Wu, K. & Borden, K. L. Structure of the C-terminal RING finger from a RING-IBR-RING/TRIAD motif reveals a novel zinc-binding domain distinct from a RING. *J Mol Biol* **340**, 1117-1129, doi:10.1016/j.jmb.2004.05.035 (2004).
469 Yamanaka, K. *et al.* Identification of the ubiquitin-protein ligase that recognizes oxidized IRP2. *Nat Cell Biol* **5**, 336-340, doi:10.1038/ncb952 (2003).
470 van Well, E. M. *et al.* A protein quality control pathway regulated by linear ubiquitination. *Embo j* **38**, doi:10.15252/embj.2018100730 (2019).
471 Duda, D. M. *et al.* Structure of HHARI, a RING-IBR-RING ubiquitin ligase: autoinhibition of an Ariadne-family E3 and insights into ligation mechanism. *Structure* **21**, 1030-1041, doi:10.1016/j.str.2013.04.019 (2013).
472 Yagi, H. *et al.* A non-canonical UBA-UBL interaction forms the linear-ubiquitin-chain assembly complex. *EMBO Rep* **13**, 462-468, doi:10.1038/embor.2012.24 (2012).
473 Marín, I., Lucas, J. I., Gradilla, A. C. & Ferrús, A. Parkin and relatives: the RBR family of ubiquitin ligases. *Physiological genomics* **17**, 253-263, doi:10.1152/physiolgenomics.00226.2003 (2004).
474 Boisson, B. *et al.* Human HOIP and LUBAC deficiency underlies autoinflammation, immunodeficiency, amylopectinosis, and lymphangiectasia. *J Exp Med* **212**, 939-951, doi:10.1084/jem.20141130 (2015).
475 Wang, P., Dai, X., Jiang, W., Li, Y. & Wei, W. RBR E3 ubiquitin ligases in tumorigenesis. *Seminars in cancer biology*, doi:10.1016/j.semcancer.2020.05.002 (2020).
476 Finney, N. *et al.* The cellular protein level of parkin is regulated by its ubiquitin-like domain. *J Biol Chem* **278**, 16054-16058, doi:10.1074/jbc.C300051200 (2003).
477 Trempe, J. F. *et al.* SH3 domains from a subset of BAR proteins define a Ubl-binding domain and implicate parkin in synaptic ubiquitination. *Mol Cell* **36**, 1034-1047, doi:10.1016/j.molcel.2009.11.021 (2009).
478 Fallon, L. *et al.* A regulated interaction with the UIM protein Eps15 implicates parkin in EGF receptor trafficking and PI(3)K-Akt signalling. *Nat Cell Biol* **8**, 834-842, doi:10.1038/ncb1441 (2006).
479 Sakata, E. *et al.* Parkin binds the Rpn10 subunit of 26S proteasomes through its ubiquitin-like domain. *EMBO Rep* **4**, 301-306, doi:10.1038/sj.embor.embor764 (2003).
480 Bai, J. J., Safadi, S. S., Mercier, P., Barber, K. R. & Shaw, G. S. Ataxin-3 is a multivalent ligand for the parkin Ubl domain. *Biochemistry* **52**, 7369-7376, doi:10.1021/bi400780v (2013).

481 Shiba-Fukushima, K. *et al.* PINK1-mediated phosphorylation of the Parkin ubiquitin-like domain primes mitochondrial translocation of Parkin and regulates mitophagy. *Sci Rep* **2**, 1002, doi:10.1038/srep01002 (2012).
482 Kondapalli, C. *et al.* PINK1 is activated by mitochondrial membrane potential depolarization and stimulates Parkin E3 ligase activity by phosphorylating Serine 65. *Open biology* **2**, 120080-120080, doi:10.1098/rsob.120080 (2012).
483 Koyano, F. *et al.* Ubiquitin is phosphorylated by PINK1 to activate parkin. *Nature* **510**, 162-166, doi:10.1038/nature13392 (2014).
484 Panicker, N., Dawson, V. L. & Dawson, T. M. Activation mechanisms of the E3 ubiquitin ligase parkin. *Biochem J* **474**, 3075-3086, doi:10.1042/BCJ20170476 (2017).
485 Chakraborty, J., Basso, V. & Ziviani, E. Post translational modification of Parkin. *Biol Direct* **12**, 6-6, doi:10.1186/s13062-017-0176-3 (2017).
486 LaVoie, M. J., Cortese, G. P., Ostaszewski, B. L. & Schlossmacher, M. G. The effects of oxidative stress on parkin and other E3 ligases. *J Neurochem* **103**, 2354-2368, doi:10.1111/j.1471-4159.2007.04911.x (2007).
487 Meng, F. *et al.* Oxidation of the cysteine-rich regions of parkin perturbs its E3 ligase activity and contributes to protein aggregation. *Mol Neurodegener* **6**, 34, doi:10.1186/1750-1326-6-34 (2011).
488 Winklhofer, K. F., Henn, I. H., Kay-Jackson, P. C., Heller, U. & Tatzelt, J. Inactivation of parkin by oxidative stress and C-terminal truncations: a protective role of molecular chaperones. *J Biol Chem* **278**, 47199-47208, doi:10.1074/jbc.M306769200 (2003).
489 Yao, D. *et al.* Nitrosative stress linked to sporadic Parkinson's disease: S-nitrosylation of parkin regulates its E3 ubiquitin ligase activity. *Proc Natl Acad Sci U S A* **101**, 10810-10814, doi:10.1073/pnas.0404161101 (2004).
490 Chung, K. K. *et al.* S-nitrosylation of parkin regulates ubiquitination and compromises parkin's protective function. *Science* **304**, 1328-1331, doi:10.1126/science.1093891 (2004).
491 Chung, K. K., Dawson, V. L. & Dawson, T. M. S-nitrosylation in Parkinson's disease and related neurodegenerative disorders. *Methods Enzymol* **396**, 139-150, doi:10.1016/S0076-6879(05)96014-X (2005).
492 Ozawa, K. *et al.* S-nitrosylation regulates mitochondrial quality control via activation of parkin. *Sci Rep* **3**, 2202, doi:10.1038/srep02202 (2013).
493 Wong, E. S. *et al.* Relative sensitivity of parkin and other cysteine-containing enzymes to stress-induced solubility alterations. *J Biol Chem* **282**, 12310-12318, doi:10.1074/jbc.M609466200 (2007).
494 Kahns, S. *et al.* Caspase-1 and caspase-8 cleave and inactivate cellular parkin. *J Biol Chem* **278**, 23376-23380, doi:10.1074/jbc.M300495200 (2003).
495 Yu, J. *et al.* Inflammasome activation leads to Caspase-1-dependent mitochondrial damage and block of mitophagy. *Proc Natl Acad Sci U S A* **111**, 15514-15519, doi:10.1073/pnas.1414859111 (2014).
496 Rubio de la Torre, E. *et al.* Combined kinase inhibition modulates parkin inactivation. *Hum Mol Genet* **18**, 809-823, doi:10.1093/hmg/ddn407 (2009).
497 Imam, S. Z. *et al.* Novel regulation of parkin function through c-Abl-mediated tyrosine phosphorylation: implications for Parkinson's disease. *J Neurosci* **31**, 157-163, doi:10.1523/jneurosci.1833-10.2011 (2011).
498 Ko, H. S. *et al.* Phosphorylation by the c-Abl protein tyrosine kinase inhibits parkin's ubiquitination and protective function. *Proc Natl Acad Sci U S A* **107**, 16691-16696, doi:10.1073/pnas.1006083107 (2010).
499 Vandiver, M. S. *et al.* Sulfhydration mediates neuroprotective actions of parkin. *Nat Commun* **4**, 1626, doi:10.1038/ncomms2623 (2013).
500 Um, J. W. & Chung, K. C. Functional modulation of parkin through physical interaction with SUMO-1. *J Neurosci Res* **84**, 1543-1554, doi:10.1002/jnr.21041 (2006).
501 Um, J. W. *et al.* Neddylation positively regulates the ubiquitin E3 ligase activity of parkin. *J Neurosci Res* **90**, 1030-1042, doi:10.1002/jnr.22828 (2012).
502 Cookson, M. R. *et al.* RING finger 1 mutations in Parkin produce altered localization of the protein. *Hum Mol Genet* **12**, 2957-2965, doi:10.1093/hmg/ddg328 (2003).
503 Zhang, Y. *et al.* Parkin functions as an E2-dependent ubiquitin- protein ligase and promotes the degradation of the synaptic vesicle-associated protein, CDCrel-1. *Proc Natl Acad Sci U S A* **97**, 13354-13359, doi:10.1073/pnas.240347797 (2000).
504 Chung, K. K. *et al.* Parkin ubiquitinates the alpha-synuclein-interacting protein, synphilin-1: implications for Lewy-body formation in Parkinson disease. *Nat Med* **7**, 1144-1150, doi:10.1038/nm1001-1144 (2001).
505 Imai, Y. *et al.* An unfolded putative transmembrane polypeptide, which can lead to endoplasmic reticulum stress, is a substrate of Parkin. *Cell* **105**, 891-902 (2001).
506 Shimura, H. *et al.* Ubiquitination of a new form of alpha-synuclein by parkin from human brain: implications for Parkinson's disease. *Science* **293**, 263-269, doi:10.1126/science.1060627 (2001).
507 Choi, P. *et al.* SEPT5_v2 is a parkin-binding protein. *Molecular Brain Research* **117**, 179-189, doi:10.1016/S0169-328X(03)00318-8 (2003).

508 Huynh, D. P., Scoles, D. R., Nguyen, D. & Pulst, S. M. The autosomal recessive juvenile Parkinson disease gene product, parkin, interacts with and ubiquitinates synaptotagmin XI. *Hum Mol Genet* **12**, 2587-2597, doi:10.1093/hmg/ddg269 (2003).
509 Ren, Y., Zhao, J. & Feng, J. Parkin binds to alpha/beta tubulin and increases their ubiquitination and degradation. *J Neurosci* **23**, 3316-3324, doi:10.1523/jneurosci.23-08-03316.2003 (2003).
510 Staropoli, J. F. *et al.* Parkin is a component of an SCF-like ubiquitin ligase complex and protects postmitotic neurons from kainate excitotoxicity. *Neuron* **37**, 735-749, doi:10.1016/s0896-6273(03)00084-9 (2003).
511 Tsai, Y. C., Fishman, P. S., Thakor, N. V. & Oyler, G. A. Parkin facilitates the elimination of expanded polyglutamine proteins and leads to preservation of proteasome function. *J Biol Chem* **278**, 22044-22055, doi:10.1074/jbc.M212235200 (2003).
512 Kyng, K. J. *et al.* Gene expression responses to DNA damage are altered in human aging and in Werner Syndrome. *Oncogene* **24**, 5026-5042, doi:10.1038/sj.onc.1208692 (2005).
513 Ko, H. S., Kim, S. W., Sriram, S. R., Dawson, V. L. & Dawson, T. M. Identification of far upstream element-binding protein-1 as an authentic Parkin substrate. *J Biol Chem* **281**, 16193-16196, doi:10.1074/jbc.C600041200 (2006).
514 Um, J. W. *et al.* Parkin ubiquitinates and promotes the degradation of RanBP2. *J Biol Chem* **281**, 3595-3603, doi:10.1074/jbc.M504994200 (2006).
515 Henn, I. H. *et al.* Parkin mediates neuroprotection through activation of IkappaB kinase/nuclear factor-kappaB signaling. *J Neurosci* **27**, 1868-1878, doi:10.1523/jneurosci.5537-06.2007 (2007).
516 Huynh, D. P., Nguyen, D. T., Pulst-Korenberg, J. B., Brice, A. & Pulst, S.-M. Parkin is an E3 ubiquitin-ligase for normal and mutant ataxin-2 and prevents ataxin-2-induced cell death. *Experimental neurology* **203**, 531-541, doi:10.1016/j.expneurol.2006.09.009 (2007).
517 Joch, M. *et al.* Parkin-mediated monoubiquitination of the PDZ protein PICK1 regulates the activity of acid-sensing ion channels. *Mol Biol Cell* **18**, 3105-3118, doi:10.1091/mbc.e05-11-1027 (2007).
518 Lim, M. K. *et al.* Parkin interacts with LIM Kinase 1 and reduces its cofilin-phosphorylation activity via ubiquitination. *Experimental cell research* **313**, 2858-2874, doi:10.1016/j.yexcr.2007.04.016 (2007).
519 Olzmann, J. A. *et al.* Parkin-mediated K63-linked polyubiquitination targets misfolded DJ-1 to aggresomes via binding to HDAC6. *J Cell Biol* **178**, 1025-1038, doi:10.1083/jcb.200611128 (2007).
520 Moore, D. J., West, A. B., Dikeman, D. A., Dawson, V. L. & Dawson, T. M. Parkin mediates the degradation-independent ubiquitination of Hsp70. *J Neurochem* **105**, 1806-1819, doi:10.1111/j.1471-4159.2008.05261.x (2008).
521 Dehvari, N. *et al.* Parkin-mediated ubiquitination regulates phospholipase C-gamma1. *J Cell Mol Med* **13**, 3061-3068, doi:10.1111/j.1582-4934.2008.00443.x (2009).
522 Fukae, J. *et al.* Programmed cell death-2 isoform1 is ubiquitinated by parkin and increased in the substantia nigra of patients with autosomal recessive Parkinson's disease. *FEBS Lett* **583**, 521-525, doi:10.1016/j.febslet.2008.12.055 (2009).
523 Rawal, N. *et al.* Parkin protects dopaminergic neurons from excessive Wnt/beta-catenin signaling. *Biochem Biophys Res Commun* **388**, 473-478, doi:10.1016/j.bbrc.2009.07.014 (2009).
524 Chen, D. *et al.* Parkin mono-ubiquitinates Bcl-2 and regulates autophagy. *J Biol Chem* **285**, 38214-38223, doi:10.1074/jbc.M110.101469 (2010).
525 Geisler, S. *et al.* PINK1/Parkin-mediated mitophagy is dependent on VDAC1 and p62/SQSTM1. *Nat Cell Biol* **12**, 119-131, doi:10.1038/ncb2012 (2010).
526 Tanaka, A. *et al.* Proteasome and p97 mediate mitophagy and degradation of mitofusins induced by Parkin. *J Cell Biol* **191**, 1367-1380, doi:10.1083/jcb.201007013 (2010).
527 Kim, K. Y. *et al.* Parkin is a lipid-responsive regulator of fat uptake in mice and mutant human cells. *J Clin Invest* **121**, 3701-3712, doi:10.1172/jci44736 (2011).
528 Shin, J. H. *et al.* PARIS (ZNF746) repression of PGC-1alpha contributes to neurodegeneration in Parkinson's disease. *Cell* **144**, 689-702, doi:10.1016/j.cell.2011.02.010 (2011).
529 Wang, H. *et al.* Parkin ubiquitinates Drp1 for proteasome-dependent degradation: implication of dysregulated mitochondrial dynamics in Parkinson disease. *J Biol Chem* **286**, 11649-11658, doi:10.1074/jbc.M110.144238 (2011).
530 Wang, X. *et al.* PINK1 and Parkin target Miro for phosphorylation and degradation to arrest mitochondrial motility. *Cell* **147**, 893-906, doi:10.1016/j.cell.2011.10.018 (2011).
531 Johnson, B. N., Berger, A. K., Cortese, G. P. & Lavoie, M. J. The ubiquitin E3 ligase parkin regulates the proapoptotic function of Bax. *Proc Natl Acad Sci U S A* **109**, 6283-6288, doi:10.1073/pnas.1113248109 (2012).
532 Kemeny, S. *et al.* Parkin promotes degradation of the mitochondrial pro-apoptotic ARTS protein. *PLoS One* **7**, e38837, doi:10.1371/journal.pone.0038837 (2012).

533 Okatsu, K. *et al.* Mitochondrial hexokinase HKI is a novel substrate of the Parkin ubiquitin ligase. *Biochem Biophys Res Commun* **428**, 197-202, doi:10.1016/j.bbrc.2012.10.041 (2012).
534 Chung, J. Y. *et al.* Elevated TRAF2/6 expression in Parkinson's disease is caused by the loss of Parkin E3 ligase activity. *Laboratory investigation; a journal of technical methods and pathology* **93**, 663-676, doi:10.1038/labinvest.2013.60 (2013).
535 Ekholm-Reed, S., Goldberg, M. S., Schlossmacher, M. G. & Reed, S. I. Parkin-dependent degradation of the F-box protein Fbw7beta promotes neuronal survival in response to oxidative stress by stabilizing Mcl-1. *Mol Cell Biol* **33**, 3627-3643, doi:10.1128/MCB.00535-13 (2013).
536 Hebron, M. L. *et al.* Parkin ubiquitinates Tar-DNA binding protein-43 (TDP-43) and promotes its cytosolic accumulation via interaction with histone deacetylase 6 (HDAC6). *J Biol Chem* **288**, 4103-4115, doi:10.1074/jbc.M112.419945 (2013).
537 Müller-Rischart, A. K. *et al.* The E3 ligase parkin maintains mitochondrial integrity by increasing linear ubiquitination of NEMO. *Mol Cell* **49**, 908-921, doi:10.1016/j.molcel.2013.01.036 (2013).
538 Sul, J. W. *et al.* Accumulation of the parkin substrate, FAF1, plays a key role in the dopaminergic neurodegeneration. *Hum Mol Genet* **22**, 1558-1573, doi:10.1093/hmg/ddt006 (2013).
539 Bendikov-Bar, I., Rapaport, D., Larisch, S. & Horowitz, M. Parkin-mediated ubiquitination of mutant glucocerebrosidase leads to competition with its substrates PARIS and ARTS. *Orphanet journal of rare diseases* **9**, 86, doi:10.1186/1750-1172-9-86 (2014).
540 Bertolin, G. *et al.* Parkin maintains mitochondrial levels of the protective Parkinson's disease-related enzyme 17-β hydroxysteroid dehydrogenase type 10. *Cell Death Differ* **22**, 1563-1576, doi:10.1038/cdd.2014.224 (2015).
541 Cha, S. H. *et al.* Loss of parkin promotes lipid rafts-dependent endocytosis through accumulating caveolin-1: implications for Parkinson's disease. *Mol Neurodegener* **10**, 63, doi:10.1186/s13024-015-0060-5 (2015).
542 Gao, F. *et al.* The mitochondrial protein BNIP3L is the substrate of PARK2 and mediates mitophagy in PINK1/PARK2 pathway. *Hum Mol Genet* **24**, 2528-2538, doi:10.1093/hmg/ddv017 (2015).
543 Kasai, S., Torii, S., Kakita, A. & Sogawa, K. Inhibitory PAS domain protein is a substrate of PINK1 and Parkin and mediates cell death in a Parkinson's disease model. *Cell death & disease* **6**, e1886, doi:10.1038/cddis.2015.243 (2015).
544 Kurup, P. K. *et al.* STEP61 is a substrate of the E3 ligase parkin and is upregulated in Parkinson's disease. *Proc Natl Acad Sci U S A* **112**, 1202-1207, doi:10.1073/pnas.1417423112 (2015).
545 Lee, S. B. *et al.* Parkin Regulates Mitosis and Genomic Stability through Cdc20/Cdh1. *Mol Cell* **60**, 21-34, doi:10.1016/j.molcel.2015.08.011 (2015).
546 McKeon, J. E., Sha, D., Li, L. & Chin, L.-S. Parkin-mediated K63-polyubiquitination targets ubiquitin C-terminal hydrolase L1 for degradation by the autophagy-lysosome system. *Cellular and molecular life sciences : CMLS* **72**, 1811-1824, doi:10.1007/s00018-014-1781-2 (2015).
547 Liu, K. *et al.* Parkin Regulates the Activity of Pyruvate Kinase M2. *J Biol Chem* **291**, 10307-10317, doi:10.1074/jbc.M115.703066 (2016).
548 Song, P. *et al.* Parkin promotes proteasomal degradation of p62: implication of selective vulnerability of neuronal cells in the pathogenesis of Parkinson's disease. *Protein Cell* **7**, 114-129, doi:10.1007/s13238-015-0230-9 (2016).
549 Song, P., Trajkovic, K., Tsunemi, T. & Krainc, D. Parkin Modulates Endosomal Organization and Function of the Endo-Lysosomal Pathway. *J Neurosci* **36**, 2425-2437, doi:10.1523/jneurosci.2569-15.2016 (2016).
550 Cakir, Z. *et al.* Parkin promotes proteasomal degradation of misregulated BAX. *J Cell Sci* **130**, 2903-2913, doi:10.1242/jcs.200162 (2017).
551 Han, K. *et al.* Parkin regulation of CHOP modulates susceptibility to cardiac endoplasmic reticulum stress. *Scientific Reports* **7**, 2093, doi:10.1038/s41598-017-02339-2 (2017).
552 Kabayama, H. *et al.* Parkin promotes proteasomal degradation of synaptotagmin IV by accelerating polyubiquitination. *Molecular and cellular neurosciences* **80**, 89-99, doi:10.1016/j.mcn.2017.02.006 (2017).
553 Liu, J. *et al.* Parkin targets HIF-1α for ubiquitination and degradation to inhibit breast tumor progression. *Nat Commun* **8**, 1823, doi:10.1038/s41467-017-01947-w (2017).
554 Park, M. H. *et al.* Parkin Knockout Inhibits Neuronal Development via Regulation of Proteasomal Degradation of p21. *Theranostics* **7**, 2033-2045, doi:10.7150/thno.19824 (2017).
555 Scott, T. L. *et al.* Polyubiquitination of apurinic/apyrimidinic endonuclease 1 by Parkin. *Molecular carcinogenesis* **56**, 325-336, doi:10.1002/mc.22495 (2017).
556 Singh, K. *et al.* Parkin targets NOD2 to regulate astrocyte endoplasmic reticulum stress and inflammation. *Glia* **66**, 2427-2437, doi:10.1002/glia.23482 (2018).
557 Wang, Y., Shan, B., Liang, Y., Wei, H. & Yuan, J. Parkin regulates NF-κB by mediating site-specific ubiquitination of RIPK1. *Cell death & disease* **9**, 732, doi:10.1038/s41419-018-0770-z (2018).

558 Bernardini, J. P. *et al.* Parkin inhibits BAK and BAX apoptotic function by distinct mechanisms during mitophagy. *Embo j* **38**, doi:10.15252/embj.201899916 (2019).
559 Koyano, F. *et al.* Parkin-mediated ubiquitylation redistributes MITOL/March5 from mitochondria to peroxisomes. *EMBO Rep* **20**, e47728, doi:10.15252/embr.201947728 (2019).
560 Sun, T. *et al.* Parkin Regulates Programmed Necrosis and Myocardial Ischemia/Reperfusion Injury by Targeting Cyclophilin-D. *Antioxid Redox Signal* **31**, 1177-1193, doi:10.1089/ars.2019.7734 (2019).
561 Chew, K. C. M. *et al.* Parkin Mediates Apparent E2-Independent Monoubiquitination In Vitro and Contains an Intrinsic Activity That Catalyzes Polyubiquitination. *PLOS ONE* **6**, e19720, doi:10.1371/journal.pone.0019720 (2011).
562 Chin, L. S., Olzmann, J. A. & Li, L. Parkin-mediated ubiquitin signalling in aggresome formation and autophagy. *Biochem Soc Trans* **38**, 144-149, doi:10.1042/bst0380144 (2010).
563 Moore, D. J. Parkin: a multifaceted ubiquitin ligase. *Biochem Soc Trans* **34**, 749-753, doi:10.1042/bst0340749 (2006).
564 Ordureau, A. *et al.* Quantitative proteomics reveal a feedforward mechanism for mitochondrial PARKIN translocation and ubiquitin chain synthesis. *Mol Cell* **56**, 360-375, doi:10.1016/j.molcel.2014.09.007 (2014).
565 Bremm, A., Freund, S. M. & Komander, D. Lys11-linked ubiquitin chains adopt compact conformations and are preferentially hydrolyzed by the deubiquitinase Cezanne. *Nat Struct Mol Biol* **17**, 939-947, doi:10.1038/nsmb.1873 (2010).
566 Bremm, A., Moniz, S., Mader, J., Rocha, S. & Komander, D. Cezanne (OTUD7B) regulates HIF-1α homeostasis in a proteasome-independent manner. *EMBO Rep* **15**, 1268-1277, doi:10.15252/embr.201438850 (2014).
567 Komander, D. & Rape, M. The ubiquitin code. *Annu Rev Biochem* **81**, 203-229, doi:10.1146/annurev-biochem-060310-170328 (2012).
568 Durcan, T. M. *et al.* USP8 regulates mitophagy by removing K6-linked ubiquitin conjugates from parkin. *Embo j* **33**, 2473-2491, doi:10.15252/embj.201489729 (2014).
569 Liu, J., Liu, W., Li, R. & Yang, H. Mitophagy in Parkinson's Disease: From Pathogenesis to Treatment. *Cells* **8**, 712, doi:10.3390/cells8070712 (2019).
570 Meissner, C., Lorenz, H., Hehn, B. & Lemberg, M. K. Intramembrane protease PARL defines a negative regulator of PINK1- and PARK2/Parkin-dependent mitophagy. *Autophagy* **11**, 1484-1498, doi:10.1080/15548627.2015.1063763 (2015).
571 Aguirre, J. D., Dunkerley, K. M., Mercier, P. & Shaw, G. S. Structure of phosphorylated UBL domain and insights into PINK1-orchestrated parkin activation. *Proc Natl Acad Sci U S A* **114**, 298-303, doi:10.1073/pnas.1613040114 (2017).
572 Wong, Y. C. & Holzbaur, E. L. Optineurin is an autophagy receptor for damaged mitochondria in parkin-mediated mitophagy that is disrupted by an ALS-linked mutation. *Proc Natl Acad Sci U S A* **111**, E4439-4448, doi:10.1073/pnas.1405752111 (2014).
573 Wong, Y. C. & Holzbaur, E. L. Temporal dynamics of PARK2/parkin and OPTN/optineurin recruitment during the mitophagy of damaged mitochondria. *Autophagy* **11**, 422-424, doi:10.1080/15548627.2015.1009792 (2015).
574 Harper, J. W., Ordureau, A. & Heo, J. M. Building and decoding ubiquitin chains for mitophagy. *Nature reviews. Molecular cell biology* **19**, 93-108, doi:10.1038/nrm.2017.129 (2018).
575 McWilliams, T. G. *et al.* Basal Mitophagy Occurs Independently of PINK1 in Mouse Tissues of High Metabolic Demand. *Cell Metab* **27**, 439-449 e435, doi:10.1016/j.cmet.2017.12.008 (2018).
576 Villa, E., Marchetti, S. & Ricci, J. E. No Parkin Zone: Mitophagy without Parkin. *Trends in cell biology* **28**, 882-895, doi:10.1016/j.tcb.2018.07.004 (2018).
577 Hanna, R. A. *et al.* Microtubule-associated protein 1 light chain 3 (LC3) interacts with Bnip3 protein to selectively remove endoplasmic reticulum and mitochondria via autophagy. *J Biol Chem* **287**, 19094-19104, doi:10.1074/jbc.M111.322933 (2012).
578 Rogov, V. V. *et al.* Phosphorylation of the mitochondrial autophagy receptor Nix enhances its interaction with LC3 proteins. *Sci Rep* **7**, 1131, doi:10.1038/s41598-017-01258-6 (2017).
579 Liu, L. *et al.* Mitochondrial outer-membrane protein FUNDC1 mediates hypoxia-induced mitophagy in mammalian cells. *Nat Cell Biol* **14**, 177-185, doi:10.1038/ncb2422 (2012).
580 Liu, L., Sakakibara, K., Chen, Q. & Okamoto, K. Receptor-mediated mitophagy in yeast and mammalian systems. *Cell research* **24**, 787-795, doi:10.1038/cr.2014.75 (2014).
581 Chu, C. T. *et al.* Cardiolipin externalization to the outer mitochondrial membrane acts as an elimination signal for mitophagy in neuronal cells. *Nat Cell Biol* **15**, 1197-1205, doi:10.1038/ncb2837 (2013).
582 Villa, E. *et al.* Parkin-Independent Mitophagy Controls Chemotherapeutic Response in Cancer Cells. *Cell Rep* **20**, 2846-2859, doi:10.1016/j.celrep.2017.08.087 (2017).

583 Yun, J. *et al.* MUL1 acts in parallel to the PINK1/parkin pathway in regulating mitofusin and compensates for loss of PINK1/parkin. *Elife* **3**, e01958, doi:10.7554/eLife.01958 (2014).
584 Fu, C. *et al.* Quantitative analysis of redox-sensitive proteome with DIGE and ICAT. *Journal of proteome research* **7**, 3789-3802, doi:10.1021/pr800233r (2008).
585 Stolen Craig, M. *et al.* Origins of Serum Semicarbazide-Sensitive Amine Oxidase. *Circulation Research* **95**, 50-57, doi:10.1161/01.RES.0000134630.68877.2F (2004).
586 Mazzatti, D. J., Pawelec, G., Longdin, R., Powell, J. R. & Forsey, R. J. SELDI-TOF-MS ProteinChip array profiling of T-cell clones propagated in long-term culture identifies human profilin-1 as a potential bio-marker of immunosenescence. *Proteome science* **5**, 7-7, doi:10.1186/1477-5956-5-7 (2007).
587 Guy, G. R., Cairns, J., Ng, S. B. & Tan, Y. H. Inactivation of a redox-sensitive protein phosphatase during the early events of tumor necrosis factor/interleukin-1 signal transduction. *Journal of Biological Chemistry* **268**, 2141-2148, doi:10.1016/S0021-9258(18)53973-9 (1993).
588 Christopher, K. L. *et al.* Alpha-crystallin-mediated protection of lens cells against heat and oxidative stress-induced cell death. *Biochimica et biophysica acta* **1843**, 309-315, doi:10.1016/j.bbamcr.2013.11.010 (2014).
589 Fuentes-Almagro, C. A., Prieto-Álamo, M.-J., Pueyo, C. & Jurado, J. Identification of proteins containing redox-sensitive thiols after PRDX1, PRDX3 and GCLC silencing and/or glucose oxidase treatment in Hepa 1–6 cells. *Journal of Proteomics* **77**, 262-279, doi:10.1016/j.jprot.2012.08.025 (2012).
590 Wang, S.-B. *et al.* Redox regulation of mitochondrial ATP synthase: implications for cardiac resynchronization therapy. *Circulation research* **109**, 750-757, doi:10.1161/CIRCRESAHA.111.246124 (2011).
591 Stevens, F. J., Dong Li, A., Salman Lateef, S. & Anderson, L. E. Identification of potential inter-domain disulfides in three higher plant mitochondrial citrate synthases: Paradoxical differences in redox-sensitivity as compared with the animal enzyme. *Photosynthesis Research* **54**, 185-197, doi:10.1023/A:1005991423503 (1997).
592 McLain, A. L., Szweda, P. A. & Szweda, L. I. α-Ketoglutarate dehydrogenase: A mitochondrial redox sensor. *Free radical research* **45**, 29-36, doi:10.3109/10715762.2010.534163 (2011).
593 Humphries, K. M., Szweda, P. A. & Szweda, L. I. Aging: A shift from redox regulation to oxidative damage. *Free radical research* **40**, 1239-1243, doi:10.1080/10715760600913184 (2006).
594 Ghezzi, P., Bonetto, V. & Fratelli, M. Thiol–Disulfide Balance: From the Concept of Oxidative Stress to that of Redox Regulation. *Antioxidants & Redox Signaling* **7**, 964-972, doi:10.1089/ars.2005.7.964 (2005).
595 Reed, T. *et al.* Redox proteomic identification of 4-hydroxy-2-nonenal-modified brain proteins in amnestic mild cognitive impairment: insight into the role of lipid peroxidation in the progression and pathogenesis of Alzheimer's disease. *Neurobiol Dis* **30**, 107-120, doi:10.1016/j.nbd.2007.12.007 (2008).
596 Taylor, E. R. *et al.* Reversible glutathionylation of complex I increases mitochondrial superoxide formation. *J Biol Chem* **278**, 19603-19610, doi:10.1074/jbc.M209359200 (2003).
597 Kim, Y., Ingram, L. O. & Shanmugam, K. T. Dihydrolipoamide dehydrogenase mutation alters the NADH sensitivity of pyruvate dehydrogenase complex of Escherichia coli K-12. *Journal of bacteriology* **190**, 3851-3858, doi:10.1128/jb.00104-08 (2008).
598 Tsukamoto, Y., Fukushima, Y., Hara, S. & Hisabori, T. Redox Control of the Activity of Phosphoglycerate Kinase in Synechocystis sp. PCC6803. *Plant and Cell Physiology* **54**, 484-491, doi:10.1093/pcp/pct002 (2013).
599 Brandes, N., Reichmann, D., Tienson, H., Leichert, L. I. & Jakob, U. Using quantitative redox proteomics to dissect the yeast redoxome. *The Journal of biological chemistry* **286**, 41893-41903, doi:10.1074/jbc.M111.296236 (2011).
600 Santhanam, S., Venkatraman, A. & Ramakrishna, B. S. Impairment of mitochondrial acetoacetyl CoA thiolase activity in the colonic mucosa of patients with ulcerative colitis. *Gut* **56**, 1543-1549, doi:10.1136/gut.2006.108449 (2007).
601 Hempel, N., Bartling, T. R., Mian, B. & Melendez, J. A. Acquisition of the metastatic phenotype is accompanied by H2O2-dependent activation of the p130Cas signaling complex. *Molecular cancer research : MCR* **11**, 303-312, doi:10.1158/1541-7786.Mcr-12-0478 (2013).
602 Miki, H. & Funato, Y. Regulation of intracellular signalling through cysteine oxidation by reactive oxygen species. *The Journal of Biochemistry* **151**, 255-261, doi:10.1093/jb/mvs006 (2012).
603 Johnston, P. A. *et al.* Development of a 384-Well Colorimetric Assay to Quantify Hydrogen Peroxide Generated by the Redox Cycling of Compounds in the Presence of Reducing Agents. *Assay and drug development technologies* **6**, 505-518, doi:10.1089/adt.2008.151 (2008).
604 Wang, W. & Barger, S. W. Roles of quaternary structure and cysteine residues in the activity of human serine racemase. *BMC Biochemistry* **12**, 63, doi:10.1186/1471-2091-12-63 (2011).
605 Lowenstein, C. J., Morrell, C. N. & Yamakuchi, M. Regulation of Weibel–Palade Body Exocytosis. *Trends in Cardiovascular Medicine* **15**, 302-308, doi:10.1016/j.tcm.2005.09.005 (2005).

606 Lowenstein, C. J. & Tsuda, H. N-ethylmaleimide-sensitive factor: a redox sensor in exocytosis. *Biological chemistry* **387**, 1377-1383, doi:10.1515/bc.2006.173 (2006).
607 Bachnoff, N., Cohen-Kutner, M., Trus, M. & Atlas, D. Intra-membrane signaling between the voltage-gated Ca2+-channel and cysteine residues of syntaxin 1A coordinates synchronous release. *Scientific reports* **3**, 1620-1620, doi:10.1038/srep01620 (2013).
608 Hao, G., Derakhshan, B., Shi, L., Campagne, F. & Gross, S. S. SNOSID, a proteomic method for identification of cysteine S-nitrosylation sites in complex protein mixtures. *Proceedings of the National Academy of Sciences of the United States of America* **103**, 1012, doi:10.1073/pnas.0508412103 (2006).
609 Nayak, A. AN EVOLUTIONARY STUDIES AND DOMAIN BASED HOMOLOGY MODELING OF HUMAN SEPTIN-1. *Wyno Journal of Medical Sciences* **Vol-2**, 1-18 (2013).
610 Sawa, T. *et al.* S-guanylation proteomics for redox-based mitochondrial signaling. *Nitric Oxide* **27**, S11, doi:10.1016/j.niox.2012.04.041 (2012).
611 Nguyen, P., Awwad, R. T., Smart, D. D. K., Spitz, D. R. & Gius, D. Thioredoxin reductase as a novel molecular target for cancer therapy. *Cancer letters* **236**, 164-174, doi:10.1016/j.canlet.2005.04.028 (2006).
612 Pennington, J. D. *et al.* Thioredoxin and thioredoxin reductase as redox-sensitive molecular targets for cancer therapy. *Curr Pharm Des* **13**, 3368-3377 (2007).
613 Duhe, R. J. *et al.* Oxidation of critical cysteine residues of type I adenylyl cyclase by o-iodosobenzoate or nitric oxide reversibly inhibits stimulation by calcium and calmodulin. *Journal of Biological Chemistry* **269**, 7290-7296 (1994).
614 Wu, C. *et al.* Thioredoxin 1-mediated post-translational modifications: reduction, transnitrosylation, denitrosylation, and related proteomics methodologies. *Antioxidants & redox signaling* **15**, 2565-2604, doi:10.1089/ars.2010.3831 (2011).
615 Stamatakis, K., Sánchez-Gómez, F. J. & Pérez-Sala, D. Identification of Novel Protein Targets for Modification by 15-Deoxy-Δ^{12,14}-Prostaglandin J₂ in Mesangial Cells Reveals Multiple Interactions with the Cytoskeleton. *Journal of the American Society of Nephrology* **17**, 89-98, doi:10.1681/asn.2005030329 (2006).
616 Shen, H., Sikorska, M., LeBlanc, J., Walker, P. R. & Liu, Q. Y. Oxidative stress regulated expression of Ubiquitin Carboxyl-terminal Hydrolase-L1: Role in cell survival. *Apoptosis : an international journal on programmed cell death* **11**, 1049-1059, doi:10.1007/s10495-006-6303-8 (2006).
617 Castegna, A. *et al.* Proteomic identification of oxidatively modified proteins in Alzheimer's disease brain. Part II: dihydropyrimidinase-related protein 2, α-enolase and heat shock cognate 71. *Journal of Neurochemistry* **82**, 1524-1532, doi:10.1046/j.1471-4159.2002.01103.x (2002).
618 Dansen, T. B. *et al.* Redox-sensitive cysteines bridge p300/CBP-mediated acetylation and FoxO4 activity. *Nature Chemical Biology* **5**, 664-672, doi:10.1038/nchembio.194 (2009).
619 Hurd, T. R., Prime, T. A., Harbour, M. E., Lilley, K. S. & Murphy, M. P. Detection of Reactive Oxygen Species-sensitive Thiol Proteins by Redox Difference Gel Electrophoresis: IMPLICATIONS FOR MITOCHONDRIAL REDOX SIGNALING. *Journal of Biological Chemistry* **282**, 22040-22051, doi:10.1074/jbc.M703591200 (2007).
620 Parinandi, N. L., Scribner, W. M., Vepa, S., Shi, S. & Natarajan, V. Phospholipase D Activation in Endothelial Cells Is Redox Sensitive. *Antioxidants & Redox Signaling* **1**, 193-210, doi:10.1089/ars.1999.1.2-193 (1999).
621 Wang, X.-T., McCullough, K. D., Wang, X.-J., Carpenter, G. & Holbrook, N. J. Oxidative Stress-induced Phospholipase C-γ1 Activation Enhances Cell Survival. *Journal of Biological Chemistry* **276**, 28364-28371, doi:10.1074/jbc.M102693200 (2001).
622 Takahashi, R. & Goto, S. Alteration of aminoacyl-tRNA synthetase with age: Heat-labilization of the enzyme by oxidative damage. *Archives of Biochemistry and Biophysics* **277**, 228-233, doi:10.1016/0003-9861(90)90573-H (1990).
623 Ling, J. & Söll, D. Severe oxidative stress induces protein mistranslation through impairment of an aminoacyl-tRNA synthetase editing site. *Proceedings of the National Academy of Sciences* **107**, 4028, doi:10.1073/pnas.1000315107 (2010).
624 Matés, J. M., Pérez-Gómez, C., de Castro, I. N., Asenjo, M. & Márquez, J. Glutamine and its relationship with intracellular redox status, oxidative stress and cell proliferation/death. *The International Journal of Biochemistry & Cell Biology* **34**, 439-458, doi:10.1016/S1357-2725(01)00143-1 (2002).
625 Wang, Y. *et al.* Cap1p is involved in multiple pathways of oxidative stress response in Candida albicans. *Free Radical Biology and Medicine* **40**, 1201-1209, doi:10.1016/j.freeradbiomed.2005.11.019 (2006).
626 Briolat, V. & Reysset, G. Identification of the Clostridium perfringens Genes Involved in the Adaptive Response to Oxidative Stress. *Journal of bacteriology* **184**, 2333-2343, doi:10.1128/jb.184.9.2333-2343.2002 (2002).

627 Giraud, E., Van Aken, O., Uggalla, V. & Whelan, J. REDOX regulation of mitochondrial function in plants. *Plant, Cell & Environment* **35**, 271-280, doi:10.1111/j.1365-3040.2011.02293.x (2012).
628 Haavik, J. & Toska, K. Tyrosine hydroxylase and Parkinson's disease. *Molecular Neurobiology* **16**, 285-309, doi:10.1007/BF02741387 (1998).
629 Oettl, K. & Stauber, R. E. Physiological and pathological changes in the redox state of human serum albumin critically influence its binding properties. *Br J Pharmacol* **151**, 580-590, doi:10.1038/sj.bjp.0707251 (2007).
630 Sultana, R. *et al.* Identification of nitrated proteins in Alzheimer's disease brain using a redox proteomics approach. *Neurobiol Dis* **22**, 76-87, doi:10.1016/j.nbd.2005.10.004 (2006).
631 Kaindl, A. M. *et al.* Acute and long-term proteome changes induced by oxidative stress in the developing brain. *Cell Death & Differentiation* **13**, 1097-1109, doi:10.1038/sj.cdd.4401796 (2006).
632 de la Vega, L. *et al.* A Redox-Regulated SUMO/Acetylation Switch of HIPK2 Controls the Survival Threshold to Oxidative Stress. *Molecular cell* **46**, 472-483, doi:10.1016/j.molcel.2012.03.003 (2012).
633 Baek, S. H. *et al.* Role of small heat shock protein HSP25 in radioresistance and glutathione-redox cycle. *J Cell Physiol* **183**, 100-107, doi:10.1002/(sici)1097-4652(200004)183:1<100::Aid-jcp12>3.0.Co;2-f (2000).
634 Greco, T. M. *et al.* Identification of S-nitrosylation motifs by site-specific mapping of the S-nitrosocysteine proteome in human vascular smooth muscle cells. *Proceedings of the National Academy of Sciences* **103**, 7420-7425, doi:10.1073/pnas.0600729103 (2006).
635 Fiaschi, T. *et al.* Redox Regulation of β-Actin during Integrin-mediated Cell Adhesion. *Journal of Biological Chemistry* **281**, 22983-22991, doi:10.1074/jbc.M603040200 (2006).
636 Filomeni, G., Rotilio, G. & Ciriolo, M. R. Cell signalling and the glutathione redox system. *Biochem Pharmacol* **64**, 1057-1064, doi:10.1016/s0006-2952(02)01176-0 (2002).
637 Menon, S. G. & Goswami, P. C. A redox cycle within the cell cycle: ring in the old with the new. *Oncogene* **26**, 1101-1109, doi:10.1038/sj.onc.1209895 (2007).
638 Ziegler, D. M. Role of reversible oxidation-reduction of enzyme thiols-disulfides in metabolic regulation. *Annu Rev Biochem* **54**, 305-329, doi:10.1146/annurev.bi.54.070185.001513 (1985).
639 Lee, C.-F., Paull, T. T. & Person, M. D. Proteome-wide detection and quantitative analysis of irreversible cysteine oxidation using long column UPLC-pSRM. *Journal of proteome research* **12**, 4302-4315, doi:10.1021/pr400201d (2013).
640 Feany, M. B. & Pallanck, L. J. Parkin: a multipurpose neuroprotective agent? *Neuron* **38**, 13-16 (2003).
641 Jiang, H., Ren, Y., Zhao, J. & Feng, J. Parkin protects human dopaminergic neuroblastoma cells against dopamine-induced apoptosis. *Hum Mol Genet* **13**, 1745-1754, doi:10.1093/hmg/ddh180 (2004).
642 Casarejos, M. J. *et al.* Susceptibility to rotenone is increased in neurons from parkin null mice and is reduced by minocycline. *J Neurochem* **97**, 934-946, doi:10.1111/j.1471-4159.2006.03777.x (2006).
643 Yasuda, T. *et al.* Parkin-mediated protection of dopaminergic neurons in a chronic MPTP-minipump mouse model of Parkinson disease. *J Neuropathol Exp Neurol* **70**, 686-697, doi:10.1097/NEN.0b013e3182269ecd (2011).
644 Creed, R. B. & Goldberg, M. S. New Developments in Genetic rat models of Parkinson's Disease. *Mov Disord* **33**, 717-729, doi:10.1002/mds.27296 (2018).
645 Shlevkov, E., Kramer, T., Schapansky, J., LaVoie, M. J. & Schwarz, T. L. Miro phosphorylation sites regulate Parkin recruitment and mitochondrial motility. *Proc Natl Acad Sci U S A* **113**, E6097-e6106, doi:10.1073/pnas.1612283113 (2016).
646 Ziviani, E., Tao, R. N. & Whitworth, A. J. Drosophila parkin requires PINK1 for mitochondrial translocation and ubiquitinates mitofusin. *Proc Natl Acad Sci U S A* **107**, 5018-5023, doi:10.1073/pnas.0913485107 (2010).
647 McLelland, G. L., Soubannier, V., Chen, C. X., McBride, H. M. & Fon, E. A. Parkin and PINK1 function in a vesicular trafficking pathway regulating mitochondrial quality control. *EMBO J* **33**, 282-295, doi:10.1002/embj.201385902 (2014).
648 Soubannier, V. *et al.* A vesicular transport pathway shuttles cargo from mitochondria to lysosomes. *Curr Biol* **22**, 135-141, doi:10.1016/j.cub.2011.11.057 (2012).
649 Manzanillo, P. S. *et al.* The ubiquitin ligase parkin mediates resistance to intracellular pathogens. *Nature* **501**, 512-516, doi:10.1038/nature12566 (2013).
650 Xu, L., Lin, D. C., Yin, D. & Koeffler, H. P. An emerging role of PARK2 in cancer. *J Mol Med (Berl)* **92**, 31-42, doi:10.1007/s00109-013-1107-0 (2014).
651 Liu, J., Zhang, C., Hu, W. & Feng, Z. Parkinson's disease-associated protein Parkin: an unusual player in cancer. *Cancer Commun (Lond)* **38**, 40-40, doi:10.1186/s40880-018-0314-z (2018).
652 Hu, H. H. *et al.* PARKIN Inactivation Links Parkinson's Disease to Melanoma. *Journal of the National Cancer Institute* **108**, doi:10.1093/jnci/djv340 (2016).

653 Cesari, R. *et al.* Parkin, a gene implicated in autosomal recessive juvenile parkinsonism, is a candidate tumor suppressor gene on chromosome 6q25-q27. *Proc Natl Acad Sci U S A* **100**, 5956-5961, doi:10.1073/pnas.0931262100 (2003).
654 Denison, S. R. *et al.* Alterations in the common fragile site gene Parkin in ovarian and other cancers. *Oncogene* **22**, 8370-8378, doi:10.1038/sj.onc.1207072 (2003).
655 Picchio, M. C. *et al.* Alterations of the tumor suppressor gene Parkin in non-small cell lung cancer. *Clin Cancer Res* **10**, 2720-2724, doi:10.1158/1078-0432.ccr-03-0086 (2004).
656 Tay, S. P. *et al.* Parkin enhances the expression of cyclin-dependent kinase 6 and negatively regulates the proliferation of breast cancer cells. *J Biol Chem* **285**, 29231-29238, doi:10.1074/jbc.M110.108241 (2010).
657 Veeriah, S. *et al.* Somatic mutations of the Parkinson's disease-associated gene PARK2 in glioblastoma and other human malignancies. *Nat Genet* **42**, 77-82, doi:10.1038/ng.491 (2010).
658 Veeriah, S., Morris, L., Solit, D. & Chan, T. A. The familial Parkinson disease gene PARK2 is a multisite tumor suppressor on chromosome 6q25.2-27 that regulates cyclin E. *Cell Cycle* **9**, 1451-1452, doi:10.4161/cc.9.8.11583 (2010).
659 Lee, Seung B. *et al.* Parkin Regulates Mitosis and Genomic Stability through Cdc20/Cdh1. *Molecular cell* **60**, 21-34, doi:10.1016/j.molcel.2015.08.011 (2015).
660 Carroll, R. G., Hollville, E. & Martin, S. J. Parkin sensitizes toward apoptosis induced by mitochondrial depolarization through promoting degradation of Mcl-1. *Cell Rep* **9**, 1538-1553, doi:10.1016/j.celrep.2014.10.046 (2014).
661 Wang, H. *et al.* Parkin regulates paclitaxel sensitivity in breast cancer via a microtubule-dependent mechanism. *The Journal of pathology* **218**, 76-85, doi:10.1002/path.2512 (2009).
662 Harrison, C. A., Gray, P. C., Vale, W. W. & Robertson, D. M. Antagonists of activin signaling: mechanisms and potential biological applications. *Trends in endocrinology and metabolism: TEM* **16**, 73-78, doi:10.1016/j.tem.2005.01.003 (2005).
663 Fujiwara, M. *et al.* Parkin as a tumor suppressor gene for hepatocellular carcinoma. *Oncogene* **27**, 6002-6011, doi:10.1038/onc.2008.199 (2008).
664 Toma, M. I. *et al.* PARK2 and PACRG are commonly downregulated in clear-cell renal cell carcinoma and are associated with aggressive disease and poor clinical outcome. *Genes, chromosomes & cancer* **52**, 265-273, doi:10.1002/gcc.22026 (2013).
665 Sun, X. *et al.* Parkin deficiency contributes to pancreatic tumorigenesis by inducing spindle multipolarity and misorientation. *Cell Cycle* **12**, 1133-1141, doi:10.4161/cc.24215 (2013).
666 Ni, H. *et al.* Inactivation of parkin by promoter methylation correlated with lymph node metastasis and genomic instability in nasopharyngeal carcinoma. *Tumour biology : the journal of the International Society for Oncodevelopmental Biology and Medicine* **39**, 1010428317695025, doi:10.1177/1010428317695025 (2017).
667 LaGory, E. L. & Giaccia, A. J. The ever-expanding role of HIF in tumour and stromal biology. *Nat Cell Biol* **18**, 356-365, doi:10.1038/ncb3330 (2016).
668 da Costa, C. A. *et al.* Transcriptional repression of p53 by parkin and impairment by mutations associated with autosomal recessive juvenile Parkinson's disease. *Nat Cell Biol* **11**, 1370-1375, doi:10.1038/ncb1981 (2009).
669 Zhang, C. *et al.* Parkin, a p53 target gene, mediates the role of p53 in glucose metabolism and the Warburg effect. *Proc Natl Acad Sci U S A* **108**, 16259-16264, doi:10.1073/pnas.1113884108 (2011).
670 Warburg, O. On the origin of cancer cells. *Science* **123**, 309-314, doi:10.1126/science.123.3191.309 (1956).
671 Sunico, C. R. *et al.* S-Nitrosylation of parkin as a novel regulator of p53-mediated neuronal cell death in sporadic Parkinson's disease. *Mol Neurodegener* **8**, 29, doi:10.1186/1750-1326-8-29 (2013).
672 Alves da Costa, C., Duplan, E., Rouland, L. & Checler, F. The Transcription Factor Function of Parkin: Breaking the Dogma. *Frontiers in neuroscience* **12**, 965-965, doi:10.3389/fnins.2018.00965 (2019).
673 Jin, H. S. *et al.* The PARK2 gene is involved in the maintenance of pancreatic β-cell functions related to insulin production and secretion. *Molecular and cellular endocrinology* **382**, 178-189, doi:10.1016/j.mce.2013.09.031 (2014).
674 Cairó, M. *et al.* Parkin controls brown adipose tissue plasticity in response to adaptive thermogenesis. *EMBO Rep* **20**, doi:10.15252/embr.201846832 (2019).
675 Chen, C. C. W., Erlich, A. T., Crilly, M. J. & Hood, D. A. Parkin is required for exercise-induced mitophagy in muscle: impact of aging. *Am J Physiol Endocrinol Metab* **315**, E404-e415, doi:10.1152/ajpendo.00391.2017 (2018).
676 Mira, M. T. *et al.* Susceptibility to leprosy is associated with PARK2 and PACRG. *Nature* **427**, 636-640, doi:10.1038/nature02326 (2004).
677 Ali, S. *et al.* PARK2/PACRG polymorphisms and susceptibility to typhoid and paratyphoid fever. *Clinical and experimental immunology* **144**, 425-431, doi:10.1111/j.1365-2249.2006.03087.x (2006).

678 Mooster, J. L. *et al.* Immune deficiency caused by impaired expression of nuclear factor-kappaB essential modifier (NEMO) because of a mutation in the 5' untranslated region of the NEMO gene. *The Journal of allergy and clinical immunology* **126**, 127-132.e127, doi:10.1016/j.jaci.2010.04.026 (2010).
679 Matheoud, D. *et al.* Parkinson's Disease-Related Proteins PINK1 and Parkin Repress Mitochondrial Antigen Presentation. *Cell* **166**, 314-327, doi:10.1016/j.cell.2016.05.039 (2016).
680 Mouton-Liger, F. *et al.* Parkin deficiency modulates NLRP3 inflammasome activation by attenuating an A20-dependent negative feedback loop. *Glia* **66**, 1736-1751, doi:10.1002/glia.23337 (2018).
681 Li, J. *et al.* Parkin Impairs Antiviral Immunity by Suppressing the Mitochondrial Reactive Oxygen Species-Nlrp3 Axis and Antiviral Inflammation. *iScience* **16**, 468-484, doi:10.1016/j.isci.2019.06.008 (2019).
682 Sliter, D. A. *et al.* Parkin and PINK1 mitigate STING-induced inflammation. *Nature*, doi:10.1038/s41586-018-0448-9 (2018).
683 Martinon, F., Burns, K. & Tschopp, J. The inflammasome: a molecular platform triggering activation of inflammatory caspases and processing of proIL-beta. *Mol Cell* **10**, 417-426, doi:10.1016/s1097-2765(02)00599-3 (2002).
684 Yang, Y., Wang, H., Kouadir, M., Song, H. & Shi, F. Recent advances in the mechanisms of NLRP3 inflammasome activation and its inhibitors. *Cell death & disease* **10**, 128, doi:10.1038/s41419-019-1413-8 (2019).
685 Heid, M. E. *et al.* Mitochondrial reactive oxygen species induces NLRP3-dependent lysosomal damage and inflammasome activation. *J Immunol* **191**, 5230-5238, doi:10.4049/jimmunol.1301490 (2013).
686 Ishikawa, H. & Barber, G. N. STING is an endoplasmic reticulum adaptor that facilitates innate immune signalling. *Nature* **455**, 674-678, doi:10.1038/nature07317 (2008).
687 Chen, Q., Sun, L. & Chen, Z. J. Regulation and function of the cGAS-STING pathway of cytosolic DNA sensing. *Nat Immunol* **17**, 1142-1149, doi:10.1038/ni.3558 (2016).
688 Zarate-Lagunes, M. *et al.* Parkin immunoreactivity in the brain of human and non-human primates: An immunohistochemical analysis in normal conditions and in Parkinsonian syndromes. *Journal of Comparative Neurology* **432**, 184-196, doi:10.1002/cne.1096 (2001).
689 Schlossmacher, M. G. *et al.* Parkin localizes to the Lewy bodies of Parkinson disease and dementia with Lewy bodies. *Am J Pathol* **160**, 1655-1667, doi:10.1016/S0002-9440(10)61113-3 (2002).
690 Pawlyk, A. C. *et al.* Novel monoclonal antibodies demonstrate biochemical variation of brain parkin with age. *J Biol Chem* **278**, 48120-48128, doi:10.1074/jbc.M306889200 (2003).
691 Berg JM, T. J., Stryer L. in *Biochemistry* (W H Freeman and Company, 2002).
692 Kurutas, E. B. The importance of antioxidants which play the role in cellular response against oxidative/nitrosative stress: current state. *Nutrition journal* **15**, 71, doi:10.1186/s12937-016-0186-5 (2016).
693 Valko, M. *et al.* Free radicals and antioxidants in normal physiological functions and human disease. *Int J Biochem Cell Biol* **39**, 44-84, doi:10.1016/j.biocel.2006.07.001 (2007).
694 Go, Y. M. & Jones, D. P. The redox proteome. *J Biol Chem* **288**, 26512-26520, doi:10.1074/jbc.R113.464131 (2013).
695 Alcock, L. J., Perkins, M. V. & Chalker, J. M. Chemical methods for mapping cysteine oxidation. *Chem Soc Rev* **47**, 231-268, doi:10.1039/c7cs00607a (2018).
696 Townsend, D. M., Tew, K. D. & Tapiero, H. The importance of glutathione in human disease. *Biomed Pharmacother* **57**, 145-155, doi:10.1016/s0753-3322(03)00043-x (2003).
697 Wang, S. & Kaufman, R. J. The impact of the unfolded protein response on human disease. *J Cell Biol* **197**, 857-867, doi:10.1083/jcb.201110131 (2012).
698 Lee, S. J., Kim, D. G., Lee, K. Y., Koo, J. S. & Lee, B. J. Regulatory mechanisms of thiol-based redox sensors: lessons learned from structural studies on prokaryotic redox sensors. *Arch Pharm Res* **41**, 583-593, doi:10.1007/s12272-018-1036-0 (2018).
699 Apel, K. & Hirt, H. Reactive oxygen species: metabolism, oxidative stress, and signal transduction. *Annu Rev Plant Biol* **55**, 373-399, doi:10.1146/annurev.arplant.55.031903.141701 (2004).
700 Reinheckel, T. *et al.* Comparative resistance of the 20S and 26S proteasome to oxidative stress. *Biochem J* **335 (Pt 3)**, 637-642, doi:10.1042/bj3350637 (1998).
701 Pajares, M. *et al.* Redox control of protein degradation. *Redox Biol* **6**, 409-420, doi:10.1016/j.redox.2015.07.003 (2015).
702 Scherz-Shouval, R. *et al.* Reactive oxygen species are essential for autophagy and specifically regulate the activity of Atg4. *Embo j* **26**, 1749-1760, doi:10.1038/sj.emboj.7601623 (2007).
703 Wani, W. Y. *et al.* Regulation of autophagy by protein post-translational modification. *Laboratory investigation; a journal of technical methods and pathology* **95**, 14-25, doi:10.1038/labinvest.2014.131 (2015).

704 Shendelman, S., Jonason, A., Martinat, C., Leete, T. & Abeliovich, A. DJ-1 is a redox-dependent molecular chaperone that inhibits alpha-synuclein aggregate formation. *PLoS Biol* **2**, e362, doi:10.1371/journal.pbio.0020362 (2004).
705 Xu, C.-Y. *et al.* DJ-1 Inhibits α-Synuclein Aggregation by Regulating Chaperone-Mediated Autophagy. *Front Aging Neurosci* **9**, 308-308, doi:10.3389/fnagi.2017.00308 (2017).
706 Li, W. W., Li, J. & Bao, J. K. Microautophagy: lesser-known self-eating. *Cell Mol Life Sci* **69**, 1125-1136, doi:10.1007/s00018-011-0865-5 (2012).
707 Burwell, L. S., Nadtochiy, S. M., Tompkins, A. J., Young, S. & Brookes, P. S. Direct evidence for S-nitrosation of mitochondrial complex I. *Biochem J* **394**, 627-634, doi:10.1042/bj20051435 (2006).
708 Kensler, T. W., Wakabayashi, N. & Biswal, S. Cell survival responses to environmental stresses via the Keap1-Nrf2-ARE pathway. *Annu Rev Pharmacol Toxicol* **47**, 89-116, doi:10.1146/annurev.pharmtox.46.120604.141046 (2007).
709 Harvey, C. J. *et al.* Nrf2-regulated glutathione recycling independent of biosynthesis is critical for cell survival during oxidative stress. *Free Radic Biol Med* **46**, 443-453, doi:10.1016/j.freeradbiomed.2008.10.040 (2009).
710 Alam, J. *et al.* Nrf2, a Cap'n'Collar transcription factor, regulates induction of the heme oxygenase-1 gene. *J Biol Chem* **274**, 26071-26078 (1999).
711 Nioi, P., McMahon, M., Itoh, K., Yamamoto, M. & Hayes, J. D. Identification of a novel Nrf2-regulated antioxidant response element (ARE) in the mouse NAD(P)H:quinone oxidoreductase 1 gene: reassessment of the ARE consensus sequence. *The Biochemical journal* **374**, 337-348, doi:10.1042/BJ20030754 (2003).
712 Kerins, M. J. & Ooi, A. The Roles of NRF2 in Modulating Cellular Iron Homeostasis. *Antioxidants & redox signaling* **29**, 1756-1773, doi:10.1089/ars.2017.7176 (2018).
713 Chen, Z. H. *et al.* 4-Hydroxynonenal induces adaptive response and enhances PC12 cell tolerance primarily through induction of thioredoxin reductase 1 via activation of Nrf2. *J Biol Chem* **280**, 41921-41927, doi:10.1074/jbc.M508556200 (2005).
714 Ishii, T. Close teamwork between Nrf2 and peroxiredoxins 1 and 6 for the regulation of prostaglandin D2 and E2 production in macrophages in acute inflammation. *Free Radic Biol Med* **88**, 189-198, doi:10.1016/j.freeradbiomed.2015.04.034 (2015).
715 Matte, A. *et al.* The Interplay Between Peroxiredoxin-2 and Nuclear Factor-Erythroid 2 Is Important in Limiting Oxidative Mediated Dysfunction in β-Thalassemic Erythropoiesis. *Antioxid Redox Signal* **23**, 1284-1297, doi:10.1089/ars.2014.6237 (2015).
716 Hawkins, K. E. *et al.* NRF2 Orchestrates the Metabolic Shift during Induced Pluripotent Stem Cell Reprogramming. *Cell Rep* **14**, 1883-1891, doi:10.1016/j.celrep.2016.02.003 (2016).
717 Budanov, A. V. The role of tumor suppressor p53 in the antioxidant defense and metabolism. *Subcell Biochem* **85**, 337-358, doi:10.1007/978-94-017-9211-0_18 (2014).
718 Sporn, M. B. & Liby, K. T. NRF2 and cancer: the good, the bad and the importance of context. *Nature Reviews Cancer* **12**, 564-571, doi:10.1038/nrc3278 (2012).
719 Minakami, R. & Sumimoto, H. Phagocytosis-Coupled Activation of the Superoxide-Producing Phagocyte Oxidase, a Member of the NADPH Oxidase (Nox) Family. *International Journal of Hematology* **84**, 193-198, doi:10.1532/IJH97.06133 (2006).
720 Lambeth, J. D. NOX enzymes and the biology of reactive oxygen. *Nature Reviews Immunology* **4**, 181-189, doi:10.1038/nri1312 (2004).
721 Takeda, K. & Akira, S. Toll-like receptors in innate immunity. *International immunology* **17**, 1-14, doi:10.1093/intimm/dxh186 (2005).
722 Kohchi, C., Inagawa, H., Nishizawa, T. & Soma, G. ROS and innate immunity. *Anticancer research* **29**, 817-821 (2009).
723 Matthews, J. R., Wakasugi, N., Virelizier, J. L., Yodoi, J. & Hay, R. T. Thioredoxin regulates the DNA binding activity of NF-kappa B by reduction of a disulphide bond involving cysteine 62. *Nucleic acids research* **20**, 3821-3830, doi:10.1093/nar/20.15.3821 (1992).
724 Hirota, K. *et al.* AP-1 transcriptional activity is regulated by a direct association between thioredoxin and Ref-1. *Proceedings of the National Academy of Sciences* **94**, 3633-3638, doi:10.1073/pnas.94.8.3633 (1997).
725 Kumagai, Y., Akiyama, M. & Unoki, T. Adaptive Responses to Electrophilic Stress and Reactive Sulfur Species as their Regulator Molecules. *Toxicol Res* **35**, 303-310, doi:10.5487/TR.2019.35.4.303 (2019).
726 Drobnica, L. & Sturdík, E. The reaction of carbonyl cyanide phenylhydrazones with thiols. *Biochim Biophys Acta* **585**, 462-476, doi:10.1016/0304-4165(79)90091-6 (1979).
727 Esterbauer, H., Schaur, R. J. & Zollner, H. Chemistry and biochemistry of 4-hydroxynonenal, malonaldehyde and related aldehydes. *Free Radic Biol Med* **11**, 81-128, doi:10.1016/0891-5849(91)90192-6 (1991).

728 Sawa, T. *et al.* Protein S-guanylation by the biological signal 8-nitroguanosine 3',5'-cyclic monophosphate. *Nat Chem Biol* **3**, 727-735, doi:10.1038/nchembio.2007.33 (2007).
729 Paris, I. *et al.* Aminochrome induces disruption of actin, alpha-, and beta-tubulin cytoskeleton networks in substantia-nigra-derived cell line. *Neurotox Res* **18**, 82-92, doi:10.1007/s12640-009-9148-4 (2010).
730 Forman, H. J., Zhang, H. & Rinna, A. Glutathione: overview of its protective roles, measurement, and biosynthesis. *Mol Aspects Med* **30**, 1-12, doi:10.1016/j.mam.2008.08.006 (2009).
731 Molavian, H., Madani Tonekaboni, A., Kohandel, M. & Sivaloganathan, S. The Synergetic Coupling among the Cellular Antioxidants Glutathione Peroxidase/Peroxiredoxin and Other Antioxidants and its Effect on the Concentration of H2O2. *Scientific Reports* **5**, 13620, doi:10.1038/srep13620 (2015).
732 Sies, H. Oxidative stress: a concept in redox biology and medicine. *Redox Biol* **4**, 180-183, doi:10.1016/j.redox.2015.01.002 (2015).
733 Sheng, Y. *et al.* Superoxide dismutases and superoxide reductases. *Chemical reviews* **114**, 3854-3918, doi:10.1021/cr4005296 (2014).
734 Nakamura, H., Nakamura, K. & Yodoi, J. Redox regulation of cellular activation. *Annual review of immunology* **15**, 351-369, doi:10.1146/annurev.immunol.15.1.351 (1997).
735 Wang, X. & Quinn, P. J. The location and function of vitamin E in membranes (review). *Molecular membrane biology* **17**, 143-156, doi:10.1080/09687680010000311 (2000).
736 Kojo, S. Vitamin C: basic metabolism and its function as an index of oxidative stress. *Curr Med Chem* **11**, 1041-1064, doi:10.2174/0929867043455567 (2004).
737 Lloyd, R. V., Hanna, P. M. & Mason, R. P. The origin of the hydroxyl radical oxygen in the Fenton reaction. *Free Radic Biol Med* **22**, 885-888, doi:10.1016/s0891-5849(96)00432-7 (1997).
738 Birk, J. *et al.* Endoplasmic reticulum: reduced and oxidized glutathione revisited. *J Cell Sci* **126**, 1604-1617, doi:10.1242/jcs.117218 (2013).
739 Sun, Y. & Li, H. Functional characterization of SAG/RBX2/ROC2/RNF7, an antioxidant protein and an E3 ubiquitin ligase. *Protein Cell* **4**, 103-116, doi:10.1007/s13238-012-2105-7 (2013).
740 Chan, T. *et al.* Oxidative stress effect of dopamine on α-synuclein: electroanalysis of solvent interactions. *ACS chemical neuroscience* **3**, 569-574, doi:10.1021/cn300034t (2012).
741 Noronha, C., Perfeito, R., Laço, M., Wüllner, U. & Rego, A. C. Expanded and Wild-type Ataxin-3 Modify the Redox Status of SH-SY5Y Cells Overexpressing α-Synuclein. *Neurochem Res* **42**, 1430-1437, doi:10.1007/s11064-017-2199-7 (2017).
742 Miyata, Y. *et al.* Cysteine reactivity distinguishes redox sensing by the heat-inducible and constitutive forms of heat shock protein 70. *Chem Biol* **19**, 1391-1399, doi:10.1016/j.chembiol.2012.07.026 (2012).
743 Choi, J. *et al.* Oxidative modifications and down-regulation of ubiquitin carboxyl-terminal hydrolase L1 associated with idiopathic Parkinson's and Alzheimer's diseases. *J Biol Chem* **279**, 13256-13264, doi:10.1074/jbc.M314124200 (2004).
744 Carroll, B. *et al.* Oxidation of SQSTM1/p62 mediates the link between redox state and protein homeostasis. *Nat Commun* **9**, 256, doi:10.1038/s41467-017-02746-z (2018).
745 Silverstein, R. L. & Febbraio, M. CD36, a scavenger receptor involved in immunity, metabolism, angiogenesis, and behavior. *Sci Signal* **2**, re3, doi:10.1126/scisignal.272re3 (2009).
746 Bobst, C. E., Thomas, J. J., Salinas, P. A., Savickas, P. & Kaltashov, I. A. Impact of oxidation on protein therapeutics: conformational dynamics of intact and oxidized acid-β-glucocerebrosidase at near-physiological pH. *Protein Sci* **19**, 2366-2378, doi:10.1002/pro.517 (2010).
747 Kallenborn-Gerhardt, W. *et al.* Rab7-a novel redox target that modulates inflammatory pain processing. *Pain* **158**, 1354-1365, doi:10.1097/j.pain.0000000000000920 (2017).
748 Marciniak, S. J. *et al.* CHOP induces death by promoting protein synthesis and oxidation in the stressed endoplasmic reticulum. *Genes & development* **18**, 3066-3077, doi:10.1101/gad.1250704 (2004).
749 Lee, J.-Y. *et al.* Nucleotide-Binding Oligomerization Domain 2 Contributes to Limiting Growth of Mycobacterium abscessus in the Lung of Mice by Regulating Cytokines and Nitric Oxide Production. *Front Immunol* **8**, 1477-1477, doi:10.3389/fimmu.2017.01477 (2017).
750 Wilson, C. & González-Billault, C. Regulation of cytoskeletal dynamics by redox signaling and oxidative stress: implications for neuronal development and trafficking. *Frontiers in cellular neuroscience* **9**, 381, doi:10.3389/fncel.2015.00381 (2015).
751 Xu, Q., Huff, L. P., Fujii, M. & Griendling, K. K. Redox regulation of the actin cytoskeleton and its role in the vascular system. *Free Radical Biology and Medicine* **109**, 84-107, doi:10.1016/j.freeradbiomed.2017.03.004 (2017).

752 Dong, Z. *et al.* Dopamine-dependent neurodegeneration in rats induced by viral vector-mediated overexpression of the parkin target protein, CDCrel-1. *Proc Natl Acad Sci U S A* **100**, 12438-12443, doi:10.1073/pnas.2132992100 (2003).
753 Umeda-Kameyama, Y. *et al.* Thioredoxin Suppresses Parkin-associated Endothelin Receptor-like Receptor-induced Neurotoxicity and Extends Longevity in Drosophila. *Journal of Biological Chemistry* **282**, 11180-11187, doi:10.1074/jbc.M700937200 (2007).
754 Arango Duque, G., Fukuda, M. & Descoteaux, A. Synaptotagmin XI regulates phagocytosis and cytokine secretion in macrophages. *J Immunol* **190**, 1737-1745, doi:10.4049/jimmunol.1202500 (2013).
755 Shi, Y. *et al.* Redox-regulated lipid membrane binding of the PICK1 PDZ domain. *Biochemistry* **49**, 4432-4439, doi:10.1021/bi100269t (2010).
756 Kato, M. *et al.* Redox State Controls Phase Separation of the Yeast Ataxin-2 Protein via Reversible Oxidation of Its Methionine-Rich Low-Complexity Domain. *Cell* **177**, 711-721.e718, doi:10.1016/j.cell.2019.02.044 (2019).
757 Deb, I., Poddar, R. & Paul, S. Oxidative stress-induced oligomerization inhibits the activity of the non-receptor tyrosine phosphatase STEP61. *J Neurochem* **116**, 1097-1111, doi:10.1111/j.1471-4159.2010.07165.x (2011).
758 Mougeolle, A. *et al.* Oxidative stress induces caveolin 1 degradation and impairs caveolae functions in skeletal muscle cells. *PloS one* **10**, e0122654-e0122654, doi:10.1371/journal.pone.0122654 (2015).
759 Han, J. M. *et al.* AIMP2/p38, the scaffold for the multi-tRNA synthetase complex, responds to genotoxic stresses via p53. *Proceedings of the National Academy of Sciences* **105**, 11206, doi:10.1073/pnas.0800297105 (2008).
760 Corroyer, S., Maitre, B., Cazals, V. & Clement, A. Altered regulation of G1 cyclins in oxidant-induced growth arrest of lung alveolar epithelial cells. Accumulation of inactive cyclin E-DCK2 complexes. *J Biol Chem* **271**, 25117-25125, doi:10.1074/jbc.271.41.25117 (1996).
761 Liu, J. *et al.* JTV1 co-activates FBP to induce USP29 transcription and stabilize p53 in response to oxidative stress. *Embo j* **30**, 846-858, doi:10.1038/emboj.2011.11 (2011).
762 Cho, K. I., Yi, H., Tserentsoodol, N., Searle, K. & Ferreira, P. A. Neuroprotection resulting from insufficiency of RANBP2 is associated with the modulation of protein and lipid homeostasis of functionally diverse but linked pathways in response to oxidative stress. *Dis Model Mech* **3**, 595-604, doi:10.1242/dmm.004648 (2010).
763 Kyng, K. J. *et al.* Gene expression responses to DNA damage are altered in human aging and in Werner Syndrome. *Oncogene* **24**, 5026-5042, doi:10.1038/sj.onc.1208692 (2005).
764 Funato, Y., Michiue, T., Asashima, M. & Miki, H. The thioredoxin-related redox-regulating protein nucleoredoxin inhibits Wnt-beta-catenin signalling through dishevelled. *Nat Cell Biol* **8**, 501-508, doi:10.1038/ncb1405 (2006).
765 Iguchi, Y. *et al.* Oxidative stress induced by glutathione depletion reproduces pathological modifications of TDP-43 linked to TDP-43 proteinopathies. *Neurobiol Dis* **45**, 862-870, doi:10.1016/j.nbd.2011.12.002 (2012).
766 Li, X. *et al.* E3 ligase Fbw7 participates in oxidative stress□induced myocardial cell injury via interacting with Mcl□1. *Mol Med Rep* **20**, 1561-1568, doi:10.3892/mmr.2019.10394 (2019).
767 Zhang, J., Wang, S., Kern, S., Cui, X. & Danner, R. L. Nitric oxide down-regulates polo-like kinase 1 through a proximal promoter cell cycle gene homology region. *J Biol Chem* **282**, 1003-1009, doi:10.1074/jbc.M607609200 (2007).
768 Villeneuve, N. F., Sun, Z., Chen, W. & Zhang, D. D. Nrf2 and p21 regulate the fine balance between life and death by controlling ROS levels. *Cell Cycle* **8**, 3255-3256, doi:10.4161/cc.8.20.9565 (2009).
769 Reynaert, N. L. *et al.* Dynamic redox control of NF-kappaB through glutaredoxin-regulated S-glutathionylation of inhibitory kappaB kinase beta. *Proc Natl Acad Sci U S A* **103**, 13086-13091, doi:10.1073/pnas.0603290103 (2006).
770 Shen, H. M. *et al.* Essential roles of receptor-interacting protein and TRAF2 in oxidative stress-induced cell death. *Mol Cell Biol* **24**, 5914-5922, doi:10.1128/mcb.24.13.5914-5922.2004 (2004).
771 Corona, J. C. & Duchen, M. R. PPARγ and PGC-1α as therapeutic targets in Parkinson's. *Neurochemical research* **40**, 308-316, doi:10.1007/s11064-014-1377-0 (2015).
772 Reingewertz, T. H. *et al.* Mechanism of the interaction between the intrinsically disordered C-terminus of the pro-apoptotic ARTS protein and the Bir3 domain of XIAP. *PLoS One* **6**, e24655, doi:10.1371/journal.pone.0024655 (2011).
773 Snyder, C. M., Shroff, E. H., Liu, J. & Chandel, N. S. Nitric oxide induces cell death by regulating anti-apoptotic BCL-2 family members. *PLoS One* **4**, e7059, doi:10.1371/journal.pone.0007059 (2009).
774 Susnow, N., Zeng, L., Margineantu, D. & Hockenbery, D. M. Bcl-2 family proteins as regulators of oxidative stress. *Seminars in cancer biology* **19**, 42-49, doi:10.1016/j.semcancer.2008.12.002 (2009).
775 Yu, C., Kim, B. S. & Kim, E. FAF1 mediates regulated necrosis through PARP1 activation upon oxidative stress leading to dopaminergic neurodegeneration. *Cell Death Differ* **23**, 1873-1885, doi:10.1038/cdd.2016.99 (2016).

776 Wuerzberger-Davis, S. M., Nakamura, Y., Seufzer, B. J. & Miyamoto, S. NF-kappaB activation by combinations of NEMO SUMOylation and ATM activation stresses in the absence of DNA damage. *Oncogene* **26**, 641-651, doi:10.1038/sj.onc.1209815 (2007).
777 Fujino, G. *et al.* Thioredoxin and TRAF family proteins regulate reactive oxygen species-dependent activation of ASK1 through reciprocal modulation of the N-terminal homophilic interaction of ASK1. *Molecular and cellular biology* **27**, 8152-8163, doi:10.1128/MCB.00227-07 (2007).
778 Canal, M., Romaní-Aumedes, J., Martín-Flores, N., Pérez-Fernández, V. & Malagelada, C. RTP801/REDD1: a stress coping regulator that turns into a troublemaker in neurodegenerative disorders. *Frontiers in cellular neuroscience* **8**, 313-313, doi:10.3389/fncel.2014.00313 (2014).
779 Torii, S. *et al.* Involvement of inhibitory PAS domain protein in neuronal cell death in Parkinson's disease. *Cell death discovery* **1**, 15015, doi:10.1038/cddiscovery.2015.15 (2015).
780 Li, H. S. *et al.* HIF-1α protects against oxidative stress by directly targeting mitochondria. *Redox Biol* **25**, 101109, doi:10.1016/j.redox.2019.101109 (2019).
781 Jang, K. H., Jang, T., Son, E., Choi, S. & Kim, E. Kinase-independent role of nuclear RIPK1 in regulating parthanatos through physical interaction with PARP1 upon oxidative stress. *Biochimica et biophysica acta. Molecular cell research* **1865**, 132-141, doi:10.1016/j.bbamcr.2017.10.004 (2018).
782 Folda, A. *et al.* Mitochondrial Thioredoxin System as a Modulator of Cyclophilin D Redox State. *Scientific Reports* **6**, 23071, doi:10.1038/srep23071 (2016).
783 Reina, S., Guarino, F., Magrì, A. & De Pinto, V. VDAC3 As a Potential Marker of Mitochondrial Status Is Involved in Cancer and Pathology. *Front Oncol* **6**, 264-264, doi:10.3389/fonc.2016.00264 (2016).
784 Zimmermann, A. K. *et al.* Glutathione binding to the Bcl-2 homology-3 domain groove: a molecular basis for Bcl-2 antioxidant function at mitochondria. *J Biol Chem* **282**, 29296-29304, doi:10.1074/jbc.M702853200 (2007).
785 Ryan, M. T. & Stojanovski, D. Mitofusins 'bridge' the gap between oxidative stress and mitochondrial hyperfusion. *EMBO Rep* **13**, 870-871, doi:10.1038/embor.2012.132 (2012).
786 Kim, Y. M. *et al.* Redox Regulation of Mitochondrial Fission Protein Drp1 by Protein Disulfide Isomerase Limits Endothelial Senescence. *Cell Rep* **23**, 3565-3578, doi:10.1016/j.celrep.2018.05.054 (2018).
787 Debattisti, V., Gerencser, A. A., Saotome, M., Das, S. & Hajnóczky, G. ROS Control Mitochondrial Motility through p38 and the Motor Adaptor Miro/Trak. *Cell Rep* **21**, 1667-1680, doi:10.1016/j.celrep.2017.10.060 (2017).
788 Heneberg, P. Redox Regulation of Hexokinases. *Antioxidants & Redox Signaling* **30**, 415-442, doi:10.1089/ars.2017.7255 (2018).
789 Carlson, E. A. *et al.* Overexpression of 17β-hydroxysteroid dehydrogenase type 10 increases pheochromocytoma cell growth and resistance to cell death. *BMC cancer* **15**, 166, doi:10.1186/s12885-015-1173-5 (2015).
790 Chinnadurai, G., Vijayalingam, S. & Gibson, S. B. BNIP3 subfamily BH3-only proteins: mitochondrial stress sensors in normal and pathological functions. *Oncogene* **27**, S114-S127, doi:10.1038/onc.2009.49 (2008).
791 Mitchell, A. R. *et al.* Redox regulation of pyruvate kinase M2 by cysteine oxidation and S-nitrosation. *The Biochemical journal* **475**, 3275-3291, doi:10.1042/BCJ20180556 (2018).
792 Yonashiro, R. *et al.* Mitochondrial ubiquitin ligase MITOL blocks S-nitrosylated MAP1B-light chain 1-mediated mitochondrial dysfunction and neuronal cell death. *Proceedings of the National Academy of Sciences* **109**, 2382, doi:10.1073/pnas.1114985109 (2012).
793 Sian, J. *et al.* Alterations in glutathione levels in Parkinson's disease and other neurodegenerative disorders affecting basal ganglia. *Ann Neurol* **36**, 348-355, doi:10.1002/ana.410360305 (1994).
794 Andersen, J. K. Iron dysregulation and Parkinson's disease. *J Alzheimers Dis* **6**, S47-52, doi:10.3233/jad-2004-6s602 (2004).
795 Jiang, H. *et al.* Parkin controls dopamine utilization in human midbrain dopaminergic neurons derived from induced pluripotent stem cells. *Nat Commun* **3**, 668, doi:10.1038/ncomms1669 (2012).
796 Kasten, M. *et al.* Genotype-Phenotype Relations for the Parkinson's Disease Genes Parkin, PINK1, DJ1: MDSGene Systematic Review. *Mov Disord* **33**, 730-741, doi:10.1002/mds.27352 (2018).
797 Berger, A. K. *et al.* Parkin selectively alters the intrinsic threshold for mitochondrial cytochrome c release. *Hum Mol Genet* **18**, 4317-4328, doi:10.1093/hmg/ddp384 (2009).
798 Matsuda, N. *et al.* PINK1 stabilized by mitochondrial depolarization recruits Parkin to damaged mitochondria and activates latent Parkin for mitophagy. *J Cell Biol* **189**, 211-221, doi:10.1083/jcb.200910140 (2010).
799 Barodia, S. K., Creed, R. B. & Goldberg, M. S. Parkin and PINK1 functions in oxidative stress and neurodegeneration. *Brain Res Bull* **133**, 51-59, doi:10.1016/j.brainresbull.2016.12.004 (2017).
800 Gong, G. *et al.* Parkin-mediated mitophagy directs perinatal cardiac metabolic maturation in mice. *Science* **350**, aad2459, doi:10.1126/science.aad2459 (2015).

801 Whitworth, A. J. *et al.* Increased glutathione S-transferase activity rescues dopaminergic neuron loss in a Drosophila model of Parkinson's disease. *Proceedings of the National Academy of Sciences* **102**, 8024-8029, doi:10.1073/pnas.0501078102 (2005).
802 Ge, P., Dawson, V. L. & Dawson, T. M. PINK1 and Parkin mitochondrial quality control: a source of regional vulnerability in Parkinson's disease. *Mol Neurodegener* **15**, 20, doi:10.1186/s13024-020-00367-7 (2020).
803 Liguori, I. *et al.* Oxidative stress, aging, and diseases. *Clin Interv Aging* **13**, 757-772, doi:10.2147/CIA.S158513 (2018).
804 Ali, S. F., David, S. N., Newport, G. D., Cadet, J. L. & Slikker, W., Jr. MPTP-induced oxidative stress and neurotoxicity are age-dependent: evidence from measures of reactive oxygen species and striatal dopamine levels. *Synapse* **18**, 27-34, doi:10.1002/syn.890180105 (1994).
805 Krężel, A. & Maret, W. The biological inorganic chemistry of zinc ions. *Arch Biochem Biophys* **611**, 3-19, doi:10.1016/j.abb.2016.04.010 (2016).
806 Cox, J. & Mann, M. MaxQuant enables high peptide identification rates, individualized p.p.b.-range mass accuracies and proteome-wide protein quantification. *Nat Biotechnol* **26**, 1367-1372, doi:10.1038/nbt.1511 (2008).
807 Ferrari, E. *et al.* Synthesis and structural characterization of soluble neuromelanin analogs provides important clues to its biosynthesis. *Journal of biological inorganic chemistry : JBIC : a publication of the Society of Biological Inorganic Chemistry* **18**, 81-93, doi:10.1007/s00775-012-0951-7 (2013).
808 Ferrari, E. *et al.* Synthesis, Structure Characterization, and Evaluation in Microglia Cultures of Neuromelanin Analogues Suitable for Modeling Parkinson's Disease. *ACS Chem Neurosci* **8**, 501-512, doi:10.1021/acschemneuro.6b00231 (2017).
809 Kano, M. *et al.* Reduced astrocytic reactivity in human brains and midbrain organoids with PRKN mutations. *NPJ Parkinsons Dis* **6**, 33, doi:10.1038/s41531-020-00137-8 (2020).
810 Gu, W. J. *et al.* The C289G and C418R missense mutations cause rapid sequestration of human Parkin into insoluble aggregates. *Neurobiol Dis* **14**, 357-364 (2003).
811 Hyun, D. H. *et al.* Effect of wild-type or mutant Parkin on oxidative damage, nitric oxide, antioxidant defenses, and the proteasome. *J Biol Chem* **277**, 28572-28577, doi:10.1074/jbc.M200666200 (2002).
812 Okarmus, J. *et al.* Lysosomal perturbations in human dopaminergic neurons derived from induced pluripotent stem cells with PARK2 mutation. *Sci Rep* **10**, 10278, doi:10.1038/s41598-020-67091-6 (2020).
813 Xiao, H. *et al.* A Quantitative Tissue-Specific Landscape of Protein Redox Regulation during Aging. *Cell* **180**, 968-983.e924, doi:10.1016/j.cell.2020.02.012 (2020).
814 Jordan, G. M., Yoshioka, S. & Terao, T. The aggregation of bovine serum albumin in solution and in the solid state. *J Pharm Pharmacol* **46**, 182-185, doi:10.1111/j.2042-7158.1994.tb03774.x (1994).
815 Paris, G., Kraszewski, S., Ramseyer, C. & Enescu, M. About the structural role of disulfide bridges in serum albumins: evidence from protein simulated unfolding. *Biopolymers* **97**, 889-898, doi:10.1002/bip.22096 (2012).
816 Maret, W. Zinc coordination environments in proteins as redox sensors and signal transducers. *Antioxid Redox Signal* **8**, 1419-1441, doi:10.1089/ars.2006.8.1419 (2006).
817 Yi, W. *et al.* The landscape of Parkin variants reveals pathogenic mechanisms and therapeutic targets in Parkinson's disease. *Hum Mol Genet* **28**, 2811-2825, doi:10.1093/hmg/ddz080 (2019).
818 Klein, C. & Lohmann, K. Parkinson disease(s): is "Parkin disease" a distinct clinical entity? *Neurology* **72**, 106-107, doi:10.1212/01.wnl.0000333666.65522.8d (2009).
819 Lesage, S. *et al.* Characterization of recessive Parkinson's disease in a large multicenter study. *Ann Neurol*, doi:10.1002/ana.25787 (2020).
820 Flynn, J. M. & Melov, S. SOD2 in mitochondrial dysfunction and neurodegeneration. *Free Radic Biol Med* **62**, 4-12, doi:10.1016/j.freeradbiomed.2013.05.027 (2013).
821 Rodríguez-Navarro, J. A. *et al.* Mortality, oxidative stress and tau accumulation during ageing in parkin null mice. *J Neurochem* **103**, 98-114, doi:10.1111/j.1471-4159.2007.04762.x (2007).
822 Damiano, M. *et al.* Tissue- and cell-specific mitochondrial defect in Parkin-deficient mice. *PLoS One* **9**, e99898, doi:10.1371/journal.pone.0099898 (2014).
823 Kitada, T. *et al.* Impaired dopamine release and synaptic plasticity in the striatum of parkin-/- mice. *J Neurochem* **110**, 613-621, doi:10.1111/j.1471-4159.2009.06152.x (2009).
824 Gibb, W. R., Narabayashi, H., Yokochi, M., Iizuka, R. & Lees, A. J. New pathologic observations in juvenile onset parkinsonism with dystonia. *Neurology* **41**, 820-822, doi:10.1212/wnl.41.6.820 (1991).
825 Yamamura, Y. *et al.* Clinical, pathologic and genetic studies on autosomal recessive early-onset parkinsonism with diurnal fluctuation. *Parkinsonism Relat Disord* **4**, 65-72, doi:10.1016/s1353-8020(98)00015-7 (1998).
826 Gouider-Khouja, N. *et al.* Autosomal recessive parkinsonism linked to parkin gene in a Tunisian family. Clinical, genetic and pathological study. *Parkinsonism Relat Disord* **9**, 247-251, doi:10.1016/s1353-8020(03)00016-6 (2003).

827 Wang, Y. Q. *et al.* Association analysis of STK39, MCCC1/LAMP3 and sporadic PD in the Chinese Han population. *Neurosci Lett* **566**, 206-209, doi:10.1016/j.neulet.2014.03.007 (2014).
828 Sun, Y., Tan, M., Duan, H. & Swaroop, M. SAG/ROC/Rbx/Hrt, a zinc RING finger gene family: molecular cloning, biochemical properties, and biological functions. *Antioxid Redox Signal* **3**, 635-650, doi:10.1089/15230860152542989 (2001).
829 Rosen, K. M. *et al.* Parkin protects against mitochondrial toxins and beta-amyloid accumulation in skeletal muscle cells. *J Biol Chem* **281**, 12809-12816, doi:10.1074/jbc.M512649200 (2006).
830 Dawson, T. M. & Dawson, V. L. Parkin plays a role in sporadic Parkinson's disease. *Neurodegener Dis* **13**, 69-71, doi:10.1159/000354307 (2014).
831 Ratan, R. R. in *Cell Death and Diseases of the Nervous System* (ed V.E. Koliatsos, Ratan, R. R.) (Humana Press, 1999).
832 Polman, C. H. *et al.* Diagnostic criteria for multiple sclerosis: 2010 revisions to the McDonald criteria. *Ann Neurol* **69**, 292-302, doi:10.1002/ana.22366 (2011).
833 Dhaeze, T. *et al.* CD70 defines a subset of proinflammatory and CNS-pathogenic TH1/TH17 lymphocytes and is overexpressed in multiple sclerosis. *Cell Mol Immunol* **16**, 652-665, doi:10.1038/s41423-018-0198-5 (2019).
834 Kuhlmann, T. *et al.* An updated histological classification system for multiple sclerosis lesions. *Acta Neuropathol* **133**, 13-24, doi:10.1007/s00401-016-1653-y (2017).
835 Dong, X. *et al.* Enhancers active in dopamine neurons are a primary link between genetic variation and neuropsychiatric disease. *Nat Neurosci* **21**, 1482-1492, doi:10.1038/s41593-018-0223-0 (2018).
836 Unger, T., Jacobovitch, Y., Dantes, A., Bernheim, R. & Peleg, Y. Applications of the Restriction Free (RF) cloning procedure for molecular manipulations and protein expression. *Journal of structural biology* **172**, 34-44, doi:10.1016/j.jsb.2010.06.016 (2010).
837 Kiss, R. *et al.* Structural features of human DJ-1 in distinct Cys106 oxidative states and their relevance to its loss of function in disease. *Biochim Biophys Acta Gen Subj* **1861**, 2619-2629, doi:10.1016/j.bbagen.2017.08.017 (2017).
838 Solti, K. *et al.* DJ-1 can form β-sheet structured aggregates that co-localize with pathological amyloid deposits. *Neurobiol Dis* **134**, 104629, doi:10.1016/j.nbd.2019.104629 (2020).
839 Micsonai, A. *et al.* Accurate secondary structure prediction and fold recognition for circular dichroism spectroscopy. *Proc Natl Acad Sci U S A* **112**, E3095-3103, doi:10.1073/pnas.1500851112 (2015).
840 Micsonai, A. *et al.* BeStSel: a web server for accurate protein secondary structure prediction and fold recognition from the circular dichroism spectra. *Nucleic acids research* **46**, W315-w322, doi:10.1093/nar/gky497 (2018).
841 Shevchenko, A., Tomas, H., Havlis, J., Olsen, J. V. & Mann, M. In-gel digestion for mass spectrometric characterization of proteins and proteomes. *Nat Protoc* **1**, 2856-2860, doi:10.1038/nprot.2006.468 (2006).
842 Muller, C. H., Lee, T. K. & Montano, M. A. Improved chemiluminescence assay for measuring antioxidant capacity of seminal plasma. *Methods Mol Biol* **927**, 363-376, doi:10.1007/978-1-62703-038-0_31 (2013).
843 Schlossmacher, M. G. & Shimura, H. Parkinson's disease: assays for the ubiquitin ligase activity of neural Parkin. *Methods Mol Biol* **301**, 351-369, doi:10.1385/1-59259-895-1:351 (2005).
844 Mori, H. *et al.* Pathologic and biochemical studies of juvenile parkinsonism linked to chromosome 6q. *Neurology* **51**, 890-892, doi:10.1212/wnl.51.3.890 (1998).
845 Martinez, T. N. & Greenamyre, J. T. Toxin models of mitochondrial dysfunction in Parkinson's disease. *Antioxid Redox Signal* **16**, 920-934, doi:10.1089/ars.2011.4033 (2012).
846 Tokarew, J. M. *et al.* Age-associated insolubility of parkin in human midbrain is linked to redox balance and sequestration of reactive dopamine metabolites. *Acta Neuropathologica*, doi:10.1007/s00401-021-02285-4 (2021).
847 Lebovitz, R. M. *et al.* Neurodegeneration, myocardial injury, and perinatal death in mitochondrial superoxide dismutase-deficient mice. *Proc Natl Acad Sci U S A* **93**, 9782-9787, doi:10.1073/pnas.93.18.9782 (1996).
848 Hinerfeld, D. *et al.* Endogenous mitochondrial oxidative stress: neurodegeneration, proteomic analysis, specific respiratory chain defects, and efficacious antioxidant therapy in superoxide dismutase 2 null mice. *J Neurochem* **88**, 657-667, doi:10.1046/j.1471-4159.2003.02195.x (2004).
849 Hennis, M. R., Seamans, K. W., Marvin, M. A., Casey, B. H. & Goldberg, M. S. Behavioral and neurotransmitter abnormalities in mice deficient for Parkin, DJ-1 and superoxide dismutase. *PLoS One* **8**, e84894, doi:10.1371/journal.pone.0084894 (2013).
850 Dumont, B. L., White, M. A., Steffy, B., Wiltshire, T. & Payseur, B. A. Extensive recombination rate variation in the house mouse species complex inferred from genetic linkage maps. *Genome Res* **21**, 114-125, doi:10.1101/gr.111252.110 (2011).
851 Wiese, A. G., Pacifici, R. E. & Davies, K. J. Transient adaptation of oxidative stress in mammalian cells. *Arch Biochem Biophys* **318**, 231-240, doi:10.1006/abbi.1995.1225 (1995).

852 Jones, B. J. & Roberts, D. J. The quantiative measurement of motor inco-ordination in naive mice using an acelerating rotarod. *J Pharm Pharmacol* **20**, 302-304, doi:10.1111/j.2042-7158.1968.tb09743.x (1968).
853 Deacon, R. M. Measuring motor coordination in mice. *J Vis Exp*, e2609, doi:10.3791/2609 (2013).
854 Metz, G. A. & Whishaw, I. Q. Cortical and subcortical lesions impair skilled walking in the ladder rung walking test: a new task to evaluate fore- and hindlimb stepping, placing, and co-ordination. *J Neurosci Methods* **115**, 169-179, doi:10.1016/s0165-0270(02)00012-2 (2002).
855 Amende, I. *et al.* Gait dynamics in mouse models of Parkinson's disease and Huntington's disease. *J Neuroeng Rehabil* **2**, 20, doi:10.1186/1743-0003-2-20 (2005).
856 Kravitz, A. V. *et al.* Regulation of parkinsonian motor behaviours by optogenetic control of basal ganglia circuitry. *Nature* **466**, 622-626, doi:10.1038/nature09159 (2010).
857 Lu, W. *et al.* Genetic deficiency of the mitochondrial protein PGAM5 causes a Parkinson's-like movement disorder. *Nat Commun* **5**, 4930, doi:10.1038/ncomms5930 (2014).
858 Gustafsson, H., Aasly, J., Strahle, S., Nordstrom, A. & Nordstrom, P. Low muscle strength in late adolescence and Parkinson disease later in life. *Neurology* **84**, 1862-1869, doi:10.1212/WNL.0000000000001534 (2015).
859 Deacon, R. Assessing burrowing, nest construction, and hoarding in mice. *J Vis Exp*, e2607, doi:10.3791/2607 (2012).
860 Fleming, S. M. *et al.* Early and progressive sensorimotor anomalies in mice overexpressing wild-type human alpha-synuclein. *J Neurosci* **24**, 9434-9440, doi:10.1523/JNEUROSCI.3080-04.2004 (2004).
861 Sikalidis, A. K. *et al.* Upregulation of capacity for glutathione synthesis in response to amino acid deprivation: regulation of glutamate-cysteine ligase subunits. *Amino Acids* **46**, 1285-1296, doi:10.1007/s00726-014-1687-1 (2014).
862 Tietze, F. Enzymic method for quantitative determination of nanogram amounts of total and oxidized glutathione: applications to mammalian blood and other tissues. *Anal Biochem* **27**, 502-522, doi:10.1016/0003-2697(69)90064-5 (1969).
863 Frasier, C. R. *et al.* Redox-dependent increases in glutathione reductase and exercise preconditioning: role of NADPH oxidase and mitochondria. *Cardiovasc Res* **98**, 47-55, doi:10.1093/cvr/cvt009 (2013).
864 Espinosa-Diez, C. *et al.* Antioxidant responses and cellular adjustments to oxidative stress. *Redox Biol* **6**, 183-197, doi:10.1016/j.redox.2015.07.008 (2015).
865 Sengupta, R., Coppo, L., Mishra, P. & Holmgren, A. Glutathione-glutaredoxin is an efficient electron donor system for mammalian p53R2-R1-dependent ribonucleotide reductase. *J Biol Chem* **294**, 12708-12716, doi:10.1074/jbc.RA119.008752 (2019).
866 Sircar, E., Rai, S. R., Wilson, M. A., Schlossmacher, M. G. & Sengupta, R. Neurodegeneration: Impact of S-nitrosylated Parkin, DJ-1 and PINK1 on the pathogenesis of Parkinson's disease. *Archives of Biochemistry and Biophysics* **704**, 108869, doi:10.1016/j.abb.2021.108869 (2021).
867 Wu, G., Fang, Y. Z., Yang, S., Lupton, J. R. & Turner, N. D. Glutathione metabolism and its implications for health. *J Nutr* **134**, 489-492, doi:10.1093/jn/134.3.489 (2004).
868 Han, D., Antunes, F., Canali, R., Rettori, D. & Cadenas, E. Voltage-dependent anion channels control the release of the superoxide anion from mitochondria to cytosol. *J Biol Chem* **278**, 5557-5563, doi:10.1074/jbc.M210269200 (2003).
869 Cenci, M. A. & Crossman, A. R. Animal models of l-dopa-induced dyskinesia in Parkinson's disease. *Mov Disord* **33**, 889-899, doi:10.1002/mds.27337 (2018).
870 Finberg, J. P. M. Inhibitors of MAO-B and COMT: their effects on brain dopamine levels and uses in Parkinson's disease. *J Neural Transm (Vienna)* **126**, 433-448, doi:10.1007/s00702-018-1952-7 (2019).
871 Taylor, T. N. *et al.* Nonmotor symptoms of Parkinson's disease revealed in an animal model with reduced monoamine storage capacity. *J Neurosci* **29**, 8103-8113, doi:10.1523/jneurosci.1495-09.2009 (2009).
872 Carballo-Carbajal, I. *et al.* Brain tyrosinase overexpression implicates age-dependent neuromelanin production in Parkinson's disease pathogenesis. *Nat Commun* **10**, 973, doi:10.1038/s41467-019-08858-y (2019).
873 Go, Y. M., Chandler, J. D. & Jones, D. P. The cysteine proteome. *Free Radic Biol Med* **84**, 227-245, doi:10.1016/j.freeradbiomed.2015.03.022 (2015).
874 Yang, Y. *et al.* Initial characterization of the glutamate-cysteine ligase modifier subunit Gclm(-/-) knockout mouse. Novel model system for a severely compromised oxidative stress response. *J Biol Chem* **277**, 49446-49452, doi:10.1074/jbc.M209372200 (2002).
875 Watanabe, T. *et al.* A novel model of continuous depletion of glutathione in mice treated with L-buthionine (S,R)-sulfoximine. *J Toxicol Sci* **28**, 455-469 (2003).
876 Zhao, Y. *et al.* Effects of glutathione reductase inhibition on cellular thiol redox state and related systems. *Archives of biochemistry and biophysics* **485**, 56-62, doi:10.1016/j.abb.2009.03.001 (2009).

877 Moosmann, B. & Behl, C. Antioxidants as treatment for neurodegenerative disorders. *Expert Opin Investig Drugs* **11**, 1407-1435, doi:10.1517/13543784.11.10.1407 (2002).
878 Uttara, B., Singh, A. V., Zamboni, P. & Mahajan, R. T. Oxidative stress and neurodegenerative diseases: a review of upstream and downstream antioxidant therapeutic options. *Curr Neuropharmacol* **7**, 65-74, doi:10.2174/157015909787602823 (2009).
879 Brooks, S. P. & Dunnett, S. B. Tests to assess motor phenotype in mice: a user's guide. *Nat Rev Neurosci* **10**, 519-529, doi:10.1038/nrn2652 (2009).
880 Cabin, D. E. *et al.* Exacerbated synucleinopathy in mice expressing A53T SNCA on a Snca null background. *Neurobiol Aging* **26**, 25-35, doi:10.1016/j.neurobiolaging.2004.02.026 (2005).
881 Kuo, Y. M. *et al.* Extensive enteric nervous system abnormalities in mice transgenic for artificial chromosomes containing Parkinson disease-associated alpha-synuclein gene mutations precede central nervous system changes. *Hum Mol Genet* **19**, 1633-1650, doi:10.1093/hmg/ddq038 (2010).
882 Laurindo, F. R., Fernandes, D. C. & Santos, C. X. Assessment of superoxide production and NADPH oxidase activity by HPLC analysis of dihydroethidium oxidation products. *Methods Enzymol* **441**, 237-260, doi:10.1016/S0076-6879(08)01213-5 (2008).
883 Gundersen, H. J. *et al.* Some new, simple and efficient stereological methods and their use in pathological research and diagnosis. *APMIS* **96**, 379-394, doi:10.1111/j.1699-0463.1988.tb05320.x (1988).
884 Hu, J. & Li, S. Electroporation formulation for cell therapy. *Methods Mol Biol* **1121**, 55-60, doi:10.1007/978-1-4614-9632-8_4 (2014).
885 Rahman, I., Kode, A. & Biswas, S. K. Assay for quantitative determination of glutathione and glutathione disulfide levels using enzymatic recycling method. *Nat Protoc* **1**, 3159-3165, doi:10.1038/nprot.2006.378 (2006).
886 Diaz, D. *et al.* Tissue specific changes in the expression of glutamate-cysteine ligase mRNAs in mice exposed to methylmercury. *Toxicol Lett* **122**, 119-129, doi:10.1016/s0378-4274(01)00341-1 (2001).
887 Shi, S. Y. *et al.* DJ-1 links muscle ROS production with metabolic reprogramming and systemic energy homeostasis in mice. *Nat Commun* **6**, 7415, doi:10.1038/ncomms8415 (2015).
888 Casagrande, S. *et al.* Glutathionylation of human thioredoxin: a possible crosstalk between the glutathione and thioredoxin systems. *Proc Natl Acad Sci U S A* **99**, 9745-9749, doi:10.1073/pnas.152168599 (2002).
889 Narendra, D., Tanaka, A., Suen, D. F. & Youle, R. J. Parkin-induced mitophagy in the pathogenesis of Parkinson disease. *Autophagy* **5**, 706-708, doi:10.4161/auto.5.5.8505 (2009).
890 Ng, A. C., Baird, S. D. & Screaton, R. A. High-content functional genomic screening to identify novel regulators of the PINK1-Parkin pathway. *Methods Enzymol* **547**, 1-20, doi:10.1016/b978-0-12-801415-8.00001-1 (2014).
891 Imanishi, M. *et al.* Zn(II) binding and DNA binding properties of ligand-substituted CXHH-type zinc finger proteins. *Biochemistry* **51**, 3342-3348, doi:10.1021/bi300236m (2012).
892 Maynard, A. T. & Covell, D. G. Reactivity of zinc finger cores: analysis of protein packing and electrostatic screening. *Journal of the American Chemical Society* **123**, 1047-1058, doi:10.1021/ja0011616 (2001).
893 D'Abrosca, G. *et al.* The (unusual) aspartic acid in the metal coordination sphere of the prokaryotic zinc finger domain. *Journal of inorganic biochemistry* **161**, 91-98, doi:10.1016/j.jinorgbio.2016.05.006 (2016).
894 Kluska, K., Adamczyk, J. & Krężel, A. Metal binding properties, stability and reactivity of zinc fingers. *Coordination Chemistry Reviews* **367**, 18-64, doi:10.1016/j.ccr.2018.04.009 (2018).
895 Kochańczyk, T., Drozd, A. & Krężel, A. Relationship between the architecture of zinc coordination and zinc binding affinity in proteins--insights into zinc regulation. *Metallomics* **7**, 244-257, doi:10.1039/c4mt00094c (2015).
896 Maret, W. New perspectives of zinc coordination environments in proteins. *Journal of inorganic biochemistry* **111**, 110-116, doi:10.1016/j.jinorgbio.2011.11.018 (2012).
897 Dyson, H. J. *et al.* Effects of buried charged groups on cysteine thiol ionization and reactivity in Escherichia coli thioredoxin: structural and functional characterization of mutants of Asp 26 and Lys 57. *Biochemistry* **36**, 2622-2636, doi:10.1021/bi961801a (1997).
898 Namuswe, F. & Berg, J. M. Secondary interactions involving zinc-bound ligands: roles in structural stabilization and macromolecular interactions. *Journal of inorganic biochemistry* **111**, 146-149, doi:10.1016/j.jinorgbio.2011.10.018 (2012).
899 Perutz, M. F. Electrostatic effects in proteins. *Science* **201**, 1187-1191, doi:10.1126/science.694508 (1978).
900 Gupta, V. & Carroll, K. S. Sulfenic acid chemistry, detection and cellular lifetime. *Biochimica et Biophysica Acta (BBA) - General Subjects* **1840**, 847-875, doi:10.1016/j.bbagen.2013.05.040 (2014).
901 Reisz, J. A., Bechtold, E., King, S. B., Poole, L. B. & Furdui, C. M. Thiol-blocking electrophiles interfere with labeling and detection of protein sulfenic acids. *Febs j* **280**, 6150-6161, doi:10.1111/febs.12535 (2013).
902 Wu, D. & Yotnda, P. Production and detection of reactive oxygen species (ROS) in cancers. *J Vis Exp*, doi:10.3791/3357 (2011).

903 Gonos, E. S. *et al.* Origin and pathophysiology of protein carbonylation, nitration and chlorination in age-related brain diseases and aging. *Aging (Albany NY)* **10**, 868-901, doi:10.18632/aging.101450 (2018).
904 Kane, J. F. Effects of rare codon clusters on high-level expression of heterologous proteins in Escherichia coli. *Current Opinion in Biotechnology* **6**, 494-500, doi:10.1016/0958-1669(95)80082-4 (1995).
905 Baca, A. M. & Hol, W. G. J. Overcoming codon bias: A method for high-level overexpression of Plasmodium and other AT-rich parasite genes in Escherichia coli. *International Journal for Parasitology* **30**, 113-118, doi:10.1016/S0020-7519(00)00019-9 (2000).
906 Hartinger, D. *et al.* Enhancement of solubility in Escherichia coli and purification of an aminotransferase from Sphingopyxis sp. MTA144 for deamination of hydrolyzed fumonisin B1. *Microbial Cell Factories* **9**, 62, doi:10.1186/1475-2859-9-62 (2010).
907 Mieyal, J. J., Gallogly, M. M., Qanungo, S., Sabens, E. A. & Shelton, M. D. Molecular Mechanisms and Clinical Implications of Reversible Protein S-Glutathionylation. *Antioxidants & Redox Signaling* **10**, 1941-1988, doi:10.1089/ars.2008.2089 (2008).
908 Kirkman, H. N. & Gaetani, G. F. Mammalian catalase: a venerable enzyme with new mysteries. *Trends Biochem Sci* **32**, 44-50, doi:10.1016/j.tibs.2006.11.003 (2007).
909 Meister, A. Glutathione metabolism and its selective modification. *J Biol Chem* **263**, 17205-17208 (1988).
910 Zhou, Z. D. & Lim, T. M. Glutathione conjugates with dopamine-derived quinones to form reactive or non-reactive glutathione-conjugates. *Neurochem Res* **35**, 1805-1818, doi:10.1007/s11064-010-0247-7 (2010).
911 Bayır, H. *et al.* Peroxidase Mechanism of Lipid-dependent Cross-linking of Synuclein with Cytochrome c*. *Journal of Biological Chemistry* **284**, 15951-15969, doi:10.1074/jbc.M900418200 (2009).
912 Chernivec, E., Cooper, J. & Naylor, K. Exploring the Effect of Rotenone-A Known Inducer of Parkinson's Disease-On Mitochondrial Dynamics in Dictyostelium discoideum. *Cells* **7**, doi:10.3390/cells7110201 (2018).
913 Begaye, A. & Sackett, D. L. Measurement of ligand binding to tubulin by sulfhydryl reactivity. *Methods Cell Biol* **95**, 391-403, doi:10.1016/S0091-679X(10)95021-8 (2010).
914 Sowmiah, S., Esperança, J. M. S. S., Rebelo, L. P. N. & Afonso, C. A. M. Pyridinium salts: from synthesis to reactivity and applications. *Organic Chemistry Frontiers* **5**, 453-493, doi:10.1039/C7QO00836H (2018).
915 Xiong, Y., Uys, J. D., Tew, K. D. & Townsend, D. M. S-glutathionylation: from molecular mechanisms to health outcomes. *Antioxid Redox Signal* **15**, 233-270, doi:10.1089/ars.2010.3540 (2011).
916 Go, Y. M. & Jones, D. P. Redox biology: interface of the exposome with the proteome, epigenome and genome. *Redox Biol* **2**, 358-360, doi:10.1016/j.redox.2013.12.032 (2014).
917 Stepanenko, A. A. & Heng, H. H. Transient and stable vector transfection: Pitfalls, off-target effects, artifacts. *Mutation Research/Reviews in Mutation Research* **773**, 91-103, doi:10.1016/j.mrrev.2017.05.002 (2017).
918 Hurd, T. R., James, A. M., Lilley, K. S. & Murphy, M. P. in *Methods Enzymol* Vol. 456 343-361 (2009).
919 Hwang, C., Lodish, H. F. & Sinskey, A. J. in *Methods in Enzymology* Vol. 251 212-221 (Academic Press, 1995).
920 Su, D. *et al.* Proteomic identification and quantification of S-glutathionylation in mouse macrophages using resin-assisted enrichment and isobaric labeling. *Free Radic Biol Med* **67**, 460-470, doi:10.1016/j.freeradbiomed.2013.12.004 (2014).
921 Cook, J. A., Iype, S. N. & Mitchell, J. B. Differential specificity of monochlorobimane for isozymes of human and rodent glutathione S-transferases. *Cancer Res* **51**, 1606-1612 (1991).
922 Butturini, E., Boriero, D., Carcereri de Prati, A. & Mariotto, S. Immunoprecipitation methods to identify S-glutathionylation in target proteins. *MethodsX* **6**, 1992-1998, doi:10.1016/j.mex.2019.09.001 (2019).
923 Jessop, C. E. & Bulleid, N. J. Glutathione directly reduces an oxidoreductase in the endoplasmic reticulum of mammalian cells. *J Biol Chem* **279**, 55341-55347, doi:10.1074/jbc.M411409200 (2004).
924 Ittisoponpisan, S. *et al.* Can Predicted Protein 3D Structures Provide Reliable Insights into whether Missense Variants Are Disease Associated? *Journal of molecular biology* **431**, 2197-2212, doi:10.1016/j.jmb.2019.04.009 (2019).
925 Mårtensson, J., Steinherz, R., Jain, A. & Meister, A. Glutathione ester prevents buthionine sulfoximine-induced cataracts and lens epithelial cell damage. *Proc Natl Acad Sci U S A* **86**, 8727-8731, doi:10.1073/pnas.86.22.8727 (1989).
926 Lee, K. J., Kang, D. & Park, H.-S. Site-Specific Labeling of Proteins Using Unnatural Amino Acids. *Molecules and cells* **42**, 386-396, doi:10.14348/molcells.2019.0078 (2019).
927 Farzam, A. *et al.* A functionalized hydroxydopamine quinone links thiol modification to neuronal cell death. *Redox biology* **28**, 101377-101377, doi:10.1016/j.redox.2019.101377 (2020).

Appendix C-Additional data

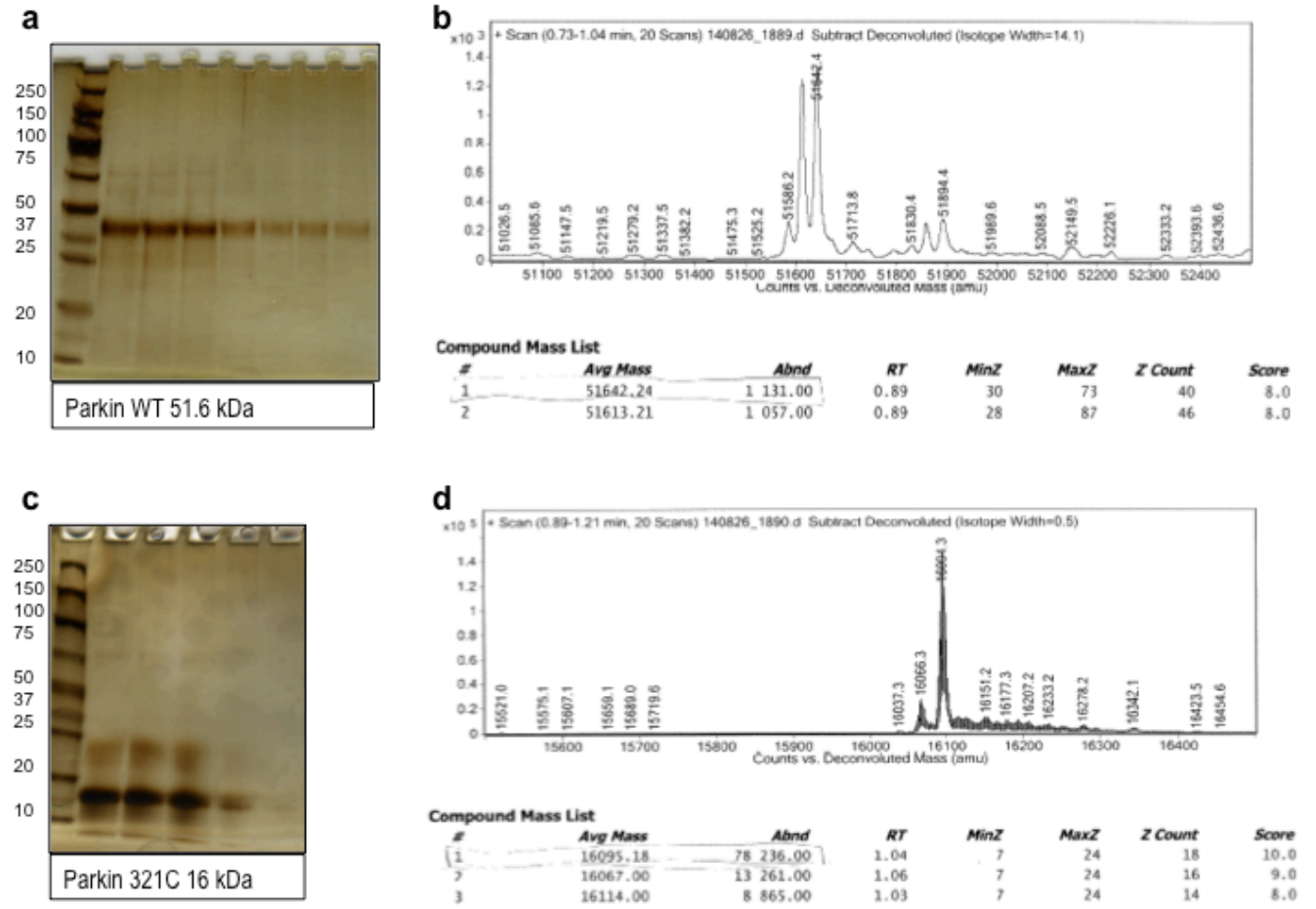

Figure C1. Examples of purity and exact masses of parkin proteins expressed in pET-SUMO vectors
(**a**) Full-length wild type (WT) Parkin, containing amino acids 1-465, run on silver stained SDS-PAGE (under reducing conditions) following expression in and purification from *E coli,* with corresponding electron-spray ionization mass spectrometry results in (**b**) indicating predicted mass of 51642.24 m/z. Truncated wild type Parkin, containing amino acids 321-465 and denoted 321C, run on silver stained SDS-PAGE (under reducing conditions) following expression in and purification from *E. coli*, (**c**) with corresponding electron-spray ionization mass spectrometry results in (**d**) indicating predicted mass of 16095.18 m/z.

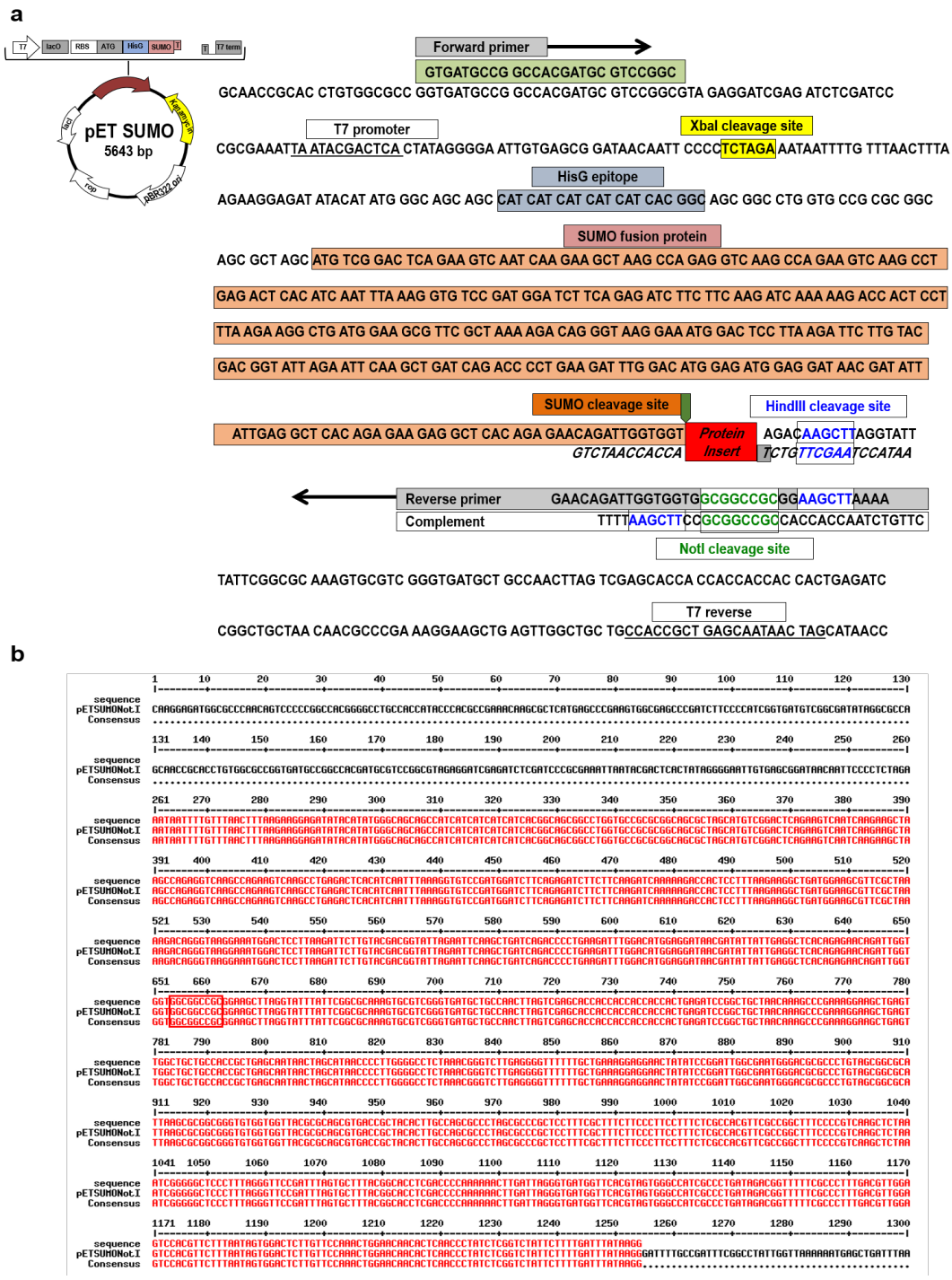

Figure C2. Insertion of Not1 restriction enzyme site into the pET-SUMO construct

(**a**) Expansion of cloning region in pET-SUMO vector including location of sequences for: T7 promoter/reverse, poly-His tag and SUMO protein upstream of protein of interest, and restriction enzyme cleavage sites for XbaI and HindIII. Addition of NotI cleavage site was incorporated by sequential cloning using the above forward and reverse primers which allowed for subsequent introduction of different protein sequences using sequential restriction enzyme cloning. (**b**) Sequencing results of isolated plasmid DNA aligned against theoretical sequence of pET-SUMO with NotI restriction enzyme site. Sequencing was performed using a standard T7 primer and alignment performed using Multialin online tool version 5.4.1. Location of NotI sequence indicated by red box (GGCGGCCGC). Sequence of pET-SUMO obtained from manufacturer (Invitrogen).

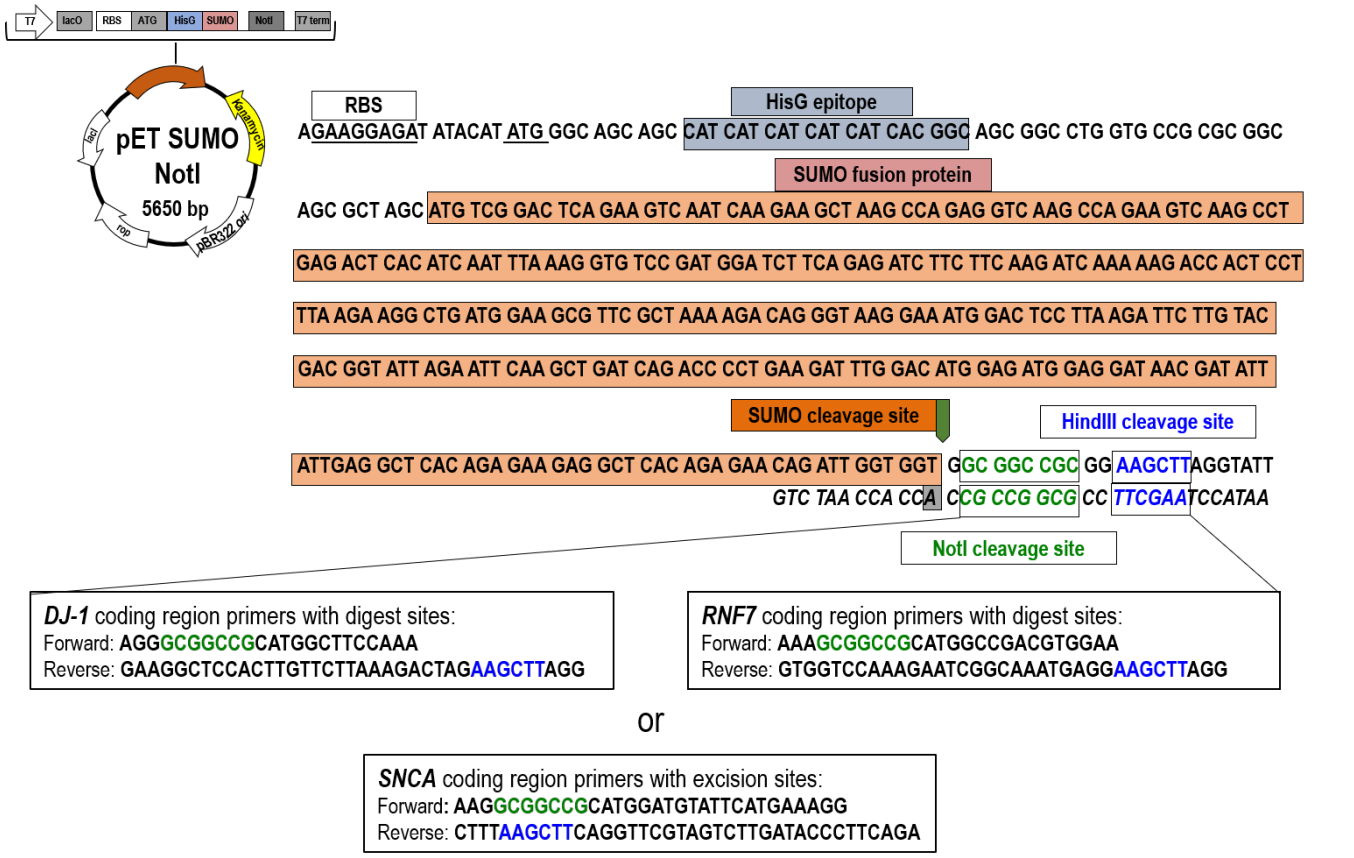

Figure C3. Cloning strategy used to insert *DJ-1*, *RNF7* and *SNCA* sequences into the pET-SUMO construct
Sequences for desired proteins were inserted between the NotI and HindIII restriction sites found in the newly formed pET-SUMO NotI expression plasmid. Forward and reverse primers, shown above, were used to amplify *DJ-1*, *SNCA* (α-synuclein) and *RNF7* (ring finger protein 7 or sensitive to apoptosis gene, SAG) protein expression sequences for insertion into pET-SUMO NotI.

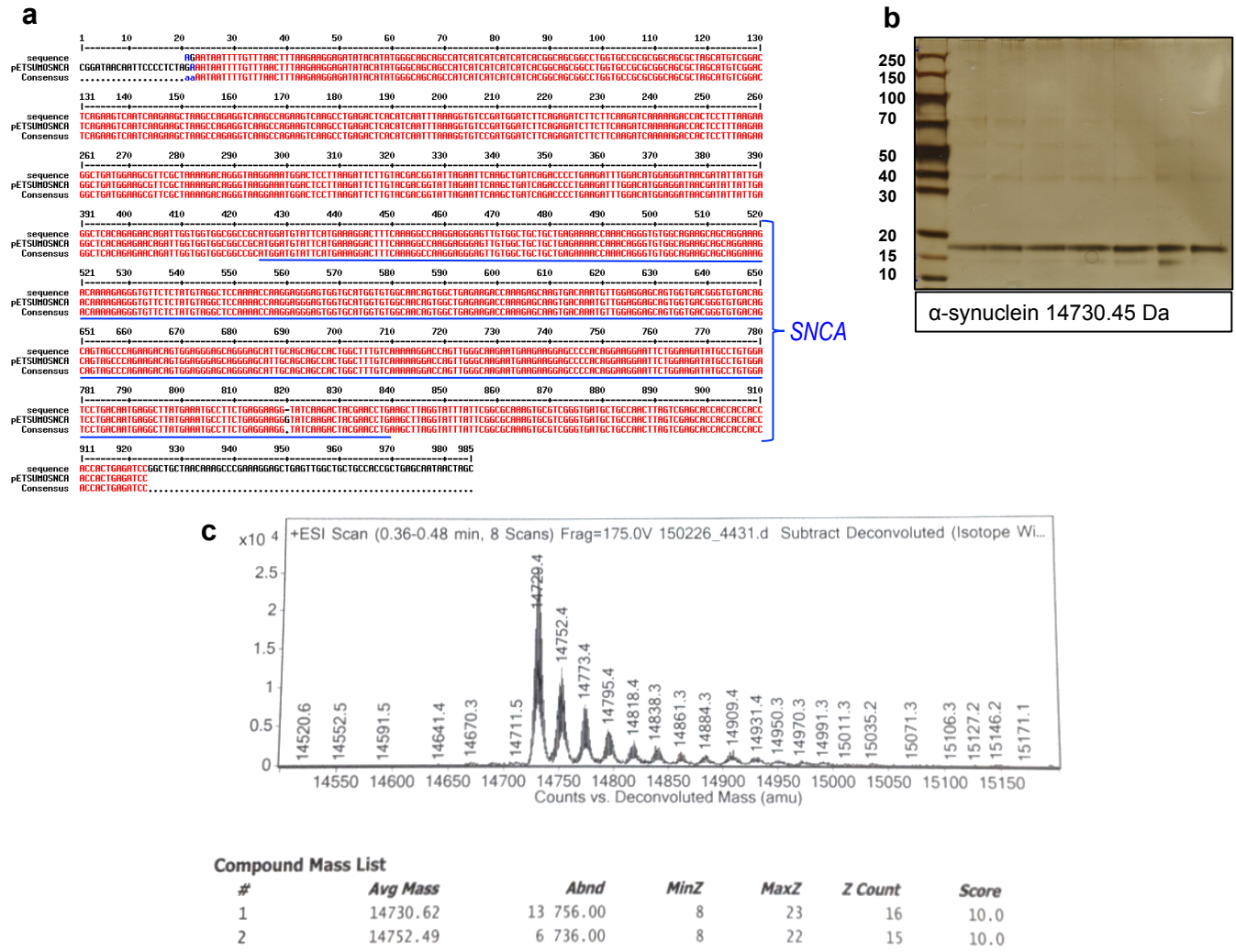

Figure C4. DNA sequence, purity and exact mass of pET-SUMO *SNCA* ligation product

(**a**) Sequencing results of isolated plasmid DNA aligned against theoretical pET-SUMO with inserted sequence for *SNCA* (NCBI Nucleotide GenBank ID # CR457058.1) using standard T7 primer and Multialin online tool version 5.4.1. Location of *SNCA* sequence insertion is indicated by blue underline. (**b**) Silver stained SDS-PAGE reducing gel of α-synuclein protein expressed and purified using the pET-SUMO *SNCA* ligation product in *E. coli*. (**c**) Expected protein molecular weight was calculated using ExPasy protein parameter calculator. Electron-spray ionization mass spectrometry results of purified protein identifies mass of 14730.62 m/z.

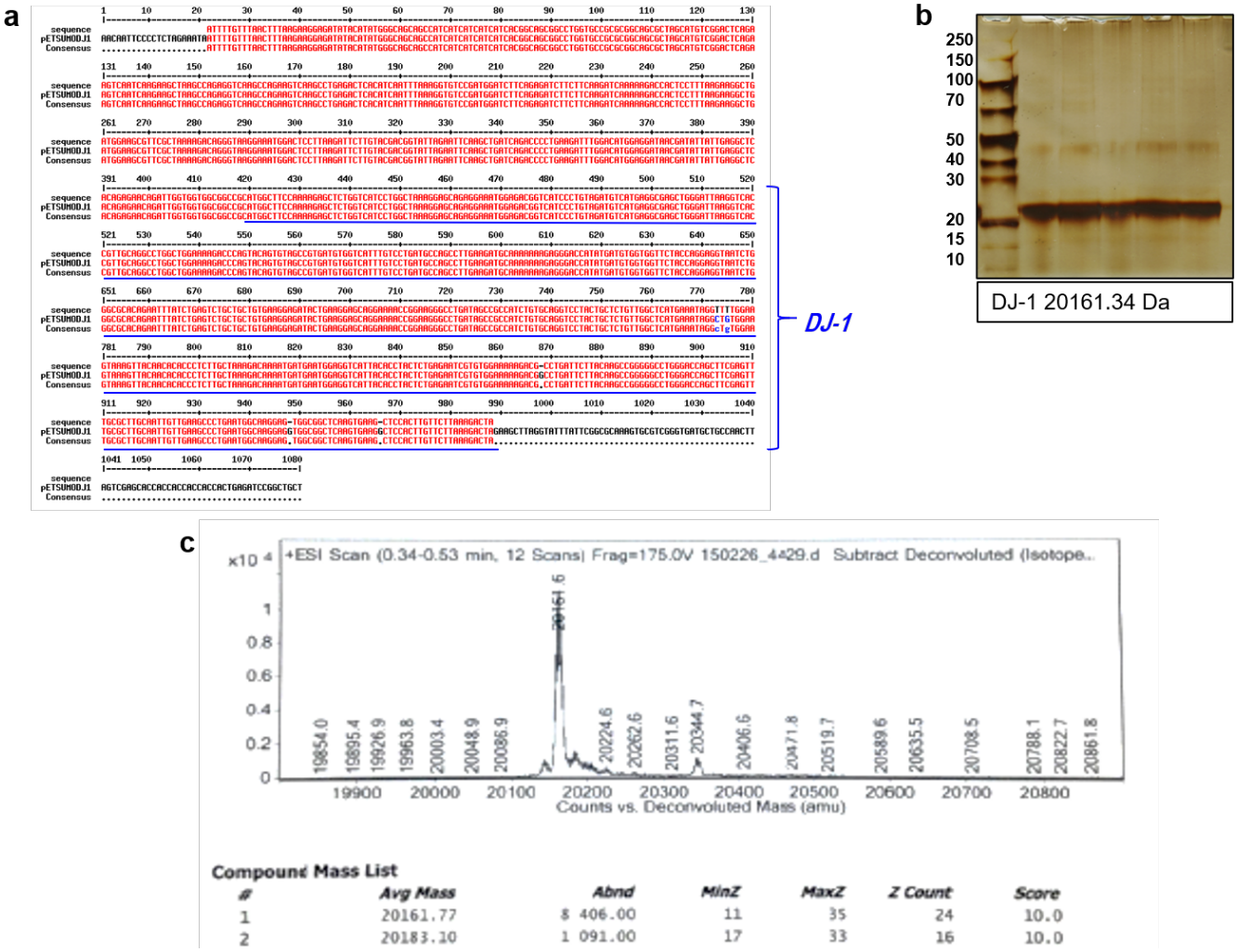

Figure C5. DNA sequence, purity and exact mass of pET-SUMO *DJ-1* ligation product
(**a**) Sequencing results of isolated plasmid DNA aligned against theoretical pET-SUMO with inserted sequence for *DJ-1* (NCBI Nucleotide GenBank ID # D61380.1) using standard T7 primer and Multialin online tool version 5.4.1. Location of *DJ-1* sequence insertion is indicated by blue underline. (**b**) Silver stained SDS-PAGE reducing gel of DJ-1 protein expressed and purified using the pET-SUMO *DJ-1* ligation product in *E. coli*. (**c**) Expected protein molecular weight was calculated using ExPasy protein parameter calculator. Electron-spray ionization mass spectrometry results of purified protein identifies mass of 20161.77 m/z, C. DJ-1, deglycase 1

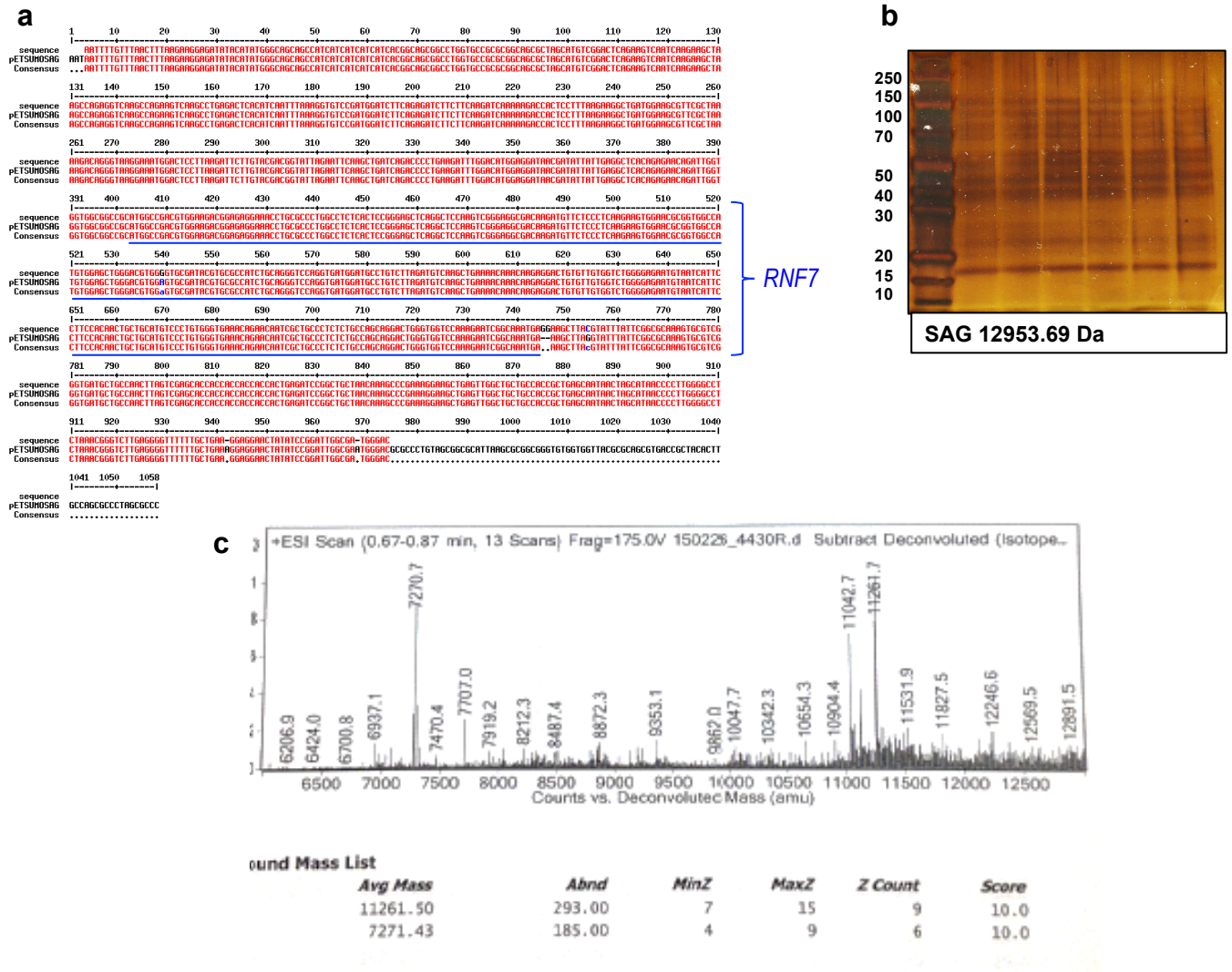

Figure C6. DNA sequence, purity and exact mass of pET-SUMO *RNF7* ligation product

(**a**) Sequencing results of isolated plasmid DNA aligned against theoretical pET-SUMO with inserted sequence for *RNF7* (NCBI Nucleotide GenBank ID # NM_014245.5, 45 to 386) using standard T7 primer and Multialin online tool version 5.4.1. Location of *RNF7* sequence insertion is indicated by blue underline. (**b**) Silver stained SDS-PAGE reducing gel of SAG protein expressed and purified using the pET-SUMO *RNF7* ligation product in *E. coli*. (**c**) Expected protein molecular weight was calculated using ExPasy protein parameter calculator. Electron-spray ionization mass spectrometry results of purified protein identifies mass of 11261.50 m/z.

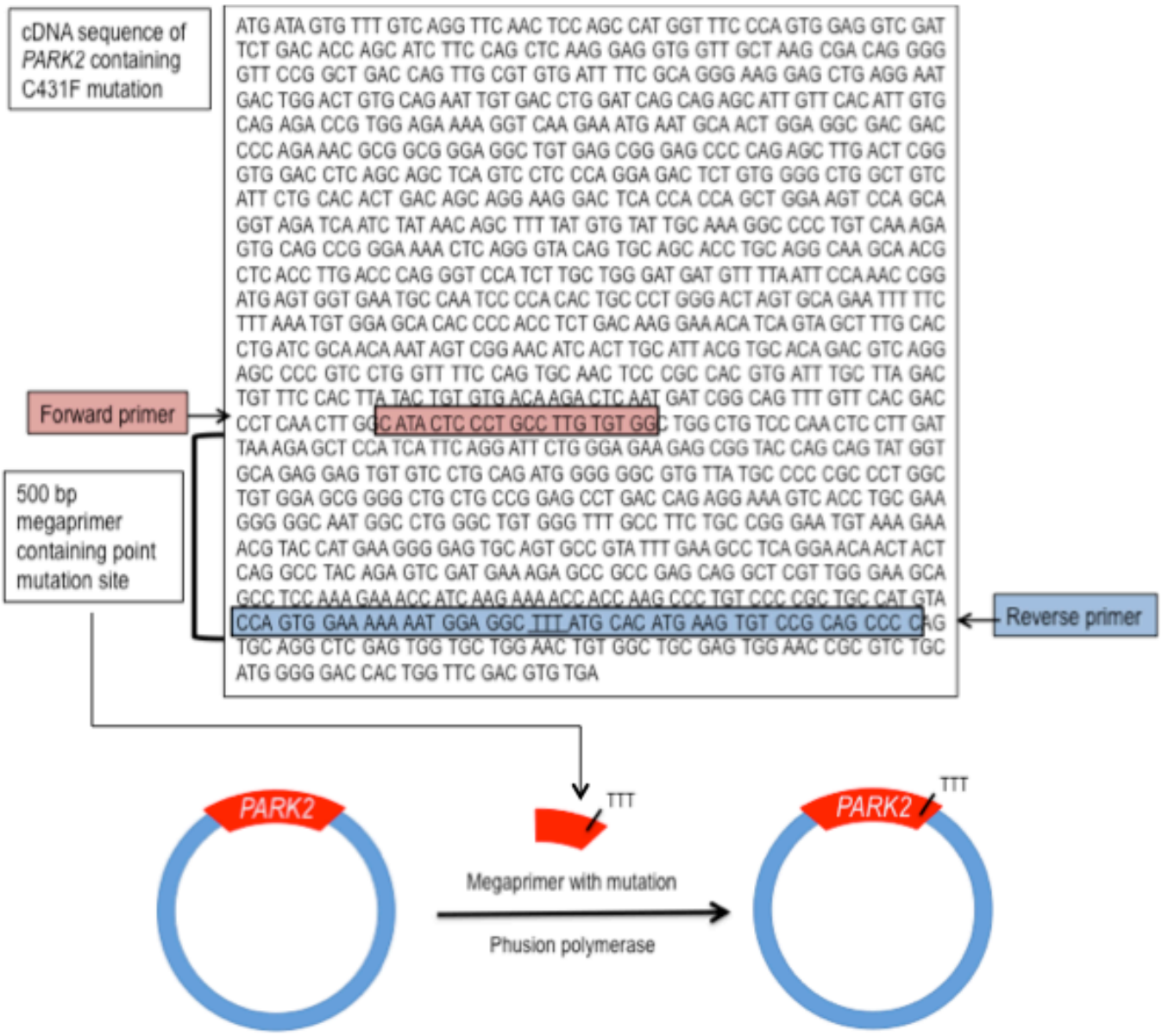

Figure C7. Cloning strategy used to incorporate PD-linked point mutations in *PRKN* sequence
Parkin protein point mutations C95A, C289G, G328E, C431F and W453X were introduced into the pET-SUMO (bacterial) or pcDNA (mammalian) expression vectors using: vectors containing the full wild-type *PKRN* sequence, a megaprimer (about 500 bp) containing the desired point mutation, and high-fidelity DNA polymerase Phusion. The megaprimers were generated using forward and reverse primers designed using A plasmid Editor (ApE) version 2.0.49. An example is shown above for C431F.

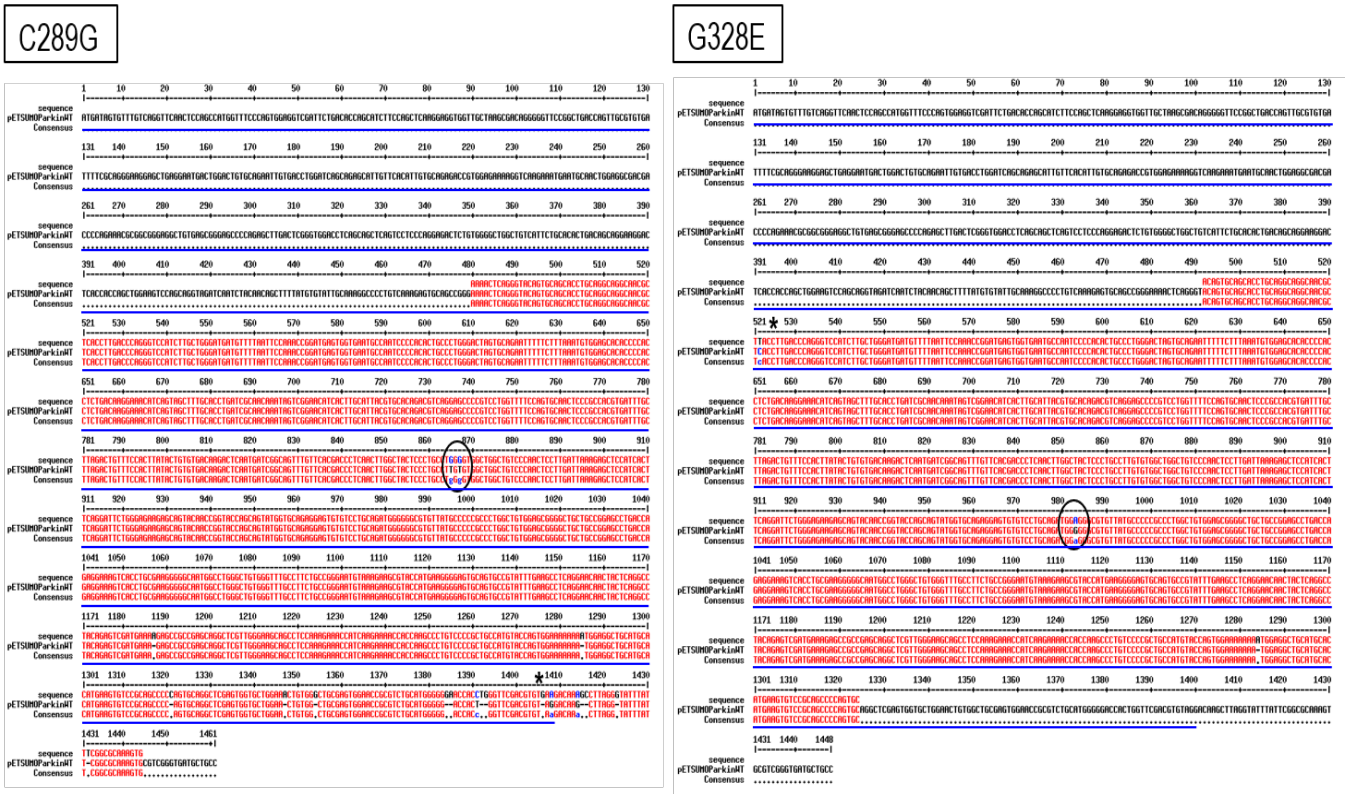

Figure C8. DNA sequencing of pET-SUMO Parkin with point mutations C289G and G328E

Sequencing results of isolated plasmid DNA aligned against theoretical sequence of pET-SUMO containing *PRKN* mRNA transcript gene sequence (underlined in blue). Sequencing was performed using a custom designed primer (P500) that starts at nucleotide 500 on the *PRKN* sequence (5' GCAGTACAACCGGTACCAGC 3') and alignment performed using Multialin online tool version 5.4.1. Sequence of pET-SUMO obtained from manufacturer (Invitrogen) and *PRKN* gene obtained from NCBI (GenBank ID# NM_004562.3 nucleotides 99-1496 for Parkin WT). Location of point mutation is indicated with a black circle. Mismatches indicated by * confer no point mutation.

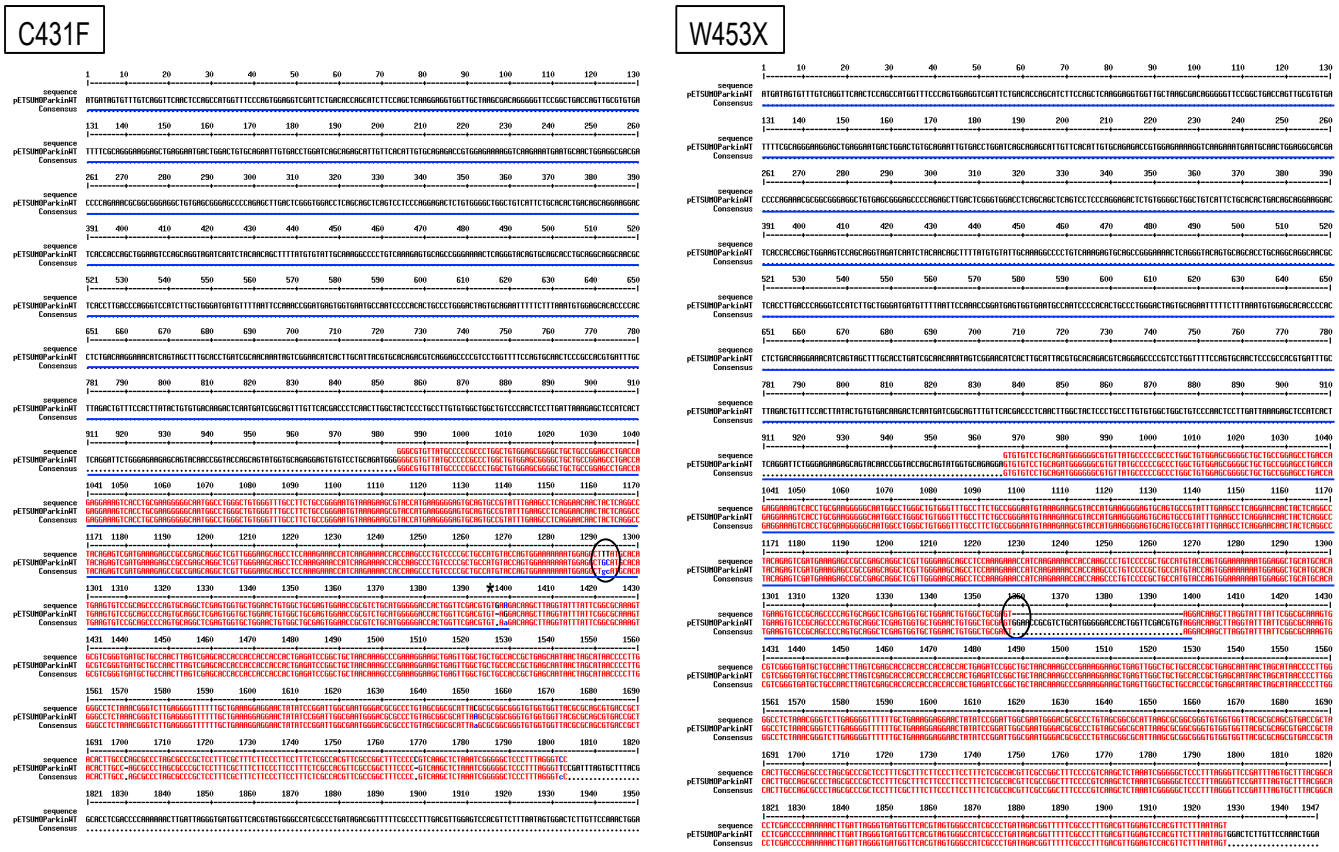

Figure C9. DNA sequencing of pET-SUMO Parkin with point mutations C431F and W453X
Sequencing was performed as in Fig. C8 using a custom designed primer (P1000) that starts at nucleotide 1000 on the *PRKN* sequence (5' GCTGGAAGTCCAGCAGGTAGATC 3')

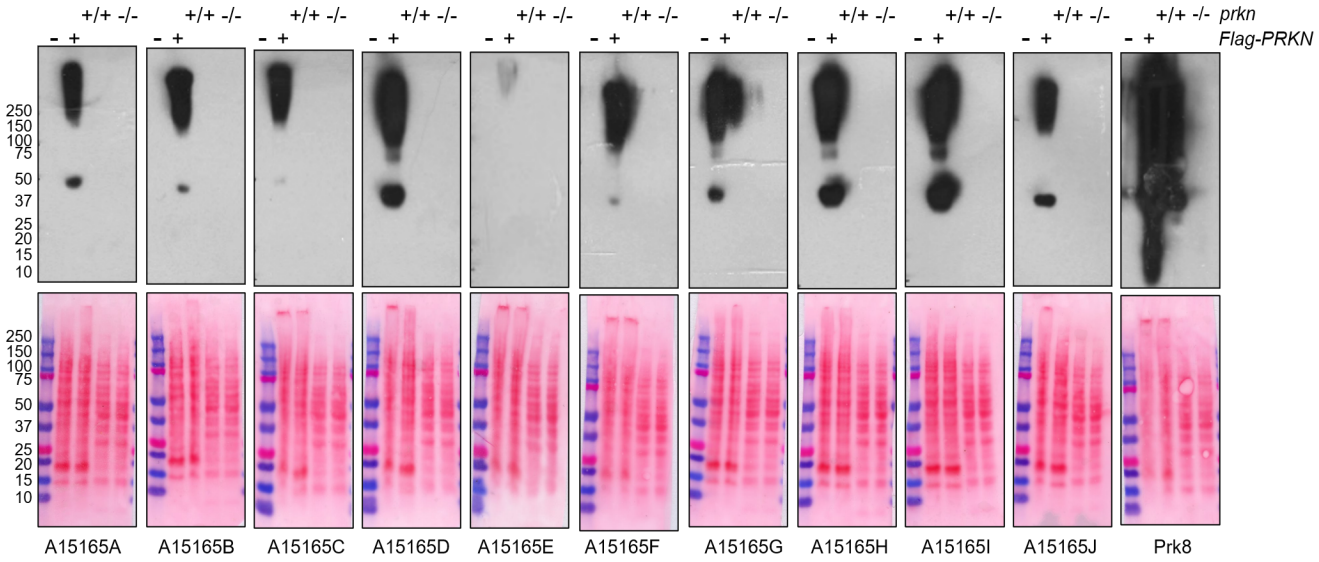

Figure C10. Immunoblotting of parkin in HEK-293 cells and mouse brain lysates using clones A15165A-J generated by BioLegend Inc.

SDS-PAGE of HEK-293 cell lysates overexpressing FLAG *PRKN* (+) vs. FLAG vector control (-) (lanes 1 and 2, 15 µg), and wild type (+/+) vs. *prkn* knockout (-/-) mouse brain lysates (lanes 3 and 4, 20 µg). Samples were run under reducing conditions and immunoblotted using BioLegend clones A15165A-J and Prk8 as parkin control, followed by 1:10000 α-mouse secondary antibody. Corresponding Ponceau S is below each blot. Concentrations of primary antibodies are as follows: A (1:5000), B (1:1000), C (1:1000), D (1:1000), E (1:500), F (1:1000), G (1:1000), H (1:1000), I (1:1000), J (1:1000) and Prk8 (1:20k). See methods (section 4.7) in Chapter 4 for antibody concentrations in µg/mL.

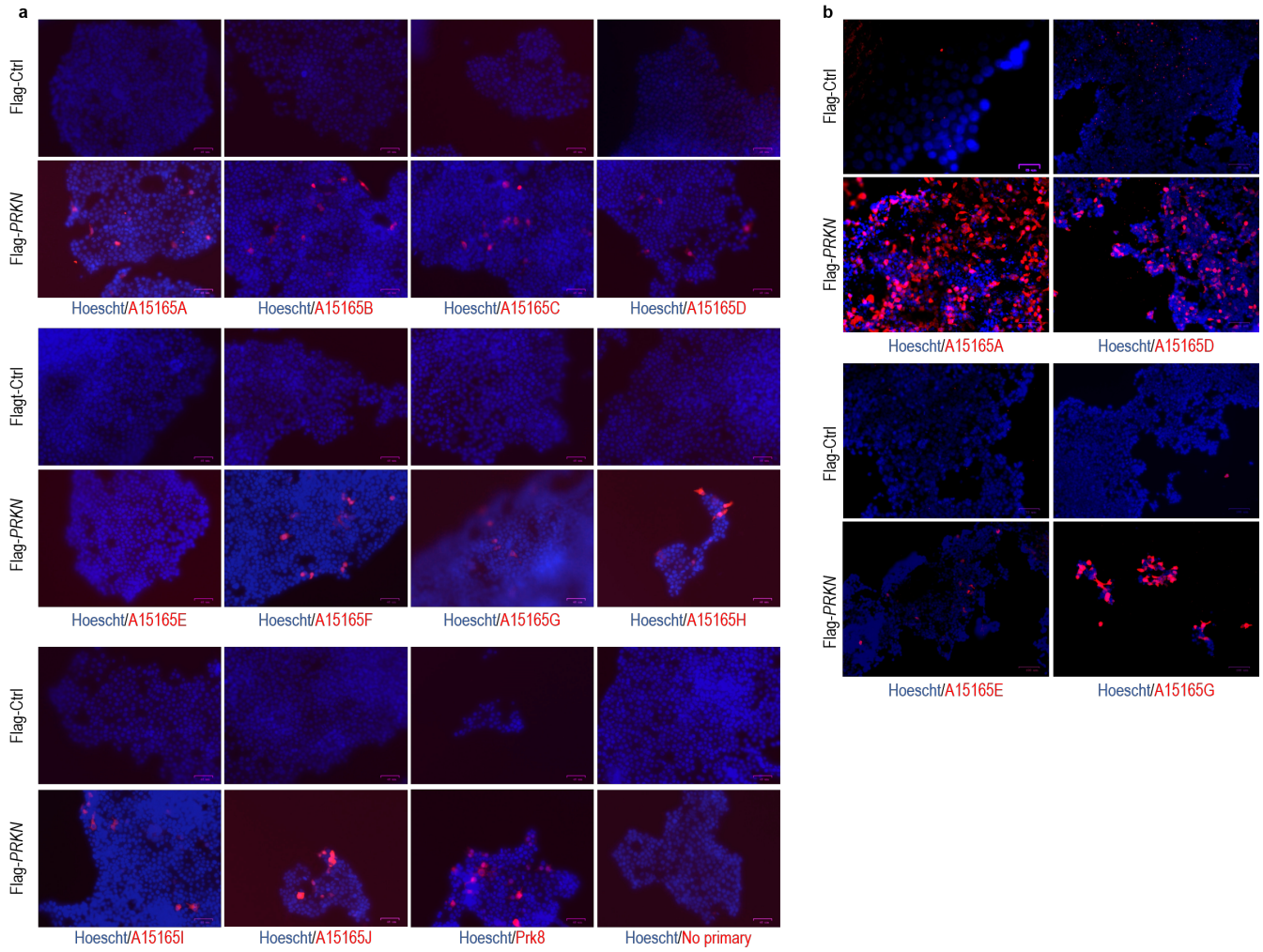

Figure C11. Immunofluorescent detection of parkin in HEK-293 cells using clones A15165A-J generated by BioLegend Inc.

Two examples of immunofluorescence trials using HEK-293 cells transfected with FLAG-*PRKN* or FLAG vector control and stained with primary anti-parkin monoclonal antibodies A15165A-J (1: 100) and Prk8 (1:100). Alexa fluor 594 -conjugated goat anti-mouse served as secondary antibody and cells were counterstained with Hoescht. Scale bars in (**a**) represent 46 µm and in (**b**) represent 100 µm except FLAG-Ctrl for A15165A (25 µm), FLAG-*PRKN* for A15165A (84 µm) and FLAG-Ctrl for A15165E (72 µm). See methods (section 4.7) in Chapter 4 for antibody concentrations in µg/mL.

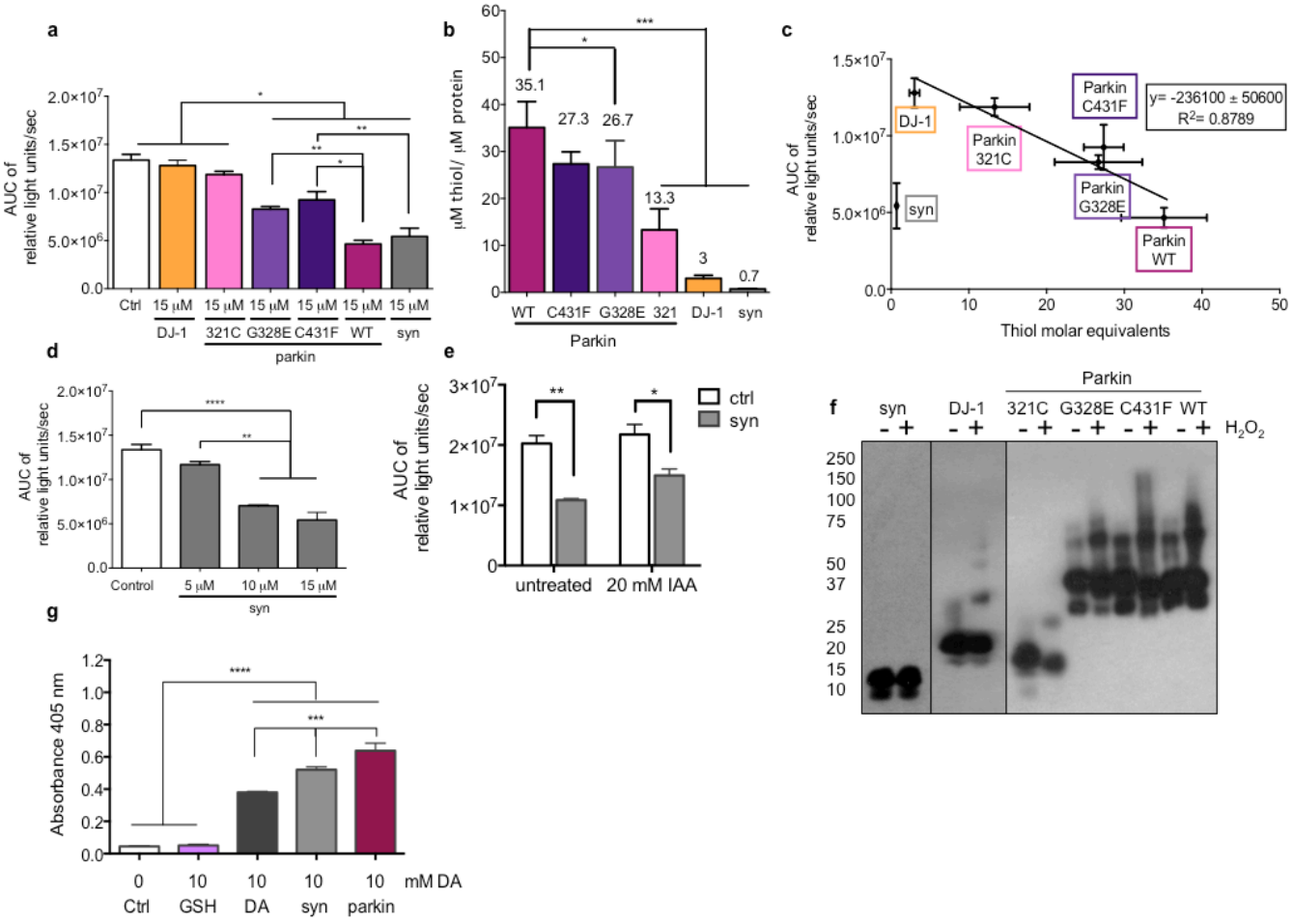

Figure C12. Reactive oxygen species and melanin produced in the presence of α-synuclein

(**a**) Chemiluminescence assay results for tagless proteins produced by pET-SUMO plasmid expression as in **Fig. 2.5e** with addition of results for α-synuclein. (**b**) Proteins in (**a**) were measured for total thiol content using Ellman's colorimetric assay as in **Fig. 2.5f** with addition of results for α-synuclein. (**c**) Regression plot as found in **Fig. 2.5g** with addition of results for α-synuclein. (**d**) Chemiluminescence assay results of tagless α-synuclein run at 5, 10 and 15 μM. (**e**) Chemiluminescence assay results of tagless α-synuclein run at 15 μM in the presence of 1 mM H_2O_2 and 20 mM iodoacetamide (IAA). (**f**) SDS-PAGE of proteins exposed to 1 mM H_2O_2 run under non-reducing conditions and blotted for parkin (Prk8, 1: 20k), DJ-1 (1: 2000) and α-synuclein (syn-1, 1:1000). Proteins were loaded at a concentration of 20 μM. (**g**) Formation of melanin after 60 min in the presence of tagless recombinant α-synuclein and WT parkin. Data in (**a**, **b**, **d**, and **g**) represent a total of three trials run in triplicate and was analyzed using one-way ANOVA with Tukey's post hoc test, (**a**): [$F(8,19)=78.88$], $p<0.0001$; (**b**): [$F(5,20)=53.23$], $p<0.0001$; (**d**): [$F(3,9)=45.79$], $p<0.0001$; and (**g**): [$F(4,10)=406.7$], $p<0.0001$. Data in **e** was analyzed by two-way ANOVA with Tukey's post hoc test, [$F\ (1,\ 8)\ =\ 45.31$, $p<\ 0.0001$], *$p<0.05$, **$p<0.001$. *$p<0.05$, **$p<0.01$, ***$p<0.001$ and ****$p<0.0001$. WT, Wild type parkin; 321C, truncated parkin (aa 321-465); G328E, PD-linked parkin point mutation; C431F, PD-linked parkin point mutant; syn, α-synuclein; DJ-1, deglycase 1; DA, dopamine; and GSH, glutathione.

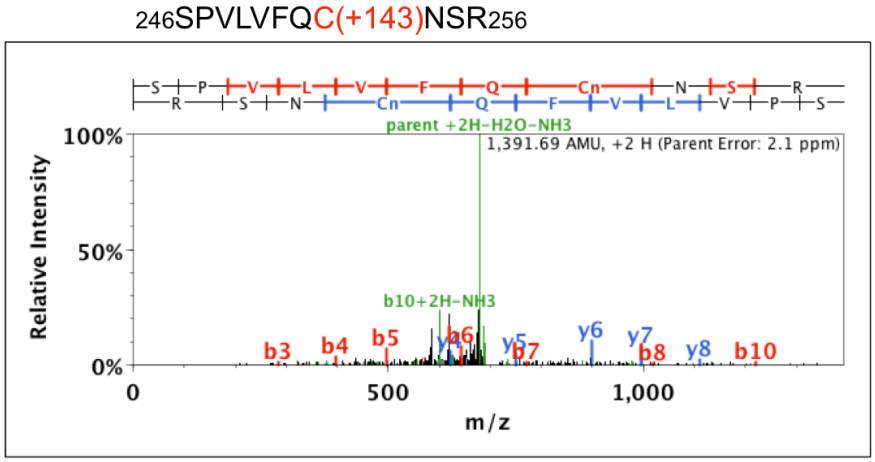

Peptide sequence	Variable modification identified by spectrum	Observed m/z	Spectrum charge	Actual peptide mass (AMU)	Predicted unmodified mass (AMU)	Peptide Identification Probability	Mascot Ion Score	Scaffold Peptide Score
246 SPVLVFQcNSR 256	C253 N-ethylmaleimide + water (+143)	696.852	2	1391.68	1248.63	100%	32.84	70.46

Figure C13. C253 N-ethylmaleimide modification detected on immunoprecipitated parkin from older human cortex. Parkin protein was immunoprecipitated as described in Chapter 2 from iodoacetamide treated human cortical SDS soluble extract derived from a 37-year-old patient (corresponding to sample ID #19 in **Supplementary Table 2.1**) Sample was eluted in Laemmli buffer containing100 mM dithiothreitol and treated with 500 mM N-ethylmaleimide overnight at 4°C before trypsin digestion and analysis by LC-MS/MS as described in Chapter 2. Shown is the LC-MS/MS spectrum and details for the peptide sequence containing N-ethylmaleimide + water on residue C253 with actual mass of 1391.68 amu. The observed m/z (696.852) corresponds to the actual mass divided by 2 with loss of both water (18 amu) and ammonia (17 amu), corresponding to peak 679.42 m/z, which is labeled in green.

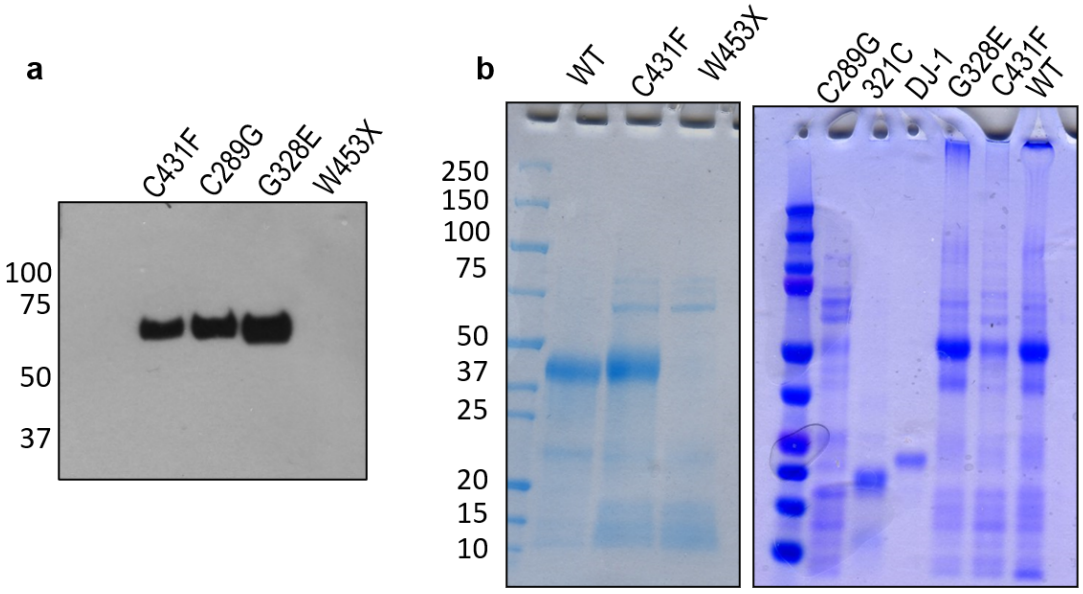

Figure C14. Bacterial expression of Parkinson disease-linked parkin point mutants
(**a**) Samples (10 µL) of crude extracts, from *E. coli* transformed with pET-SUMO Parkinson disease-linked parkin mutant plasmids, run on Western blot under reducing conditions and blotted for Parkin (2132S 1: 5000). Note that samples appear large in molecular weight (about 60 kDa) due to presence of poly-His tag. (**b**) Samples (10 µL) of purified protein, from *E. coli* transformed with pET-SUMO plasmids, run on Coomassie Blue-stained SDS-PAGE in reducing conditions. WT, Wild type and 321, truncated (aa 321-465) parkin.

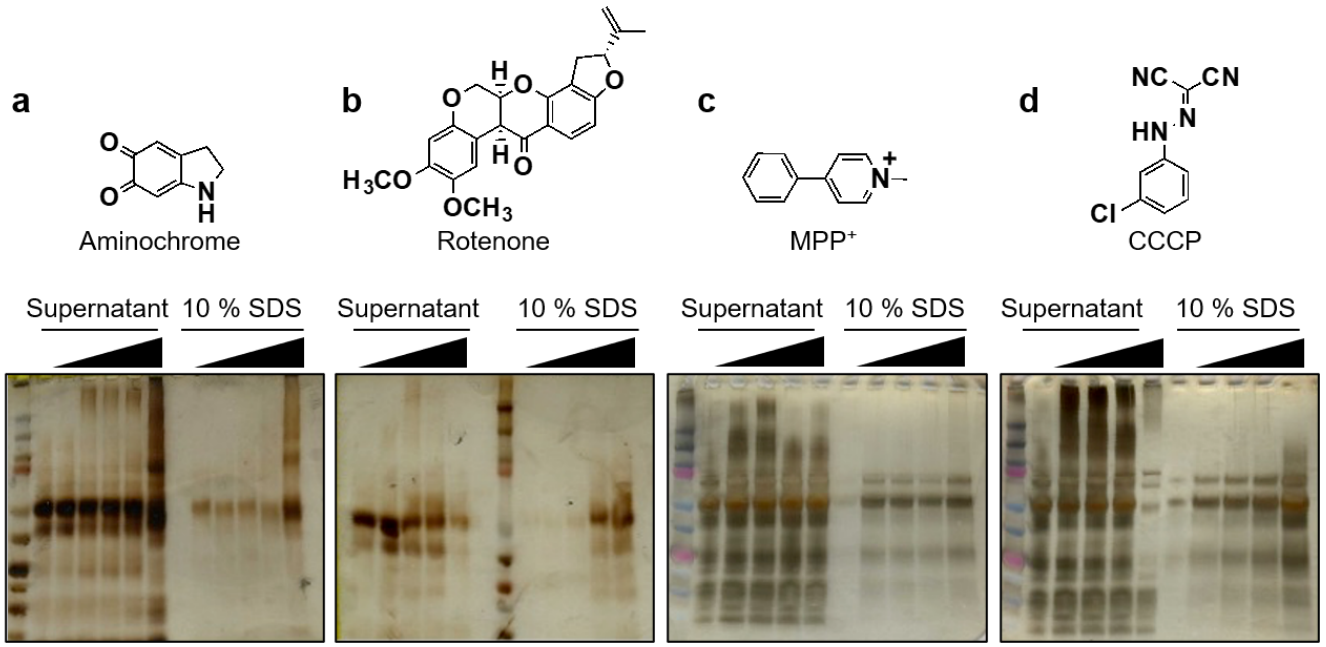

Figure C15. Effect of mitochondrial toxins on parkin solubility

Silver stained SDS-PAGE of recombinant parkin (10 µL of 20 µM, or 10 µg) reacted with the following increasing concentrations of mitochondrial toxins: (**a**) aminochrome at 2, 20, 50 and 200 µM, (**b**) rotenone and (**c**)1-methyl-4-phenylpyridinium (MPP+) at 10, 20, 200 and 2000 µM; and (**d**) carbonyl cyanide 3-chlorophenylhydrazone (CCCP) at 2, 20, 50 and 200 µM. Samples were treated for 30 min at 37ºC, spun at 21,000 x g for 15 min and resulting pellet and supernatant were loaded using Laemmli buffer containing 100 mM mercaptoethanol. Molecular structure of mitochondrial toxins is shown above corresponding gels.

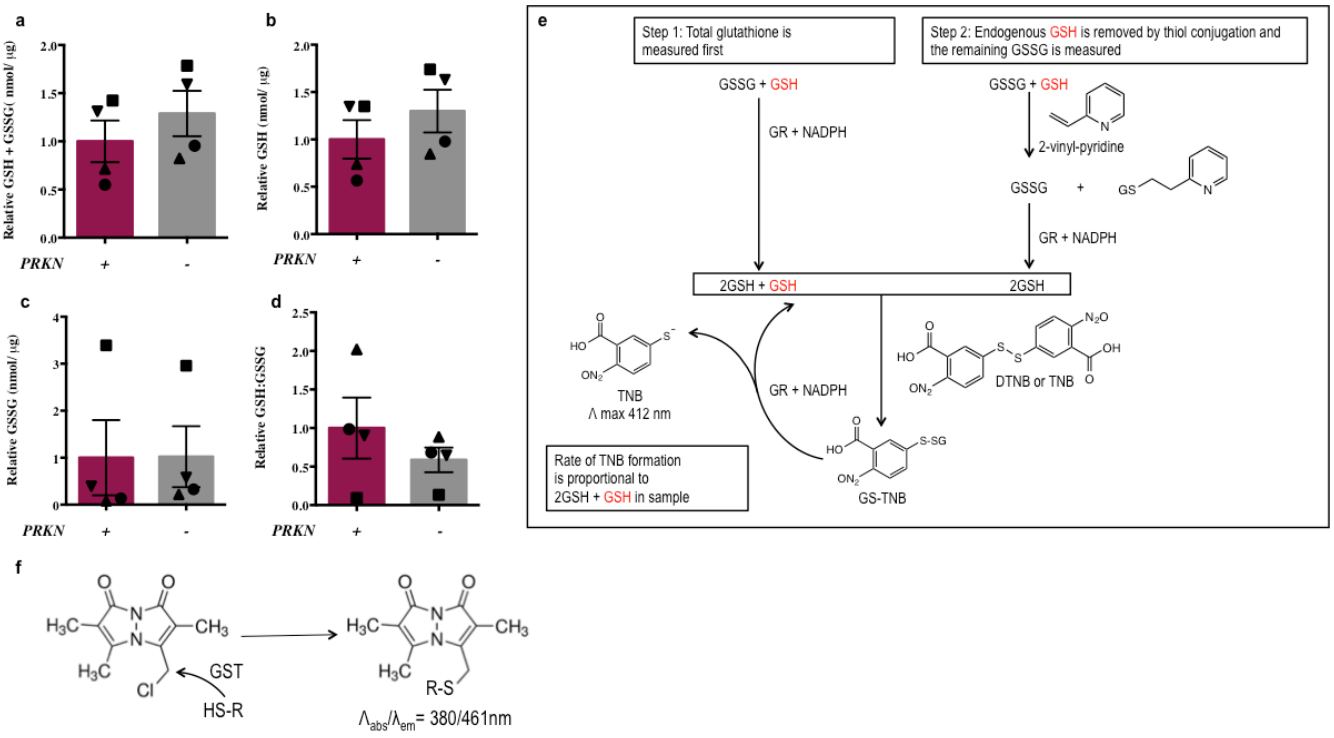

Figure C16. Enzymatic measurement of glutathione in cell and brain lysates
Total GSH + GSSG (**a**), GSH (**b**), GSSG (**c**) and GSH: GSSG (**d**) levels in HEK-293 cells expressing FLAG-*PRKN* or FLAG vector control, n=4. Raw values were measured by Tietze glutathione reductase recycling method, described in (**e**), and normalized to FLAG-*PRKN*. Tietze assay uses the reversible thiol-conjugating compound 5,5′-dithiobis-2-nitrobenzoic acid (DTNB) and the GSH-regenerating properties of glutathione reductase (GR) to measure GSH and GSSG levels in cell and tissue lysates. DNTB reacts with free GSH and produces GS-TNB. GR requires NADPH as co-factor to regenerate GSH and release 2-nitro-5-thiobenzoic acid (TNB). The rate of TNB produced represents the level of GSH and GSSG within the sample. For GSSG measurements, GSH is removed from the sample by irreversible conjugation to 2-vinyl-pyridine. (**f**) The monochlorobimane assay uses glutathione-*S*-transferase (GST) to conjugate free GSH to monochlorobimane, producing a fluorescently-active molecule. Unpaired Student T-test was used to measure statistical significance of (**a-d**). p=0.0576 for (**a**), p=0.0540 for (**b**), p=0.1300 for (**c**), and p=0.3367 for (**d**).

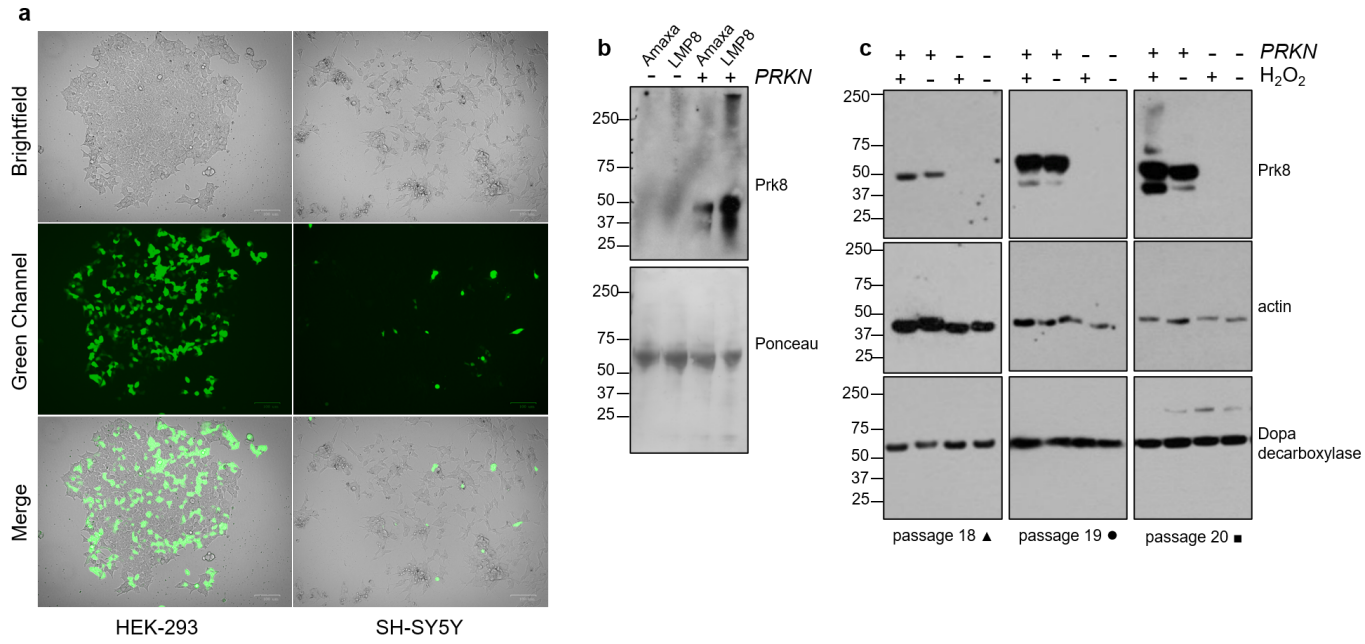

Figure C17. Transient parkin expression level in HEK-293 and SH-SY5Y cells
(**a**) Brightfield and green fluorescence images of HEK-293 and SH-SY5Y cells transfected using Lipofectamine2000 and polyoxamer 188. Scale bars represent 100 µm. Average transfection efficiency was 45.5 % and 6.1 % for HEK-293 and SH-SY5Y cells, respectively, and was calculated using cell counts from three images on ImageJ software (version 1.51j8).
(**b**) SDS-PAGE of SH-SY5Y cells transfected with FLAG-*PRKN* (+) or FLAG vector control (-) using commercially available Amaxa electroporation kit (Lonza) vs. polyoxamer 188 (LMP8), **b**. Cell lysates (20 µg/well) were run under reducing conditions and blotted for parkin using Prk8 (1:500). Parkin signal intensity (measured as pixel by ImageJ software) was normalized to Ponceau S staining, with the LMP8 method having approximately a 4-fold increase in parkin expression compared to the Amaxa method. (**c**) Parkin expression level in SH-SY5Y cells transfected with FLAG-*PRKN* or FLAG vector control, treated with or without 1 mM H_2O_2 and used to measure glutathione levels (n=3, see Figure 3.4f). Samples were loaded at 2.5 µg/well and blotted for parkin (Prk8, 1:1000), actin (1:500) and dopa decarboxylase (*aka* aromatic L-amino acid decarboxylase or L-AADC, 1:1000). Symbols shown next to passage numbers correspond to data points in **Fig. 3.4f.**

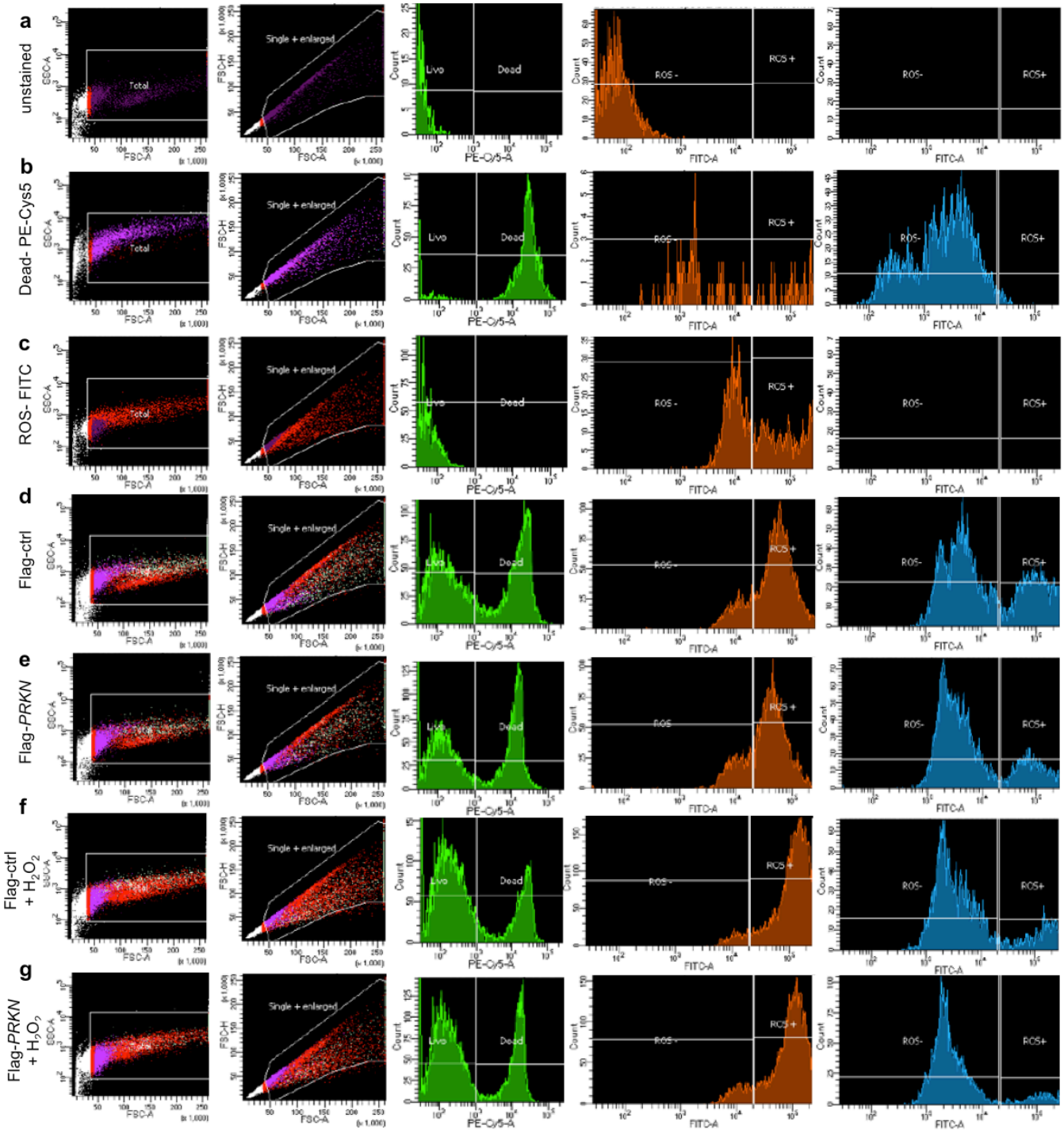

Figure C18. Example of gating used in flow cytometry measurements of intracellular reactive oxygen species
HEK-293 cells untreated in (**a**), treated with ethanol and stained with ethidium bromide (PE-Cys5 channel, shown in green) in (**b**), treated with H_2O_2 (2 mM) and stained with ROS fluorophore 2',7'-dichlorodihydrofluorescein diacetate, DCFDA, (appears in FITC channel, shown in orange) in (**c**), transfected with FLAG-control expression vector, treated with 0 mM (**d**) or 2 mM H_2O_2 (**f**) and stained with ethidium bromide and DCFDA, transfected with FLAG-*PRKN* expression vector, treated with 0 mM (**e**) or 2 mM H_2O_2 (**g**) and stained with ethidium bromide and DCFDA. Images in blue represent the level of ROS (FITC positive) in dead cells (PE-Cys5 positive). Note gating for FITC was based on transfected cells. Mean FITC (images in orange) was used to measure the level of ROS in live cells, see **Supplementary Fig. 3.4e**.

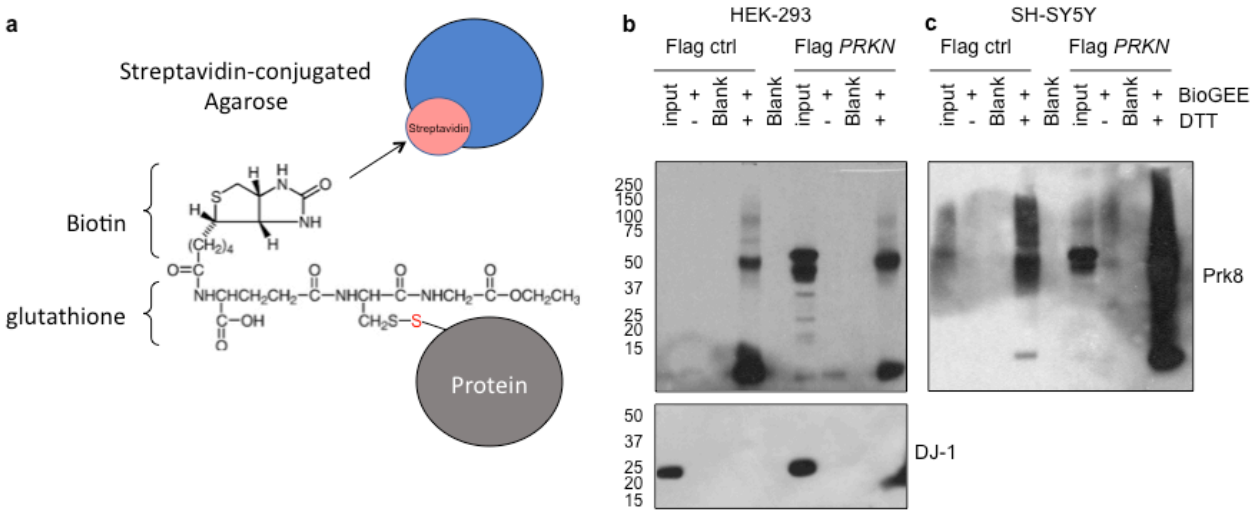

Figure C19. Protein thiol pull-down assay with glutathione ethyl ester biotin amide (BioGEE) pull-down assay.
(**a**) After BioGEE binds to free thiols, cells are lysed and BioGEE is pulled down using streptavidin bound agarose. Proteins that are bound to BioGEE via disulfide bonds are pulled down as well and are then removed from beads using 10 mM dithiolthreitol (DTT) and identified by SDS-PAGE immunoblotting. (**b**) Results from pull-down assay using HEK-293 cells overexpressing FLAG *PRKN* or vector control and 3 h incubation with 1.8 uM BioGEE (Invitrogen). Cells were wahed with 50 mM iodoacetamide in phosphate buffered saline (PBS) to quench excess BioGEE and lysed in RIPA buffer using sonication. Biotin-conjugated streptavidin was prepared by incubating D-biotin (3 mg/mL) with streptavidin conjugated agarose (0.5 mL) and incubated with lysates at 50 uL/mg protein to remove non-specific binding. Streptavidin agarose (100 µL/mg protein, Sigma) was added to the remaining lysate and incubated for 2 h with rocking. Following several washes with 0.1% SDS in PBS bound proteins were eluted with 10 mM DTT. Total protein elute and washes were concentrated using centrifugation (21 000 x g, for 20 min) in Amicon Ultra 10 kDa MWCO filters (Millipore) and run on reducing SDS-PAGE (100 mM DTT). Membrane was blotted for parkin (Prk8 1:20k) and DJ-1 (1:2000), n=1. Input represents 0.5 % of pull-down. (**c**) Results from pull-down assay using SH SY5Y cells overexpressing FLAG *PRKN* or vector control and 3 h incubation with 5 uM BioGEE. Experimental protocol is identical to **b**. Membrane was blotted for parkin (Prk8 1:20k) and input represents 2.5 % of pull-down., n=1.

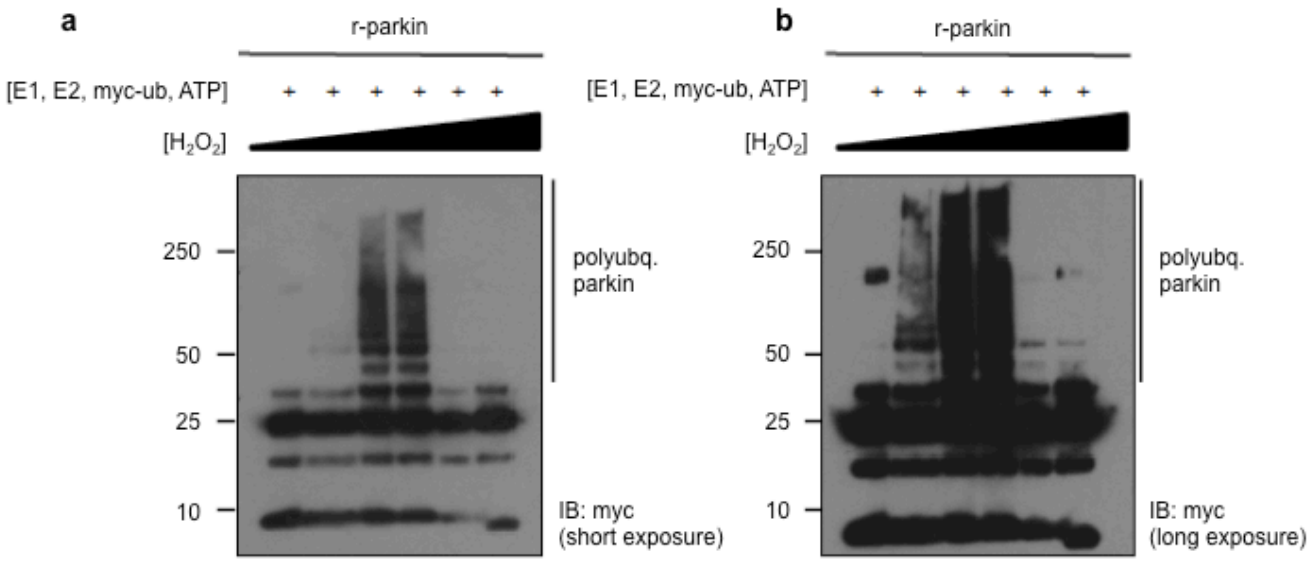

Figure C20. Biphasic effect of oxidation on parkin autoubiquitination of parkin.
The autoubiquitination of parkin was dependent on the presence of myc-tagged ubiquitin (myc-ub), ub activating (E1) and conjugating (E2) enzymes, as well as, ATP. The ubiquitination activity was monitored by immunoblotting for myc to visualize high molecular weight parkin species containing myc-tagged polyubiquitin chains. Parkin (1 μM) was incubated with increasing concentrations of H_2O_2 (0, 2μM, 20μM, 200μM, 2 mM and 20mM). Short exposure is shown in (**a**), vs. long exposure in (**b**). Assay performed by Daniel El-Kodsi.